Synthesis of sulfur and selenium doped anthanthrene

and

PXX catalysed photoredox aryl coupling reactions

Thesis by

Oliwia MATUSZEWSKA

Under the supervision of Prof. Davide BONIFAZI

Presented to the School of Chemistry of Cardiff University in Partial Fulfillment of the Requirements for the degree of Doctor of Philosophy (PhD) in Chemistry

November, 2021

Acknowledgements

First, I would like to thank my supervisor Prof. Davide Bonifazi, for placing his trust in me and giving me the opportunity to work in an international scientific environment.

I am very grateful to Dr Antoine Stopin for the proofreading of the thesis. I would like to thank Dr Rodolfo Tondo and Stephanie Wallace for their useful comments.

Special thanks to Cristofer Pezzetta for our fruitful collaboration and all the help and good times during our secondments. Many thanks to Robert Davidson and all the people at Dr. Reddys for making the secondment possible. I would also like to thank Prof. Paolo Melchiorre for allowing me to shortly join his group. Thank you to Danielle Mazzarella and all Melchiorre Group for making me feel at home in Tarragona.

I would also like to thank all the people who helped to make this work possible. Thank you to Dr Grazia Bezzu for the collaboration on PXX project. Special thanks to Tommaso Battisti and Ruben Ferreira for photophysical and electrochemical characterization. Many thanks to Dr Benson Kariuki, Dr Nicola Demitri, Dr Nicolas Biot, Dr Deborah Romito and Dr Magali Allain for all the help and support on the X-ray diffraction analysis. Thank you to Cecile Mézière and Prof Marc Sallé for their work and expertise on mixed valence complexes. Many thanks to Dr Samuel Mañas-Valero and Prof Eugenio Coronado for work and expertise on conductivity measurements. Thank you to Elisa Fresta and Prof Rubén D. Costa for their work and expertise on LEC devices.

Numerous thanks to all the past and present members of Bonifazi Group who made it an unforgettable experience. Thank you to Rodolfo, Melina, Tanja, Olesia, Cataldo, Andre, Maria, Francesco, Andrey, Jacopo, Andrea S, Jack, Alex, Davide, Andrea F, Lou, Dmytro and Diem, it was a pleasure to work and learn with you. Thanks to all the visiting PhDs and students Alexandra, Adiel, Francois, Matteo, Paolo, Tooba and Komal for all the time spent together.

Serdeczne podziękowania dla mojej rodziny, której niegasnące wsparcie umożiliwiło mi osiągnięcie tego celu. Mamo dziękuję za motywację, godziny rozmów i wiarę w to że mi się uda, tato dziękuję za zaszczepienie we mnie miłości do czytania i nauki.

Podziękowania dla moich przyjaciółek Doroty, Patycji, Asi K, Kaludii, Magdy i Asi W za to, że zawsze miały dla mnie czas i słowa otuchy.

Acknowledgements

Specjalne podziękowania dla Piotrka za wiarę we mnie, wsparcie we wszystkich trudnych momentach i sprawienie, że ten okres stał się wyjątkowy, dziękuję!

I would also like to acknowledge the financial support from the European Union's Horizon 2020 Research and Innovation Program under the Marie Sklodowska-Curie Actions H2020-MSCA-ITN-2016-722591 (PHOTOTRAIN).

List of abbreviations

Å	Angstrom
Aq	Aqueous
a.u.	Arbitrary unit
bpy	2,2′-Bipyridine
°C	Degree Celsius (0 °C = 273.16 K)
CV	Cyclic voltammetry
DDQ	2,3-Dichloro-5,6-dicyano-1,4-benzoquinone
DIPEA	*N,N*-Diisopropylethylamine
DMF	*N,N*-Dimethylformamide
DMSO	Dimethylsulfoxide
dppf	1,1'-Bis(diphenylphosphino)ferrocene
dtbpf	1,1′-Bis(di-tert-butylphosphino)ferrocene
Et al.	*Et alia* (latin) and others
EI	Electron ionization
EDG	Electron donating group
EnT	Energy transfer
E_{ox}	Oxidation potential
EPR	Electron paramagnetic spectroscopy
E_{red}	Reduction potential
ESI	Electrospray ionization
ET	Electron transfer
Et	Ethyl
Et_2O	Diethyl ether
EtOAc	Ethyl acetate
EtOH	Ethanol
eq.	Equivalent
eV	Electronvolt (1eV = 1.602 x 10-19 J)
EWG	Electron withdrawing group
*E**	Redox potential in excited state
fac	Facial
Fc	Ferrocene
h	Hour
HAT	Hydrogen atom transfer

HOMO	Highest occupied molecular orbital
HPLC	High-performance liquid chromatography
HR	High resolution
hv	Light
IR	Infrared spectroscopy
i.e.	Id est (latin) that is
k_f	Fragmentation rate constant
LED	Light emitting diode
LR	Low resolution
LUMO	Lowest unoccupied molecular orbital
m-	*meta*
M	Molar
m-CPBA	Meta-chloroperoxybenzoic acid
Me	Methyl
MeCN	Acetonitrile
MeOH	Methanol
min	Minute
m.p.	Melting point
MS	Mass spectrometry
m/z	Mass-to-charge ratio
nm	Nanometer
NMR	Nuclear magnetic resonance
ns	Nanosecond
o-	*ortho*
OFET	Organic field-effect transistor
OLED	Organic light emitting diode
OTFT	Organic thin film transistor
p-	*para*
PAH	Polycyclic aromatic hydrocarbon
PD	Photodynamic therapy
PDI	Perylene diimide
pH	Potential of hydrogen
Ph	Phenyl
PivOH	Pivalic acid
PTXTX	*Peri*-thioxanthenothioxanthene
PXX	*Peri*-xanthenoxanthene
rt	Room temperature

SCE	Saturated calomel electrode
SET	Single electron transfer
SN2	Bimolecular nucleophilic substitution
S_EAr	Electrophilic Aromatic Substitution
$TBAPF_6$	Tetrabutylammonium hexafluorophosphate
t-Bu	*Tert*-butyl
Tf	Trifluoromethanesulfonyl group
THF	Tetrahydrofuran
TLC	Thin layer chromatography
TMEDA	Tetramethylethylenediamine
TMSCN	Trimethylsilyl cyanide
UV-Vis	Ultraviolet-visible
XRD	X-Ray Diffraction
λ	Wavelength
ε	Molar extinction coefficient
τ	Lifetime
Φ	Quantum yield

Abstract

Polycyclic aromatic hydrocarbons (PAHs) have been widely studied, as they have found multiple applications in the field of organic electronics. Among various methods of influencing the properties of PAHs, doping with heteroatoms was found to be a versatile strategy. One such PAH is *peri*-xanthenoxanthne (PXX), which is an O doped anthanthrene investigated as an organic semiconductor by SONY.

The first part of this thesis focuses on the synthesis of sulfur- (PTXTX) and selenium-doped PXX derivatives. PTXTX and a range of its derivatives with solubilising groups and different oxidation levels have been synthesised. It has been also shown that electrophilic aromatic substitution can be utilised towards the synthesis of Se doped PAHs. The X-ray crystal structures and optoelectronic properties of synthetised compounds have been investigated. The applications of PTXTX in multivalence complexes and LEC devices have been shortly described.

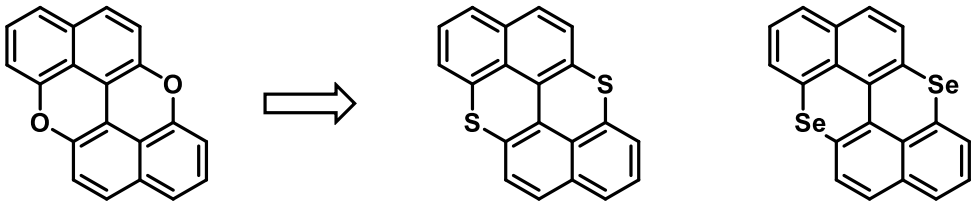

PXX **PTXTX** **36**

In the second project, our goal was to utilise PXX as a photoredox catalyst. PXX is strongly reducing in the singlet excited state, metal-free and easy to synthesise, making it a potentially useful chromophore. PXX was able to photoredox catalyse intermolecular coupling of electron-poor aryl halides with electron-rich radical traps.

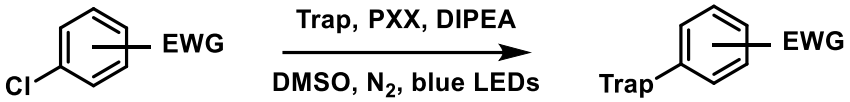

Additionally, a novel cyclisation reaction of aryl chlorides, leading to the synthesis of PAHs has been shown. Under blue light irradiation, PXX catalysed intramolecular coupling of *o*-terphenyl chlorides possessing electron-withdrawing group (EWG) on the ring with a chlorine atom. A range of mono and disubstituted triphenylenes was achieved in good yields. Products with different substituents, such as EWGs and electron-donating groups (EDGs) as well as structures with heteroarenes were successfully obtained.

A double cyclisation led to an unexpected disubstituted tetraphenylene derivative, achieving a new route towards this important class of compounds.

Table of Contents

Chapter 1
Synthesis and characterisation of S- and Se- doped anthanthrenes and their derivatives

This Thesis is formed by two different projects namely S and Se-doped PAHs and PXX photoredox catalysis, therefore separate introduction sections will be discussed in each dedicated chapter.

This chapter describes the synthesis and characterization of S-doped **PTXTX**, its oxidised derivatives, Se-doped compound **36** and dibenzoselenophene **40**. It is divided into seventeen main sections: *i)* section 1.1 gives a general introduction on organic semiconductors; *ii)* section 1.2 gives an introduction on the synthesis of PAHs containing S-doped 5 and 6-membered rings; *iii)* section 1.3 gives an introduction on Se doped PAHs; *iv)* section 1.4 gives a short introduction on anthanthrenes *v)* section 1.5 describes the aim of the project; *vi)* section 1.6 reports the synthesis of **PTXTX**; *vii)* section 1.7 reports the synthesis of **PTXTX** structures with solubilising moieties; *viii)* section 1.8 reports the synthesis of **PTXTX** oxidised derivatives; *ix)* section 1.9 reports the synthesis of molecule **36** through triflic acid mediated cyclisation; *ix)* section 1.10 reports the synthesis of dibenzoselenophene **40** using triflic acid mediated cyclisation *xi)* section 1.11 discusses literature reports on **PTXTX** derivatives; *xii)* section 1.12 reports X-ray crystal structures of **PTXTX** and its derivatives and of compound **36**; *xiii)* section 1.13 reports a photophysical characterisation of **PTXTX** and its derivatives and of compound **36**; *xiv)* section 1.14 reports an electrochemical characterisation of **PTXTX** and its derivatives and of compound **36**; *xv)* section 1.15 discusses mixed valence crystals based on **PTXTX**; *xvi)* section 1.16 discusses electroluminescent devices build on **PTXTX**; *xvii)* section 1.17 concludes the chapter.

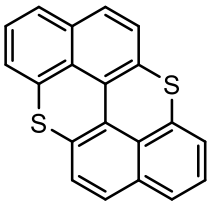

PTXTX

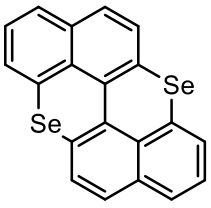

36

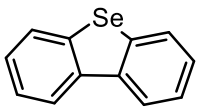

40

Synthesis and characterisation of S- and Se- doped anthanthrenes and their derivatives

The work presented in this chapter is published in the following article:

Matuszewska, O., Battisti, T., Ferreira, R. R., Biot, N., Demitri, N., Mézière, C., Allain, M., Sallé, M., Mañas-Valero, S., Coronado, E., Fresta, E., Costa, R. D., Bonifazi, D., *Chem. Eur. J.* 2023, e202203115.

The photophysical and electrochemical characterisation presented in this chapter was performed by *Tommaso Battisti* (*Cardiff University, School of Chemistry, Cardiff*) and *Ruben Ferreira* (*University of Vienna, Faculty of Chemistry, Vienna, Austria*), the X-ray analysis by *Nicolas Biot* (*Cardiff University, School of Chemistry, Cardiff*), *Nicola Demitri* (*Elettra Synchrotron, Trieste, Italy*) and *Deborah Romito* (*University of Vienna, Faculty of Chemistry, Vienna, Austria*), the mixed valence complexes were prepared by *Cecile Mézière* (*University of Angers, Angers, France*), their X-ray analysis was performed by *Magali Allain* (*University of Angers, Angers, France*) while the results were analyzed by *Marc Sallé* (*University of Angers, Angers, France*), conductivity of MV crystals was measured by *Samuel Mañas-Valero* (*University of València, València, Spain*), while the results were analyzed by *Eugenio Coronado* (*University of València, València, Spain*), LEC devices were prepared by Elisa Fresta (*Technical University, Munich, Germany*) while the results were analyzed by Rubén D. Costa (*Technical University, Munich, Germany*).

1.1 Organic semiconducting materials

1.1.1 General introduction: chemistry of the excited states

The electronic state of a molecule is built from closely packed vibrational energy levels. Upon absorption of a photon an excitation occurs, from the lowest vibrational energy level of the ground state to one of the excited electronic states, through a vertical transition (according to the Frank-Condon rule).

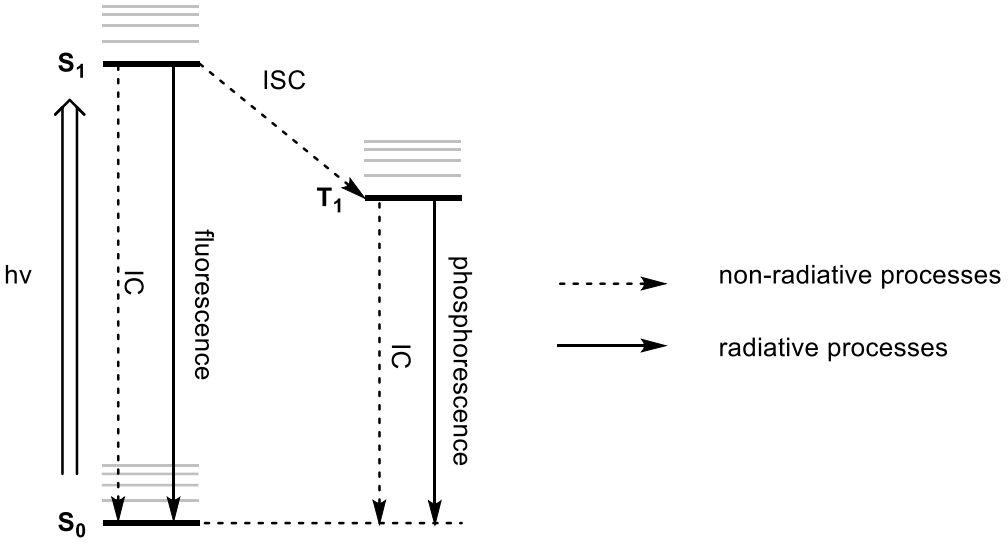

Figure 1.1. Jablonski diagram showing the electronic states of a molecule and the transitions between them. ISC – intersystem crossing, IC – internal conversion.[1]

However, the first excited state is most important for consideration, as relaxation from higher electronic states to the lowest excited electronic state is faster than any other measurable process (Kasha's rule).[1] Depending on its spin multiplicity, an excited state can either be a singlet (S) or a triplet (T). It is a singlet when the spins of electrons are antiparallel – paired, or a triplet when they are parallel – unpaired. As the transitions between states of different multiplicity are spin forbidden, an electron is usually excited from the singlet ground state S_0 to the singlet excited state S_1 (Figure 1.1).[1]

An excited state tends to quickly deactivate following one of two pathways, either photophysical or photochemical. In a photophysical process, an organic molecule in an excited state R* returns back to R. This can occur either through a non-radiative process (R*→R), or a radiative process where light is emitted (R*→R + hv). In a non-radiative pathway, internal conversion (IC), energy is lost as heat. It is also possible for a spin forbidden transition to occur – an intersystem crossing (ISC), where electron proceeds from S_1 to an excited triplet state T_1 in a non-radiative process. A radiative relaxation pathway is called fluorescence if it comes from the deactivation of a singlet

excited state, or phosphorescence in case of the deactivation of a triplet. Since $T_1 \rightarrow S_0$ transition is spin forbidden, T_1 is longer living than S_1 (usually in the microsecond to millisecond range). The efficiency of fluorescence and phosphorescence is calculated with a quantum yield - Φ, which is the number of events occurring per photon absorbed by a system. For example, a quantum yield of fluorescence - Φ_F, is the number of photons emitted divided by the number of photons absorbed (Eq. 1).[1]

$$\Phi_F = \frac{number\ of\ photons\ emmited}{number\ of\ photons\ absorbed} \qquad \text{Eq. 1}$$

Similarly, the quantum yield of phosphorescence Φ_P can be calculated. Measuring the quantum yield of fluorescence or phosphorescence gives information on the population of these excited states. However, not all excited triplet states are emissive, in which case the deactivation can take place through IC and not phosphorescence. In that case, a singlet oxygen sensitization experiment can be used to measure the population of T_1. Unlike most molecules, oxygen is a triplet ($^3\Sigma_g^-$) in its lowest energy ground state, while it has two higher energy excited singlet states ($^1\Delta_g$, $^1\Sigma_g^+$). $^1\Delta_g$ is more stable from these two states, and it is responsible for many reactions in chemistry and biology. Singlet oxygen can be produced through a photochemical activation of a sensitizer. The sensitizer is excited with visible light, enters a triplet state through ISC, and transfers its energy to the ground state oxygen ($^3O_2$) which generates singlet state oxygen ($^1O_2$) (Figure 1.2). In a singlet oxygen sensitization experiment a fullerene C_{60} is utilized as a reference since its quantum yield (Φ_T) of singlet excited state ($^1C_{60}$*) conversion to triplet excited state ($^3C_{60}$*) is close to 1. Excitation of fullerene leads to the generation of singlet oxygen ($^1O_2$). $^1O_2$ intensity of luminescence at 1270 nm was measured and allowed to measure quantum yield (Φ_Δ) for $^1O_2$ generation by C_{60}, which is close to unity. This allows elucidation of the triplet yield (Φ_T) of the sensitizer in question. C_{60} is used as a reference, with the luminescence of $^1O_2$ at 1270 nm generated by the sensitizer compared to the luminescence of $^1O_2$ generated by C_{60}.[2]

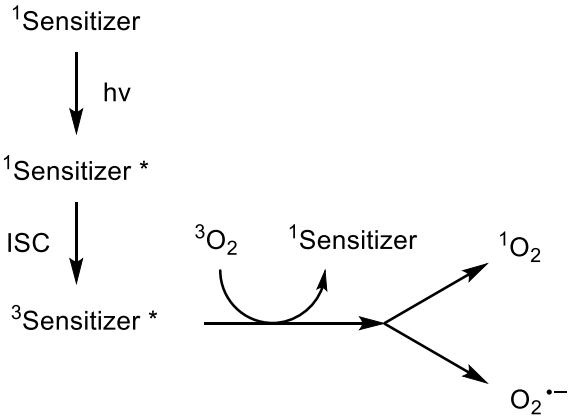

Figure 1.2. Mechanism of singlet oxygen sensitization.[2]

One of the methods of increasing triplet yield is the employment of the "heavy atom effect" which is an increase of a spin-forbidden process by the presence of an atom of high atomic number. Heavy atom effect can be external or internal.[3] In the case of the external effect, a molecule containing a heavy atom, such as CH_3I, is added to the system to increase triplet yield. Internal effect means that a heavy atom is included in the structure of the sensitizer. For example replacement of oxygen with sulphur and selenium in chalcogenoxanthylium dyes leads to an increase in triplet yield from Φ_T^O=0.09 for oxygen doped compound to Φ_T^S=0.23 for sulfur and Φ_T^{Se}=0.97 for selenium doped derivatives.[4]

1.1.2 Organic semiconducting materials

According to the IUPAC Gold Book, a semiconductor is a *"material whose conductivity, due to charges of both signs, is normally in the range between that of metals and insulators and in which the electric charge carrier density can be changed by external means."*[3] Semiconductors have basic insulating properties but can exhibit electrical conductivity upon injection of charges. This injection of charges can happen due to doping, electrodes material, or photoexcitation.[5] Organic semiconductors (OSCs) have recently received much attention due to their mechanical flexibility, light weight, low-cost production, and low-temperature processing.[6] Easy processability such as spin coating, ink-jet printing and reel-to-reel fabrication helped OSCs find applications in organic electronics. OSCs have been applied in transistors,[7–12] organic light-emitting diodes (OLEDs),[13–16] lasers,[17,18] solar cells[19–21] and photodetectors.[22,23] Organic semiconductors can be categorised into two main groups: polymers and small molecules. Conjugated polymers are usually prepared with weight distribution, as an exact number of monomers cannot be precisely controlled. They are generally soluble in organic solvents, which means they can be deposited on substrate materials using

solution processing approaches. On the other hand, organic molecules have precise and much lower weights. However, they often display low solubility in organic solvents meaning that they need to be deposited through thermal evaporation under a high vacuum.[6] The chemical structure of small molecules can be modified to influence their properties, such as bandgap, solubility and chemical stability. By introducing substituents to the structure of small molecules, researchers can increase their solubility. This approach allows the use of solution processing techniques, reducing the cost and simplifying the handling and processability of the compounds.

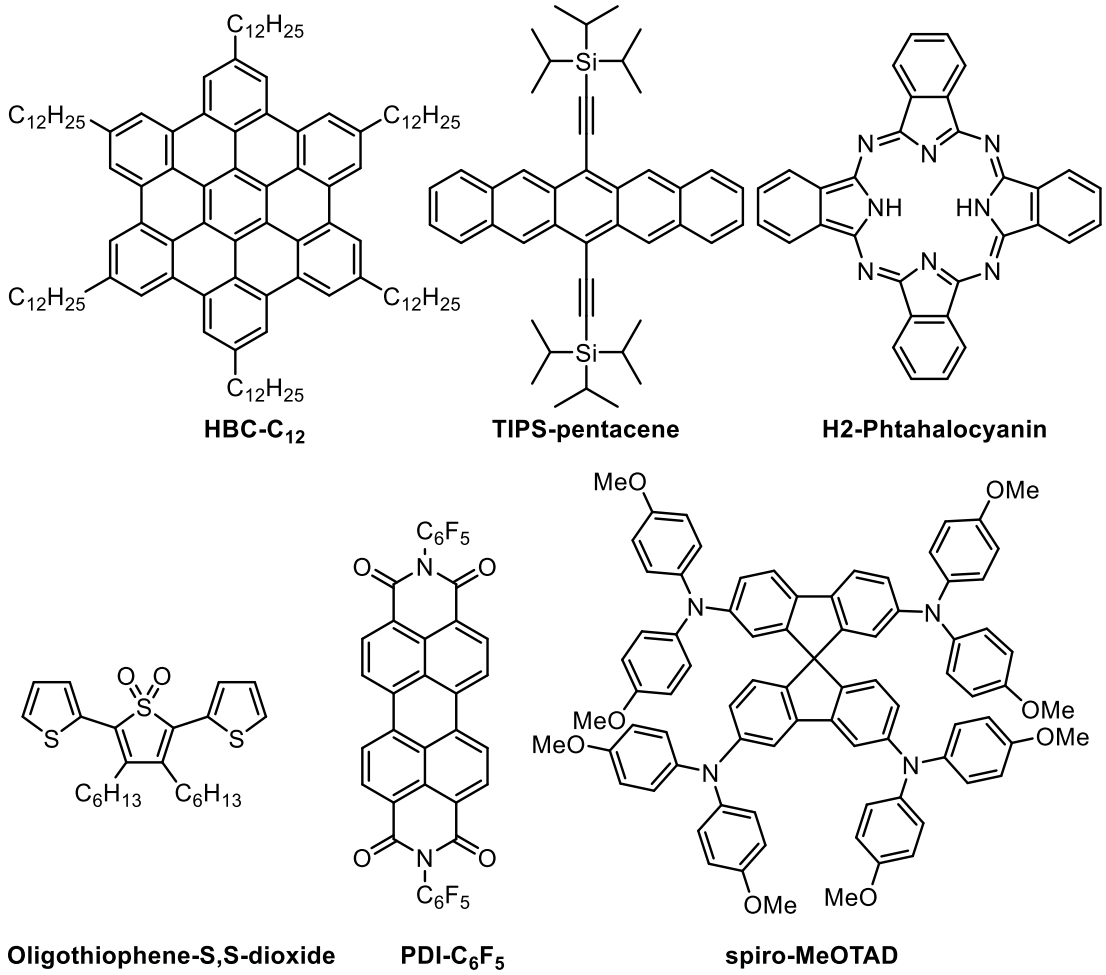

Figure 1.3. Small molecule OSCs, **HBC-C_{12}**,[24] **TIPS-pentacene**,[11] **H2-Phthalocyanian**,[9] **oligothiophene-S,S-dioxide**,[13] **PDI-C_6F_5**,[10] **Spiro-MeOTAD**.[20]

The introduction of substituents can also influence the properties of the molecules. For example, the introduction of alkyl chains to the **HBC** structure led not only to soluble derivative **HBC-C_{12}**, but also allowed for self-organisation of the molecules, leading to the formation of liquid crystals with hexagonal columnar mesophases (Figure 1.3).[24] Substituents can also increase the chemical stability of the compound, as in the case of **TIPS-pentacene**, where the introduction of TIPS substituents to the pentacene

structure increased the oxidative stability, as well as the solubility of the molecule in organic solvents (Figure 1.3).[11] Some other examples of small molecules possessing organic semiconducting properties have been presented in Figure 1.3.

Since OSCs are built from either alkene or aryl-based molecules, they have sp^2 hybridised carbon atoms. The π electrons in P_z orbitals are delocalised all over the conjugated alkene or aryl structure, and are responsible for the charge transport in OSCs. These π electrons usually have the highest energy in the molecule, occupying orbitals called HOMO - the highest occupied molecular orbitals. Meanwhile, the lowest unoccupied molecular orbitals – LUMO are empty orbitals which are the lowest in energy. The energy difference between these orbitals is called the energy gap, and it is the energy required to excite an electron in the molecule from its HOMO to LUMO.

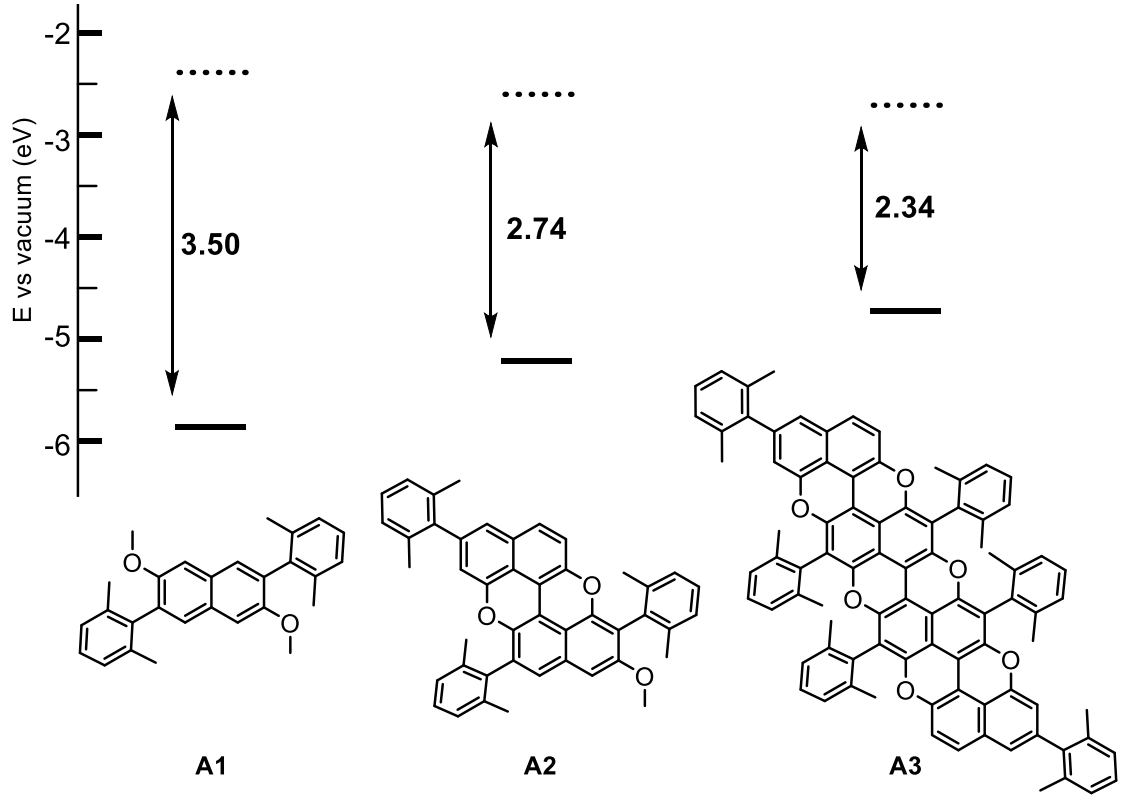

Figure 1.4. Bandgap, as well as HOMO (plain) and LUMO (dashed) energy levels of naphthalene **A1**, **A2** and molecular ribbon **A3**.[25]

The energy gap is lowered with the increased conjugation of the system and extended delocalisation of π electrons. The HOMO-LUMO gap is an important feature of OSCs, and controlling the degree of conjugation allows tuning of the energy gap and of OSCs properties.[6] For example, the synthesis of extended PXX zig-zag molecular ribbon led to the decrease of bandgap with the increased size of the molecule (Figure 1.4).[25] While the bandgap for naphthalene derivative **A1** is 3.50 eV, it falls to 2.74 eV for PXX

derivative **A2** and drops even further to 2.34 eV for molecular ribbon **A3**. Apart from increasing the conjugation, the HOMO-LUMO gap can also be tailored by doping small molecules with heteroatoms, such as O, N, S, Se, etc. One of the important OSCs groups is the S containing polycyclic aromatic hydrocarbons (PAHs), and the following sections will describe their synthesis and applications in organic electronics.

1.1.3 Charge transfer in organic semiconductors

OSCs based on π-conjugated neutral compounds have intermolecular interactions governed by Pauli repulsion and attractive London dispersion forces. Their charge transport properties are strongly influenced by the strength of the electronic coupling between neighbouring cores. The highest coupling is expected to be present in perfectly π-stacked molecules, although it rarely happens as the destabilizing exchange is highest in this conformation.[26,27] In larger oligoacenes Pauli repulsion is balanced by attractive dispersion, such as charge penetration. Charge penetration occurs when electron clouds of interacting molecules overlap, and the nuclei of one of the entities becomes deshielded. Charge penetration has been shown to be an important factor in the electrostatic stabilization of PAH dimers.[28] Electronic coupling, exchange, and charge penetration increase down the chalcogen group O<S<Se, potentially explaining the good charge transfer abilities of many S-doped PAHs. Sulfur rich PAHs, such as PTA and ETTDM-TTF, also show considerable π-stacking in their crystals and have the exchange and charge penetration large enough to compete with dispersion. Predictably the electronic coupling in these dimers is also substantial.[27]

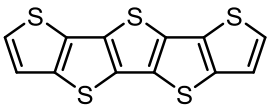

PTA

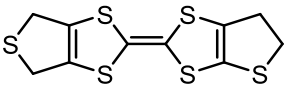

ETTDM-TTF

Figure 1.5. Structure of some S-doped PAHs.[27]

1.2 S-doped PAHs

Preferable properties described in the previous section make S-doped PAHs widely used in materials chemistry. Applications include organic field effect transistors (OFETs)[29–36], organic light emitting diodes (OLEDs)[37–40], micro-supercapacitors,[41] perovskite solar cells[42] and bulk heterojunction photovoltaics.[43–46] Interested readers can find more details about the synthesis and applications of S-doped PAHs in the following reviews.[47–50] Selected synthetic approaches will be described in the following sections, first for PAHs containing S-doped 5-membered rings, and next for 6-membered rings. As the chapter will focus on the structure of **PTXTX**, which has two

6-membered rings containing S atoms, the introduction will focus more on the latter case.

1.2.1 Synthesis of PAHs with S-doped 5-membered ring

1.2.1.1 Thiophene based synthesis

One of the most straightforward approaches towards the synthesis of the 5-membered S-doped ring in the PAHs structure is using thiophene derivatives as starting materials.[14] One example of such a method is presented in Scheme 1.1.[12]

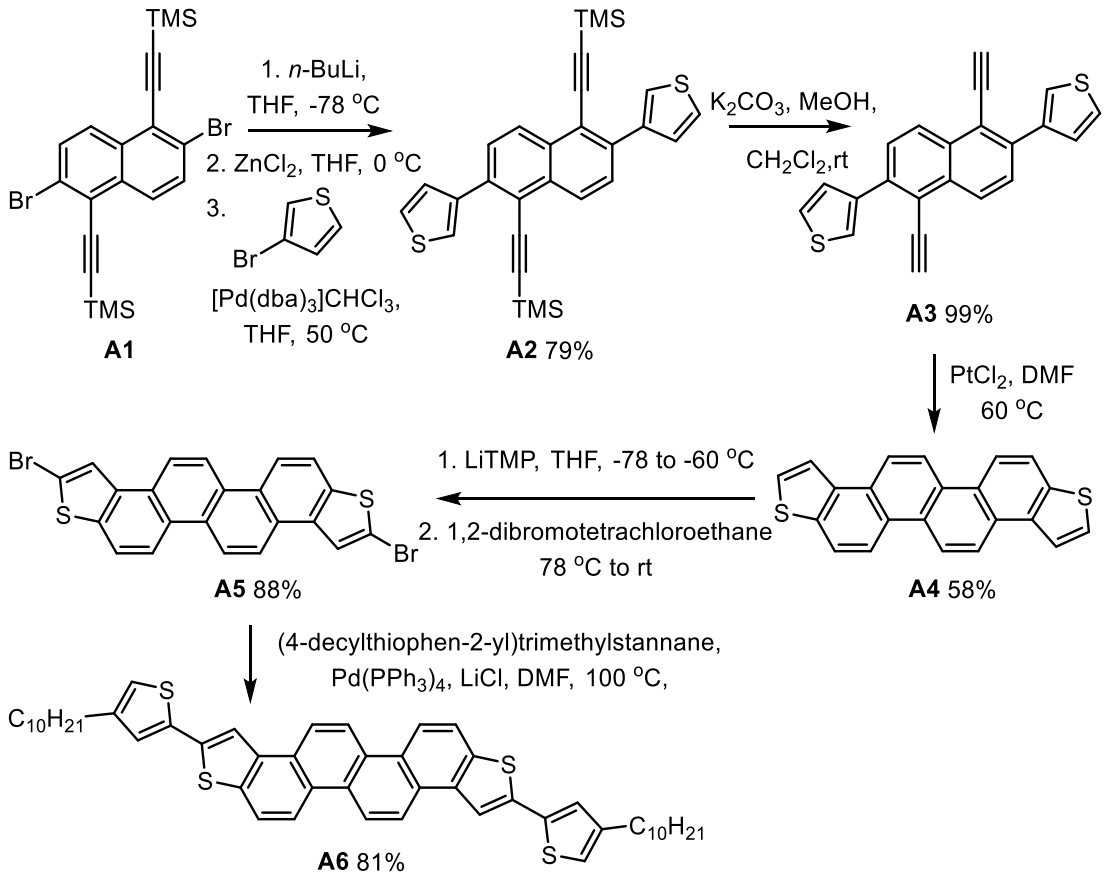

Scheme 1.1. Synthesis of molecule **A6**.[12]

First, bromonaphthalene **A1** underwent lithium-halogen exchange, followed by transmetalation with $ZnCl_2$, and Negishi coupling with 3-bromothiophene to give molecule **A2** in 79% yield. Subsequent removal of TMS protecting groups in basic conditions afforded alkyne **A3** in 99% yield. Two 6-*exo-dig* double cyclisations were catalysed by $PtCl_2$ to give molecule core **A4** in 58 % yield. Bromination of thiophene moieties was performed with 88% yield through lithiation, using LiTMP and 1,2-tetrachlorodibromoethane. Finally, 4-decylthiophen groups were introduced in Stille coupling to give **A6** in 81% yield. The molecule **A6** exhibited high electron mobility (μ_{max}

= 10 $cm^2V^{-1}s^{-1}$) in single-crystalline OFET devices, making it suitable for potential practical applications.

1.2.1.2 Newman-Kwart rearrangement

Molecule **A10** was synthesised using the Newman-Kwart rearrangement as the cyclisation step (Scheme 1.2).[12] The first step was selective lithiation, followed by transmetalation with $ZnCl_2$. Arylzinc intermediate was then reacted with 1,4-dibromo-2,5-dimethoxybenzene through the Negishi coupling, which after demethylation with BBr_3 gave molecule **A8** in 78% yield. Next, the reaction with thiocarbamoyl chloride led to compound **A9** in 72% yield. Finally, the Newman-Kwart thermal rearrangement afforded **A10** in 64% yield. **A10** was found to have large charge mobility (μ_{max} = 16 cm^2 V^{-1} s^{-1}) in an air-stable p-channel OFET device.

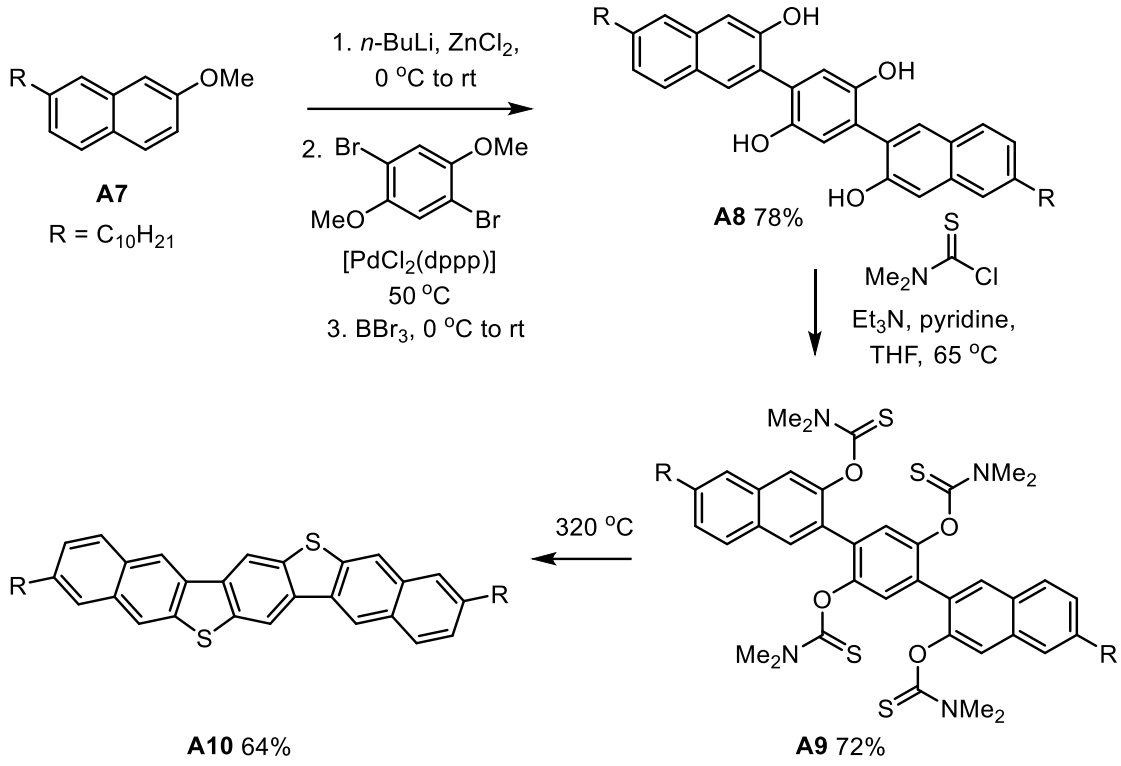

Scheme 1.2. Synthesis of thienoacene **A10**.[12]

The cyclisation of compound **A9** starts with Newman-Kwart rearrangement, which mechanism has been presented in Scheme 1.3. The rearrangement can be considered an intramolecular aromatic nucleophilic substitution reaction. The mechanism of the following cyclisation has been proposed by Woodward *et al*.[51] based on the BINOL cyclisation via a keto-tautomer.[52]

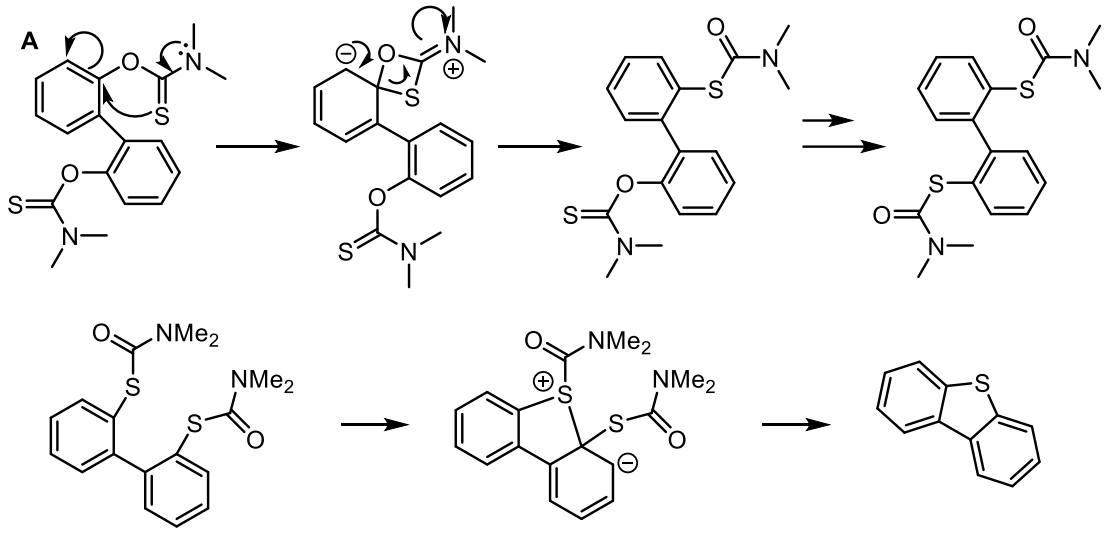

Scheme 1.3. A Plausible mechanism for Newman-Kwart rearengment followed by cyclisation.[51]

1.2.1.3 S-annulation of perylene

5-membered ring can also be achieved in the bay annulation reaction of perylene (Scheme 1.4). Perylenothiophene **A12** was synthesised in the reaction of **A11** with sulfur in NMP, at 180 °C, giving the product **A12** in 70% yield.[53] Tetraester derivatives of **A12** found application as luminescent columnar liquid crystals.[54] This reaction has also been applied in the synthesis of S-annulated perylene diimides for organic solar cells application.[46]

A11 **A12** 70%

Scheme 1.4. Chalcogen annulation with S powder.[53]

1.2.1.4 Triflic acid mediated cyclisation

Triflic acid has been reported to mediate electrophilic aromatic substitution of sulfoxides, leading to triflic salts. When followed by demethylation with a base, an aryl sulfide bond is obtained. While first reports showcased intermolecular polymerisation reaction,[55,56] an intramolecular version of this reaction was also developed to give dibenzothiophene moiety (**DBT)** (Scheme 1.5).[57–61] The reaction consists of two steps, first sulfoxide **A13** is protonated with strong triflic acid, and electrophilic aromatic substitution leads to triflic acid salt **A14**. This salt can be isolated and was characterised

Synthesis and characterisation of S- and Se- doped anthanthrenes and their derivatives

by Haryono *et al.*[58] The second step is demethylation with a base, usually pyridine, which leads to **DBT**.

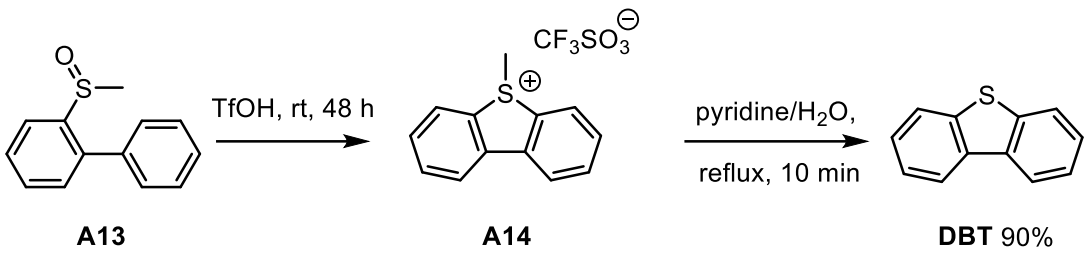

Scheme 1.5. TfOH mediated cyclisation giving **DBT**.[57]

1.2.1.5 Pd-catalysed cyclisation

Tobisu *et al*. reported Pd(II) catalysed C-S bond formation leading to dibenzothiophene moiety.[62] They synthesised a range of dibenzothiophenes **DBT** from biphenyl phenylsulfides **A15**, using $Pd(OAc)_2$ as a catalyst and 2,6-dimethylbenzoic acid as a ligand (Scheme 1.6). Various substituents were well tolerated, including EDGs, EWGs, and halogens.

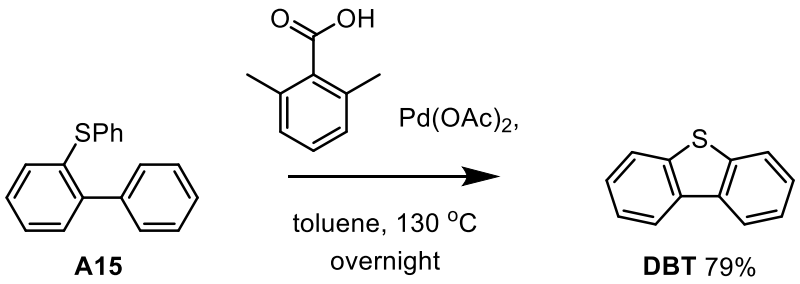

Scheme 1.6. Pd (II) catalysed dibenzothiophenes synthesis.[62]

The authors proposed that the reaction mechanism involves the formation of a 6-membered palladacycle **A** (Scheme 1.7).[62]

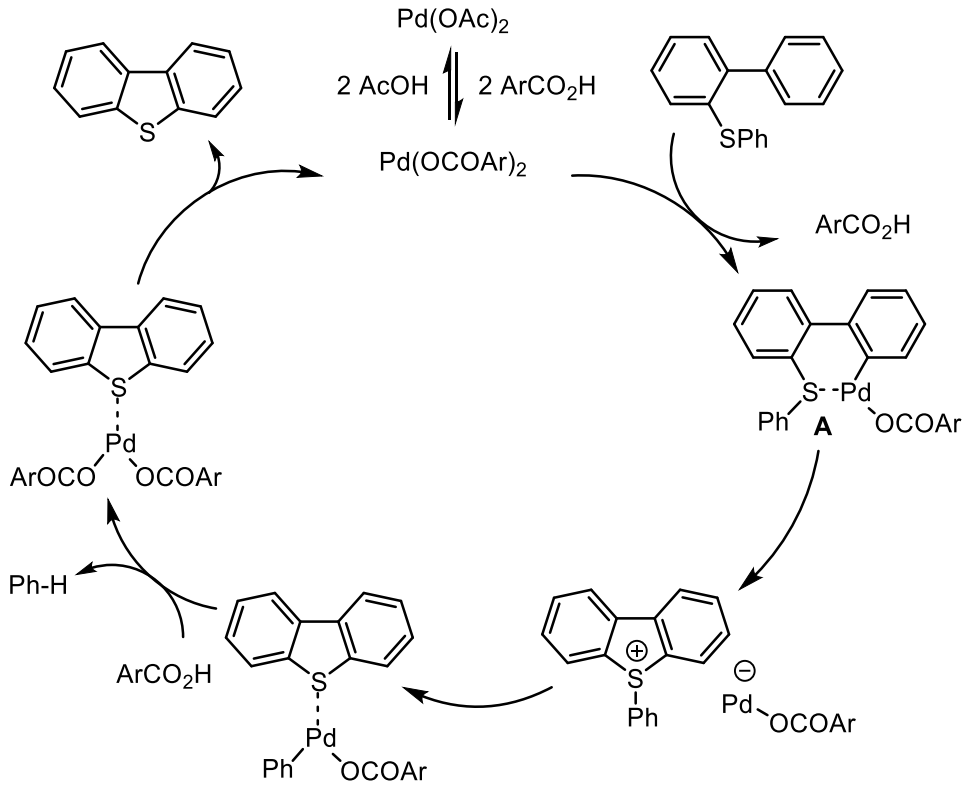

Scheme 1.7. Reaction mechanism proposed for Pd(II) catalysed dibenzothiophene formation. Ar = 2,6-dimethylphenyl.[62]

1.2.2 Synthesis of PAHs with S-doped 6-membered ring

Several approaches can be applied towards the synthesis of PAHs, with 6-membered ring containing sulfur. They can be formed through C-C or C-S bond formation, or based on a substrate already containing 6-membered ring with S atom, such as thioxanthone. The following sections will give examples of these synthetic pathways.

1.2.2.1 Cyclisation through C-C bond formation

Cyclisation can be performed through the formation of a C-C bond on a thiophenyl group. This can be realised through the diazotisation reaction, followed by thermal or Cu-catalysed cyclisation, which will be described in the following sections.

1.2.2.1.1 Cyclisation via diazonium salt formation

Solvent orange 63, which is an industrial dye, has been achieved through the synthesis of diazonium salt from amine **A16** and nitrosulfuric acid, followed by thermal cyclisation (Scheme 1.8).[63]

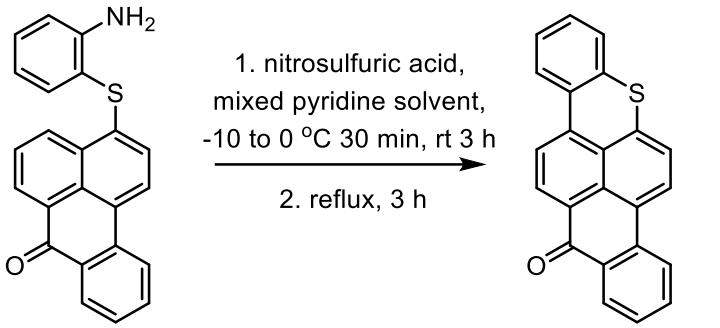

A16 **Solvent Orange 63**

Scheme 1.8. Synthesis of industrial dye **Solvent Orange 63**.[63]

Thiocylic naphthalimides are usually synthesised through Pschorr cyclisation.[64–68] A representative example of the synthesis is shown in Scheme 1.9. The reaction between bromide **A18** and thiol **A17** led to thioether **A19** in 77% yield.[65] Next, diazonium salt was formed, which underwent Pschorr cyclisation giving compound **A20**. Finally, condensation reaction between **A20** and amine allowed for the synthesis of thiocyclic fused naphtalimides **A21**. This class of compounds has been applied as DNA photocleavers[64,65,67,68] and fluorescent probes.[66]

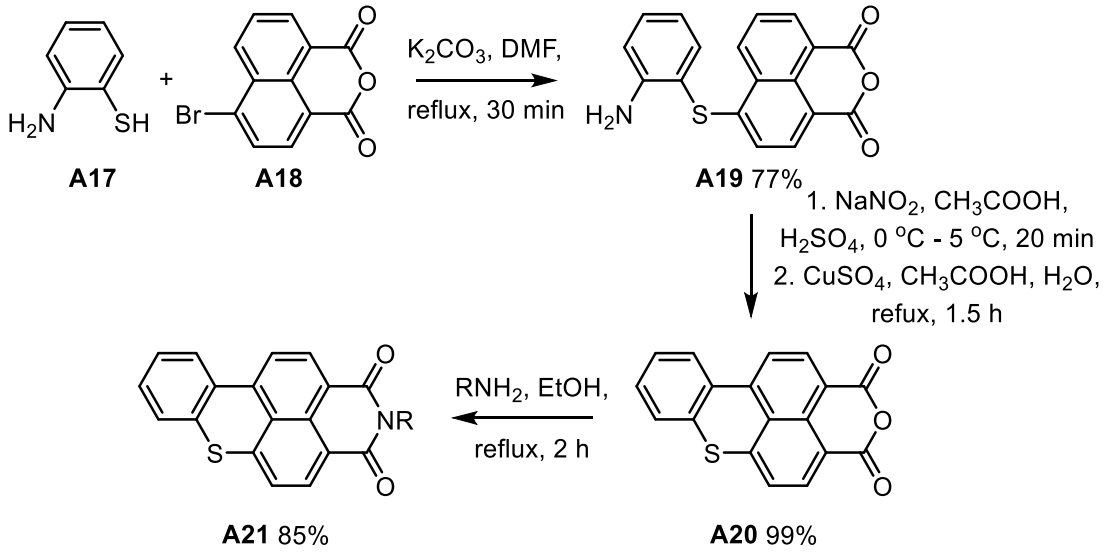

Scheme 1.9. Synthesis of thio-heterocylic naphthalimides **A21**.[65]

1.2.2.2 Pd-catalysed synthesis

A range of 5, 6 and 7-membered S-bridged PAHs were synthesised through a Pd-catalysed reaction.[69] Synthesis of pyrene-thienoacene **A24** is shown as an example in Scheme 1.10. C-C bond is formed through a Pd catalysed dehydrogenative cyclisation between a phenylsulfoxide group and a perylene moiety of **A22**. After the reduction of sulfoxide **A23** with $NiCl_2$ and Al powder, thienoacene **A24** was obtained.

Photophysical properties of both **A23** and **A24** were compared. Absorption of **A24** was red shifted compared to **A23**, λ_{max} = 425 nm vs λ_{max} = 385 nm, respectively. Quantum yield of fluorescence was tested for both molecules, and while it is moderate for **A23** Φ_F = 0.17, it is relatively high for **A24** Φ_F = 0.48.

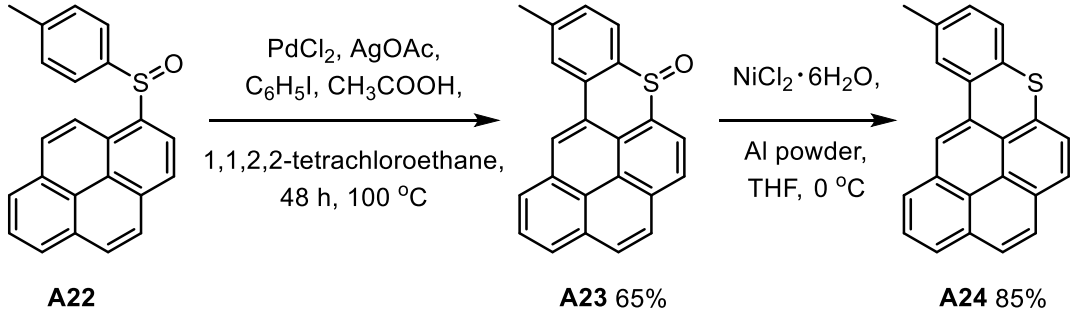

Scheme 1.10. Synthesis of pyrene-thienoacene **A24**.[69]

The reaction is deemed to work through a palladacycle with sulfoxides as chelating groups, while the AgOAc salt has been used for the regeneration of Pd(II) catalyst (Scheme 1.11).

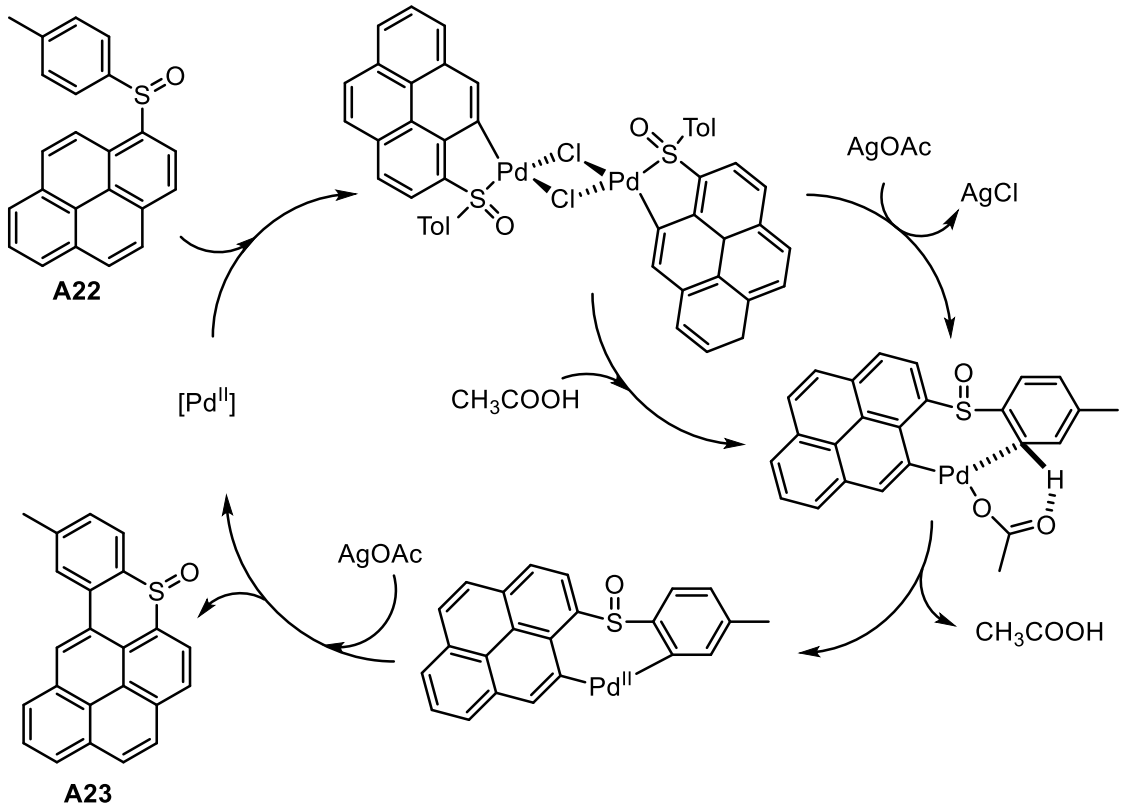

Scheme 1.11. Postulated mechanism for Pd catalysed dehydrogenative cyclisation.[69]

1.2.2.3 Aromatization

Wu *et al.* synthesised O- and S-doped positively charged PAHs.[70] The first step in the synthesis of S-doped **BNATX** salt was triflic acid catalysed ether-sulfide exchange between thiol **A25** and ether **A26**, leading to sulfide **A27** (Scheme 1.12). The product was condensed with benzaldehyde to give **A28**. After oxidation, followed by dehydrative aromatization, BF_4^- salt **A30** was obtained. Finally, UV light promoted cyclisation led to **BNATX** salt. **BNATX** salt showed red shifted absorption spectra compared to O doped **BNAX** salt, with $\lambda_{max\ BNTAX}$= 600 nm vs $\lambda_{max\ BNAX}$= 573 nm.

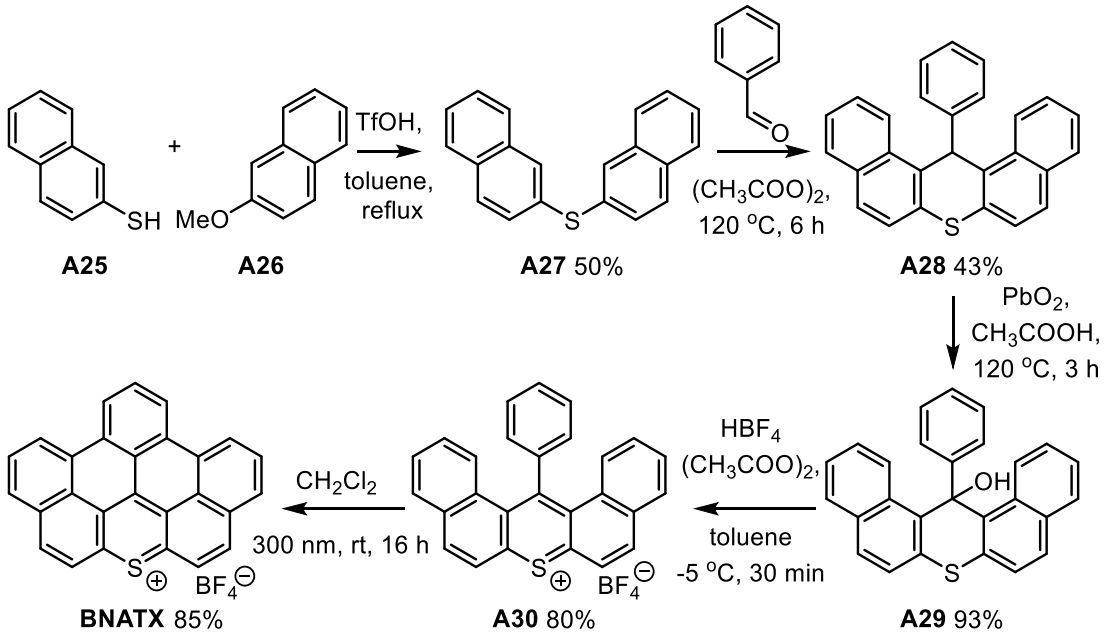

Scheme 1.12. Synthesis of **BNATX** salt.[70]

1.2.2.4 Cyclisation through C-S bond formation

1.2.2.4.1 Triflic acid mediated cyclisation

6-membered rings[71–75] can be achieved by a triflic acid mediated cyclisation similar to the formation of 5-membered rings in dibenzothiophene synthesis (paragraph 1.2.1.4). In the first step, triflic salt is achieved in TfOH mediated cyclisation, which after demethylation with a base gives the desired compound. One example of this synthetic pathway is presented in Scheme 1.13. Pyrene−thienoacene **A32** was achieved with TfOH mediated cyclisation of **A31**, followed by demethylation with pyridine, in 65% yield.[74] The formation of isomer **A34** with 5-membered ring was not observed, although authors managed to obtain it from a different precursor **A33**. **A32** exhibits a broad absorption band red-shifted to 433 nm, compared to 384 nm for **A34**. **A32** also shows a significantly higher quantum yield of fluorescence Φ_F= 0.6 compared to Φ_F= 0.1 for isomer **A34**.

Synthesis and characterisation of S- and Se- doped anthanthrenes and their derivatives

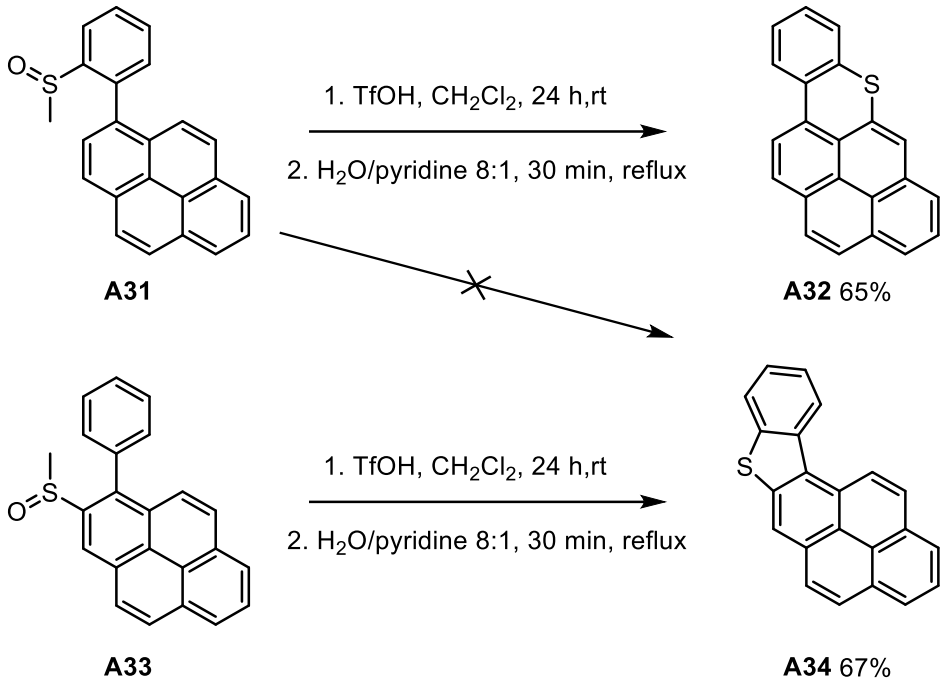

Scheme 1.13. Synthesis of thiopyran derivatives.[74]

1.2.2.4.2 I_2 mediated cyclisation

C-S bond formation has also been achieved in I_2 mediated cyclisation. Zhang *et al.* reported the synthesis of pyrene-fused thioxanthenes with one (**A36**) and two (**A38**) S-doped rings (Scheme 1.14).[76] Excess of iodine in $CHCl_3$ was used to promote the cyclisation of substrates containing *o*-methylthio moieties (**A35** and **A37**).

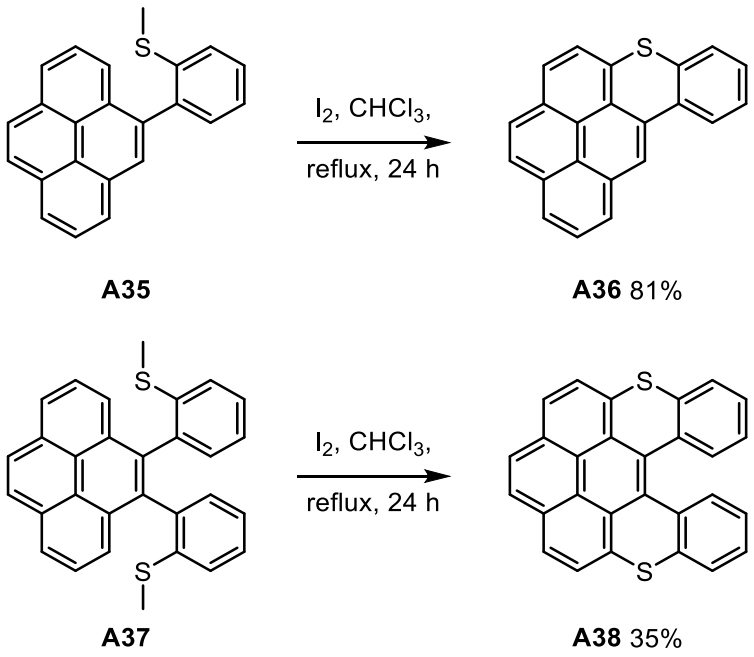

Scheme 1.14. Iodine mediated cyclisation leading to pyrene-fused thioxanthenes.[76]

More extended product **A38** showed red shifted absorption compared to **A36**, with λ_{max} = 498 nm and λ_{max} = 427 nm, respectively. Iodine mediated cyclisation has also been used in the synthesis of chalcogenophene based compounds through the formation of C-S and C-Se bonds from stilbene derivatives.[77–79]

1.2.2.5 Cyclisation through C-S and C-C bonds formation

S-doped PAHs can also be achieved through the formation of both C-S and C-C bonds in a single reaction. Thioxanthene **A40** has been achieved in the reaction between **A39** and sodium *p*-toluenethiolate, under UV light irradiation (Scheme 1.15).[80]

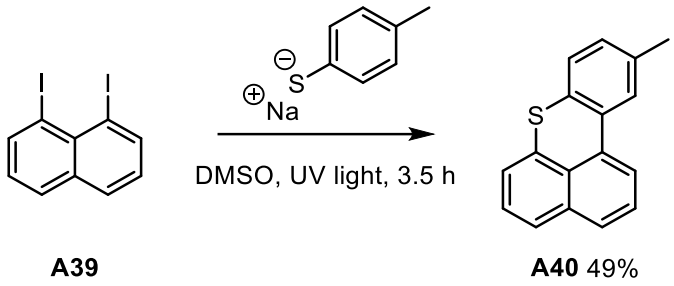

A39 **A40** 49%

Scheme 1.15. Synthesis of **A40** through $S_{NR}1$ reaction. 500 W Mercury lamp used as a light source.[80]

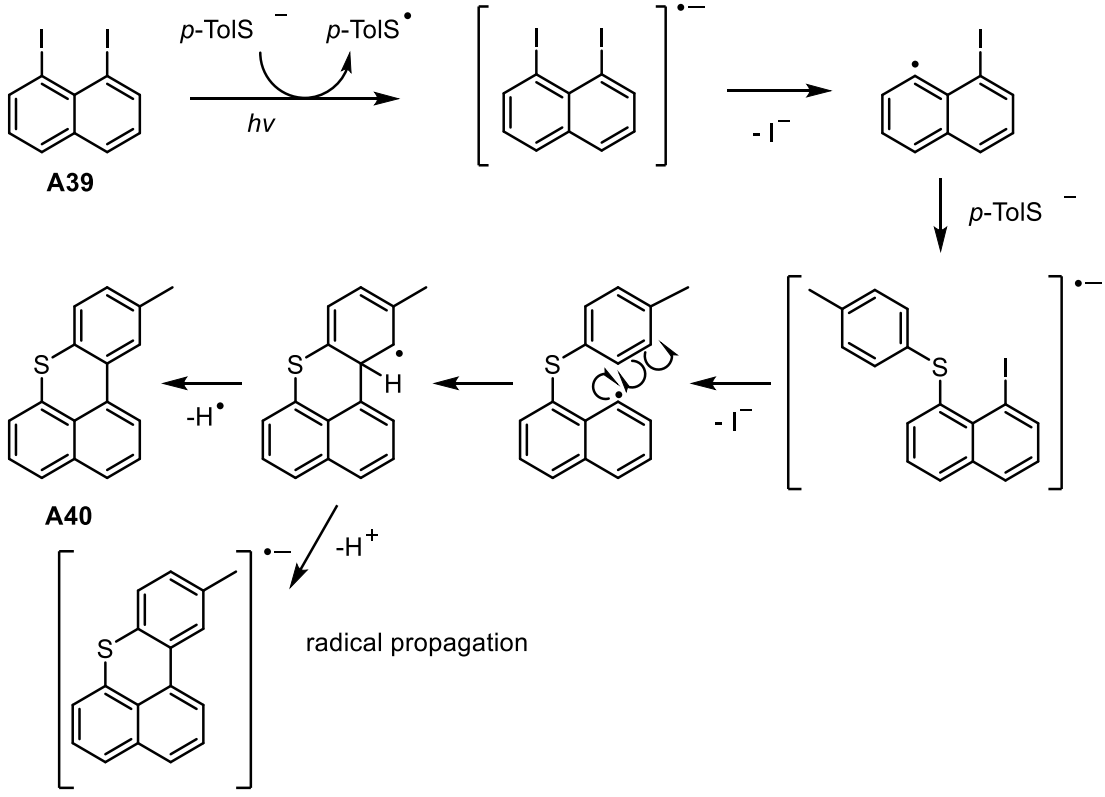

A39 **A40**

Scheme 1.16. The proposed mechanism for SNR_1 synthesis of thioxanthene A40.[80]

The postulated mechanism involves a radical-nucleophilic aromatic substitution ($S_{NR}1$), followed by an intramolecular homolytic aromatic substitution (Scheme 1.16).[80,81] The reaction likely involves a radical propagation step.

1.2.2.6 Through thioxanthone

1.2.2.6.1 Thioxanthone synthesis

Thioxanthone is often used as a photocatalyst for energy transfer (EnT), single electron transfer (SET) and hydrogen atom transfer (HAT) reactions.[82] While the compound is commercially available, its derivatives are traditionally synthesised through acid mediated condensation of a 2-sulfanylbenzoic acid **A41** with an arene **A42** (Scheme 1.17).[83]

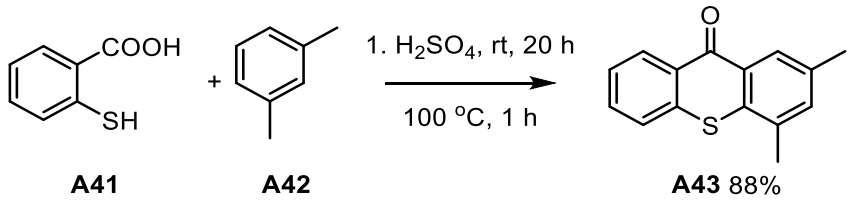

Scheme 1.17. Condensation of a 2-sulfanylbenzoic acid with an arene.[83]

However, this condensation often suffers from low yields, and other methods were developed to achieve higher yields in more mild conditions.[84] For example, thioxanthones **A45** can also be obtained in a reaction between **A44** and $Na_2S{\cdot}9H_2O$ in DMF at 60 °C. Thioxanthones bearing halo or methoxy substituents were achieved in high yields (77-95%) (Scheme 1.18).[85]

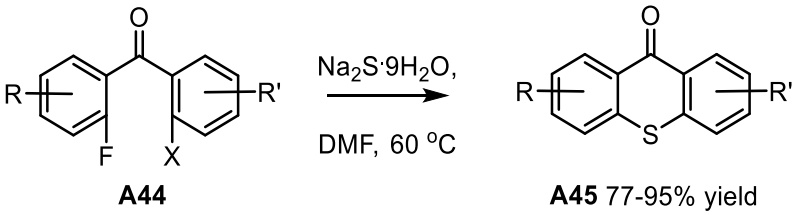

Scheme 1.18. Synthesis of thioxanthone derivatives.[85]

1.2.2.6.2 Thioxanthone in the synthesis of PAHs

Thioxanthone has also been applied as a substrate in the synthesis of PAHs containing thioxanthene moiety. Compound **A50** has been obtained through a 4-step synthesis (Scheme 1.19).[86] First, thioxanthone **A46** has been subjected to conditions of Corey-Fuchs olefination, yielding compound **A47** in 53% yield. Next, Sonogashira coupling,

and desilylation with Bu_4NF gave alkyne **A49**. Finally, [Ru] catalysed cycloisomerisation allowed for the synthesis of **A50** in 95% yield. Compounds based on **A50** structure have been applied as materials for OLEDs.[87]

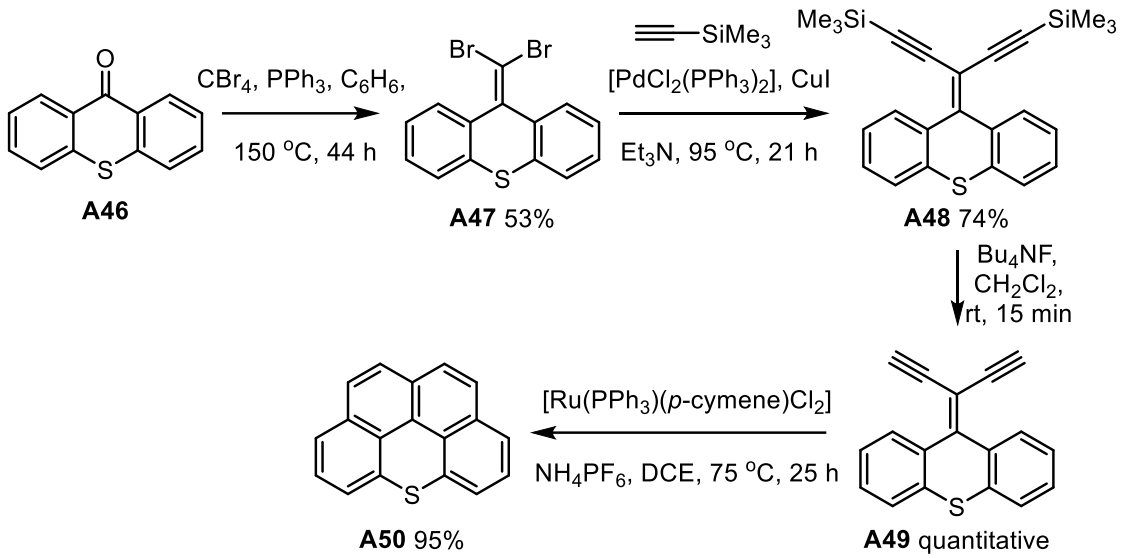

Scheme 1.19. Synthesis of *peri*-naphthothioxanthene **A50**.[86]

The [Ru] catalysed cyclisation has been proposed to work through the formation of the ruthenium-vinylidene (Scheme 1.20).

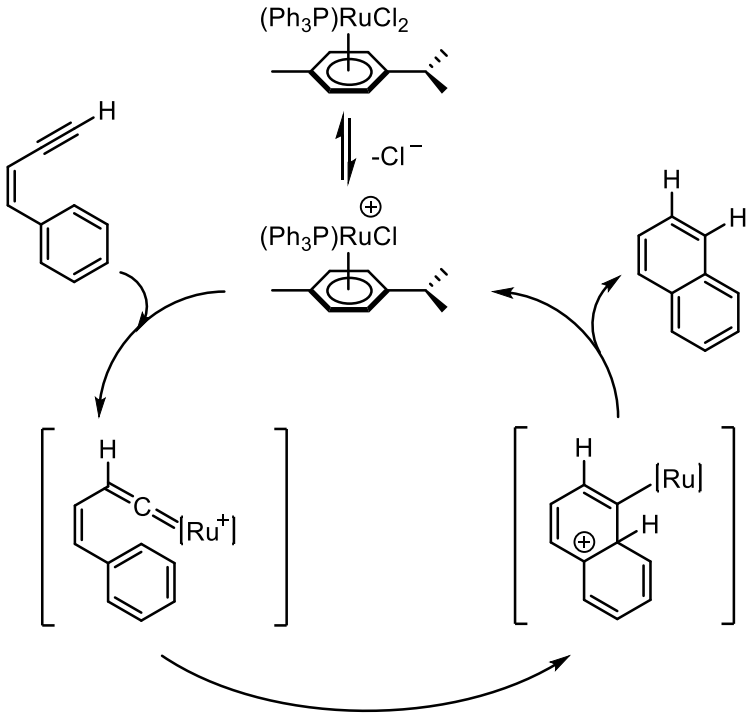

Scheme 1.20. Proposed mechanism for [Ru] catalysed cycloisomerisation.[86]

Synthesis and characterisation of S- and Se- doped anthanthrenes and their derivatives

Another example of the use of thioxanthone in PAHs synthesis is presented in Scheme 1.21.

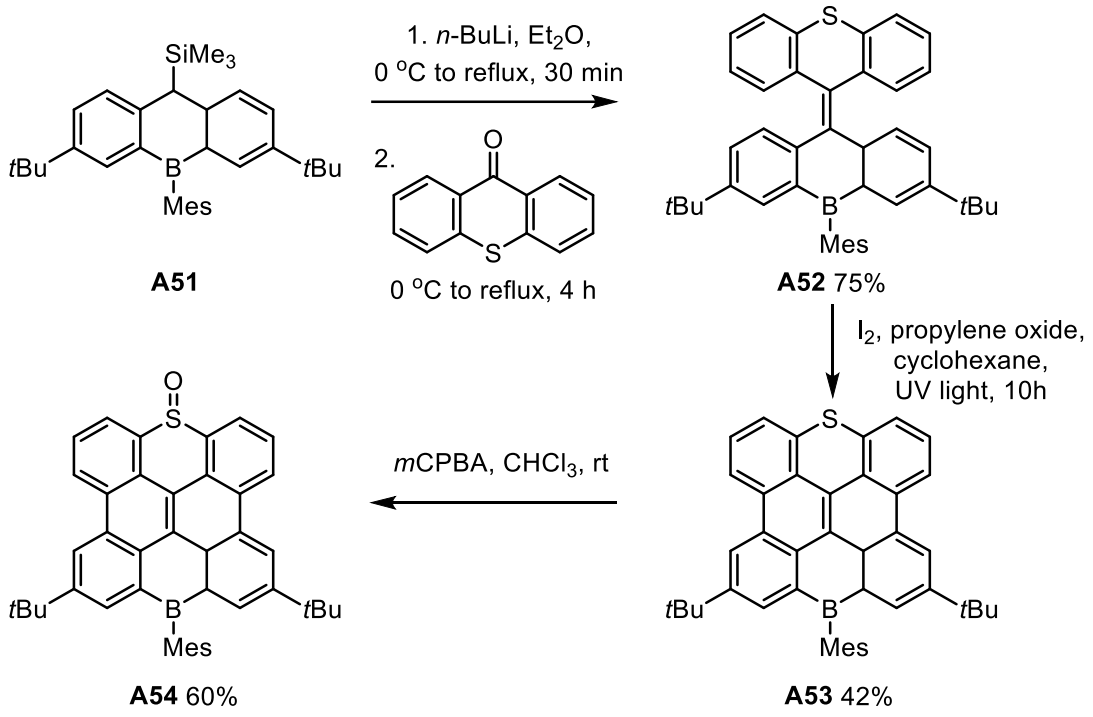

Scheme 1.21. UV light mediated synthesis of S-doped arylborane **A53**. Medium pressure Hg lamp used as UV light source.[88]

The first synthetic step was Peterson olefination between **A51** and thioxanthone.[88] Next, annulation was achieved through I_2 catalysed Mallory reaction giving PAH **A53** in 42% yield. The authors decided to oxidise sulfide **A53** with *m*CPBA in $CHCl_3$ to achieve sulfoxide **A54**. However, further oxidation to sulfone with excess *m*CPBA was unsuccessful. Oxidation caused blue shift of absorption maximum, with λ_{max}= 397 nm for sulfoxide **A54** and λ_{max}= 513 nm for **A53**.

1.3 Introduction on Se doped PAHs

Se-doped PAHs have found applications in the field of materials chemistry, in OLEDs,[89–92] OFETs[78,93] organic thin film transistors (OTFTs),[94,95] proton sponges[96] and organic solar cells.[97,98] They have also been studied in medicinal biology, including photodynamic therapy (PDT)[99–103] and viral inhibition.[104] While a range of selenium-containing PAHs has been studied, this introduction will focus on synthesis and applications of dibenzoselenophenes and selenoxanthene derivatives, as relevant to the work presented later in this chapter.

1.3.1 Synthetic routes towards dibenzoselenophene

Dibenzoselenophenes have been usually synthesised similarly to dibenzothiophenes, often appearing in the same study. Synthesis of substituted dibenzoselenophenes has only been demonstrated in a few cases.[105–107] In most studies, the reaction mechanism has been probed for the dibenzothiophenes and deemed to work alike for the selenium analogues. Selected synthetic examples will be described in this section, while an interested reader can find more details in the following reviews.[108–111]

1.3.1.1 Diselenide substrates

Dibenzoselenophene **DBSe** can be obtained from 2-biphenyl diselenide **B1** using a range of mediators, following different reaction pathways (Scheme 1.22). First developed conditions required the use of Br_2 in CCl_4.[112] Later I_2, in the presence of K_2CO_3 as a base, allowed for greener conditions.[113] The reaction has been proposed to work through oxidative cleavage of Se - Se bond by I_2, followed by a subsequent C - Se bond formation, through an intramolecular aromatic electrophilic substitution (S_EAr). Pd(II)-catalysed reaction also allowed a similar transformation.[114] It has been proposed to work through an oxidative insertion of [$PdCl_2$] into a Se - Se bond, followed by the formation of a 6-membered palladacycle. Another transition metal catalysed synthesis utilised $MoCl_5$.[115] The authors proposed a single electron transfer (SET) reaction mechanism.

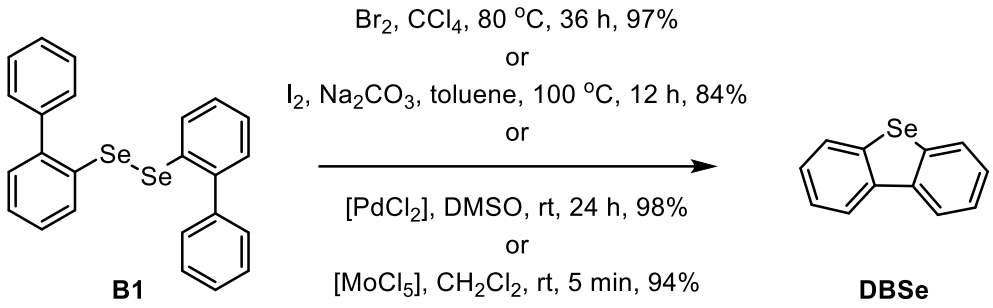

Scheme 1.22. Dibenzoselenophene synthesis from 2-biphenylyl diselenide.[112–115]

1.3.1.2 Diiodophenyl substrates

Diiodobiphenyl **B2** reacts with elemental Se to give disbenzoselenophene, in a CuI catalysed reaction in the presence of K_2CO_3 in NMP (Scheme 1.23).[116,117] The reaction has also been applied to the synthesis of ladder-type π-conjugated systems.[117] These conditions have been built from the previously developed CuI catalysed coupling reactions with sulfur giving thiols[118] and dibenzoselenophene synthesis with Na_2Se, used together with elemental Se, CuI and NMP mixture.[119,120]

Synthesis and characterisation of S- and Se- doped anthanthrenes and their derivatives

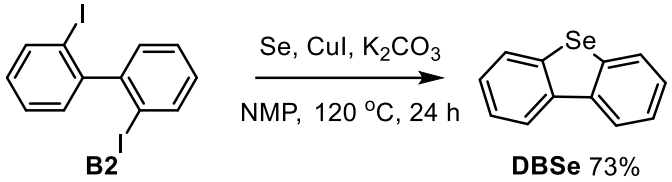

Scheme 1.23. Dibenzoselenophene synthesis through CuI catalysed reaction.[116]

1.3.1.3 Iodonium substrates

Dibenzoselenophenes can also be obtained from iodonium salts **B3**, in the reaction with elemental selenium and a strong base (Scheme 1.24).[105] A broad range of substituents was well tolerated, including EDGs, EWGs, halogens and aryls, yielding dibenzoselenophene derivatives in 49-90% yields. Chalcogen - iodine exchange has been proposed to involve an anion/radical dual activation.

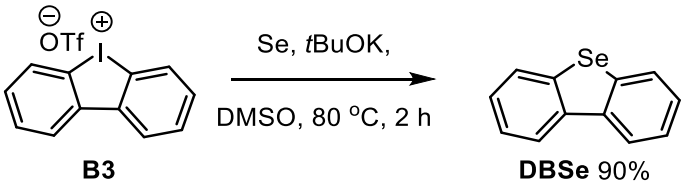

Scheme 1.24. Dibenzoselenophene synthesis through iodonium salt.[105]

1.3.1.4 Dilithiated substrates

Dibenzoselenophene and its derivatives can also be prepared through dilithiated biphenyls, although reported yields are generally low.[96,121,122] One example has been presented in Scheme 1.25. Lithiation of 2,2'-dibromobiphenyl **B4**, followed by the reaction with elemental Se, led to the formation of dibenzodiselenin **B5**. After oxidative bond cleavage through bromination, followed by the reaction with PhLi, dibenzoselenophene was achieved.[122]

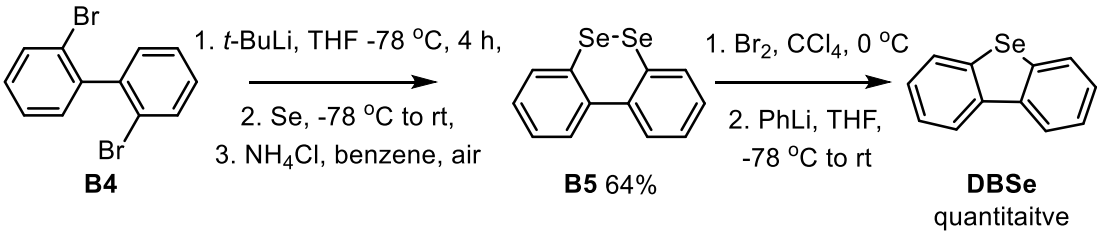

Scheme 1.25. Dibenzoselenophene synthesis from bis(bromoselanyl)biphenyl.[122]

1.3.1.5 Benzannulation substrates

Dibenzoselenophene has also been achieved in the Lewis acid catalysed benzannulation reaction of selenophene (Scheme 1.26).[123] 2,5-dimethoxytetrahydrofuran (DMTHF) has acted as a four-carbon synthon and $ZnBr_2$ as

a catalyst. The reaction has been proposed to occur through an intermediate, where elimination of -OMe groups as MeOH would lead to bbenzannulation.

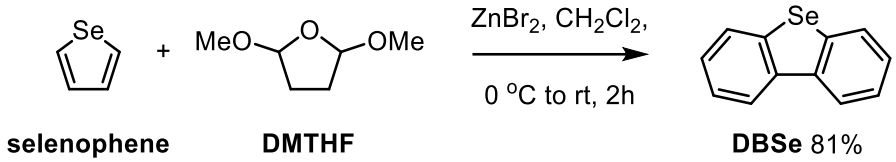

Scheme 1.26. Benzannulation of selenophene.[123]

1.3.1.6 Arylboronic acid substrates

Recently arylboronic acids **B6** were demonstrated to give selenaheterocycles in $AgNO_2$ catalysed reaction with elemental Se, in the presence of $K_2S_2O_8$ and air as oxidants (Scheme 1.27).[106] Synthesis of dibenzoselenophenes with a wide range of substituents was achieved. While the presence of EDGs, halogens and polycycles was well tolerated on the aryl ring without $B(OH)_2$ group, EWGs such as -CN or -COOMe shut down the reaction. The presence of substituents on the ring containing $B(OH)_2$ led to slightly diminished yields, although examples of products with $-CF_3$, -OMe and -F were demonstrated. A radical reaction mechanism was proposed, which has been corroborated by control experiments with TEMPO.

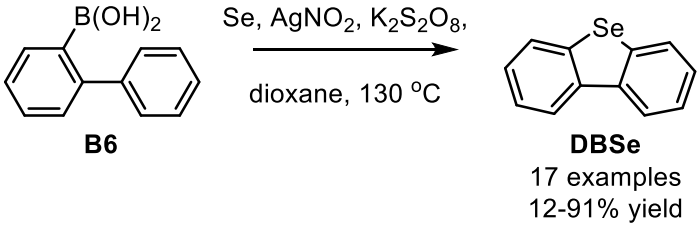

Scheme 1.27. Ag(I) catalysed synthesis of dibenzoselenophenes.[106]

Simultaneously a similar transformation was achieved by Zhang *et al.*, where dibenzoselenophenes were achieved in a metal-free reaction of arylboronic acids (Scheme 1.28).[107] A range of dibenzoselenophenes was achieved by reacting arylboronic acids **B6** with elemental Se and trimethylsilyl cyanide (TMSCN). EDGs, EWG, halogens and polycycles were well tolerated as substituents, giving products in high yields (56-98%). A radical reaction mechanism was proposed based on control experiments with TEMPO.

Synthesis and characterisation of S- and Se- doped anthanthrenes and their derivatives

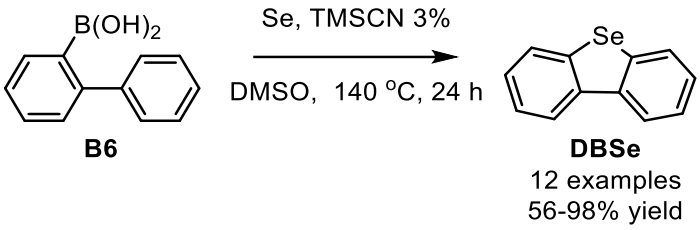

Scheme 1.28. TMSCN catalysed dibenzoselenophene synthesis.[107]

1.3.2 Synthesis of 6-membered Se doped PAHs

1.3.2.1 Selenorhodamines

Selenorhodamines have been widely studied for applications in photodynamic therapy (PDT),[124] dye sensitised solar cells[125] and singlet oxygen sensitisers for photocatalytic reactions.[126] In particular, research in the area of PDT of cancer cells has led to the development of a large amount of new selenorhodamine derivatives (Figure 1.6).[99–103] Due to the incorporation of a heavy atom, their λ_{max} is red shifted, compared to O and S doped derivatives, and lies in the range optimal for tissue penetration (600-800 nm).[124] The synthesis of an extended selenorhodamine **B7**, as a representative example of this group, is depicted in Scheme 1.29.[100]

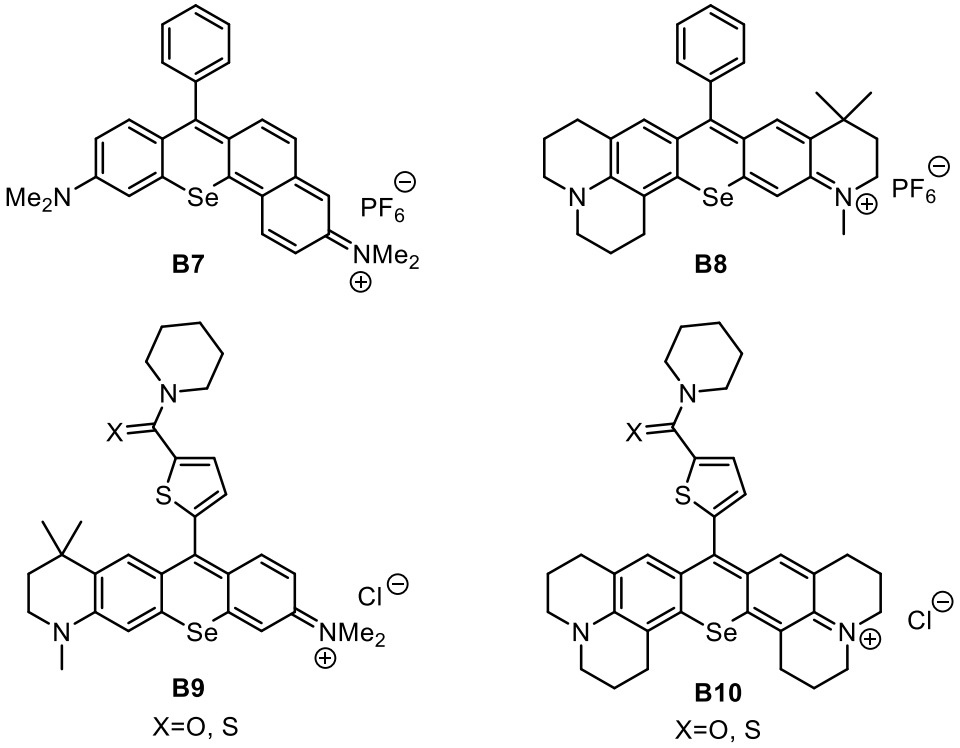

Figure 1.6. Se containing rhodamine derivatives studied as photosensitisers.[124]

The first step of the synthesis was *o*-lithiation of **B11** with *s*-BuLi/TMEDA mixture, followed by quenching with a diselenide. An obtained regioisomeric mixture of

selenoethers **B12** was treated with $POCl_3/Et_3N$, to give extended xanthone **B13**, isolated in 41% yield. Treatment with PhMgBr, followed by the workup with aqueous HPF_6 gave selenorhodamine salt **B7** in 84% yield.

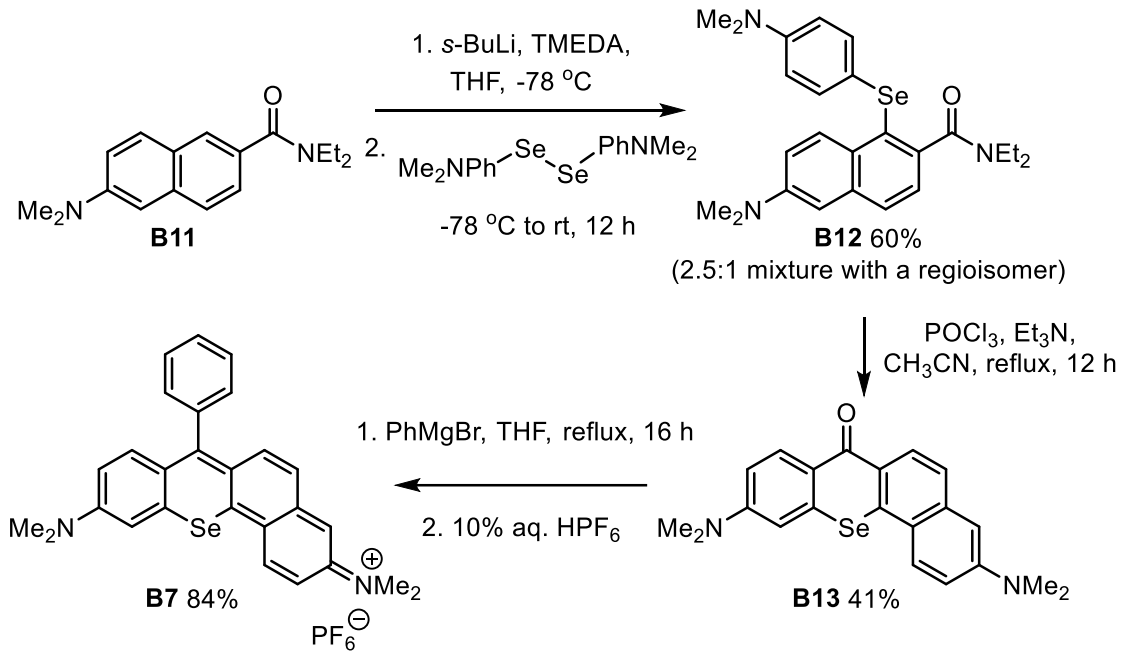

Scheme 1.29. Synthesis of selenorhodamine B7.[100]

Compound **B7** showed an absorption band at λ = 647 nm, and high singlet oxygen sensitisation $\Phi(^1O_2) = 0.65$, which allowed it to be used as an effective photosensitiser for photodynamic therapy of colon cancer cells.[100] In further studies, the synthesis of selenorhodamine derivatives was optimised by introducing TMS group to the starting material, to block the formation of a regioisomer.[127]

Efficient singlet oxygen sensitisation allowed selenorhodamine **B16** to photocatalyse the Aza-Henry reaction of aryl-1,2,3,4-tetrahydroisoquinolines **B14** with nitromethane, in moderate to high yields (62-84%) (Scheme 1.30).[126] The significantly reduced reactivity under N_2 atmosphere has corroborated the singlet oxygen sensitisation mechanism.

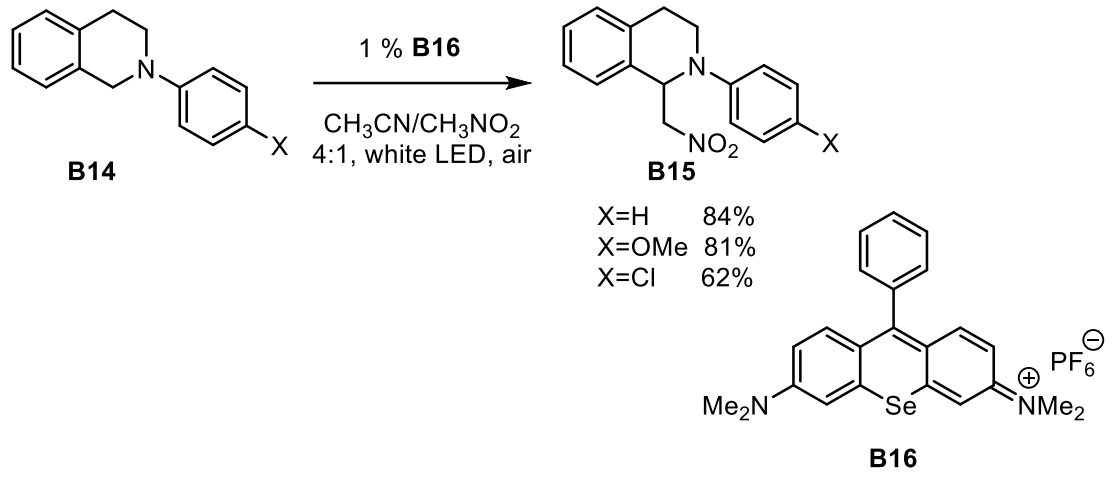

Scheme 1.30. Aza-Henry reaction utilising selenorhodamine B16 as the photocatalyst. Reaction times varied between 5 to 11 h.[126]

1.3.2.2 Selenopyrylium salts

Selenopyrylium salts found applications as polymerisation and crosslinking photoinitiators, reversible inhibitors of cholinesterases and photosensitisers for PDT.[128] Synthesis and applications of selenopyrylium salts have been described in the following reviews.[124,128–130] One example of selenopyrylium salt synthesis is presented in Scheme 1.31, in the synthesis of dicationic pentacene **B22**.[131]

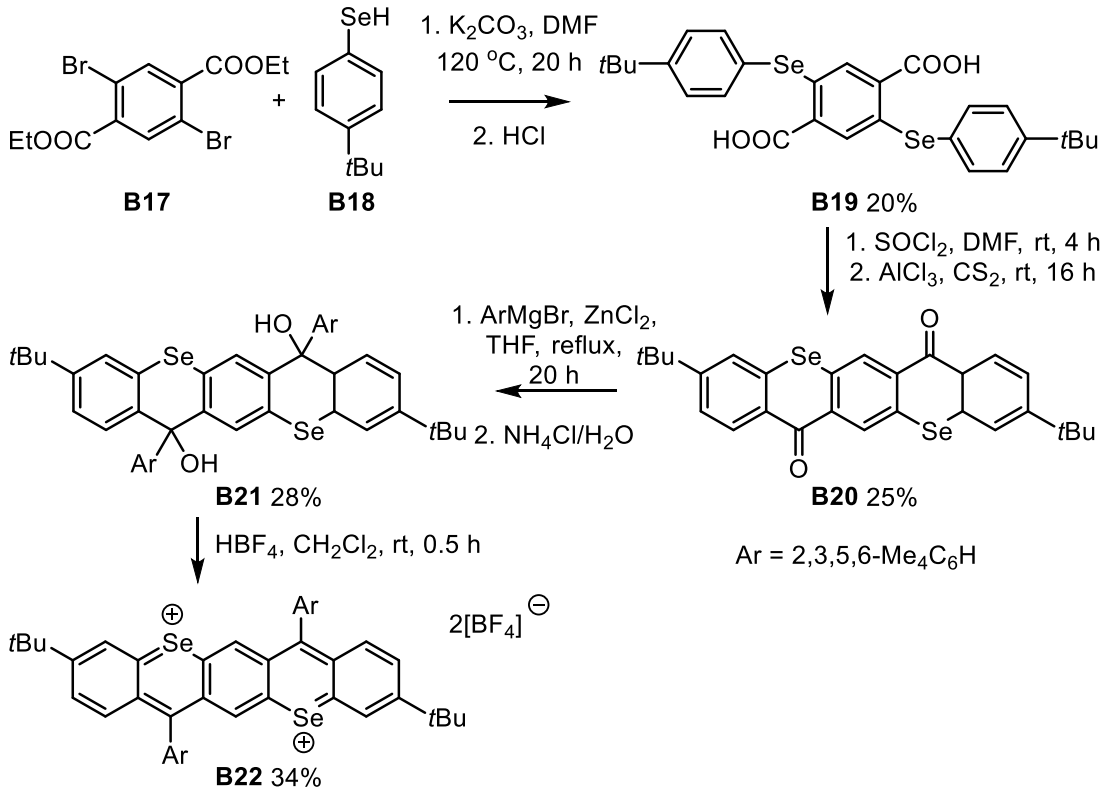

Scheme 1.31. Synthesis of dicationic selenopyrylium salts.[131]

Synthesis and characterisation of S- and Se- doped anthanthrenes and their derivatives

The first synthetic step was a nucleophilic substitution of dibrominated compound **B17** with benzeneselenol **B18**. Next, chlorination and Friedel-Crafts acylation led to dione **B20** in 25% yield. Treatment with the Grignard reagent in the presence of $ZnCl_2$ allowed alcohol **B21** in 28% yield. Finally, dehydration with HBF_4 led to selenopyrylium salt **B22** in 34% yield. Spectroscopic analysis and theoretical calculations suggest 22π-electrons aromaticity distributed over the whole pentacene framework.

1.3.2.3 Selenoxanthene derivatives

Selenoxanthene and selenoxanthone derivatives have been synthesised as precursors for selenorhodamine derivatives,[124] room-temperature phosphorescence materials[132,133] and antiviral inhibitors.[134] Their synthesis has also been described in the following reviews and publications.[135–138]

Recently selenoxanthene derivatives **B26** have been studied as antiviral inhibitors (Scheme 1.32).[134] Amine **B23** has been cyclised in the reaction with isoamyl nitrite in 87% yield. Next, naphthalene anhydride moiety of **B24** has been converted into naphthalene imide **B25** in 85% yield, after refluxing with diamine. Finally, the reaction of **B25** with HCl gas led to the formation of chloride salts **B26** in 75% yield. Obtained benzoselenoxanthenes **B26** showed inhibiting activity towards Influenza A virus.

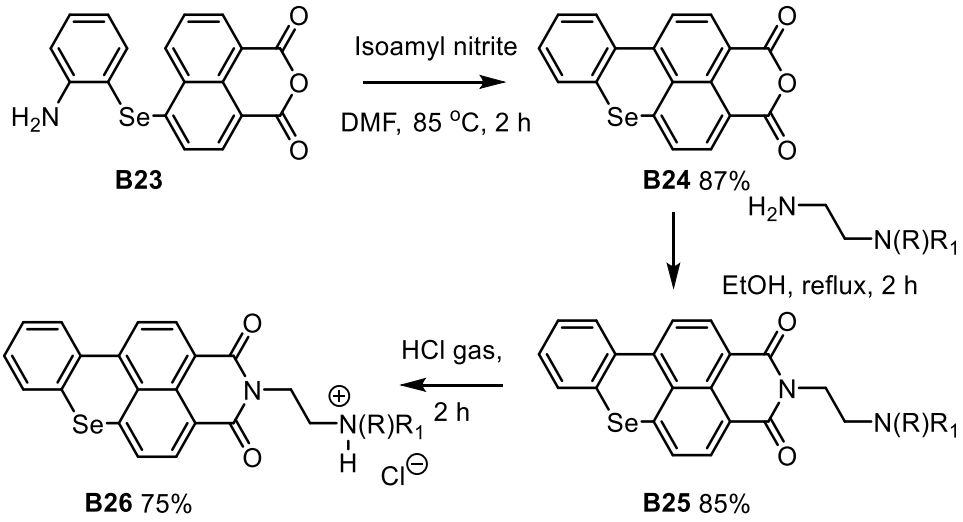

Scheme 1.32. Synthesis of benzoselenoxanthenes.[134]

1.3.3 S_EAr in the synthesis of Se containing compounds

Even though S_EAr reactions are widely used in the intramolecular synthesis of S doped PAHs, with examples in the synthesis of dibenzothiophenes (paragraph 1.1.1.2) and thioxanthene derivatives (paragraph 1.1.2.3.1), they have been rarely used in the cyclisations forming C-Se bond. There is a single example of an acid-mediated S_EAr reaction leading to the dibenzoselenophene (**DBSe**). Thioether **B30** has been treated

with concentrated sulfuric acid and then refluxed with zinc giving dibenzoselenophene in 60% yield (Scheme 1.33).[139]

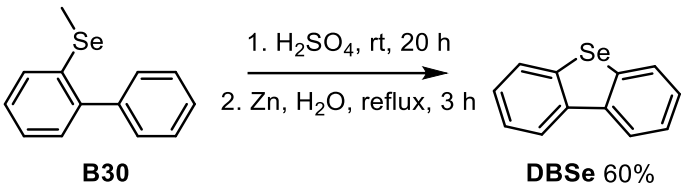

B30 **DBSe** 60%

Scheme 1.33. H_2SO_4 mediated dibenzoselenophene synthesis.[139]

An example of S_EAr reaction utilising trifluoromethyl selenoxide **B31** as starting material has been presented in (Scheme 1.34).[140] Tf_2O was used as a mediator to achieve triflic salt **B32**.

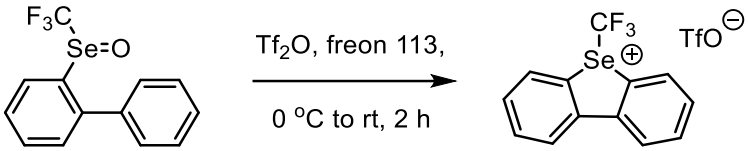

B31 **B32** 94%

Scheme 1.34. Synthesis of Se-(trifluoromethyl)-dibenzoselenophenium triflate **B32**.[140]

1.4 Anthanthrenes

Anthanthrene based PAHs are widely studied for applications as a semiconducting material in optoelectronics, as they are more stable than linear acenes. They have lower diradical character and are less prone to oxidation, which is a leading cause of linear acenes decomposition.[141] Anthrantrene based PAHs have been used in OFETs[142] and solar cells.[142,143] Derivatization of anthanthrene has been applied to increase its solubility, to influence its bandgap and environmental stability to oxidation.[144] The derivatization of anthanthrene has been achieved through the introduction of substituents,[142,143,145,146] extension of structure through annulation[143,144,147] and doping with different heteroatoms, such as Si,[148] N,[149] B[150] and O.[151,152] Especially doping with O was found to give PXX, a derivative more environmentally stable than anthanthrene.[152]

1.4.1 PXX

Peri-xanthenoxanthene (**PXX**) is an O-doped anthanthrene derivative, that absorbs blue light (λ_{max} = 444 nm) with an excitation coefficient of 17300 $M^{-1}cm^{-1}$ and exhibits a relatively high quantum yield of fluorescence Φ_F = 0.62.[153] **PXX** can be synthesised

in a Cu catalysed reaction from **BINOL** (Scheme 1.35).[154,155] Different Cu catalysts, such as $Cu(OAc)_2$,[156–158] CuI[154,155] and CuCl[159] were used to promote this reaction.

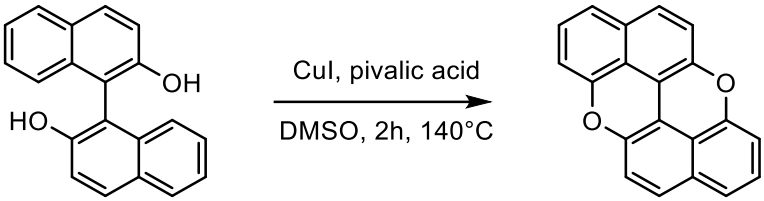

BINOL **PXX** 86%

Scheme 1.35. Synthesis of **PXX** through CuI promoted **BINOL** cyclisation.[154,155]

PXX and its derivatives were investigated in the organic semiconductors field[158,160,161] for their excellent carrier-transport and electron injection properties.[155] In recent years our group became interested in **PXX** motif and developed various **PXX** based structures, such as pyrene derivatives,[155] **PXX** mono- and diimide derivatives[153,162] and molecular ribbons[25,154] (Figure 1.7). The synthesis of various extended and doped **PXX** derivatives allowed for fine tuning of the HOMO-LUMO gap. Extension of π-system (**B33**, **B34**, **B37**, **A3**)[25] as well as the introduction of EWG imide groups (**PXXDI**, **PXXMI**),[153,162] led to the shrinking of the bandgap resulting in red shift of absorption spectra. Another approach towards tuning of the HOMO-LUMO gap, that our group investigated, lies in doping. The introduction of N atoms into **PXX** structure (**B35**, **B36**) led to the blue shift of absorption maxima ($\lambda_{max\ PXX}$ = 443 nm, $\lambda_{max\ 57}$ = 437 nm, $\lambda_{max\ 58}$ = 413 nm).[149]

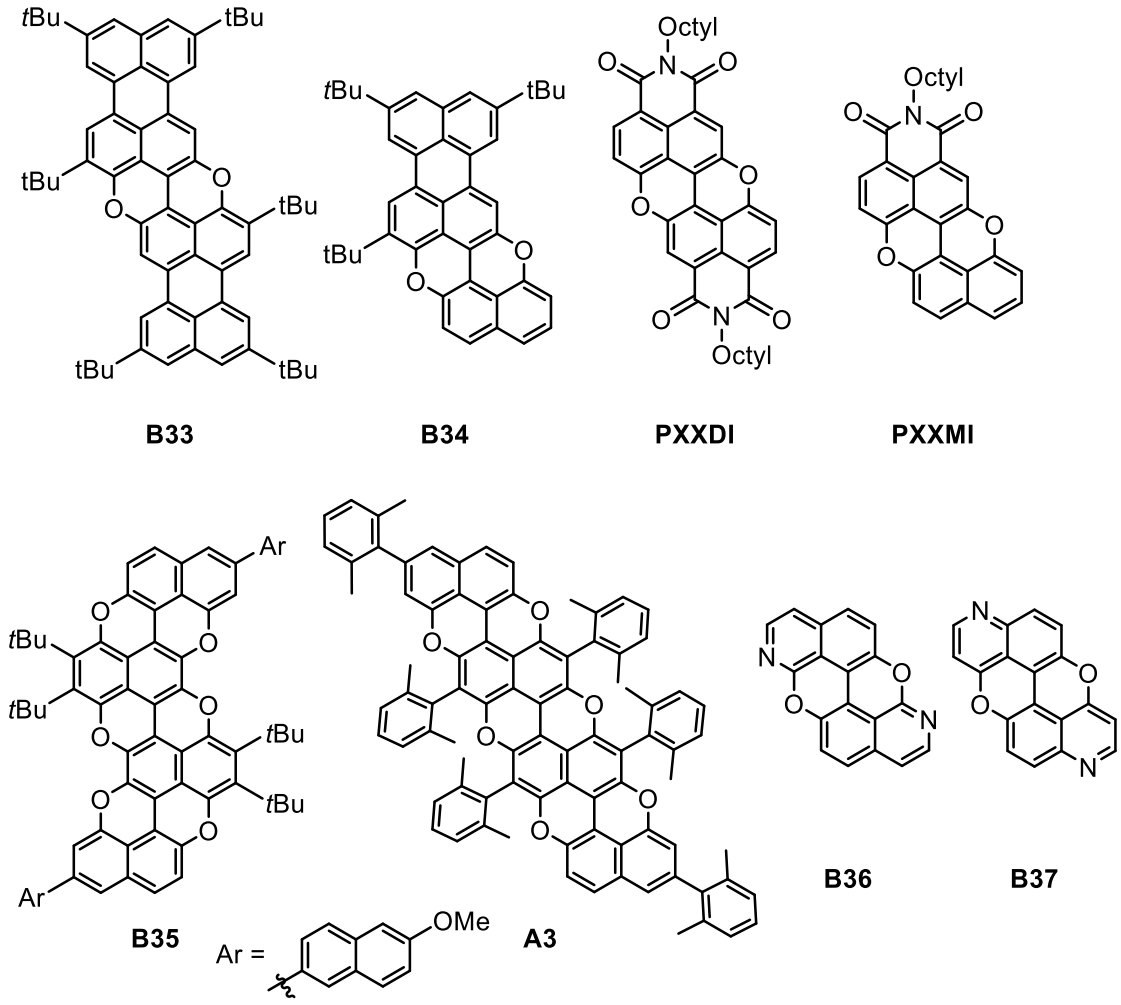

Figure 1.7. Different **PXX** derivatives.[25, 154,155,162,163]

The introduction of N atoms also affected solid state interactions, with new hydrogen bonding between N and O atoms and hydrogens in the crystal structure of compound **B36** (Figure 1.8). These hydrogen bonds prevented the typical herringbone arrangement seen in the **PXX** crystals, which has been connected with lower charge transport properties in organic semiconductors.

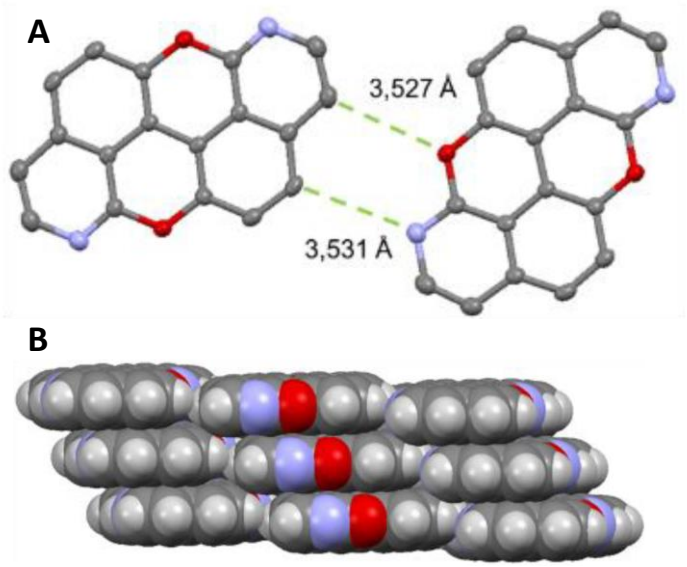

Figure 1.8. A hydrogen bonding and **B** crystal packing in molecule **B36**.[149]

1.5 Aim of the project

In O-doped PAHs oxidation (either chemical with BAHA[164] or electrochemical[165]) of the molecules leads to the formation of stable pyrylium cations, displaying significantly red shifted UV-VIS spectra, compared to the neutral species. However, oxygen doped PAHs cannot be structurally changed through oxidation, restricting structural and optoelectronic variabilities which could be accessed through derivatization. On the other hand, other chalcogen atoms, such as S and Se, can have three different oxidation states.[166] Peri-thiaxanthenothiaxanthene (**PTXTX**),[167] the S-doped analogue of **PXX** in which the oxygen atoms are replaced by sulfur atoms, could be an example of PAH whose optoelectronic properties would be influenced through the oxidation of chalcogen. Mono- and di-oxidation of the sulfur atoms (Figure 1.9) could lead to the widening of the HOMO-LUMO gap, rising of the ionization potential and affecting the solid-state organization.

As explained in paragraph 1.2, S-doped PAHs display higher charge penetration than their O-doped counterparts, as well as higher π-stacking, leading to larger electronic coupling and better charge transfer properties. Exchanging O-atoms in PXX with S-atoms could lead to a beneficial self organization in the solid state and to better charge transfer properties in OSCs.

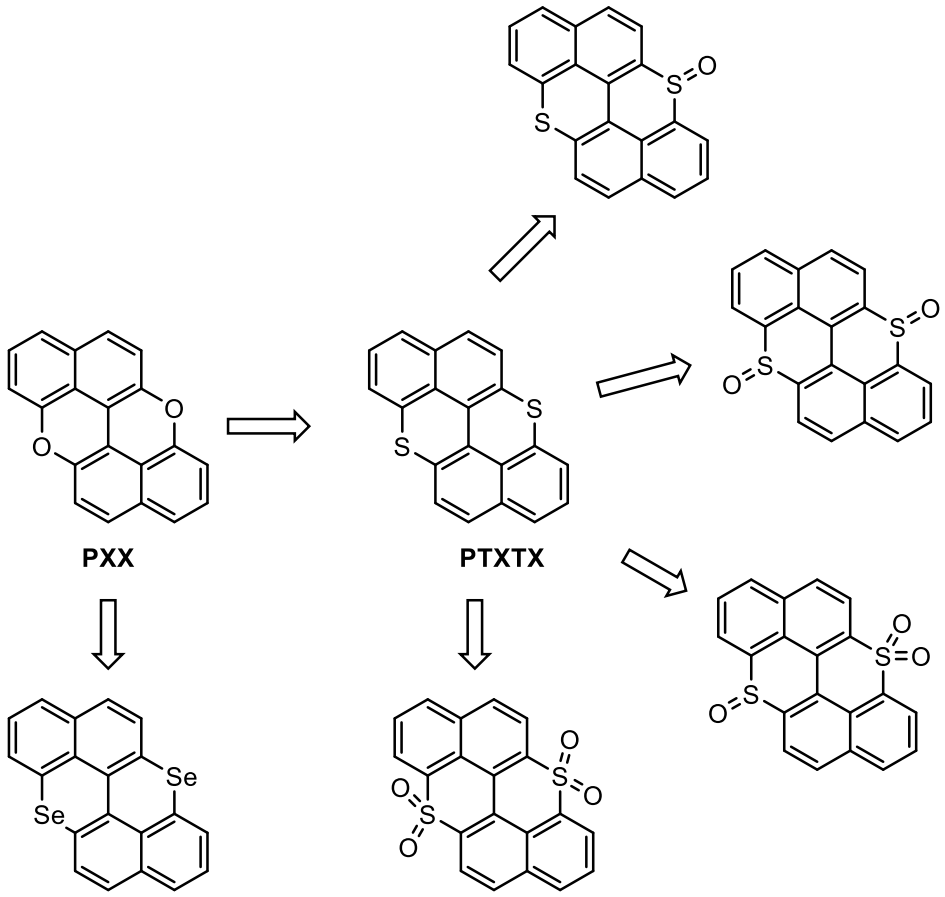

Figure 1.9. PTXTX and possible oxidised derivatives.

1.6 Synthesis of PTXTX

1.6.1 Triflic acid mediated synthesis of PTXTX

Synthesis of **PTXTX** through triflic acid mediated cyclisation has been reported previously in the literature.[167] We decided to use this reaction as the main synthetic step to obtain **PTXTX** and test its photophysical and electrochemical properties. **PTXTX** amine derivative has recently been applied as a hole transporter in perovskite solar cells.[168]

1.6.1.1 Retrosynthesis

A retrosynthetic pathway to **PTXTX** is presented in Scheme 1.36. **PTXTX** can be obtained through triflic acid mediated cyclisation of disulfoxide **2**, which could be obtained through oxidation of thioether **1**. While there are many available methods of obtaining thioethers we decided to use metal halogen exchange, followed by quenching with dimethyldisulfide, as it could give **1** in just one reaction, from commercially available 2,2'-dibromo-1,1-binaphthyl.

Synthesis and characterisation of S- and Se- doped anthanthrenes and their derivatives

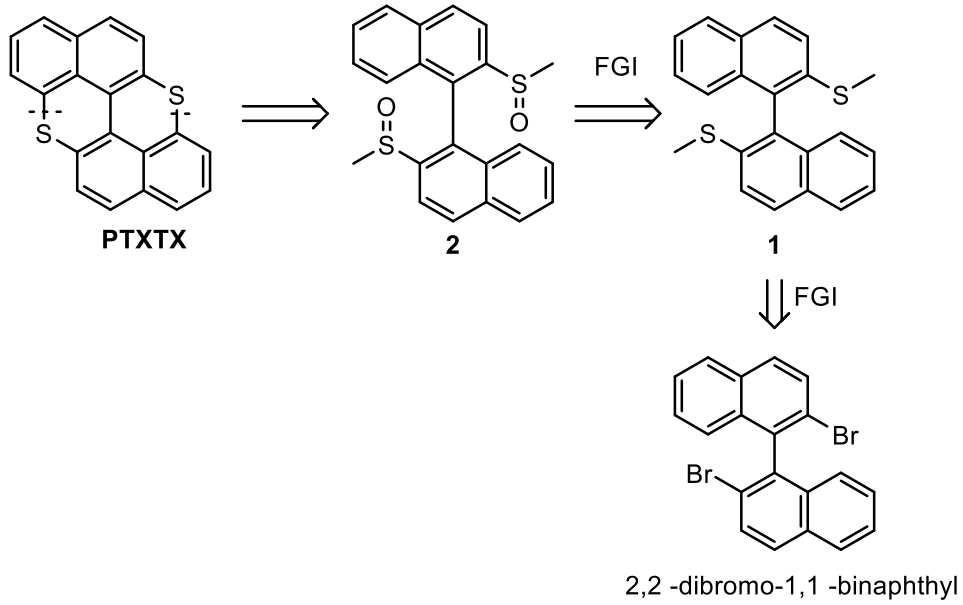

Scheme 1.36. Retrosynthetic pathway to **PTXTX**.

1.6.1.2 PTXTX synthesis - results

We proceeded with the lithium halogen exchange of 2,2'-dibromonaphthalene, followed by a reaction with dimethyldisulfide to give thioether **1** (Scheme 1.37). At first, *t*-BuLi was tested as lithiating reagent with TMEDA as a ligand. After quenching with dimethyldisulfide, **1** was obtained with 79% yield. However, safer *n*-BuLi could also be used towards this reaction without a loss of reactivity, giving **1** in 82% yield. The second necessary step was oxidation of thioether **1** to disulfoxide **2**. Several oxidation methods were tested, such as oxidation with *t*-BuOOH/$VO(acac)_2$, $Ti(OiPr)_4$/*t*-BuOOH, *m*CPBA and H_2O_2/CH_3COOH (in situ generated peracetic acid). The best results were obtained with H_2O_2/CH_3COOH. Compound **2** was achieved as a mixture of diastereoisomers, due to the presence of three centers of chirality, namely two sulfoxide moieties and axial chirality originating from the binaphthalene backbone.

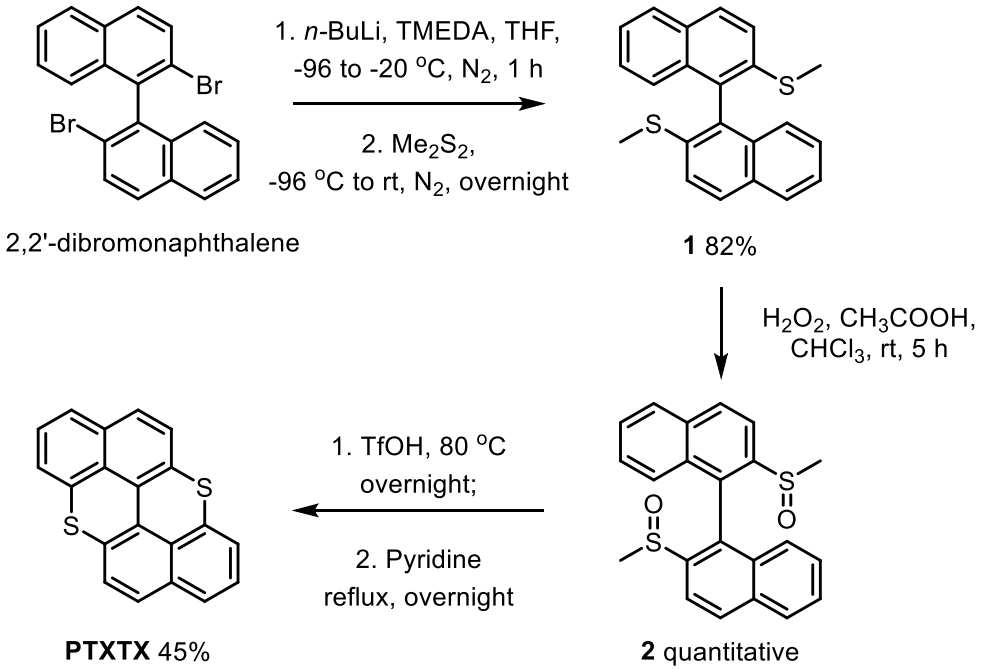

Scheme 1.37. Synthesis of **PTXTX**.

A quantitatively obtained mixture of diastereoisomers was used directly in the next step. The neat triflic acid was used to cyclise the molecule through electrophilic aromatic substitution, and then pyridine was added to act as a base and demethylate the bis-sulfonium salt. Several attempts were made to isolate the triflic salt after the first step, but they were unsuccessful. This hindered our attempts to optimise the reaction, as both steps could not be separated and optimised independently. However, the biggest problem we encountered with this reaction was the purification of the desired product. Early on, we managed to obtain the desired product, although its reliable isolation and purification were found to be difficult. **PTXTX** was found to partially decompose in chlorinated solvents, such as CH_2Cl_2 and $CHCl_3$, but it proved to have low solubility in most of the other organic solvents. CH_2Cl_2 and $CHCl_3$ are known to be slightly acidic and to have a high lifetime of singlet oxygen.[169] Since we envisioned that this molecule would have a highly populated triplet state, we thought that it could efficiently produce singlet oxygen under irradiation with light. **PTXTX** is a thioether and its sulfur atoms can potentially be oxidised to sulfoxide or sulfone. So possibly the decomposition could be caused by oxidation with the singlet oxygen it would produce. This prompted us to avoid using chlorinated solvents and attempt to use toluene, as **PTXTX** has a relatively high solubility in it, and the lifetime of singlet oxygen is an order of magnitude lower in toluene than in $CHCl_3$ ($2.9 \cdot 10^{-5}$ s vs $2.5 \cdot 10^{-4}$ s).[169] Another issue was the high degree of decomposition that was happening during isolation by column chromatography. Several other methods of isolation were tested,

such as recrystallisation and sublimation, but they were unsuccessful. A small amount of pure product was isolated using long columns of biobeads, used commonly in GPC – gel permeation chromatography. Although they allowed isolation of low quantities of pure product, this method is rather more appropriate to large molecules that stay shorter time in the polymer pores of GPC column. The high cost of biobeads, large amounts of toluene that were used and the long separation time that was necessary prompted us to look for other methods of purification. Different stationary phases for column chromatography were tested, such as silica treated with NEt_3 or basic alumina and in the end, neutral alumina Brockman activity I led to the best result.

During the synthesis of the **PTXTX** we also encountered a reproducibility issue. The cyclisation reaction (Scheme 1.38) worked only with an old batch of triflic acid (entry 1 Table 1.1). This old batch had a layer of solid on the bottom of the flask, that could possibly be triflic acid monohydrate, which is a solid that forms when the acid is exposed to moisture from air. When instead a new, fresh reagent was used (entry 2), the reaction did not give the desired product, and most of the starting material was recovered. To investigate the problem, the reaction was also performed with distilled TfOH (entry 3) and with 1.2 eq. of water (entry 4), but the desired product was not obtained in both cases.

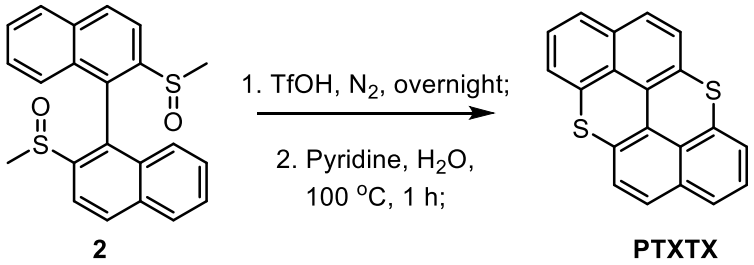

2 **PTXTX**

Scheme 1.38. Triflic acid mediated cyclisation reaction in the synthesis of **PTXTX**.

Table 1.1. Optimisation of cyclisation reaction to obtain **PTXTX**. *second step with pyridine, for 24h.

entry	TfOH batch	Temp	Outcome and yield
1	Old (partially hydrated)	rt	35% **PTXTX**
2	new	rt	Mostly starting material
3	distilled	rt	Mostly starting material
4	new + 1.2 eq. of water	rt	Mostly starting material
5	new*	80°C	45% **PTXTX**

The reproducibility problem was solved by heating the reaction at 80°C,[75] allowing the formation of the product with new triflic acid and affording a higher 45% yield (entry 5).

The need for high temperature could be explained with the reaction mechanism. Based on the reaction mechanism reported in the literature, we propose an electrophilic aromatic substitution, followed by demethylation with pyridine of the resulting salt.[170,171] First, triflic acid protonates the sulfoxide, which is then attacked by an electron pair from a neighbouring ring (Scheme 1.39). Next, dehydration leads to the formation of the corresponding sulfonic salt. The same steps would apply to the other sulfoxide moiety. Pyridine added in the second stage demethylates the salt giving a sulfide bond. The high temperature might help the dehydration step (Scheme 1.39).

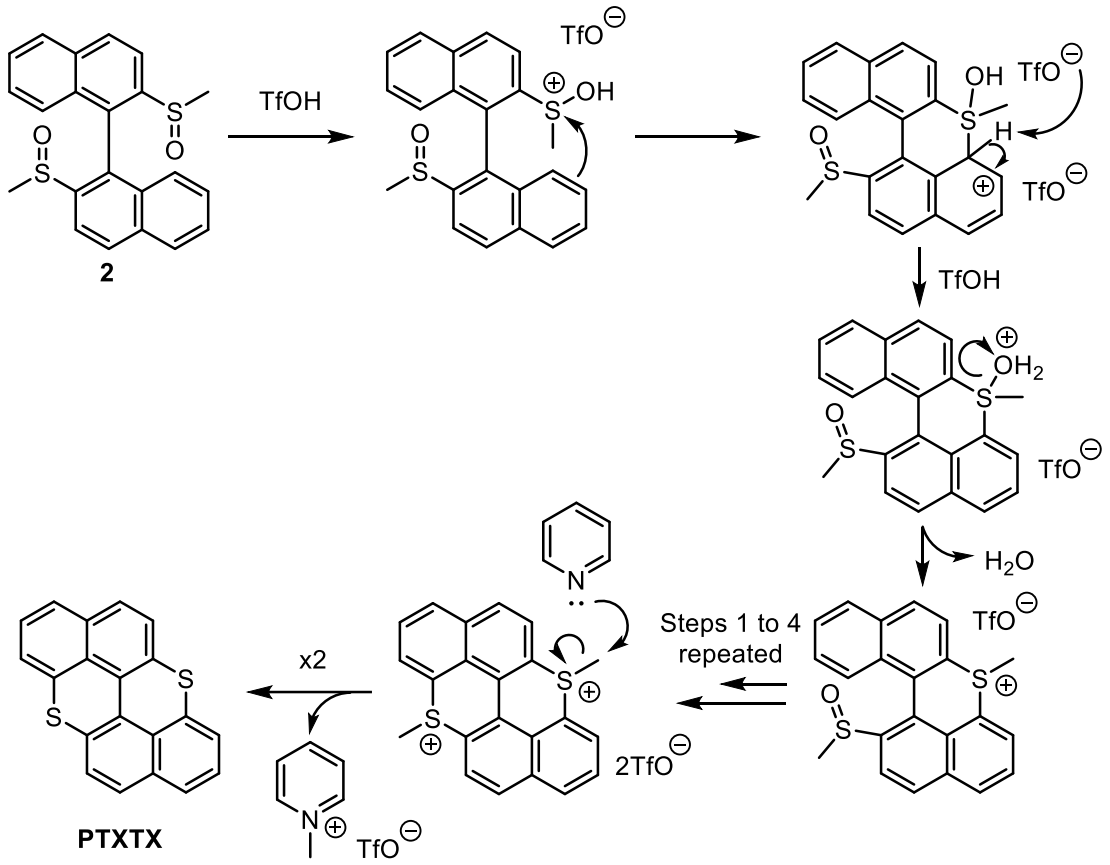

Scheme 1.39. Part of the proposed mechanism of TfOH mediated cyclisation of sulfoxide **2**.

The formation of **PTXTX** was confirmed by full characterisation, as well as through the analysis of the single crystal X-ray structure.

^{1}H NMR spectra of **PTXTX** is presented in Figure 1.10. As expected from a symmetrical molecule, 5 peaks are visible in the typical aromatic part of the spectrum. 2 peaks, 7.27 and 6.78 ppm are doublets, coupled with the same J = 8.7 Hz coupling constant, corresponding to protons *d* and *e*. A doublet of doublets at 7.01 ppm is coupled with two other signals, with J = 8.1 and 7.3 Hz, which are both ortho coupling constants, indicating it can be assigned to protons *b*. Doublets of doublets at 7.13 and at 6.86 ppm

are coupled together with J = 1.4 Hz, which is a meta coupling constant, and they correspond to protons *c* and *a*.

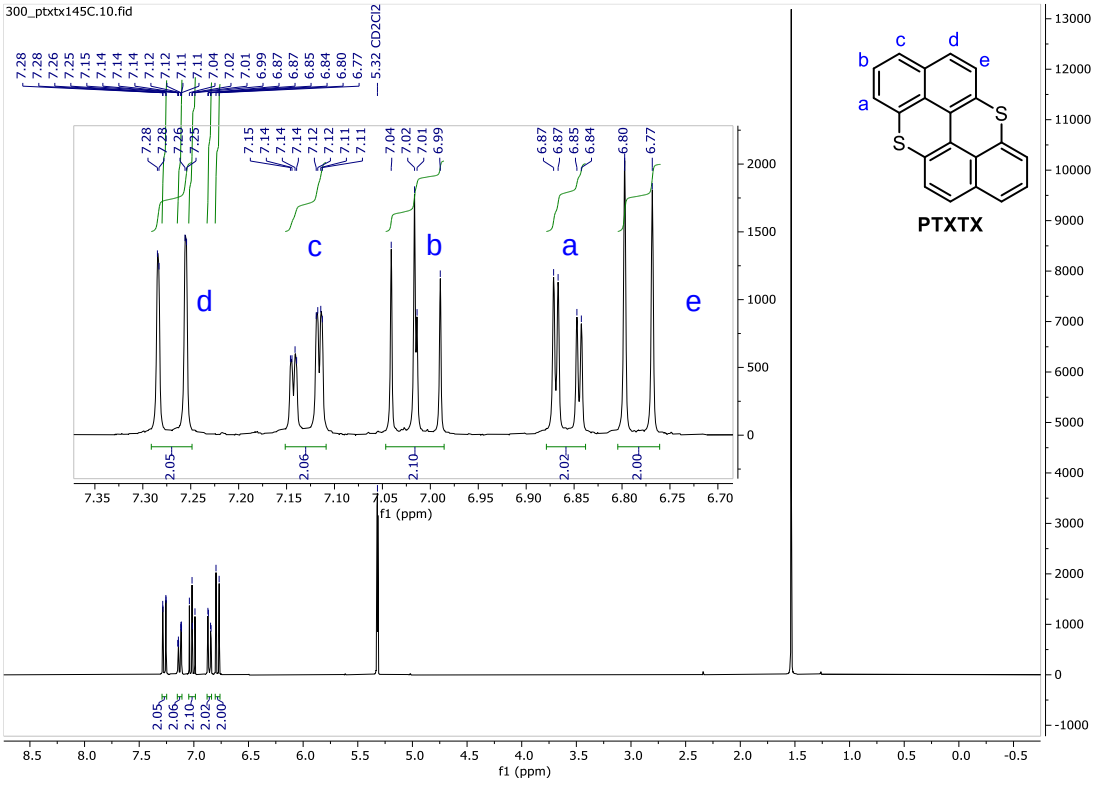

Figure 1.10. ^{1}H NMR of **PTXTX**, 300 MHz, CD_2Cl_2.

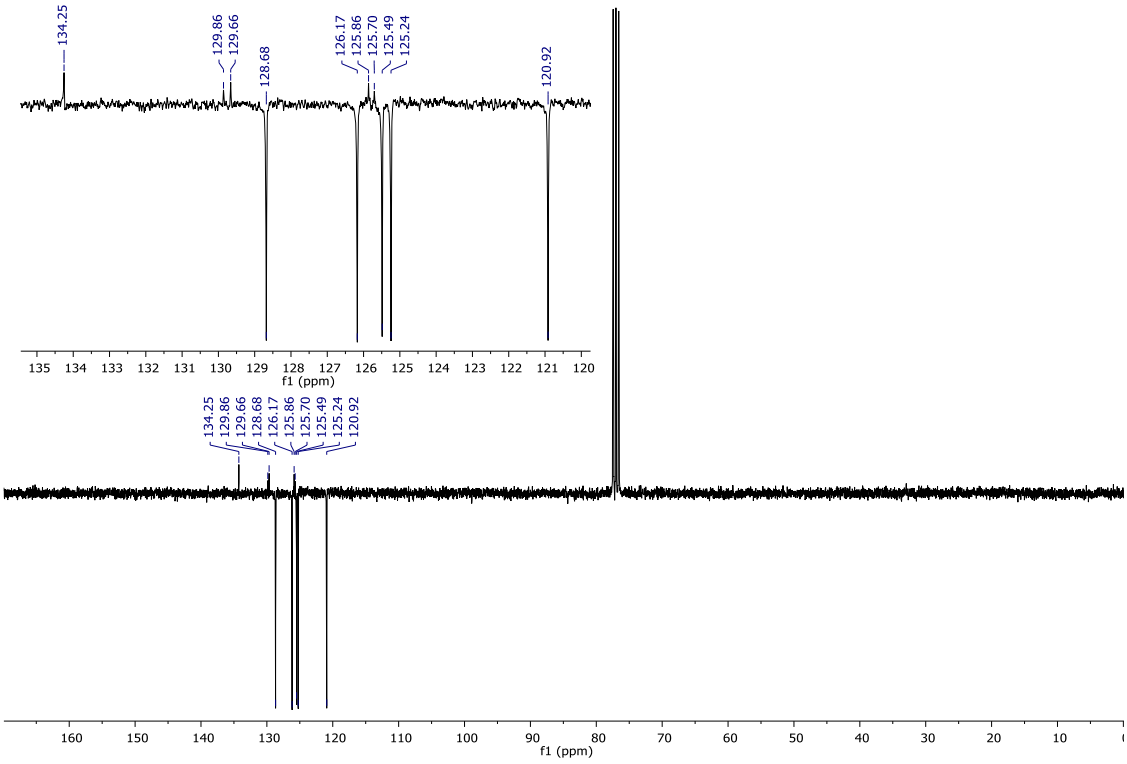

Figure 1.11. APT ^{13}C NMR of **PTXTX**, 125 MHz, CD_2Cl_2.

In the Attached Proton Test - APT ^{13}C NMR spectrum (Figure 1.11), as expected 10 peaks are visible in the typical aromatic part of the spectrum. 5 peaks are C atoms without protons (pointing up), and 5 are CH carbon atoms (pointing down). Correct mass was also found in HR mass spectrometry.

Due to the low yields, as well as issues with purification and reproducibility we encountered, simultaneously we pursued other methods to try to obtain **PTXTX** and the results are reported in the following sections.

1.6.2 Other attempts at the synthesis of PTXTX

1.6.2.1 H_2SO_4 mediated cyclisation attempt

Since electrophilic aromatic substitution with triflic acid successfully yielded **PTXTX**, we decided to test if other mediators could be used towards this cyclisation reaction. H_2SO_4 has been reported to mediate electrophilic aromatic substitution of sulfoxides leading to various dibenzothiophenes, so it was tested first.[171,172]

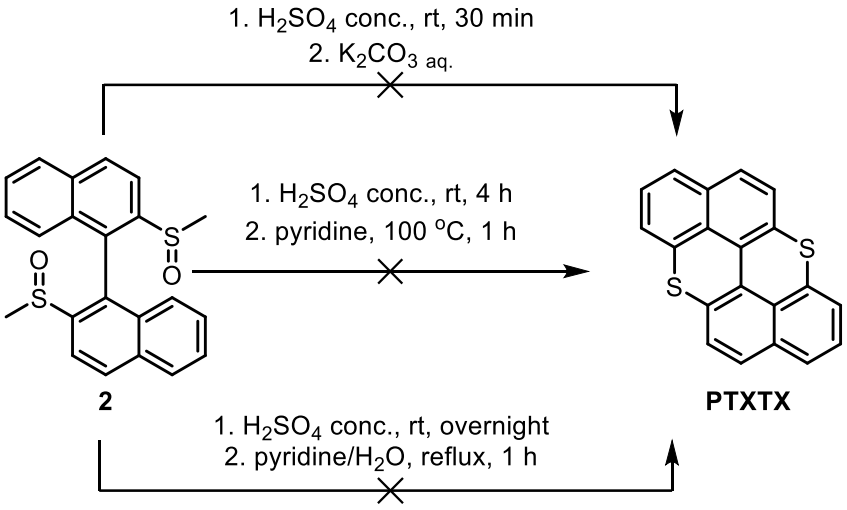

Scheme 1.40. Attempts at H_2SO_4 mediated cyclisation of sulfoxide **2**.

Concentrated H_2SO_4 was used at room temperature to mediate cyclisation of sulfoxide **2**, and then either K_2CO_3, pyridine or pyridine/water were used as demethylating agents (Scheme 1.40). When K_2CO_3 was used as a demethylating agent, the formation of desired product was not observed. The starting material was partially recovered, and an insoluble, dark precipitate was achieved, possibly the product of intermolecular coupling. When pyridine or a mixture of pyridine and water were used, only traces of the desired product were observed on TLC, although mostly unreacted starting material was recovered, and again insoluble dark precipitate was formed. Seeing how this method failed to give **PTXTX** we decided to move to other reactions.

1.6.2.2 Tf_2O mediated cyclisation attempt

It has been first described by Balenkova,[170] and later utilised by others,[173,174] that triflic anhydride can mediate intermolecular electrophilic aromatic substitution of aryl sulfoxides with arenes. In the first step, triflic anhydride mediates the coupling, giving a sulfonium salt, which after demethylation with a base gives a thioether. An intramolecular version of this reaction has also been reported, leading to benzothiophene derivatives.[175–177]

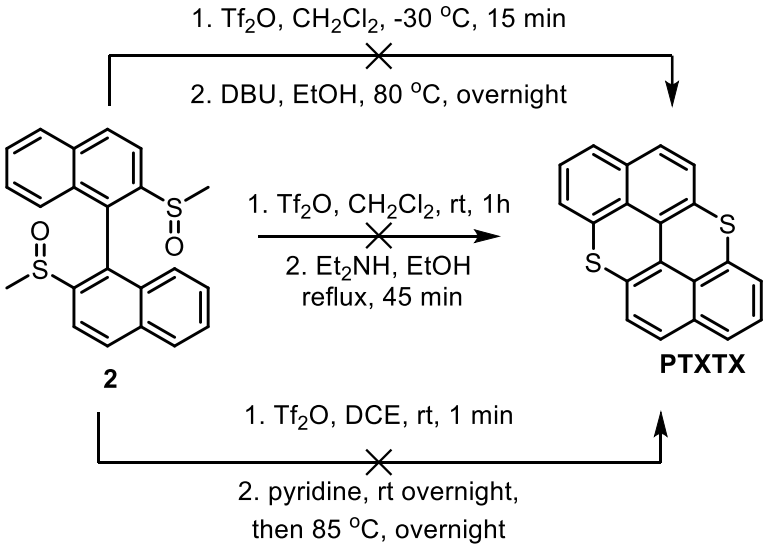

Scheme 1.41. Attempts at Tf_2O mediated cyclisation of sulfoxide **2**.

We decided to test if Tf_2O/base protocol can mediate cyclisation giving **PTXTX** structure. Several variants of the reaction were tested, using either low or room temperature, different solvents and bases, such as DBU[173], Et_2NH[174] or pyridine[176] (Scheme 1.41). However, the desired product was not obtained in any of the cases, and some unreacted starting material was recovered. A dark, insoluble precipitate was formed as well, potentially the result of the intermolecular rather than intramolecular reaction.[170,173,174]

1.6.2.3 Cu catalysed cyclisation attempt

Copper(I) catalysed cyclization of aryl thiol has been reported to give thioxanthene derivative, applied as an OLED material.[178] We were interested to see if we could apply copper catalysed cyclisation reaction conditions to our target sulfur doped **PTXTX**. We decided to test the conditions that allow the synthesis of **PXX** (paragraph 1.4). First, we needed to obtain dithiol **6**, the synthesis of which has been previously described in the literature (Scheme 1.42).[179] The reaction between commercially

available **BINOL**, NaH and N,N'-dimethylthiocarbamoyl chloride afforded compound **3** with 75% yield (Scheme 1.42).

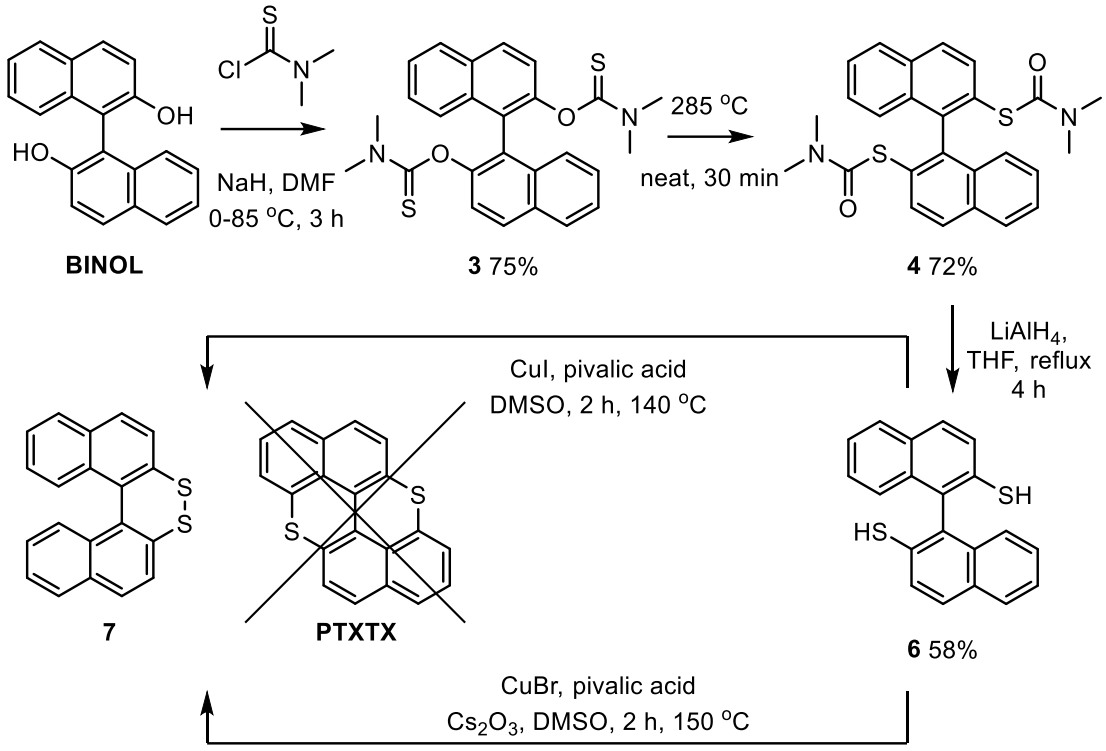

Scheme 1.42. Synthesis and attempt at cyclisation of dithiol **6**.

Subsequent Newman-Kwart thermal rearrangement was found to give a mediocre yield when the temperature was too low. When the temperature was lower than 285°C (referring to the temperature of a metal bath that the reaction vessel was immersed in), a formation of side product **5** was detected, and only a low amount of desired product **4** was achieved (32%) (Scheme 1.43).

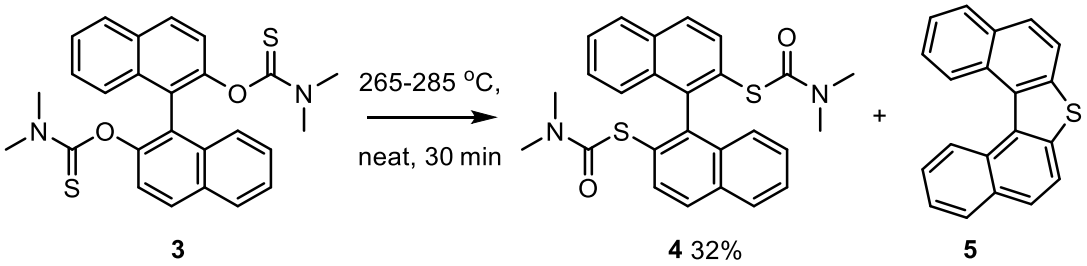

Scheme 1.43. Side product formed from Newman-Kwart thermal rearrangement of compound **3** when the reaction temperature was lower than 285 °C.

However, when the temperature was stable at 285 °C, ensured by the layer of thermoinsulating material around the reaction vessel, the rearranged bis-thiocarbamate **4** was obtained with 72% yield (Scheme 1.42). Finally, reduction with

$LiAlH_4$ in refluxing THF yielded dithiol **6** with 58% yield. The cyclisation of compound **6** (Scheme 1.42) was attempted with the use of CuI, pivalic acid and DMSO[154,155] at 140°C. The desired compound was not achieved, and alternative conditions were tested as well, with CuBr, pivalic acid and Cs_2O_3 in DMSO at 150°C. Unfortunately, desired **PTXTX** was not obtained and only the formation of disulfide **7** was detected in both cases (Scheme 1.42). The disulfide could have been formed through oxidation with either DMSO[180,181] or Cu(I) and DMSO combina tion,[182] as literature reports synthesis of sulfoxides with both these systems.

1.6.2.4 I_2 mediated cyclisation attempt

We decided to test if I_2 mediated cyclisation reaction,[76] described in paragraph 1.2.2.4.2, could be applied to the direct transformation of thioether **1** into **PTXTX** (Scheme 1.44). Two literature reported reaction conditions were tested, using either boiling chloroform[76,183] or boiling glacial acetic acid.[77] However, in both cases no conversion was observed, and only unreacted starting material was recovered.

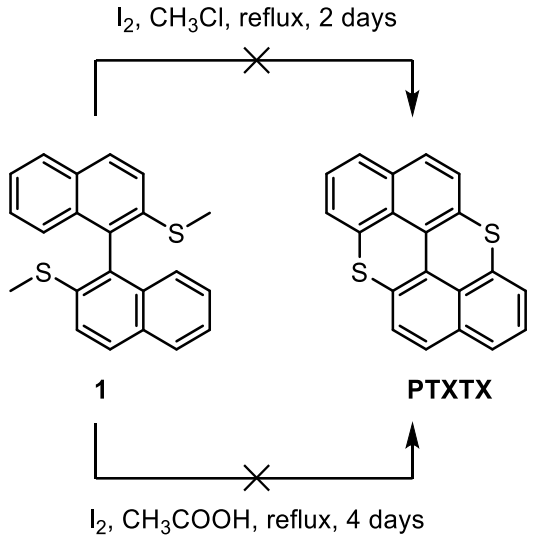

Scheme 1.44. An attempt at the direct cyclisation of thioether **1** with iodine (synthesis of compound **1** was presented in Scheme 1.37).

1.6.2.5 Pd(II) catalysed cyclisation attempt

Next, we decided to test if the Pd-catalysed reaction, developed for the synthesis of dibenzothiophenes[62] (paragraph 1.2.2.2), could be applied towards the formation of desired **PTXTX**. The synthesis of phenylsulfide **8** was achieved by the reaction of 2,2'-dibromonaphthalene with *n*-BuLi, followed by the addition of diphenyldisulfide, to give compound **8** in 69% yield (Scheme 1.45). However, when the palladium catalysed cyclisation was tested, it was unsuccessful, giving mostly unreacted starting material.

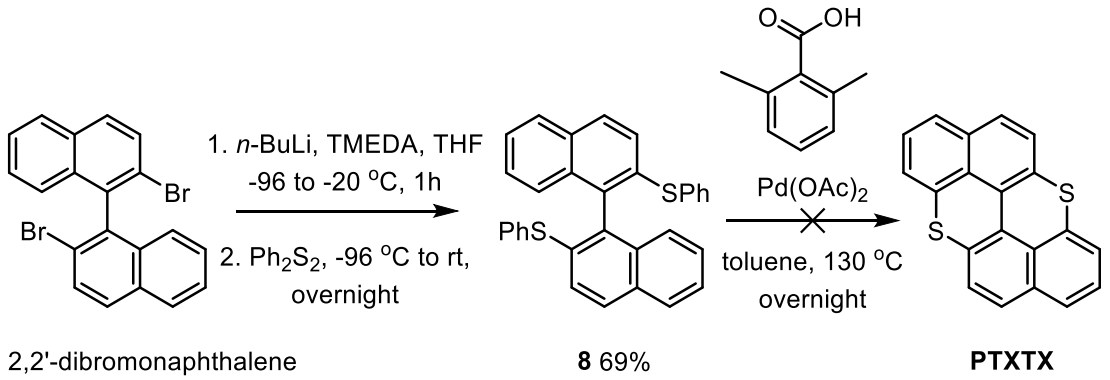

Scheme 1.45. Synthesis of phenylsulfide **8** and Pd(II) catalysed cyclisation attempt.

One explanation for the lack of reactivity in the case of **PTXTX** could derive from the postulated reaction mechanism (paragraph 1.2.2.2, Scheme 1.7).[62] While during the synthesis of dibenzothiophene 6-membered palladacycle would form, in the case of **PTXTX** the analogous intermediate would have to contain 7-membered palladacycle. However, the formation of 7-membered palladacycles has been shown to be disfavoured.[184]

As we could not find alternative ways of obtaining **PTXTX**, we decided to keep using triflic acid mediated synthesis, and moved to the synthesis of derivatives bearing solubilising groups.

1.7 Synthesis of PTXTX derivatives bearing solubilising groups

1.7.1 Synthesis of PTXTX derivatives bearing solubilising groups - retrosynthesis

Since we observed low solubility of **PTXTX** in most organic solvents, we decided to include solubilising groups. In solid states, molecules of **PTXTX** interact with each other through π- π stacking, as confirmed through X-ray crystal structure we managed to obtain (paragraph 1.12.1). So we decided to include mesitylene moieties in positions 2 and 8, hoping they would assume perpendicular positions to the plane of **PTXTX** and so efficiently break interactions between the molecules, similarly as reported for **PXX** derivatives.[25] Solubilising moieties could be introduced through Suzuki coupling, which would require the introduction of bromine atoms in the molecule. They could be introduced at three different stages, either to a sulfide, sulfoxide or to a parent **PTXTX** structure. All three retrosynthetic pathways have been presented in Scheme 1.46.

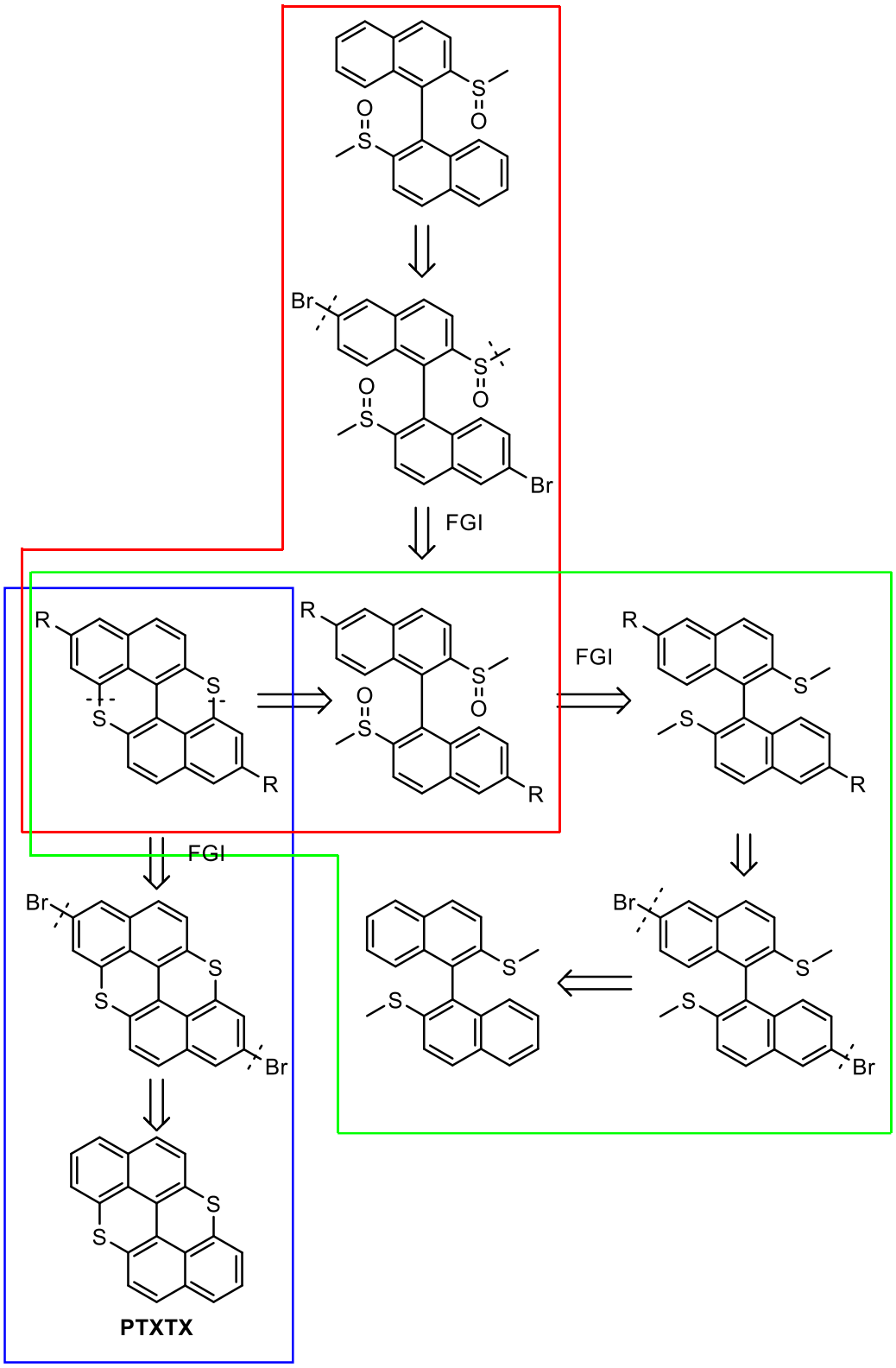

Scheme 1.46. Retrosynthetic pathways to substituted **PTXTX**.

Introduction of bromine atoms to a parent **PTXTX**, the blue route, would require two additional steps, while introducing them at the stage of sulfoxide, the red route, three additional steps and to a sulfide, the green route, four steps. We decided to first test

the blue route as it has fewer new steps, and also potentially allows easy introduction of other substituents using the bromo derivative.

1.7.2 Synthesis of PTXTX derivatives bearing solubilising groups – results

1.7.2.1 Introduction of mesitylene groups to the PTXTX structure

We commenced the blue route with bromination of **PTXTX**, using bromine in CH_2Cl_2 (Scheme 1.47). However, the obtained mixture of products was not possible to separate due to low solubility in organic solvents. Mass analysis of the sample suggested that a combination of products with up to four bromine atoms was achieved. We decided to test if the substituted products would be easier to separate and submitted the mixture of bromides **9*** to the Suzuki reaction conditions with mesitylene boronic acid. Although the Suzuki coupling was successful, and the mixture of obtained compounds **10*** was soluble, the products proved to be inseparable.

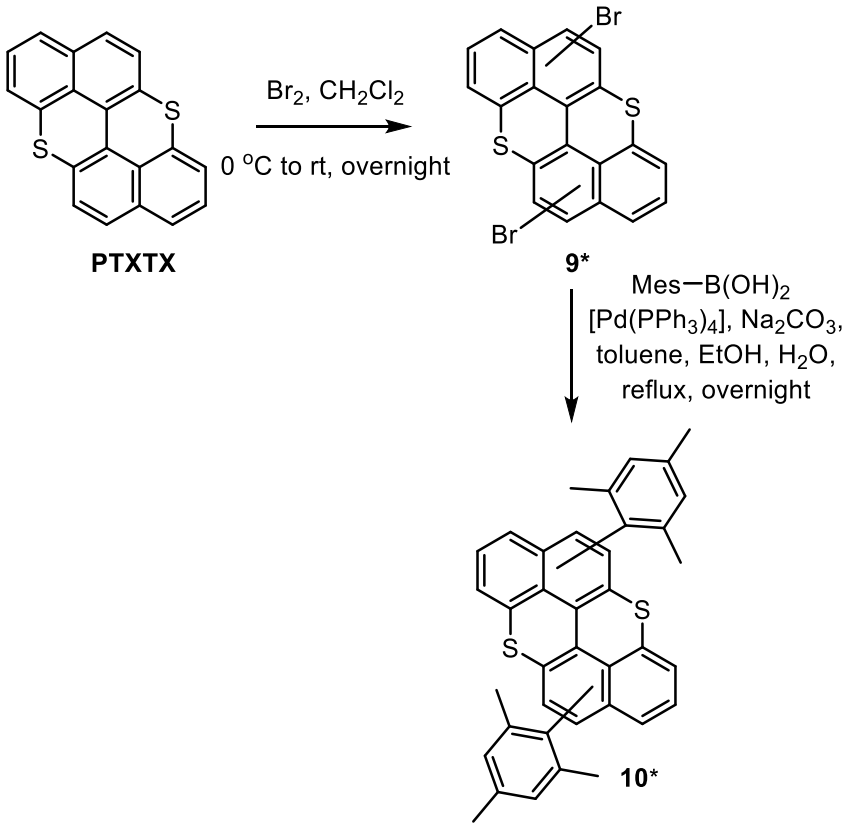

Scheme 1.47. An attempt at the synthesis of compound **10*** a mixture of inseparable products was obtained, the position of bromine atoms was not confirmed.

Since the bromination of **PTXTX** was found to not be selective and products highly insoluble, we decided to move to other retrosynthetic pathways.

Next, the red route (Scheme 1.46) was employed, as it requires fewer steps than the green route.

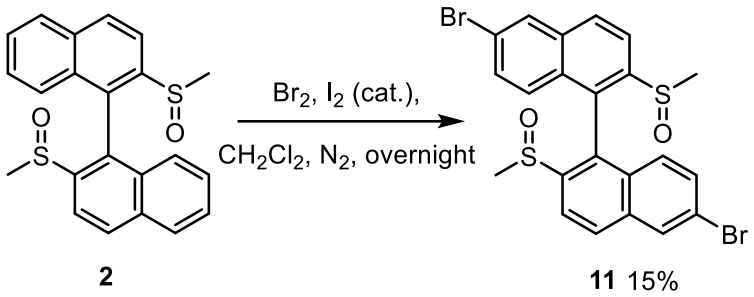

2 **11** 15%

Scheme 1.48. Bromination of sulfoxide **2**.

Bromination of sulfoxide **2** with bromine in CH_2Cl_2 led to a negligible conversion after overnight reaction time. A catalytic amount of iodine was used to push the reaction forward, but **11** was still isolated only in a low yield of 15% (Scheme 1.48). As the bromination works through an electrophilic aromatic substitution mechanism, it should give better results when a substrate is electron-rich. Since a thioether is more electron-rich than a sulfoxide, it should be brominated more efficiently. And so, we decided to move to the green route, which starts with the bromination of thioether **1** (Scheme 1.46).

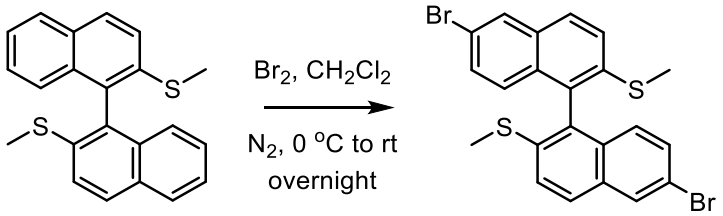

1 **12** 90%

Scheme 1.49. Bromination of thioether **1**.

When thioether **1** was brominated with Br_2 in CH_2Cl_2, **12** was obtained in 90% yield (Scheme 1.49). Having achieved brominated product **12**, we moved further with the green route (Scheme 1.46). Next, mesitylene groups were introduced through a Suzuki coupling, obtaining **13** in 81% yield (Scheme 1.50). Thioether **13** was then oxidised, using previously described conditions with H_2O_2 (1.6.1.2). Compound **14** was obtained quantitatively as a mixture of diastereoisomers and used directly in the next step. However, triflic acid mediated cyclisation allowed isolation of only trace amounts of product **15** (2 mg, 4% yield). The conversion was low, and some decomposition of the product was observed during the isolation. Heating the reaction mixture to 80°C in neat triflic acid did not improve the result. Finally, cyclisation with TfOH in acetonitrile at 80°C was tested, but apart from a low amount of desired product, multiple side products were formed, making isolation of a pure product impossible.

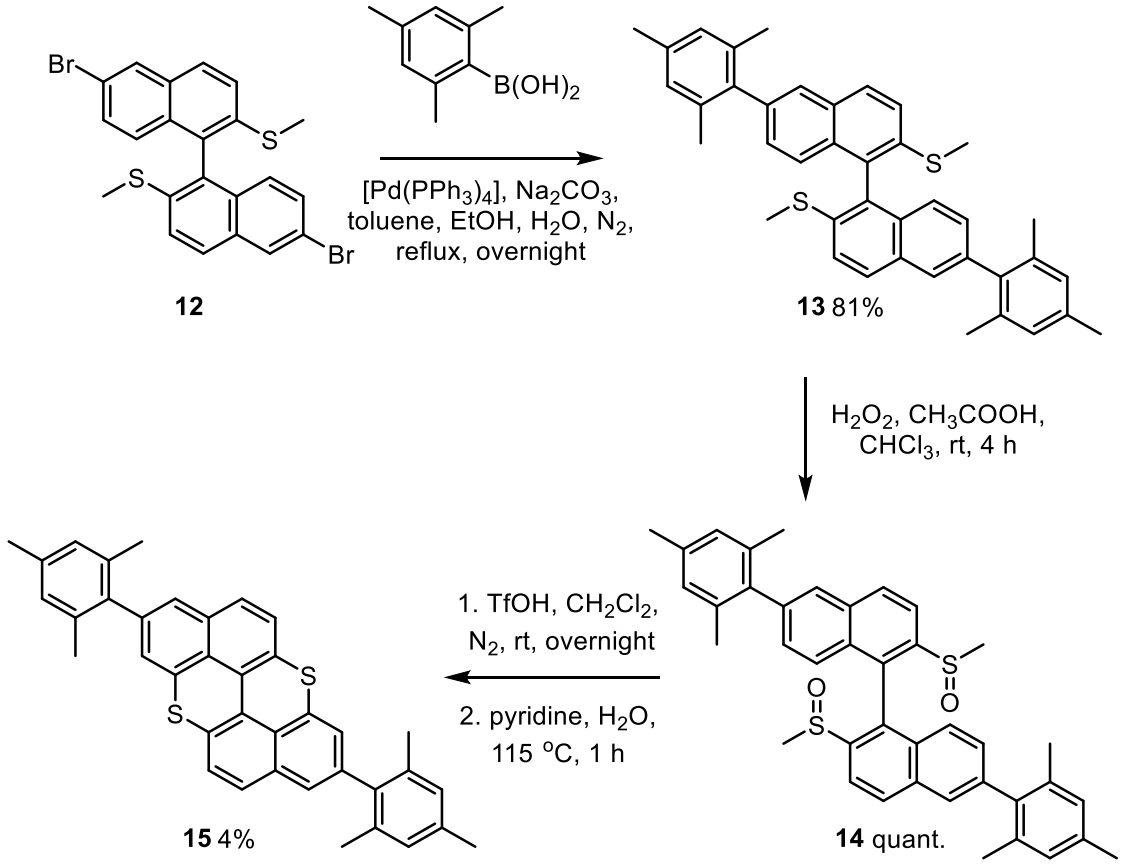

Scheme 1.50. Synthesis of molecule **15**.

Seeing how all the tested routes failed to give a significant amount of mesitylene substituted product, we decided to test another approach. We were interested to see if cyclisation of bromo-substituted sulfoxide, followed by a Suzuki coupling, could lead to a better result. Previously synthesised brominated thioether **12** was oxidised to the sulfoxide using H_2O_2, achieving quantitatively **11** as a mixture of diastereoisomers (Scheme 1.51). The diastereoisomeric mixture was used directly in the triflic acid mediated cyclisation step, leading to the extremely insoluble product. After several attempts at crystallisation, a small sample of crystalline product **16** was obtained from hot *o*-dichlorobenzene, and the expected mass of the compound was achieved through HR mass spectrometry. However, full characterisation was impossible due to the extreme insolubility of the material in most organic solvents. The crystallisation did not allow purification of the sufficient amount of sample for the following reaction, so a crude material was subjected to the Suzuki coupling condition. The reaction gave a mixture of soluble, orange products, but their separation was unsuccessful.

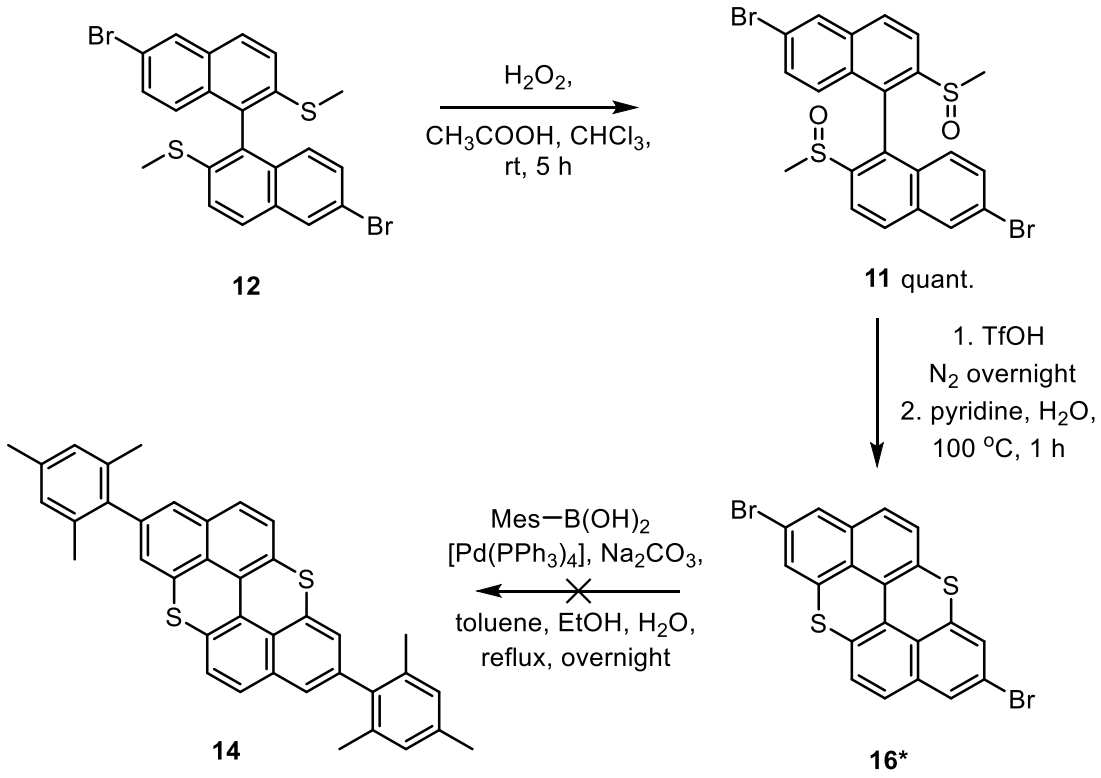

Scheme 1.51. A synthetic attempt at **14**. ***16** insoluble and not fully characterised.

1.7.2.2 An attempt at the introduction of *p*-tertbutylphenyl groups to the PTXTX structure

As the synthesis of mesitylene substituted **PTXTX** allowed only a trace amount of product, we decided to study other moieties as solubilising groups. First, we tested *p*-tertbutylphenyl groups, which could be introduced similarly as mesitylene moieties. *P*-tertbutylphenyl groups were introduced through the Suzuki coupling (Scheme 1.52), leading to product **17** with a high yield (92%). Subsequent oxidation with H_2O_2 led to the sulfoxide **18**, obtained quantitatively as a mixture of diastereoisomers, used directly in the next cyclisation step. Finally, triflic acid mediated cyclisation, followed by demethylation with pyridine/ water mixture, was attempted. However, desired product **19** was not obtained and some starting material was recovered, as well as some dark, insoluble precipitate, possibly the result of intermolecular coupling. Raising the temperature of the cyclisation step to 80 °C did not change the reaction outcome.

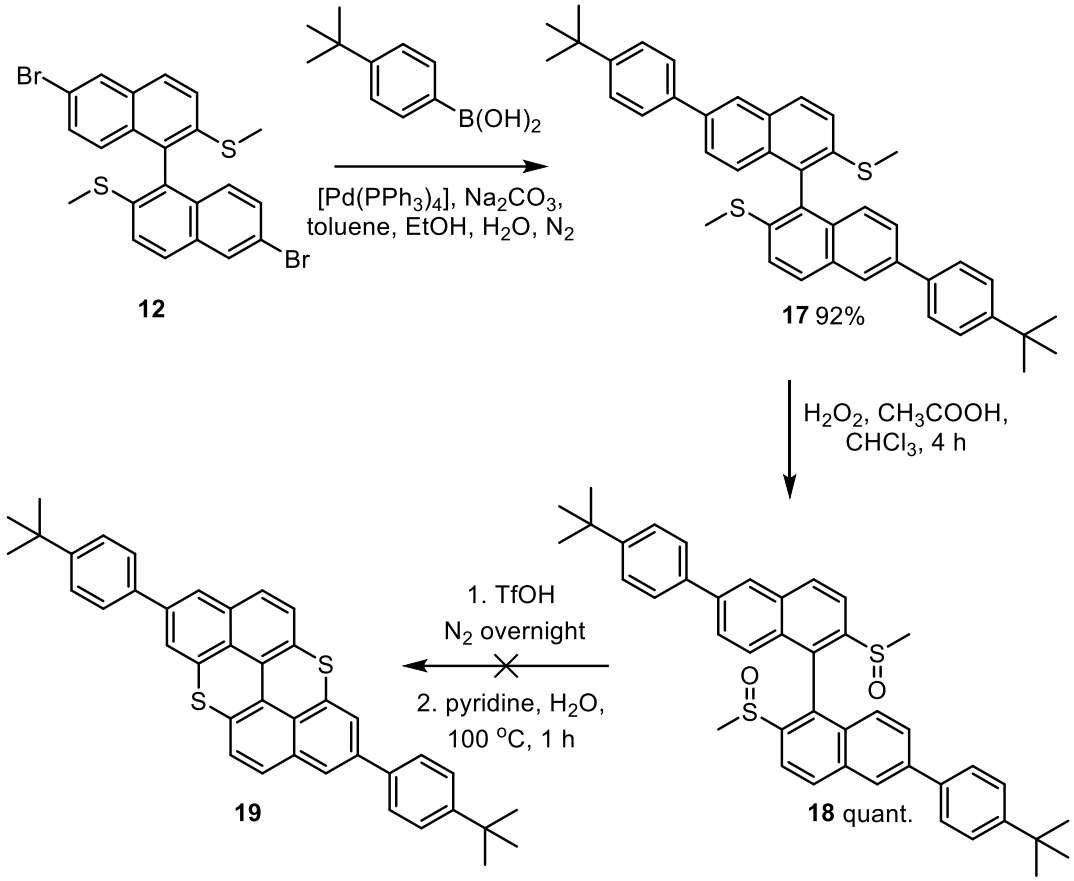

Scheme 1.52. Attempted synthesis of **19**.

1.7.2.3 Introduction of *p*-trifluoromethylphenyl groups to the PTXTX structure

As triflic acid mediated cyclization works through an electrophilic aromatic substitution, the reactivity of the molecule could be increased by electron-rich substituents. Since both tested groups were electron-rich, we were concerned that an intermolecular side reaction was possibly happening instead of intramolecular cyclization. This prompted us to test more electron-poor substituent instead. We decided to study *p*-trifluoromethylphenyl groups, as they could be introduced through a standard Suzuki reaction. Suzuki coupling between compound **12** and *p*-trifluoromethylphenyl boronic acid led to product **20** in 75% yield (Scheme 1.53). Subsequent oxidation with H_2O_2 gave quantitatively a diastereoisomeric mixture of **21**, which was used directly in the next step. However, the triflic acid mediated cyclisation reaction, followed by demethylation with pyridine, produced an insoluble, dark red precipitate. Recrystallisation trials were unsuccessful, so purification of the product was attempted by washing with several organic solvents. The full characterisation was not possible due to the very low solubility of the product in organic solvents, but HR mass spectrometry suggests that the desired product was obtained. As the product was not soluble enough, it was also not suitable for further analysis.

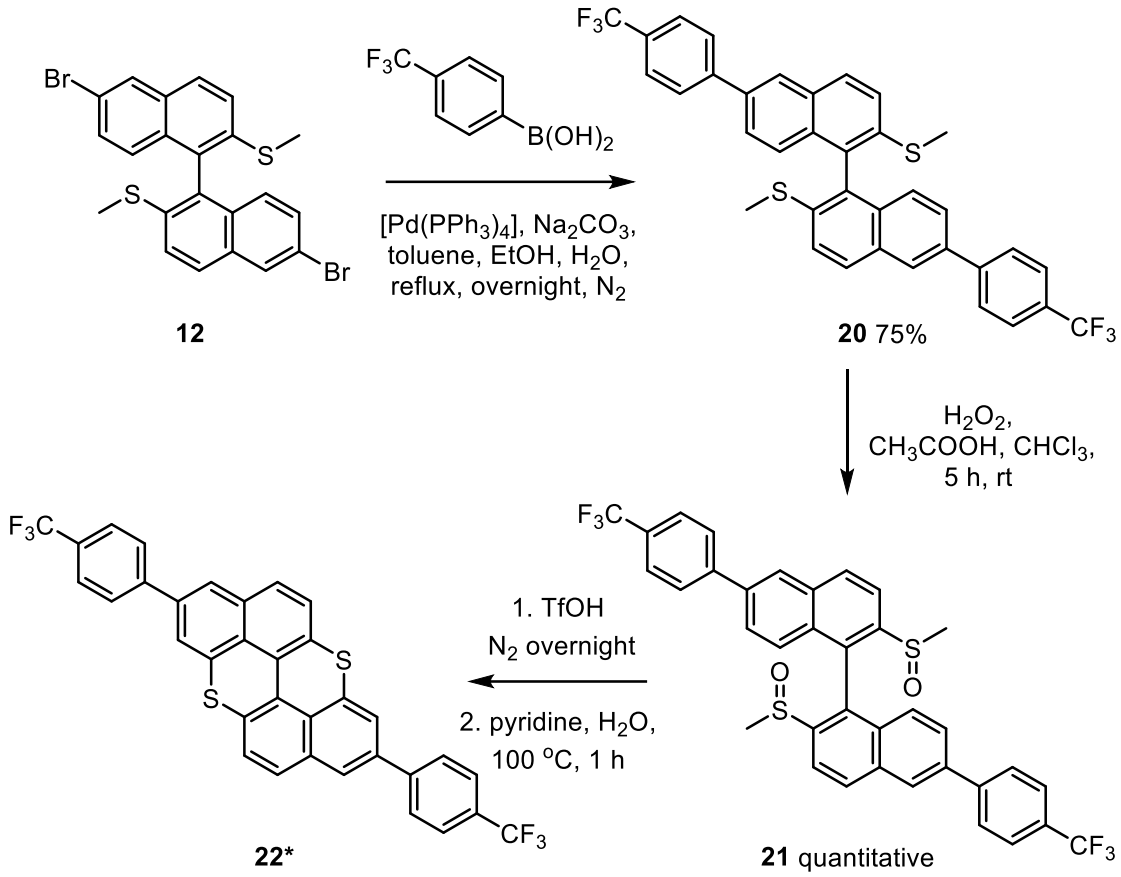

Scheme 1.53. Synthesis of **22**. ***22** insoluble and not fully characterised.

1.7.2.4 Introduction of *n*-octyl groups to the PTXTX structure

Finally, we attempted to use *n*-octyl chains as substituents. They were introduced through the Kumada coupling between compound **12** and *n*-octyl Grignard reagent, giving **23** with 70% yield (Scheme 1.54). After quantitative oxidation with H_2O_2, sulfoxide **24** was obtained as a mixture of diastereoisomers, used directly in the next step. Cyclisation with triflic acid, at room temperature, followed by the demethylation with pyridine led to successful isolation of compound **25**. However, similarly as in the case of **PTXTX**, we encountered reproducibility issues with the cyclisation reaction.

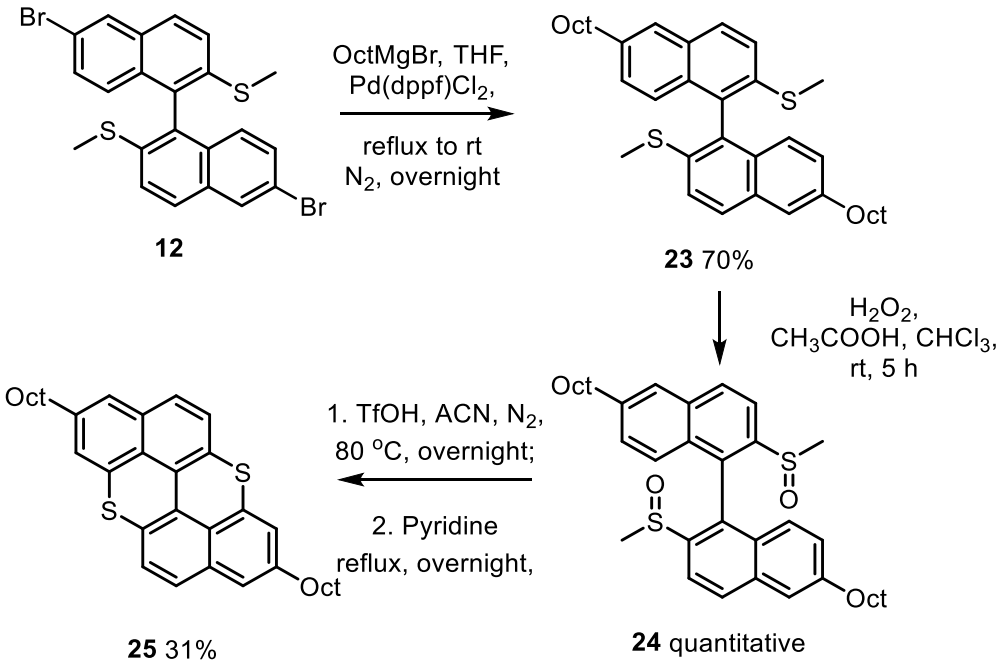

Scheme 1.54. Synthesis of compound **25**.

Again, the reaction worked only with partially hydrated old triflic acid (Table 1.2 entry 1) and did not work with a new batch (entry 2). However, in this case heating to 80°C (entry 3) or to 120°C (entry 4) did not restore reactivity, and only side products were obtained. It is possible that these harsh conditions led to the isomerisation of *n*-octyl chains. Indeed, triflic acid can be used as a catalyst for the cracking of hydrocarbons at elevated temperatures (80-120°C).[185,186] Therefore, it is possible that *n*-octyl chains in molecule **25** underwent partial isomerisation, which led to the formation of a mixture of side products. Dilution of triflic acid with different solvents was studied, to test if milder, diluted conditions would solve the issue (Table 1.2 entries 5-10). High conversion with **25** as the main product was achieved in acetonitrile at 80°C (entry 10). The reaction was repeated on a larger scale, and product **25** isolated in 31% yield.

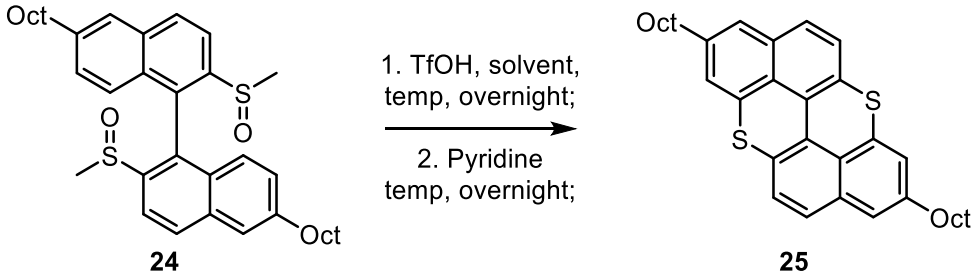

Scheme 1.55. Synthesis of molecule **25**.

Table 1.2. Optimisation of cyclisation reaction to obtain **25**. Screening on 0.04 mmol scale of **24**, in second step 1 ml of pyridine added, temperature of the 2nd step the same as in 1st step unless otherwise stated, [(a)] yield from reaction performed on 0.72 mmol scale of **24**, [(b)] yield from reaction performed on 0.83 mmol scale of **24**.

entry	TfOH	Solvent	Temp	Outcome and yield
1	Old (partially hydrated)	-	rt (2nd step 100 °C)	29% **25** [(a)]
2	new	-	rt (2nd step 100 °C)	Mostly starting material
3	new	-	80 °C	Side products
4	new	-	120 °C	Side products
5	new 0.2 mL	DCE	80 °C	Side products
6	new, 5 eq.	$CHCl_3$	reflux	Mostly starting material
7	new, 0.2 mL	$CHCl_3$	reflux	Mostly starting material
8	new, 0.2 mL	DMF	120 °C	Mostly starting material
9	new, 5 eq.	CH_3CN	80 °C	Mostly starting material
10	new, 1 mL	CH_3CN	80 °C	31% **25** [(b)]

During the purification of molecule **25** problems with a decomposition of the molecule were encountered, similarly as with **PTXTX**. However, just as with **PTXTX**, chromatography on neutral alumina Brockmann activity 1 led to the successful isolation of **25** with 31% yield.

The structure of **25** was confirmed through full characterization and single crystal X-ray structure.

^{1}H NMR spectrum shows 4 peaks in the aromatic part of the spectrum (7.18-6.72 ppm), with similar shifts as for the parent **PTXTX** (7.27-6.78 ppm). Two doublets, 7.18 and 6.74 ppm, are coupled with J = 8.7 Hz, which is an ortho coupling constant, so they can be assigned to protons *c* and *d*. The other two peaks, 6.88 and 6.72 ppm are doublets coupled with J = 1.6 Hz, a meta coupling constant, meaning they correspond to protons *b* and *a*. In the 2.5 – 0.8 ppm part of the spectrum, we can observe multiplets which can be assigned to the 34 protons in the aliphatic chains. Analysing the ^{13}C NMR spectrum (Figure 1.13) we can see 10 peaks in the aromatic part of spectrum, from 141 to 122 ppm, similarly as for the **PTXTX** (134-120 ppm). We can also notice 8 peaks in the aliphatic part of spectrum, between 35 and 14 ppm, which can be assigned to octyl chains. The molecular ion has been observed in HR mass spectrometry.

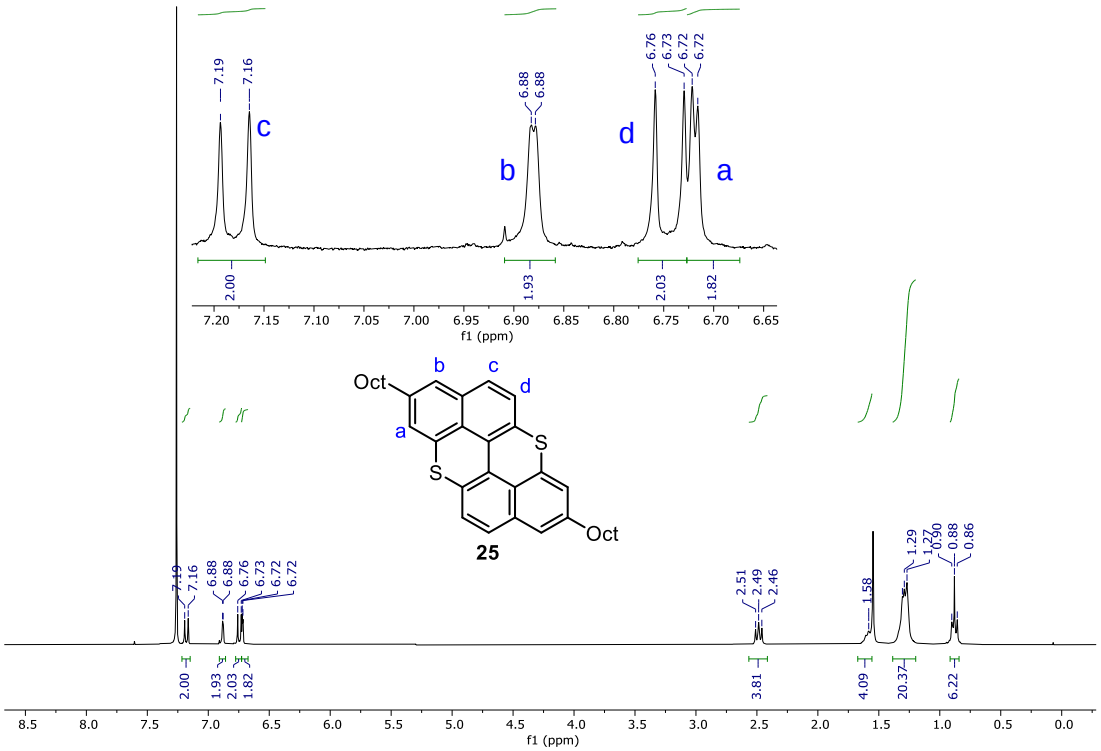

Figure 1.12. ^{1}H NMR spectra of compound **25**, 300 MHz, $CDCl_3$.

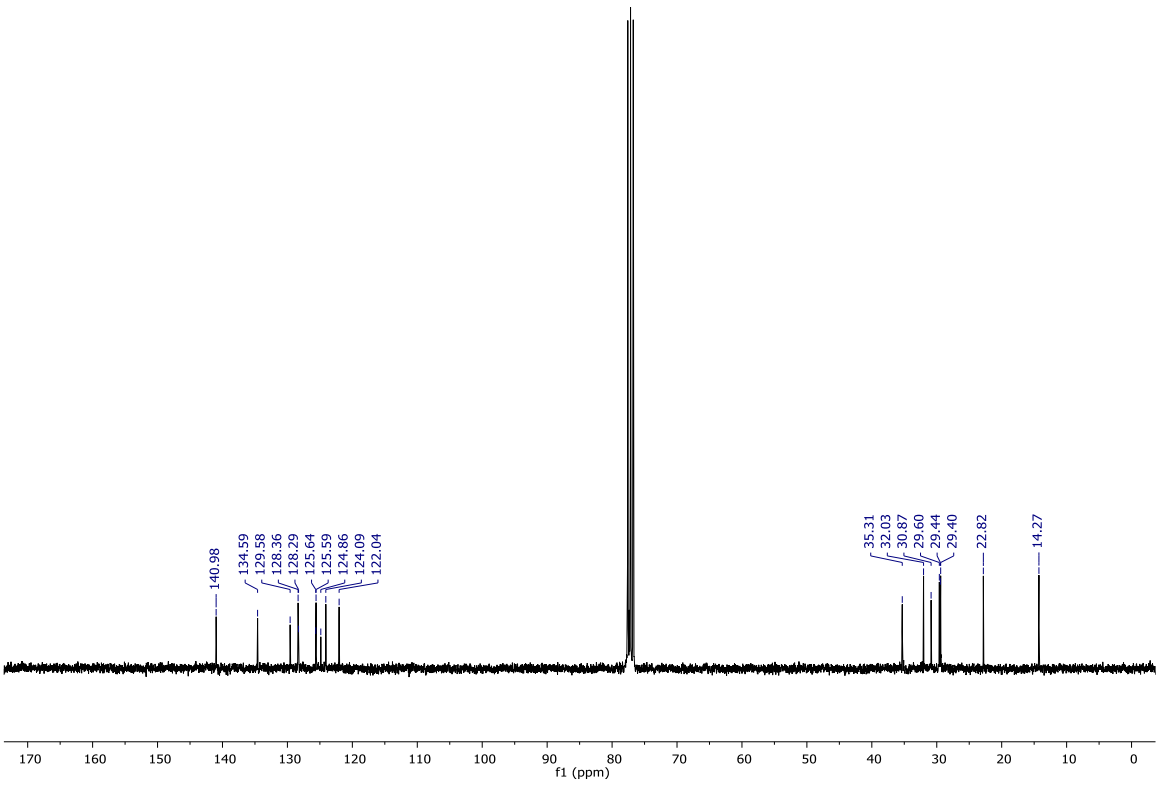

Figure 1.13. ^{13}C NMR spectra of compound **25**, 75 MHz, $CDCl_3$.

1.7.3 Introduction of aldehyde groups into PTXTX structure - retrosynthesis

During our synthetic trials at the substituted **PTXTX**, we observed that cyclisation of molecules bearing EWGs (bromine and *p*-trifluoromethylphenyl groups) were more successful than when EDGs were present. However, they proved to be insoluble in organic solvents, making their full characterisation impossible. We decided to introduce a solubilizing group that would have both a linker and EWG moiety to try to increase the yield of the cyclisation reaction and the solubility of the molecule. As we were interested in potentially using **PTXTX** derivatives in photoredox catalysis, we wanted to improve its solubility in solvents typically used in these reactions, which are most often polar solvents such as CH_3CN.[187,188] We decided to introduce polar groups, and we chose nitriles, as they could be easily introduced through a Knoevenagel condensation with an aldehyde (Scheme 1.56).

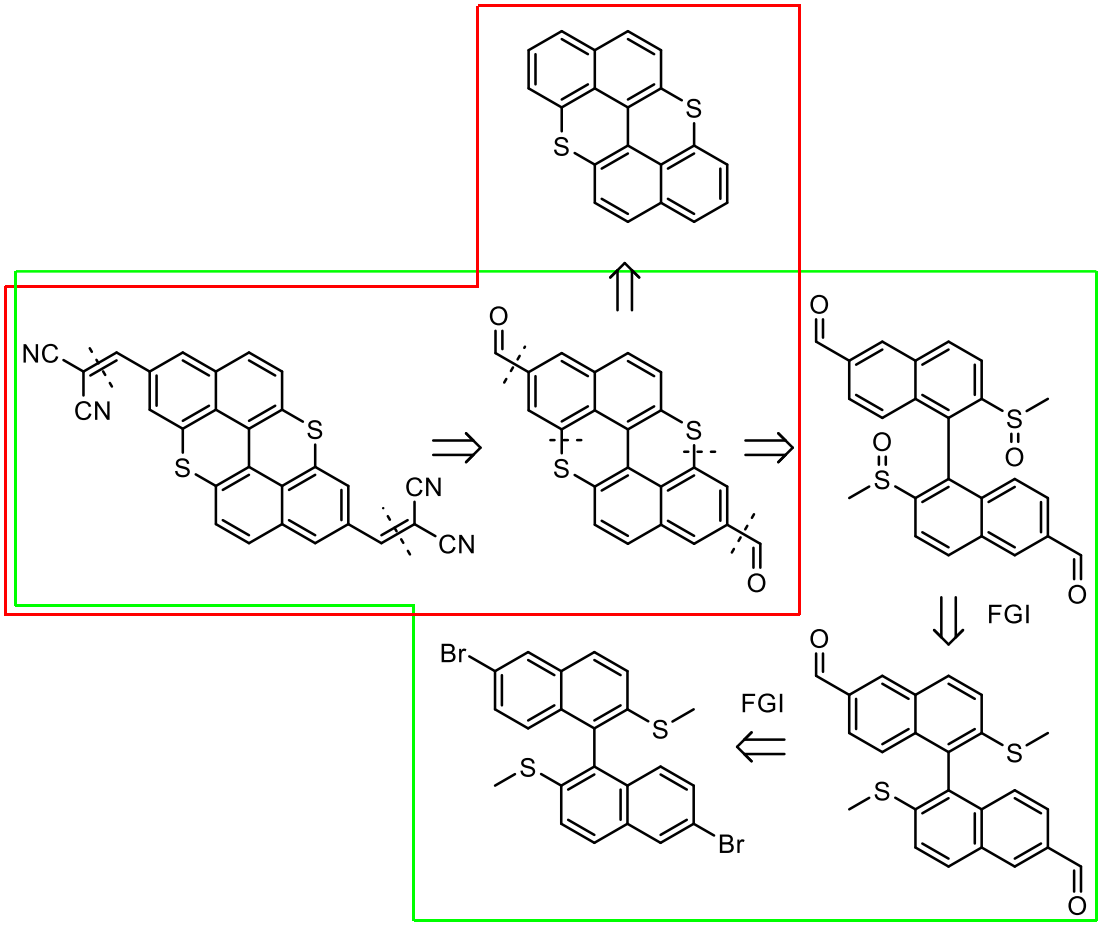

Scheme 1.56. Retrosynthetic pathways to nitrile substituted **PTXTX**.

The aldehyde can be introduced through two retrosynthetic pathways (Scheme 1.56). In pathway red aldehyde moiety could be introduced to **PTXTX** structure through a

direct formylation, either with a Vilsmeier-Haack reagent or with $TiCl_4$ and dichloromethyl methyl ether. In pathway green aldehydic moieties would be introduced to the thioether structure through a metal halogen exchange followed by quenching with DMF. We decided to first attempt the retrosynthetic pathway red as it requires fewer steps.

1.7.4 Introduction of aldehyde groups into PTXTX structure – results

1.7.4.1 Red route, Vilsmeyer-Haack reaction

Direct formylation of **PTXTX** was attempted through a sonicator assisted Vilsmeyer-Haack reaction, reported to require lower temperatures and give higher yields than standard conditions.[189]

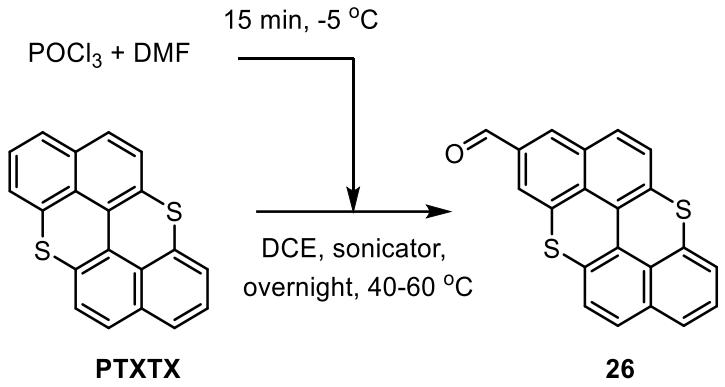

Scheme 1.57. An attempt at formylation of **PTXTX** with Vlismeyer-Haack reagent.

The Vilsmeyer-Haack reagent, generated in the reaction between $POCl_3$ and DMF, was added to **PTXTX**, and the reaction mixture was sonicated overnight, at 40-60 °C. Only partial formation of monoaldehyde (as judged from NMR of the crude) was observed, and full conversion could not be obtained. Isolation of molecule **26** was hindered by the decomposition of the product during the chromatography. This prompted us to move to other formylation reactions, hoping they would give higher conversions and facilitate purification.

1.7.4.2 Red route, formylation with $TiCl_4$ and dichloromethylmethylether

Next, formylation of **PTXTX** with $TiCl_4$ and dichloromethyl methyl ether was attempted (Scheme 1.58).[190] Only partial conversion to the mono formylated product was achieved. However, side products were formed as well and the desired product could not be isolated, as it decomposed during the column chromatography, which prompted us to move to the green route.

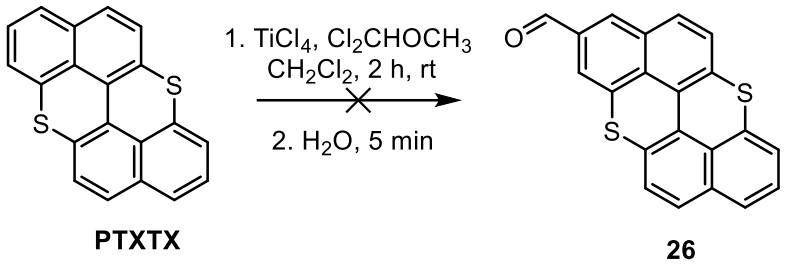

Scheme 1.58. An attempt at formylation of **PTXTX** with $TiCl_4$ and dichloromethyl methyl ether.

1.7.4.3 Green route, metalation and formylation protocol.

The first step of pathway green (Scheme 1.56) required the transformation of bromide **11** into aldehyde **27**, which could be achieved through lithium halogen exchange, followed by quenching with DMF (Scheme 1.59).

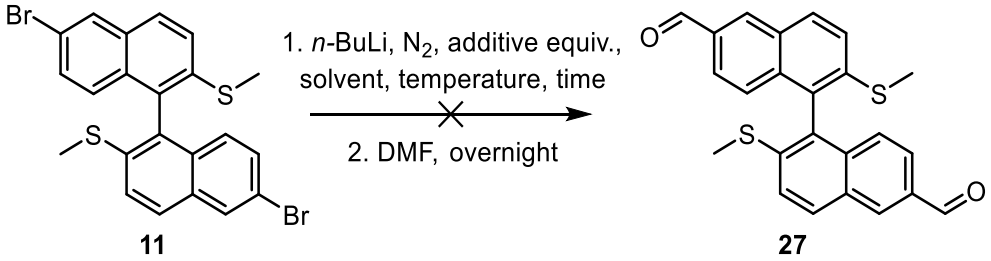

Scheme 1.59. Synthesis of molecule **27**.

Table 1.3. Attempts at dialdehyde synthesis through lithium halogen exchange and quenching with DMF. Formation of aldehydes detected by developing TLCs in 2,4-dinitrophenylhydrazine and/or through NMR.

entry	Additive	Eq.	Solvent	Temperature	Time	Outcome
1	TMEDA	4.2	THF	-96 °C to -20 °C	1h	mixture of aldehydes, traces of desired product observed
2	-	3.8	THF	-78 °C to -20 °C	1h	no aldehydes detected
3	TMEDA	2.1	THF	-96 °C	1h	mixture of aldehydes, desired product not observed
4	TMEDA	2.1	Et_2O	-78 °C to rt	16h	Starting material not soluble, no conversion

The first attempt (Table 1.3 entry 1) was performed with conditions used for lithium halogen exchange that led to thioether **1** (paragraph 1.6.1.2). A small amount of an impure dialdehyde was obtained, along with other aldehydes. The presence of an aldehydic moiety was confirmed by developing TLC in 2,4-dinitrophenylohydrazine, and by observing a peak at 10.1 ppm in ^{1}H NMR. However, the presence of multiple side products did not allow the isolation of a pure sample. Side products could be the result of an ortho-lithiation reaction or a metalation of the methyl group of a

thioether.[191,192] We decided to test the reaction without TMEDA (entry 2), but no aldehyde formation was detected. To avoid the formation of side products, the excess of *n*-BuLi was diminished to 2.1 equivalents (entry 3). However, only undesired aldehydic products were obtained, while compound **27** was not detected in the reaction mixture. Literature suggests that using Et_2O as a solvent favours lithium-halogen exchange over deprotonation, which is facilitated in THF.[192] Unfortunately, the starting material **11** was not soluble in Et_2O at the desired range of temperatures and no conversion was observed (entry 4). These difficulties in obtaining desired compound **27** prompted us to abandon the synthesis of nitrile substituted **PTXTX**.

1.8 Synthesis of PTXTX oxidised derivatives

The presence of sulfur atoms in **PTXTX** structure offers an opportunity to obtain a scope of oxidised molecules, that could display a range of different optoelectronic properties, potentially interesting for photocatalysis and electronics. We decided to attempt the synthesis of mono, di, tri and tetra oxidised **PTXTX** derivatives for both parent and the *n*-octyl substituted molecules. We chose H_2O_2/CH_3COOH as an oxidant since it afforded the best result for the oxidation of thioether **1**.

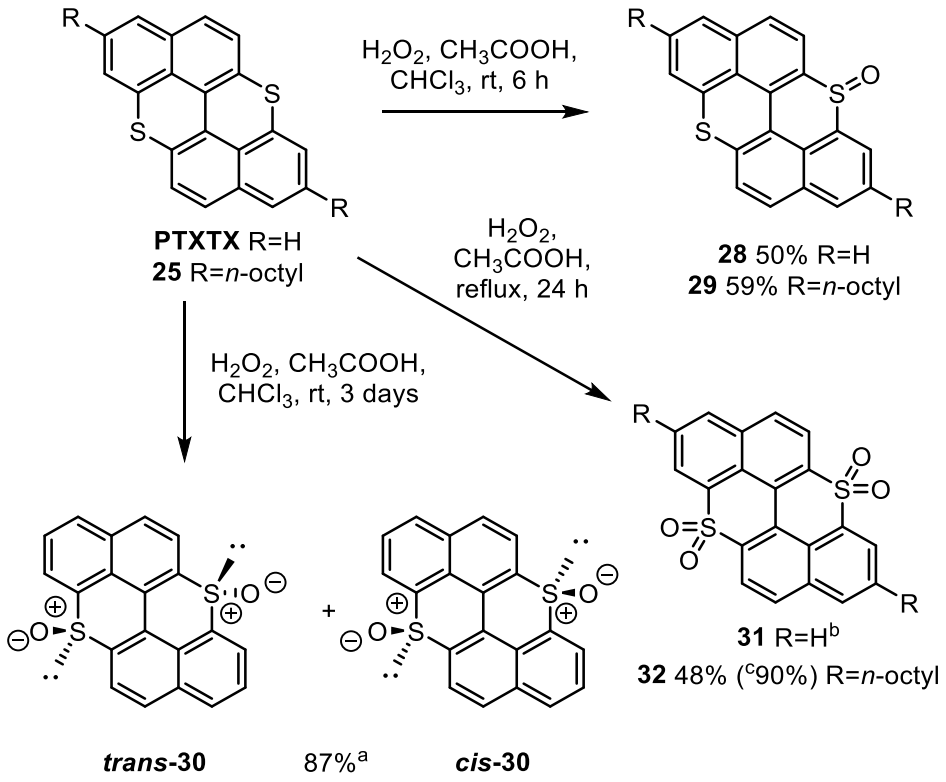

Scheme 1.60. Oxidation of **PTXTX** and **25** to a mono, and disulfoxide and sulfones. [a] yield of diastereoisomeric mixture, [b] insoluble product obtained impure, full characterisation not possible, [c] yield obtained using *m*CPBA, $CHCl_3$, reflux, 24h

Monooxidation was achieved with 6 equivalents of H_2O_2, after 6 h, giving compounds **28** (unsubstituted) and **29** (with octyl chains) with 50% and 59% yield, respectively. Having synthesised monosulfoxides we confirmed that the decomposition of **PTXTX** and compound **25** we observed on the silica (paragraph 1.6.1) was due to the oxidation. Indeed, both monosulfoxides have the same retention factors (rf) as the respective decomposition products observed when **PTXTX** and **25** come in contact with silica gel.

The synthesis of disulfoxide **30** required an extension of the reaction time to three days to achieve full conversion. Disulfoxide was achieved in 87% yield as a mixture of diastereoisomers, since sulfoxide is a centre of chirality. Separation of the diastereoisomers was found to be possible using a recycling HPLC. However, the products were found to decompose during the isolation process. Only a ***trans*-30** isomer was achieved pure and could be used in further characterisation. Due to the low stability of the disulfoxide **30** and difficulties with its isolation, the synthesis of octyl substituted molecule was not attempted. During isolation of **30**, traces of highly unstable sulfoxide-sulfone were isolated with structure confirmed through X-Ray crystallography. However, low stability made full characterisation impossible.

Finally, the synthesis of sulfones was performed. Oxidation of **PTXTX** was performed with H_2O_2/CH_3COOH, and full conversion was achieved after 24 h. However, product **31** was found to be highly insoluble in organic solvents, making its purification and characterisation unachievable. The structure was confirmed through analysis of single crystals suitable for X-ray diffraction. To solve the solubility issue, oxidation of octyl substituted **25** was performed using the same reaction conditions that gave compound **31**. Product **32** was achieved in 48% yield and was found to have better solubility in organic solvents. The reaction yield was increased to 90% when oxidation with *m*CPBA in refluxing $CHCl_3$ was used instead.

Analysis of ^{1}H NMR spectrum of compound **32** (Figure 1.14) shows the presence of 8 aromatic and 34 aliphatic protons (Figure 1.14). 8.45 ppm and 8.27 ppm doublets are coupled with ortho coupling constant J = 8.7 Hz and they correspond to protons *d* and *c*. 8.50 ppm and 8.11 ppm doublets are coupled with para coupling constant J = 1.8 Hz, and they can be assigned to protons *a* and *b*. These coupling constants correspond to values obtained for a not oxidised compound **25** (8.7 Hz and 1.6 Hz, respectively). However, a large shift is evident, from 7.19 – 6.72 ppm in compound **25** (Figure 1.12) to 8.50 – 8.11 ppm in sulfone **32**. Such a shift can be expected, as the introduction of electron withdrawing sulfone moieties leads to the deshielding of the neighbouring

protons. ^{13}C NMR spectrum of compound **32** shows the presence of 10 aromatic and 8 aliphatic protons (Figure 1.15), with shifts similar to those in compound **25** (Figure 1.13).

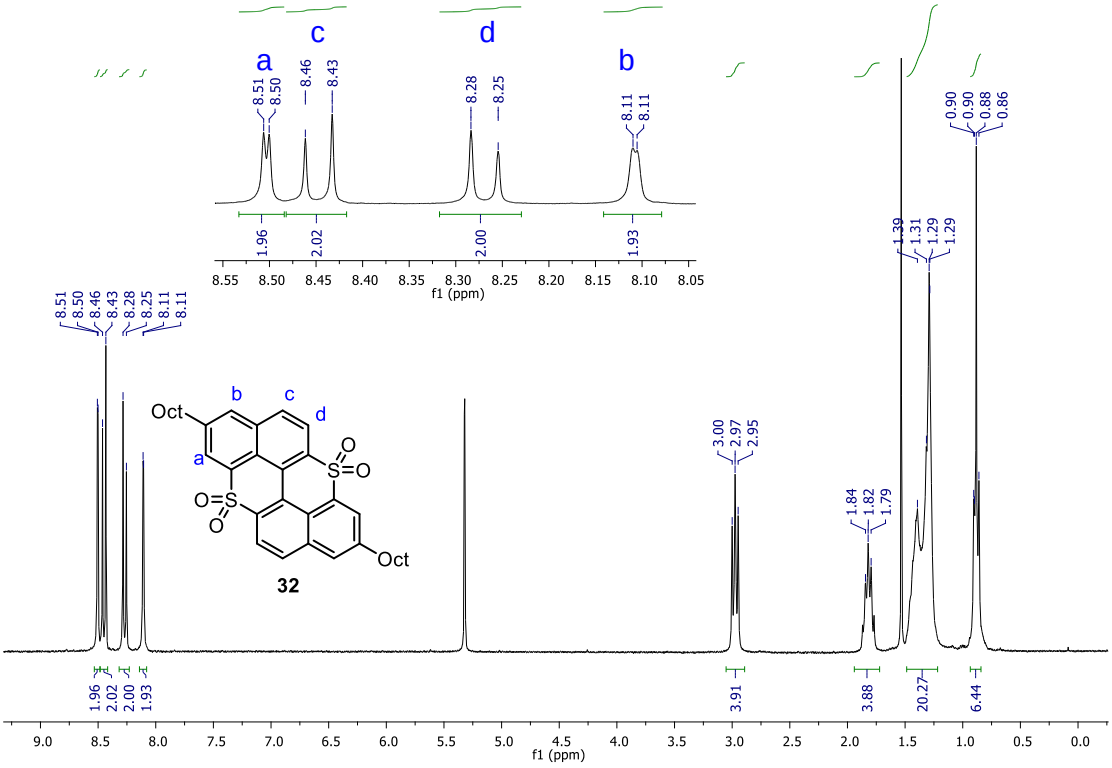

Figure 1.14. ^{1}H NMR spectra of compound **32**, 300 MHz, CD_2Cl_2.

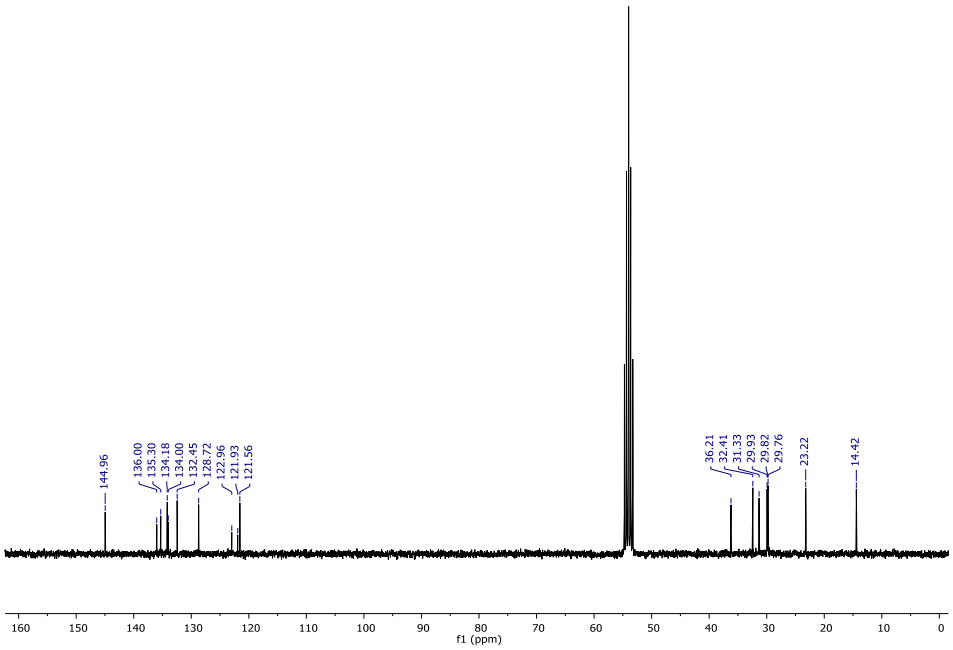

Figure 1.15. ^{13}C NMR spectra of compound **32**, 75 MHz, CD_2Cl_2.

Crystals suitable for X-Ray diffraction were grown for all the products, and the results will be discussed in section 1.12. Photophysical and electrochemical characterisation of isolated molecules will be discussed in sections 1.13 and 1.14, respectively.

1.9 Synthesis of Se doped anthrantrene (36) using TfOH mediated electrophilic aromatic substitution

Inspired by the successful synthesis of **PTXTX** and its oxidised derivatives we decided to test if Se doped derivative could be achieved in a similar manner. Although few intramolecular S_EAr reactions were reported in the literature to form C-Se bonds, existing examples prompted us to test TfOH mediated cyclisation, followed by demethylation with pyridine, in the synthesis of *peri*-selenoxanthenoselenoxanthene **36** and dibenzoselenophene **40**. Molecule **36** is an interesting material for optoelectronic applications, with its derivatives containing arylamine substituents recently applied in OLED devices. They have been reported in a patent, which did not disclose the route towards molecule **36** itself.[193]

1.9.1 Retrosynthetic route towards *peri*-selenoxanthenoselenoxanthene 36

We devised two retrosynthetic routes, red and green, to obtain compound **36** (Scheme 1.61). The red route includes diselenide based synthesis, which is often used to obtain dibenzoselenophenes (paragraph **Error! Reference source not found.**). The d iselenide **33** could be obtained from 2,2'-dibromo-1,1'-binaphthalene in the lithium – halogen exchange followed by the reaction with elemental Se.[122] The green route uses the same steps that allowed the synthesis of sulfur-doped **PTXTX** in paragraph 1.2.1.2, utilising electrophilic aromatic substitution in the cyclisation step. This route requires the synthesis of selenoxide **35**, which could be obtained through the oxidation of compound **34**. Selenoether **34** could be achieved from 2,2'-dibromo-1,1'-binaphthalene in the lithium – halogen exchange, followed by the reaction with dimethydiselenide.

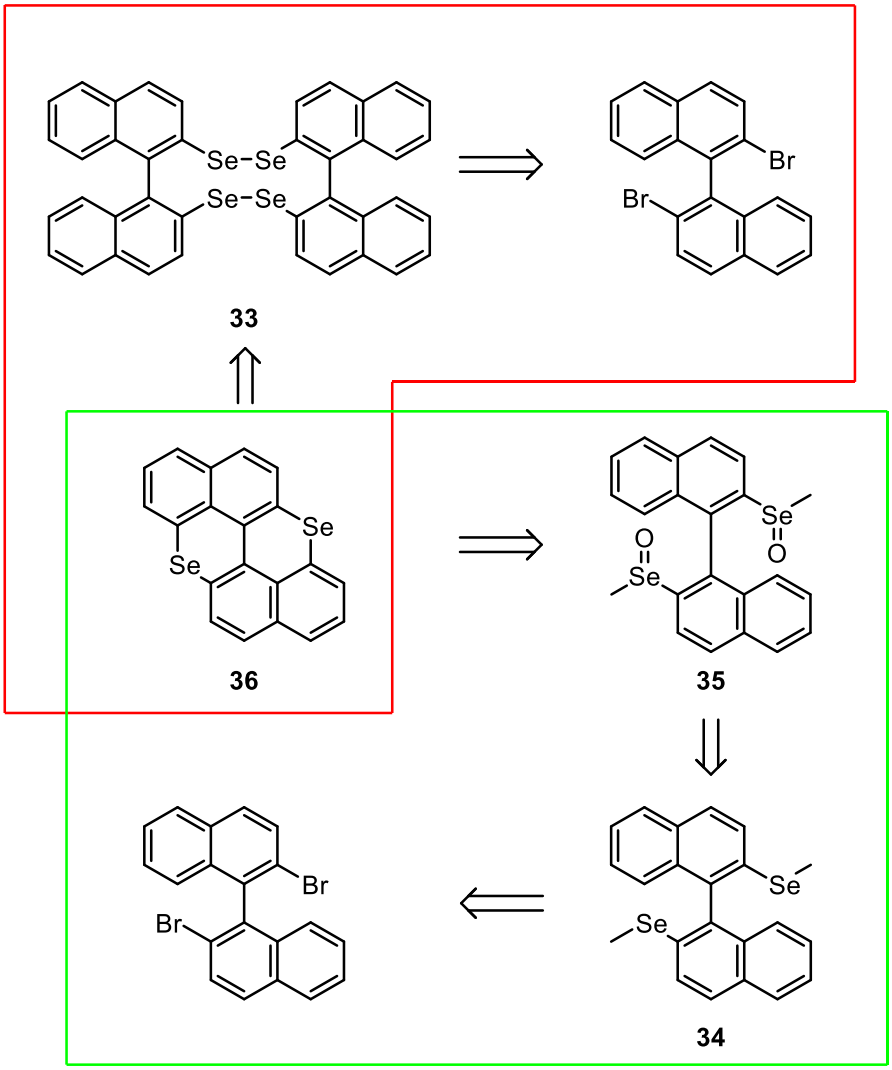

Scheme 1.61. Two retrosynthetic routes, red and green, towards molecule **36**.

1.9.2 Synthesis of *peri*-selenoxanthenoselenoxanthene 36

1.9.2.1 Red route - a metalation/selenylation method

First, we decided to test the red retrosynthetic route, as it requires fewer steps than the green route. The synthesis of diselenides can be performed through lithium halogen exchange, followed by the reaction with elemental selenium and oxidation (Scheme 1.62). Molecule **33** has been previously reported as one of the products of the reaction between 2,2'-dibromo-1,1'-binaphthalene and *t*-BuLi, followed by elemental Se addition and quenching with NH_4Cl and benzene under air.[122] However, in our hands these conditions led to the complex and inseparable mixture of products (Table 1.4, entry 1). Next, $K_3Fe(CN)_6$ was tested as an oxidant (entry 2), but led to the same result. Finally, TMEDA was added in the first step to facilitate the lithium–halogen exchange, while NH_4Cl was used in the oxidation step (entry 3). Unfortunately, an inseparable mixture of products was achieved again.

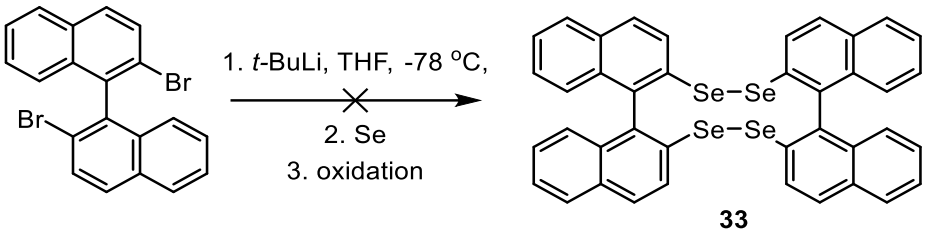

33

Scheme 1.62. Synthetic attempts at molecule **33**.

Table 1.4. Conditions tested for the synthesis of diselenide **33**.

entry	additive in step 1	Step 3	Outcome
1	-	Air, NH_4Cl, benzene	Inseparable mixture of products
2	-	$K_3Fe(CN)_6$	Inseparable mixture of products
3	TMEDA	Air, NH_4Cl	Inseparable mixture of products

Not being able to obtain diselenide **33**, we decided to abandon the red route and pursue the green route.

1.9.2.2 Green route - electrophilic aromatic substitution

The synthesis of compound **36** using the green route is described in Scheme 1.63. First, lithium - halogen exchange of 2,2'-dibromo-1,1'-binaphthalene with *n*-BuLi and TMEDA, followed by addition of Me_2Se_2, led to selenoether **34** in 65% yield. Oxidation of **34** was performed with H_2O_2 in $CH_3COOH/CHCl_3$ mixture, leading quantitatively to selenoxide **35**. Compound **35** was achieved as a mixture of diastereoisomers, since selenoxides are chirality centres and the presence of binaphthalene introduces axial chirality. Diastereoisomeric mixture was directly used in the cyclisation attempt. The cyclisation was conducted using neat triflic acid at 80 °C, followed by the demethylation with pyridine at 100 °C leading to the molecule **36** in 44%. The isolation was achieved by the recrystallisation from a hot mixture of hexane and toluene.

Synthesis and characterisation of S- and Se- doped anthanthrenes and their derivatives

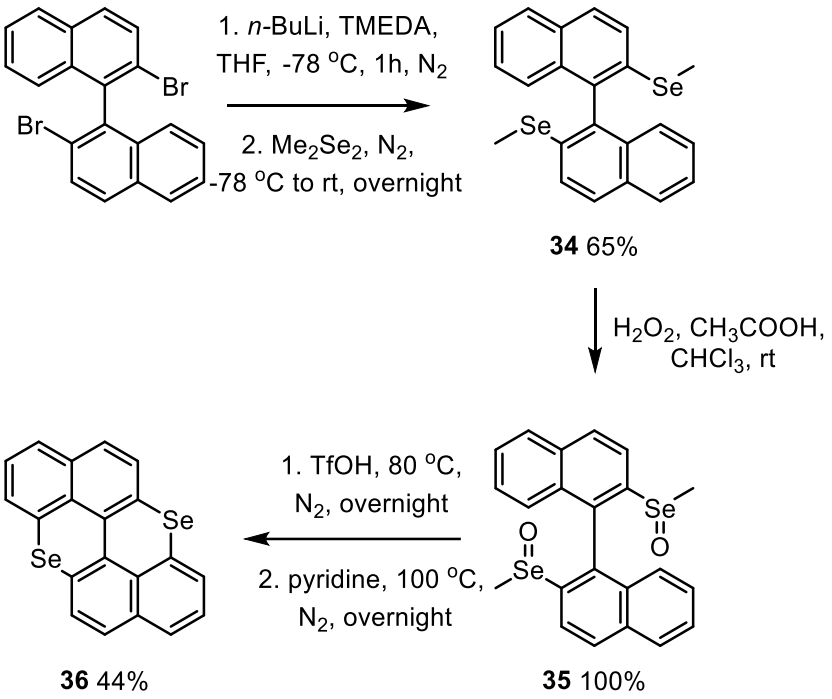

Scheme 1.63. Synthesis of **36** through a TfOH mediated electrophilic aromatic substitution.

^{1}H NMR spectra of compound **36** shows 5 peaks in the typical aromatic part of the spectrum, showing similar coupling patterns as in S doped derivative **PTXTX** (Figure 1.16).

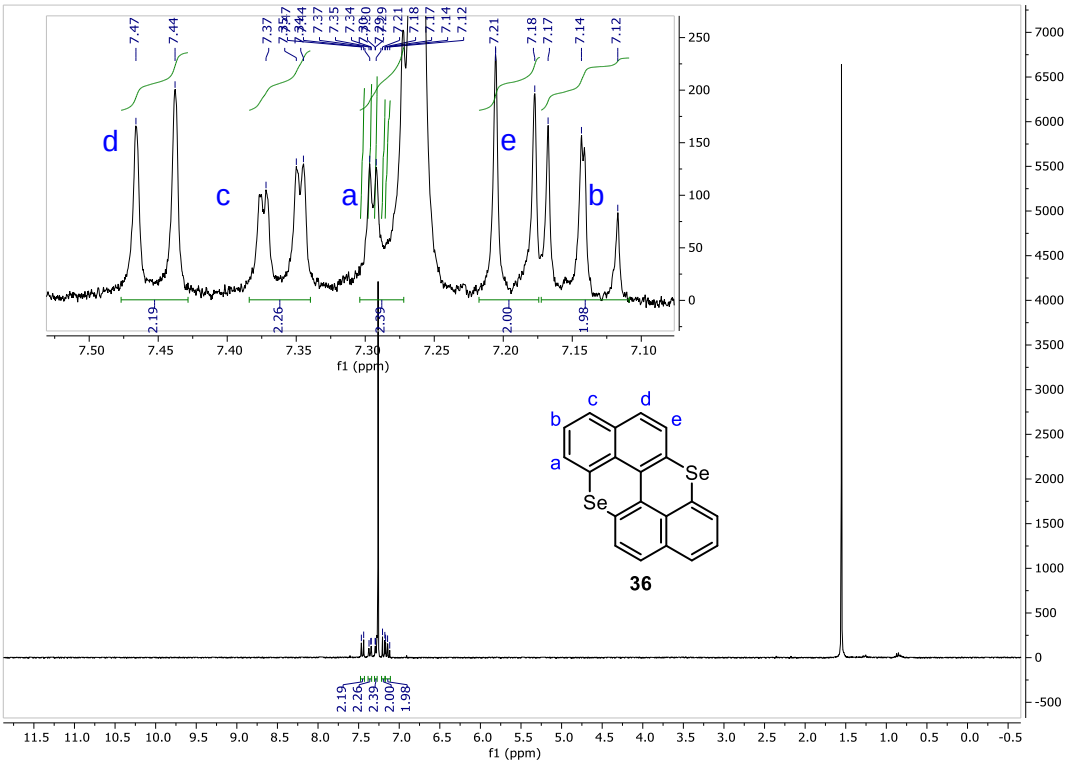

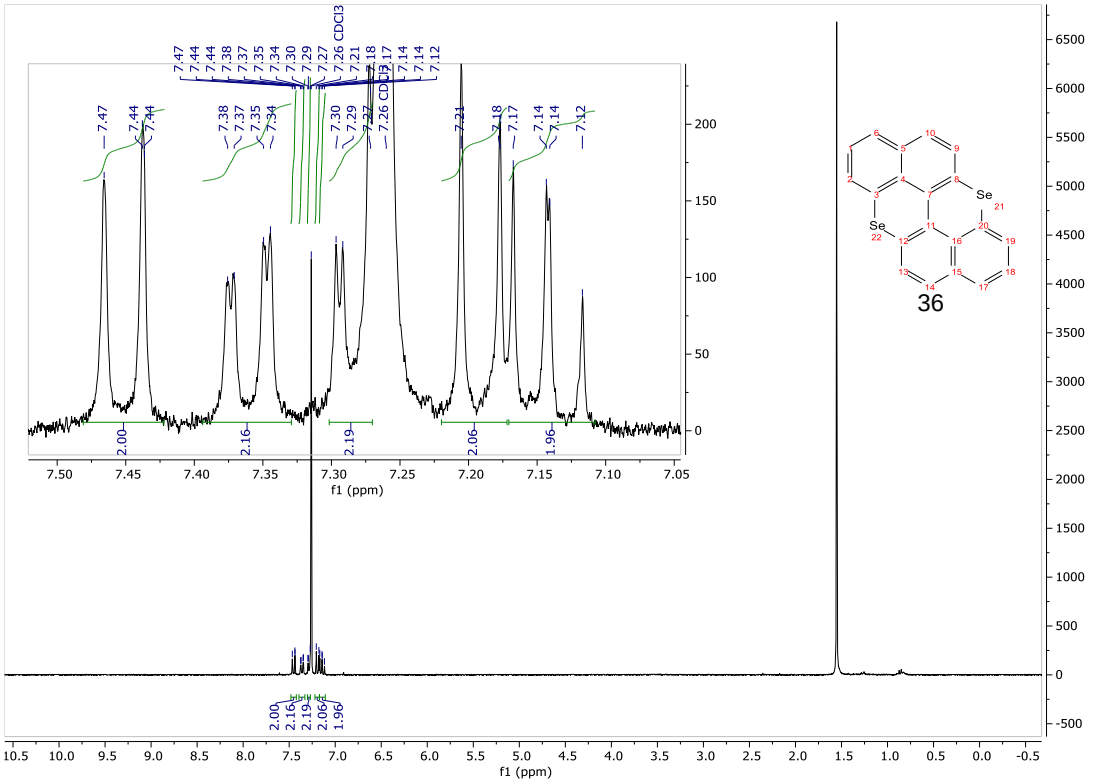

Figure 1.16. ^{1}H NMR of compound **36**, 300 MHz, $CDCl_3$.

Doublets at 7.46 ppm and 7.19 ppm are coupled with J = 8.5 Hz, which is an ortho coupling constant. These peaks can be assigned as protons *d* and *e*. Doublet of doublets at 7.14 ppm shows two typical ortho coupling constants with J = 7.9 Hz and 7.3 Hz, corresponding to protons *b*. Doublets of doublets which are coupled with 7.14 ppm peak, 7.36 ppm and 7.28 ppm are coupled together with meta coupling constant J = 1.3 Hz, and can be assigned as protons *c* and *a*. Chemical shifts of Se doped **36** (7.46 – 7.14 ppm) are moved downfield in comparison to S doped **PTXTX** (7.28 – 6.77 ppm). Deshielding is known to occur when moving down the chalcogen group, and is ascribed to the heavy atom effect, originating in spin-orbit coupling at the heavy atom.[194] The structure of the compound was also confirmed through HR mass spectrometry.

We were interested in achieving oxidised derivatives of compound **36**, like in the case of **PTXTX** derivatives (paragraph 1.6), to study the influence of oxidation on the photophysical properties. Attempts at the oxidation of compound **36** with H_2O_2, to achieve selenoxide **37**, suffered from stability issues (Scheme 1.64). Although oxidation seemed successful on TLC, decomposition occurred during isolation, possibly due to photodegradation. More studies are necessary to achieve compound **37** and other oxidised derivatives. Shielding from light and oxygen could potentially help avoid decomposition.

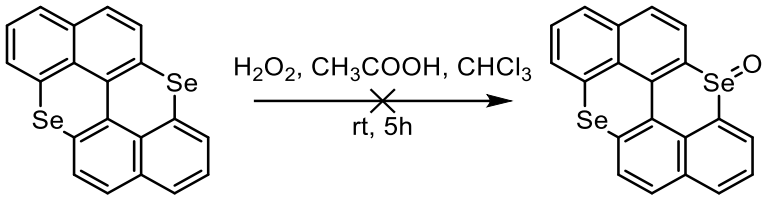

36 **37**

Scheme 1.64. Attempt at the oxidation of molecule **36**.

Due to the fact that low amount of compound **36** was possible to synthesise and decomposition was observed after storing the sample it was not tested in mixed valence crystals or electrochemical devices,

1.10 Synthesis of dibenzoselenophene using TfOH mediated electrophilic aromatic substitution

Seeing how triflic acid-mediated cyclisation was successful in the synthesis of molecule **36**, we decided to test if it can also give 5-membered rings through the synthesis of dibenzoselenophene. Even though dibenzothiophenes have been achieved through a triflic acid mediated S_EAr cyclisation of sulfoxides (paragraph 1.1.1.2), a similar reaction has not been reported for the dibenzoselenophene synthesis.

First, 2-bromo-1,1'-biphenyl was converted into a lithiated intermediate using *n*-BuLi with TMEDA, which after quenching with dimethyl diselenide gave compound **38** in 84% yield (Scheme 1.65). Oxidation with H_2O_2 gave selenoxide **39** quantitatively. Finally, TfOH mediated cyclisation at 80 °C, followed by demethylation with pyridine led to dibenzoselenophene **40**, isolated in 90% yield.

Synthesis and characterisation of S- and Se- doped anthanthrenes and their derivatives

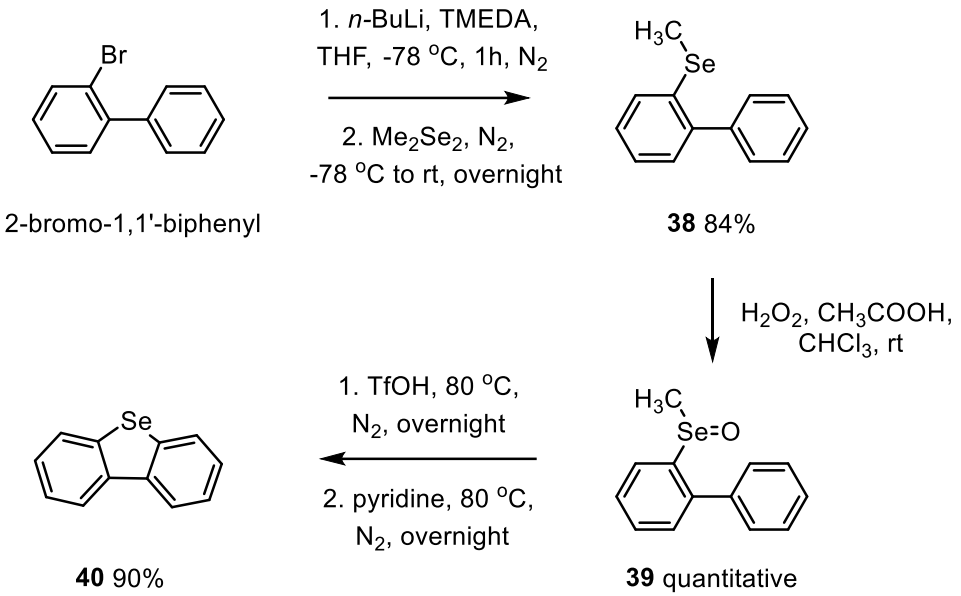

Scheme 1.65. Synthesis of dibenzoselenophene **39** using TfOH mediated electrophilic aromatic substitution.

Although ladder-type thienoacenes have been synthesised using triflic acid mediated cyclisation of sulfoxides,[58,195] similar reaction has, to the best of our knowledge, not been reported for selenoxide derivatives. Triflic acid mediated cyclisation of selenoxides, followed by demethylation, could potentially be used to prepare Se - doped ladder-type oligomers, which are interesting for optoelectronic applications.[196]

1.11 Literature reports for S and Se-doped anthanthrenes

During the time this work was prepared a patent and a publication featuring S and Se doped anthanthrenes were published and the results will be shortly described here. Reports of **PTXTX** and Se doped Se-doped anthanthrene derivatives compounds have been synthesised and applied in OLEDs.[197] **PTXTX** based material have been also synthetised as semiconducting material for TFTs.[167]

The following patent application describes OLED materials with S (**B38**) and Se (**B39**) doped xanthene derivatives, possessing carbazole groups, used as hole transporting layers (Figure 1.17).[197] The current efficiency of such achieved devices (13.8 cd/A and 14.0 cd/A for **B38** and **B39** respectively) was higher than for device with reference material **NBP** used as hole transporting layer (13 cd/A). The operating voltage was also improved, from 5.2 V for reference material **NPB** to 4.3 and 4.2 V for S and Se derivatives respectively.

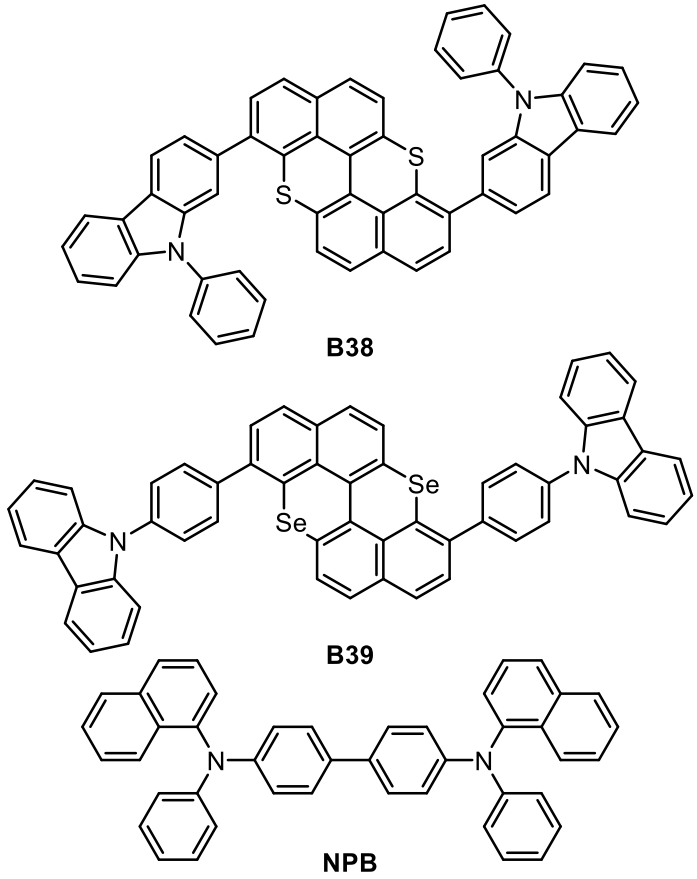

Figure 1.17. Structure of xanthene based hole transporting materials and of reference material.[197]

PTXTX based molecules were used as hole transporters for perovskite solar cells and compared to previously achieved O doped derivatives.[168] **PTXTX** molecules were achieved as described in this chapter (Scheme 1.37) so the synthesis will not be reported again. Next, the molecules were brominated with NBS at -78 °C and coupled with bis(4-methoxyphenyl)amine in a Buchwald-Hartwig cross-coupling to achieve difunctionalized **PTXTX-OMe-DPA** derivative in 83% yield.

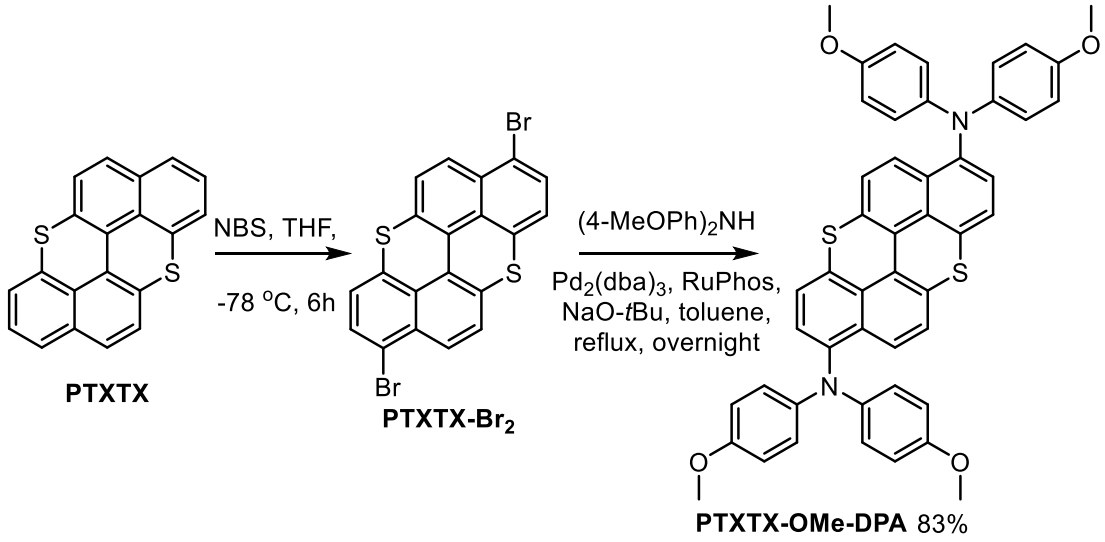

Figure 1.18. Part of the synthesis of **PTXTX-OMe-DPA**. Synthesis of **PTXTX** achieved as in Scheme 1.37.[168]

The hole mobility of single crystals of **PTXTX-OMe-DPA** was calculated as $3.9 \cdot 10^{-2}$ cm^2 V^{-1} s^{-1}, lower than for an O-doped derivative **spiro-OMeTAD** ($6.3 \cdot 10^{-2}$ cm^2 V^{-1} s^{-1}). However, in spin-coated thin films there is a different arrangement of molecules than in crystals. **PTXTX-OMeDPA** and **spiro-OMeTAD** thin films were spin-coated on PEDOT:PSS substrate, and thin films of S-doped material were found to have a larger averaged domain of molecule aggregates, which is desirable for good charge transport. This resulted in the average hole mobility for **PTXTX-OMeDPA** thin films being over five times higher than that of **spiro-OMeTAD** ($9.5 \cdot 10^{-4}$ cm^2 V^{-1} s^{-1} vs $1.8 \cdot 10^{-4}$ cm^2 V^{-1} s^{-1}, respectively). The hole transport is much slower in thin-films than in single crystals, as there is a large disorder in almost amorphous films. Next, perovskite solar cells with **PTXTX-OMeDPA** as a hole transporter were constructed, with a structure of glass|FTO|TiO2|FA-based perovskite|hole-transporter|Au. These solar cells exhibited a power conversion efficiency (PCE) of 22.2%, which is higher than for **spiro-OMeTAD** based device (20.8%). Finally, the **PTXTX-OMeDPA** based device achieved better stability, during dark storage at 60 °C and while operating under light-soaking at 60 °C, than the O-doped based device.[168]

1.12 Crystal structures

1.12.1 Crystal structures of PTXTX

PTXTX has been crystalised by the slow diffusion of EtOH into **PTXTX** solution in CH_2Cl_2, yielding two types of polymorphic crystals, yellow plates and red needles. Both crystal structures belong to P 2_1/c space group. In both polymorphic structures, **PTXTX**

has almost identical lengths of bonds and angles, so in the text only values for yellow plate polymorph will be reported (Figure 1.19).

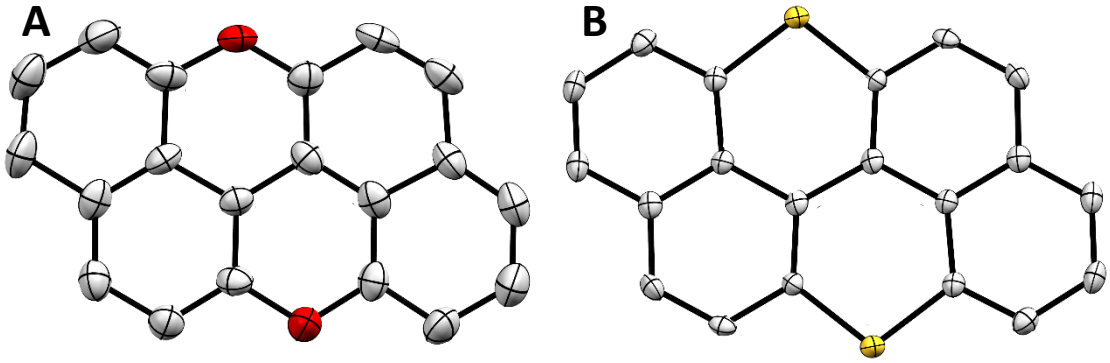

Figure 1.19. A PXX ORTEP representation (50% probability ellipsoids) crystallisation method vacuum sublimation;[157] **B PTXTX** ORTEP representation (50% probability ellipsoids), yellow plate polymorph, crystals grown by slow diffusion of EtOH into the solution of **PTXTX** in CH_2Cl_2.

Ring containing sulfur atom is slightly larger than other rings, with S atoms sticking 3.3° out of both sides of the molecule's plane. While in **PXX** C-O-C angle is 122°,[157] in **PTXTX** the corresponding C-S-C angle decreases to 104°. At the same time, while in **PXX** length of C-O bond is 1.39 Å, in **PTXTX** C-S bond length is extended to 1.741(3) Å (and 1.742(3) Å). Both differences can be attributed to the large size of the sulfur atom.

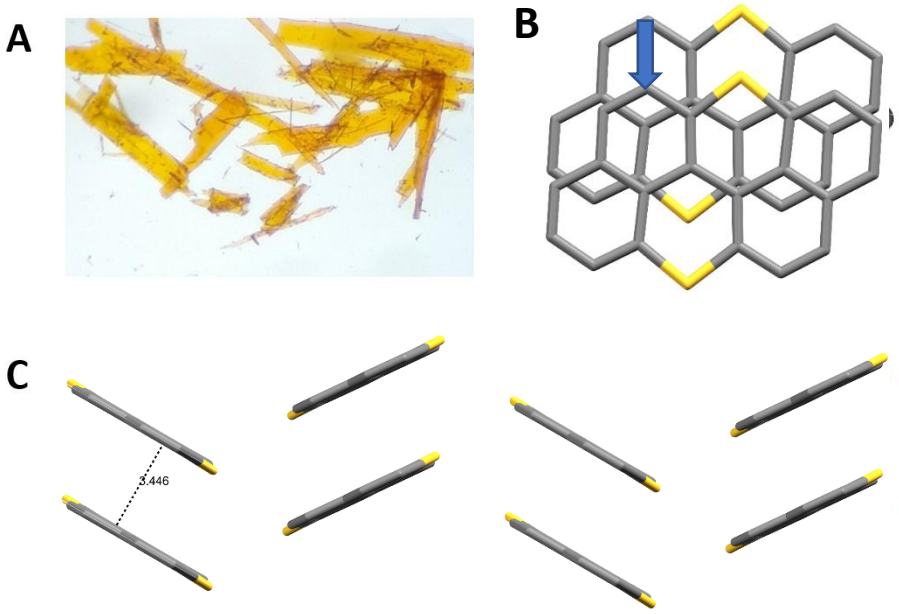

Figure 1.20. Yellow plate **PTXTX** polymorph. **A** picture of crystals. **B** π-π stacking top view with 1.79 Å displacement. **C** crystal packing side view, the distance between stacked molecules 3.45 Å. Monoclinic system, P $2_1/c$ space group, R factor 5.73%.

In both polymorphic forms, **PTXTX** molecules are interacting with parallel displaced π-π stacking.[198] In yellow plates the molecules are displaced with 1.79 Å, in an arrangement called slip, while the distance between stacked molecules is 3.45 Å (Figure 1.20). In red needles, displacement between stacked molecules is 2.80 Å, and resembles arrangement in graphite which is called glike (Figure 1.21).[199] The distance between stacked molecules is 3.41 and 3.51 Å. In both polymorphs, the distance between the planes of the molecules lies in a range typically reported for π-π stacking: 3.3–3.8 Å.[200]

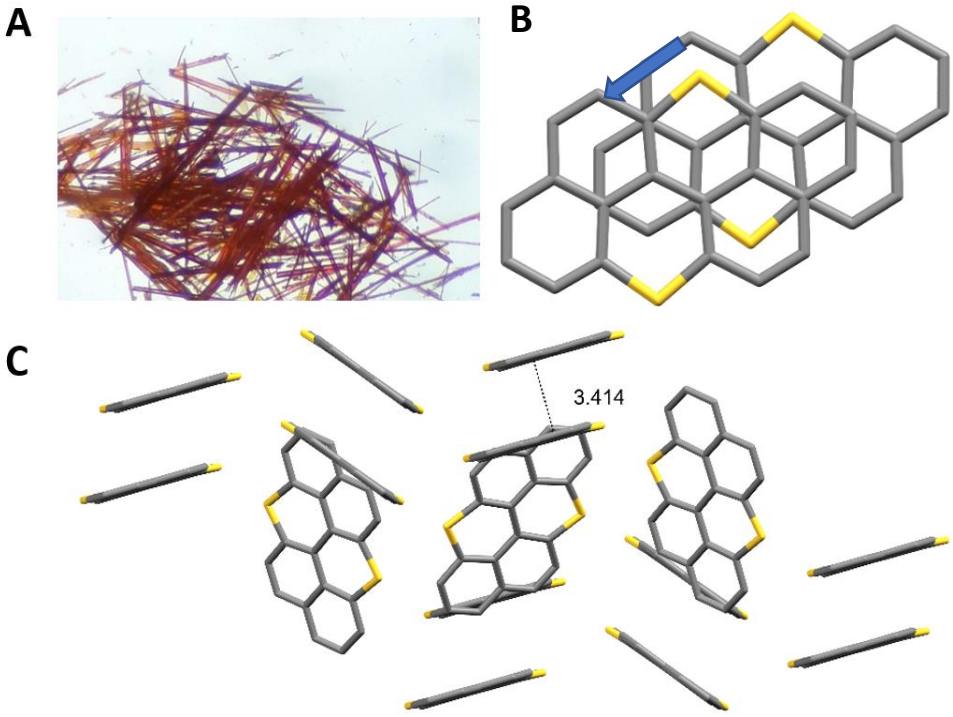

Figure 1.21. Red needle **PTXTX** polymorph. **A** picture of crystals. **B** π-π stacking top view with 2.80 Å displacement. **C** crystal packing side view, distances between stacked molecules 3.41 Å and 3.51 Å. Monoclinic system, P $2_1/c$ space group.

1.12.2 Crystal structure of sulfoxide 28

Crystals of molecule **28** suitable for X-Ray diffraction were obtained by hot recrystallisation from CH_3CN, and they belong to the P $2_12_12_1$ space group.

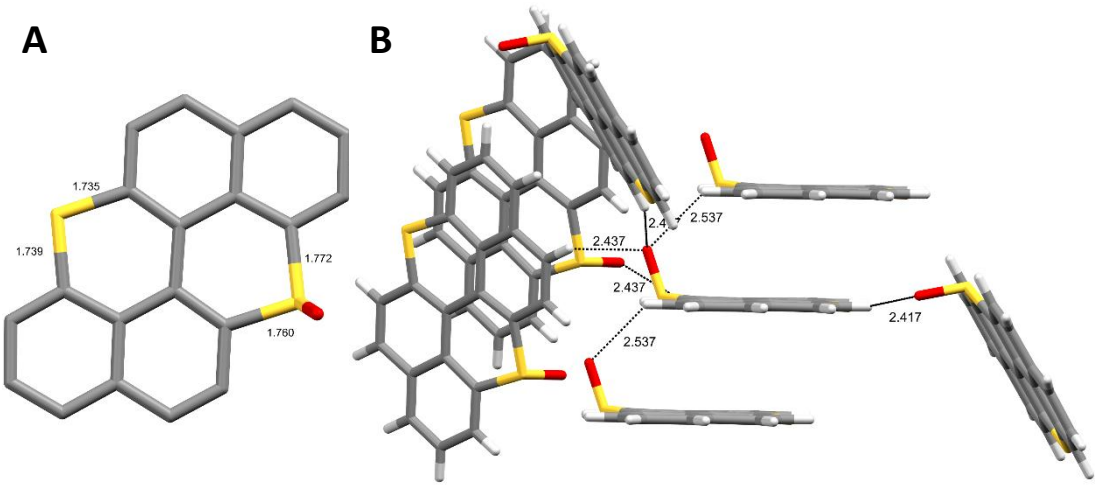

Figure 1.22. Crystal structure of molecule **28**, **A** Length of C-S bonds, **B** selected short contacts highlighted. Orthorhombic system, P $2_12_12_1$ space group, R factor 6.53%.

Molecules are flat, with sulfur atoms distorted from the molecule's plane on its opposite sides (Figure 1.22). The presence of sulfoxide group increases the distortion to 7° angle, while the angle of distortion for the sulfur of thioether is 2.6°. The lengths of S-C bonds in the thioether part (1.739(6) Å and 1.736(6) Å) are very similar as in **PTXTX** (~1.74 Å), whereas they are slightly longer in the sulfoxide part (1.771(6) Å and 1.760(6) Å). A net of short contacts can be observed between oxygen atom of sulfoxide and hydrogen atoms, measuring between 2.42 and 2.54 Å. These distances are consistent with typical lengths of weak hydrogen bonds seen in PAHs.[201]

1.12.3 Crystal structure of bis-sulfoxide *trans*-30

The crystallisation of ***trans*-30** from hot DMSO afforded monoclinic crystals belonging to P $2_1/c$ space group. Molecules are flat, with oxygen atoms on opposite sides of the molecule's plane, and sulfur atoms distorted even more than in the monosulfoxide **28** (Figure 1.23). Sulfur atoms are sticking at 17° angle from the naphthylic core plane, higher compared to the monosulfoxides where the angle was just 7°. The lengths of C-S bonds (1.771(3) and 1.757(3) Å) are almost identical as the C-S bonds of sulfoxide moiety in molecule **28** (~1.77 Å and 1.76 Å). The molecules interact with a net of weak hydrogen bonds between oxygen atoms of sulfoxides and hydrogen atoms.

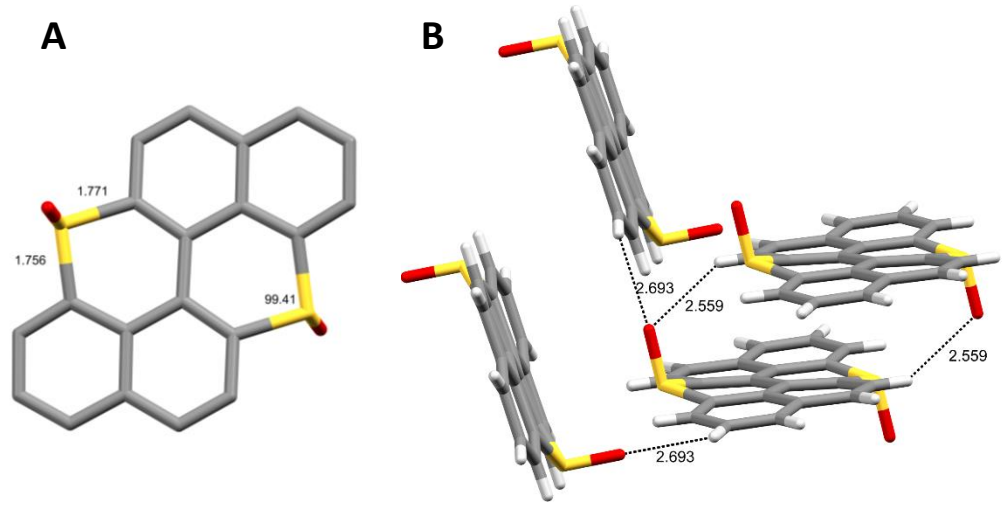

Figure 1.23. Crystal structure of ***trans*-30 A** length of C-S bonds and C-S-C angle, **B** selected short contacts highlighted. Monoclinic system, P $2_1/c$ space group, R factor 5.27%.

1.12.4 Crystal structure of sulfoxide-sulfone

Sulfoxide-sulfone crystalised in the P -1 space group. The achieved crystal suffered from so-called “twinning”. This resulted in the 50% probability of 2 oxygen atoms on either of two S atoms in the solved structure, so even though there are 3 oxygen atoms in the molecule it can look like there are 4 (Figure 1.24). Molecules are bent, with naphthylic moieties at a 159° angle. While the lengths of C-S bonds for one sulfur atom (1.766(3) Å and 1.767(4) Å) are consistent with the length observed in the sulfoxide ***trans*-30** (~1.77 Å and 1.76 Å), the other sulfur atom has C-S bond length (1.747(4) Å and 1.752(3) Å) just like in the sulfones **31** (~1.75 Å). Molecules are connected with an extensive net of weak hydrogen bonds between oxygen atoms and hydrogens.

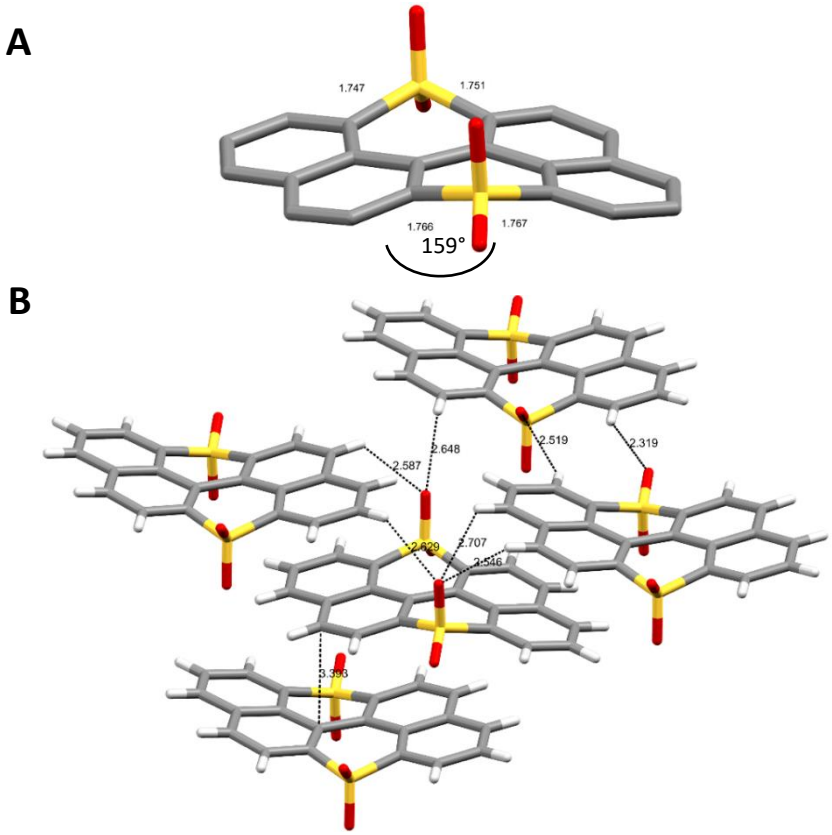

Figure 1.24. A Crystal structure of sulfoxide-sulfone **B** selected short contacts highlighted. Triclinic system, P -1 space group. (3 oxygen atoms in the molecule, 50% probability of 2 oxygen atoms on either of sulfurs), R factor 7.3%.

1.12.5 Crystal structure of bis-sulfone 31

Crystals of bis-sulfone **31** were obtained through hot crystallisation from DMSO and belong to the P -1 space group. The length of C-S bonds (1.751(2) Å and 1.749(2) Å) is the same as in the part of sulfoxide-sulfone molecule (~1.75 Å). Molecules are bent, forming a 157° angle between the naphthylic moieties, similar to sulfoxide-sulfone's corresponding 159° angle (Figure 1.25). Each molecule interacts with eight other molecules through a wide range of weak hydrogen bonds, between oxygen atoms of the sulfone and hydrogens. This high number of weak hydrogen bonds could explain the very low solubility of the compound.

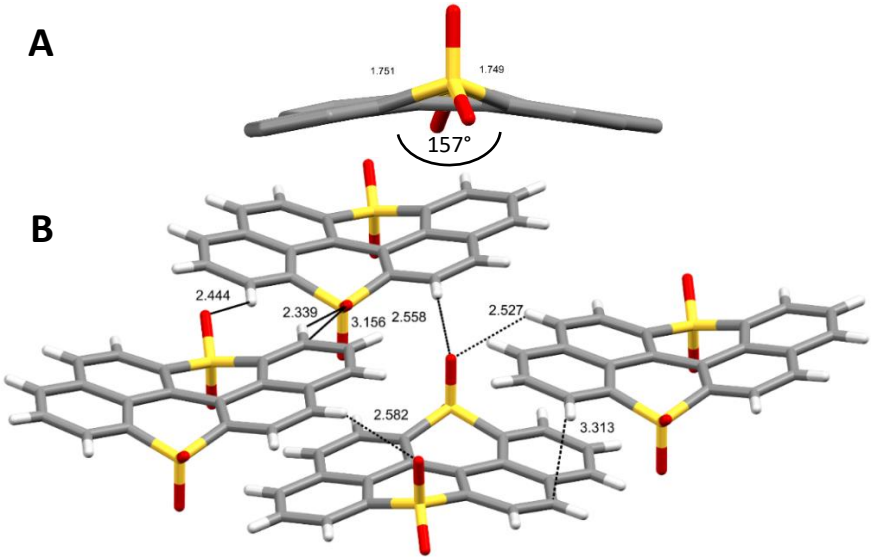

Figure 1.25. A Crystal structure of **32**. **B** selected short contacts highlighted. Triclinic system, P -1 space group, R factor 4.96%.

1.12.6 Crystal structures of bis-octyl-bis-sulfone *anti*-32

Crystals suitable for X-Ray diffraction were grown by slow diffusion of hexane into the solution of **32** in toluene. Two polymorphs were obtained from the same crystallisation batch. Thin rods consisted of polymorph ***anti*-32** (Figure 1.26), while thin plates of polymorph ***syn*-32** with hexane molecules in the crystal lattice (Figure 1.27).

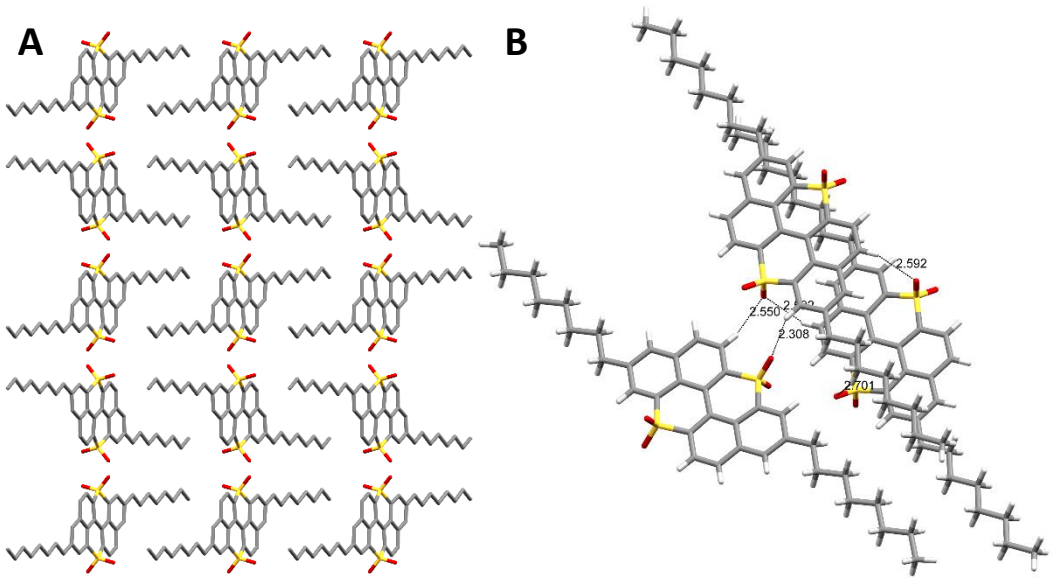

Figure 1.26. Crystal structure of polymorph ***anti*-32** selected short contacts highlighted. Monoclinic system, P 2_1/c space group **A** view along “b” axis **B** view along “a” axis, R factor 7.01%.

Crystals of polymorph ***anti*-32** (Figure 1.26) belong to P 2_1/c space group. The molecules are mostly flat with oxygen atoms in an “anti” conformation, similarly as in

sulfoxide ***trans*-30**. The sulfur atoms are distorted out of the molecule's plane, one placed 16° over and the other 16° under the molecule's core, an angle similar to ***trans*-30** 17°. Chains are tilted over and the other under the plane of the molecule core, with 6° angle. The presence of chains and different conformation of the molecule did not affect the length of C-S bonds (1.740(4) and 1.753(4) Å), which is similar in unsubstituted sulfone **31** (~1.75 Å). The molecules are segregated, the cores with sulfonic parts and octyl chains form hydrophilic and hydrophobic layers (A in Figure 1.26). The molecules are flat and interact through weak hydrogen bonds between oxygen atoms of the sulfones and hydrogens placed on cores and chains (B in Figure 1.26).

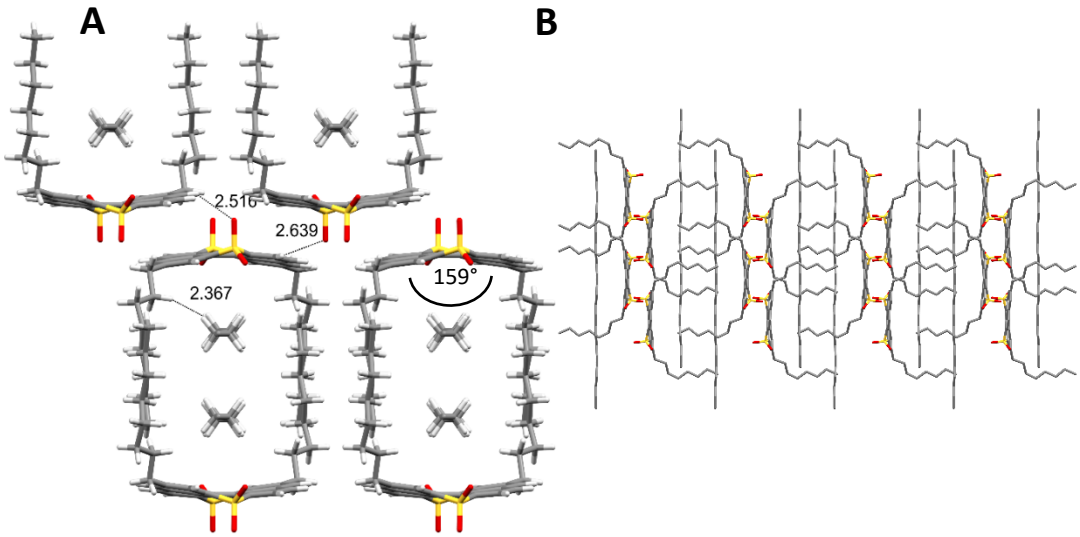

Figure 1.27. Crystal structure of polymorph ***syn*-32** with hexane molecules in the crystal structure, selected short contacts highlighted. Monoclinic system, C 2/c space group. **A** view along "c" axis **B** view along "a" axis, R factor 11.72%.

Polymorph ***syn*-32** crystalises in the C 2/c space group. While the molecules have the same syn conformation of oxygen atoms as in sulfone **31**, the length of C-S bonds is slightly different 1.770(4) Å and 1.742(4) Å vs ~1.75 Å in **31**. The molecules are bent, the two halves of the molecule's core form a 159° angle, similarly as in the crystal structure of **31**, where it was 157°. In the crystal structure, there are large, rectangular voids, which form tunnels filled with hexane. The walls of these tunnels consist of octyl chains that interact with hexane molecules via hydrophobic interactions. The main observed interactions are weak hydrogen bonds between the oxygen atoms of the sulfone groups and hydrogens of both the naphthyl core and the chains (A in Figure 1.27). It is possible to observe segregation in which all hydrophilic sulfone groups as well as hydrophobic octyl chains and hexane molecules form layers (B in Figure 1.27).

Similarly as in urea and thiourea,[202] polymorph ***syn*-32** forms an inclusion compound with hexane with 1D parallel channels running along the “c” axis. As with the urea inclusion compounds, the channel structure is based on weak host-guest interactions, and the absence of solvent in the crystal lattice in polymorph ***anti*-32** leads to the lack of pores and different molecular arrangements in the crystals.

1.12.7 Crystal structure of bis-selenide 36

Single crystals of **36**, suitable for XRD study, were prepared through a batch crystallisation from hot toluene and hexane mixture (Figure 1.28). The molecule is flat in the solid state, although the large size of selenium atoms causes them to be slightly distorted out of the molecule plane. C-Se-C angle decreased to 100°, compared to analogical angles in **PTXTX** (104°) and **PXX** (122°) (paragraph 1.9.1). The length of C-Se bond in **36** is 1.88 Å and 1.87 Å, longer than the corresponding C-S and C-O bonds in **PTXTX** (1.74 Å) and **PXX** (1.39 Å). Both changes are likely connected to the large size of the Se atom. Compound **36** crystallised in the $P2_1/c$ space group, in a herringbone arrangement, similarly as in the yellow plates polymorph of **PTXTX** (paragraph 1.9.1). The distance between Se atoms is 3.67 Å, which lies inside of the van der Waals radii of two Se atoms.[203,204] Even though both molecules have a similar crystal packing, a corresponding interaction between S atoms in **PTXTX** does not exist. The molecules of **36** interact through π-π stacking, with the 3.51 Å distance between the stacked molecules, also comparable to the corresponding distance in the **PTXTX** yellow plates (3.46 Å).

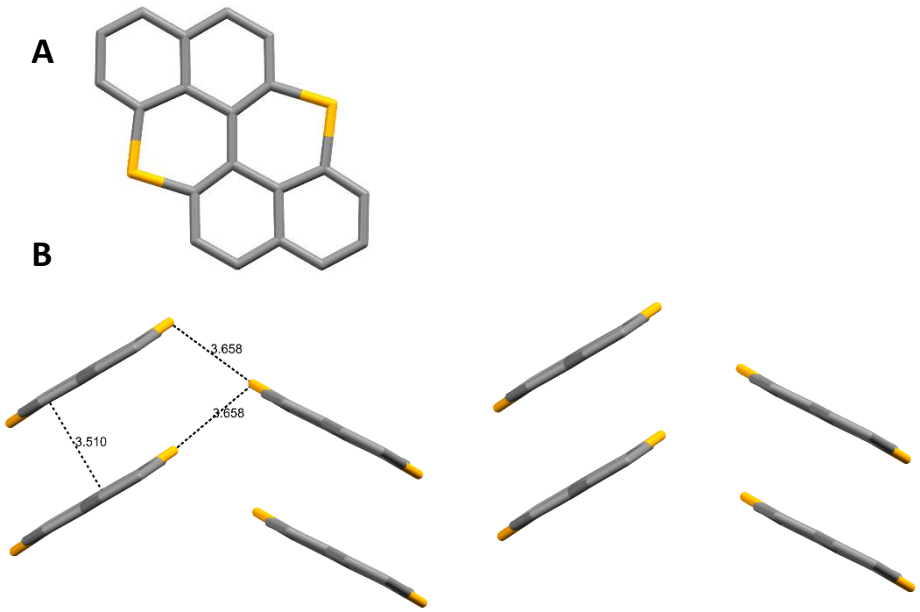

Figure 1.28. A Crystal structure of **36**. **B** selected close contacts. Monoclinic system, space group $P2_1/c$.

1.13 Photophysical characterisation

This section investigated the photophysical properties of **PTXTX** and its derivatives **28**, ***trans*-30** and **32** through UV/Vis absorption and emission spectroscopy. **PTXTX** data will also be compared with O-doped **PXX** and Se-doped **36**, to showcase the effect of doping with different chalcogens.

PTXTX shows absorption spectra red shifted when compared with **PXX** (500 nm vs 443 nm) (Figure 1.29). The presence of heavier S-atoms leads to reduced oscillator strength of the $S_0 \rightarrow S_1$ transition, resulting in broader and less intense absorption bands ($\varepsilon_{max} \approx 6000$ M^{-1} cm^{-1} and 17300 M^{-1} cm^{-1}[153] for **PTXTX** and **PXX**, respectively, Table 1.6).

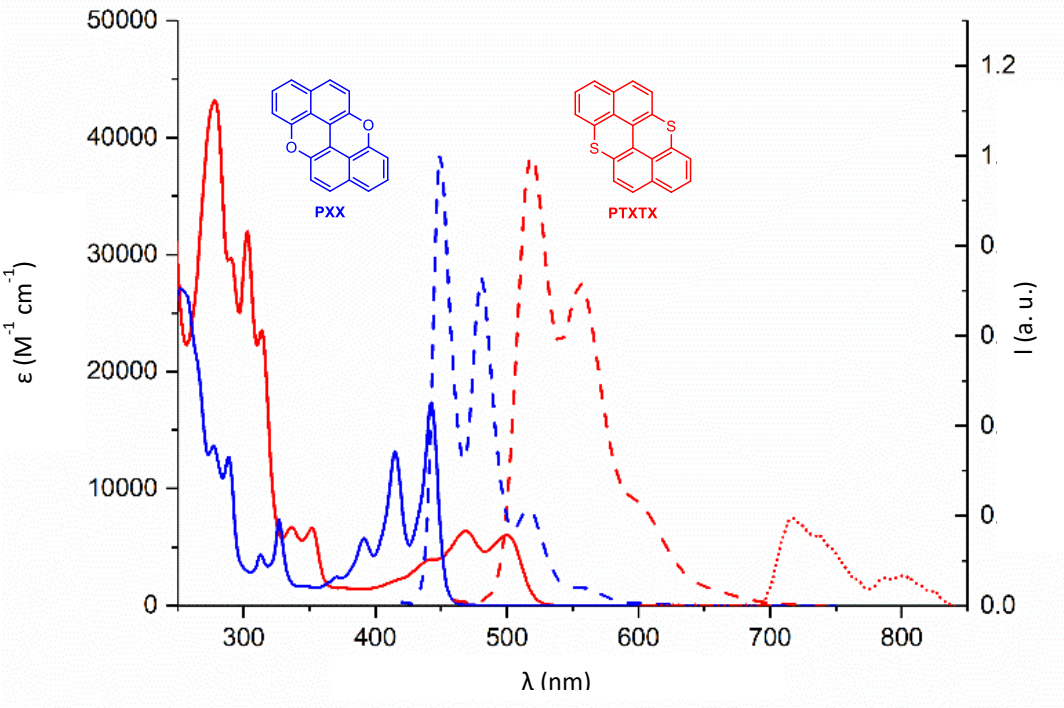

Figure 1.29. UV-Vis (—) and luminescence spectra (- - -) of **PXX** (blue, λ_{exc} = 389 nm) and **PTXTX** (red, λ_{exc} = 445 nm), recorded in CH_2Cl_2 at rt. Phosphorescence (⋯) intensity has been magnified and measured after the addition of CH_3I, at 77K.

Quantum yield of fluorescence was reduced from 0.62 in the case of **PXX** to 0.02 for **PTXTX** (Table 1.6), which could be explained by an efficient non-radiative deactivation via triplet population. However, only a weak phosphorescence could be observed between 700-820 nm at 77 K, induced by an external heavy atom effect through the addition of CH_3I[205] (Figure 1.29). To corroborate this hypothesis a singlet oxygen sensitisation measurement was performed to study the triplet population of

PTXTX. While the quantum yield of singlet oxygen formation equals n $\Phi_{rel}(^1O_2)$ = 0.26 for **PXX**, it rose to 0.64 for **PTXTX** (Table 1.5), showing more efficient ISC.

Table 1.5. $^1O_2$ sensitization quantum yield (Φ_{rel}) recorded for **PXX** (λ_{exc} = 390 nm) and **PTXTX** (λ_{exc} = 511 nm) vs C_{60} in a CH_2Cl_2 solution at rt.[a] C_{60} Φ_{rel} ($^1O_2$) = 1[206]

Molecule	$\Phi_{rel}(^1O_2)$	
	I_{1270nm}[a]	Area
PXX	0.30	0.26
PTXTX	0.72	0.64

Oxidation of S-atoms results in a progressive blue shift of absorption spectra. While **PTXTX** has its lowest energy band at λ_{max} = 500 nm, in oxidised derivatives corresponding bands are centred at 458 nm, 414 nm and 399 nm for **28**, ***trans*-30**, and **32** respectively (

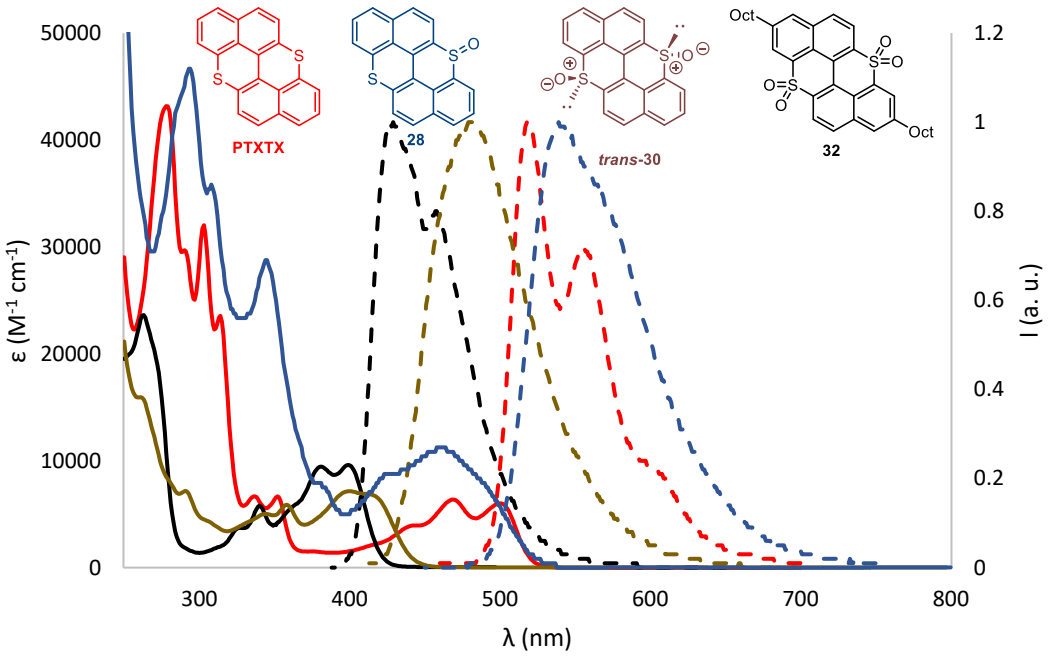

Figure 1.30, Table 1.6). Emission profiles for compounds **PTXTX**, **28**, ***trans*-30**, and **32** mirror the absorption bands, while they exhibit moderated photoluminescence quantum yields (Φ_{em}) (Φ_{em} = 2%, 22%, 4%, and 35%, respectively) and lifetimes in the nanosecond range (τ = 5.2, 11.2, 0.6, and 0.7 ns, respectively). Upon substitution of the O-atoms with S-atoms a lowering of the HOMO-LUMO energy bandgap is evident (E_{00} = 2.78 and 2.44 eV for **PXX** and **PTXTX**, respectively), as well as its widening upon progressive oxidation (E_{00} = 2.44, 2.43, 2.83, 2.99 eV for **PTXTX, 28**, ***trans*-30**, and **32**, respectively) (Table 1.6).

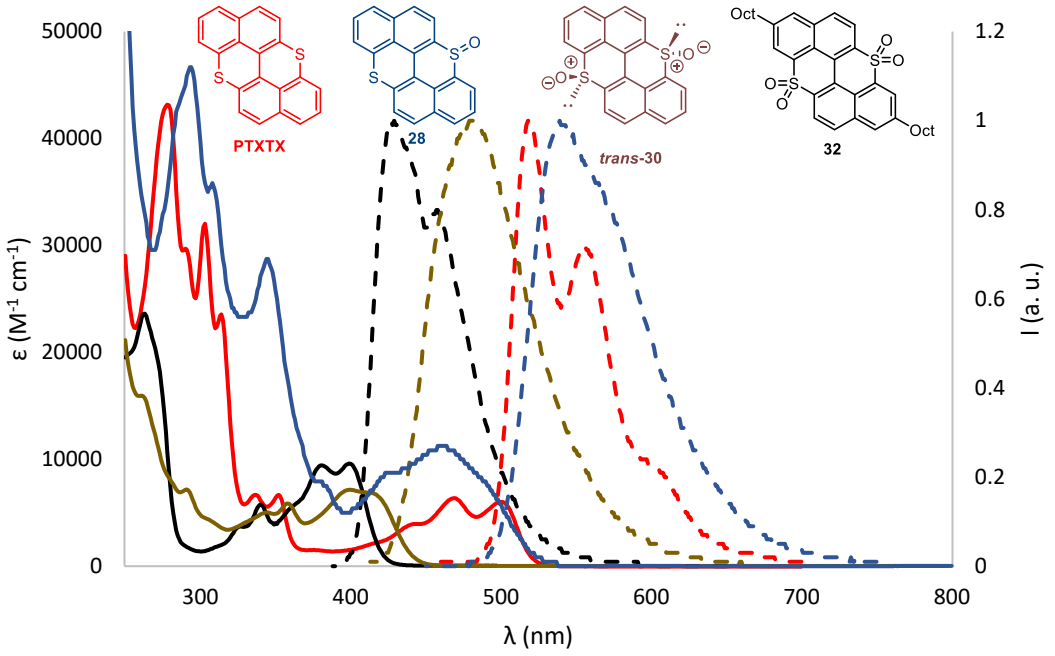

Figure 1.30. UV-VIS (—) and luminescence (- - -) spectra for **PTXTX** (red, λ_{exc} = 450 nm), **28** (blue, λ_{exc} = 345 nm), ***trans*-30** (brown, λ_{exc} = 350 nm), and **32** (black, λ_{exc} = 365 nm), recorded in CH_2Cl_2 at rt.

Table 1.6. Absorption and emission maxima, fluorescence lifetimes, Φ_{em} and energy bandgaps for molecules **PTXTX, 28**, ***trans*-30**, and **32**. Recorded in aerated CH_2Cl_2 at rt. [a] λ_{exc} = 450 or 340 nm.[b] Standard: coumarin 153 in EtOH (Φ = 0.53).[207] [c] Standard 9,10-diphenylanthracene in cyclohexane (Φ = 0.97±0.03).[208] [d] Energy calculated at the lowest energy intersection (λ_{int}) between normalised absorption and emission spectra, $E_{00} = 1240.5/\lambda_{int}$. [e] Energy gap between S_0 and T_1.

Molecule	Absorbance		Fluorescence			Energy Band Gap
	λ, nm	ε, M^{-1} cm^{-1}	λ,(nm)	τ (ns)[a]	Φ_{em}	E_{00} (eV)[d]
PXX	443	17300[153]	450[153]	5.0[153]	0.62[153][b]	2.78
PTXTX	500	6000	518	5.2	< 0.02[b]	2.44 (1.72)[e]
28	458	4050	539	11.2	0.22[b]	2.43
***trans*-30**	414	6761	483	0.6	0.04[b]	2.83
32	399	9600	430	0.7	0.35[c]	2.99

Heavier Se atoms result in lack of defined vibronic structure a in the π→π* transition in absorption spectra of **36**, which is evident in **PXX**, and less defined in **PTXTX** (Figure 1.31). For **PXX** the absorption has a maximum at 443 nm, while for **PTXTX** and compound **36** bathochromic shift to 469 nm has been observed. The fluorescence spectra are less intense in the O>S>Se direction. The fluorescence emission of

compound **36** was too weak to measure the quantum yield. Observed trends are in line with previously described reports comparing PAHs containing different chalcogens.[4,209] No phosphorescence was observed at 77 K. As only weak fluorescence and no phosphorescence was detected, a singlet oxygen sensitisation experiment would be necessary, in future, to measure the triplet state population of compound **36**.

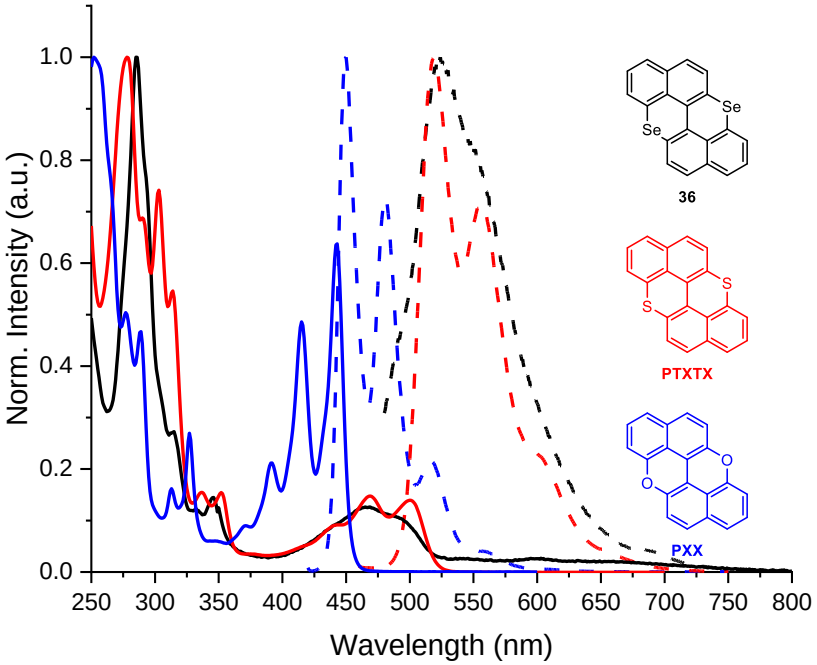

Figure 1.31. Normalized UV-VIS (—) and normalized luminescence (- - -) spectra for **36**, (black, λ_{exc} = 460 nm), **PTXTX** (red, λ_{exc} = 445 nm) and **PXX** (blue, λ_{exc} = 389nm), recorded in CH_2Cl_2 at rt.

1.14 Electrochemical investigation

1.14.1 Introduction to Cyclic Voltammetry

Cyclic voltammetry (CV) is a technique commonly employed to investigate the reduction and oxidation processes of OSCs. It allows elucidation of oxidative and reductive properties of the compound in question. Cyclic voltammogram diagrams have potential (E) on the x-axis, while the y-axis is the response - resulting current (i) passed. The current axis (y) is often not labelled, with a scale bar inset to the graph instead. Sometimes a scan rate (v) is reported in CV experiments. For example, the scan rate of 100 mV/s indicates that during the experiment the potential was linearly varied at the speed (scan rate) of 100 mV per second from high to low potentials. The equilibrium

between oxidised and reduced species during CV experiments are described by Nernst equation (Eq. 2).

$$E = E^0 + \frac{RT}{nF} ln \frac{(Ox)}{(Red)} = E^0 + 2.3026 \frac{RT}{nF} log_{10} \frac{(Ox)}{(Red)} \quad \text{Eq. 2}$$

In one electron processes n=1, activities are replaced with concentrations, while standard potential E^0 is replaced with the formal potential $E^{0\prime}$ (Eq. 3).

$$E = E^{0\prime} + \frac{RT}{F} ln \frac{[Ox]}{[Red]} = E^{0\prime} + 2.3026 \frac{RT}{F} log_{10} \frac{[Ox]}{[Red]} \quad \text{Eq. 3}$$

Formal potential $E^{0\prime}$ is estimated with the experimentally determined halfway potential value: $E_{1/2}$, which is an average potential between points A and B in Figure 1.32.

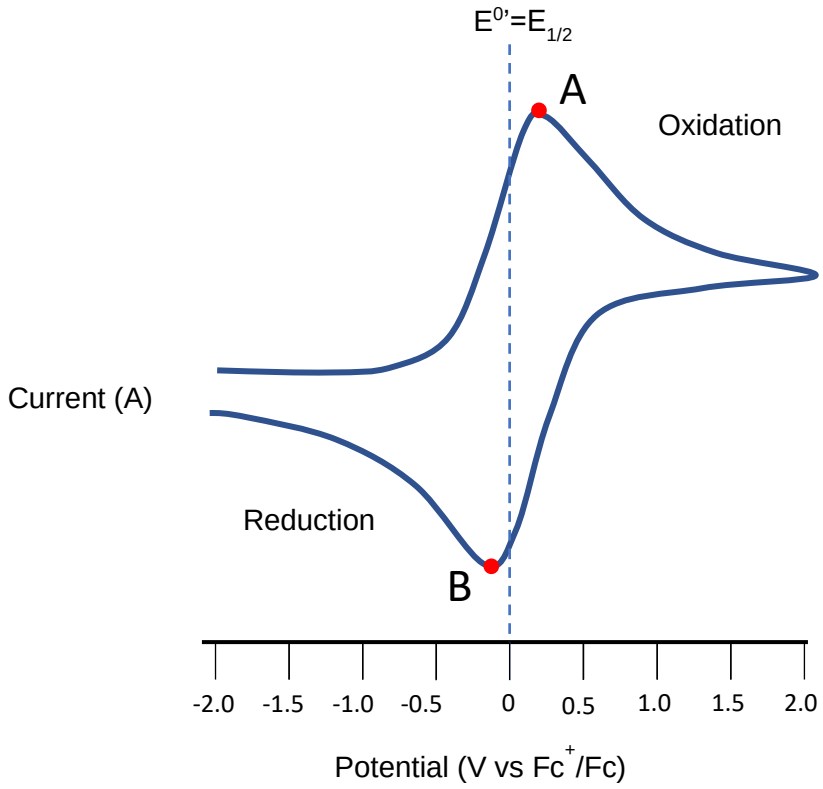

Figure 1.32. Example of cyclic voltammogram.

1.14.2 Electrochemical investigation of PTXTX, its oxidised derivatives and compound 36

Redox properties of **PTXTX** and its derivatives were investigated through cyclic voltammetry, in CH_2Cl_2 at rt, using $TBAPF_6$ as an electrolyte and either ferrocene or decamethylferrocene as internal standards. Reported values are referenced to ferrocene. The cyclic voltammograms are reported in Figure 1.33 and Figure 1.34, while corresponding data is collected in Table 1.7.

PTXTX shows a reversible oxidation wave ($E_{1/2}^{ox1}$ = 0.21 V vs $Fc^{+/0}$) at a lower potential than **PXX** ($E_{1/2}^{ox1}$ = 0.31 V vs $Fc^{+/0}$) (Figure 1.33). Sulfoxide derivatives **28** and ***trans*-30** show irreversible oxidation waves. However, all chemically oxidised derivatives have reversible reduction waves at ($E_{1/2}^{red1}$ = -1.90 V, -1.60 V and -1.34 V, for **28**, ***trans*-30** and **32** respectively). A second reduction wave is present for ***trans*-30** and **32** ($E_{1/2}^{red2}$ = -1.96 V (irreversible) and -1.82 V (reversible)), respectively.

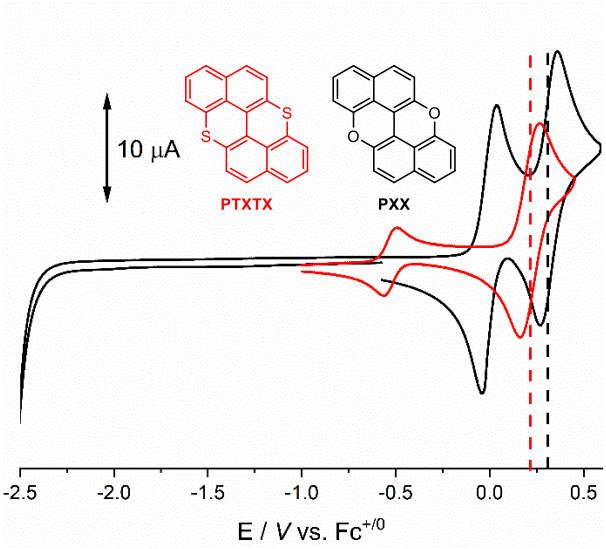

Figure 1.33. CV of **PTXTX** (red, 0.9 mM, $E_{1/2}$ $FcMe_{10}^{+/0}$ = -0.532 V vs. Fc) and **PXX** (black, 1.0 mM, Fc was used as a reference) in a CH_2Cl_2 solution at rt.

Table 1.7. Cyclic Voltammetry data of **PTXTX**, **28**, ***trans*-30** and **32** in CH_2Cl_2 at rt. Scan rate 0.05 V s^{-1}, $TBAPF_6$ was used as electrolyte, and either ferrocene[210] or decamethylferrocene (for **PTXTX**) were used as an internal references. ^{irr} irreversible peak.

Molecule	Oxidation		Reduction	
	$E_{1/2}^{ox1}$	$E_{1/2}^{ox2}$	$E_{1/2}^{red1}$	$E_{1/2}^{red2}$
PXX	0.31	/	/	/
PTXTX	0.21	/	/	/
28	0.8^{irr}	1.3^{irr}	-1.90	/
***trans*-30**	1.1^{irr}	1.3^{irr}	-1.6	-2.1
32	/	/	-1.34	-1.82

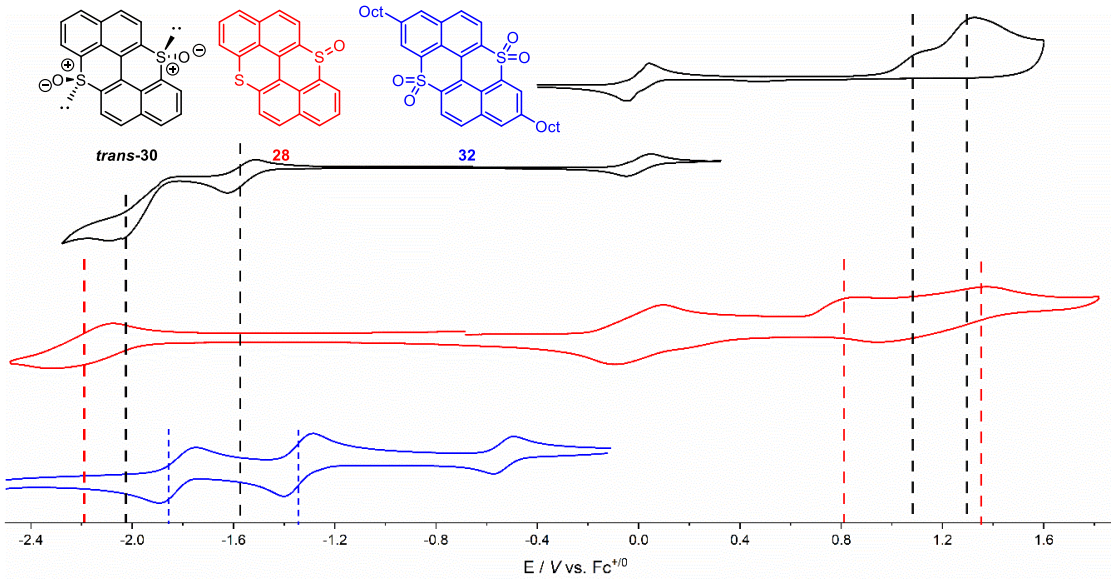

Figure 1.34. *From top to bottom*, Stacked Cyclic Voltammograms of ***trans*-30** (black), **28** (red), **32** (blue) in CH_2Cl_2 at rt. Scan rate 0.05 V/s, $TBAPF_6$ was used as electrolyte and ferrocene was used as an internal reference standard for **28**, ***trans*-30**. Decamethylferrocene was used as a reference for **32** ($E_{1/2}$ $FcMe_{10}^{+/0}$ = -0.532 V vs. Fc).[210]

To compare the potentials of **PXX**, **PTXTX** and **36**, all the values are reported vs SCE (Table 1.8). Compound **36** exhibits two oxidation waves at $E_{1/2}^{ox1}$ = 0.41 V and $E_{1/2}^{ox2}$ = 0.94 V vs SCE, with the first wave at a lower potential than in **PXX** ($E_{1/2}^{ox1}$ = 0.77 V vs SCE) and **PTXTX** (0.67 V vs SCE).

Table 1.8. Cyclic Voltammetry data of **PXX**, **PTXTX** and **36** reported vs SCE. E $Fc^{+/0}$ = 0.46 V vs. SCE in CH_2Cl_2.

Molecule	Oxidation vs SCE		Reduction vs SCE	
	$E_{1/2}^{ox1}$	$E_{1/2}^{ox2}$	$E_{1/2}^{red1}$	$E_{1/2}^{red2}$
PXX	0.77	/	/	/
PTXTX	0.67	/	/	/
36	0.41	0.94	/	/

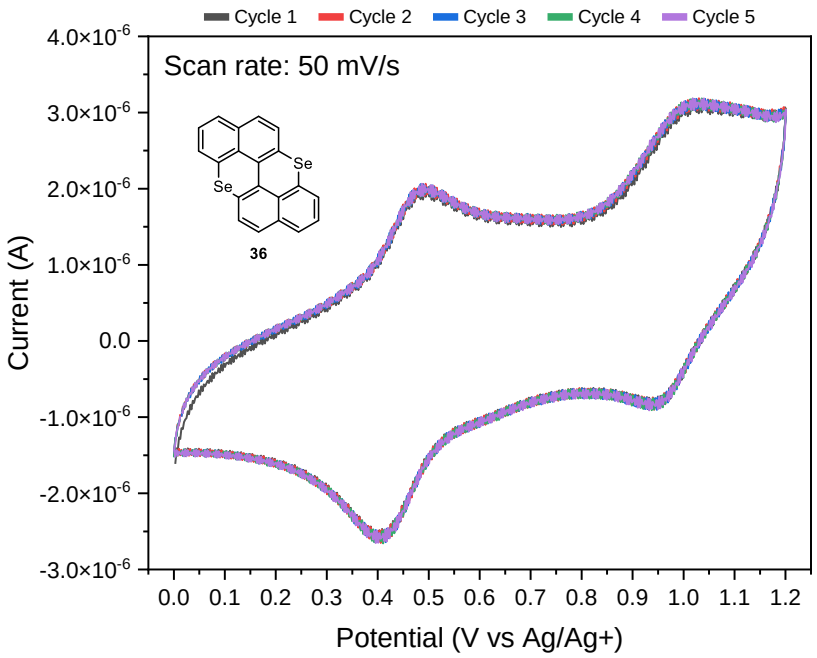

Figure 1.35. CV of molecule **36**, Ag/Ag^+ used as reference electrode, scan rate 50 mV/s, electrolyte 0.1M $TBAPF_6$ in CH_2Cl_2, working electrode glassy carbon, counter electrode Pt wire.

As expected, changing O-atoms in **PXX** to S-atoms in **PTXTX** and Se-atoms in **36** enhances the reduction behaviour of the compound.[196] The presence of reduction waves in oxidised derivatives **28**, ***trans*-30** and **32** can be attributed to the electron withdrawing properties of sulfoxide and sulfone groups.

1.15 Mixed valence crystals

Mixed valence crystals of **PTXTX** were prepared by electrooxidation experiments, from THF/EtOH solution, and compared to the similarly prepared **PXX**-based materials.[211] **PXX** gave orthorhombic crystals with two **PXX** molecules and one ClO_4^- anion $(\mathbf{PXX})_2(ClO_4)_1$. While monoclinic, black needles of **PTXTX** mixed-valence (MV) complexes were obtained with three **PTXTX** molecules and two ClO_4^- anions, $(\mathbf{PTXTX})_3(ClO_4)_2$. In both materials the columnar arrangement was observed, with ClO_4^- distributed between the π-π stacked pillars (Figure 1.36). In a $(\mathbf{PXX})_2(ClO_4)_1$ crystals an average interplanar spacing is 3.33(7) Å, while in the $(\mathbf{PTXTX})_3(ClO_4)_2$ it is slightly larger, from 3.35 to 3.37 Å.

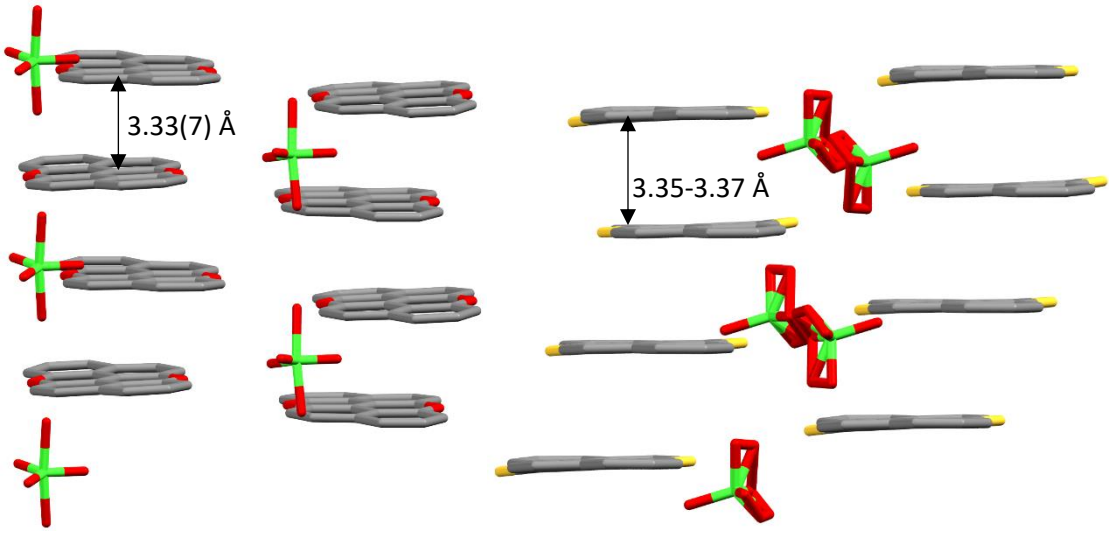

Figure 1.36. Columnar packing in crystals of $(PTXTX)_3(ClO_4)_2$ (top) and $(PXX)_2(ClO_4)$ (bottom).

This columnar packing in MV complex of **PTXTX** stands in contrast to the packing in the crystals of neutral **PTXTX**, where herringbone arrangement was observed in both polymorphic forms (Figure 1.20 and Figure 1.21). Columnar stacking is preferential to herringbone arrangement in organic semiconductors, as it enhances the electronic coupling between stacked cores and raises charge transport properties of the material.

Electric investigations of single crystals of both MV complexes were conducted, with several single crystals measured for each material. Both materials revealed a semiconducting behaviour for both measured materials. The conductivities (σ) at rt are in the order of 10^{-2} - 10^{-3} S cm-1 for $(\mathbf{PTXTX})_3(ClO_4)_2$ and 10^{-1} - 10^{-2} S cm^{-1} for $(\mathbf{PXX})_2(ClO_4)_1$. Most organic semiconducting materials are insulators or weakly conductive ($\sigma < 10^{-6}$ S cm^{-1}), with exception for TCNQ-TTF co-crystals, and several radicals and MOFs. Compared to MV complexes of O-doped PAHs[164] obtained by us previously, which displayed σ in the order of 10^{-4} - 10^{-3} S cm^{-1}, both (**PXX**)2(ClO4)1 and $(\mathbf{PTXTX})_3(ClO_4)_2$ MV complexes show one of the highest conductivity values for an organic semiconductor up to date.

1.16 Electroluminescence behaviour in LEC

Light-emitting electrochemical cells (LECs) are thin film devices generating light from an electric current (electroluminescence). They are usually composed of a blend of organic semiconductor and an ionic electrolyte sandwiched between electrodes. They display low cost, easy upscalability, as they can be fabricated with solution based techniques, and high versatility towards the type of emitters. PAHs emitters, such as pentacene, pyrene derivatives and BN-doped coronene were applied in these devices,

giving highly emitting blue and red emitting LECs. [212] However, mid-energy emitting PAH-based LECs have rarely been reported. **PTXTX** and its derivative with octyl chains **25** display yellowish green emission, and show *p*-type semiconducting properties, making them interesting materials for emissive layers in LECs. Thin films (~60 nm thick) were fabricated onto quartz and Indium Tin Oxide (ITO) substrates using a mixture of the emitters and the ionic matrix (trimethylolpropane ethoxylate - TMPE and potassium triflate - KOTf) in a 1.0 : 0.10 : 0.02 ratio (emitter: TMPE:KOTf).[211] **PTXTX** did not show high enough solubility to allow the creation of thin films. However, **PTXTX** with octyl chains - **25** and **PXX** thin films were fabricated and found to show homogenous morphology under atomic force microscopy (AFM) assay. Thin films showed similar photoluminescence spectrum (Table 1.9) compared to the solution based results (Table 1.6). Photoluminescence quantum yields Φ_{em}^{film} were 0.1 for **25** and 0.46 for **PXX**, values comparable to those measured in solution (Table 1.9) and the presence of a matrix did not affect those values.

Table 1.9. Thin-film photophysical properties of **25** and **PXX** films. (λ_{exc}=377 nm), [a] only emitter, [b] with polyelectrolyte matrix.

	λ_{max} [a] (nm)	λ_{max} [b] (nm)	$\Phi_{em}^{film\ a}$	$\Phi_{em}^{film\ b}$	τ [a] (ns)	τ [b] (ns)
25	530 571 625	533 567 627	0.07	0.10	1.0	0.9
PXX	465 504 551	450 512 546 587	0.48	0.46	6.6	5.2

The electroluminescent behaviour of **25** and **PXX** was studied in LECs built as ITO/PEDOT:PSS (90 nm)/**PXX** or **25**:TMPE:KOTf 1:0.10:0.02 (60 nm)/Al(90 nm).

Table 1.10. PXX- and **25**-based LECs measured at different pulsed currents. [a]PC: pulsed current, [b]maximum luminance, [c]time to reach 50% of the initial luminance, [d]power efficiency.

Device	**PC**[a] (mA)	**Luminance$_{max}$**[b] (cd m^{-2})	**Average Voltage** (V)	**$t_{1/2}$**[c] (h)	**Eff**[d] (cd/A)
PXX	10 mA	40.1	2.7	0.3	0.08
PXX	20 mA	74.2	3.2	0.2	0.07
25	10 mA	9.4	2.6	3.2	0.02
25	20 mA	17.3	2.7	2.2	0.01

The electroluminescence response of the devices is similar to that of the thin films and solutions, displaying a broad emission band with a maximum at 494 nm and 537 nm for **PXX** and **25**. The **PXX**- based devices show good performances with a maximum luminance of *ca*. 40 and 75 cd m^{-2}, with an average efficacy of 0.1 cd/A at 10 and 20

mA, respectively. **25**-based devices showed lower luminance values of *ca*. 10 and 17 cd m^{-2} along with lower efficiencies, as expected from the reduced Φ_{em}^{film} of **25** (Table 1.10). The device stability of a few hours is similar for both emitters. While these devices are one of the first examples of mid-emitting PAH-based LECs, their performance (efficiency and stability) is comparable to that of the reported green-emitting LECs based on small molecules (Figure 1.37).[213–216]

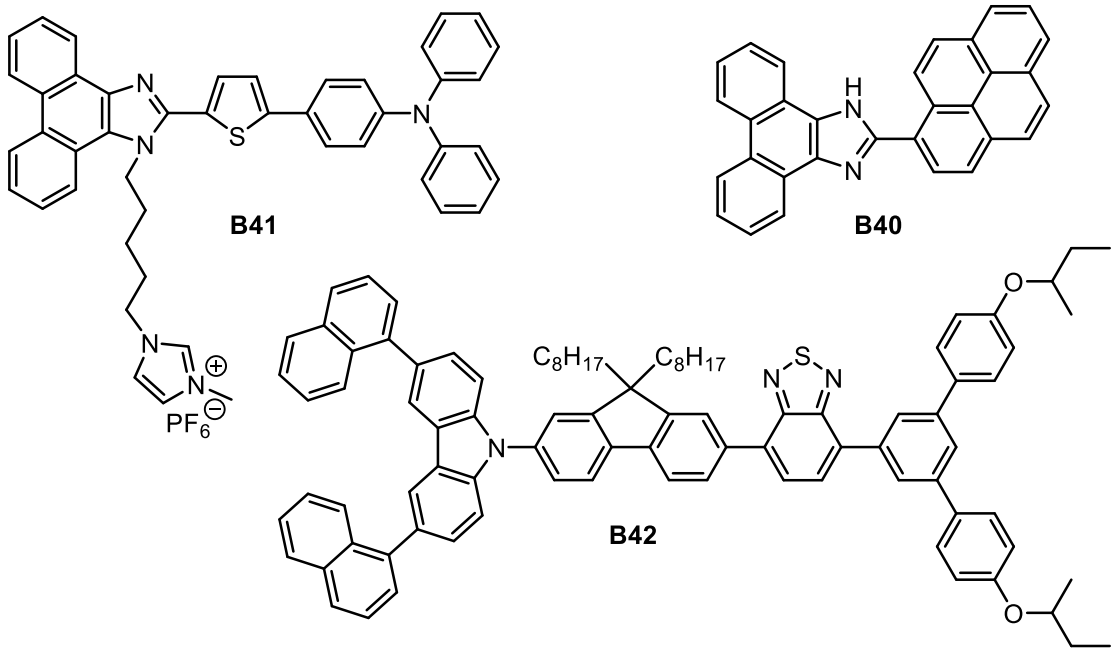

Figure 1.37. Structures of literature reported green emitting small molecules used in LEC devices.[213,215]

1.17 Conclusion

The work reported in this chapter concerned the synthesis and characterisation of a range of molecules based on the S and Se-doped anthanthrene structure. **PTXTX** was achieved in 45% yield through a triflic acid mediated cyclisation of sulfoxide **2**, followed by demethylation with pyridine. Several attempts at **PTXTX** derivatives bearing solubilising groups were made, which led to the successful synthesis of a soluble derivative bearing *n*-octyl chains – **25**. *N*-octyl chains were introduced through the Kumada coupling of bromo substituted thioether **23** with Grignard reagent in 70% yield. After quantitative oxidation to sulfoxide **24** and TfOH mediated cyclisation, compound **25** was achieved in 31% yield. Oxidation of **PTXTX** and **25** with H_2O_2 allowed the synthesis of monosulfoxides – **28** and **29** with 50 and 59% yield, respectively. Further oxidation led to disulfoxide **30** with 87% yield, and insoluble disulfone **31**. However, the presence of octyl chains in sulfone **32** led to a soluble derivative. We also demonstrated a novel intramolecular S_EAr reaction of selenoxides leading to Se-doped PAHs. Triflic

acid mediated cyclisation of selenoxides, followed by demethylation with pyridine, leads to the synthesis of selena heterocycles. We demonstrated that this reaction is suitable both for the formation of PAHs containing 6-membered (*peri*-selenoxanthenoselenoxanthene **36**) and 5-membered (dibenzoselenophene **40**) rings containing Se atom. All achieved compounds were studied through X-ray crystallography. Non-oxidised molecules (**PTXTX** and **25**), monosulfoxides (**28** and **29**), disulfoxide (**30**) and one polymorph of sulfone **32** (***anti*-32**) showed flat structures, with S atoms distorted out of the molecule's plane. However, molecules of sulfones **31** and polymorph ***syn*-32** showed bent structures, where naphthyl cores formed 157° and 159° angles, respectively. Photophysical studies of achieved molecules were conducted as well. Hypsochromic shift was observed with increased oxidation of molecules, with λ_{max} at 500 nm for **PTXTX** while for **28**, ***trans*-30**, and **32** bands lie at 458 nm, 414 nm and 399 nm, respectively. The photophysical and electrochemical properties of compound **36**, as well as its X-ray crystal structure, were demonstrated and compared to the S (**PTXTX**) and O (**PXX**) doped analogues. Molecule **36** crystallises with a similar crystal packing as **PTXTX** molecules in yellow plates polymorph. Compound **36** showed absorption and emission spectra like those of **PTXTX**, with the same λ_{max}, although without vibronic structure visible for **PTXTX**. As no phosphorescence was detected for compound **36**, the singlet oxygen sensitisation experiment is needed to assess the triplet population. Electrocrystallisation experiments were performed with **PTXTX** and **PXX** to test its potential as semiconducting material. Mixed valence crystals: $(\mathbf{PTXTX})_3(ClO_4)_2$ and $(\mathbf{PXX})_2(ClO_4)_1$ were obtained, and their conductivities were tested. The materials showed σ in order of 10^{-2} - 10^{-3} S cm^{-1} and 10^{-1} - 10^{-2} S cm^{-1} respectively, showing good semiconducting properties. Molecule **25** and **PXX** were employed in electrochemical cell (LEC) devices. Devices with emission bands at 537 nm and 494 nm, displaying maximum luminance of 17 and 75 cd m^{-2} were prepared using **25** and **PXX** as emitters, respectively.

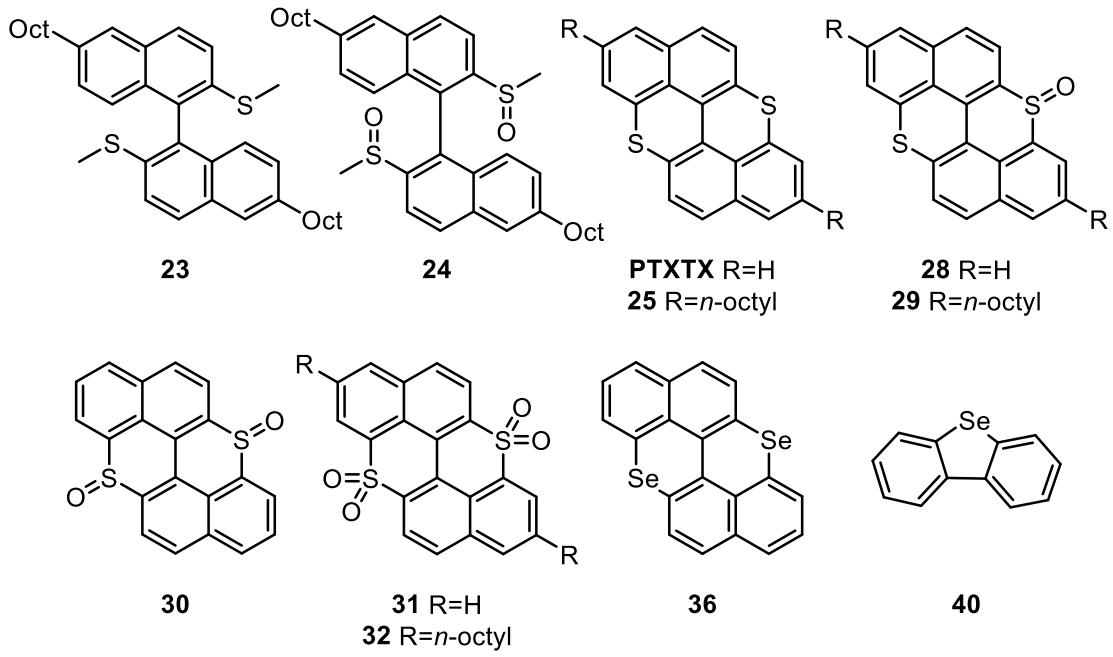

23 **24** **PTXTX** R=H **25** R=*n*-octyl **28** R=H **29** R=*n*-octyl

30 **31** R=H **32** R=*n*-octyl **36** **40**

1.18 Bibliography

[1] N. J. Turro, V. Ramamurthy, J. C. Scaiano, in *Modern Molecular Photochemistry of Organic Molecules*, University Science Books, California, **2010**, pp. 1–39.

[2] M. Orfanopoulos, *Photochem. Photobiol.* **2021**, *97*, 1182–1218.

[3] A. D. McNaught, A. Wilkinson, *IUPAC. Compendium of Chemical Terminology, 2nd Ed. (the "Gold Book").*, Blackwell Scientific Publications, Oxford, **1997**.

[4] T. Y. Ohulchanskyy, D. J. Donnelly, M. R. Detty, P. N. Prasad, *J. Phys. Chem. B* **2004**, *108*, 8668–8672.

[5] S. K. Tripathi, R. Kaur, in *Thermoelectricity and Advanced Thermoelectric Materials* (Eds.: R. Kumar, R. Singh), Woodhead Publishing, **2021**, pp. 195–231.

[6] F.-C. Chen, in *Encyclopedia of Modern Optics*, Elsevier, **2018**, pp. 220–231.

[7] Y. Zhang, X. Cai, Y. Bian, J. Jiang, in *Functional Phthalocyanine Molecular Materials* (Ed.: J. Jiang), Springer Berlin Heidelberg, Berlin, Heidelberg, **2010**, pp. 275–321.

[8] B. Lim, H. Sun, Y. Y. Noh, *Dyes Pigm.* **2017**, *142*, 17–23.

[9] Z. Bao, A. J. Lovinger, A. Dodabalapur, *Adv. Mater.* **1997**, *9*, 42–44.

[10] H. Z. Chen, M. M. Ling, X. Mo, M. M. Shi, M. Wang, Z. Bao, *Chem. Mater.* **2007**,

19, 816–824.

[11] S. K. Park, T. N. Jackson, J. E. Anthony, D. A. Mourey, *Appl. Phys. Lett.* **2007**, *91*, 3–5.

[12] T. Okamoto, C. P. Yu, C. Mitsui, M. Yamagishi, H. Ishii, J. Takeya, *J. Am. Chem. Soc.* **2020**, *142*, 9083–9096.

[13] G. Barbarella, L. Favaretto, G. Sotgiu, M. Zambianchi, A. Bongini, C. Arbizzani, M. Mastragostino, M. Anni, G. Gigli, R. Cingolani, *J. Am. Chem. Soc.* **2000**, *122*, 11971–11978.

[14] G. Turkoglu, M. E. Cinar, T. Ozturk, *Top. Curr. Chem.* **2017**, *375*, 1–45.

[15] Y. H. Jung, D. Karthik, H. Lee, J. H. Maeng, K. J. Yang, S. Hwang, J. H. Kwon, *ACS Appl. Mater. Interfaces* **2021**, *13*, 17882–17891.

[16] S. Tan, K. Jinnai, R. Kabe, C. Adachi, *Adv. Mater.* **2021**, *33*, 1–6.

[17] K. I. Sakai, T. Tsuzuki, Y. Itoh, M. Ichikawa, Y. Taniguchi, *Appl. Phys. Lett.* **2005**, *86*, 1–3.

[18] Y. Li, K. Wang, Q. Liao, L. Fu, C. Gu, Z. Yu, H. Fu, *Nano Lett.* **2021**, *21*, 3287–3294.

[19] A. Mishra, P. Bäuerle, *Angew. Chem. Int. Ed.* **2012**, *51*, 2020–2067.

[20] U. Bach, D. Lupo, P. Comte, J. E. Moser, F. Weissörtel, J. Salbeck, H. Spreitzer, M. Grätzel, *Nature* **1998**, *395*, 583–585.

[21] Y. Cai, Y. Li, R. Wang, H. Wu, Z. Chen, J. Zhang, Z. Ma, X. Hao, Y. Zhao, C. Zhang, F. Huang, Y. Sun, *Adv. Mater.* **2021**, *33*, 1–9.

[22] T. Osawa, T. Kajitani, D. Hashizume, H. Ohsumi, S. Sasaki, M. Takata, Y. Koizumi, A. Saeki, S. Seki, T. Fukushima, T. Aida, *Angew. Chem. Int. Ed.* **2012**, *51*, 7990–7993.

[23] R. Dhar, J. Ramakrishna, V. Nawani, P. K. Manda, D. Gupta, P. Venkatakrishnan, S. Dutta, *Synth. Met.* **2021**, *280*, 116883.

[24] P. Herwig, C. W. Kayser, K. Müllen, H. W. Spiess, *Adv. Mater.* **1996**, *8*, 510–513.

[25] A. Berezin, N. Biot, T. Battisti, D. Bonifazi, *Angew. Chem. Int. Ed.* **2018**, *57*, 8942–8946.

[26] C. Sutton, C. Risko, J. L. Brédas, *Chem. Mater.* **2016**, *28*, 3–16.

[27] G. Gryn'ova, C. Corminboeuf, *J. Phys. Chem. Lett.* **2016**, *7*, 5198–5204.

[28] R. Podeszwa, K. Szalewicz, *Phys. Chem. Chem. Phys.* **2008**, *10*, 2735.

[29] Y. Sun, L. Tan, S. Jiang, H. Qian, Z. Wang, D. Yan, C. Di, Y. Wang, W. Wu, G. Yu, S. Yan, C. Wang, W. Hu, Y. Liu, D. Zhu, *J. Am. Chem. Soc.* **2007**, *129*, 1882–1883.

[30] S. Zhang, X. Qiao, Y. Chen, Y. Wang, R. M. Edkins, Z. Liu, H. Li, Q. Fang, *Org. Lett.* **2014**, *16*, 342–345.

[31] L. Zöphel, D. Beckmann, V. Enkelmann, D. Chercka, R. Rieger, K. Müllen, *Chem. Commun.* **2011**, *47*, 6960–6962.

[32] R. Q. Lu, Y. N. Zhou, X. Y. Yan, K. Shi, Y. Q. Zheng, M. Luo, X. C. Wang, J. Pei, H. Xia, L. Zoppi, K. K. Baldridge, J. S. Siegel, X. Y. Cao, *Chem. Commun.* **2015**, *51*, 1681–1684.

[33] Y. Qiao, Z. Wei, C. Risko, H. Li, J. L. Brédas, W. Xu, D. Zhu, *J. Mater. Chem.* **2012**, *22*, 1313–1325.

[34] L. Chen, P. Xia, T. Du, Y. Deng, Y. Xiao, *Org. Lett.* **2019**, *21*, 5529–5532.

[35] L. Yang, N. Zhang, Y. Han, Y. Zou, Y. Qiao, D. Chang, Y. Zhao, X. Lu, J. Wu, Y. Liu, *Chem. Commun.* **2020**, *56*, 9990–9993.

[36] J. Gao, L. Li, Q. Meng, R. Li, H. Jiang, H. Li, W. Hu, *J. Mater. Chem.* **2007**, *17*, 1421–1426.

[37] C. Du, S. Ye, Y. Liu, Y. Guo, T. Wu, H. Liu, J. Zheng, C. Cheng, M. Zhu, G. Yu, *Chem. Commun.* **2010**, *46*, 8573–8575.

[38] S. H. Jeong, J. Y. Lee, *J. Mater. Chem.* **2011**, *21*, 14604–14609.

[39] S. C. Dong, L. Zhang, J. Liang, L. S. Cui, Q. Li, Z. Q. Jiang, L. S. Liao, *J. Phys. Chem. C* **2014**, *118*, 2375–2384.

[40] Y. Cai, C. Shi, H. Zhang, B. Chen, K. Samedov, M. Chen, Z. Wang, Z. Zhao, X. Gu, D. Ma, A. Qin, B. Z. Tang, *J. Mater. Chem. C* **2018**, *6*, 6534–6542.

[41] Z. S. Wu, Y. Z. Tan, S. Zheng, S. Wang, K. Parvez, J. Qin, X. Shi, C. Sun, X. Bao, X. Feng, K. Müllen, *J. Am. Chem. Soc.* **2017**, *139*, 4506–4512.

[42] J. Cao, Y. M. Liu, X. Jing, J. Yin, J. Li, B. Xu, Y. Z. Tan, N. Zheng, *J. Am. Chem.*

Soc. **2015**, *137*, 10914–10917.

[43] A. A. Gorodetsky, C. Y. Chiu, T. Schiros, M. Palma, M. Cox, Z. Jia, W. Sattler, I. Kymissis, M. Steigerwald, C. Nuckolls, *Angew. Chem. Int. Ed.* **2010**, *49*, 7909–7912.

[44] X. Li, H. Wang, H. Nakayama, Z. Wei, J. A. Schneider, K. Clark, W. Y. Lai, W. Huang, J. G. Labram, J. R. De Alaniz, M. L. Chabinyc, F. Wudl, Y. Zheng, *ACS Appl. Energy Mater.* **2019**, *2*, 3805–3814.

[45] H. Choi, S. Paek, J. Song, C. Kim, N. Cho, J. Ko, *Chem. Commun.* **2011**, *47*, 5509–5511.

[46] W. Fan, N. Liang, D. Meng, J. Feng, Y. Li, J. Hou, Z. Wang, *Chem. Commun.* **2016**, *52*, 11500–11503.

[47] X. Y. Wang, X. Yao, A. Narita, K. Müllen, *Acc. Chem. Res.* **2019**, *52*, 2491–2505.

[48] A. Narita, X. Y. Wang, X. Feng, K. Müllen, *Chem. Soc. Rev.* **2015**, *44*, 6616–6643.

[49] A. Nelson, in *Categ. 2, Hetarenes Relat. Ring Syst.* (Ed.: Thomas), Georg Thieme Verlag, Stuttgart, **2003**, pp. 787–816.

[50] M. Stępień, E. Gońka, M. Żyła, N. Sprutta, *Chem. Rev.* **2017**, *117*, 3479–3716.

[51] V. Albrow, K. Biswas, A. Crane, N. Chaplin, T. Easun, S. Gladiali, B. Lygo, S. Woodward, *Tetrahedron Asymmetry* **2003**, *14*, 2813–2819.

[52] M. Cavazza, M. Zandomeneghi, **1996**, *7863*, 9990–9991.

[53] W. Jiang, H. Qian, Y. Li, Z. Wang, *J. Org. Chem.* **2008**, *73*, 7369–7372.

[54] R. K. Gupta, B. Pradhan, S. K. Pathak, M. Gupta, S. K. Pal, A. Ammathnadu Sudhakar, *Langmuir* **2015**, *31*, 8092–8100.

[55] K. Yamamoto, E. Shouji, H. Nishide, E. Tsuchida, *J. Am. Chem. Soc.* **1993**, *115*, 5819–5820.

[56] E. Tsuchida, E. Shouji, K. Yamamotot, **1993**, *812*, 7144–7148.

[57] H. Sirringhaus, R. H. Friend, C. Wang, J. Leuninger, K. Müllen, *J. Mater. Chem.* **1999**, *9*, 2095–2101.

[58] A. Haryono, K. Miyatake, J. Natori, E. Tsuchida, *Macromolecules* **1999**, *32*,

3146–3149.

[59] C. Du, S. Ye, J. Chen, Y. Guo, Y. Liu, K. Lu, Y. Liu, T. Qi, X. Gao, Z. Shuai, G. Yu, *Chem. Eur. J.* **2009**, *15*, 8275–8282.

[60] P. Gao, D. Beckmann, H. N. Tsao, X. Feng, V. Enkelmann, W. Pisula, K. Müllen, *Chem. Commun.* **2008**, 1548.

[61] Y. Zhang, F. Peng, R. He, L. Ying, W. Yang, Y. Cao, *New J. Chem.* **2018**, *42*, 2750–2757.

[62] M. Tobisu, Y. Masuya, K. Baba, N. Chatani, *Chem. Sci.* **2016**, *7*, 2587–2591.

[63] J. Lander, E. Spietschka, *Process for Preparing Compounds of the Benzothioxanthene Series.*, **1974**, US3828072A.

[64] P. H. Grayshan, A. M. Kadhim, A. T. Perters, *J. Heterocycl. Chem.* **1974**, *11*, 33–38.

[65] X. Qian, Y. Li, Y. Xu, Y. Liu, B. Qu, *Bioorganic Med. Chem. Lett.* **2004**, *14*, 2665–2668.

[66] J. Kollar, Štefan Chmela, P. Hrdlovič, *J. Photochem. Photobiol. A Chem.* **2013**, *270*, 28–36.

[67] Q. Yang, P. Yang, X. Qian, L. Tong, *Bioorganic Med. Chem. Lett.* **2008**, *18*, 6210–6213.

[68] Y. Xu, X. Qian, W. Yao, P. Mao, J. Cui, *Bioorganic Med. Chem.* **2003**, *11*, 5427–5433.

[69] B. Wang, Y. Liu, C. Lin, Y. Xu, Z. Liu, Y. Zhang, *Org. Lett.* **2014**, *16*, 4574–4577.

[70] D. Wu, W. Pisula, M. C. Haberecht, X. Feng, K. Müllen, *Org. Lett.* **2009**, *11*, 5686–5689.

[71] C. Du, S. Ye, Y. Liu, Y. Guo, T. Wu, H. Liu, J. Zheng, C. Cheng, M. Zhu, G. Yu, *Chem. Commun.* **2010**, *46*, 8573–8575.

[72] S. Moon, Y. Nishii, M. Miura, *Org. Lett.* **2019**, *21*, 233–236.

[73] E. Si, P. Zhao, L. Wang, Z. Duan, F. Mathey, *Eur. J. Org. Chem.* **2020**, *2020*, 697–701.

[74] S. Zhang, X. Qiao, Y. Chen, Y. Wang, R. M. Edkins, Z. Liu, H. Li, Q. Fang, *Org. Lett.* **2014**, *16*, 342–345.

[75] K. Oyaizu, T. Mikami, F. Mitsuhashi, E. Tsuchida, *Macromolecules* **2002**, *35*, 67–78.

[76] S. Zhang, Z. Liu, Q. Fang, *Org. Lett.* **2017**, *19*, 1382–1385.

[77] C. Ruzié, J. Karpinska, A. R. Kennedy, Y. H. Geerts, *J. Org. Chem.* **2013**, *78*, 7741–7748.

[78] T. Yamamoto, K. Takimiya, *J. Am. Chem. Soc.* **2007**, *129*, 2224–2225.

[79] K. Niimi, S. Shinamura, I. Osaka, E. Miyazaki, K. Takimiya, *J. Am. Chem. Soc.* **2011**, *133*, 8732–8739.

[80] R. K. Norris, J. A. McMahon, *Arkivoc* **2003**, *2003*, 139–155.

[81] B. Janhsen, C. G. Daniliuc, A. Studer, *Chem. Sci.* **2017**, *8*, 3547–3553.

[82] N. F. Nikitas, P. L. Gkizis, C. G. Kokotos, *Org. Biomol. Chem.* **2021**, *19*, 5237–5253.

[83] I. Okabayashi, M. Kimura, H. Fujiwara, A. Kato, *Chem. Pharm. Bull.* **1987**, *35*, 2545–2549.

[84] A. M. Paiva, M. M. Pinto, E. Sousa, *Curr. Med. Chem.* **2013**, *20*, 2438–2457.

[85] K. Kobayashi, T. Komatsu, K. Nakagawa, E. Hara, S. Yuba, *Heterocycles* **2013**, *87*, 2577–2587.

[86] P. M. Donovan, L. T. Scott, *J. Am. Chem. Soc.* **2004**, *126*, 3108–3112.

[87] G. Jianhua, Q. Zhao, *Naphtho-Thioxanthene Derivative as Well as Preparation Method and Application Thereof*, **2017**, CN106349212A.

[88] V. M. Hertz, J. G. Massoth, M. Bolte, H. W. Lerner, M. Wagner, *Chem. Eur. J.* **2016**, *22*, 13181–13188.

[89] R. Kwong, B. Ma, C. Xia, C. Lin, *Organoselenium Materials and Their Uses in Organic Light Emitting Devices*, **2010**, US20100072887A1.

[90] W. Yeager, L. Zeng, C. Xia, *Organic Electroluminescent Materials and Devices*, **2016**, US20160329503 A1.

[91] A. Petrenko, K. Leitonas, D. Volyniuk, G. V. Baryshnikov, S. Belyakov, B. F. Minaev, H. Ågren, H. Durgaryan, J. V. Gražulevičius, P. Arsenyan, *Dalt. Trans.* **2020**, *49*, 3393–3397.

[92] A. K. Mohanakrishnan, N. Senthil Kumar, P. Amaladass, *Tetrahedron Lett.* **2008**, *49*, 4792–4795.

[93] K. Takimiya, Y. Kunugi, Y. Konda, H. Ebata, Y. Toyoshima, T. Otsubo, *J. Am. Chem. Soc.* **2006**, *128*, 3044–3050.

[94] S. Shi, L. Tang, H. Guo, M. A. Uddin, H. Wang, K. Yang, B. Liu, Y. Wang, H. Sun, H. Y. Woo, X. Guo, *Macromolecules* **2019**, *52*, 7301–7312.

[95] H. Kong, Y. K. Jung, N. S. Cho, I. N. Kang, J. H. Park, S. Cho, H. K. Shim, *Chem. Mater.* **2009**, *21*, 2650–2660.

[96] H. A. Staab, M. Höne, C. Krieger, *Tetrahedron Lett.* **1988**, *29*, 1905–1908.

[97] J. S. Wu, S. W. Cheng, Y. J. Cheng, C. S. Hsu, *Chem. Soc. Rev.* **2015**, *44*, 1113–1154.

[98] K. Ramki, N. Venkatesh, G. Sathiyan, R. Thangamuthu, P. Sakthivel, *Org. Electron.* **2019**, *73*, 182–204.

[99] M. W. Kryman, K. S. Davies, M. K. Linder, T. Y. Ohulchanskyy, M. R. Detty, *Bioorganic Med. Chem.* **2015**, *23*, 4501–4507.

[100] K. S. Davies, M. K. Linder, M. W. Kryman, M. R. Detty, *Bioorganic Med. Chem.* **2016**, *24*, 3908–3917.

[101] M. W. Kryman, G. A. Schamerhorn, J. E. Hill, B. D. Calitree, K. S. Davies, M. K. Linder, T. Y. Ohulchanskyy, M. R. Detty, *Organometallics* **2014**, *33*, 2628–2640.

[102] M. Chiba, Y. Ichikawa, M. Kamiya, T. Komatsu, T. Ueno, K. Hanaoka, T. Nagano, N. Lange, Y. Urano, *Angew. Chem. Int. Ed.* **2017**, *56*, 10418–10422.

[103] J. E. Hill, M. K. Linder, K. S. Davies, G. A. Sawada, J. Morgan, T. Y. Ohulchanskyy, M. R. Detty, *J. Med. Chem.* **2014**, *57*, 8622–8634.

[104] L.-W. Shen, M.-Q. Qian, K. Yu, S. Narva, F. Yu, Y.-L. Wu, W. Zhang, *Sci. Rep.* **2020**, *10*, 7635.

[105] M. Wang, Q. Fan, X. Jiang, *Org. Lett.* **2016**, *18*, 5756–5759.

[106] X. Zhang, X. B. Huang, W. X. Gao, Y. B. Zhou, M. C. Liu, H. Y. Wu, *Adv. Synth. Catal.* **2020**, *362*, 5639–5644.

[107] X. Zhang, X. B. Huang, Y. B. Zhou, M. C. Liu, H. Y. Wu, *Chem. Eur. J.* **2021**, *27*, 944–948.

[108] P. J. Murphy, in *Categ. 2, Hetarenes Relat. Ring Syst.* (Ed.: E.J. Thomas), Georg Thieme Verlag, Stuttgart, **2000**, pp. 307–323.

[109] M. Milen, T. Szabó, *Chem. Heterocycl. Compd.* **2019**, *55*, 936–938.

[110] V. P. Litvinov, V. D. Dyachenko, *Russ. Chem. Rev.* **1997**, *66*, 923–951.

[111] P. S. Hellwig, T. J. Peglow, F. Penteado, L. Bagnoli, G. Perin, E. J. Lenardão, *Molecules* **2020**, *25*, 5907.

[112] J. D. McCullough, T. W. Campbell, E. S. Gould, *J. Am. Chem. Soc.* **1950**, *72*, 5753–5754.

[113] K. Nishino, Y. Ogiwara, N. Sakai, *Eur. J. Org. Chem.* **2017**, *2017*, 5892–5895.

[114] K. Nishino, Y. Ogiwara, N. Sakai, *Chem. Eur. J.* **2018**, *24*, 10971–10974.

[115] P. Franzmann, S. B. Beil, D. Schollmeyer, S. R. Waldvogel, *Chem. Eur. J.* **2019**, *25*, 1936–1940.

[116] W. Li, G. Xiao, G. Deng, Y. Liang, *Org. Chem. Front.* **2018**, *5*, 1488–1492.

[117] B. Wu, N. Yoshikai, *Angew. Chem. Int. Ed.* **2015**, *54*, 8736–8739.

[118] Y. Jiang, Y. Qin, S. Xie, X. Zhang, J. Dong, D. Ma, *Org. Lett.* **2009**, *11*, 5250–5253.

[119] H. Suzuki, T. Nakamura, T. Sakaguchi, K. Ohta, *J. Org. Chem.* **1995**, *60*, 5274–5278.

[120] V. H. K. Fell, A. Mikosch, A. K. Steppert, W. Ogieglo, E. Senol, D. Canneson, M. Bayer, F. Schoenebeck, A. Greilich, A. J. C. Kuehne, *Macromolecules* **2017**, *50*, 2338–2343.

[121] L. Engman, *J. Heterocycl. Chem.* **1984**, *21*, 413–416.

[122] S. Murata, T. Suzuki, A. Yanagisawa, S. Suga, *J. Heterocycl. Chem.* **1991**, *28*, 433–438.

[123] S. M. Rafiq, R. Sivasakthikumaran, A. K. Mohanakrishnan, *Org. Lett.* **2014**, *16*, 2720–2723.

[124] M. Elsherbini, W. S. Hamama, H. H. Zoorob, *Coord. Chem. Rev.* **2017**, *330*, 110–126.

[125] M. W. Kryman, J. N. Nasca, D. F. Watson, M. R. Detty, *Langmuir* **2016**, *32*,

1521–1532.

[126] J. L. Clark, J. E. Hill, I. D. Rettig, J. J. Beres, R. Ziniuk, T. Y. Ohulchanskyy, T. M. McCormick, M. R. Detty, *Organometallics* **2019**, *38*, 2431–2442.

[127] W. Lv, S. Chi, W. Feng, T. Liang, D. Song, Z. Liu, *Chem. Commun.* **2019**, *55*, 7037–7040.

[128] G. Doddi, G. Ercolani, in *Six-Membered Hetarenes with One Chalcogen*, Georg Thieme Verlag KG, **1994**, pp. 65–195.

[129] J. Fernández-Lodeiro, M. F. Pinatto-Botelho, A. A. Soares-Paulino, A. C. Gonçalves, B. A. Sousa, C. Princival, A. A. Dos Santos, *Dyes Pigm.* **2014**, *110*, 28–48.

[130] P. J. Murphy, in *Categ. 2, Hetarenes Relat. Ring Syst.* (Ed.: Thomas), Georg Thieme Verlag, Stuttgart, **2003**, pp. 817–854.

[131] N. Nagahora, T. Kushida, K. Shioji, K. Okuma, *Organometallics* **2019**, *38*, 1800–1808.

[132] S. Wang, H. Shu, X. Han, X. Wu, H. Tong, L. Wang, *J. Mater. Chem. C* **2021**, *9*, 9907–9913.

[133] D. De Sa Pereira, D. R. Lee, N. A. Kukhta, K. H. Lee, C. L. Kim, A. S. Batsanov, J. Y. Lee, A. P. Monkman, *J. Mater. Chem. C* **2019**, *7*, 10481–10490.

[134] L. W. Shen, M. Q. Qian, K. Yu, S. Narva, F. Yu, Y. L. Wu, W. Zhang, *Sci. Rep.* **2020**, *10*, 1–12.

[135] P. J. Murphy, in *Categ. 2, Hetarenes Relat. Ring Syst.* (Ed.: Thomas), Georg Thieme Verlag, Stuttgart, **2003**, pp. 855–879.

[136] A. Mandal, S. Dana, H. Sahoo, G. S. Grandhi, M. Baidya, *Org. Lett.* **2017**, *19*, 2430–2433.

[137] N. K. Brennan, D. J. Donnelly, M. R. Detty, *J. Org. Chem.* **2003**, *68*, 3344–3347.

[138] D. J. Del Valle, D. J. Donnelly, J. J. Holt, M. R. Detty, *Organometallics* **2005**, *24*, 3807–3810.

[139] A. Dari, L. E. Christiaens, M. J. Renson, T. A. Pakkanen, J. C. Négrel, M. Chanon, C. Striley, J. Weidlein, A. Nasiri, Y. Okada, *Acta Chem. Scand.* **1993**, *47*, 208–211.

[140] T. Umemoto, S. Ishihara, *J. Am. Chem. Soc.* **1993**, *115*, 2156–2164.

[141] W. Fudickar, T. Linker, *J. Am. Chem. Soc.* **2012**, *134*, 15071–15082.

[142] J. B. Giguère, N. S. Sariciftci, J. F. Morin, *J. Mater. Chem. C* **2015**, *3*, 601–606.

[143] C. Aumaitre, J. F. Morin, *Chem. Rec.* **2019**, *19*, 1142–1154.

[144] Y. Du, H. B. Lovell, F. Lirette, J. F. Morin, K. N. Plunkett, *J. Org. Chem.* **2021**, *86*, 1456–1461.

[145] L. Zhang, B. Walker, F. Liu, N. S. Colella, S. C. B. Mannsfeld, J. J. Watkins, T. Q. Nguyen, A. L. Briseno, *J. Mater. Chem.* **2012**, *22*, 4266–4268.

[146] J. B. Giguère, J. Boismenu-Lavoie, J. F. Morin, *J. Org. Chem.* **2014**, *79*, 2404–2418.

[147] Z. Wang, R. Li, Y. Chen, Y. Z. Tan, Z. Tu, X. J. Gao, H. Dong, Y. Yi, Y. Zhang, W. Hu, K. Müllen, L. Chen, *J. Mater. Chem. C* **2017**, *5*, 1308–1312.

[148] T. Delouche, G. Taifour, M. Cordier, T. Roisnel, D. Tondelier, P. Manzhi, B. Geffroy, B. Le Guennic, D. Jacquemin, M. Hissler, P. A. Bouit, *Chem. Commun.* **2022**, *58*, 88–91.

[149] C. Valentini, Tailoring Optoelectronic Properties of Anthanthrene through O- , S- , and N-Doping, Cardiff University, **2019**.

[150] J. M. Farrell, C. Mützel, D. Bialas, M. Rudolf, K. Menekse, A. M. Krause, M. Stolte, F. Würthner, *J. Am. Chem. Soc.* **2019**, *141*, 9096–9104.

[151] K. Takaishi, S. Hinoide, T. Matsumoto, T. Ema, *J. Am. Chem. Soc.* **2019**, *141*, 11852–11857.

[152] N. Lv, M. Xie, W. Gu, H. Ruan, S. Qiu, C. Zhou, Z. Cui, *Org. Lett.* **2013**, *15*, 2382–2385.

[153] A. Sciutto, A. Fermi, A. Folli, T. Battisti, J. M. Beames, D. M. Murphy, D. Bonifazi, *Chem. Eur. J.* **2018**, *24*, 4382–4389.

[154] D. Stassen, N. Demitri, D. Bonifazi, *Angew. Chem. Int. Ed.* **2016**, *55*, 5947–5951.

[155] T. Miletić, A. Fermi, I. Orfanos, A. Avramopoulos, F. De Leo, N. Demitri, G. Bergamini, P. Ceroni, M. G. Papadopoulos, S. Couris, D. Bonifazi, *Chem. Eur. J.* **2017**, *23*, 2363–2378.

[156] R. Pummerer, E. Prell, A. Rieche, *Berichte der Dtsch. Chem. Gesellschaft (A B Ser.* **1926**, *59*, 2159–2161.

[157] T. Asari, N. Kobayashi, T. Naito, T. Inabe, *Bull. Chem. Soc. Jpn.* **2001**, *74*, 53–58.

[158] N. Lv, M. Xie, W. Gu, H. Ruan, S. Qiu, C. Zhou, Z. Cui, *Org. Lett.* **2013**, *15*, 2382–2385.

[159] T. Kamei, M. Uryu, T. Shimada, *Org. Lett.* **2017**, *19*, 2714–2717.

[160] N. Kobayashi, M. Sasaki, K. Nomoto, *Chem. Mater.* **2009**, *21*, 552–556.

[161] H. Li, F. Zhang, S. Qiu, N. Lv, Z. Zhao, Q. Li, Z. Cui, *Chem. Commun.* **2013**, *49*, 10492–10494.

[162] A. Sciutto, A. Berezin, M. Lo Cicero, T. Miletić, A. Stopin, D. Bonifazi, *J. Org. Chem.* **2018**, *83*, 13787–13798.

[163] A. Sciutto, A. Fermi, A. Folli, T. Battisti, J. M. Beames, D. M. Murphy, D. Bonifazi, *Chem. Eur. J.* **2018**, *24*, 4382–4389.

[164] L. Đorđević, C. Valentini, N. Demitri, C. Mézière, M. Allain, M. Sallé, A. Folli, D. Murphy, S. Mañas-Valero, E. Coronado, D. Bonifazi, *Angew. Chem. Int. Ed.* **2020**, *59*, 4106–4114.

[165] J. Fletcher-Charles, R. R. Ferreira, M. Abraham, D. Romito, M. Oppel, L. González, D. Bonifazi, *Eur. J. Org. Chem.* **2022**, *2022*, DOI 10.1002/ejoc.202101166.

[166] J. Yuan, Z. Xu, M. O. Wolf, *Chem. Sci.* **2022**, 5447–5464.

[167] A. Wigglesworth, Y. Wu, P. Liu, *Semiconductor Compound*, **2015**, US 9,123,902 B2.

[168] A. Zheng, M. Ren, Y. Zhang, Y. Cai, J. Zhang, Y. Yuan, M. Lei, P. Wang, *ACS Mater. Lett.* **2020**, *2*, 691–698.

[169] K. I. Salokhiddinov, I. M. Byteva, G. P. Gurinovich, *J. Appl. Spectrosc.* **1981**, *34*, 561–564.

[170] V. G. Nenaidenko, E. S. Balenkova, *Russ. J. Org. Chem.* **2003**, *39*, 291–330.

[171] V. B. Pandya, M. R. Jain, B. V. Chaugule, J. S. Patel, B. M. Parmar, J. K. Joshi, P. R. Patel, *Synth. Commun.* **2012**, *42*, 497–505.

[172] D. M. Chen, S. Wang, H. X. Li, X. Z. Zhu, C. H. Zhao, *Inorg. Chem.* **2014**, *53*, 12532–12539.

[173] J. A. Fernández-Salas, A. P. Pulis, D. J. Procter, *Chem. Commun.* **2016**, *52*, 12364–12367.

[174] T. Shoji, J. Higashi, S. Ito, K. Toyota, T. Asao, M. Yasunami, K. Fujimori, N. Morita, *Eur. J. Org. Chem.* **2008**, 1242–1252.

[175] S. Yoshida, H. Yorimitsu, K. Oshima, *Org. Lett.* **2007**, *9*, 5573–5576.

[176] D. Vasu, J. N. Hausmann, H. Saito, T. Yanagi, H. Yorimitsu, A. Osuka, *Asian J. Org. Chem.* **2017**, *6*, 1390–1393.

[177] D. Vasu, H. Yorimitsu, A. Osuka, *Angew. Chem. Int. Ed.* **2015**, *54*, 7162–7166.

[178] K. Jong-Woo, H. Seok-Hwan, K. Young-Kook, J. Hye-Jin, P. Jun-Ha, L. Eun-Young, L. Jin-O, H. Sang-Hyun, K. Kwang-Hyun, J. Eun-Jae, K. Soo-Yon, *Condensed Cyclic Compound and Organic Light-Emitting Device Including the Same*, **2017**, US 9,601,700 B2.

[179] H. He, L.-Y. Chen, W.-Y. Wong, W.-H. Chan, A. W. M. Lee, *Eur. J. Org. Chem.* **2010**, *2010*, 4181–4184.

[180] C. N. Yiannios, J. V. Karabinos, *J. Org. Chem.* **1963**, *28*, 3246–3248.

[181] T. J. Wallace, *J. Am. Chem. Soc.* **1964**, *86*, 2018–2021.

[182] T. Guo, H. Wang, *Synlett* **2017**, *28*, 1845–1851.

[183] T. Yamamoto, K. Takimiya, *J. Am. Chem. Soc.* **2007**, *129*, 2224–2225.

[184] J. E. Rice, Z. W. Cai, *J. Org. Chem.* **1993**, *58*, 1415–1424.

[185] G. A. Olah, *Increasing the Octane Number of Natural Gasoline with Trifluoromethanesulfonicacid*, **1985**, US4508618A.

[186] G. A. Olah, G. K. S. Prakash, A. Molnár, J. Sommer, in *Superacid Chem.*, Wiley, **1985**, pp. 524–539.

[187] N. A. Romero, D. A. Nicewicz, *Chem. Rev.* **2016**, *116*, 10075–10166.

[188] I. K. Sideri, E. Voutyritsa, C. G. Kokotos, *Org. Biomol. Chem.* **2018**, *16*, 4596–4614.

[189] M. M. Ali, S. Sana, Tasneem, K. C. Rajanna, P. K. Saiprakash, *Synth. Commun.*

2002, *32*, 1351–1356.

[190] J. Y. Hu, A. Paudel, T. Yamato, *J. Chem. Res.* **2009**, 109–113.

[191] M. G. Cabiddu, S. Cabiddu, E. Cadoni, S. De Montis, C. Fattuoni, S. Melis, *Tetrahedron* **2004**, *60*, 3915–3920.

[192] T. Kliś, J. Serwatowski, G. Wesela-Bauman, M. Zadrozna, *Tetrahedron Lett.* **2010**, *51*, 1685–1689.

[193] L. Duan, H. Fan, C. Huang, D. Hang, X. Liang, Z. Li, Z. Cao, Y. Liu, Q. Ban, J. Li, H. Zhonglin, L. Hu Jianjun, *OLED Material and Application Thereof in Organic Electroluminescent Device*, **2020**, CN111039955A.

[194] Y. Y. Rusakov, I. L. Rusakova, *Int. J. Quantum Chem.* **2019**, *119*, e25809.

[195] Z. Cai, M. A. Awais, N. Zhang, L. Yu, *Chem* **2018**, *4*, 2538–2570.

[196] H. Ebata, E. Miyazaki, T. Yamamoto, K. Takimiya, *Org. Lett.* **2007**, *9*, 4499–4502.

[197] L. DUAN, H. FAN, C. HUANG, D. HANG, X. LIANG, Z. LI, Z. CAO, Y. LIU, Q. BAN, J. LI, Z. LUO, J. HU, *Preparation of OLED Material as Host Material in Organic Electroluminescent Device*, **2020**, CN 111087407 A.

[198] R. Thakuria, N. K. Nath, B. K. Saha, *Cryst. Growth Des.* **2019**, *19*, 523–528.

[199] E. M. Cabaleiro-Lago, J. Rodríguez-Otero, *ACS Omega* **2018**, *3*, 9348–9359.

[200] C. Janiak, *J. Chem. Soc. Dalt. Trans.* **2000**, 3885–3896.

[201] T. Steiner, *Implic. Mol. Mater. Struct. New Technol.* **1999**, 185–196.

[202] K. D. M. Harris, *Supramol. Chem.* **2007**, *19*, 47–53.

[203] A. Bondi, *J. Phys. Chem.* **1964**, *68*, 441–451.

[204] L. Pauling, in *The Nature of the Chemical Bond*, Cornell University Press, Ithaca, NY, **1960**, p. 260.

[205] M. Kasha, *J. Chem. Phys.* **1952**, *20*, 71–74.

[206] Y. Rio, G. Accorsi, H. Nierengarten, C. Bourgogne, J. M. Strub, A. Van Dorsselaer, N. Armaroli, J. F. Nierengarten, *Tetrahedron* **2003**, *59*, 3833–3844.

[207] C. Würth, M. Grabolle, J. Pauli1, M. Spieles1, U. Resch-Genger1, *Nat. Protoc.* **2013**, *8*, 1535–1550.

[208] K. Suzuki, A. Kobayashi, S. Kaneko, K. Takehira, T. Yoshihara, H. Ishida, Y. Shiina, S. Oishi, S. Tobita, *Phys. Chem. Chem. Phys.* **2009**, *11*, 9850.

[209] A. Kremer, C. Aurisicchio, F. De Leo, B. Ventura, J. Wouters, N. Armaroli, A. Barbieri, D. Bonifazi, *Chem. Eur. J.* **2015**, *21*, 15377–15387.

[210] I. Noviandri, K. N. Brown, D. S. Fleming, P. T. Gulyas, P. A. Lay, A. F. Masters, L. Phillips, *J. Phys. Chem. B* **1999**, *103*, 6713–6722.

[211] O. Matuszewska, T. Battisti, R. R. Ferreira, N. Biot, N. Demitri, C. Mézière, M. Allain, M. Sallé, S. Mañas-Valero, E. Coronado, E. Fresta, R. D. Costa, D. Bonifazi, *Chem. – A Eur. J.* **2022**, DOI 10.1002/chem.202203115.

[212] E. Fresta, R. D. Costa, *J. Mater. Chem. C* **2017**, *5*, 5643–5675.

[213] S. Kanagaraj, A. Puthanveedu, Y. Choe, *Adv. Funct. Mater.* **2020**, *30*, 1907126.

[214] K. Shanmugasundaram, J. C. John, S. Chitumalla, J. Jang, Y. Choe, *Org. Electron.* **2019**, *67*, 141–145.

[215] K. Shanmugasundaram, H. Been, J. C. John, A. Puthanveedu, N. N. T. Pharm, S. G. Lee, Y. Choe, *New J. Chem.* **2021**, *45*, 19338–19346.

[216] E. Fresta, J. Dosso, J. Cabanillas-Gonzalez, D. Bonifazi, R. D. Costa, *ACS Appl. Mater. Interfaces* **2020**, *12*, 28426–28434.

Chapter 2

PXX as a photocatalyst for aryl-aryl coupling reactions

This chapter describes PXX photoredox catalysed aryl-aryl couplings of aryl halides. It is divided in five main sections: *i)* section 3.1 gives a general introduction on photoredox catalysis; *ii)* section 3.2 is a short introduction on PXX as a photoredox catalyst; *iii)* section 3.3 describes intermolecular PXX photoredox catalysed aryl-aryl coupling of aryl halides; *iv)* section 3.4 gives an introduction on the synthesis of PAHs; *v)* section 3.5 describes the PXX photoredox catalysed cyclisation of aryl chlorides leading to triphenylenes and tetraphenylene, *vi)* section 3.6 concludes the Chapter.

The research work described in section 3.3 was performed in collaboration with *Dr Cristofer Pezzetta* (*Cardiff University, School of Chemistry, Cardiff* and *Dr. Reddy's Laboratories, Cambridge*) who performed experiments leading to compounds **42**, **48**, **49** and **51**. The results were published in the following article:

C. Pezzetta, A. Folli, O. Matuszewska, D. Murphy, R. W. M. Davidson, D. Bonifazi, *Adv. Synth. Catal.* **2021**, *363*, 4740–4753.

The research work described in section 3.4 was performed in collaboration with *Dr Grazia Bezzu* (*Cardiff University, School of Chemistry*), who performed experiments leading to compounds **70** and **73**.

The X-ray analysis presented in this chapter has been performed by *Dr Benson Kariuki* (*Cardiff University, School of Chemistry, Cardiff*).

2.1 Introduction on photoredox catalysis

2.1.1 Photoredox catalysis

Most organic molecules are able only to absorb UV and not visible light. Due to its high energy, the use of UV light can lead to the breaking of multiple bonds and degradation of organic molecules, so photocatalysts able to absorb visible light are used instead. After IUPAC "Gold Book" a photocatalyst is *"able to produce, upon absorption of light, chemical transformations of the reaction partners. The excited state of the photocatalyst repeatedly interacts with the reaction partners forming reaction intermediates and regenerates itself after each cycle of such interactions."*[1] Photocatalysts that work based on electron transfer are called photoredox catalysts, and they exploit enhanced redox properties of photocatalysts in their excited state. Promotion of an electron, from the highest occupied molecular orbital (HOMO) to the lowest unoccupied molecular orbital (LUMO), lowers the ionisation potential (IP) of a molecule, and increases its electron affinity (EA). It means that removing one electron from the half-filled former LUMO, of a given excited state, is less endothermic (energetically favourable) than removing it from the filled HOMO of the ground state. Similarly, adding an electron to the half-full former HOMO of an excited state molecule is more exothermic than adding it to the empty LUMO. This leads to the fact that molecules at their excited state become more oxidising and reducing than at the ground state.

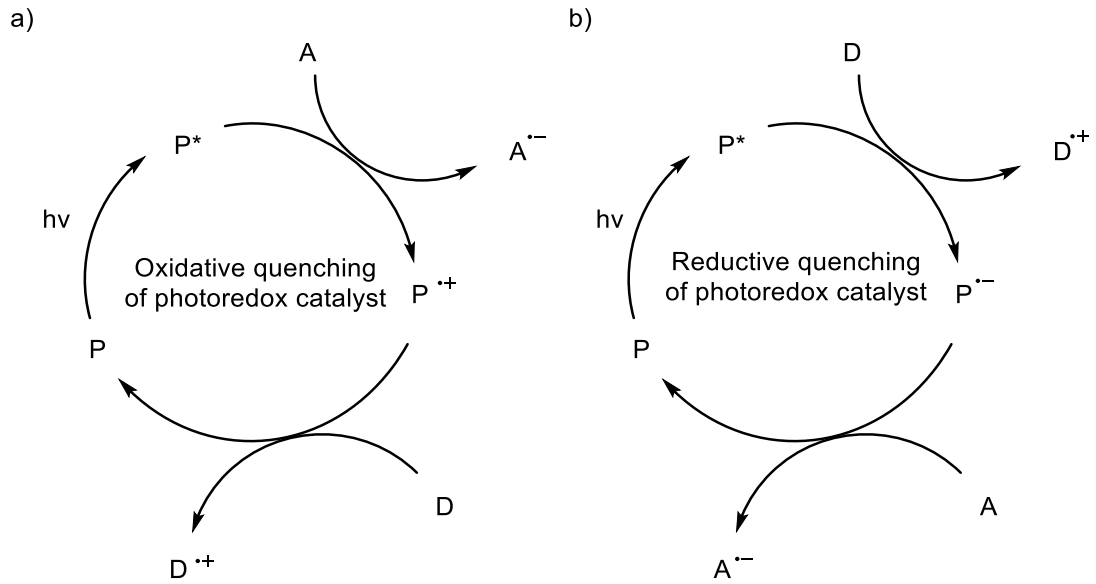

Scheme 2.1. a) Oxidative and b) reductive quenching photocatalytic cycles. P – photoredox catalyst, P* - excited state of a photoredox catalyst. A – electron acceptor, D – electron donor.[2]

An excited state photoredox catalyst (P*) can undergo either an oxidative or a reductive quenching (Scheme 2.1). In the oxidative quenching mechanism, P* is oxidised to the radical cation intermediate ($P^{\bullet+}$) by an electron acceptor (A), which can be a substrate or a sacrificial oxidant. Then the photoredox catalyst (P) is regenerated through the reduction of $P^{\bullet+}$ by an electron donor (D), which can either be a substrate or a sacrificial reductant. In the reductive quenching path, an excited state catalyst (P*) is reduced to a radical anion ($P^{\bullet-}$) by D, a substrate or a sacrificial reductant. The photoredox cycle is closed through an oxidation of $P^{\bullet-}$ back to P by A, a substrate or a sacrificial oxidant.[2]

2.1.2 Important photoredox catalysed reactions

Traditionally, radical chemistry needed high temperature, UV light or initiators to start the reactions. These conditions often led to poor selectivity and low yields. It takes advantage of radical chemistry while using mild conditions, *i.e.* visible light at room temperature, and can be considered environmentally friendly, particularly when organic chromophores are used as catalysts. Photoredox catalysis allows for late state functionalisation, which can be especially useful in pharmaceutical chemistry.[2–5] Since the seminal works by the groups of Yoon,[6] MacMillan[7] and Stephenson,[8] photoredox catalysis has been growing more and more popular. These works will be shortly described here.

Group of MacMillan reported asymmetric alfa-alkylation of aldehydes **C1**, with electron deficient alkyl bromide **C2** (Scheme 2.2).[7] $Ru(bpy)_3Cl_2$ was used as a photoredox catalyst, while imidazolidinone **C4** was used as an organocatalyst. Aldehydes with different substituents, such as alkyl chains **C5**, cyclic alkanes **C6** and benzyls **C7** could be coupled. Different electron efficient bromides were used, which gave malonates (**C5-C7**), 4-methoxyaroyl (**C8**), fluorinated ester (**C9**) and tertiary ester (**C10**). High yields (70-93%) and ee (90-99%) were achieved. The proposed reaction mechanism includes dual organocatalysis and photoredox catalysis (Scheme 2.2). In the initiation step excited state $Ru(bpy)_3^{2+*}$ can be reduced by a sacrificial amount of an enamine, resulting in the formation of $Ru(bpy)_3^{+}$. This species is capable of reducing electron deficient bromide **C2**, leading to the formation of a radical **A** and to the regeneration of the $Ru(bpy)_3^{2+}$. The organocatalytic cycle starts with the condensation of the chiral imidazolidinone **C4** with the aldehyde **C1** to form an enamine. The addition of the radical **A** to the enamine leads to the formation of a new radical **B**. SET oxidation of **B** with $Ru(bpy)_3^{2+*}$ gives iminium ion, and its hydrolysis delivers the enantioenriched α-alkylated aldehyde product **C3**.

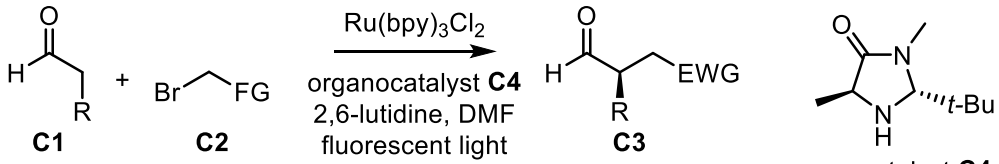

Selected examples:

Diethyl bromomalonate as bromide

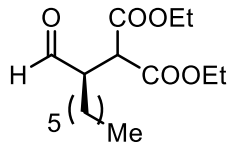

C5 93% yield, 90% ee

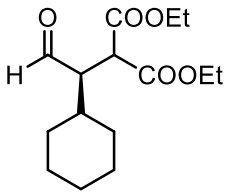

C6 83% yield, 95% ee

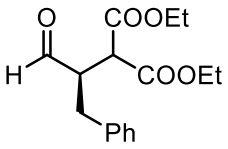

C7 92% yield, 90% ee

Octanal as an aldehyde

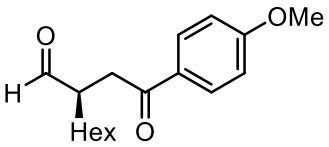

C8 87% yield, 96% ee

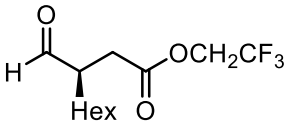

C9 80% yield, 92% ee

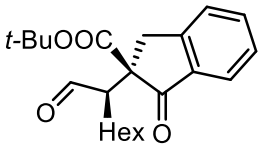

C10 70% yield, 5:1 dr, 99% ee

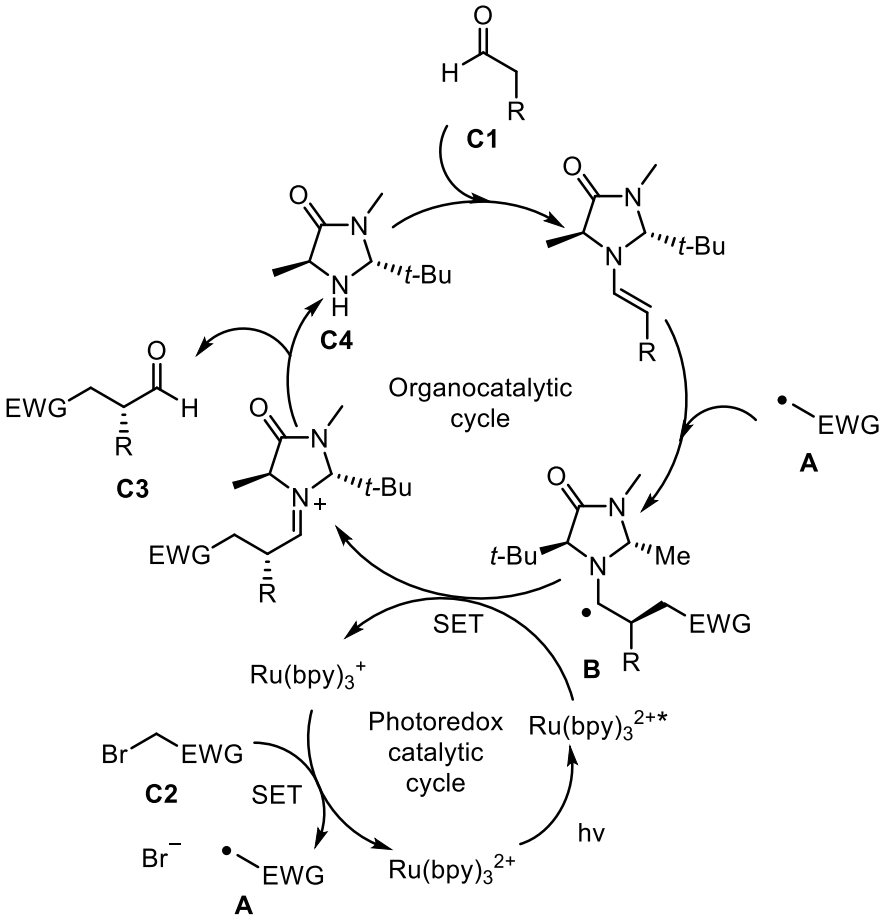

Scheme 2.2. Asymmetric α-alkylation of aldehydes, and proposed reaction mechanism.[7]

Group of Yoon reported photoredox catalysed [2+2] cycloaddition of bisenones **C11** to cyclobutane containing products **C12** (Scheme 2.3).[6]

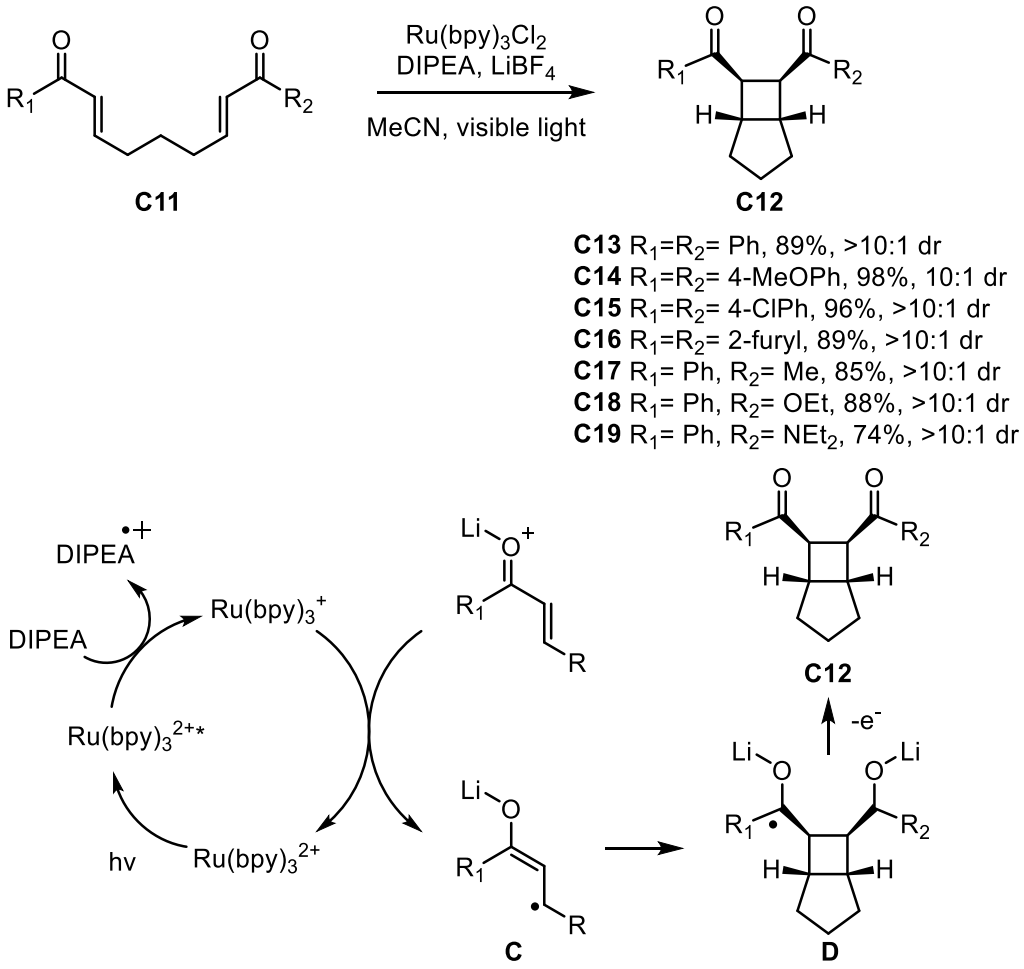

Scheme 2.3. Photoredox catalysed [2+2] enone cycloadditions.[6]

Various substituents were well tolerated on enone, giving high yields (74-98%) and diastereoselectivities (>10:1). Groups such as 4-MeOPh **C14**, 2-ClPh **C15**, Me **C17** and OEt **C18** were included in the structure, but at least one aryl group was needed for the reaction to occur. In the proposed reaction mechanism excited state $Ru(bpy)_3^{2+*}$ is reduced by DIPEA to $Ru(bpy)_3^{+}$. $Ru(bpy)_3^{+}$ reduces a Lewis acid activated enone to a radical **C** and $Ru(bpy)_3^{2+}$ is regenerated. Radical **C** undergoes [2+2] cycloaddition resulting in the ketyl radical **D**. The oxidation of this radical gives the product **C12**.

After these reports, photoredox catalysis has become much more popular, with more and more transformations being reported. Selected important photoredox catalysed transformations reported in the last 10 years have been presented in Scheme 2.4.

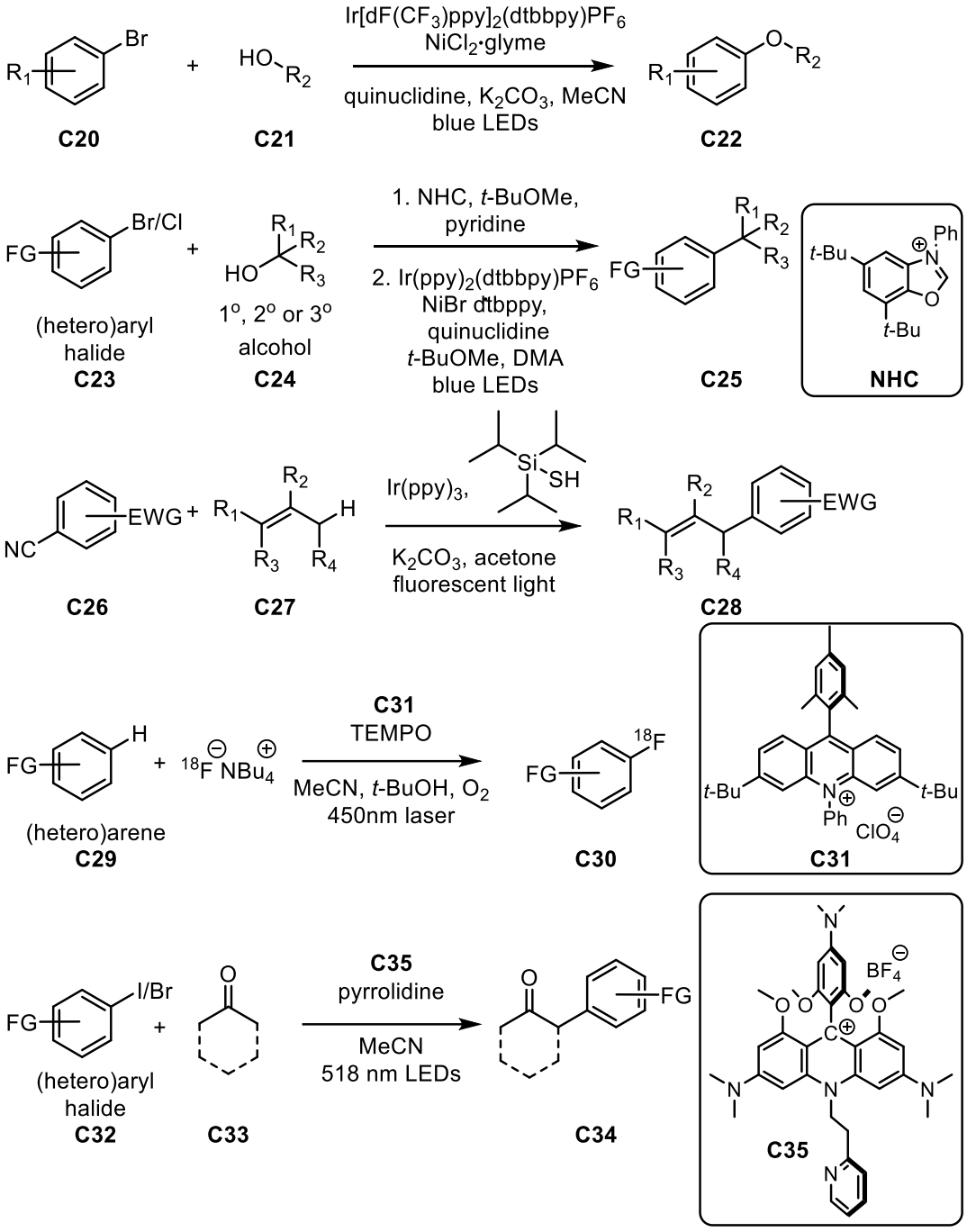

Scheme 2.4. Selected important photoredox reactions from the last 10 years. From the top: alcohol arylation,[9] deoxygenative arylation of alcohols,[10] allylic arylation,[11] fluorination with ^{18}F,[12] α-arylation of cyclic ketones.[13]

The first reaction is a dual Nickel-photoredox catalysed arylation of alcohols.[9] It allowed for the coupling of aryl bromides **C20** with primary and secondary alcohols **C21** at room temperature and under visible light irradiation. This report inspired also other dual Nickel/photoredox catalysed transformations, such as C-N[14,15] and C-S[15,16] couplings. It also led to the development of deoxygenative arylation of alcohols, allowing for the cross-coupling of aryls with sp^3 hybridized carbons.[10] Alcohols activated in situ with *N*-heterocyclic carbene (NHC) react in a dual Nickel/photoredox

catalysed transformation. Primary, secondary and tertiary alcohols **C24** can react with aryl or heteroaryl bromides and chlorides **C23**. The third presented transformation is a dual organo/photoredox catalysed allylic arylation. There, cyanoaryls **C26** react with either cyclic or acyclic olefins **C27**, under the influence of $Ir(ppy)_3$ photoredox catalyst and thiol organocatalyst.[11] The next presented transformation is a direct radiolabelling of arenes with ^{18}F, an important radioisotope for PET tomography.[12] C-H functionalisation of arenes and heteroarenes **C29** was conducted with $^{18}F^{-}NBu_4^{+}$ as the 18-fluorine source and with acridinium-based photooxidant **C31**. Another important reaction is α-arylation of cyclic ketones.[13] Aryl or heteroaryl halides **C32** bearing mainly EWGs were coupled with 6 or 5 membered cyclic ketones **C33**, using an acridinium type photoredox catalyst **C35**.

2.1.3 Metal coordination complexes in dehalogenation reactions

Given their long-living triplet excited states (τ=1100 ns for $[Ru(bpy)_3]^{2+}$),[17] iridium and ruthenium-based polypyridyl complexes are widely utilised as photoredox catalysts.[18,19] They show high chemical stability and can be used in loadings as low as 1%.[18]

2.1.1.1 Ruthenium

One of the most commonly employed photoredox catalysts is $[Ru(bpy)_3Cl_2]$. It has been widely used in both oxidation and reduction reactions, with the moderate oxidising potential of E^*_{red} = 0.77 V vs SCE in the excited state, and the reduction potential E^*_{ox} = -0.81 V vs SCE.[18] $[Ru(bpy)_3Cl_2]$ has been also used in the reductive dehalogenation of various activated (benzylic or α-carbonyl) alkyl halides **C36** (Scheme 2.5).[8] The protocol included DIPEA as the stoichiometric reductant with either HCOOH or Hantzsch ester, under visible light irradiation. Both alkyl bromides and chlorides have been successfully dehalogenated, although the protocol is limited to activated (benzylic **C38**, **C40** or α-carbonyl **C39**) halides.

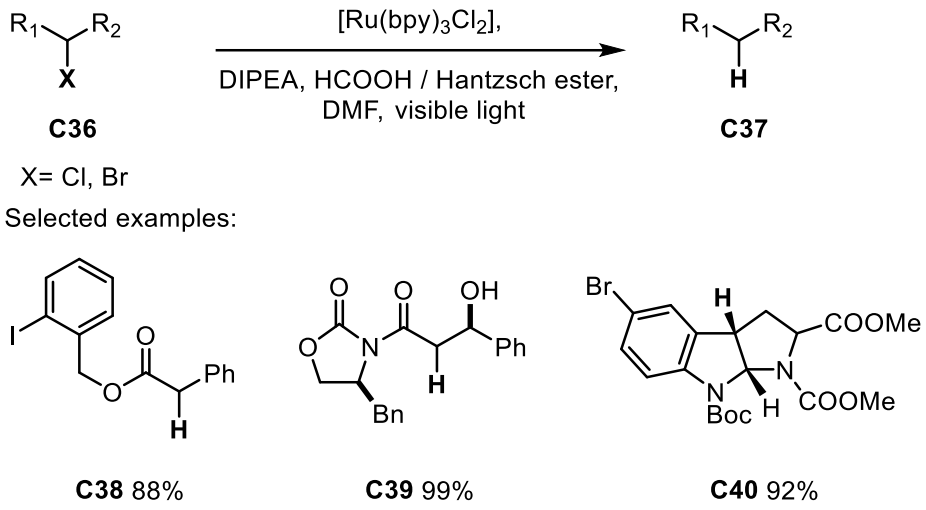

Scheme 2.5. [Ru(bpy)$_3$Cl$_2$] photoredox catalysed dehalogenation. 14W fluorescent bulb used as the light source.[8]

2.1.1.2 Iridium

Among the different complexes *fac*-[Ir(ppy)$_3$] is particularly interesting, due to its highly reducing properties in the excited state (E^*_{ox} = -1.73 V vs SCE).[20] They allow for the reduction of various alkyl and aryl halides.[21–23] [Ir(ppy)$_3$] was used for the photoredox catalysed reductive dehalogenation of aryl iodides **C41**, with HCOOH used as the proton source and Bu_3N as the sacrificial reductant (Scheme 2.6).[21] Both aryl iodides activated towards reduction – those possessing electron-withdrawing groups (EWG) **C43**, **C45** as well as deactivated ones – with electron-donating groups (EDG) **C44**, **C46** gave high yields (92-98%). However, in the latter case irradiation had to be prolonged up to 44h to achieve complete conversion.

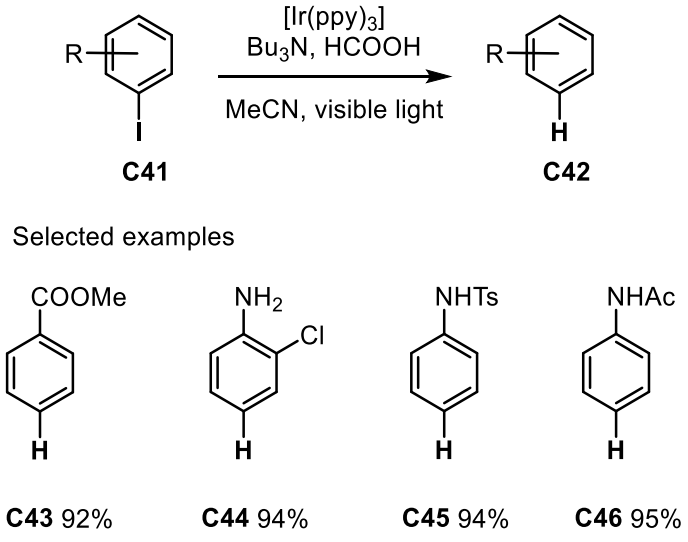

Scheme 2.6. Reductive dehalogenation of aryl iodides photoredox catalysed by [Ir(ppy)$_3$]. Blue or white LEDs used as the light source. Reaction time varied from 6 h, in the case of activated iodides, to 44h in the case of deactivated ones.[21]

Given the topic of the thesis, the introduction will focus more on organic photoredox catalysts.

2.1.4 Organic Chromophores

The high cost of the transition metals, especially iridium, their low abundance, as well as high environmental impact of their extraction[24] encouraged researchers to look for alternatives, such as fully organic compounds. Organic chromophores offer not only a metal free alternative to either iridium or ruthenium-based catalysts, but also a possibility of introducing chromophores possessing enhanced redox properties. For example, an organic chromophore 9-mesityl-10-methylacridinium, Mes-Acr-Me^+, is one of the most oxidizing photoredox catalysts (E^*_{red} ~ 2.1 V vs. SCE),[25] while 2,4,5,6-tetra(9H-carbazol-9-yl)isophthalonitrile - 4CzIPN displays one of the largest photoredox window (E^*_{ox} = -1.04 V vs SCE, E^*_{red} = 1.35 V vs SCE).[26] The latter could be used for both oxidation and reduction events in the same reaction. Even though many organic chromophores have been developed as photoredox catalysts, few of them are strongly reducing enough to replace *fac*-[$Ir(ppy)_3$]. Strongly reducing photoredox catalysts are necessary for various organic reactions, one of them being an aryl-aryl coupling. It is one of the most widely used organic chemistry reactions, traditionally performed with transition metal catalysts. The use of organic-based photoredox catalysis has been explored as a potentially cheaper, milder and more sustainable alternative,[2] and will be presented in the following section.

2.1.5 Photoredox catalysed aryl – aryl couplings

Photoredox catalysed aryl-aryl couplings can be performed using a variety of radical precursors, such as diazonium salts,[27] diaryliodonium salts,[28] aryl sulfonyl chlorides[29], aryl sulfonium salts[30] and aryl halides.[31] From Figure 2.1 one can notice that aryl diazonium salts and sulfonium salts have reduction potentials between 0.0 to -1.0 V vs SCE, which can be easily accessed by many photoredox catalysts. However, these radical precursors display low environmental stability, and are not commercially available.[32] On the contrary, aryl halides are usually bench-stable, commercially available and cheap, but difficult to be reduced (E_{red}< -1.8 V vs SCE). Only catalysts having strong reductive power, E^*_{ox} lower than -1.8 V vs SCE can be utilised.

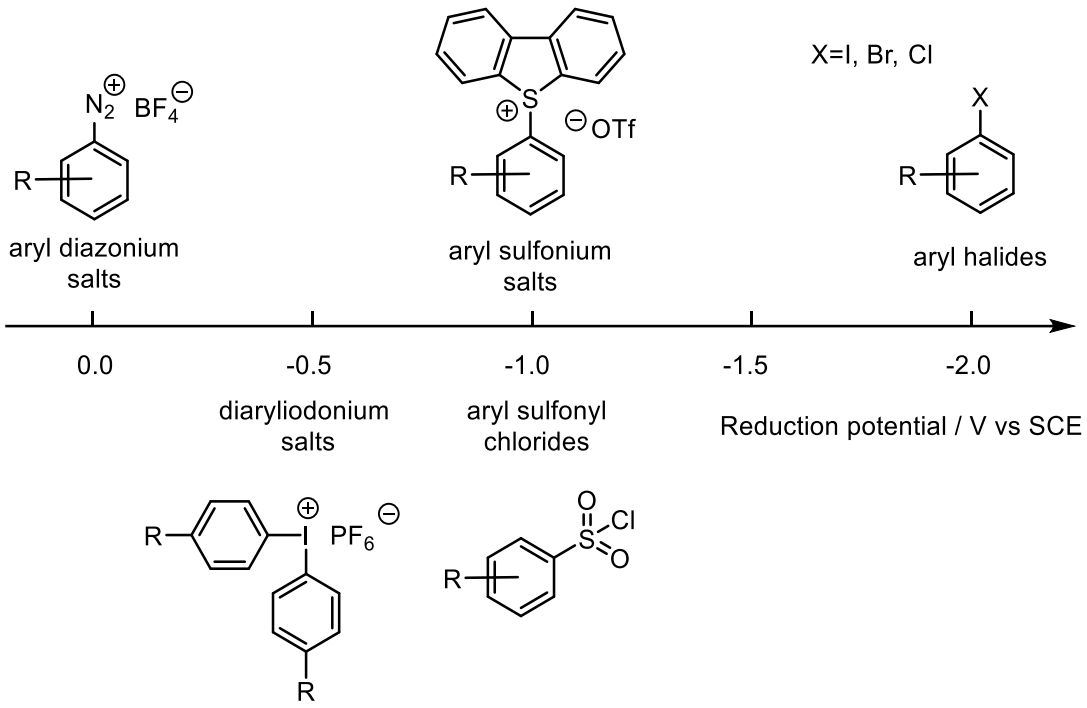

Figure 2.1. The reduction potentials of radical precursors used in photoredox catalysed aryl-aryl couplings. While the precursors become more difficult to reduce in order: aryl diazonium salts < diaryliodonium salts < aryl sulfonium salts ≈ aryl sulfonyl chlorides < aryl halides, they also become more bench stable, cheap and commercially available in the presented order.[32]

The general scheme and mechanism of coupling between a radical precursor **C47** (aryl -diazonium salt, -sulfonium salt or -halide) and a radical trap **C48** (usually heteroaryl) is presented in Scheme 2.7. Only the mechanism with oxidative quenching of the catalyst is presented, although reductive quenching happens as well.

Upon absorption of a photon of appropriate energy, the photoredox catalyst P is excited to P*. P* reduces a radical precursor **C47**, and upon the fragmentation, an aryl radical **A** is produced. This radical reacts with a radical trap **C48** (usually electron-rich heteroaryl), forming another aryl radical **B**. Subsequently, an electron donor D can reduce $P^{\bullet+}$ to regenerate P. D can be either a sacrificial amine or the previously formed radical species (**B**). In either case, it is possible that a reaction between the starting material **C47** and the radical **B** can occur, leading to the radical propagation, starting a chain type reaction. After deprotonation, the desired product **C49** is obtained.

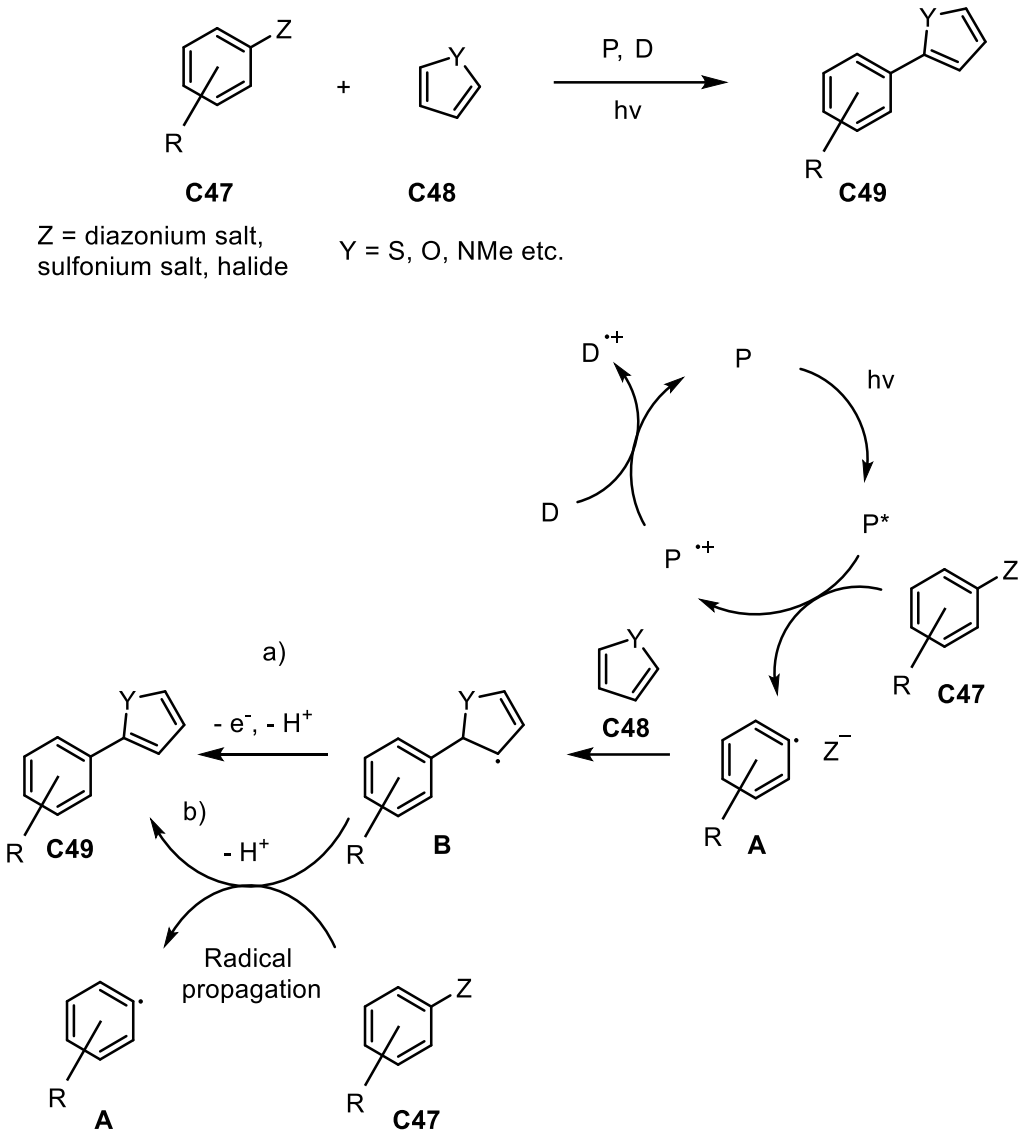

Scheme 2.7. General scheme and mechanism of photoredox catalysed aryl-aryl coupling with oxidative quenching of the catalyst, using different radical precursors, such as aryl diazonium salts, sulfonium salts or halides. D – electron donor, P -photoredox catalyst.

In the following sections, the topic of aryl-aryl couplings photoredox catalysed by chromophores will be developed. Examples of reactions utilising aryl diazonium salts, sulfonium salts and aryl halides as radical precursors will be described. More details can be found in the following reviews.[2,32–35]

2.1.1.3 Aryl diazonium salts

Aryl diazonium salts are widely used as substrates for photoredox catalysed aryl-aryl couplings, as they can be easily reduced with a reduction potential $E_{red} \approx -0.1$ V to −0.3 V vs SCE.[36] This makes them suitable radical precursors and allows moderately reducing photoredox catalysts to be employed towards this reaction, such as Eosin Y[27] or $[Ru(bpy)_3]^{2+}$.[37] Upon SET reduction by a photoredox catalyst, aryl diazonium salt fragments into an aryl radical and N_2 molecule. However, there is a risk

connected with the use of diazonium salts, as they are thermally unstable and sensitive to friction and shock, which can lead to violent decomposition and explosion. Most aryl diazonium salts are not commercially available and have to be stored at low temperatures.

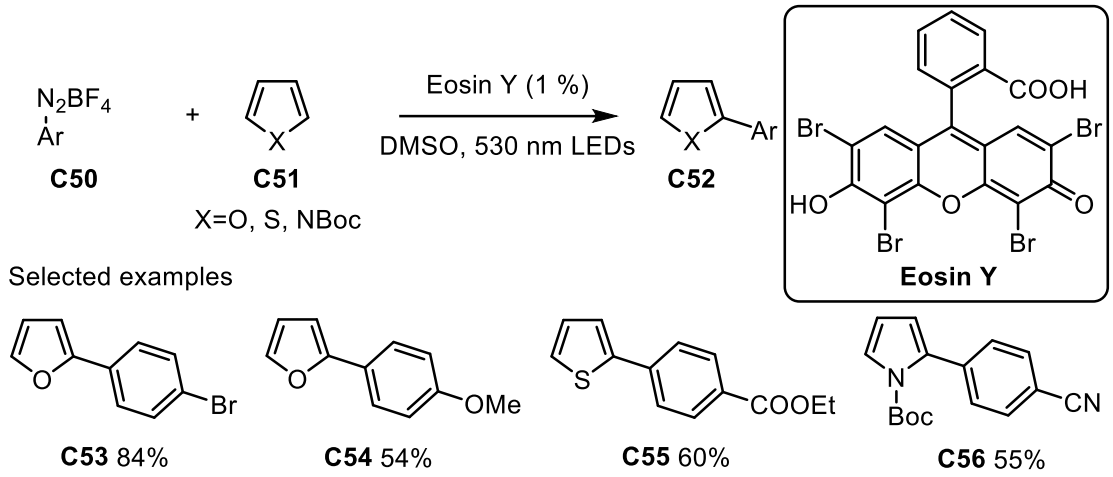

Scheme 2.8. Arylation of various heteroarenes with aryl diazonium salts, using Eosin Y as the photoredox catalyst.[27]

Coupling between aryl diazonium salts **C50** and different heteroarenes **C51**, such as furan, thiophene and *N*-Boc-pyrrole, was achieved using Eosin Y as the photoredox catalyst (Scheme 2.8).[27] Moderate to high yields of coupled products **C52** were achieved (40-86%), and examples with either EDGs or EWGs on the aryl diazonium salts were studied. Trapping tests with TEMPO confirmed that the reaction follows a radical pathway.

To overcome issues connected with the use of diazonium salts, such as lack of commercial availability, low stability and risk of explosion, a method employing *in situ* generation of diazonium salts was developed.

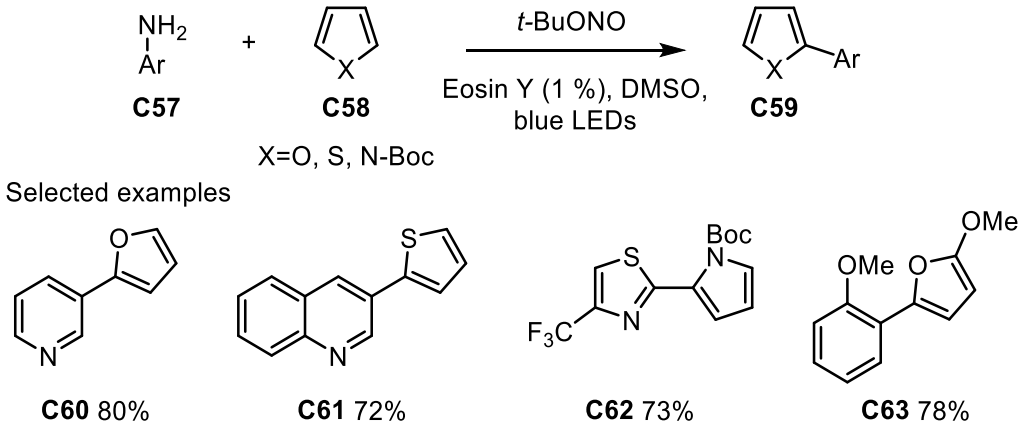

Scheme 2.9. *In situ* generation of aryl diazonium salts and their C−H heteroarylation by photoredox catalysis with Eosin Y.[38]

This one-pot procedure involved the generation of aryl diazonium salts using aryl amines **C57** and *t*-BuONa, followed by the coupling reaction with heteroarenes **C58**, using Eosin Y as the photoredox catalyst (Scheme 2.9).[38] Different heteroarenes and arenes, bearing either EWGs or EDGs, were coupled with furan, thiophene or *N*-Boc-pyrrole, giving the desired products **C59** in high yields (66-88%).

2.1.1.4 Aryl sulfonium salts

One-pot, two-step arylation reaction, employing arylsulfonium salts as a radical source, was recently reported by the group of Procter.[30]

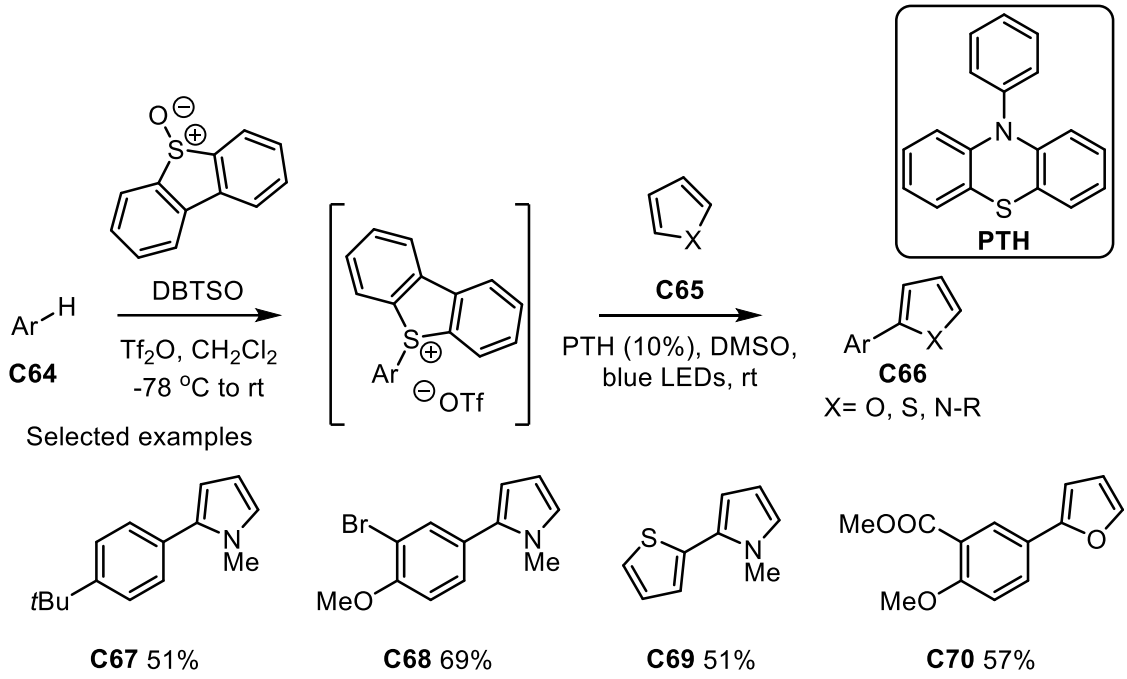

Scheme 2.10. Generation of arylsulfonium salts and their coupling with heteroaryls using PTH as the photoredox catalyst. Kessil 34 W blue LED lamp used as the light source.[30]

The first step was the preparation of a sulfonium salt in an interrupted Pummerer reaction between the dibenzothiophene-S-oxide (DBTSO) and aryl compound **C64** (Scheme 2.10). In the second step, couplings of these sulfonium salts with various heteroaryl substrates **C65**, employing 10-phenylphenothiazine (PTH) as the photoredox catalyst, gave biaryls **C66** in moderate to high yields (40-86%). The reaction could also be applied towards the coupling of two unsubstituted heteroarenes, giving compound **C69** in 51% yield.

2.1.1.5 Aryl halides

Due to their low cost, stability and commercial availability, aryl halides, and especially aryl chlorides, could be the perfect radical source for photoredox catalysed arylation

reactions.[32] However, strongly negative reduction potentials of aryl chlorides (E_{red} ≈ -1.8 to -2.9 V vs SCE)[39] suggest that up to date, only a few photoredox catalysts can be used to trigger this reaction. To solve this problem, researchers are using two approaches. The first is to generate strongly reducing species through so-called "consecutive photoinduced electron transfer", where photogenerated, stable radical anion of a photoredox catalyst is excited by another photon of light.[31] Another approach consists of developing new, strongly reducing photoredox catalysts, such as triazole based chromophore Py-BTz-Py.[40] Examples of both methods will be described in the following sections.

Consecutive photoinduced electron transfer

In 2014 the group of König utilised perylene diimide (PDI) to trigger photoredox catalysed reduction of aryl halides, as well as their coupling with different pyrroles (Scheme 2.11).[31]

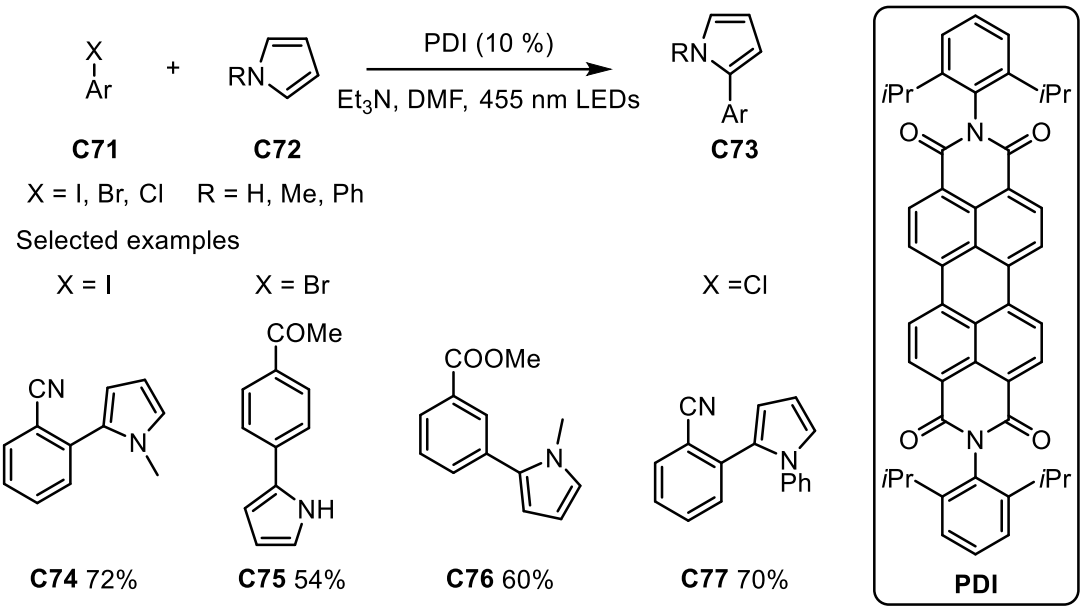

Scheme 2.11. Photoredox couplings of aryl halides with pyrroles, catalysed by PDI.[31]

Using Et_3N as a sacrificial electron donor, while irradiating with blue LEDs, the authors managed to couple aryl iodides (**C74**), bromides (**C75**, **C76**) and chlorides (**C77**) possessing different EWGs with a range of pyrroles **C72**, achieving moderate to high yields (52-74%). The mechanism of this reaction includes two consecutive photoinduced electron transfers (Scheme 2.12). An excited state photoredox catalyst PDI* oxidises a sacrificial amine, acting as an electron donor (Et_3N), which authors confirmed through quenching studies. This forms a radical anion $PDI^{\bullet-}$, which is stable enough to be excited, forming highly reducing $PDI^{\bullet-}$*. $PDI^{\bullet-}$* is a coloured radical, studied through spectroscopy with absorption bands between 600-1000 nm.[31] The

potential value of $PDI^{-\bullet}$*/PDI half-reaction was subsequently measured by the Schanze group, using quenching studies, as −1.87 V vs SCE, corroborating the proposed reaction mechanism.[41] Given the high reducing potential of $PDI^{\bullet-}$*, it can reduce aryl iodides and electron-deficient aryl bromides and chlorides.[31]

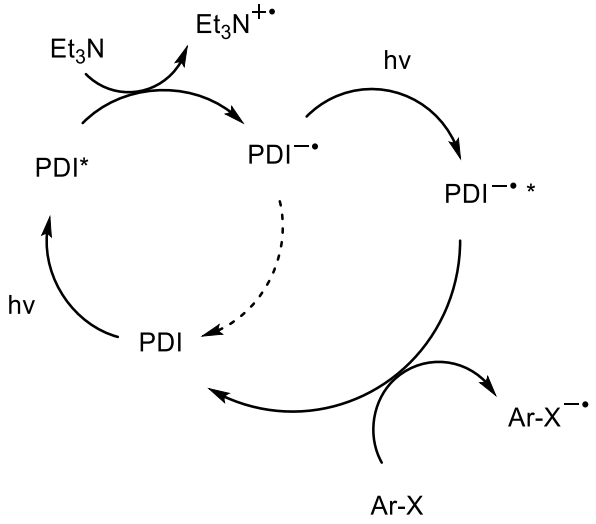

Scheme 2.12. Mechanism of reduction of aryl halides employing a consecutive photoinduced electron transfer with PDI.[31]

In the follow-up work, the group of König showed that rhodamine-6G (Rh-6G) can also be used as a catalyst in a consecutive photoinduced electron transfer reaction.[42] The investigation has shown that using Rh-6G allows for a high degree of control over the reaction outcome. The authors managed to regulate the redox power of the photocatalyst by utilising light of different wavelengths. When green light (530 nm) is used, Rh-6G* is obtained, and in the presence of DIPEA, acting as a sacrificial amine, reduced to a radical anion $Rh\text{-}6G^{\bullet-}$. Both Rh-6G* and $Rh\text{-}6G^{\bullet-}$ can engage in reductive processes, with moderate reduction potential of respectively ~ -0.8 V and -1.0 V vs SCE. However, when blue light (455 nm) is used $Rh\text{-}6G^{\bullet-}$ is excited to $Rh\text{-}6G^{\bullet-}$*, which has a powerful reduction potential value of E^*_{ox} ~ -2.4 V vs SCE. Using this method, researchers managed to selectively achieve either mono **C79** or bi **C80** functionalisation of tribromobenzene **C78** (Scheme 2.13). When the green light was used, moderately reducing $Rh\text{-}6G^{\bullet-}$ led to the mono substitution. However, when the blue light was applied, the strongly reducing $Rh\text{-}6G^{\bullet-}$* species gave access to disubstitution.[42]

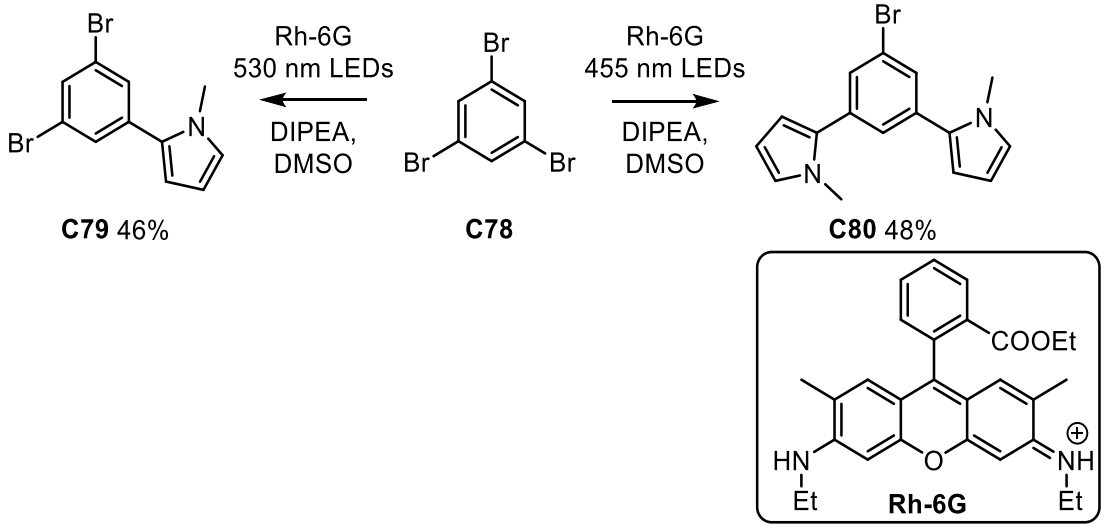

Scheme 2.13. Rh-6G photoredox catalysed selective functionalisation of tribromobenzene using either green (530 nm) or blue (455 nm) light.[42]

Triazole based photoredox catalyst - Py-BTz-Py

Recently Wang *et al.* developed a new photoredox catalyst with a high reductive power, which can reduce aryl halides.[40] They designed a series of donor-acceptor type organic photocatalysts, including Py-BTz-Py (2-butyl-4,7-bis(1- methyl-1H-pyrrol-2-yl)-2H-benzo[d][1,2,3]triazole) (Scheme 2.14).

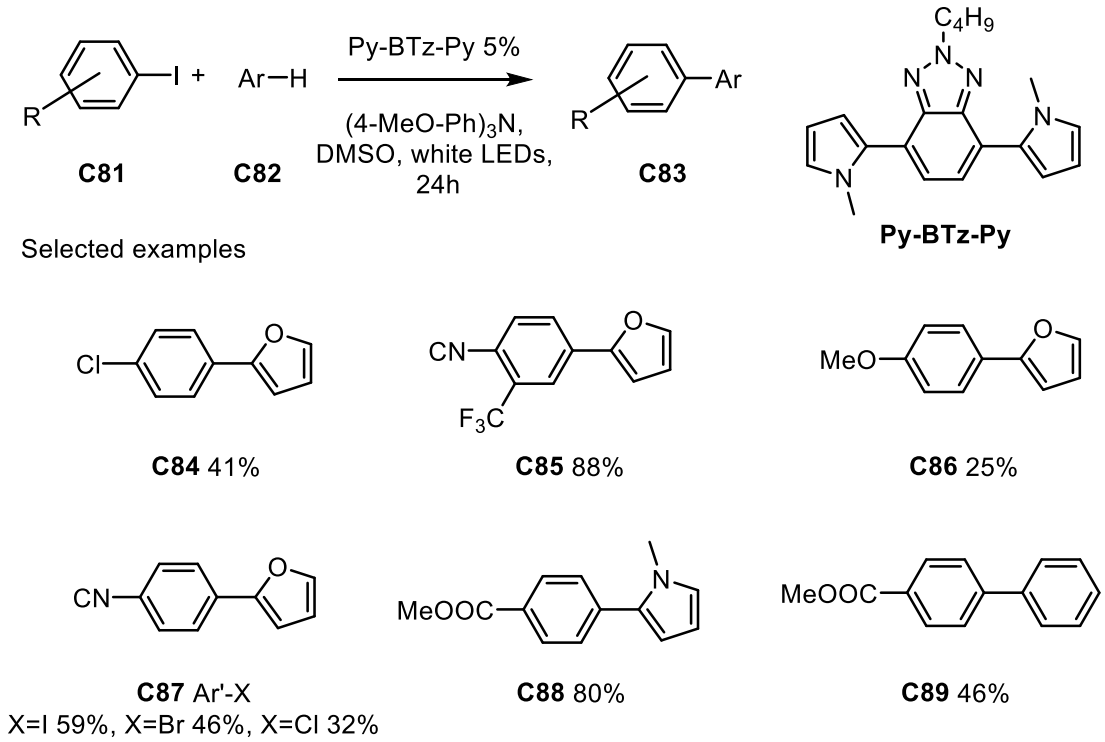

Scheme 2.14. Photoredox catalysed coupling of various aryl iodides with different radical traps, mostly heteroarenes. White light LEDs > 420 nm used.[40]

Py-BTz-Py, which has two *N*-methylpyrrole moieties, depicts a very strong reducing power E^*_{ox} = -2.04 V vs SCE at the excited state. A wide range of couplings of aryl iodides **C81** with radical traps **C82**, such as furan, benzene and *N*-methylpyrrole, was demonstrated (Scheme 2.14).[40] The use of aryl iodides bearing EWGs gave desired products in moderate to high yields (41 – 88% **C84**, **C85**, **C88**), while the use of electron-neutral and electron-rich aryl iodides led to the reduction of yield (**C86** 25%). Bromide and chloride derivatives could also be used, although with lower yields **C87**.

2.2 PXX in photoredox catalysis

2.2.1 Introduction on PXX

As few strongly photoreducing organic catalysts are available to chemists, we decided to investigate already known chromophore *peri*-xanthenoxanthene (PXX) described in more detail in section 1.4. PXX itself has a very strong reducing potential in the singlet excited state (E^*_{ox} = -2 V vs SCE).[43] It can be easily prepared in just one step (synthesis of PXX presented in section 1.4, on Scheme 1.36)[44] and at a low cost (£2.3/mmol for raw materials)[45]. These characteristics make PXX a good candidate for use as a green, cheap, easy to synthesise and strongly reducing photoredox catalyst. As PXX* (-2V vs SCE)[43] is more strongly reducing than [Ir(ppy)$_3$] in the excited state (-1.73 V vs SCE)[20], it could offer a cheap and metal-free alternative to this widely used photocatalyst.

2.2.2 PXX in photoredox catalysed reactions

2.2.2.1 Reductive dehalogenation

The use of PXX as the photoredox catalyst has been previously reported, by our group, to dehalogenate activated alkyl and aryl bromides **C51** (Scheme 2.15).[43]

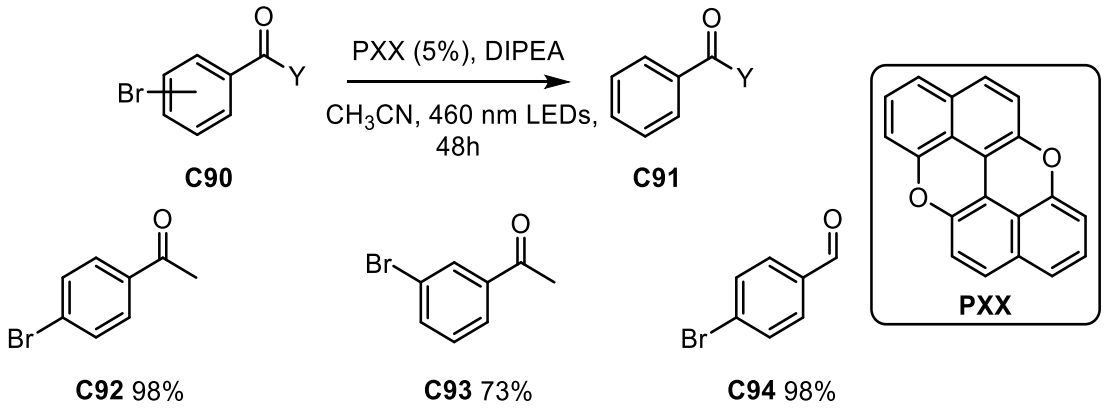

Scheme 2.15. Dehalogenation of aryl bromides photoredox catalysed by PXX. Conversions determined by GC-MS analysis.[43]

Under the blue light irradiation (460 nm), and with the use of DIPEA, PXX was able to dehalogenate *p*- (**C92**) and *m*-bromoacetophenone (**C93**) as well as *p*-bromobenzaldehyde (**C94**).

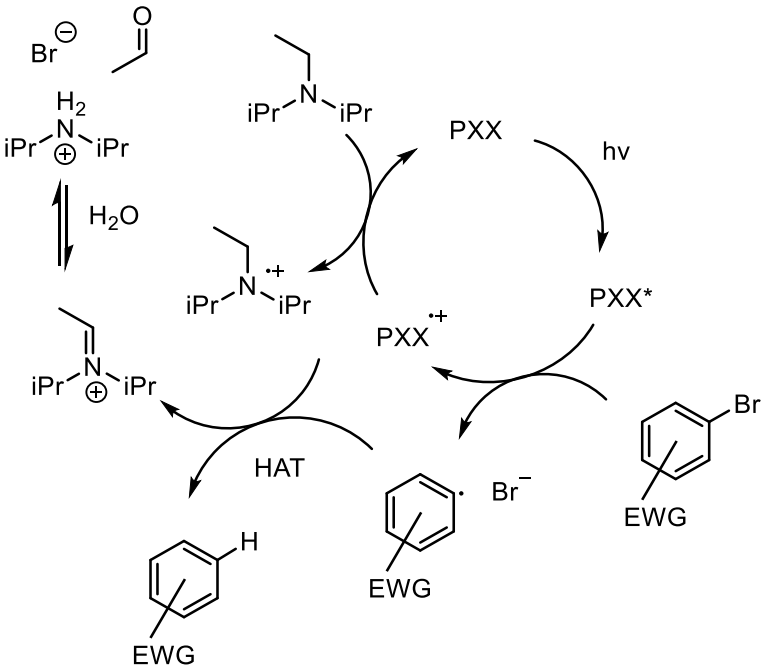

Scheme 2.16. Mechanism of reductive dehalogenation of aryl bromides photoredox catalysed by PXX.[43]

Quenching studies were performed to elucidate the reaction mechanism. An investigation has shown that the quenching constant between PXX* and *p*-bromoacetophenone (k_q=1.3x10^{10} M^{-1}s^{-1}) is three orders of magnitude higher than that with DIPEA (k_q=3.5x10^{7} M^{-1}s^{-1}). This suggests that PXX* can reduce aryl bromides, and that the mechanism is photoreductive (Scheme 2.16). It has been proposed that the excited state PXX* reduces an aryl bromide to a radical anion, which then fragments into a bromine anion and an aryl radical. This aryl radical is then hydrogenated through hydrogen atom transfer (HAT), possibly with DIPEA$^{\bullet+}$. This has been suggested by isolation, from the reaction mixture, of the single crystals of diisopropyl ammonium bromide, confirmed by X-ray analysis. EPR studies confirmed the presence of photogenerated aryl radicals.

2.2.2.2 Iododifluoromethylation of alkenes

More recently PXX has been used as the photoredox catalyst by Trifonov *et al*. in the iododifluoromethylation of alkenes (Scheme 2.17).[46] Terminal alkenes **C95** were reacted with phosphonium salt **C96**, using 0.5% PXX as the catalyst under blue LEDs irradiation. After protodephosphorylation under basic conditions, the desired products **C97** were obtained in moderate to high yields (40-78%).

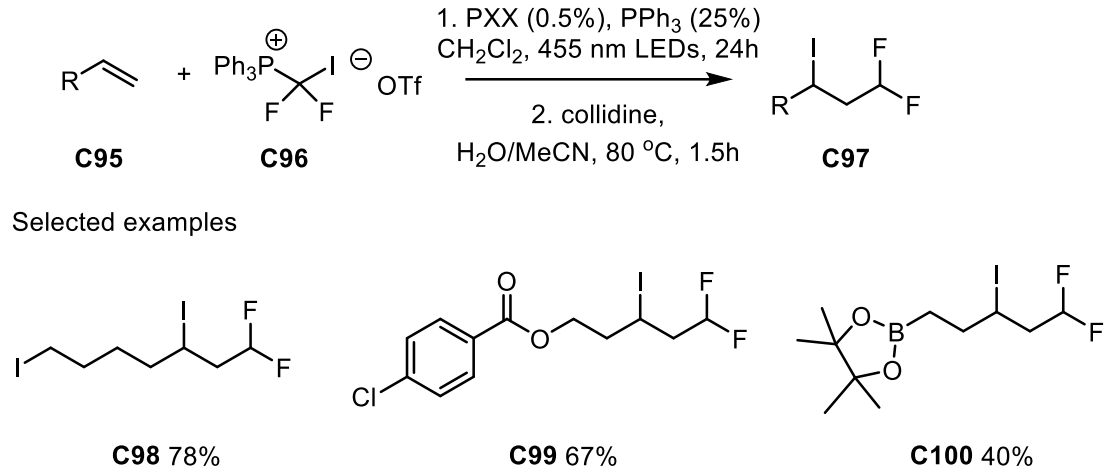

Scheme 2.17. Iododifluoromethylation of terminal alkenes, employing PXX as the photoredox catalyst.[46]

In the proposed mechanism (Scheme 2.18), the excited state PXX* reduces the starting material, leading to the cleavage of C-I bond and formation of the radical cation **A** and an iodide anion. The addition of radical cation **A** to the double bond of **C95** leads to radical **B**. After oxidation of I^- to $I^\bullet$ by $PXX^{\bullet+}$, iodine radical reacts with the radical cation **B** to give the product **C**. After hydrolysis of **C** product **C97** is obtained.

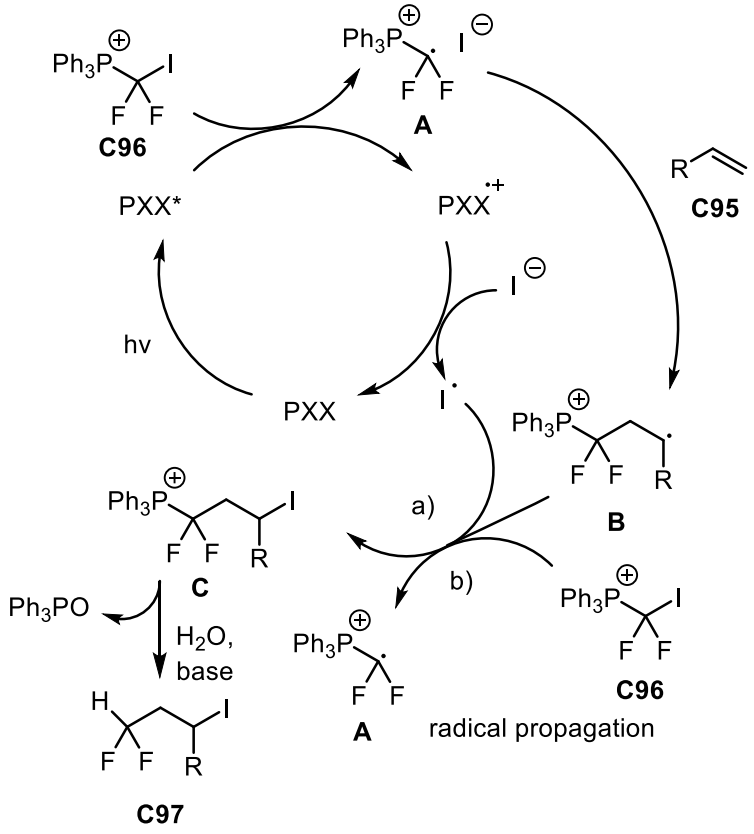

Scheme 2.18. Mechanism of the iododifluoromethylation of alkenes, photoredox catalysed by PXX.[46]

Alternatively, (path b)) radical **B** can abstract iodine from **C96**, leading to the radical chain process, which is supported by the determination of quantum yield having the value of 3.1. It is worth mentioning that other photoredox catalysts, such as [$Ir(ppy)_3$] and 4CzIPN, were also screened for this reaction. On a model reaction, using 4-phenyl-1-butene as the starting material, they gave inferior yields, respectively 25% and 46%, compared to 75% achieved with PXX. The high efficiency of PXX in the reaction has been ascribed to the stacking interaction between phenyl rings of phosphonium cation and electron-rich aromatic rings of PXX. This interaction could facilitate the reduction of the phosphonium cation by bringing it close to the catalyst.[46]

2.2.2.3 PXX catalysed couplings

Our group decided to show PXX as a strongly reducing and versatile photoredox catalyst, by employing it in several different classes of reactions.[45] While aryl-aryl couplings will be described in more detail in section 2.3, a short description of other reactions that PXX can catalyse, which appeared in our paper, will be presented in this section.

β-Arylation of Carbonyl Compounds

PXX was used as a photoredox catalyst in β-arylation of carbonyl compounds, originally reported by MacMillan.[47] PXX replaced more expensive $Ir(ppy)_3$ as a photoredox catalyst, and led to the coupling of cyclic ketones with cyanoarenes (Scheme 2.19). 5 and 6 membered cyclic ketones could be effectively used, while 1,4-dicyanobenzene and 4-cyanophthalide could be used as cyanoarenes. Mechanistic studies suggest that both oxidative and reductive mechanisms are possible.

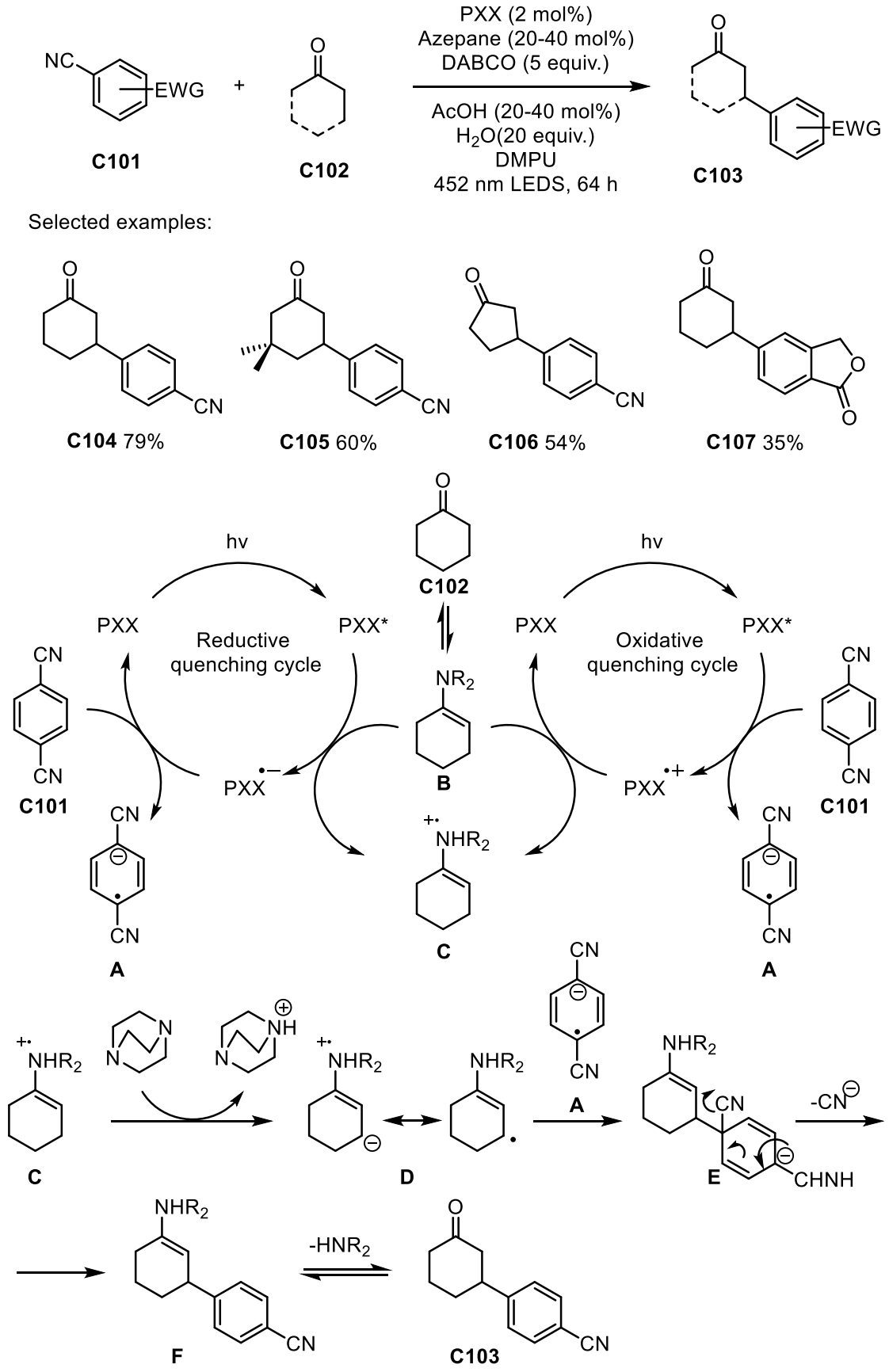

Scheme 2.19. β-Arylation of carbonyl compounds and proposed reaction mechanism.[45]

Nickel-PXX dual catalysis cross-coupling

Dual Nickel-photoredox cross-couplings have been previously demonstrated for the formation of C-N[14,15] and C-S[15,16] bonds using different photoredox catalysts. PXX has been demonstrated to also work in Ni-photoredox dual catalysis. It was possible to use low loading of PXX catalyst (0.2%.) Different aryl bromides were coupled with secondary amines giving products with high yields (69-87%) (Scheme 2.20).

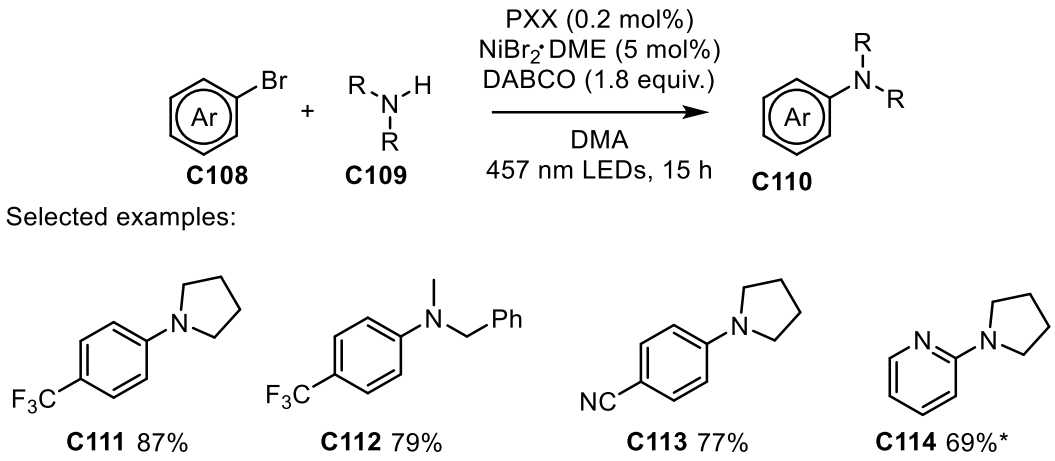

Scheme 2.20. Coupling of aryl bromides with amines,*reaction time 64h.[45]

The proposed reaction mechanism involves the reduction of Ni(II) amino complex to Ni(I) with excited state PXX* (Scheme 2.21). Next, the oxidative addition of aryl bromide **C108** leads to Ni(III) aryl complex, which undergoes reductive elimination to give the C-N bond. Finally, the turnover of PXX can be accomplished by the oxidation of DABCO.

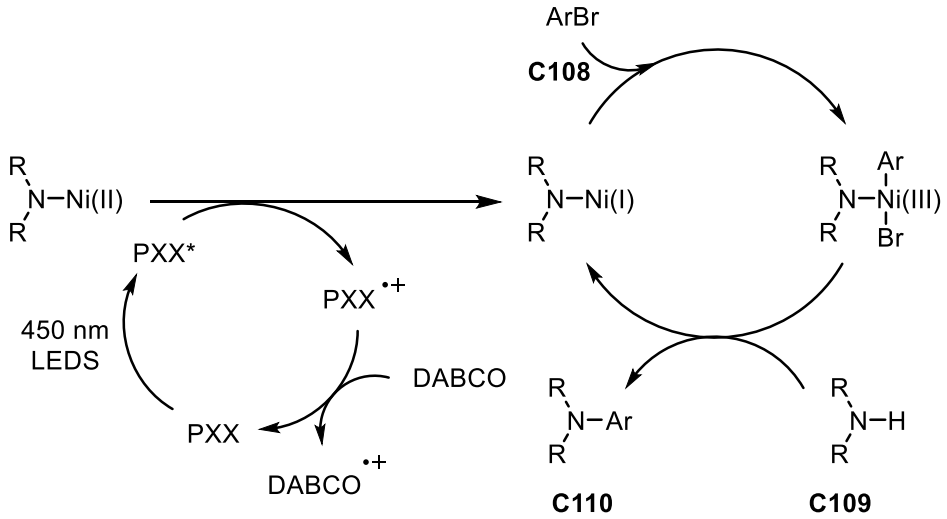

Scheme 2.21. Reaction mechanism proposed for coupling of aryl bromides with amines.[45]

C-S cross-coupling has also been achieved using PXX, in dual Ni-photoredox catalysis (Scheme 2.22). Very high yields (85-98%) were achieved in the coupling of both aliphatic (**C118**, **C119**, **C121**) as well as aromatic (**C120**) thiols. Both aryl bromides possessing EWGs and EDGs gave good results.

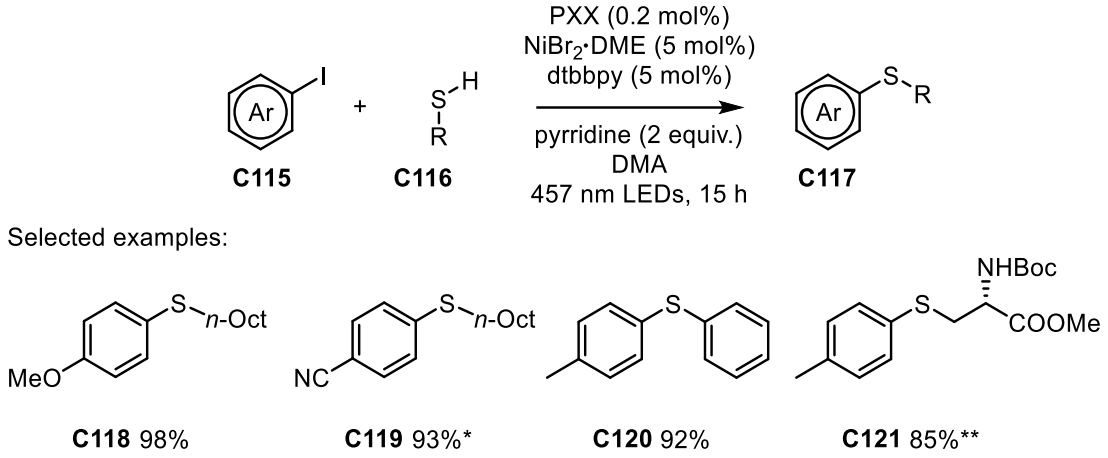

Scheme 2.22. Coupling of aryl bromides with thiols, *****4-Bromobenzonitrile used as a substrate, **reaction time 40 h.[45]

2.3 Intermolecular photoredox aryl couplings catalysed by PXX

2.3.1 Project aim

Looking at the reductive power of the excited state PXX* (E^*_{ox} = -2 V vs SCE),[43] we realised that it should reduce not only aryl bromides, as was demonstrated by our group,[43] but also electron-poor aryl chlorides, such as *p*-chlorocyanobenzene (E_{red} = -1.88 V vs SCE).[48] We were interested to see if an aryl coupling could be achieved instead of simple dehalogenation. As mentioned in section 2.1.1.5, aryl chlorides are very interesting for photoredox catalysed aryl couplings thanks to their stability, low cost and commercial availability. However, their high reduction potentials and low fragmentation rates make their use in these couplings limited.[32] Thus, we decided to showcase the potential of PXX as a green, cheap and strongly reducing photoredox catalyst in the arylation of aryl chlorides.

2.3.2 Results on intermolecular aryl coupling photoredox catalysed by PXX

We envisioned that PXX should be able to catalyse aryl-aryl couplings, following a photoreductive mechanism similar to that described by our group previously, for the dehalogenation of aryl chlorides (Scheme 2.16).[43] However, here the photogenerated radical would react with an electron-rich trap instead of undergoing HAT. To limit the dehalogenation, an excess of 10 eq. of an electron-rich trap was used. We began our

tests with a coupling between *o*-chlorocyanobenzene and *N*-methylpyrrole, acting as an electron-rich radical trap. 2% of PXX as the photoredox catalyst, and 1.4 eq. of DIPEA as a sacrificial amine were used, with overnight irradiation using blue LEDs (457 nm, setup described in experimental section), in DMSO (Scheme 2.23). We were satisfied to see that **41** was isolated with high yield (69%). We proceeded to check the scope and limitations of this reaction, by testing how different aryl chlorides, as well as different electron-rich radical traps performed as starting materials. After overnight irradiation, an internal standard (tetrachloroethane) was added, and NMR yield was estimated, using signals of *N*-methylpyrrole moiety (**41**-**47**) or chlorocyanobenzene moiety (**48**-**51**). Where sufficient NMR yield (at least 50%) was obtained, the products were isolated and unless stated otherwise isolated yields are reported.

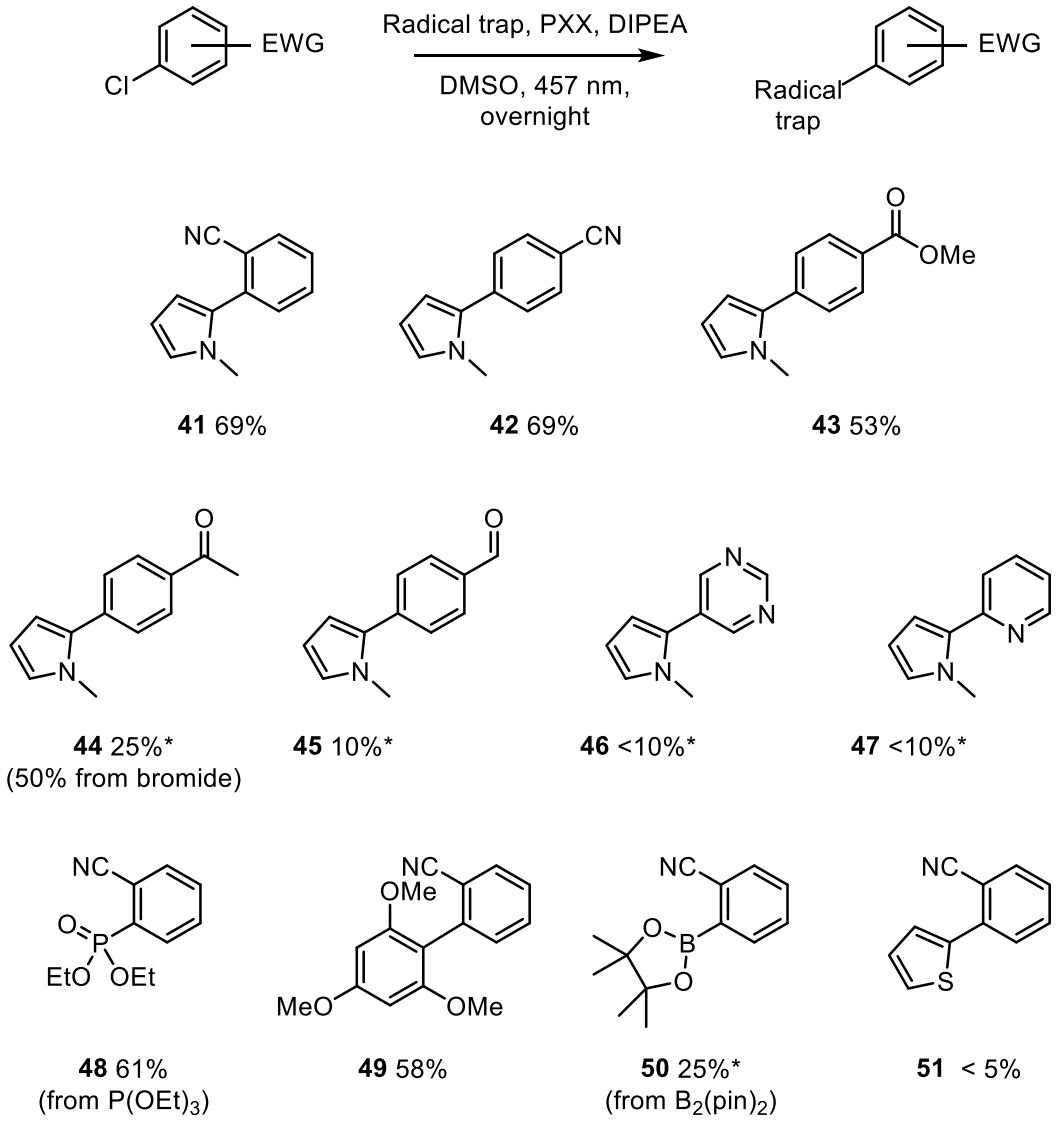

Scheme 2.23. PXX photoredox catalysed aryl-aryl couplings. Conditions: 10 eq. of a radical trap, 2% of PXX, 1.4 eq. of DIPEA, 1 ml of DMSO, on 0.2 mmol scale of aryl halide, overnight irradiation with blue light LEDs, freeze-pump-thaw performed, under N_2. *NMR yield determined using tetrachloroethane as an internal standard.

We began studying the reaction scope by testing different aryl chlorides. Using *para* **42**, rather than *ortho* isomer of chlorocyanobenzene did not affect the yield (69%) (Scheme 2.23). Ester group **43** gave 53% yield. Both ketone **44** and aldehyde **45** allowed for very low conversion (25 and 10% NMR yield, respectively). However, since it has been previously shown that PXX can reduce *p*-bromoacetophenone,[43] we decided to test if using a bromide derivative would increase the yield. Indeed, when *p*-bromoacetophenone was used as the starting material, product **44** was isolated with 50% yield. Since *p*-bromoacetophenone and *p*-chloroacetophenone have very similar reduction potentials: -1.89 and -1.91 V vs SCE respectively,[49] the potential itself cannot be used to explain different results obtained with these starting materials. However, when we look at fragmentation rate constants for *p*-bromo and *p*-chloroacetophenone we can see that the latter is two orders of magnitude slower ($k_{f\,p\text{-}Br} = 3.2 \cdot 10^7\ s^{-1}$, $k_{f\,p\text{-}Cl} = 3.2 \cdot 10^5\ s^{-1}$).[49] A low fragmentation rate means that even though the radical anion is readily formed the cleavage of C-Cl bond is slow, limiting the formation of aryl radical and hampering reaction progress.[39] Both pyrimidine **46** and pyridine **47** gave poor results (<10% NMR yield), which shows that aryl chlorides without EWGs are not viable substrates for this reaction, as their reduction potential is too negative for PXX to reach ($E_{red\ o\text{-}Cl\text{-}pyridine} = -2.6$ V vs SCE).[50] Subsequently, we proceeded to study the scope of electron-rich radical traps. Triethylphosphite **48** and trimethoxybenzene **49** gave good results – respectively 61% and 58% yield. B_2Pin_2 **50** also was tested as a trap, although only a very low conversion of around 10% was obtained in standard conditions. Changing the solvent to CH_3CN/H_2O 19:1, with Bu_3N as a base, did not improve the result. Finally, using DMSO/H2O 9:1 solvent system and 3 eq. of B_2Pin_2 led to a slight improvement, giving 25% NMR yield. When thiophene was used as a radical trap, only traces of product **51** were isolated (5%).

Building on the mechanism of PXX catalysed dehalogenation,[43] discussed in section 2.2.1 (Scheme 2.16), we propose the mechanism of this reaction (Scheme 2.24). Upon excitation, PXX* reduces an aryl halide, which undergoes heterolytic cleavage yielding an aryl radical A and a halide anion, while $PXX^{\bullet+}$ is formed. The reaction of the radical A with an electron-rich trap gives a new aryl radical B, which upon rearomatisation yields a coupling product. Regeneration of PXX can take place upon the reduction of $PXX^{\bullet+}$ by either DIPEA or the aryl radical B.

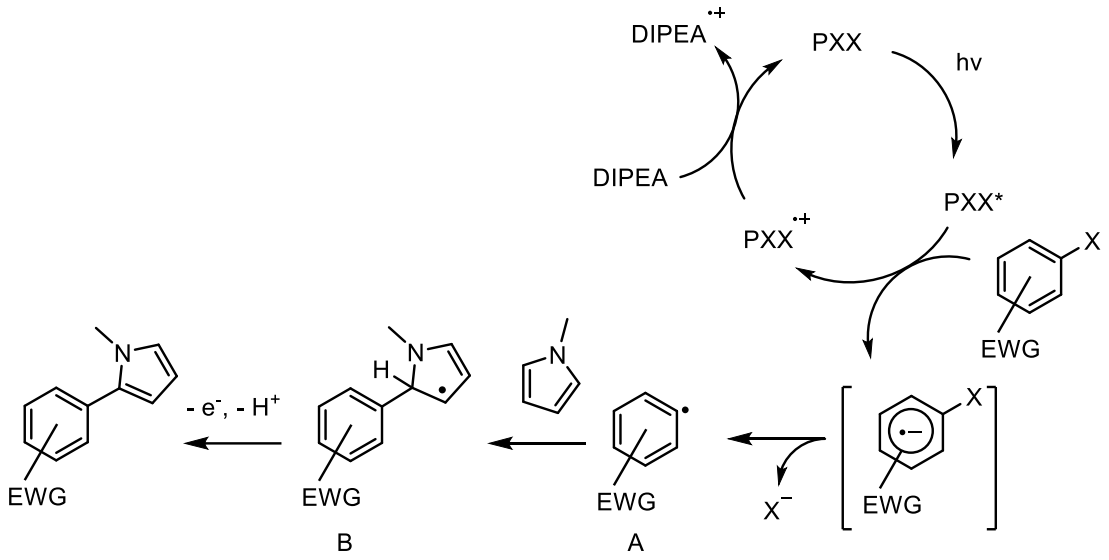

Scheme 2.24. Proposed mechanism of intermolecular coupling photoredox catalysed by PXX.

We decided to also test PTXTX as a photoredox catalyst, to compare its efficiency to those of PXX.

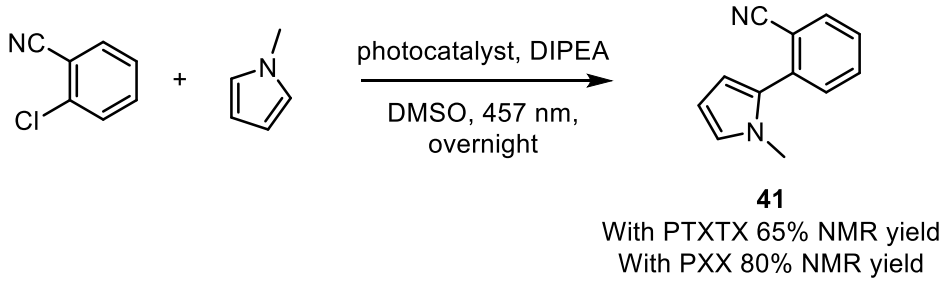

Scheme 2.25. Comparison of PTXTX and PXX efficiency as a photoredox catalyst in a coupling reaction of 1-chloro-2-isocyanobenzene with pyrrole. Conditions: 10 eq. of a radical trap, 2% of photocatalyst, 1.4 eq. of DIPEA, 1 ml of DMSO, on 0.2 mmol scale of aryl halide, overnight irradiation with blue light LEDs, freeze-pump-thaw performed, under argon. *NMR yield determined using tetrachloroethane as an internal standard.

Using the same reaction conditions, PTXTX was less effective than PXX in a coupling of 1-chloro-2-isocyanobenzene with N-methylpyrrole. While the NMR yield was 80% when PXX was used, it dropped to 65% in the case of PTXTX (Scheme 2.25). There can be several possible reasons for such a result. The solubility of PTXTX is lower than solubility of PXX in most organic solvents, which can lead to a lower concentration of the catalyst. PTXTX has also a lower excitation coefficient than PXX (ε_{PTXTX} = 6000 M^{-1} cm^{-1} vs ε_{PXX} = 17300 M^{-1} cm^{-1}), which means that PTXTX absorbs less light than PXX, and cannot be as effectively excited. PTXTX is also less reducing in the excited state than PXX ($E^*_{1/2}{}^{ox}{}_{PTXTX}$ = -1,72V vs SCE vs $E^*_{1/2}{}^{ox}{}_{PXX}$ = -2 vs SCE). Se doped anthanthrene **36** was not checked as a photoredox catalyst, as it was found to be only weakly absorbing, and was synthesised only in small amounts.

The positive results of the intermolecular aryl-aryl couplings photocatalysed by PXX led us to consider if the intramolecular version of the coupling reaction could be possible. The intramolecular version of the reaction would be a cyclisation that would lead to the synthesis of polycyclic aromatic hydrocarbons – PAHs. Exceptional optoelectronic properties of PAHs make them crucial in material chemistry, and new methods to obtain them are constantly developed and improved.[51–55] To the best of our knowledge, photoredox catalysed cyclisation of aryl halides has not been previously used to synthesise PAHs.

The introduction concerning pathways to obtain PAHs and the results of our experiments will be described in the following sections.

2.4 Introduction to the synthesis of PAHs

PAHs have attracted growing interest due to their unique electronic and optoelectronic properties. They have been widely used in dye-sensitised solar cells, organic light emitting diodes and organic field effect transistors.[51, 53,54,56] Following sections will describe selected methods that allow obtaining PAHs, highlighting reactions based on photocyclisation. More details on the synthesis of PAHs can be found in the following reviews.[51–55]

2.4.1 The Scholl reaction and oxidative coupling

One of the first and commonly used reactions leading to PAHs is the Scholl reaction. This Lewis acid promoted coupling was first described in 1910 by Scholl and Mansfeld, who used neat $AlCl_3$ at 140-145°C to obtain extended quinone **C123** (Scheme 2.26).[57]

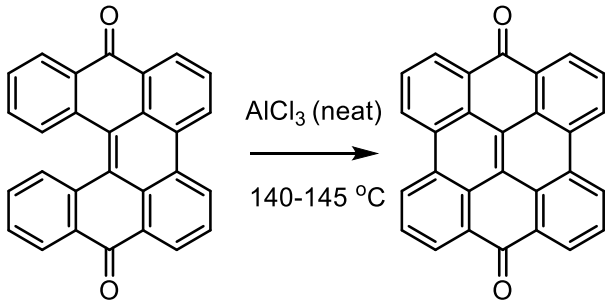

C122 **C123**

Scheme 2.26. First report of the Scholl reaction (yield not reported).[57]

Various protocols have been implemented since then to optimise the Scholl reaction. The introduction of $AlCl_3$/NaCl melt, and later use of high boiling solvents such as dichlorobenzene or nitrobenzene, made the handling of the reaction easier.[58] The addition of $CuCl_2$[59] and then CS_2 as a solvent led to the development of improved

conditions, $AlCl_3/CuCl_2/CS_2$[60] and $AlCl_3/Cu(SO_3CF_3)_2/CS_2$.[61] The introduction of these conditions allowed performing reactions at room temperature and gave higher yields.

The reaction mechanism is still debated, with two mechanisms being proposed. While some researchers use the terms the Scholl reaction and oxidising coupling interchangeably, others suggest that they are two different reactions.[58] The latter implies that the Scholl reaction name should be applied only to those reactions where a strong Lewis acid, such as $AlCl_3$ is used, and that the mechanism involves an arenium cation. However, when oxidising reagents such as $FeCl_3$ or $MoCl_5$ are used at room temperature, they suggest that a radical mechanism prevails.[58] The fact that oxidising reagents are often weak Lewis acids fuels difficulties in distinguishing these reactions.

Apart from $FeCl_3$ or $MoCl_5$, other oxidants routinely used for cyclodehydrogenative couplings are DDQ/acid and phenyliodine bis(trifluoroacetate) – $PIFA/BF_3{\cdot}Et_2O$ systems. There have been numerous examples of annulation reactions in the synthesis of both small PAHs and large nanographenes. For example, various hexabenzocoronenes – **HBC**s have been synthesised using a $FeCl_3/CH_3NO_2/CH_2Cl_2$ mixture (Scheme 2.27).[62,63]

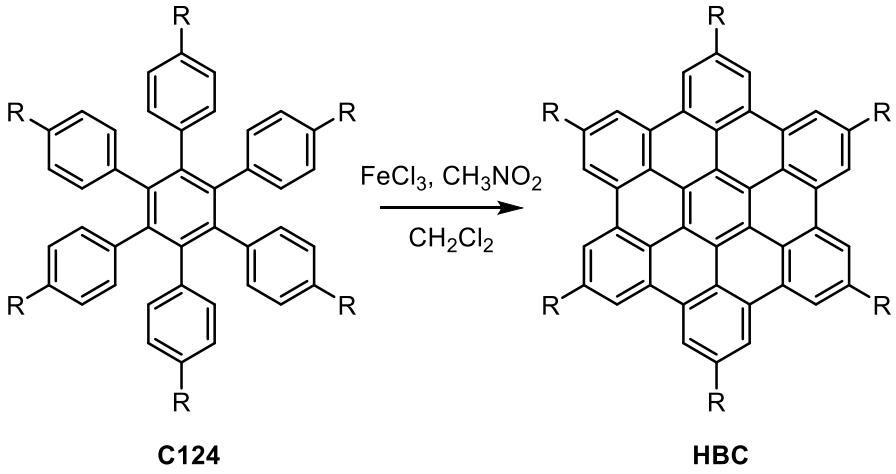

Scheme 2.27. HBC synthesis.[62]

The Scholl reaction is particularly useful to obtain large PAHs, where multiple annulations must be obtained. One of the biggest molecules obtained by the Scholl reaction is the 222 carbon graphite sheet, where 108 hydrogen atoms were removed under the influence of $AlCl_3$ and $Cu(SO_3CF_3)_2$ in CS_2 at 30°C.[61]

Although oxidative cyclodehydrogenation and the Scholl reaction are extremely useful, they present several drawbacks. They can suffer from polymerisation when small substrates, such as triphenylenes, are used. Also, the presence of the EWGs can often suppress reactivity.[64]

2.4.2 Pd-catalysed C-H activation

Pd-catalysed C-H activation can be used to synthesise small PAHs using Pd(II) source, ligands, strong base and high temperature. This reaction is regioselective towards the creation of 5-membered rings. For example, when aryl triflate **C125** was subjected to $[PdCl_2(PPh_3)_2]$, LiCl and DBU conditions, it gave only product containing 5-membered ring **C126**, and not perylene (Scheme 2.28).[65]

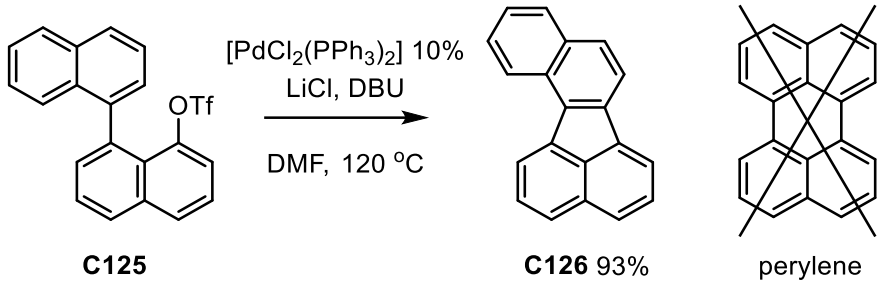

Scheme 2.28. Pd-catalysed intramolecular aryl coupling.[65]

Preference towards the formation of 5-membered rings can be the result of the reaction mechanism, which has been proposed to work through a palladacycle (Scheme 2.29). The creation of a 5-membered ring would work through a 6-membered palladacycle, which would be preferable to a 7-membered cycle, required to obtain a 6-membered ring.[66]

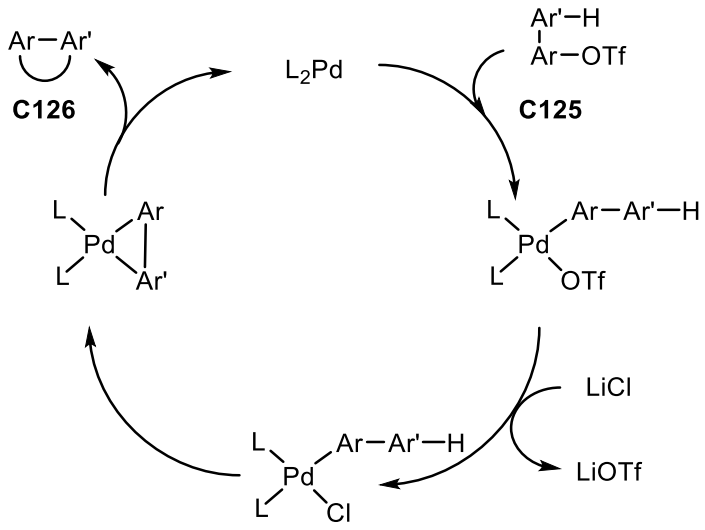

Scheme 2.29. Reaction mechanism proposed for Pd-catalysed intramolecular aryl coupling.[65]

The creation of 6-membered rings was achieved in a synthesis of substituted picenes[67] and [6]phenacens.[68] They were achieved in a double cyclisation, catalysed by $[PdCl_2(NCPh)_2]$ with PCy_3 as a ligand, Cs_2CO_3 and PivOH, in DMA at 150°C (Scheme 2.30). Unsubstituted **C128** as well as electron-rich products were achieved, using these conditions, with moderate yields (24-47%).

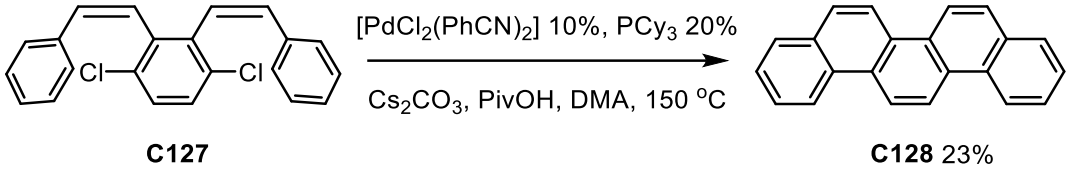

C127 **C128** 23%

Scheme 2.30. Pd catalysed picene synthesis.[67]

2.4.3 Base induced coupling

C-H activation employing strong bases, such as KO*t*-Bu and NaO*t*-Bu, has been proven to lead to both inter[69] and intramolecular[70,71] aryl couplings of aromatic compounds to aryl halides. Although at first it was reported that transition metals, such as iridium,[72] are needed in base induced aryl couplings, it has been subsequently proven that metal catalysts are not necessary. The Itami group showed that when microwave irradiation or high temperature are applied, KO*t*-Bu alone is enough to promote the coupling of electron-deficient nitrogen heterocycles with aryl iodides.[69]

The intramolecular version of base induced coupling has been reported as well, leading to 6-membered heteroarenes. Various additives, such as neocuproine,[73] pyridine[70] or pyridine with phenanthroline combination[70] have been used to promote the reaction. 6- and 7-membered phenanthridinones could also be obtained with the use of phenanthroline.[74]

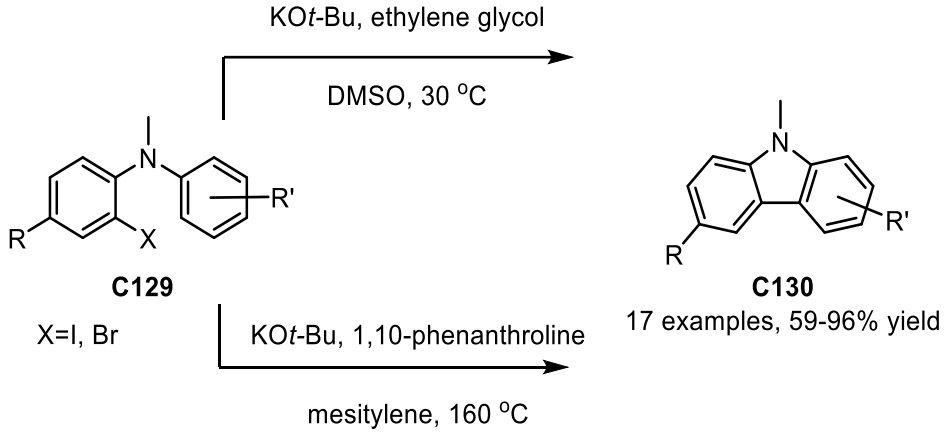

C129 X=I, Br

C130 17 examples, 59-96% yield

Scheme 2.31. Carbazole synthesis through KO*t*-Bu promoted intramolecular coupling. Conditions with 1,10-phenanthroline gave higher yields when bromides were used as starting materials.[71]

More recently, KO*t*-Bu with either ethylene glycol or 1,10-phenanthroline was used to synthesise carbazoles **C130** (Scheme 2.31).[71] Products with -Me, -OMe and -F substituents were synthesised with high yields (59-96%). Control experiments with radical scavengers, such as TEMPO, suggest a radical mechanism for both an inter-[69] and intramolecular[71] version of the reaction. In the proposed mechanism KO*t*-

But, in the presence of different additives such as amines, led to the generation of aryl radicals, with KO*t*-Bu assisting the deprotonation.[75,76] The reactions are deemed to involve a radical chain propagation mechanism.[77]

2.4.4 Oxidative photocyclisation

Oxidative photocyclisation, also called the Mallory reaction, allows the conversion of molecules containing stilbene-like motives into phenanthrene structures.[78–80] The reaction requires UV light and an oxidant, which can be either air or a catalytic amount of I_2. For example, this methodology has been used in one step of the circumanthracene **C132** synthesis (Scheme 2.32).[81] Scheme 2.33 depicts a fragment of the likely reaction mechanism, which allows the synthesis of compound **C132**. In the first step, the stilbene derivative is excited with UV light. Then it undergoes a [6π] photocyclisation reaction to dihydrophenanthrene, and under oxidation with I_2 gives a phenanthrene motive. Similar steps are repeated, to yield a product of another photocyclisation reaction.[78,79]

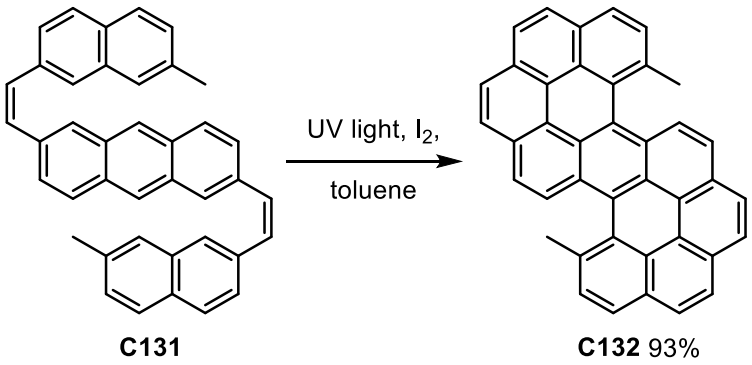

Scheme 2.32. Example of a photocyclisation in a synthesis of circumanthracene. 450 W mercury arc lamp used.[81]

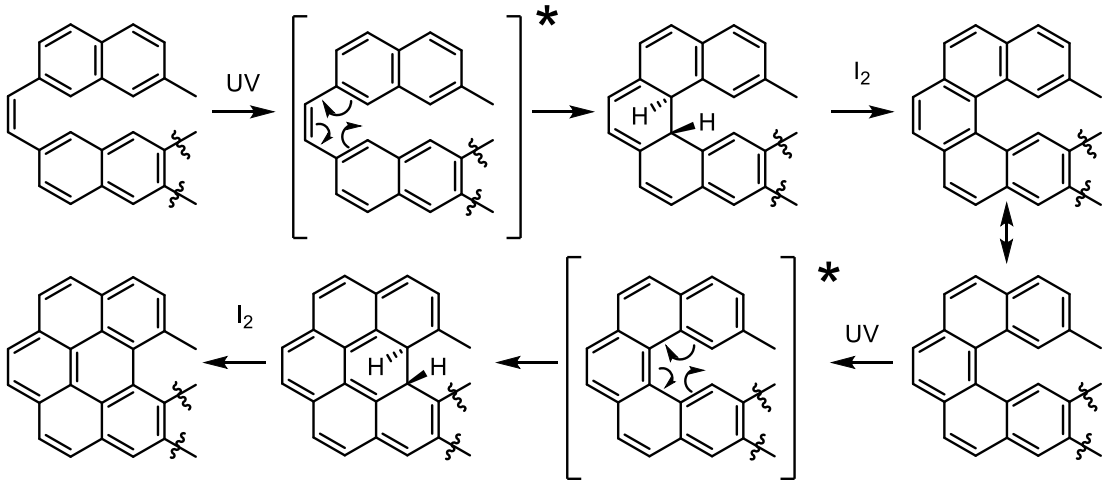

Scheme 2.33. Fragment of the mechanism of Mallory cyclization, to achieve compound **C72**.[81]

Sato *et al*. discovered that *o*-terphenyl motive can also undergo a related reaction, yielding a triphenylene structure.[82]

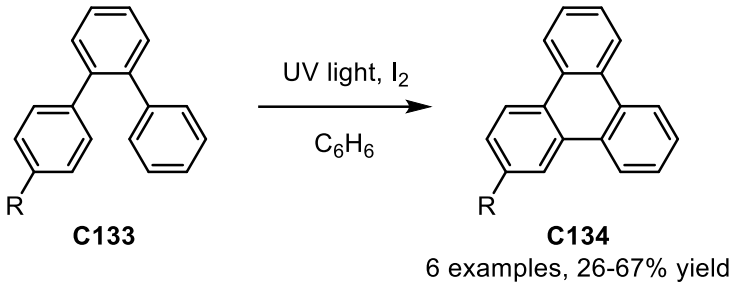

C133 **C134**
6 examples, 26-67% yield

Scheme 2.34. Photocyclisation of *o*-terphenyls, high pressure mercury lamp used.[82]

Unlike in the stilbene cyclisation, cyclisation of *o*-terphenyls **C133** requires an equimolar amount of I_2 and an inert atmosphere. These conditions allowed the synthesis of triphenylenes **C134** with various substituents, such as -Br, -OCH_3 or -$COOC_2H_5$ in moderate to good yields (26-67%) (Scheme 2.34).[82,83]

2.4.5 UV light promoted photochemical cyclodehydrohalogenation

PAHs can also be obtained with UV light promoted cyclodehydrohalogenation. Different halogens, such as I[84], Br[82], Cl[82,85,86] and even F[87] can be employed in this reaction. For example, UV light promoted cyclodehydrochlorination was used to synthesise phenanthro[9,10-c]thiophenes **C136** (Scheme 2.35).[85] Several substituents such as -Me, -OMe, -CF_3 and -F were successfully included in the structure, leading to products **C136** in high yields (66-82%).

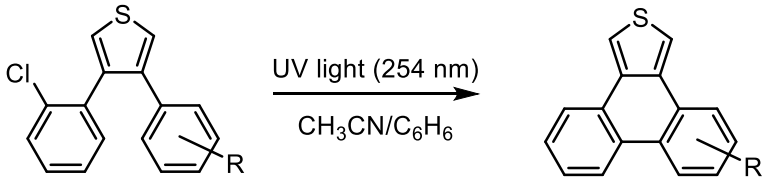

C135
R=Me, OMe, CF_3, F

C136
66-82% yield

Scheme 2.35. UV light promoted photochemical cyclodehydrochloriantion.[85]

The photocyclisation has been proposed to work through the UV light promoted, conrotatory [10π] pericyclic reaction mechanism, followed by the elimination of the HCl molecule (Scheme 2.36).

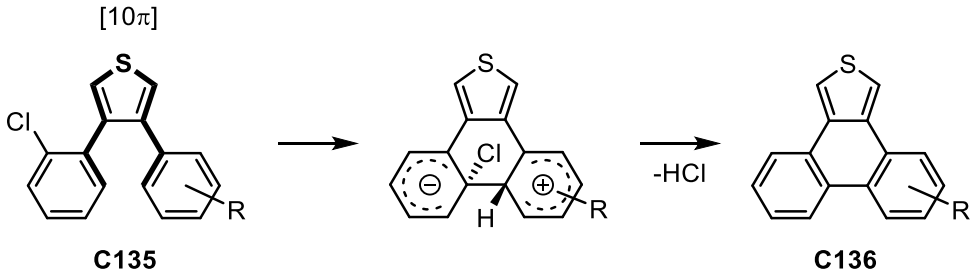

Scheme 2.36. Proposed reaction mechanism of the thiophene **C135** photocyclization.[85]

Multiple photochemical cyclodehydrochlorination reactions can be carried out simultaneously. Daigle *et al*. obtained mono, di- and tetracyclisation **C138** reaction products in a similar reaction (Scheme 2.37).[86]

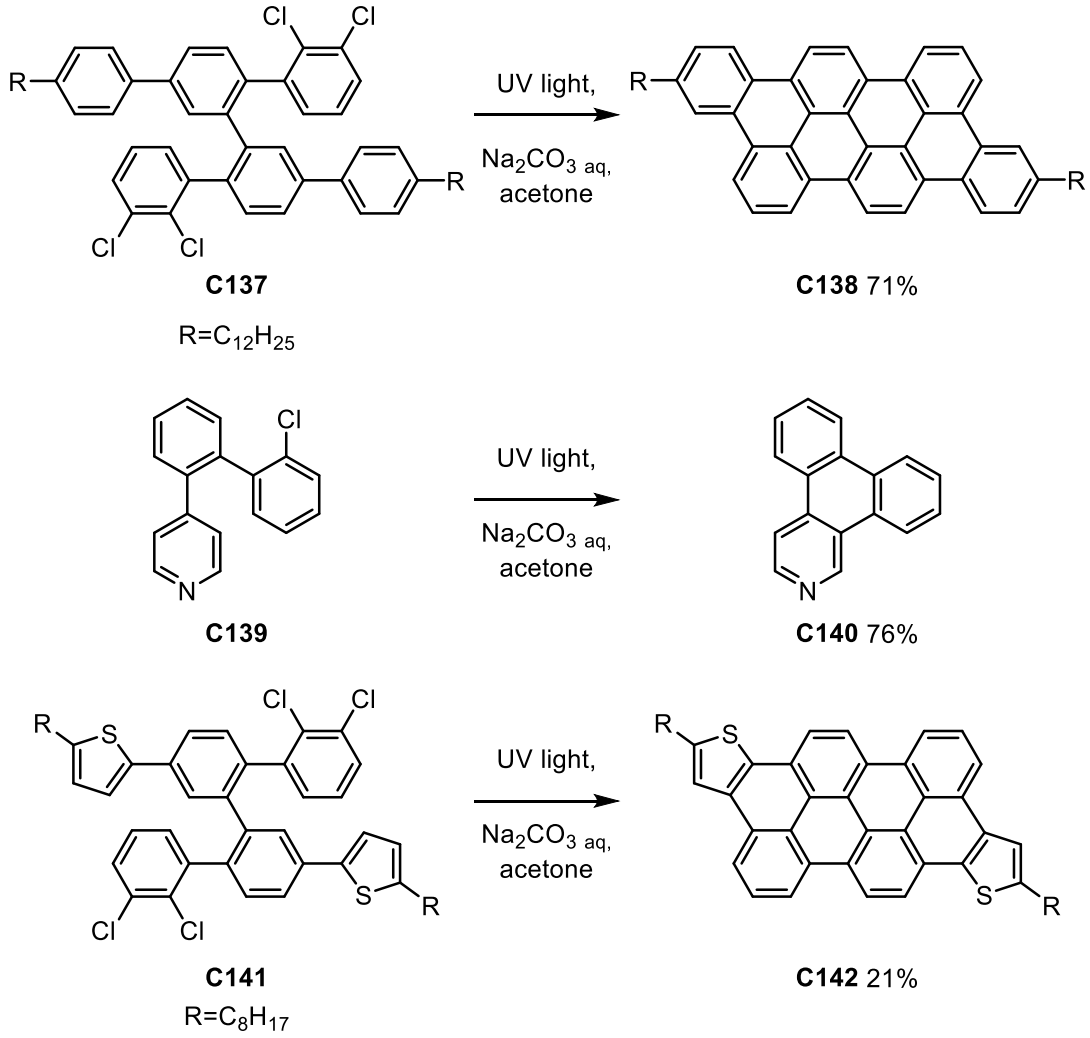

Scheme 2.37. Photochemical cyclodehydrochlorination reaction promoted by UV light. 450 W medium pressure mercury lamp used.[86]

Moderate to high yields (21-95%) were obtained, although only alkyl chains have been demonstrated as substituents. However, pyridine **C140** and thiophene **C142** moieties could be successfully included in the structure of achieved nanographenes.

The reaction mechanism is proposed to be a conrotatory [4n+2] π photocyclisation, followed by HCl elimination, similar to the mechanism described in Scheme 2.36. The alternative radical mechanism is thought to be possible for bromo and iodo derivatives, although not applicable in the case of chlorine or fluorine containing materials.[82,85,86]

2.4.6 Photoredox catalysed Pschorr like reaction

A photoredox catalysed version of the Pschorr reaction, utilising visible light irradiation, was achieved using $[Ru(bpy)_3]^{2+}$ as the photocatalyst (Scheme 2.38).[88] Phenanthrene derivatives **C144** bearing different substituents, such as Br or OCH_3, were synthesised quantitatively, using diazonium salts of stilbenes **C143** as starting materials.

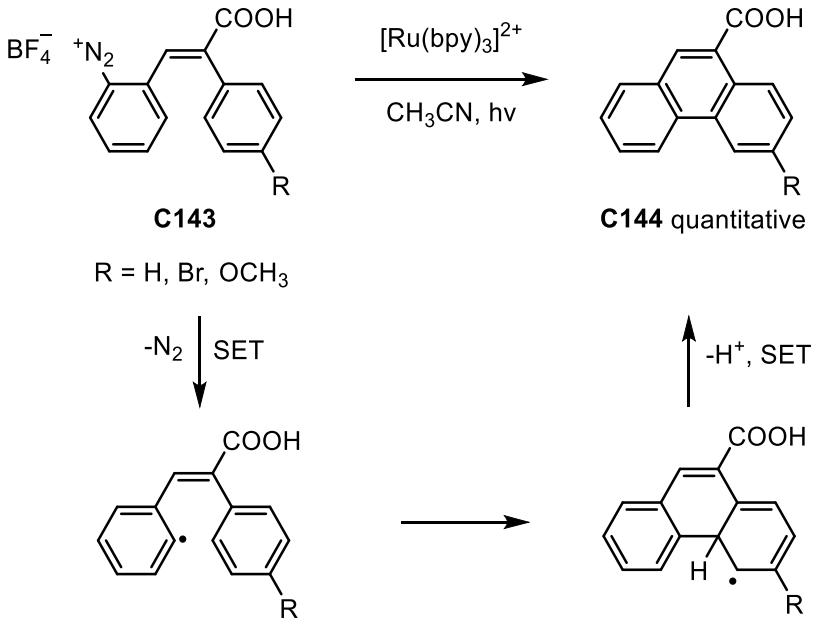

Scheme 2.38. Photoredox catalysed Pschorr reaction and plausible reaction mechanism. Visible light > 410 nm used.[88]

More recently, 6-arylphenanthridines **C146** were synthesised in the Pschorr like reaction, also using $[Ru(bpy)_3]^{2+}$ as the photoredox catalyst (Scheme 2.39).[89] Diazonium salts have been formed *in situ* from amines **C145** and *t*-BuONO, and then served as a radical precursor in the photoredox catalysed coupling. A range of products **C146** bearing either EWGs or EDGs were synthesised with high yields (85-94%). The reaction mechanism is proposed to follow a SET reduction of a diazonium salt with $*[Ru(bpy)_3]^{2+}$, similarly to the general mechanism for photoredox catalysed aryl-aryl couplings depicted in section 2.1.5 (Scheme 2.7). The difference is that as the reaction is intramolecular, the aryl ring in the molecule takes the role of an electron-rich radical trap.

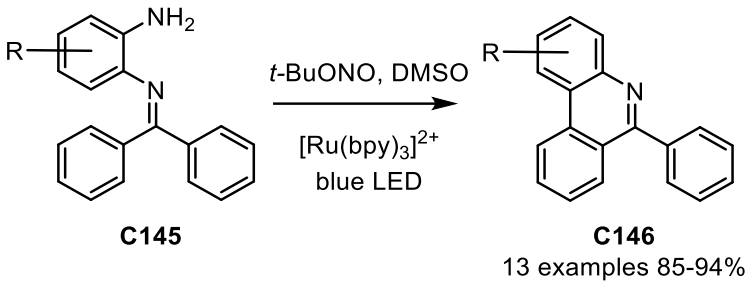

Scheme 2.39. Photoredox catalysed 6-arylphenanthridines synthesis.[89]

2.5 Cyclisation of aryl chlorides photoredox catalysed by PXX

2.5.1 Aim of the project

Even though many pathways to synthesise PAHs have been developed, new improved methods are still necessary. Existing methodologies can suffer from harsh conditions (namely UV light, high temperature or strong base), often employ expensive Pd or Ir based transition metal catalysts and can present low efficiency in electron-poor or small substrates. This creates space for the development of new highly effective but mild and green synthetic pathways toward PAHs. Photoredox catalysis, employing chromophores, meets these conditions as a powerful but mild method, where reactions are catalysed with light and usually take place at room temperature. Few examples of the use of photoredox catalysis towards intramolecular aryl-aryl couplings have been reported,[88,89] and to the best of our knowledge, none employed aryl halides as radical precursors.

Our proposal is a cyclisation of aryl halides, photoredox catalysed by PXX, leading to the synthesis of PAHs (Scheme 2.40). The reaction is an intramolecular version of the coupling we demonstrated in section 2.3.2.

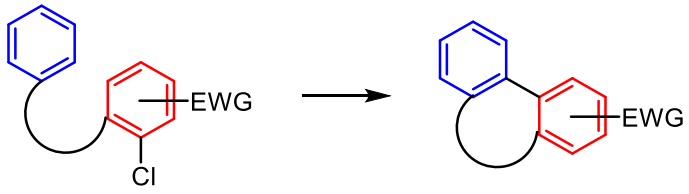

Scheme 2.40. Scheme for intramolecular aryl-aryl coupling leading to the synthesis of PAHs.

The reaction requires the incorporation of EWG in the ring containing Cl atom, as electron-poor aryl chlorides have reduction potential achievable by PXX. As methods to synthesise PAHs often do not perform well on electron-deficient starting materials, for example oxidative coupling, our reaction could be complementary to them.

2.5.2 Triphenylene

Triphenylene is one of the simplest PAHs which could be achieved using the proposed PXX photoredox catalysed cyclisation reaction. Triphenylene has been widely studied for liquid crystal applications[90–92] and organic light-emitting diodes (OLEDs)[93,94]. Triphenylene based symmetrical hexaethers **C147** (Figure 2.2) are the most commonly studied materials for discotic liquid crystals applications. Various groups have been tested as ether substituents R, from paraffinic side chains with ionic liquid pendants, to benzyl and biphenyl ethers.[95] Triphenylene based hexaesters **C148** (Figure 2.2) have been widely investigated as well. Branched and not-branched fluorinated phenyls, as well as dialkoxy benzoates and azobenzene moieties, have been applied as substituents R.[95]

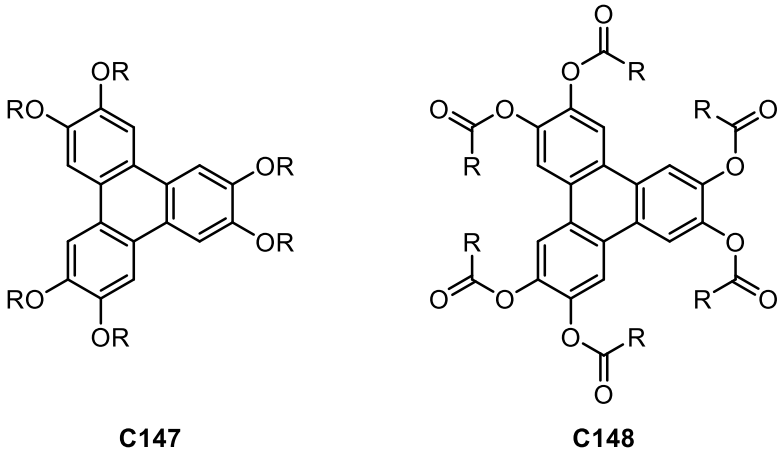

Figure 2.2. The general structure of triphenylene based hexaethers and hexaesters.[95]

Triphenylene derivatives are also used as electron transport materials in OLEDs since the planar triphenylene core provides good electron transport abilities.[93,94] One example of triphenylene tested for electron transport applications is compound **C156**, a triphenylene disubstituted with bipyridine to provide good electron injection ability (Scheme 2.41).[94] In the first step, double Suzuki coupling led to molecule **C151** in 40% yield. Ipso bromination of trimethylsilyl substituted moieties led to molecule **C152** in 86% yield. **C152** underwent oxidative coupling with $MoCl_5$, leading to triphenylene **C153** in 9% yield. Then Miyaura borylation reaction allowed compound **C154** in 70% yield, which after Suzuki coupling yielded desired product **C156** in 60% yield.

As shown, triphenylenes are an important class of compounds for application in optoelectronics, although their synthesis often suffers from low yields. So we want to propose another pathway towards the synthesis of substituted triphenylenes.

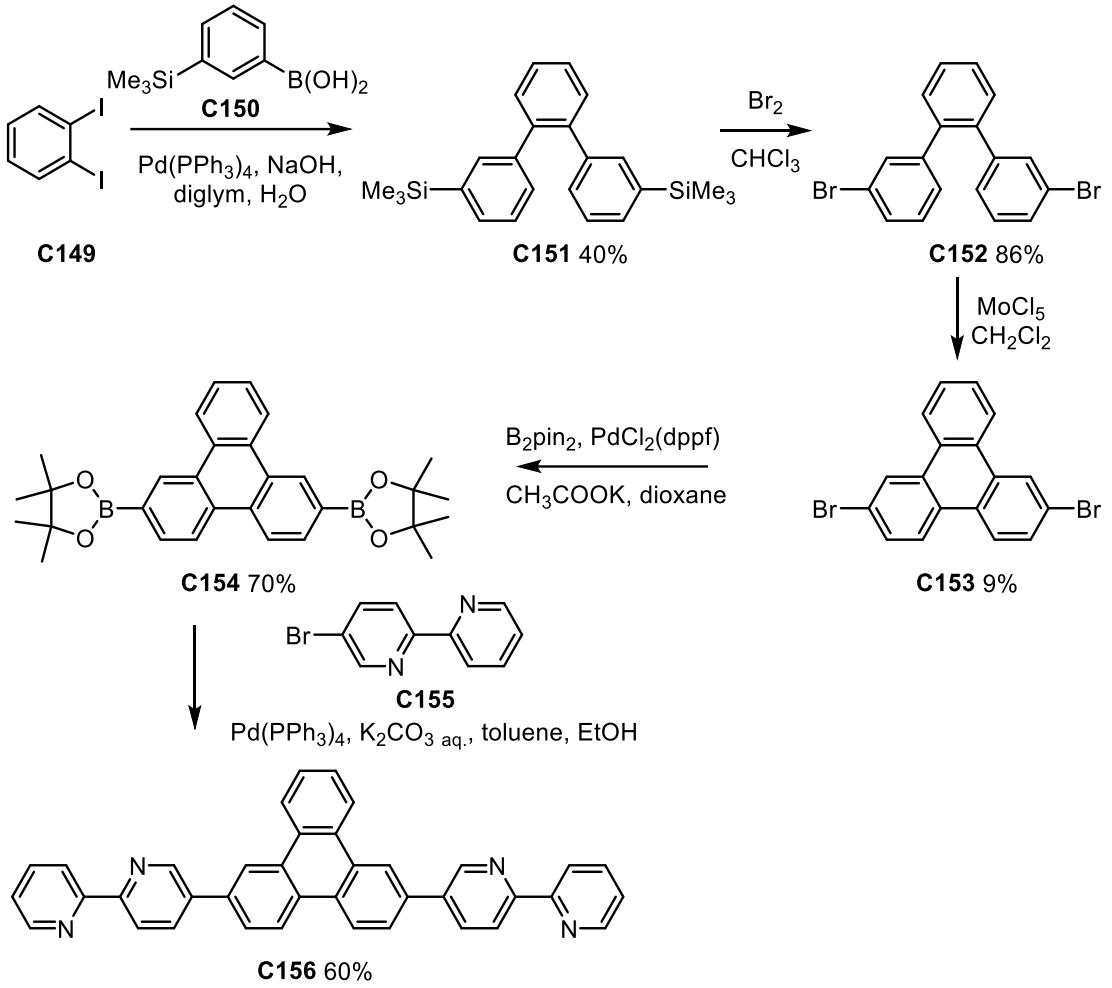

Scheme 2.41. Synthesis of triphenylene derivative.[94]

2.5.3 Tetraphenylenes

As we achieved a tetraphenylene structure during our attempt at a double photocyclization reaction (section 2.5.7), a short introduction about tetraphenylenes is given in the following section.

Substituted tetraphenylenes are chiral molecules, which prompted studies on their use as ligands in asymmetric catalysis. For example, asymmetric hydrogenation of olefins **C157** was realised with $Rh(COD)_2BF_4$, using ***(S,S)*-C159** as a ligand (Scheme 2.42).[96] All reactions were quantitative, and the products were achieved with high enantioselectivity (94.9–99.0% ee).

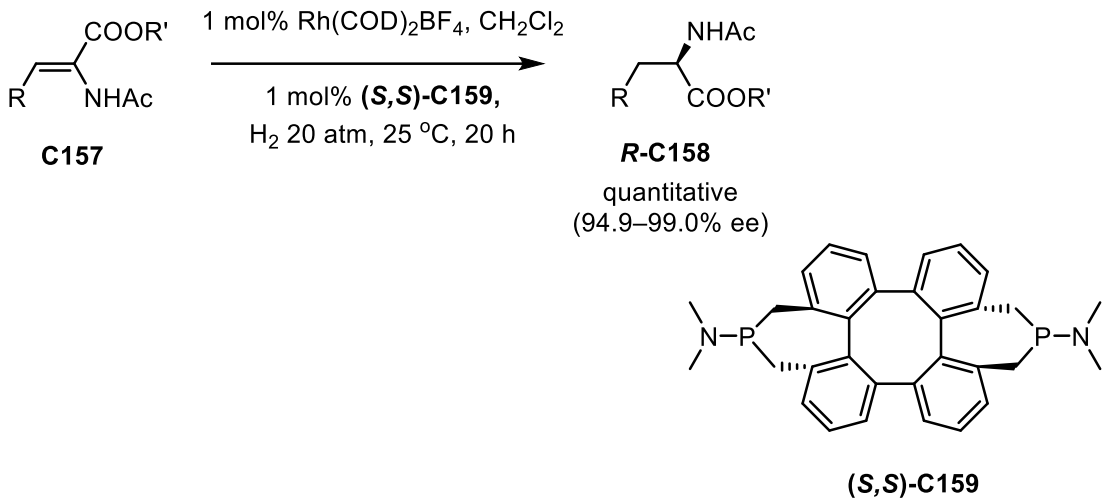

Scheme 2.42. Asymmetric hydrogenation of olefins.[96]

Not substituted tetraphenylene can classically be achieved in Pd[97] and Pt[97,98] catalysed reactions of biphenylene. Substituted tetraphenylenes can also be achieved through transition metal catalysed reactions of biphenylene, with Ni[99,100] and Pd[101] catalysed reaction of biphenylene with biaryl halides. The reaction was developed further to give a wide range of mono and disubstituted tetraphenylenes (Scheme 2.43).[102] Various EWGs and EDGs can be applied as substituents to give the products **C163** in high yields (60-84%). It was also possible to introduce two different substituents into the structure of tetraphenylene (**C163e**, **C1636**).

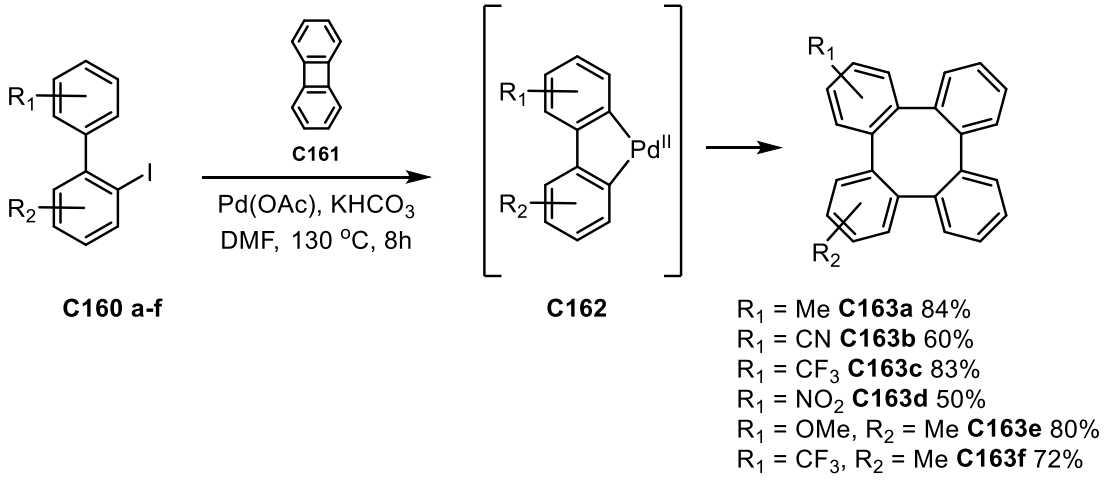

Scheme 2.43. Synthesis of monosubstituted tetraphenylene derivatives.[102]

Pd-catalysed C-H activation can also be applied to achieve tetra substituted tetraphenylenes (Scheme 2.44). Tetra, di and monosubstituted products **C165** were achieved with moderate to good yields (21-68%).[103] Various substituents, such as -Me, -Ph, -Cl, -F and -OMe were well tolerated. The reaction has been proposed to work

through a Pd complex, similar to **C162**, which could later react with another molecule of starting material.

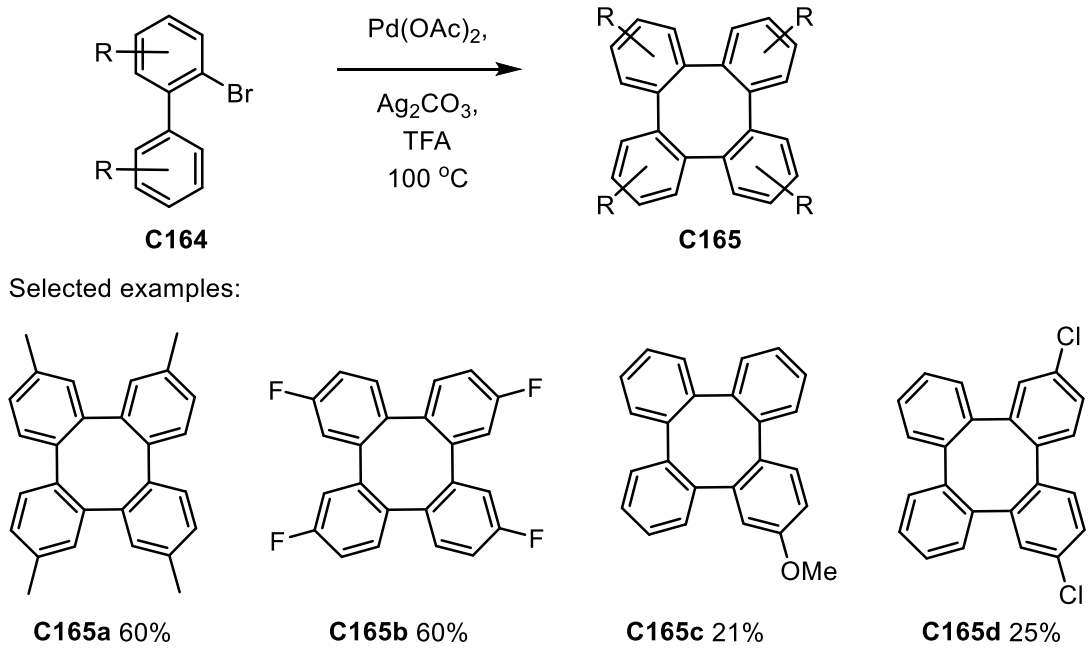

Scheme 2.44. Pd-catalyzed C–H activation of 2-iodobiphenyls.[103]

Tetraphenylene derivatives can also be achieved in the oxidative coupling of dilithiobiphenyl derivatives with different metal catalysts, such as $CuCl_2$[104] and $CuBr_2$.[105] More recently the method has been used to achieve hydroxy-substituted tetraphenylenes.[106,107] Stereoselective variant of the reaction was developed as well, where sparteine was added to achieve substituted tetraphenylenes **C167** with moderate enantioselectivity (Scheme 2.45).[105]

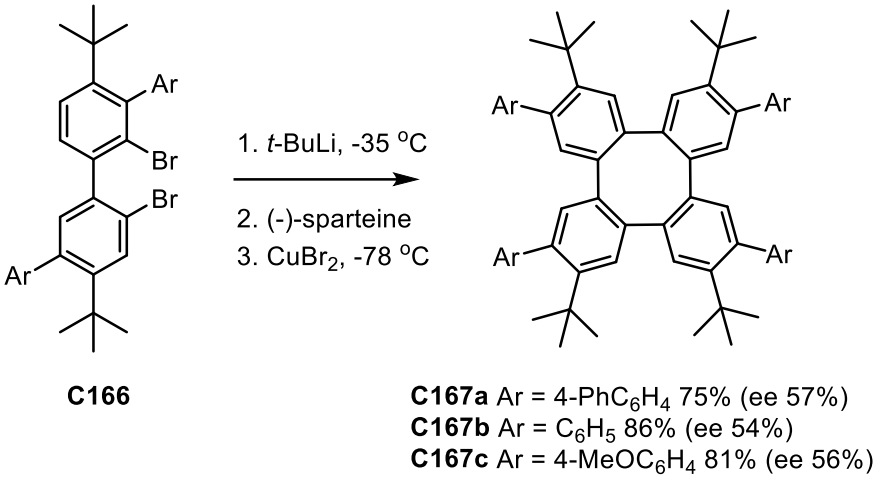

Scheme 2.45. $CuBr_2$ catalysed stereoselective tetraphenylene synthesis.[105]

2.5.4 Retrosynthesis

In the retrosynthetic pathway, shown in Scheme 2.46, breaking the indicated bond in triphenylene leads to a substituted *o*-terphenyl.

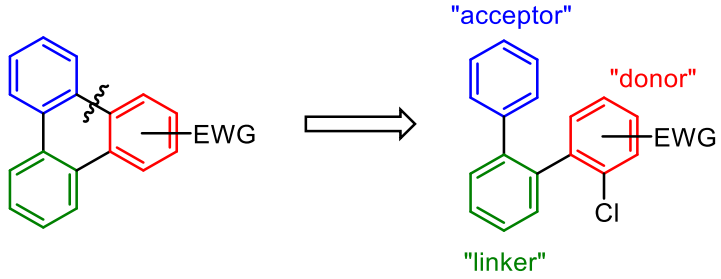

Scheme 2.46. Retrosynthetic route to triphenylenes using an intramolecular PXX photoredox catalysed aryl coupling.

The blue aryl group in *o*-terphenyl acts as an electron-rich radical trap and will be called an acceptor. The red ring, which will be called a donor, has a chlorine atom in position 2, which acts as a radical source after the reduction. For the chloride to have a reduction potential accessible by PXX* (E^*_{ox} = -2 V vs SCE), an EWG is necessary in a donor ring. Meanwhile, the green aryl group acts as a linker.

If we assume that each aryl group (acceptor, donor and linker) can bear different substituents, we can see that a large number of substituted triphenylenes can be potentially synthesised. To show the scope and limitations of the reaction, we decided to synthesise a range of substituted substrates for cyclisation reactions by Suzuki couplings, preferably in one or up to two Suzuki reactions. There are two retrosynthetic pathways, route A and route B, we can follow to achieve *o*-terphenyl structure (Scheme 2.47). Route A places a bromine atom on the phenyl ring containing EWG, while in route B bromine is present on a biphenyl.

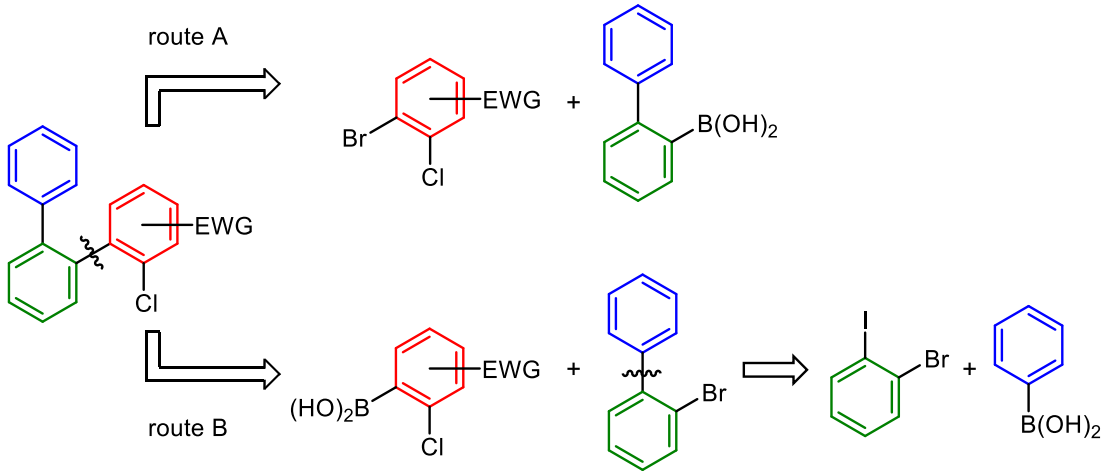

Scheme 2.47. Retrosynthetic routes to *o*-terphenyl structure: route A (top) and route B (bottom).

Route A places a bromine atom on an electron-poor donor ring and a boronic acid on a biphenyl. The Suzuki coupling works best when an aryl halide is electron-poor, as it promotes oxidative addition, and when an aryl boronic acid is electron-rich, since it promotes transmetalation step,[108] making route A preferable. The presence of both chlorine and bromine atoms on a donor ring raises a question about a risk of a double coupling. To avoid this potential issue, a moderately active Pd catalyst, such as [$Pd(PPh_3)_4$], was used, and equimolar amounts of bromide and boronic acid were employed. In route B, on the other hand, an aryl bromide would be more electron-rich and an aryl boronic acid electron-poor, which is unpreferable in the Suzuki couplings.[109–111] However, this route gives access to easy modification of a biphenylene core. It allows the construction of biphenylenes with different substituents on both linker and donor rings in another Suzuki coupling. After considering these facts, we decided to use route A when required starting materials were commercially available and route B when they had to be synthesised.

2.5.5 Synthesis of starting materials for intramolecular photoredox coupling – use of Suzuki couplings

To test the boundaries of the PXX catalysed photoredox cyclisation reaction, we decided to prepare materials with different EWGs, EDGs as well as with heterocycles. First, we decided to test which EWGs can be included in a donor ring to activate the chloride. We started with a nitrile as an EWG, both in positions para and ortho to the chloride (**52** and **53**), since it gave a high yield in an intermolecular coupling (section 2.3.2). We also planned to test if a para-ester group (**54**) as well as a nitro substituent (**55**) could activate the chloride. To test if five-membered rings can be created with this methodology, we decided to synthesise **56**. To study which structures will be tolerated on an acceptor ring, playing the role of a radical trap, we planned to include heteroaromatic moieties pyrrole **57** and furan **58**, as well as EDGs dimethoxy **59** and tert-butyl **60**. Planned structures also included EWGs on either the acceptor **61** (ester) **62** (nitrile) or the linker of **63**.

The synthesis of these materials will be described below. As the focus of our studies was on the photoredox cyclisation reaction, rather than on the Suzuki couplings, these reactions were not optimised if the desired compound was obtained in a sufficient amount for the cyclisation reaction.

2.5.5.1 Route A

As the necessary starting materials were commercially available, structures **52** - **56** were prepared using route A (Scheme 2.48). To avoid the potential formation of doubly

substituted products, equimolar amounts of boronic acid and aryl bromide were used. Precursors with a nitrile group, **52** and **53** were obtained with 23% and 30% yields, respectively. Ester **54** was achieved in 32% yield, while compound **55** with a nitro group was synthesised with 38% yield. The synthesis of **56** was performed with 1-naphthalene boronic acid, instead of 2-biphenylboronic acid, and led to a high yield (88%). The fact that **56** was synthesised with a significantly higher yield (88%) than products **52** - **55** (23-38%), could derive from a lower steric hindrance in a reaction with naphthalene boronic acid than with 2-biphenylboronic acid.

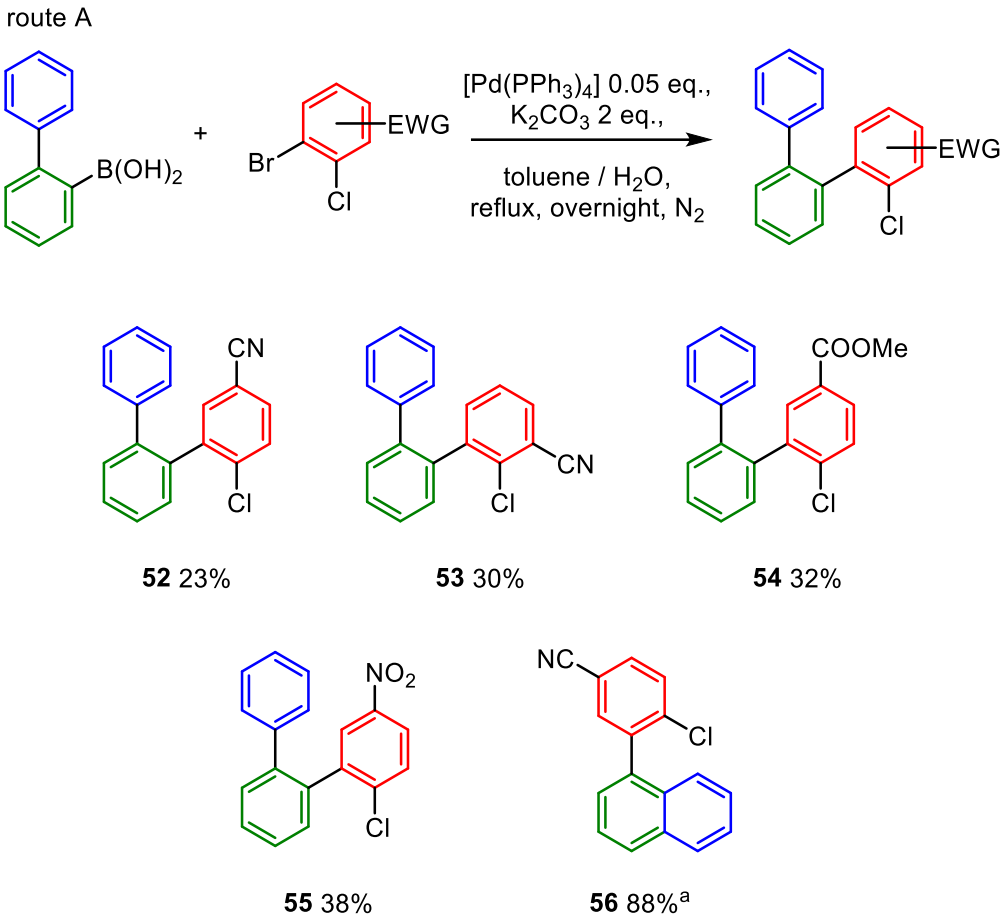

Scheme 2.48. *O*-terphenyls prepared in Suzuki couplings using route A. Equimolar amounts of boronic acid and bromide used. [a]1-naphthalene boronic acid used instead of 2-biphenylboronic acid.

2.5.5.2 Route B

Synthesis of compounds **57** - **62** required route B (Scheme 2.49). In the case of compounds **57** and **58** only step II was necessary, as suitable aryl bromides were commercially available. Meanwhile, both steps were necessary for compounds **59** – **62**, as substituted biphenyls had to be synthesised. To achieve molecule **57**, the conditions applied in route A (Scheme 2.48) were tested first, namely [$Pd(PPh_3)$] as a catalyst in toluene/H_2O mixture. Unfortunately, no conversion was observed.

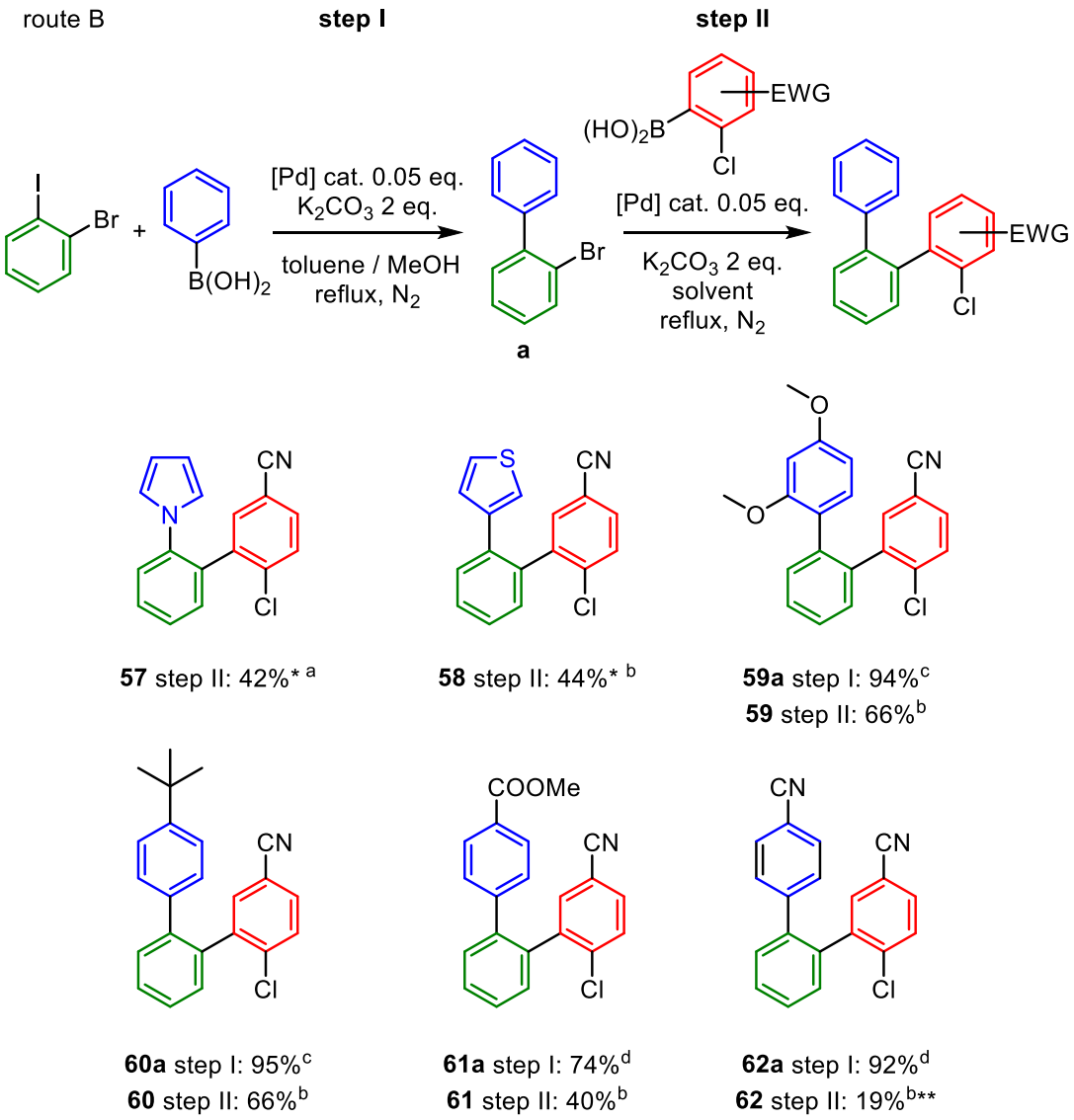

Scheme 2.49. *o*-terphenyls prepared in Suzuki couplings using route B. Step I, 1 eq. aryl bromide, 1.2 eq. boronic acid; step II 1 eq. aryl bromide, 1.5 eq. boronic acid; *only step II was necessary; **reaction time 3 days; [a] $[Pd(PPh_3)Cl_2]$, DME/H_2O; [b] $[Pd(dppf)Cl_2]$, dioxane/H_2O; [c] $[Pd(PPh_3)Cl_2]$; [d] $[Pd(dppf)Cl_2]$. Products from step I are marked with "a" after the number.

As described in section 2.5.4, an electron-poor aryl boronic acid and an electron-rich aryl bromide are not preferable in Suzuki couplings.[108] Here, the nitrile group on an arylboronic acid makes it electron-poor, and a sterically hindered aryl bromide can also pose an issue.[108] Eventually, $[Pd(PPh_3)_2Cl_2]$ as a catalyst was tested in DME/H_2O mixture, and a moderate yield (42%) of **57** was obtained this time.

A challenge with using electron-deficient aryl boronic acids in Suzuki couplings is that although several procedures have been developed,[109–111] they cannot be generally applied to all starting materials. The introduction of an EWG on the donor ring is necessary though, to obtain molecules with reduction potential achievable by PXX, so

we decided to test different conditions reported to be effective with electron-deficient boronic acids.

Synthesis of **59** required two consecutive Suzuki couplings. The first one needed to be selective, so only iodine would react. Only a small excess (1.2 eq.) of boronic acid was used, and the reaction was monitored by TLC, to stop at a monosubstitution step. This approach has led to 94% yield of the resulting precursor **59a**. However, the second step posed a challenge, as the use of [$Pd(PPh_3)_4$] as the catalyst did not lead to the desired product formation. [$Pd(dba)_3$] with SPhos ligand has been tested, as this catalytic system was reported to work effectively in Suzuki reactions with electron-poor substrates,[111] although in our case no conversion was observed. Finally, conditions with [$Pd(dppf)Cl_2$] in dioxane/H_2O were applied, and compound **59** was obtained in 66% yield.

To synthesise molecule **60** two steps were necessary. In the step I tert-butyl substituted biphenyl bromide **60a** was obtained in an excellent yield (95%). Moving to the step II, [$Pd(PPh_3)_4$] as a catalyst again gave no conversion. However, when [$Pd(dppf)Cl_2$] was used, complete conversion was obtained after 5.5 h, and **60** was achieved with 67% yield. In further reactions we decided to use the following conditions, as they gave high yields: 0.05 eq. of [$Pd(dppf)Cl_2$], 1 eq. of aryl bromide, 1.5 eq. of boronic acid, 2 eq. of K_2CO_3 in dioxane/H_2O 5:1.

Preparation of material **58** including thiophene ring needed only the step II, as an appropriate bromide was commercially available. The desired product was isolated with 44% yield.

To study how EWGs present in an acceptor ring would affect the cyclisation reaction, *o*-terphenyls bearing ester **61** and nitrile **62** groups on the acceptor ring were prepared. Synthesis of precursor with ester group **61** required two consecutive Suzuki reactions. The step I gave **61a** in a good yield of 74%, while the step II led to the isolation of **61** with a moderate yield of 40%. Similar results were obtained in the case of compounds with a nitrile group on the acceptor ring **62**. Again, the step I gave **62a** in a very high yield of 92%, while the step II needed prolonged reaction time (3 days), to obtain sufficient conversion and still gave **62** in a low yield of 19%.

To study the influence of an EWG present on a linker ring, we decided to synthesise an isomer of **61** with the ester group on the linker ring (**63**). Two steps were necessary to synthesise this compound. However, in the step I, even the slight excess of boronic acid (1.2 eq.) led to an inseparable mixture of mono and disubstituted products. The mixture of compounds was subjected to conditions from the step II, in hope that the

introduction of an electron-poor aryl ring would facilitate the isolation of the desired product **63** from the side product. However, low conversion was observed in the step II and the reaction time had to be extended to 3 days. Unfortunately, substantial hydrolysis occurred, and carboxylic acid was obtained rather than the ester **63** (Scheme 2.50).

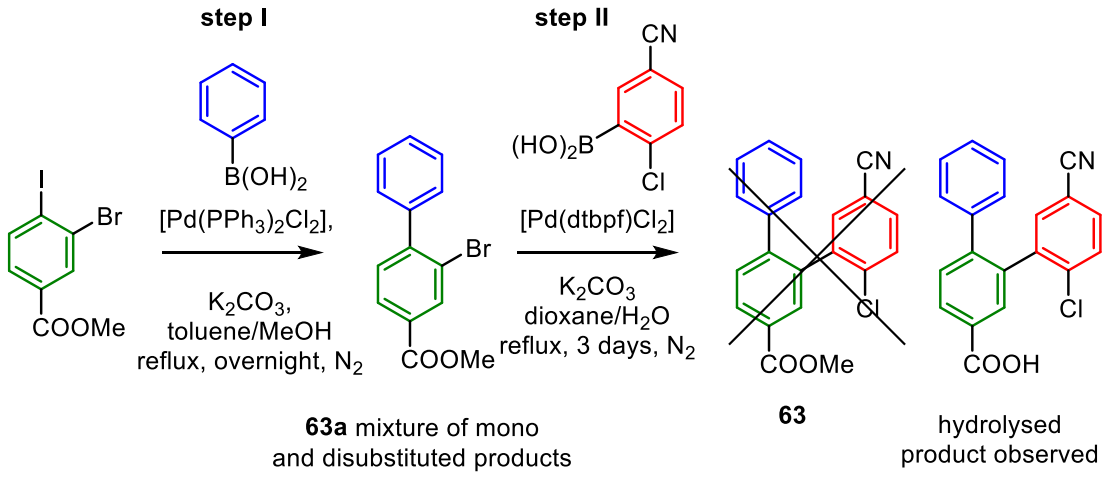

Scheme 2.50. The failed attempt at the synthesis of **63**. Step I 1.2 eq. of boronic acid, step II 1.5 eq. of boronic acid.

The issue with low conversion and hydrolysis in the step II prompted us to look for mild but effective conditions to achieve desired compound **63**.

Emulsion conditions for Suzuki coupling

We decided to try the Suzuki coupling in emulsion, where the reaction is conducted in a small amount of emulsion, rather than in a large amount of organic solvent and water. After IUPAC "Gold Book" an emulsion is "*a fluid colloidal system in which liquid droplets and/or liquid crystals are dispersed in a liquid. The droplets often exceed the usual limits for colloids in size.*"[1] These conditions are modifications of micellar systems,[112] where reactions are taking place in micelles formed from water and surfactant. The Suzuki coupling reactions performed in emulsion have been shown to be very effective for the preparation of polyphenyl derivatives, with decreased temperatures, higher yields and shorter reaction times compared to classical conditions.[113] Additionally the use of selected surfactants, such as Kolliphor EL, allows to conduct these couplings under air, rather than in an inert atmosphere.[113] For our system, we decided to use 2% of [Pd(dtbpf)Cl_2] catalyst, 6 eq. of Et_3N as a base and 0.5M emulsion as a reaction medium (2% of Kolliphor EL and 10% of toluene in water), at 60°C, under air.[113]

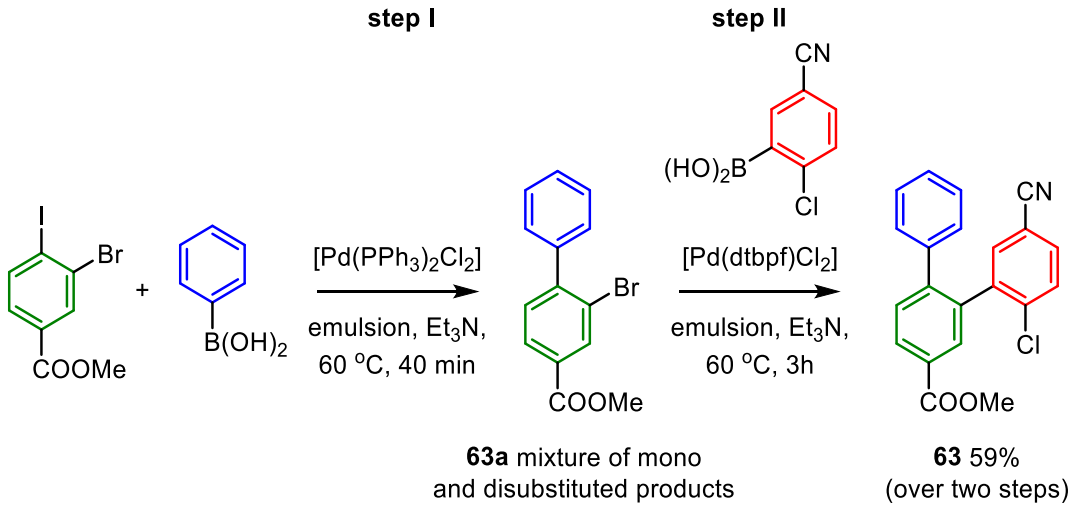

Scheme 2.51. Synthesis of compound **63** using emulsion conditions. [Pd] cat 0.02 eq., Et_3N 6 eq., emulsion 0.5M: 2% of Kolliphor EL and 10% toluene in water, under air. Step I 1.1 eq. of boronic acid. Step II 1.5 eq. of boronic acid.

Indeed, when emulsion conditions were applied to the first step, full conversion was observed in only 40 min, leading to ester-bearing precursor **63a** (Scheme 2.51). Slightly modified conditions were applied, where only 1.1 eq. of boronic acid and $[Pd(PPh_3)_2Cl_2]$ were used to avoid double substitution, but still a small amount of disubstituted product was obtained and proved difficult to separate. The impure precursor was subjected to the conditions of the step II, using $[Pd(dtbpf)Cl_2]$ as a catalyst. The full conversion was obtained after 3 h, and **63** was isolated with 59% yield over two steps (Scheme 2.51).

2.5.6 Cyclisation photoredox catalysed by PXX

Having prepared a range of necessary precursors, we proceeded to test the intramolecular coupling photoredox catalysed by PXX. We employed conditions used in section 2.3.2. Experiments were performed on a 0.2 mmol scale of previously prepared aryl chloride (**52**-**63**), with 2% of PXX as the photoredox catalyst, 1.4 eq. of DIPEA as the sacrificial electron donor in DMSO, under an inert atmosphere and with blue light irradiation (457 nm), achieved using UltraLEDs Blue 120 high intensity LED strips coiled around a 250 ml glass beaker. The results are presented in Scheme 2.52.

First, the reaction on a substrate **52** bearing a nitrile group in *para* position to chlorine atom was tested, as nitriles were most successful in case of an intermolecular coupling. Indeed, compound **64** was isolated with 70% yield after overnight irradiation (Scheme 2.52). We proceeded to check the scope of EWG on the donor ring. Placing the nitrile group in an *ortho* position to the chlorine atom in the precursor led to a high yield of **65** (72%) as well. The ester group was also found to be highly activating, with **66** obtained with 72% yield.

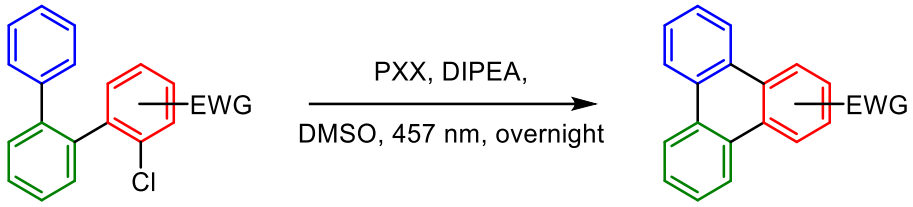

Different EWG in a donor ring

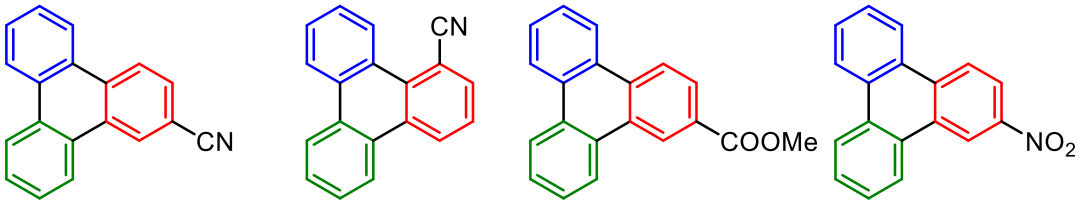

64 70% **65** 72% **66** 72% **67** 0%

Heterocycles

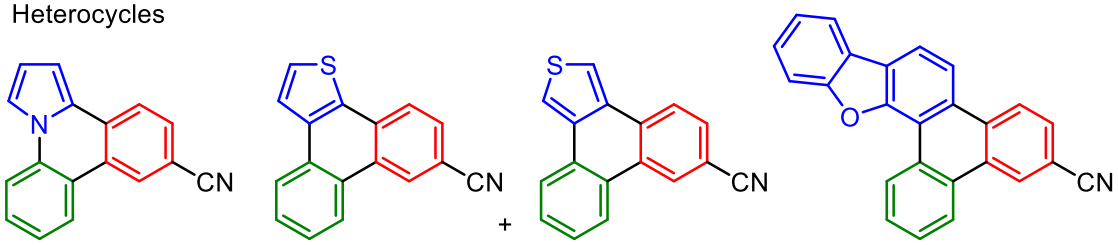

68 83% **69a** **69b** **70** 40%

Combined yield 48% 1 : 1.16 ratio

EDG in an acceptor ring

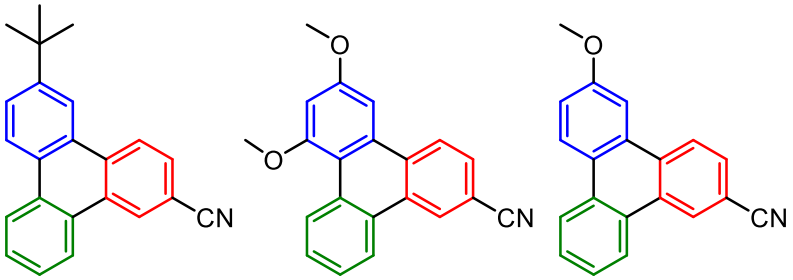

71 69% **72** 0% **73** 70%

EWG in an acceptor ring EWG in a linker ring 5 membered ring

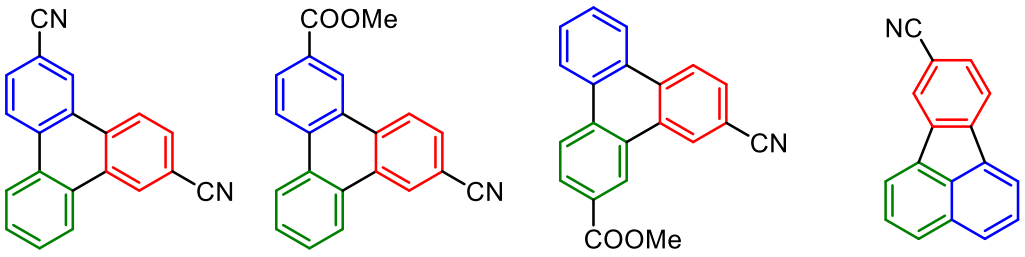

74 0%* **75** 38% **76** 66% **77** 0%

Scheme 2.52. PXX catalysed cyclisation. 0.2 mmol scale of aryl halide, 2% of PXX, 1.4 eq. of DIPEA and 1 ml of DMSO, unless stated otherwise. Blue LED strips (457 nm) used as the light source, reactions performed after degassing with freeze pump thaw and under N_2, isolated yields reported.* reaction performed on 0.14 mmol scale of aryl chloride.

The use of nitro group as EWG did not allow the formation of **67**, with no conversion of starting material observed. The radical formation should be possible, as chlorides with NO_2 group have reduction potential easily achievable by PXX (-1.05 eV vs SCE for *p*-chloronitrobenzene).[49] However, the presence of NO_2 on aryl chlorides is correlated with a slow C-Cl fragmentation kinetics $k_{f\,p\text{-chloronitrobenzene}} = 10^{-2}\ s^{-1}$),[49] which can hamper the formation of aryl radicals.[39]

Next, we moved to molecules containing heterocyclic structures acting as electron-rich radical traps (Scheme 2.52). When pyrrole was used as an acceptor ring, **68** was obtained with 83% yield. The use of thiophene containing structure led to cyclisation in both positions 2 **69a** and 3 **69b**. The combined yield was 48%, and the products were isolated in proportion 1 to 1.16. Structures of these isomers were assigned using ^{1}H NMR, with the product isolated in a slightly smaller amount proposed to be **69a**, cyclised in position 2. The doublet signal *a* at 7.98 ppm is coupled with *J*= 5.4 Hz (coupling partner in multiplet 7.76 – 7.66 3H) (Figure 2.3, top), which is a typical coupling constant between protons 2 and 3 in thiophene (usually 5.4 Hz).[114] Additionally doublet of doublets signal *g* at 8.92 ppm is coupled with doublet of doublets *i* at 8.13 ppm with a para coupling constant *J*=0.5 Hz, and with doublet of doublets *h* at 7.76 ppm with a meta coupling constant 1.5 Hz. Signals *i* and *h* are coupled together with the same coupling constant *J* = 8.3 Hz. Meanwhile, in the other isomer **69b**, the doublets *a* and *b* at 8.12 and 8.07 ppm are coupled with the same coupling constant *J* = 3 Hz (Figure 2.3, bottom), which is a typical coupling constant in thiophene, between protons 2 and 5 (usually 3.4 Hz).[114] Additionally doublet *g* at 8.62 ppm is coupled with doublet of doublets *h* at 7.69 ppm with a meta coupling constant 1.5 Hz. As the isolated yield of both isomers was compared with crude NMR not analysed and the scale was small, the difference in the distribution of isomers can derive from an experimental error. HR mass spectroscopy indicated the same molecular ion for **69a** and **69b**, suggesting they are indeed isomers.

When dibenzofuran was acting as an acceptor, **70** was obtained with 40% yield. However, the observed conversion was high, and probably low solubility of the product led to some loss of product during the isolation.

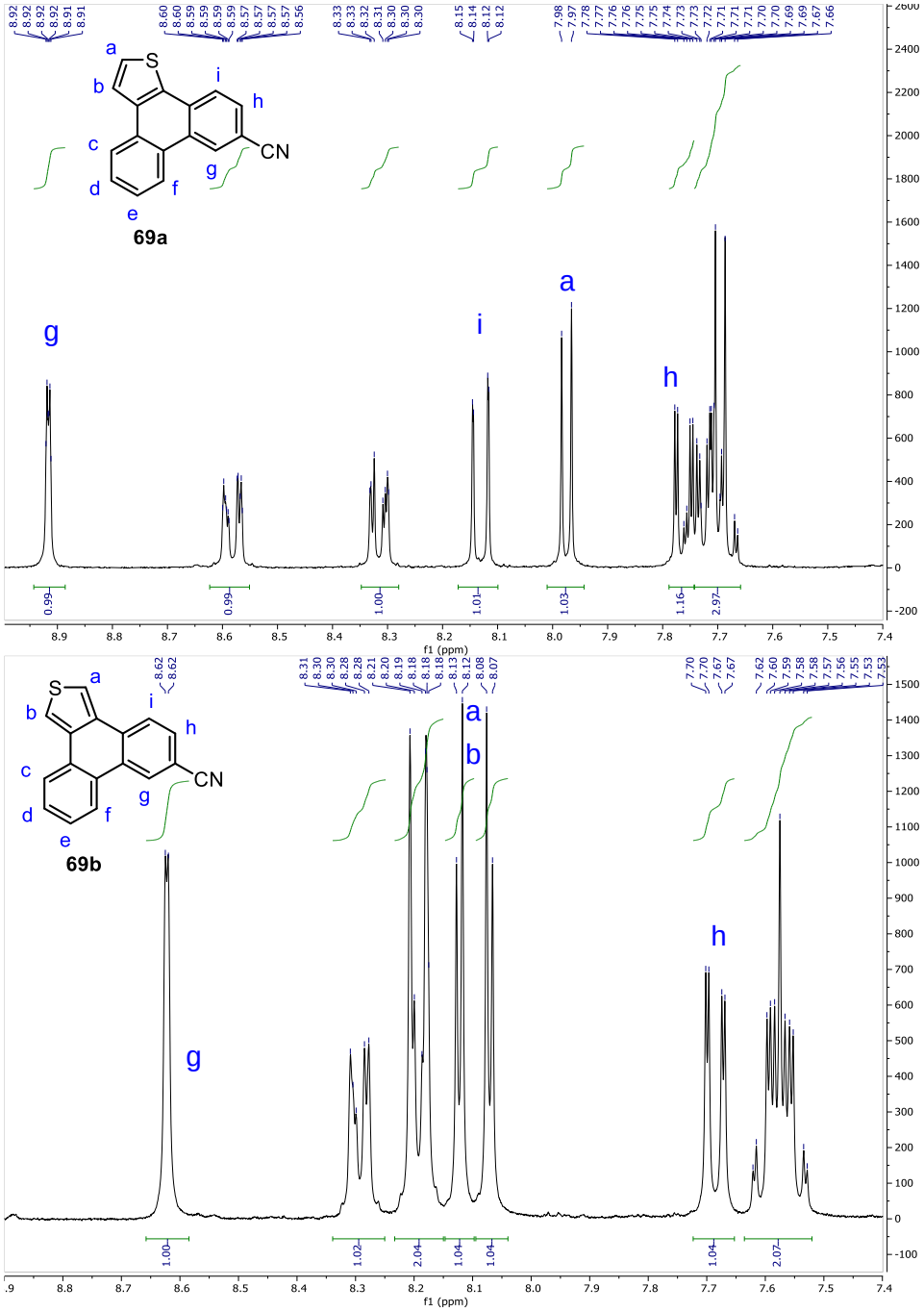

Figure 2.3. Part of ^{1}H NMR for compounds **69a** (up) and **69b** (down), 300 MHz, $CDCl_3$.

We proceeded to study the effect of EDGs in an acceptor ring on the reaction outcome. EDGs are expected to be well tolerated since an acceptor ring should be electron-rich to act as an effective radical trap. Product with a tert-butyl group **71** was isolated in 69% yield. However, when the precursor bearing two methoxy groups (**59**), was subjected to the cyclisation conditions, product **72** was not obtained, with only unreacted starting material isolated from the reaction mixture. The issue at place could be a possible steric hindrance between the methoxy group and the hydrogen atom in molecule **59**, underlined in Figure 2.4.

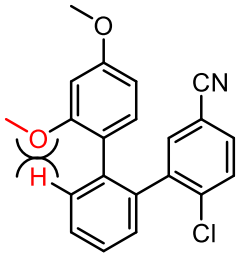

59

Figure 2.4. Structure of molecule **59** with potential steric hindrance indicated.

To test if this methoxy group was to blame for the lack of reactivity, the cyclisation on a terphenyl with only one methoxy group in *para* position to the linker ring was performed. Indeed, **73** was obtained in 70% yield, suggesting that the steric hindrance could be responsible for a failure to achieve product **72**.

Next, we studied the influence of EWGs in the acceptor ring on a reaction outcome. Since the acceptor ring should be electron-rich to trap the radical effectively, the presence of an EWG is expected to diminish the reaction yield. When nitrile was introduced, product **74** was not obtained, although some conversion was achieved. However, issues with the solubility of the product made isolation problematic and the reaction outcome is not clear. When the ester group was introduced, **75** was isolated in 38% yield, which is lower compared to the naked acceptor cycle in **64** (70%). To confirm that the decrease of the yield was due to the presence of the ester group in the acceptor cycle, an isomer with the ester group in a linker group was synthesised. Indeed, the reactivity was restored, and **76** was obtained in 66% yield.

The formation of compound **77** containing a five-membered ring was attempted, but it failed. Only dehalogenated product and unreacted starting material were obtained under standard reaction conditions. Increasing the reaction time to 3 days and doubling the PXX loading yielded a fully dehalogenated molecule.

Finally, control experiments were also performed to ensure that both PXX and light are necessary for the reaction (Scheme 2.53). When the light was excluded, no conversion of **52** was observed, with 100% of starting material remaining unchanged (NMR yield). When the reaction was performed under light but without PXX, around 10% of the product **64** and 90% of starting material were achieved (NMR yield). Possibly this small amount of product could be a result of photochemical cyclodehydrochlorination, similar to the reactions described in section 2.4.5. Performed experiments show that both light and PXX are necessary for the effective photoredox catalysed intramolecular aryl-aryl coupling.

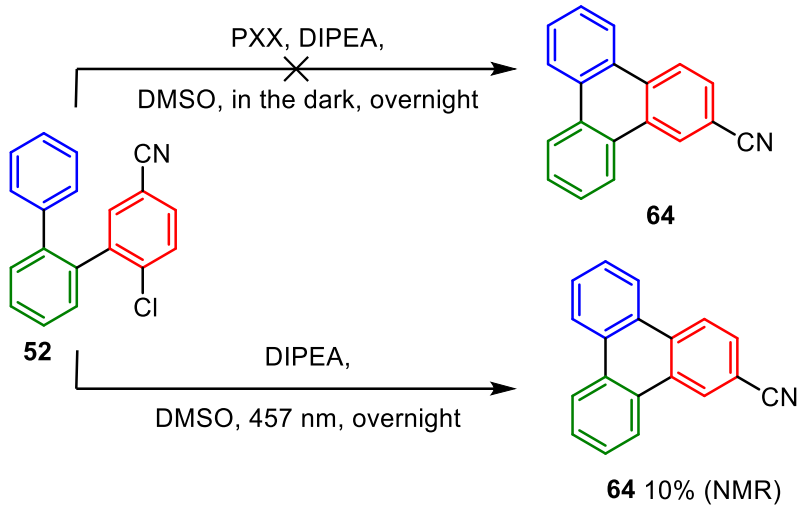

Scheme 2.53. Control experiments in the dark (up), or without PXX (down). Yield determined by NMR, using tetrachloroethane as an internal standard. Reactions were performed on 0.2 mmol scale of aryl halide, with 1.4 eq. of DIPEA and 1 ml of DMSO, with 2% of PXX (up) in the dark (up) or with blue LED strips (457 nm) irradiation (down). Reactions were performed after degassing with freeze pump thaw and under N_2.

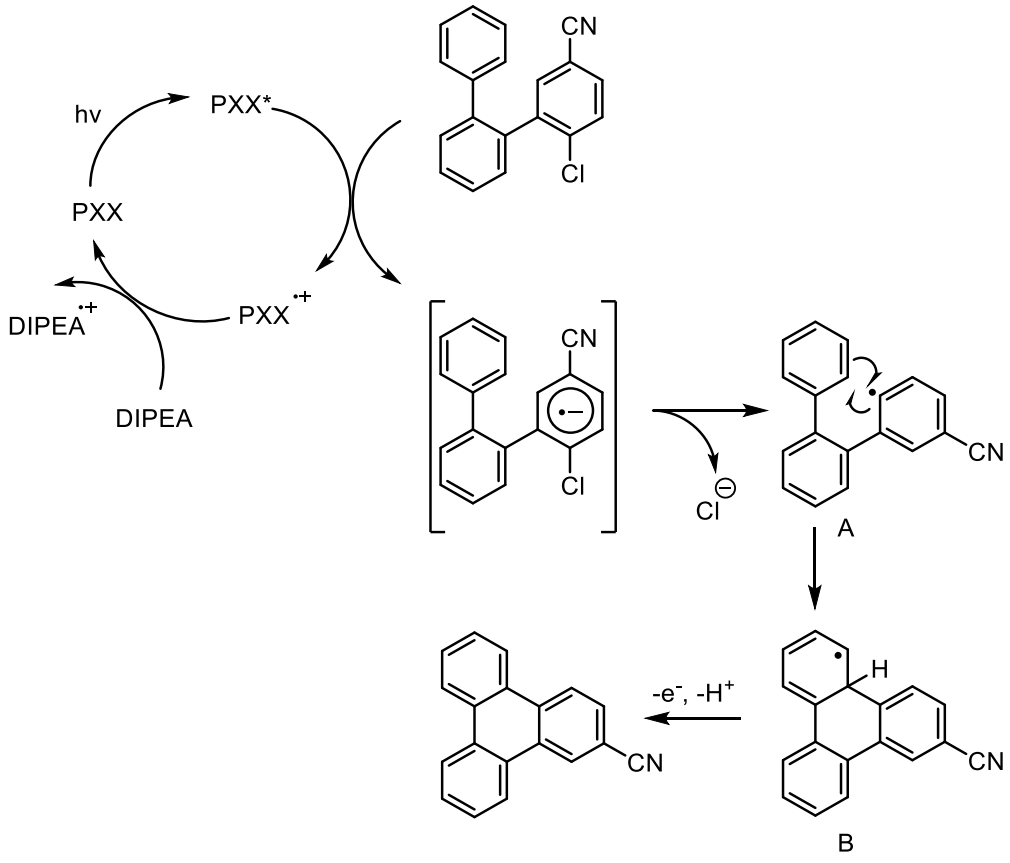

Scheme 2.54. The reaction mechanism proposed for PXX photoredox catalysed cyclisation.

On the basis of these control experiments and previous studies[45,115] we propose a reaction mechanism (Scheme 2.54). After photoreduction of an aryl halide by PXX* an aryl radical A is formed, which is then trapped by a donor aryl ring. After oxidation and

deprotonation of the resulting radical B, a triphenylene structure is achieved. Regeneration of the PXX catalyst can take place in reaction with DIPEA or the aryl radical B.

2.5.7 Towards double photocyclisation reactions

Having developed a variety of mono and disubstituted triphenylenes through a mono cyclisation, we decided to study the possibility of using this photoredox catalysed coupling in a double cyclisation reaction. Achieving double cyclisation would be a first step toward studying multiple cyclisations, leading to an alternative way of synthesising large PAHs.

One of the simplest PAHs which could be obtained through a double photoredox cyclisation is compound **79** (Scheme 2.55). Molecule **78**, which would be a precursor for this double cyclisation, could be synthesised in a double Suzuki coupling from commercially available 2,2'-dibromo-1,1'-biphenyl.

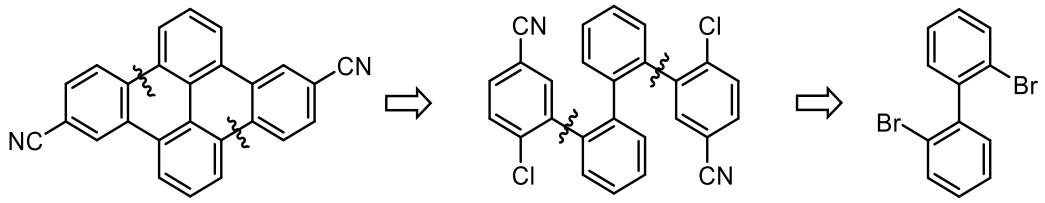

79 **78**

Scheme 2.55. Retrosynthetic routes to a double cyclisation product **79**.

To synthesise compound **78** a double Suzuki reaction was necessary (Scheme 2.56). First, the reaction conditions developed for a single Suzuki coupling (section 2.5.5.2) were tested, with [Pd(dppf)Cl_2] used as a catalyst. However, a complex mixture of products was obtained, which could not be separated and identified, even when prolonged reaction time (3 days) and high boronic acid loading (4.5 eq.) were used (Table 2.1 entry 1). Possibly a mono substituted product, as well as dehalogenated side products, were achieved. [Pd(dtbpf)Cl_2] was also tested as a more efficient catalyst,[116] but still a similar result was obtained (Table 2.1 entry 2). Finally, emulsion conditions, which were described in section 2.5.5.2 ([Pd(dtbpf)Cl_2], emulsion with 2% Kolliphor EL and 10% of toluene in water, Et_3N), were tested and full conversion was achieved after 3.5 h, with desired compound **78** isolated in 66% yield (Table 2.1 entry 3). The use of Kolliphor EL allowed the reaction to be carried out under air, instead of N_2, and isolation was performed through crystallisation without the need for column chromatography.

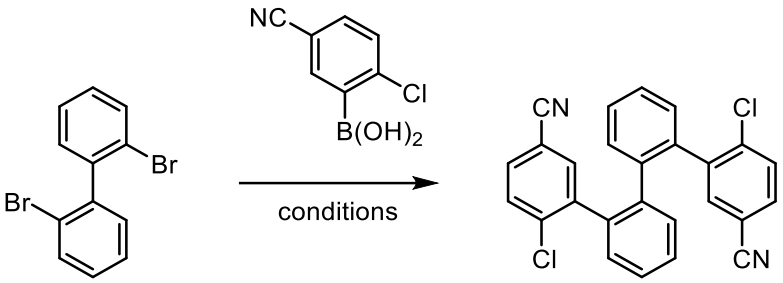

78

Scheme 2.56. Double Suzuki coupling to synthesise **78**.

Table 2.1. Conditions tested for Suzuki coupling to obtain **78**. (*2% Kolliphor EL and 10% of toluene in water).

entry	Conditions	Boronic acid eq.	Outcome
1	[Pd(dppf)Cl_2], K_2CO_3, dioxane/H_2O, reflux, 3 days, N_2	4.5	Complex mixture of products
2	[Pd(dtbpf)Cl_2], K_2CO_3, toluene/H_2O, reflux, 2 days, N_2	3	Complex mixture of products
3	[Pd(dtbpf)Cl_2], emulsion*, Et_3N, 60 °C, 3.5 h, air	3	66% yield

Having successfully prepared precursor **78**, double cyclisation reaction was attempted (Scheme 2.57). First, the reaction conditions reported for mono cyclisation reaction in section 2.5.6 were applied. After overnight irradiation mostly unreacted starting material was recovered (Table 2.2 entry 1). This could result from low solubility of **78** in DMSO. Complete solubilisation of starting materials is essential in photocatalysis since it can affect light penetration, and photoreaction can only occur where the light penetrates the reaction medium. We tried to solve this issue by testing the reaction in a solvent in which **78** is more soluble – DMF, as well as experimenting with a lower concentration in DMSO. Diluting the reaction mixture to 0.025 M in DMSO led to full solubilisation of the substrate. After 4 days of irradiation, complete conversion was achieved, and compound **80** was isolated in 28% yield (Table 2.2 entry 2). To try to increase the reaction yield, overnight irradiation in DMF was attempted, but it led to negligible conversion (Table 2.2 entry 3). However, after 2 days of irradiation **80** was isolated in 11% yield (Table 2.2 entry 4). Interestingly, the formation of molecule **79**, which was the expected product, has not been observed. The structure of **80**, a disubstituted tetraphenylene, was confirmed by full characterisation and X-ray crystallography.

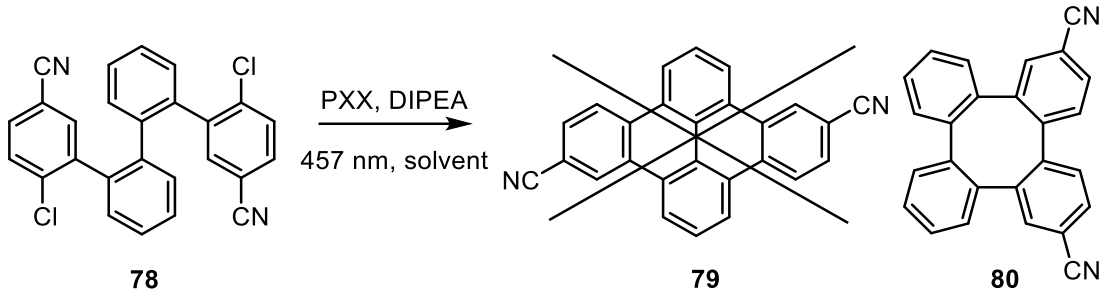

Scheme 2.57. Double photoredox cyclisation reaction.

Table 2.2. Conditions tested for the cyclisation of substrate **78**. 0.1 mmol scale of **78,** 2.8 eq. DIPEA, irradiation with 457 nm LEDs, freeze-pump-thaw performed, under N_2.

entry	Solvent	PXX loading	Time	Outcome
1	DMSO 0.2 M	4%	overnight	mostly starting material
2	DMSO 0.025 M	6%	4 days	28% **80**
3	DMF 0.1 M	8%	overnight	mostly starting material
4	DMF 0.1 M	8%	2 days	11% **80**

In the ^{1}H-NMR spectrum of compound **80** (Figure 2.5), the peaks appear between 7.65 ppm and 7.12 ppm, which falls in a similar range to the monosubstituted 2-cyanotetraphenylene (between 7.56 and 7.12 ppm).[102]

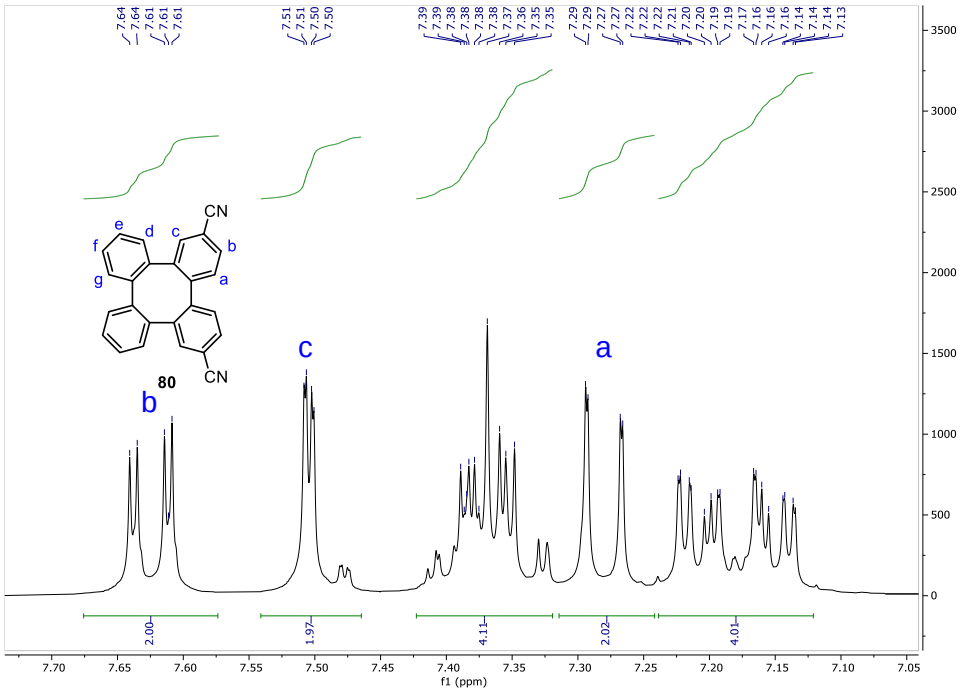

Figure 2.5. Part of the ^{1}H-NMR spectrum of compound **80**.

The doublet of doublets at 7.50 ppm can be assigned to protons *c*, as it is coupled with J = 1.7, 0.5 Hz, which are standard meta and para coupling constants. This signal is coupled with the meta coupling constant 1.7 Hz to the doublet of doublets *a* at 7.62

ppm. Peak at 7.50 ppm is also coupled to the doublet of doublets *b* at 7.28 ppm with *J* = 0.5 Hz, which is typical for para protons. Signals *a* and *b* are coupled with identical ortho coupling constant *J*=7.9 Hz. The multiplet peaks will be responsible for protons in the unsubstituted phenyl rings.

The ^{13}C NMR shows 13 peaks, as expected from a symmetrical molecule with 26 carbon atoms (Figure 2.6). The peak at 119 ppm falls in the standard region for nitriles (115-125 ppm), while the other twelve peaks fall at the range typical for aromatic carbons.[114]

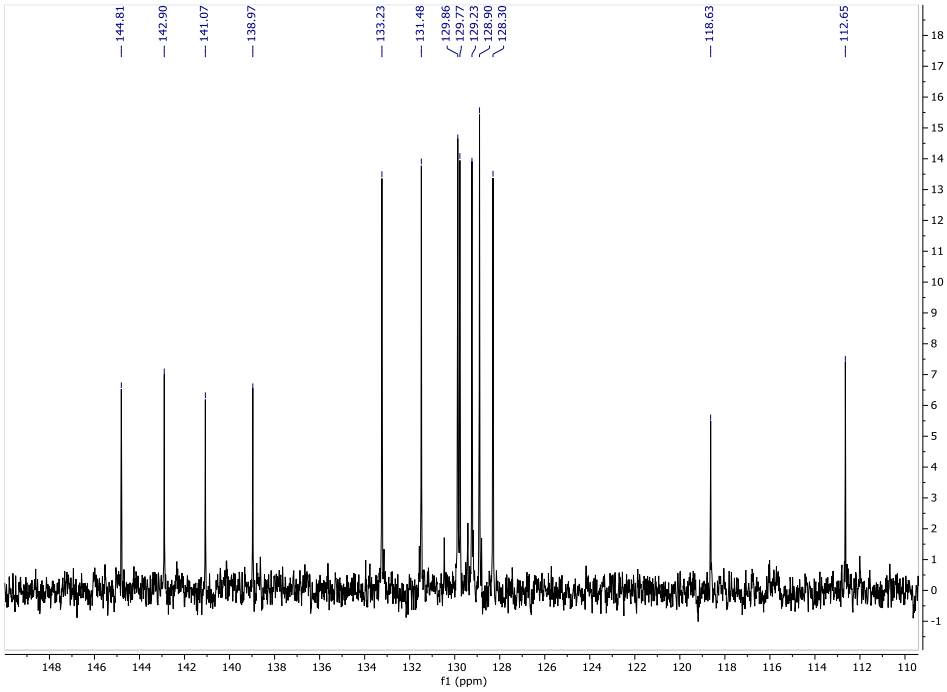

Figure 2.6. Part of the ^{13}C NMR of compound **80**, 75 MHz, CD_2Cl_2.

The crystal structure shows a distinct saddle-shaped framework, typical for a tetraphenylene structure[117] (Figure 2.7). HR mass spectroscopy also confirmed the mass of the compound.

Compound **80** could be a result of a radical SNAr reaction (Scheme 2.58). After photoreduction of **79** by PXX*, and loss of a chloride anion, an aryl radical would be formed, which could intramolecularly attack a second chloroaryl moiety. Loss of a chlorine radical would lead to formation of tetraphenylene **80**. Chlorine radical could abstract a proton from DIPEA and lead to formation of HCl.

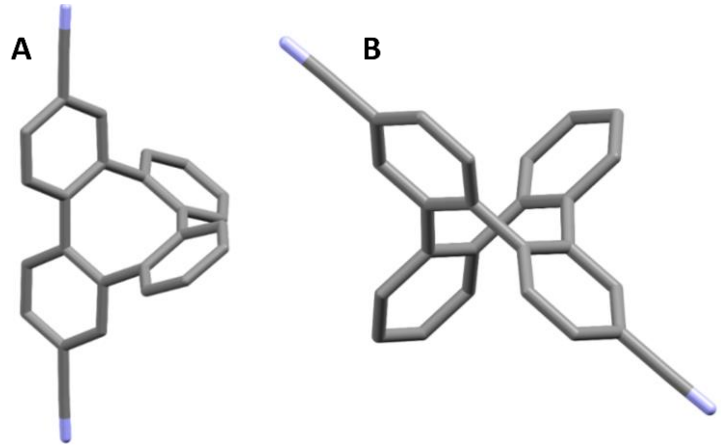

Figure 2.7. Crystal structure of **80**. Tetragonal system, I $4_1/a$ space group.

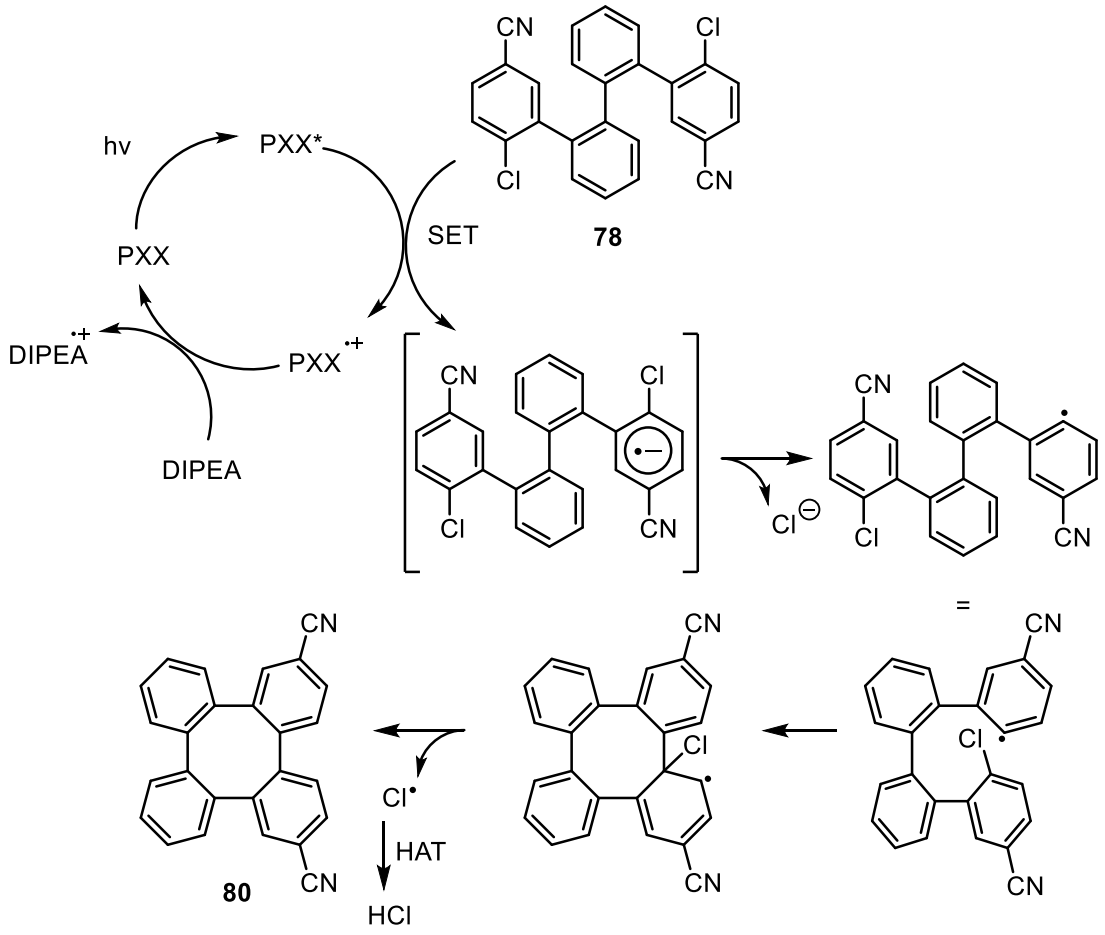

Scheme 2.58. Reaction mechanism proposed for the formation of product **80**.

Although desired molecule **79** has not been synthesised, we achieved a novel synthetic pathway towards substituted tetraphenylenes. As explained in section 2.5.3, the synthesis of tetraphenylene and its derivatives has recently witnessed extensive progress, with applications in the fields of asymmetric catalysis, organic light-emitting diodes and liquid crystalline materials.[119] However, to the best of our knowledge, this is the first photoredox catalysed reaction that led to a tetraphenylene structure.

2.6 Conclusion

The work reported in this chapter demonstrated the ability of PXX to promote photoredox catalysed aryl-aryl couplings of aryl chlorides. PXX is a photoredox catalyst that is metal-free, easy to synthesise and strongly reducing in the singlet excited state. We have illustrated its ability to promote intermolecular couplings of electron-poor aryl chlorides with electron-rich radical traps. Aryl chlorides with nitrile and ester groups gave high yields, while effective traps included *N*-methylpyrrole, triethylphosphite and trimethoxybenzene. We have also developed a novel intramolecular photoredox catalysed coupling, where PXX mediated cyclisation of various chloro-*o*-terphenyls, possessing an EWG, into triphenylenes. While a nitrile or an ester group must be present on the chloride bearing ring, a range of substituents can be tolerated on other aryl moieties. Structures without a substituent or bearing EDG on an acceptor ring, gave desired products in high yields (~70%). Heterocycles such as pyrrole, thiophene and dibenzofuran also could be used as acceptor rings with varying yields (40-83%). While the introduction of an EWG (an ester) to an acceptor ring led to a diminished yield (38%), its presence was well tolerated on the linker ring (66%). Based on the reported reaction mechanisms[43,45] and control tests, both intermolecular and intramolecular reactions were proposed to follow a radical photoreductive mechanism. We also attempted a double cyclisation reaction, which followed an unexpected reaction pathway, giving a tetraphenylene derivative **80**. Instead of the expected C-H coupling, a product of what could be the diradical recombination was obtained. In this way, we achieved a new route toward substituted tetraphenylenes. In the future, we aim to study multicyclisation reactions as well as optimise the synthesis of tetraphenylene derivatives and study the reaction mechanism.

2.7 Literature

[1] A. D. McNaught, A. Wilkinson, *IUPAC. Compendium of Chemical Terminology, 2nd Ed. (the "Gold Book").*, Blackwell Scientific Publications, Oxford, **1997**.

[2] N. A. Romero, D. A. Nicewicz, *Chem. Rev.* **2016**, *116*, 10075–10166.

[3] D. Ravelli, M. Fagnoni, A. Albini, *Chem. Soc. Rev.* **2013**, *42*, 97–113.

[4] M. H. Shaw, J. Twilton, D. W. C. MacMillan, *J. Org. Chem.* **2016**, *81*, 6898–6926.

[5] S. G. E. Amos, M. Garreau, L. Buzzetti, J. Waser, *Beilstein J. Org. Chem.* **2020**, *16*, 1163–1187.

[6] M. A. Ischay, M. E. Anzovino, J. Du, T. P. Yoon, *J. Am. Chem. Soc.* **2008**, *130*, 12886–12887.

[7] D. A. Nicewicz, D. W. C. MacMillan, *Science* **2008**, *322*, 77–80.

[8] J. M. R. Narayanam, J. W. Tucker, C. R. J. Stephenson, *J. Am. Chem. Soc.* **2009**, *131*, 8756–8757.

[9] J. A. Terrett, J. D. Cuthbertson, V. W. Shurtleff, D. W. C. MacMillan, *Nature* **2015**, *524*, 330–334.

[10] Z. Dong, D. W. C. MacMillan, *Nature* **2021**, *598*, 451–456.

[11] J. D. Cuthbertson, D. W. C. MacMillan, *Nature* **2015**, *519*, 74–77.

[12] W. Chen, Z. Huang, N. E. S. Tay, B. Giglio, M. Wang, H. Wang, Z. Wu, D. A. Nicewicz, Z. Li, *Science* **2019**, *364*, 1170–1174.

[13] M. M. Hossain, A. C. Shaikh, J. Moutet, T. L. Gianetti, *Nat. Synth.* **2022**, *1*, 147–157.

[14] E. B. Corcoran, M. T. Pirnot, S. Lin, S. D. Dreher, D. A. Dirocco, I. W. Davies, S. L. Buchwald, D. W. C. Macmillan, *Science* **2016**, *353*, 279–283.

[15] Y. Du, R. M. Pearson, C. Lim, S. M. Sartor, M. D. Ryan, H. Yang, N. H. Damrauer, G. M. Miyake, *Chem. – A Eur. J.* **2017**, *23*, 10962–10968.

[16] M. S. Oderinde, M. Frenette, D. W. Robbins, B. Aquila, J. W. Johannes, *J. Am. Chem. Soc.* **2016**, *138*, 1760–1763.

[17] A. Juris, V. Balzani, P. Belser, A. von Zelewsky, *Helv. Chim. Acta* **1981**, *64*, 2175–2182.

[18] C. K. Prier, D. A. Rankic, D. W. C. MacMillan, *Chem. Rev.* **2013**, *113*, 5322–5363.

[19] Y. Xi, H. Yi, A. Lei, *Org. Biomol. Chem.* **2013**, *11*, 2387–2403.

[20] L. Flamigni, A. Barbieri, C. Sabatini, B. Ventura, F. Barigelletti, in *Photochem. Photophysics Coord. Compd. II*, Springer Berlin Heidelberg, Berlin, Heidelberg, **2007**, pp. 143–203.

[21] J. D. Nguyen, E. M. D'Amato, J. M. R. Narayanam, C. R. J. Stephenson, *Nat. Chem.* **2012**, *4*, 854–859.

[22] Y. Cheng, X. Gu, P. Li, *Org. Lett.* **2013**, *15*, 2664–2667.

[23] H. W. Shih, M. N. Vander Wal, R. L. Grange, D. W. C. MacMillan, *J. Am. Chem. Soc.* **2010**, *132*, 13600–13603.

[24] P. Nuss, M. J. Eckelman, *PLoS One* **2014**, *9*, 1–12.

[25] S. Fukuzumi, H. Kotani, K. Ohkubo, S. Ogo, N. V. Tkachenko, H. Lemmetyinen, *J. Am. Chem. Soc.* **2004**, *126*, 1600–1601.

[26] H. Uoyama, K. Goushi, K. Shizu, H. Nomura, C. Adachi, *Nature* **2012**, *492*, 234–238.

[27] D. P. Hari, P. Schroll, B. König, *J. Am. Chem. Soc.* **2012**, *134*, 2958–2961.

[28] Y. X. Liu, D. Xue, J. Di Wang, C. J. Zhao, Q. Z. Zou, C. Wang, J. Xiao, *Synlett* **2013**, *24*, 507–513.

[29] P. Natarajan, A. Bala, S. K. Mehta, K. K. Bhasin, *Tetrahedron* **2016**, *72*, 2521–2526.

[30] M. H. Aukland, M. Šiaučiulis, A. West, G. J. P. Perry, D. J. Procter, *Nat. Catal.* **2020**, *3*, 163–169.

[31] I. Ghosh, T. Ghosh, J. I. Bardagi, B. Konig, *Science* **2014**, *346*, 725–728.

[32] I. Ghosh, L. Marzo, A. Das, R. Shaikh, B. König, *Acc. Chem. Res.* **2016**, *49*, 1566–1577.

[33] V. Balzani, G. Bergamini, P. Ceroni, *Angew. Chem. Int. Ed.* **2015**, *54*, 11320–11337.

[34] D. Ravelli, M. Fagnoni, A. Albini, *Chem. Soc. Rev.* **2012**, *42*, 97–113.

[35] C. S. Wang, P. H. Dixneuf, J. F. Soulé, *Chem. Rev.* **2018**, *118*, 7532–7585.

[36] M. Raicopol, L. Necula, M. Ionita, L. Pilan, *Surf. Interface Anal.* **2012**, *44*, 1081–1085.

[37] D. Xue, Z.-H. Jia, C.-J. Zhao, Y.-Y. Zhang, C. Wang, J. Xiao, *Chem. – A Eur. J.* **2014**, *20*, 2960–2965.

[38] P. Maity, D. Kundu, B. C. Ranu, *Eur. J. Org. Chem.* **2015**, *2015*, 1727–1734.

[39] C. Costentin, M. Robert, J. M. Savéant, *J. Am. Chem. Soc.* **2004**, *126*, 16051–16057.

[40] L. Wang, J. Byun, R. Li, W. Huang, K. A. I. Zhang, *Adv. Synth. Catal.* **2018**, *360*,

4312–4318.

[41] C. J. Zeman, S. Kim, F. Zhang, K. S. Schanze, *J. Am. Chem. Soc.* **2020**, *142*, 2204–2207.

[42] I. Ghosh, B. König, *Angew. Chem. Int. Ed.* **2016**, *55*, 7676–7679.

[43] A. Sciutto, A. Fermi, A. Folli, T. Battisti, J. M. Beames, D. M. Murphy, D. Bonifazi, *Chem. Eur. J.* **2018**, *24*, 4382–4389.

[44] T. Kamei, M. Uryu, T. Shimada, *Org. Lett.* **2017**, *19*, 2714–2717.

[45] C. Pezzetta, A. Folli, O. Matuszewska, D. Murphy, R. W. M. Davidson, D. Bonifazi, *Adv. Synth. Catal.* **2021**, *363*, 4740–4753.

[46] A. L. Trifonov, L. I. Panferova, V. V. Levin, V. A. Kokorekin, A. D. Dilman, *Org. Lett.* **2020**, *22*, 2409–2413.

[47] M. T. Pirnot, D. A. Rankic, D. B. C. Martin, D. W. C. MacMillan, *Science* **2013**, *340*, 1593–1596.

[48] D. E. Bartak, K. J. Houser, B. C. Rudy, M. D. Hawley, *J. Am. Chem. Soc.* **1972**, *94*, 7526–7530.

[49] C. P. Andrieux, J. M. Saeveant, D. Zann, *Nouv. J. Chim.* **1984**, *8*, 107.

[50] G. Lefèvre, A. Jutand, *Chem. Eur. J.* **2014**, *20*, 4796–4805.

[51] X. Feng, W. Pisula, K. Müllen, *Pure Appl. Chem.* **2009**, *81*, 2203–2224.

[52] M. Stępień, E. Gońka, M. Żyła, N. Sprutta, *Chem. Rev.* **2017**, *117*, 3479–3716.

[53] A. Bodzioch, E. Kowalska, J. Skalik, P. Bałczewski, *Chem. Heterocycl. Compd.* **2017**, *53*, 11–20.

[54] B. P. Mathew, M. R. Kuram, *Inorg. Chim. Acta* **2019**, *490*, 112–129.

[55] O. T. Dyan, G. I. Borodkin, P. A. Zaikin, *Eur. J. Org. Chem.* **2019**, *2019*, 7271–7306.

[56] Y. Yamamoto, A. I. Almansour, N. Arumugam, R. S. Kumar, *Arkivoc* **2015**, *2016*, 9–41.

[57] R. Scholl, J. Mansfeld, *Ber. Dtsch. Chem. Ges.* **1910**, *43*, 1734–1746.

[58] M. Grzybowski, K. Skonieczny, H. Butenschön, D. T. Gryko, *Angew. Chem. Int. Ed.* **2013**, *52*, 9900–9930.

[59] P. Kovacic, A. Kyriakis, *Tetrahedron Lett.* **1962**, *3*, 467–469.

[60] M. Müller, H. Mauermann-Düll, M. Wagner, V. Enkelmann, K. Müllen, *Angew. Chem. Int. Ed.* **1995**, *34*, 1583–1586.

[61] C. D. Simpson, J. D. Brand, A. J. Berresheim, L. Przybilla, H. J. Räder, K. Müllen, *Chem. Eur. J.* **2002**, *8*, 1424–1429.

[62] M. Müller, C. Kübel, K. Müllen, *Chem. Eur. J.* **1998**, *4*, 2099–2109.

[63] X. Feng, W. Pisula, L. Zhi, M. Takase, K. Müllen, *Angew. Chem. Int. Ed.* **2008**, *47*, 1703–1706.

[64] B. T. King, J. Kroulík, C. R. Robertson, P. Rempala, C. L. Hilton, J. D. Korinek, L. M. Gortari, *J. Org. Chem.* **2007**, *72*, 2279–2288.

[65] J. E. Rice, Z. W. Cai, *J. Org. Chem.* **1993**, *58*, 1415–1424.

[66] T. Jin, J. Zhao, N. Asao, Y. Yamamoto, *Chem. Eur. J.* **2014**, *20*, 3554–3576.

[67] N. H. Chang, X. C. Chen, H. Nonobe, Y. Okuda, H. Mori, K. Nakajima, Y. Nishihara, *Org. Lett.* **2013**, *15*, 3558–3561.

[68] N. H. Chang, H. Mori, X. C. Chen, Y. Okuda, T. Okamoto, Y. Nishihara, *Chem. Lett.* **2013**, *42*, 1257–1259.

[69] S. Yanagisawa, K. Ueda, T. Taniguchi, K. Itami, *Org. Lett.* **2008**, *10*, 4673–4676.

[70] D. S. Roman, Y. Takahashi, A. B. Charette, *Org. Lett.* **2011**, *13*, 3242–3245.

[71] S. Lin, X. He, J. Meng, H. Gu, P. Zhang, J. Wu, *Eur. J. Org. Chem.* **2017**, *2017*, 443–447.

[72] K. I. Fujita, M. Nonogawa, R. Yamaguchi, *Chem. Commun.* **2004**, *10*, 1926–1927.

[73] C. L. Sun, Y. F. Gu, W. P. Huang, Z. J. Shi, *Chem. Commun.* **2011**, *47*, 9813–9815.

[74] B. S. Bhakuni, A. Kumar, S. J. Balkrishna, J. A. Sheikh, S. Konar, S. Kumar, *Org. Lett.* **2012**, *14*, 2838–2841.

[75] S. Zhou, E. Doni, G. M. Anderson, R. G. Kane, S. W. Macdougall, V. M. Ironmonger, T. Tuttle, J. A. Murphy, *J. Am. Chem. Soc.* **2014**, *136*, 17818–17826.

[76] G. Nocera, J. A. Murphy, *Synthesis* **2020**, *52*, 327–336.

[77] A. Studer, D. P. Curran, *Angew. Chem. Int. Ed.* **2011**, *50*, 5018–5022.

[78] F. B. Mallory, C. S. Wood, J. T. Gordon, *J. Am. Chem. Soc.* **1964**, *86*, 3094–3102.

[79] F. B. Mallory, C. W. Mallory, in *Organic Reactions Vol. 30* (Ed.: W.G. Dauben), John Wiley & Sons, Inc., Hoboken, **1984**, pp. 1–456.

[80] K. B. Jørgensen, *Molecules* **2010**, *15*, 4334–4358.

[81] R. D. Broene, F. Diederich, *Tetrahedron Lett.* **1991**, *32*, 5227–5230.

[82] T. Sato, S. Shimada, K. Hata, *Bull. Chem. Soc. Jpn.* **1971**, *44*, 2484–2490.

[83] T. Sato, S. Shimada, K. Hata, *Bull. Chem. Soc. Jpn.* **1969**, *42*, 766–772.

[84] Q. Chen, S. Thoms, S. Stöttinger, D. Schollmeyer, K. Müllen, A. Narita, T. Basché, *J. Am. Chem. Soc.* **2019**, *141*, 16439–16449.

[85] I. Schnapperelle, T. Bach, *Chem. Eur. J.* **2014**, *20*, 9725–9732.

[86] M. Daigle, A. Picard-Lafond, E. Soligo, J.-F. Morin, *Angew. Chem. Int. Ed.* **2016**, *55*, 2042–2047.

[87] Z. Li, R. J. Twieg, *Chem. Eur. J.* **2015**, *21*, 15534–15539.

[88] H. Cano-Yelo, A. Deronzier, *J. Chem. Soc., Perkin Trans. 2* **1984**, 1093–1098.

[89] P. Natarajan, N. Kumar, M. Sharma, *Org. Chem. Front.* **2016**, *3*, 1265–1270.

[90] T. Osawa, T. Kajitani, D. Hashizume, H. Ohsumi, S. Sasaki, M. Takata, Y. Koizumi, A. Saeki, S. Seki, T. Fukushima, T. Aida, *Angew. Chem. Int. Ed.* **2012**, *51*, 7990–7993.

[91] S. Ukai, K. Hirose, *Chem. Pharm. Bull.* **1968**, *16*, 195–201.

[92] M. Gupta, S. K. Pal, *Langmuir* **2016**, *32*, 1120–1126.

[93] M. Saleh, M. Baumgarten, A. Mavrinskiy, T. Schäfer, K. Müllen, *Macromolecules* **2010**, *43*, 137–143.

[94] K. Togashi, S. Nomura, N. Yokoyama, T. Yasuda, C. Adachi, *J. Mater. Chem.* **2012**, *22*, 20689.

[95] S. K. Pal, S. Setia, B. S. Avinash, S. Kumar, *Liq. Cryst.* **2013**, *40*, 1769–1816.

[96] H. Y. Peng, C. K. Lam, T. C. W. Mak, Z. Cai, W. T. Ma, Y. X. Li, H. N. C. Wong, *J. Am. Chem. Soc.* **2005**, *127*, 9603–9611.

[97] B. L. Edelbach, D. A. Vicic, R. J. Lachicotte, W. D. Jones, *Organometallics* **1998**, *17*, 4784–4794.

[98] B. L. Edelbach, R. J. Lachicotte, W. D. Jones, *J. Am. Chem. Soc.* **1998**, *120*, 2843–2853.

[99] J. J. Eisch, A. M. Piotrowski, K. I. Han, C. Krüger, Y. H. Tsay, *Organometallics* **1985**, *4*, 224–231.

[100] H. Schwager, S. Spyroudis, K. P. C. Vollhardt, *J. Organomet. Chem.* **1990**, *382*, 191–200.

[101] D. Masselot, J. P. H. Charmant, T. Gallagher, *J. Am. Chem. Soc.* **2006**, *128*, 694–695.

[102] B. Wan, Y. Zhang, *Synthesis* **2021**, *53*, 3299–3306.

[103] H. Jiang, Y. Zhang, D. Chen, B. Zhou, Y. Zhang, *Org. Lett.* **2016**, *18*, 2032–2035.

[104] U. R. Von, V. G. Wittig, **1967**, *108*, 91–108.

[105] A. Rajca, H. Wang, P. Bolshov, S. Rajca, *Tetrahedron* **2001**, *57*, 3725–3735.

[106] J. F. Cui, H. Huang, H. N. C. Wong, *Synlett* **2011**, 1018–1022.

[107] C. W. Lai, C. K. Lam, H. K. Lee, T. C. W. Mak, H. N. C. Wong, *Org. Lett.* **2003**, *5*, 823–826.

[108] D. Blakemore, in *RSC Drug Discovery Series*, **2016**, pp. 1–69.

[109] F. Batool, A. H. Emwas, X. Gao, M. A. Munawar, G. A. Chotana, *Synthesis* **2017**, *49*, 1327–1334.

[110] K. M. Clapham, A. S. Batsanov, M. R. Bryce, B. Tarbit, *Org. Biomol. Chem.* **2009**, *7*, 2155–2161.

[111] D. Bulfield, S. M. Huber, *J. Org. Chem.* **2017**, *82*, 13188–13203.

[112] G. La Sorella, G. Strukul, A. Scarso, *Green Chem.* **2015**, *17*, 644–683.

[113] M. Rooney, S. Mattiello, R. Stara, A. Sanzone, P. Brazzo, M. Sassi, L. Beverina, *Dyes Pigm.* **2018**, *149*, 893–901.

[114] D. J. K. Robert M. Silverstein, Francis X. Webster, *J. Mol. Struct.* **2005**, 512.

[115] A. Sciutto, A. Fermi, A. Folli, T. Battisti, J. M. Beames, D. M. Murphy, D. Bonifazi, *Chem. Eur. J.* **2018**, *24*, 4382–4389.

[116] A. Sanzone, A. Calascibetta, E. Ghiglietti, C. Ceriani, G. Mattioli, S. Mattiello, M. Sassi, L. Beverina, *J. Org. Chem.* **2018**, *83*, 15029–15042.

[117] H. Irngartinger, W. R. K. Reibel, *Acta Crystallogr. Sect. B Struct. Crystallogr. Cryst. Chem.* **1981**, *37*, 1724–1728.

[118] D. V. Preda, L. T. Scott, *Org. Lett.* **2000**, *2*, 1489–1492.

[119] J. W. Han, X. S. Peng, H. N. C. Wong, *Natl. Sci. Rev.* **2017**, *4*, 892–916.

[120] *CrysAlisPro, Agilent Technologies, Version 1.171.37.33 c (Release 27-03-2014 CrysAlis171 .NET)*, **n.d.**

[121] G. M. Sheldrick, *SHELX-2013: Program for the Solution of Crystal Structures*, University Of Göttingen, **2013**.

[122] A. Lausi, M. Polentarutti, S. Onesti, J. R. Plaisier, E. Busetto, G. Bais, L. Barba, A. Cassetta, G. Campi, D. Lamba, A. Pifferi, S. C. Mande, D. D. Sarma, S. M. Sharma, G. Paolucci, *Eur. Phys. J. Plus* **2015**, *130*, 43.

[123] W. Kabsch, *Acta Crystallogr. Sect. D* **2010**, *66*, 125–132.

[124] G. Sheldrick, *Acta Crystallogr. Sect. A* **2015**, *71*, 3–8.

[125] G. Sheldrick, *Acta Crystallogr. Sect. C* **2015**, *71*, 3–8.

[126] P. Emsley, B. Lohkamp, W. G. Scott, K. Cowtan, *Acta Crystallogr. Sect. D* **2010**, *66*, 486–501.

[127] G. A. Crosby, J. N. Demas, *J. Phys. Chem.* **1971**, *75*, 991–1024.

[128] N. Armaroli, F. Diederich, C. O. Dietrich-Buchecker, L. Flamigni, G. Marconi, J. F. Nierengarten, J. P. Sauvage, *Chem. Eur. J.* **1998**, *4*, 406–416.

[129] Y. Rio, G. Accorsi, H. Nierengarten, C. Bourgogne, J. M. Strub, A. Van Dorsselaer, N. Armaroli, J. F. Nierengarten, *Tetrahedron* **2003**, *59*, 3833–3844.

[130] H. He, L.-Y. Chen, W.-Y. Wong, W.-H. Chan, A. W. M. Lee, *Eur. J. Org. Chem.* **2010**, *2010*, 4181–4184.

[131] R. Mariz, A. Poater, M. Gatti, E. Drinkel, J. J. Bürgi, X. Luan, S. Blumentritt, A.

Linden, L. Cavallo, R. Dorta, *Chem. Eur. J.* **2010**, *16*, 14335–14347.

[132] M. Tiecco, L. Testaferri, M. Tingoli, D. Chianelli, M. Montanucci, *J. Org. Chem.* **1983**, *48*, 4289–4296.

[133] K. Nishino, Y. Ogiwara, N. Sakai, *Chem. Eur. J.* **2018**, *24*, 10971–10974.

[134] B. Yiğit, N. Gürbüz, M. Yiğit, Z. Dağdeviren, İ. Özdemir, *Inorg. Chim. Acta* **2017**, *465*, 44–49.

[135] D. S. Lee, C. S. Kim, N. Iqbal, G. S. Park, K. S. Son, E. J. Cho, *Org. Lett.* **2019**, *21*, 9950–9953.

[136] T. F. Wang, C. L. Lin, C. N. Chen, T. C. Wang, *J. Chinese Chem. Soc.* **2007**, *54*, 811–816.

[137] J. Song, F. Wei, W. Sun, K. Li, Y. Tian, C. Liu, Y. Li, L. Xie, *Org. Lett.* **2015**, *17*, 2106–2109.

[138] M. Nishimura, M. Ueda, N. Miyaura, *Tetrahedron* **2002**, *58*, 5779–5787.

[139] P. H. Gore, F. S. Kamounah, A. Y. Miri, *Tetrahedron* **1979**, *35*, 2927–2929.

[140] J. Tu, G. Li, X. Zhao, F. Xu, *Tetrahedron Lett.* **2019**, *60*, 44–47.

Chapter 3
Experimental part

3.1 Instrumentation

Melting points (m.p.): were measured on a Gallenkamp apparatus in open capillary tubes.

Nuclear magnetic resonance (NMR): spectra were recorded on a Bruker Fourier 300 MHz spectrometer equipped with a dual (^{13}C, ^{1}H) probe, a Bruker AVANCE III HD 400 MHz NMR spectrometer equipped with a Broadband multinuclear (BBFO) SmartProbe™ or a Bruker AVANCE III HD 500 MHz Spectrometer equipped with Broadband multinuclear (BBO) Prodigy CryoProbe. ^{1}H spectra were obtained at 300, 400 or 500 MHz, C spectra were obtained at 75 or 100 MHz. All spectra were obtained at room temperature (rt) unless otherwise stated. Chemical shifts are reported in ppm, using the solvent residual signal as an internal reference ($CDCl_3$: δH = 7.26 ppm, δC = 77.16 ppm; CD_2Cl_2: δH = 5.32 ppm, δC = 53.84). Coupling constants (*J*) are given in Hz. Resonance multiplicity is described as s (singlet), d (doublet), dd (doublet of doublets), ddd (doublet of doublets of doublets) and m (multiplet). Carbon spectra were acquired with a complete decoupling for the proton. The Attached Proton Test (APT) experiments were used to determine C-H multiplicities in carbon spectra and the peaks assigned as (C) for quaternary, (CH) for tertiary, (CH_2) for secondary and (CH_3) for primary carbon atoms.

Infrared spectra (IR): were recorded on a Shimadzu IR-Affinity 1S FTIR spectrometer in ATR mode with a diamond mono-crystal.

Mass spectrometry (HRMS): ESI mass spectra were performed on a Waters LCT HR time of flight mass spectrometer in the positive ion mode. EI mass spectra were performed on Waters GCT Premier micromass time of flight spectrometer. APCI mass spectra were performed on a Waters LCT Premier quadrupole time of flight mass spectrometer operating in the atmospheric pressure chemical ionisation mode.

XRD: crystallographic studies were undertaken at Cardiff University were performed on single crystal mounted in paratone and studied on an Agilent SuperNova Dual three-circle diffractometer using Cu-Kα (λ = 1.540598 Å) or Mo-Kα (λ = 0.7093187 Å) radiation and a CCD detector. Measurements were typically made at 150(2) K or 293(2) K with temperatures maintained using an Oxford Cryostream unless otherwise stated.

Data were collected, integrated and corrected for absorption using a numerical absorption correction based on gaussian integration over a multifaceted crystal model within CrysAlisPro.[120] The structures were solved by direct methods and refined against F2 within SHELXL-2013.[121] For compound **32** data collections were performed at the X-ray diffraction beamline (XRD1) of the Elettra Synchrotron, Trieste (Italy)[122]. The crystals were dipped in NHV oil (Jena Bioscience, Jena, Germany) and mounted on the goniometer head with kapton loops (MiTeGen, Ithaca, USA). Complete datasets were collected at 100 K (nitrogen stream supplied through an Oxford Cryostream 700 - Oxford Cryosystems Ltd., Oxford, United Kingdom) through the rotating crystal method. Data were acquired using a monochromatic wavelength of 0.700 Å, on a Pilatus 2M hybrid-pixel area detector (DECTRIS Ltd., Baden-Daettwil, Switzerland). The diffraction data were indexed and integrated using XDS.[123] The structures were solved by the dual space algorithm implemented in the SHELXT code.[124] Fourier analysis and refinement were performed by the full-matrix least-squares methods based on F^2 implemented in SHELXL (Version 2018/3)[125]. The Coot program was used for modeling.[126] A summary of crystallographic data are available as ESI and the structures deposited with the Cambridge Structural Database (CCDC deposition numbers 1869239-1869246). These data can be obtained free of charge from The Cambridge Crystallographic Data Centre via www.ccdc.cam.ac.uk/data_request/cif.

HPLC: purification was performed on Japan analytical industry NEXT recycling preparative HPLC with Japan analytical industry column JAIGEL-SIL,SH-043-10(20φx25) and pre column JAIGEL-SIL-P-SH-043-10(20φ).

Electrochemical Analysis: Cyclic voltammetry measures were carried out at rt in nitrogen-purged dry CH_2Cl_2 with a Model 800 potentiostat (CH instruments), AUTOLAB EcoChemie 30 multipurpose instrument and AUTOLAB PGSTAT 204. Glassy carbon electrode with a 3 mm diameter has been used as a working electrode, Ag wire has been used as a pseudo-reference electrode (AgQRE) and Pt spiral has been used as a counter electrode. Working electrode and AgQRE electrodes were polished on a felt pad with 0.05 or 0.3 µm alumina suspension and sonicated in deionised water for few minutes before each experiment; the Pt wire was flame-cleaned. Tetrabutylammonium hexafluorophosphate ($TBAPF_6$) has been exploited as a supporting electrolyte at concentration around 0.1 M. Ferrocene (Fc) and Decamethylferrocene ($FcMe_{10}$) have been added as internal reference ($E\ Fc^{+/0}$ = 0.46 V vs. SCE in CH_2Cl_2; $E(FcMe_{10}^{+/0}$ = -0.072 V vs. SCE in CH_2Cl_2). HOMO and LUMO energies were calculated from the first formal redox potentials (half-wave potentials) using equations: E HOMO = - (5.1 eV + $E_{1/2\ ox.1}$ vs. $Fc^{+/0}$) and E LUMO = - (5.1 eV + $E_{1/2\ red.1}$ vs. $Fc^{+/0}$). In the cases where

oxidation or reduction waves were not detected by means of cyclic voltammetry, HOMO or LUMO levels have been calculated using the optical gap $\Delta E_{0\text{-}0}$, considering the lowest energy intersection between normalised absorption and emission spectra $eV = 1240.5/\lambda_{int\ (nm)}$.

Photophysical analysis: Absorption spectra of compounds were recorded on air equilibrated CH_2Cl_2 solutions at rt with Agilent Cary 5000 UV-Vis spectrophotometer, using quartz cells with path length of 1.0 cm. Emission spectra were recorded on an Agilent Cary Eclipse fluorescence spectrofluorometer. Emission lifetime measurements were performed on a JobinYvon-Horiba FluoroHub single photon counting module, using Nano-LED pulsed source at 459 nm or 340 nm and with an Edinburgh FLS920 spectrofluorimeter equipped with a TCC900 card for data acquisition in time-correlated single photon counting experiments (0.5 ns time resolution) with a PicoQuant pulsed diode laser 340 ± 20 nm. Quantum yield values were calculated using 9,10-diphenylanthracene in air equilibrated cyclohexane or coumarin153 in air equilibrated ethanol (ϕ = 0.97 and 0.53 respectively), following the method of Demas and Crosby.[127] Low temperature emission spectra were recorded on CH_2Cl_2:$CHCl_3$ 1:1 (v/v) rigid matrixes immersed in liquid nitrogen contained in a quartz Dewar flask. Measures on sensitisation of singlet-oxygen luminescence ($^1\Delta_g$) were performed with the $^1O_2$ luminescence band centred at 1270 nm, which was monitored under steady-state irradiation for the samples (x) and reference standard (st), which ϕ_Δ is known. [128] Exciting at an isoabsorbing wavelength and working in the same solvent, $\phi_\Delta x$ could be calculated with equation $\phi_{\Delta x} = \phi_{\Delta x} \frac{I_x}{I_{st}}$. Where I_x and I_{st} are the emission intensities of respectively sample and standard at 1270 nm, while $\phi_{\Delta x}$ is the singlet oxygen production yield of the standard. A solution of C_{60} in CH_2Cl_2 was used as a reference ($\phi_{\Delta st} = 1$).[129]

3.2 Materials and methods

Thin layer chromatography (TLC) was conducted on pre-coated aluminium sheets with 0.20 mm *Merk Millipore* Silica gel 60 with fluorescent indicator F254. Column chromatography was carried out using Merck Gerduran silica gel 60 (particle size 63-200 µm). Chemicals were purchased from Sigma Aldrich, Acros Organics, Alfa Aesar, Apollo Scientific, TCI, ABCR and Fluorochem and were used as received. Hydrochloric acid (HCl 32%) was purchased from Fischer Scientific. Pyridine was purchased from Acros Organics. MeOH, $CHCl_3$ and acetone were purchased as reagent-grade and used without further purification. Solvents were purchased from Sigma Aldrich, while deuterated solvents from Eurisotop. Where it was indicated that dry THF, Et_2O, toluene

or CH_2Cl_2 were used, HPLC grade solvents were dried using a Braun MB SPS-800 solvent purification system. Dry DMSO was purchased from Sigma Aldrich and Acros and used as received. When indicated that other dry solvents were used, they were dried upon placing for at least 24h upon molecular sieves that were previously heated to 160 °C overnight under vacuum, cooled down and stored under N_2.

When indicated that dry solvent was used, anhydrous conditions were achieved by drying Schlenk tubes or 2-neck flasks by flaming with a heat gun under vacuum and then purging with N_2. The inert atmosphere was maintained using N_2-filled balloons equipped with a syringe and a needle that was used to penetrate the silicon stoppers used to close the flask's necks. Additions of liquid reagents were performed using plastic or Hamilton syringes.

Low temperature baths were prepared using different solvent mixtures depending on the desired temperature: -96 °C with acetone/liquid N_2, -78 °C with acetone/dry ice, -10 °C with ice/NaCl and 0 °C with ice/water.

Emulsion for micellar conditions was prepared by mixing water and toluene in 9:1 proportions, adding 2% by weight of Kolliphor EL and sonicating until the white mixture was obtained. It was subsequently stored in a tightly closed bottle.

Freeze-pump-thaw was performed in Schlenk tubes closed with greased glass corks. Schlenk tube was inserted in a liquid N_2 for 1 minute, then placed under a high vacuum for 5 minutes. After the vacuum was closed, the Schlenk tube was removed from liquid N_2 until the solution thawed. The process was repeated 3 times, and at the end the tube was backfilled with N_2.

Photoredox reactions were performed under blue LED (457 nm) irradiation. UltraLEDs Blue 120 high intensity LED strip was coiled around a 250 ml beaker, and up to 4 Schlenk tubes with reaction mixtures were placed inside. An electric fan was placed over the reactor to maintain rt. Tetrachloroethane was used as an internal standard to check the NMR yield.

The progress of reactions was checked by TLC using UV light, $KMnO_4$, p-anisaldehyde or PMA as stains.

3.3 Experimental procedures

3.3.1 General procedures

General procedure A – Suzuki coupling

Aryl bromide or iodide (1eq), K_2CO_3 (1.2 - 4eq) and solvent mixture (toluene/water, toluene/MeOH, dioxane/water or DME/water) were degassed in a sonicator with N_2 flow for 15 min. Pd catalyst ([$Pd(PPh_3)_4$], [$Pd(dppf)Cl_2$], [$Pd(PPh_3)_2Cl_2$] or [$Pd(dtbpf)Cl_2$] 0.05-0.1 eq) and boronic acid (1-4 eq) were added and the mixture degassed for 5 more min. The reaction mixture was refluxed for an indicated amount of time. After cooling down to rt, water was added and the mixture extracted with EtOAc 3 times. The combined organic phases were washed with brine, dried with $MgSO_4$, filtered and concentrated under reduced pressure. The product was isolated by silica gel chromatography with an indicated solvent system. In cases when the products were not isolated pure, obtained materials were recrystallised or reprecipitated from an indicated solvent.

General procedure B – Micellar Suzuki coupling

An aryl bromide (1 eq), boronic acid (1.1 - 3 eq), Pd catalyst ([$Pd(dtbpf)Cl_2$] or [$Pd(PPh_3)_2Cl_2$] (0.02 – 0.04 eq) and an emulsion (0.5 M) (water:toluene 9:1 with 2% Kolliphor) were placed in a screw top vial with stirring bar and sonicated for 30 s. Et_3N (6 eq) was added, the top screwed tightly, and the mixture stirred at 60 °C for an indicated period of time. After cooling down to rt the mixture was diluted with CH_2Cl_2 and loaded on the silica gel column/filter for purification.

General procedure C – Photoredox coupling

An aryl halide (1 eq, 0.2 mmol) and PXX (0.02 eq, 0.04 mmol) were placed in a Schlenk tube and set under vacuum for 5 min. After backfilling with N_2 and under N_2 flow, they were dissolved in 1 mL of dry DMSO. DIPEA (1.4 eq, 0.28 mmol) and a radical trap (10 eq, 2 mmol) were added, and the mixture freeze-pump-thawed 3 times (frozen with liquid N_2, set under vacuum for 5 min, thawed) and then backfilled with N_2. The reaction mixture was stirred overnight with irradiation from blue (457 nm) LEDs. Tetrachloroethane (0.2 mmol) was added to the reaction mixture as an internal standard, and an aliquot was used to perform NMR. If the conversion was deemed sufficient (at least 50%), the purification was performed. Water (10 mL) and brine (2 mL) were added to the combined reaction mixture, and it was extracted with EtOAc 3 times. The combined organic phases were washed with brine, dried with $MgSO_4$,

filtered and concentrated under reduced pressure. The pure product was isolated by silica gel chromatography with an indicated solvent system.

General procedure D – Photoredox cyclisation

An aryl chloride (1 eq, 0.2 mmol) and PXX (0.02 eq, 0.04 mmol) were placed in a Schlenk tube and set under vacuum for 5 min. After backfilling with N_2 and with N_2 flow, they were suspended in 1 mL of dry DMSO. DIPEA (1.4 eq, 0.28 mmol) was added, and the mixture freeze-pump-thawed 3 times (frozen with liquid N_2, set under vacuum for 5 min, thawed) and then backfilled with N_2. The reaction mixture was stirred overnight with irradiation from blue (457 nm) LEDs. Water (10 mL) and brine (2 mL) were added, and the mixture was extracted with EtOAc 3 times. The combined organic phases were washed with brine, dried with $MgSO_4$, filtered and concentrated under reduced pressure. The pure product was isolated by silica gel chromatography with an indicated solvent system.

General procedure E - disulfide and diselenide use

$(MeS)_2$, $(PhS)_2$ and $(MeSe)_2$ are toxic and extremely smelly, all procedures were performed under the fume hood, all materials (glassware, gloves, syringes, etc.) that came in contact with the substance, or the reaction mixture, bleached for 48 h.

3.3.2 Synthetic procedures

Synthesis of 2,2'-bis(methylthio)-1,1'-binaphthalene 1

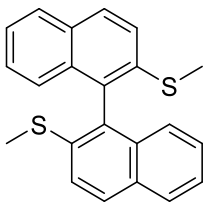

1

General procedure E applied. To a solution of 2,2'-dibromonaphthalene (4 g, 9.71 mmol) in dry THF (130 mL) TMEDA (3.2 mL, 21.85 mmol) was added under N_2. *n*-BuLi (1.6 M solution in hexanes) (14.7 mL, 23.30 mmol) was added dropwise at -96 °C and the reaction mixture stirred for 1h. To the green slurry which formed $(MeS)_2$ (4.4 mL, 48.5 mmol) was added at -96 °C, and the yellow mixture was stirred overnight while allowed to slowly return back to rt. Water (50 mL) was added and the mixture extracted with CH_2Cl_2 (3 × 50 mL). The organic phase was dried with $MgSO_4$, filtered and concentrated in vacuo with a liquid N_2 trap. The crude was purified through silica gel chromatography (petroleum ether/CH_2Cl_2, 4:1) to give **1** as a white solid (2.76 g, 82%).

M.p.: 182-183 °C; IR (ATR) ν (cm^{-1}): 3051, 2980, 2914, 1616, 1580, 1557, 1499, 1421, 1335, 1310, 1258,1211, 1200, 1159, 1132, 1117, 1057, 1024, 951, 943, 856, 800, 777, 772, 745, 737, 691, 669, 610, 559; ^{1}H NMR (400 MHz, CD_2Cl_2): δ = 8,01 (d, *J* = 8.8 Hz, 2H), 7.92 (d, *J* = 8.2 Hz, 2H), 7.62 (d, *J* = 8.8 Hz, 2H), 7.41 (ddd, *J* = 8.2, 6.8, 1.3 Hz, 2H), 7.25 (ddd, *J* = 8.5, 6.8, 1.3 Hz, 2H), 6.96 (d, *J* = 8.5 Hz, 2H), 2.44 (*s*, 6H); ^{13}C NMR (100 MHz, $CDCl_3$): δ = 136.7, 132.7, 132.6, 131.5, 129.0, 128.3, 127.1, 125.3, 125.0, 132.3, 15.9; HRMS (ES^+): m/z $[M+H]^+$ calcd for ($C_{22}H_{19}S_2$): 347.0928; found 347.0928.

Synthesis of 2,2'-bis(methylsulfinyl)-1,1'-binaphthalene 2

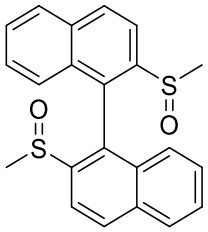

2

To a solution of compound **1** (1 g, 2.89 mmol) in 80 mL of 1:1 $CHCl_3$:CH_3COOH mixture, H_2O_2 (1.46 mL, 17 mmol, 35% in water) was added and the mixture stirred for 5 h at rt. The reaction mixture was quenched with saturated NaOH aq. solution at 0 °C, until pH~12. The mixture was extracted with $CHCl_3$ (3 × 50 mL). The combined organic phases were washed with brine, dried over $MgSO_4$, filtered and concentrated in vacuo. The product was dried under vacuum to compound **2** as a white solid in a quantitative yield (1.149 g). The product was used as a diastereoisomeric mixture in the next step.

M.p.: 142-145 °C; IR (ATR) ν (cm^{-1}): 3055, 2997, 2913, 1584, 1503, 1412, 1403, 1308, 1256, 1161, 1032, 951, 872, 818, 787, 775, 748, 692, 677, 637, 496, 463; ^{1}H NMR (300 MHz, CD_2Cl_2) and ^{13}C NMR (75 MHz, $CDCl_3$) spectra of the diastereoisomeric mixture attached in the Appendix A; HRMS (ES^+): m/z $[M+H]^+$ calcd for ($C_{22}H_{19}O_2S_2$): 379.0826; found 379.0829.

Synthesis of thioxanthenothioxanthene PTXTX

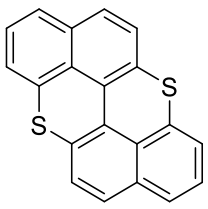

PTXTX

To an oven dried flask containing compound **2** (100 mg, 0.264 mmol), TfOH (1 mL) was added under N_2, and the mixture stirred at 80 °C overnight. To the reaction mixture, which over time changed colour from deep purple to deep brown, pyridine (5 mL) was added and the mixture, now deep orange, stirred overnight at 80 °C. After cooling to rt, pyridine was removed in vacuo, the residue dissolved in CH_2Cl_2, washed with water and brine, dried with $MgSO_4$, filtered and concentrated. The crude product was purified by column chromatography (neutral alumina Brockman activity 1, hexane/CH_2Cl_2 20:1, gradient to pure CH_2Cl_2) to afford **PTXTX** as an orange solid (37 mg, 45%).

M.p.: 211-213 °C; IR (ATR) ν (cm^{-1}): 3042, 2920, 2851, 1593, 1543, 1508, 1499, 1474, 1458, 1414, 1358, 1315, 1281, 1206, 1163, 1155, 1115, 1074, 995, 966, 959, 874, 812, 777, 758, 744, 640, 630, 557, 550, 530; ^{1}H NMR (300 MHz, CD_2Cl_2): δ = 7.27 (d, J = 8.7 Hz, 2H), 7.13 (dd, J = 8.1 Hz, 1.43 Hz 2H), 7.01 (dd, J = 8.1, 7.3 Hz, 2H), 6.86 (dd, J = 7.3 Hz, 1.4 Hz, 2H), 6.79 (d, J = 8.7 Hz, 2H); ^{13}C NMR (75 MHz, $CDCl_3$): δ = 134.3 (C), 129.9 (C), 129.7 (C), 128.7 (CH), 126.2 (CH), 125.9 (C), 125.7 (C), 125.5 (CH), 125.2 (CH), 120.9 (CH); HRMS (APCI$^+$): m/z $[M+H]^+$ calcd for ($C_{20}H_{11}S_2$): 315.0302; found 315.0293. Crystals suitable for X-ray diffraction were grown by slow diffusion of EtOH into solution of **PTXTX** in CH_2Cl_2, see section 4.4.

Synthesis of 1,1'-Binaphthalene-2,2'-diyl-O,O'-bis(N,N'-dimethylthiocarbamate) 3

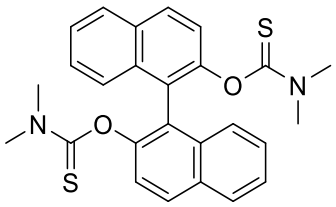

3

BINOL (1 g, 3.492 mmol) was placed in a dry Schlenk tube under N_2, and 16 mL of dry DMF was added. The mixture was cooled in an ice bath, and NaH 60 % in mineral oil (0.335 g, 8.38 mmol) was added in portions. To a resulting suspension at 0 °C dimethylthiocarbamoyl chloride (0.992 g, 8.03 mmol) was added in one portion. The resulting mixture was stirred for 3 h at 85 °C under N_2. After that, the mixture was cooled to rt and poured into 30 mL of 3% KOH solution. The white precipitate that formed was filtered and washed with water. The precipitate was dissolved in CH_2Cl_2, washed with brine, and the organic phase was dried with $MgSO_4$. After concentration, the yellow precipitate was recrystallised from a mixture of CH_2Cl_2 and petroleum ether to give **3** as a white solid with 75% yield (1.204 g, 2.614 mmol).

^{1}H NMR (300 MHz, $CDCl_3$): δ = 7.97 (d, *J* = 8.9 Hz, 2H), 7.90 (d, *J* = 8.4 Hz, 2H), 7.62 (d, *J* = 8.9 Hz, 2H), 7.47 – 7.42 (m, 4H), 7.32 – 7.27 (m, 2H), 3.08 (s, 6H), 2.52 (s, 6H); ^{13}C NMR (75 MHz, $CDCl_3$) δ =186.3, 149.6, 133.4, 131.5, 128.4, 127.9, 126.9, 126.5, 125.9, 124.1, 123.8, 42.9, 38.2 ; LRMS (ES^+): m/z $[M+Na]^+$ calcd for ($C_{26}H_{24}N_2O_2S_2Na$): 483.11; found: 482.89; In agreement with literature data.[130]

Synthesis of 1,1'-Binaphthalene-2,2'-diyl-S,S'-bis(N,N'-dimethylthiocarbamate) 4

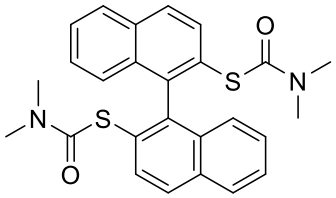

4

Compound **3** (0.680 g, 1.476 mmol) was placed carefully at the bottom of a dry Schlenk tube, set under N_2 and immersed into a metal bath heated previously to 295 °C. The reagent melted and was stirred at 285 °C for 30 min, keeping the temperature constant by wrapping the reaction container and bath in an aluminium foil. After cooling to rt the solid was dissolved in CH_2Cl_2, and the product separated by column chromatography (SiO_2, gradient chloroform to chloroform/EtOAC 10:3). The resulting material was recrystallised from CH_2Cl_2/petroleum ether mixture to afford **4** with 72% yield (487 mg, 1.057 mmol).

^{1}H NMR (300 MHz, $CDCl_3$): δ = 7.98 (d, *J* = 8.6 Hz, 2H), 7.91 (d, *J* = 8.1 Hz, 2H), 7.80 (d, *J* = 8.6 Hz, 2H), 7.49 – 7.44 (m, 2H), 7.26 – 7.20 (m, 2H), 7.08 (d, *J* = 8.4 Hz, 2H), 2.82 – 2.73 (br, 12H); ^{13}C NMR (100 MHz, $CDCl_3$) δ = 166.3, 141.0, 133.4, 133.3, 133.3, 128.5, 128.3, 128.0, 127.1, 126.7, 126.6, 37.0, 35.2; LRMS (ES^+): m/z $[M+Na]^+$ calcd for ($C_{26}H_{24}N_2O_2S_2Na$): 483.11; found: 482.90; In agreement with literature data.[130]

Synthesis of 1,1'-Binaphthalene-2,2'-dithiol 6

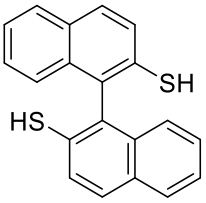

6

Compound **4** (480 mg, 1.042 mmol) was added to ice cooled suspension of $LiAlH_4$ (238 mg, 6.253 mmol) in 5 mL of dry THF, under N_2. The mixture was refluxed for 4 h and

then cooled to rt. The ice-cold water was added carefully through a condenser to quench the reaction, and 10% HCl solution was added until acidic pH was achieved. The mixture was then extracted with Et_2O, the combined organic phases dried with $MgSO_4$ and concentrated. The crude product was recrystallised from CH_2Cl_2/petroleum ether mixture to afford **6** with 58% yield (192 mg, 0.693 mmol).

^{1}H NMR (300 MHz, $CDCl_3$): δ = 7.90 – 7.87 (m, 4H), 7.57 (d, *J* = 8.6 Hz, 2H), 7.45 – 7.40 (m, 2H), 7.31 – 7.28 (m, 2H), 7.01 (d, *J* = 8.5 Hz, 2H), 3.28 (s, 2H); ^{13}C NMR (100 MHz, $CDCl_3$) δ = 132.8, 132.1, 132, 131.5, 129.2, 128.4, 127.6, 127.3, 125.7, 125,0; LRMS (ASAP+): m/z $[M+H]^+$ calcd for ($C_{20}H_{15}S_2$): 319.06; found: 318.89; In agreement with literature data.[130]

Synthesis of 2,2'-bis(phenylthio)-1,1'-binaphthalene 8

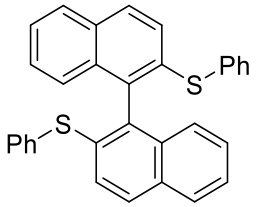

8

General procedure E applied. To a solution of 2,2'-dibromo-1,1'-binaphthalene (300 mg, 0.73 mmol) in dry THF (15 mL) TMEDA (0.24 mL, 1.64 mmol) was added under N_2. *n*-BuLi (1.6 M solution in hexanes) (1.1 mL, 1.75 mmol) was added dropwise at -78°C and the mixture stirred for 1h. To the slurry that formed $(PhS)_2$ (800 mg, 3.65 mmol) was added in one portion at -78°C. The mixture was stirred overnight while allowed to heat slowly back to rt. Water (20 mL) was added and the mixture extracted with CH_2Cl_2 (3 x 20 mL). The combined organic phases were dried with $MgSO_4$, filtered and concentrated under reduced pressure. Purified by silica gel chromatography with eluent petroleum ether/CH_2Cl_2 4:1 to give desired product **8** as a white precipitate (237 mg, 69% yield).

^{1}H NMR (300 MHz, CD_2Cl_2): δ = 7.91 (d, *J* = 8.1 Hz, 2H), 7.87 (d, *J* = 8.8 Hz, 2H), 7.49 – 7.42 (m, 6H), 7.37 – 7.27 (m, 10 H), 7.13 (d, *J* = 8.4 Hz, 2H); ^{13}C NMR (75 MHz, CD_2Cl_2) δ = 135.9, 135.1, 134.9, 133.2, 133, 132.2, 129.3, 129.1, 128.3, 127.7, 127.6, 127.2, 126.0, 125.7; LRMS (ES^+): m/z $[M+H]^+$ calcd for ($C_{32}H_{23}S_2$): 471.12; found: 471.12; In agreement with literature data.[131]

Synthesis of 6,6'-dibromo-2,2'-bis(methylsulfinyl)-1,1'-binaphthalene 11

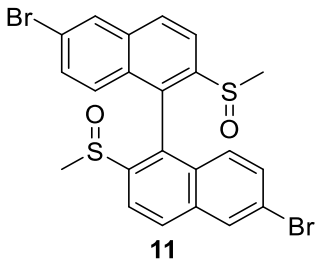

11

Synthesis through bromination

To a solution of compound **2** (120 mg, 0.317 mmol) in dry CH_2Cl_2 (4 mL) 3 mg of iodine was added under N_2, at 0 °C. 0.1 mL of Br_2 was dissolved in 9.9 mL of dry CH_2Cl_2, and 4.3 mL of this solution (0.86 mmol) was added dropwise to the reaction mixture. The mixture was stirred overnight, allowing it to reach rt. The reaction mixture was quenched with a saturated $Na_2S_2O_3$ solution (10 mL) and extracted with CH_2Cl_2 (3 x 10 mL). The combined organic phases were washed with brine, dried over $MgSO_4$, filtered and concentrated in vacuo. The crude was purified by silica gel chromatography (petroleum ether/EtOAc 5:1, gradient to EtOAc) to afford **11** as a white solid (27 mg, 15%).

M.p.: 178-180 °C; IR (ATR) v (cm^{-1}): 3055, 2920, 1607, 1576, 1551, 1485, 1412, 1400, 1302, 1190, 1152, 1038, 951, 872, 860, 804, 702, 675, 646, 501, 428, 419, 403; ^1H NMR (400 MHz, $CDCl_3$): δ = 8.05 (d, J = 2.0 Hz, 2H), 7.90 (d, J = 8.8 Hz, 2H), 7.59 (d, J = 8.8 Hz, 2H), 7.31 (dd, J = 9.0, 2.0 Hz, 2H), 6.82 (d, J = 9.0 Hz, 2H), 2.44 (s, 6H); HRMS (APCI$^+$): m/z $[M+H]^+$ calcd for ($C_{22}H_{17}O_2S_2Br_2$): 534.9037; found 534.9047.

Synthesis through oxidation

To a solution of compound **12** (400 mg, 0.793 mmol) in 280 mL of 1:1 $CHCl_3$:CH_3COOH mixture, H_2O_2 (466 µL, 4.76 mmol, 35% in water) was added and the mixture stirred for 5 h at rt. The reaction mixture was quenched with saturated NaOH aq. solution at 0 °C, until pH~12. The mixture was extracted with $CHCl_3$ (3 × 20 mL), the organic phase washed with brine, dried over $MgSO_4$, filtered and concentrated in vacuo. The crude product was dried under vacuum to obtain compound **11** as a white solid in a quantitative yield (425 mg). The product was used as a diastereoisomeric mixture in the next step.

^{13}C NMR (100 MHz, $CDCl_3$) spectra of the diastereoisomeric mixture attached in the Appendix A.

Synthesis of (6,6'-dibromo-[1,1'-binaphthalene]-2,2'-diyl)bis(methylsulfane) 12

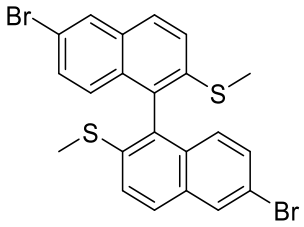

12

To a solution of compound **1** (1 g, 2.89 mmol) in dry CH_2Cl_2 (10 mL) a bromine solution was added dropwise (0.4 mL, 7.8 mmol of bromine in 9.6 mL of dry CH_2Cl_2) at 0 °C, under N_2. The mixture was stirred overnight while allowed to slowly reach rt. The reaction mixture was quenched by the addition of saturated $Na_2S_2O_3$ solution (20 mL) and extracted with CH_2Cl_2 (3 x 50 mL). The combined organic phases were washed with brine, dried over $MgSO_4$, filtered and concentrated in vacuo. The crude was purified by silica gel chromatography (petroleum ether/CH_2Cl_2 5:1) to afford **12** as a white solid (1.307 g, 90%).

M.p.: 247-250 °C (decomposition); IR (ATR) v (cm^{-1}): 3067, 3048, 2957, 2916, 2853, 1730, 1724, 1719, 1576, 1558, 1545, 1485, 1429, 1331, 1308, 1287, 1273, 1263, 1254, 1153, 1142, 1123, 1072, 1065, 972, 947, 870, 818, 808, 795, 760, 737, 702, 671, 646, 517; ^{1}H NMR (300 MHz, CD_2Cl_2): δ = 8.08 (d, J = 2.1 Hz, 2H), 7.92 (d, J = 8.8 Hz, 2H), 7.63 (d, J = 8.8 Hz, 2H), 7.32 (dd, J = 9.0, 2.1 Hz, 2H), 6.81 (d, J = 9.0, 2H), 2.43 (s, 6H); ^{13}C NMR (100 MHz, $CDCl_3$): δ = 137.6, 132.5, 131.7, 131.0, 130.6, 130.4, 128.3, 126.5, 124.2, 119.4, 15.7; HRMS (EI^+): m/z $[M]^+$ calcd for ($C_{22}H_{16}{}^{79}Br^{81}BrS_2$): 503.9040; found 503.9036.

Synthesis of 6,6'-dimesityl-[1,1'-binaphthalene]-2,2'-diyl)bis(methylsulfane) 13

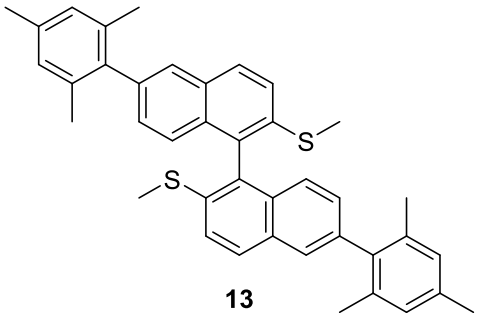

13

To a Schlenk tube compound **12** (370 mg, 0.734 mmol), 2,4,6-trimethylphenylboronic acid (289 mg, 1.761 mmol), Na_2CO_3 (233 mg, 2.202 mmol), toluene (12 mL), EtOH (6 mL) and water (2 mL) were added, and the mixture degassed for 30 min in a sonicator, with N_2 flow. [$Pd(PPh_3)_4$] (51 mg, 0.044 mmol) was added, and the reaction mixture

degassed for an additional 5 min. The reaction mixture was refluxed overnight under N_2. The mixture was cooled to rt, and the organic solvents evaporated under reduced pressure. The mixture was diluted with water and extracted with CH_2Cl_2. The combined organic phases were washed with brine, dried with $MgSO_4$ and concentrated under reduced pressure. The product was purified by column chromatography (SiO_2, petroleum ether/CH_2Cl_2 3:1) to afford **13** as a white solid (345 mg, 81%).

M.p.: 176-178 °C; IR (ATR) v (cm^{-1}): 3051, 2997, 2914, 1585, 1560, 1541, 1503, 1412, 1308, 1298, 1258, 1211, 1163, 1138, 1115, 1028, 961, 947, 930, 908, 880, 872, 816, 791, 775, 760, 731, 694, 675, 637, 606, 583, 563, 534, 523, 515; ^{1}H NMR (400 MHz, CD_2Cl_2.): δ = 7.99 (d, *J* = 8.8 Hz, 2H), 7.66 (m, 2H), 7.64 (d, *J* = 8.8 Hz, 2H), 7.10 (d, *J* = 8.6 Hz, 2H), 7.07 (dd, *J* = 8.6, 1.6 Hz, 2H), 6.95 (m, 2H), 6.94 (m, 2H), 2.47 (s, 6H), 2.31 (s, 6H), 2.03 (s, 6H), 2.00 (s, 6H); ^{13}C NMR (100 MHz, $CDCl_3$): δ = 138.8, 138.1, 136.8, 136.5, 136.3, 133.1, 131.7, 131.7, 129.2, 129.0, 128.3, 128.3, 128.2, 125.2, 123.9, 21.2, 21.1, 21.1, 16.3; Additional two ^{13}C peaks are present, as mesitylene groups in ortho position to naphthalene ring are not equivalent. HRMS (EI^+): m/z $[M]^+$ calcd. for ($C_{40}H_{38}S_2$): 582.2415; found 582.2415.

Synthesis of 6,6'-dimesityl-2,2'-bis(methylsulfinyl)-1,1'-binaphthalene 14

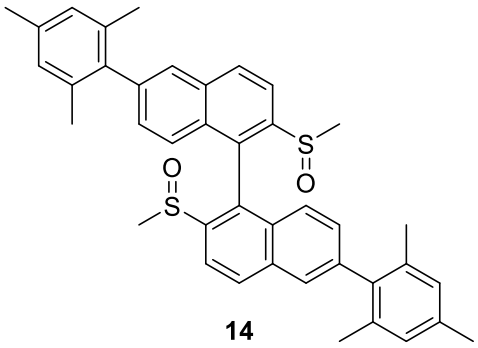

14

Compound **13** (341 mg, 0.585 mmol) was dissolved in 50 mL of 1:1 $CHCl_3$:CH_3COOH mixture. To a stirred solution H_2O_2 (500 µL, 5.82 mmol) was added, and the mixture stirred for 4 h. The reaction was cooled in an ice bath, and NaOH was added until pH ~ 12. The mixture was extracted with $CHCl_3$. The combined organic phases were washed with $NaHCO_3$ and brine, dried with $MgSO_4$ and concentrated. Compound **14** was obtained as a white solid in a quantitative yield (360 mg). The product was used as a diastereoisomeric mixture in the next step.

M.p.: 154-156 °C; IR (ATR) v (cm^{-1}): 2914, 2855, 1620, 1481, 1377, 1312, 1159, 1059, 949, 899, 854, 833, 814, 706, 698, 646, 581, 505, 444; ^{1}H NMR (400 MHz, CD_2Cl_2) and ^{13}C NMR (100 MHz, $CDCl_3$) spectra of the diastereoisomeric mixture attached in

the Appendix A. HRMS (ES$^+$): m/z calcd. for ($C_{40}H_{39}O_2S_2$): $[M+H]^+$ 615.2391; found 615.2394.

Synthesis of 2,8-dimesitylthioxanthenothioxanthene 15

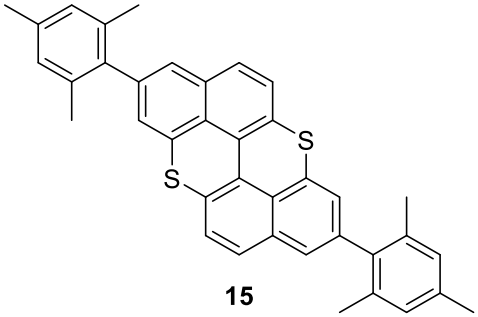

15

Compound **14** (55 mg, 0.09 mmol) was set under N_2, and TfOH was added (200 µL). The mixture was stirred overnight at rt. A condenser was added, and the system was set under N_2 again. Pyridine (1 mL) and water (8 mL) were added, and the mixture stirred for 1 h at 115 °C. After the mixture was cooled to rt, it was filtered, and the solid was washed with water. The solid was then dissolved in CH_2Cl_2 and purified first by column chromatography (SiO_2 petroleum ether, gradient to petroleum ether/CH_2Cl_2 10:1 and then by preparative TLC on a standard TLC plate, to obtain **15** as an orange solid (2 mg, 4%).

M.p., IR and carbon spectra could not be performed due to small amount of a sample.^{1}H NMR (400 MHz, CD_2Cl_2): δ = 7.29 (d, J = 8.9 Hz, 2H), 6.93 (s, 4H), 6.91 (d, J = 1.7 Hz, 2H), 6.84 (d, J = 8.6 Hz, 2H), 6.70 (d, J = 1.6 Hz, 2H), 2.30 (s, 6H), 2.05 (s, 12H); HRMS (ES$^+$): m/z $[M+H]^+$ calcd. for ($C_{38}H_{31}S_2$) 551.1867; found 551.1862.

Synthesis of 2,8-dibromothioxanthenothioxanthene 16

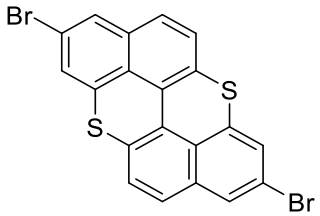

16

Diastereoisomeric mixture of compound **11** (200 mg, 0.37 mmol) was set under N_2 in a dry, two-neck flask equipped with a condenser. TfOH was added (1.2 mL) and the mixture was stirred overnight at rt. Pyridine (4 mL) and water (32 mL) were added, and the mixture stirred for 1 h at 100 °C. After the mixture was cooled to rt it was filtered, the solid washed with water and dried under a high vacuum. Highly insoluble in most

organic solvents crude (130 mg) was recrystallised from hot *o*-dichlorobenzene to obtain 29 mg of **16** as gold coloured crystalline material. The product turned out to be impossible to dissolve in any solvent, including hot *o*-dichlorobenzene, which made full characterisation impossible.

M.p.: 230-232 °C; IR (ATR) v (cm^{-1}): 3046, 1682, 1576, 1541, 1481, 1456, 1435, 1356, 1312, 1277, 1202, 1161, 1123, 1096, 1084, 1034, 951, 878, 837, 791, 770, 748, 731, 675, 658, 629, 546, 492, 457, 426; HRMS (ASAP+): m/z $[M]^+$ calcd for ($C_{20}H_8S_2Br_2$): 471.8414; found 471.8425.

Synthesis of (6,6'-bis(4-(tert-butyl)phenyl)-[1,1'-binaphthalene]-2,2'-diyl)bis(methylsulfane) 17

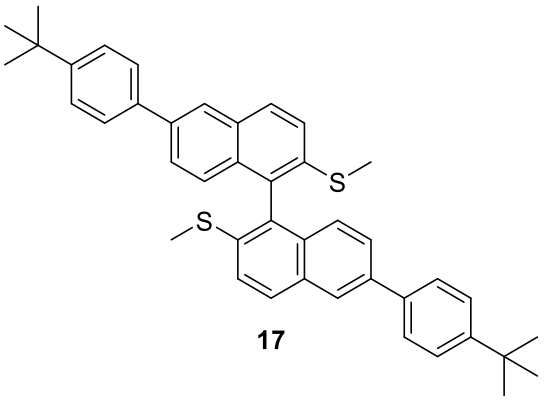

17

To a Schlenk tube compound **12** (300 mg, 0.595 mmol), 4-tertbutylphenylboronic acid (252 mg, 1.42 mmol), Na_2CO_3 (186 mg, 1.76 mmol), toluene (12 mL), EtOH (6 mL) and water (2 mL) were added, and the mixture degassed for 30 min in a sonicator, with N_2 flow. $[Pd(PPh_3)_4]$ (42 mg, 0.036 mmol) was added, and the mixture degassed for an additional 5 min. The reaction mixture was refluxed overnight under N_2. The mixture was cooled to rt, and the organic solvents evaporated under reduced pressure. The residue was diluted with water and extracted with CH_2Cl_2. The combined organic phases were washed with brine, dried with $MgSO_4$ and concentrated. The product was purified by column chromatography (SiO_2, petroleum ether/CH_2Cl_2 5:1, then 3:1) to afford **17** as a white solid (335 mg, 92%).

M.p.: 180-182 °C; IR (ATR) v (cm^{-1}): 3030, 2959, 2918, 2901, 2864, 1582, 1487, 1458, 1433, 1362, 1269, 1111, 966, 887, 841, 820, 567, 419; ^{1}H NMR (300 MHz, $CDCl_3$): δ = 8.11 (d, *J* = 1.6 Hz, 2H), 8.06 (d, *J* = 8.8 Hz, 2H), 7.66 – 7.62 (m, 6H), 7.55 (dd, *J* = 8.8, 1.8 Hz, 2H), 7.52 – 7.48 (m, 4H), 7.14 (d, *J* = 8.8 Hz, 2H), 2.48 (s, 6H), 1.39 (s, 18H); ^{13}C NMR (75 MHz, $CDCl_3$) δ 150.4, 138.1, 137.9, 136.6, 132.4, 131.8, 131.8,

129.4, 127.1, 126.9, 126.0, 125.9, 125.5, 123.7, 34.7, 31.5, 16.0; HRMS (ASAP+): m/z $[M+H]^+$ calcd. for ($C_{42}H_{43}S_2$) 611.2806; found 611.2783.

Synthesis of 6,6'-bis(4-(tert-butyl)phenyl)-2,2'-bis(methylsulfinyl)-1,1'-binaphthalene 18

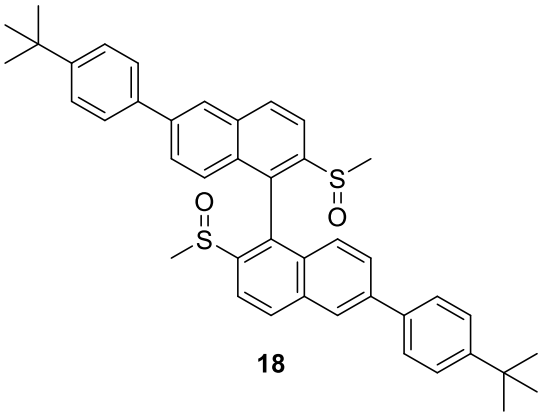

18

To a solution of compound **17** (290 mg, 0.475 mmol) in 50 mL of 1:1 $CHCl_3$:CH_3COOH mixture, H_2O_2 (240 µL, 2.8 mmol, 35% in water) was added, and the mixture stirred for 4.5 h at rt. The reaction mixture was quenched with saturated NaOH aq. solution at 0 °C, until pH~12 was reached. The mixture was extracted with $CHCl_3$ (3 × 25 mL). The combined organic phases were washed with brine, dried over $MgSO_4$, filtered and concentrated in vacuo. The crude product was dried under vacuum to obtain compound **18** as a white solid in a quantitative yield (304 mg). The product was used as a diastereoisomeric mixture in the next step.

M.p.: 169-171 °C; IR (ATR) v (cm^{-1}): 3032, 2959, 2920, 2903, 2864, 1516, 1489, 1458, 1362, 1269, 1113, 1051, 951, 887, 841, 820, 569, 419; ^1H NMR (300 MHz, $CDCl_3$) and ^{13}C NMR (100 MHz, $CDCl_3$) spectra of the diastereoisomeric mixture attached in the Appendix A. HRMS (ASAP+): m/z $[M+H]^+$ calcd. for ($C_{42}H_{43}O_2S_2$) 643.2704; found 643.2700.

Synthesis of (6,6'-bis(4-(trifluoromethyl)phenyl)-[1,1'-binaphthalene]-2,2'-diyl)bis(methylsulfane) 20

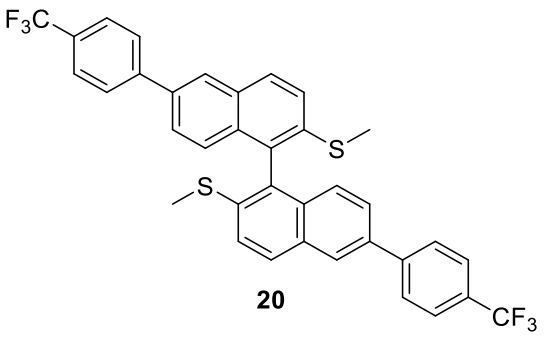

20

To a Schlenk tube compound **12** (200 mg, 0.37 mmol), 4-(trifluoromethyl)phenylboronic acid (181 mg, 0.95 mmol), Na_2CO_3 (126 mg, 1.19 mmol), toluene (8 mL), EtOH (4 mL) and water (2 mL) were added, and the mixture degassed for 25 min in a sonicator, with N_2 flow. $[Pd(PPh_3)_4]$ (28 mg, 0.024 mmol) was added and the mixture degassed for an additional 5 min. The reaction mixture was refluxed overnight under N_2. The mixture was cooled to rt, and the organic solvents evaporated under reduced pressure. The residue was diluted with water and extracted with CH_2Cl_2. The combined organic phases were washed with brine, dried with $MgSO_4$ and concentrated. The product was purified by column chromatography (SiO_2, petroleum ether/CH_2Cl_2 3:1) to afford **20** as a white solid (189 mg, 75%).

M.p.: 243-245 °C; IR (ATR) v (cm^{-1}): 3049, 2922, 1614, 1572, 1491, 1435, 1414, 1321, 1157, 1144, 1109, 1069, 1015, 887, 845, 833, 820, 812, 799, 608, 403; ^{1}H NMR (300 MHz, $CDCl_3$): δ = 8.05 (d, J = 1.9 Hz, 2H), 8.00 (d, J = 9.0 Hz, 2H), 7.70 -7.67 (m, 4H), 7.64-7.60 (m, 4H), 7.58 (d, J = 8.8 Hz, 2H), 7.44 (dd, J = 8.8, 1.9 Hz, 2H), 7.05 (d, J = 8.8 Hz, 2H), 2.41 (s, 6H); ^{13}C NMR (100 MHz, $CDCl_3$) δ = 144.5, 137.8, 136.5, 132.2, 131.8, 131.6, 129.6, 129.3, 127.6, 126.9, 126.6, 125.9 (q, J_{CF} = 3.7 Hz), 125.7, 123.8, 123.1, 15.8; HRMS (EI$^+$): m/z $[M]^+$ calcd for ($C_{36}H_{24}F_6S_2$): 634.1224; found 634.1210.

Synthesis of 2,2'-bis(methylsulfinyl)-6,6'-bis(4-(trifluoromethyl)phenyl)-1,1'-binaphthalene 21

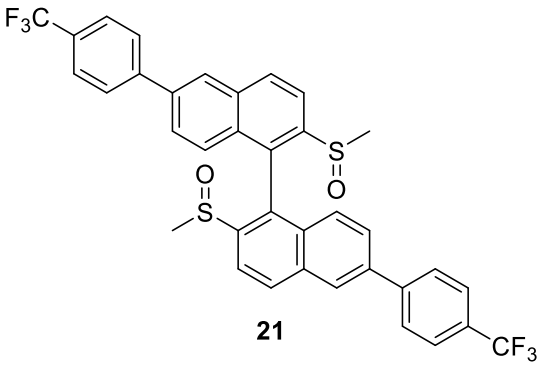

21

To a solution of **20** (156 mg, 0.246 mmol) in 24 mL of 1:1 $CHCl_3$:CH_3COOH mixture, H_2O_2 (150 µL, 1.47 mmol, 35% in water) was added, and the reaction mixture stirred for 5 h at rt. The reaction mixture was quenched with saturated NaOH aq. solution at 0 °C, until pH~12 was reached. The mixture was extracted with $CHCl_3$ (3 × 20 mL). The combined organic phases were washed with brine, dried over $MgSO_4$, filtered and concentrated in vacuo. The crude product was dried under vacuum to obtain compound **21** as a white solid in a quantitative yield (161 mg). The product was used as a diastereoisomeric mixture in the next step.

M.p.: 207-209 °C; IR (ATR) ν (cm^{-1}): 3055, 2961, 2920, 2866, 1614, 1489, 1412, 1319, 1269, 1161, 1111, 1069, 1047, 1015, 953, 887, 822, 714, 683, 610, 567, 501, 457, 442, 419, 411; ^1H NMR (400 MHz, $CDCl_3$) and ^{13}C NMR (100 MHz, $CDCl_3$) spectra of the diastereoisomeric mixture attached in the Appendix A. HRMS ($APCI^+$): m/z $[M+H]^+$ calcd for ($C_{36}H_{25}F_6O_2S_2$): 667.1200; found 667.1197.

Synthesis of 2,8-bis(4-(trifluoromethyl)phenyl)thioxanthenothioxanthene 22

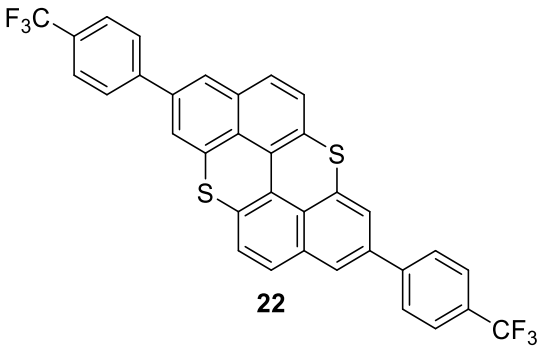

22

To a flame dried, two-neck flask equipped with a condenser compound **21** (70 mg, 0.11 mmol) was added under N_2. TfOH was added (420 µL) and the mixture, which turned dark, was stirred overnight at rt. Pyridine (1.4 mL) and water (11.2 mL) were added,

and the mixture stirred for 1 h at 100 °C. Cooling to rt caused the precipitation of a red solid, which was filtered and washed with water. As the solid was extremely insoluble in organic solvents, washing cycles with CH_2Cl_2, $CHCl_3$, EtOH, THF, acetone and petroleum ether were performed. Drying under a high vacuum led to 45 mg of product **22** as a dark red precipitate. Due to the poor solubility, a full characterisation was impossible.

M.p.: 238-240 °C; IR (ATR) v (cm^{-1}): 2974, 1682, 1605, 1551, 1422, 1317, 1290, 1180, 1119, 1107, 1015, 891, 881, 843, 802, 770, 702, 565, 538, 492; HRMS (ASAP+): m/z $[M+H]^+$ calcd for ($C_{34}H_{17}F_6S_2$): 603.0676; found 603.0665. Due to poor solubility no NMR spectroscopic characterisation could be performed.

Synthesis of (6,6'-dioctyl-[1,1'-binaphthalene]-2,2'-diyl)bis(methylsulfane) 23

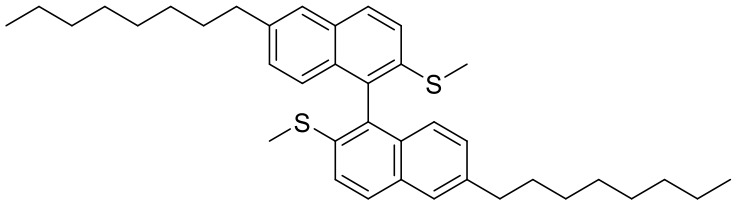

23

To a suspension of **12** (390 mg, 0.773 mmol) and [Pd(dppf)Cl_2] (29 mg, 0.039 mmol) in dry THF (25 mL) under N_2, *n*-Oct-Mg-Br was added dropwise (3.8 mL of 1 M solution in THF) at 0 °C. The mixture was stirred at reflux for 2.5 h and then at rt overnight. NH_4Cl aq. sat. solution (20 mL) was added, and the mixture extracted with EtOAc (3 x 20 mL). The combined organic phases were washed with brine, dried over $MgSO_4$, filtered and concentrated in vacuo. The crude product was purified by silica gel chromatography (petroleum ether/CH_2Cl_2 5:1), to afford **23** (310 mg, 70%) as a white glue.

IR (ATR) v (cm^{-1}): 2955, 2920, 2853, 1578, 1493, 1458, 1433, 1377, 1335, 1312, 1260, 1140, 1119, 974, 880, 843, 802, 721, 679, 420; ^{1}H NMR (300 MHz, $CDCl_3$): δ = 7.91 (d, *J* = 8.7 Hz, 2H), 7.65 (apparent doublet, 2H), 7.55 (d, *J* = 8.7 Hz, 2H), 7.09 (dd, *J* = 8.7, 1.8 Hz, 2H), 6.92 (d, *J* = 8.7 Hz, 2H), 2.72-2.62 (m, 4 H), 2.42 (s, 6H), 1.68 – 1.63 (m, 4H), 1.40 – 1.26 (m, 20H), 0.89 – 0.85 (m, 6H); ^{13}C NMR (75 MHz, $CDCl_3$): δ = 139.9, 135.3, 132.7, 131.7, 131.2, 128.7, 128.5, 126.6, 124.9, 123.4, 36.1, 32.0, 31.3, 29.6, 29.6, 29.4, 22.8, 16.0, 14.3; HRMS (APCI$^+$): m/z $[M+H]^+$ calcd for ($C_{38}H_{51}S_2$): 571.3432; found 571.3435.

Synthesis of 2,2'-bis(methylsulfinyl)-6,6'-dioctyl-1,1'-binaphthalene 24

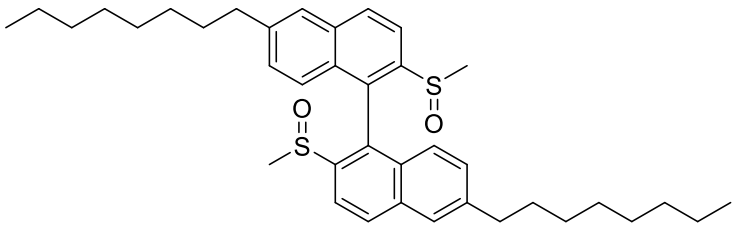

24

To a solution of **23** (199 mg, 0.35 mmol) in 30 mL of $CHCl_3$:CH_3COOH (1:1) mixture, H_2O_2 (0.18 mL, 2.06 mmol, 35% in water) was added and the reaction mixture stirred for 5 h at rt. The reaction mixture was quenched with saturated NaOH aq. solution at 0 °C, until pH~12. The mixture was extracted with $CHCl_3$ (3 × 20 mL). The combined organic phases were washed with brine, dried over $MgSO_4$, filtered and concentrated in vacuo. The crude product was dried under vacuum to obtain compound **24** in a quantitative yield (214 mg). The product was used as a diastereoisomeric mixture in the next step.

IR (ATR) ν (cm^{-1}): 29216, 2853, 2361, 2342, 1578, 1491, 1458, 1433, 1375, 1337, 1312, 1258, 1119, 1057, 880, 814, 802, 669, 419; ^1H NMR (300 MHz, $CDCl_3$) and ^{13}C NMR (75 MHz, $CDCl_3$) spectra of the diastereoisomeric mixture attached in the Appendix A. HRMS (APCI$^+$): m/z $[M+H]^+$ calcd for ($C_{38}H_{51}O_2S_2$): 603.3330; found 603.3340.

Synthesis of 2,8-dioctylthioxanthenothioxanthene 25

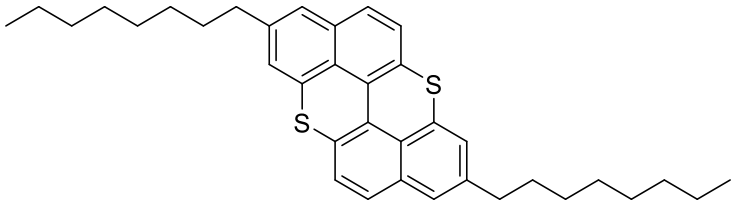

25

To a solution of compound **24** (500 mg, 0.83 mmol) in 65 mL of dry CH_3CN, TfOH (1 mL) was added under N_2, and the mixture stirred at 80 °C overnight. To the reaction mixture, which changed colour to dark brown, pyridine was added (5 mL) and the orange mixture stirred at 80 °C overnight, under N_2. After cooling to rt the solvent was removed in vacuo. The residue was dissolved in CH_2Cl_2, washed with water and brine. The combined organic phases were dried over $MgSO_4$, filtered and concentrated in vacuo. The crude product was purified by column chromatography (neutral alumina

Brockman activity 1, heptane/CH_2Cl_2 20:1, gradient to pure CH_2Cl_2) to give compound **25** as an orange solid (140 mg, 31%).

M.p.: 120-122 °C; IR (ATR) v (cm^{-1}): 3051, 2949, 2922, 2853, 1609, 1547, 1487, 1466, 1420, 1360, 1283, 1169, 1111, 1009, 941, 870, 839, 795, 773, 735, 554; ^{1}H NMR (300 MHz, $CDCl_3$): δ = 7.18 (d, *J* = 8.7 Hz, 2H), 6.88 (d, *J* = 1.6 Hz, 2H), 6.74 (d, *J* = 8.7 Hz, 2H), 6.72 (d, *J* = 1.6 Hz, 2H), 2.50 – 2.45 (m, 4H), 1.58 (m, 4H), 1.31 – 1.26 (m, 20H), 0.88 – 0.86 (m, 6H); ^{13}C NMR (75 MHz, $CDCl_3$): δ = 141, 134.6, 129.6, 128.4, 128.3, 125.6, 125.6, 124.9, 124.1, 122.0, 35.5, 32.0, 30.9, 29.6, 29.4, 29.4, 22.8, 14.3; HRMS (EI^+): m/z $[M]^+$ calcd for ($C_{36}H_{42}S_2$): 538.2728; found 538.2715. Crystals suitable for X-RAY diffraction were obtained by slow diffusion of petroleum ether into the solution of **25** in toluene, see section 4.4.

Synthesis of thioxanthenothioxanthene-6-oxide 28

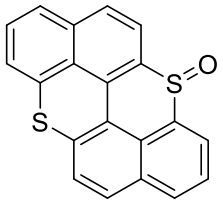

28

To a solution of **PTXTX** (19 mg, 0.06 mmol) in 20 mL of 1:1 $CHCl_3$:CH_3COOH mixture, H_2O_2 was added (31 µL, 0.36 mmol, 35% in water) and the mixture stirred at rt for 6h, in the dark. The reaction mixture was quenched with saturated NaOH aq. solution at 0 °C, until pH~12. The mixture was extracted with $CHCl_3$ (3 x 20 mL). The combined organic phases were washed with brine, dried with $MgSO_4$ and concentrated in vacuo. The crude material was purified with silica gel chromatography ($CHCl_3$) followed by HPLC ($CHCl_3$/THF 13:1) to obtain **28** as a dark red solid (10 mg, 50%).

M.p.: 240-242 °C; IR (ATR) v (cm^{-1}): 3048, 2918, 2851, 1609, 1541, 1495, 1435, 1416, 1341, 1290, 1229, 1196, 1140, 1059, 1016, 959, 874, 854, 829, 816, 783, 752, 685, 673, 646, 604, 567, 530, 515, 496, 465, 453, 434, 409; ^{1}H NMR (300 MHz, $CDCl_3$): δ = 8.38 (dd, *J* = 7.2, 1.3 Hz, 1H), 8.14 (dd, *J* = 8.0, 1.3 Hz, 1H), 7.95 (d, *J* = 8.5 Hz, 1H), 7.93 (d, *J* = 8.7 Hz, 1H), 7.81 (dd, *J* = 8.0, 7.2 Hz, 1H), 7.80 (d, *J* = 8.7 Hz,1H), 7.59 (dd, *J* = 7.6, 1.8 Hz, 1H), 7.48 – 7.43 (m, 2H), 7.41 (dd, *J* = 7.4, 1.8 Hz, 1H); ^{13}C NMR spectra could not be recorded due to low solubility of the product; HRMS ($APCI^+$): m/z $[M+H]^+$ calcd for ($C_{20}H_{11}OS_2$): 331.0251; found 331.0255. Crystals suitable for X-ray diffraction were obtained by hot recrystallization from CH_3CN, see section 4.4.

Synthesis of 2,8-dioctylthioxanthenothioxanthene-6-oxide 29

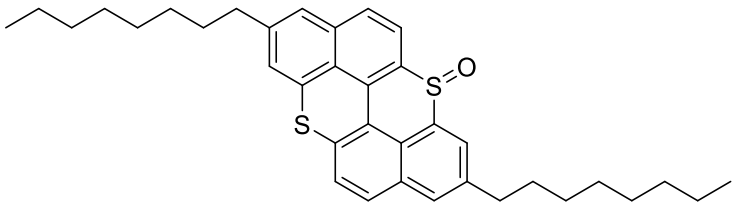

29

Compound **25** (25 mg, 0.046 mmol) was dissolved in 20 mL of 1:1 $CHCl_3$:CH_3COOH solution, H_2O_2 was added (24 µL, 0.27 mmol, 35% in water) and the mixture stirred at rt for 4 h, in the dark. A large amount of starting material was still visible on TLC, so another 10 µL of H_2O_2 was added, and the mixture stirred for another 2 h. The reaction mixture was quenched with saturated NaOH aq. solution at 0 °C, until pH~12. The mixture was extracted with $CHCl_3$ (3 x 20 mL). The combined organic phases were washed with brine, dried with $MgSO_4$ and concentrated in vacuo. The crude material was purified with silica gel chromatography (petroleum ether/EtOAc 20 :1, gradient to EtOAc) followed by HPLC ($CHCl_3$/THF 32:1) to obtain **29** as an orange solid (15 mg, 59%).

M.p.: 142-144 °C; IR (ATR) ν (cm^{-1}): 3049, 2951, 2914, 2847, 1611, 1558, 1514, 15-8, 1489, 1458, 1150, 1072, 1022, 982, 939, 880; ^{1}H NMR (500 MHz, CD_2Cl_2): δ = 8.21 (d, *J* = 1.7 Hz, 1H), 7.95 (d, *J* = 1.2 Hz, 1H), 7.92 (d, *J* = 8.7 Hz, 1H), 7.90 (d, *J* = 8.6 Hz, 1H), 7.76 (d, *J* = 8.6 Hz, 1H), 7.47 (d, *J* = 8.7 Hz, 1H), 7.41 (d, *J* = 1.2 Hz, 1H), 7.32 (d, *J* = 1.7 Hz, 1H), 2.95 – 2.91 (m, 2H), 2.75 – 2.72 (m, 2H), 1.80 – 1.77 (m, 2H), 1.72 – 1.70 (m, 2H), 1.41 – 1.27 (m, 20H), 0.89 – 0.87 (m, 6H); ^{13}C NMR (75 MHz, $CDCl_3$): δ = 142.8 (C), 141.6 (C), 137.6 (C), 134.9 (CH), 134.8 (C), 132.7 (CH), 132.6 (C), 131.7 (C), 131.1 (C), 130.8 (CH), 129.6 (CH), 128.8 (CH), 128.0 (C), 127.2, (C), 126.5 (C), 126.0 (CH), 124.1 (CH), 122.1 (CH), 121.4 (C), 119.6 (C), 35.8 (CH_2), 35.6 (CH_2), 32.0 (CH_2), 31.2 (CH_2), 31.1 (CH_2), 29.6 (CH_2), 29.5 (CH_2), 29.4 (CH_2), 22.8 (CH_2), 14.3 (CH_3) (6 carbon peaks are missing due to overlap); HRMS (APCI$^+$): m/z $[M+H]^+$ ($C_{36}H_{43}OS_2$): 555.2755; found 555.2758. Crystals suitable for X-RAY diffraction were obtained by slow diffusion of MeOH into **29** solution in CH_2Br_2, see section 4.4.

Synthesis of thioxanthenothioxanthene-6,12-dioxide 30

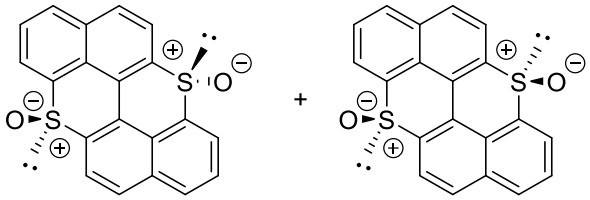

***trans*-30** ***cis*-30**

To a solution of **PTXTX** (65 mg, 0.21 mmol) in 20 mL of 1:1 $CHCl_3$:CH_3COOH mixture, H_2O_2 was added (93 µL, 0.91 mmol, 30% in water) and the mixture stirred overnight. The reaction was not finished by TLC, so another 46 µL of H_2O_2 was added, and the mixture stirred for 2 more days. The reaction mixture was quenched with saturated NaOH aq. solution at 0 °C, until pH~12. The mixture was extracted with $CHCl_3$ (3 x 30 mL). The combined organic phases were washed with brine, dried with $MgSO_4$ and concentrated in vacuo. The crude material was purified with column chromatography (SiO_2, petroleum ether/CH_2Cl_2 2:1 to pure CH_2Cl_2) to obtain a diastereoisomeric mixture of **30** (62 mg, 87%) as a yellow solid. The mixture was separated by HPLC ($CHCl_3$/THF 10:1 followed by another HPLC 7:1) to obtain 1:1 mixture of ***trans*-30** and ***cis*-30**. Diastereoisomer ***cis*-30** partially decomposed during the separation process on the HPLC, so it could not be characterised.

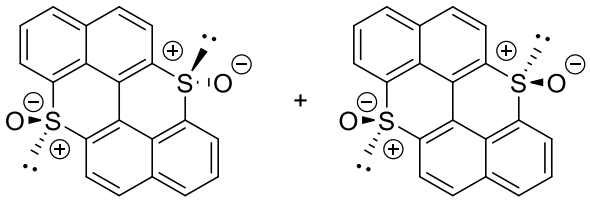

***trans*-30** ***cis*-30**

Characterisation of the diastereoisomeric mixture: m.p.: 284-286 °C (decomposition); IR (ATR) ν (cm^{-1}): 3090, 3055, 3011, 2924, 2853, 1578, 1489, 1423, 1369, 1294, 1215, 1202, 1153, 1142, 1121, 1061, 1013, 835; ^{1}H NMR (300 MHz, CD_2Cl_2): δ = 8.43 (dd, J = 7.2, 1.2 Hz, 2H), 8.38 (dd, J = 7.2, 1.2 Hz, 2H), 8.30 – 8.27 (m, 8H), 8.23 (dd, J = 8.2, 1.2 Hz, 2H), 8.16 (dd, J = 8.2, 1.2 Hz, 2H), 7.92 – 7.84 (m, 4H); ^{13}C NMR (75 MHz, $CDCl_3$): δ = 137.7 (C), 136.8 (C), 136.5 (C), 135.8 (C), 135.2 (C), 134.6 (C), 133.4 (CH), 132.6 (CH), 132.3 (CH), 132.3 (CH), 131.5 (CH), 129.2 (CH), 128.1 (CH), 128.1 (CH), 126.5 (CH), 124.5 (CH), 122.4 (C), 122.1 (C) (2 carbon peaks are missing due to overlap); HRMS (APCI$^+$): m/z $[M+H]^+$ ($C_{20}H_{11}O_2S_2$): 347.0200; found 347.0211.

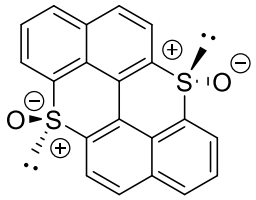

***trans*-30**

Characterisation of the ***trans*-30** diastereoisomer: m.p.: 225-227 °C; IR (ATR) ν (cm^{-1}): 2920, 2851, 1578, 1497, 1439, 1425, 1368, 1294, 1217, 1204, 1165, 1140, 1121, 1011, 926, 839, 762, 683, 660, 625, 563, 536, 525, 473, 457, 436; ^{1}H NMR (300 MHz, CD_2Cl_2): δ = 8.43 (dd, J = 7.2, 1.2 Hz, 2H), 8.32 (d, J = 8.5 Hz, 2H), 8.32 (d, J = 8.5 Hz, 2H), 8.23 (dd, J = 8.2, 1.2 Hz, 2H), 7.90 (dd, J = 8.2, 7.2 Hz, 2H); ^{13}C NMR (75 MHz, $CDCl_3$): δ = 136.8 (C), 136.5 (C), 135.2 (C), 133.4 (CH), 132.3 (CH), 131.5 (CH), 128.1 (CH), 126.5 (CH), 122.5 (C), 122.4 (C); HRMS (APCI$^+$): m/z $[M+H]^+$ ($C_{20}H_{11}O_2S_2$): 347.0200, found 347.0190 Crystals suitable for X-ray diffraction were obtained by hot recrystallization from DMSO, see section 4.4.

Synthesis of thioxanthenothioxanthene-6,6,12,12-tetraoxide 31

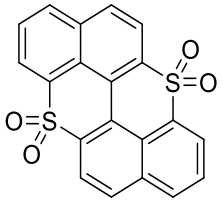

31

To a suspension of **PTXTX** (25 mg, 0.066 mmol) in CH_3COOH (5 mL), H_2O_2 (1 mL) was added, and the mixture refluxed overnight. After cooling down to rt a yellow precipitate which formed was washed with water and petroleum ether, and recrystallised from hot DMF. Recrystallisation did not allow purification, as an impurity also crystallised, and low solubility of the product did not allow purification with other methods. However, despite the crystallisation of impurity, it was possible to manually pick crystals of **31** suitable for X-RAY diffraction, see section 4.4.

Synthesis of 2,8-dioctylthioxanthenothioxanthene-6,6,12,12-tetraoxide 32

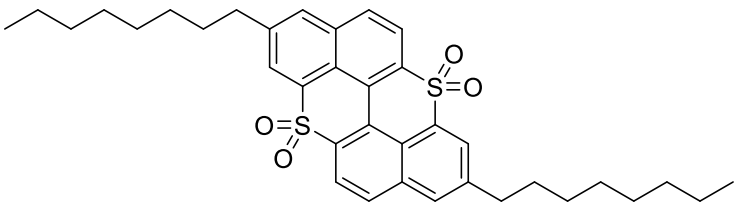

32

To a suspension of **25** (30 mg, 0.05 mmol) in $CHCl_3$ (5 mL), *m*CPBA (43 mg, 0.25 mmol) was added, and the mixture refluxed overnight. The mixture was cooled down to rt and concentrated under reduced pressure. The crude product was purified with silica gel chromatography (petroleum ether/CH_2Cl_2 1:4, gradient to 2:5) to afford **32** (27 mg, 90%) as a pale, yellowish solid.

M.p.: 184-186 °C; IR (ATR) v (cm^{-1}): 2957, 2922, 2847, 1618, 1582, 1466, 1433, 1422, 1371, 1290, 1206, 1159, 1134, 1123, 1013, 974, 895, 822, 799, 775, 719, 662, 611, 588, 569, 557, 519; ^{1}H NMR (300 MHz, CD_2Cl_2): δ = 8.50 (d, *J* = 1.8 Hz, 2H), 8.45 (d, *J* = 8.7 Hz, 2H), 8.27 (d, *J* = 8.7 Hz, 2H), 8.11 (apparent doublet, 2H), 3.00 – 2.95 (m, 4H), 1.87 – 1.77 (m, 4H), 1.45- 1.29 (m, 20H), 0.90 – 0.86 (m, 6H); ^{13}C NMR (75 MHz, CD_2Cl_2): δ = 145.0, 136.0, 135.3, 134.2, 134.0, 132.5, 128.7, 123.0, 121.9, 121.6, 36.2, 32.4, 31.3, 29.9, 29.8, 29.8, 23.2, 14.4; HRMS (APCI$^+$): m/z $[M+H]^+$ calcd for ($C_{36}H_{43}O_4S_2$): 603.2603; found 603.2603. Crystals suitable for X-RAY diffraction were obtained by slow diffusion of hexane into solution of **32** in toluene, see section 4.4.

Synthesis of 2,2'-bis(methylselanyl)-1,1'-binaphthalene 34

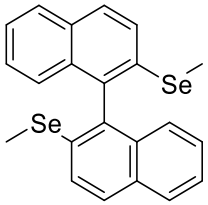

34

General procedure E applied. To a stirred solution of 2,2'-dibromo-1,1'-binaphthalene (500 mg, 1.21 mmol) in dry THF (20 mL), TMEDA (0.4 mL, 2.73 mmol) was added under N_2. *n*-BuLi (1.6 M solution in hexanes) (1.8 mL, 2.9 mmol) was added dropwise at -78 °C and the mixture stirred for 1h. To the formed, greenish slurry $(MeSe)_2$ (0.69 mL, 7.3 mmol) was added dropwise at -78 °C, and the reaction mixture was stirred overnight while slowly heating back to rt. Water (20 mL) was added and the mixture extracted with CH_2Cl_2 (3 x 20 mL). The combined organic phases were dried with $MgSO_4$, filtered and concentrated in vacuo. Purification by silica gel chromatography with petroleum ether/CH_2Cl_2 (4:1) gave desired product **34** as a white precipitate (345 mg, 65% yield).

M.p.: 174 - 176 °C; IR (ATR) v (cm^{-1}): 3049, 2980, 2928, 1614, 1578, 1555, 1499, 1420, 1395, 1373, 1339, 1317, 1273, 1254, 1165, 1150, 1134, 1125, 1107, 941, 910, 901, 843, 804, 779, 770, 743, 689, 546; ^{1}H NMR (300 MHz, $CDCl_3$): δ = 7.94 (d, *J* = 8.7 Hz, 2H), 7.90 (d, *J* = 8.2 Hz, 2H), 7.64 (d, *J* = 8.7 Hz, 2H), 7.43 (ddd, *J* = 8.2, 6.8, 1.3 Hz,

2H), 7.25 (ddd, *J* = 8.5, 6.8, 1.3 Hz, 2H), 7.04 (d, *J* = 8.5 Hz, 2H), 2.28 (s, 6H); ^{13}C NMR (75 MHz, $CDCl_3$) δ = 135.6, 132.7, 132.3, 132.0, 129.0, 128.3, 127.1, 125.8, 125.5, 125.1, 6.6; HRMS (APCI$^+$): m/z $[M+H]^+$ calcd for ($C_{22}H_{19}{}^{78}Se_2$): 438.9833; found: 438.9840.

Synthesis of 2,2'-bis(methylseleninyl)-1,1'-binaphthalene 35

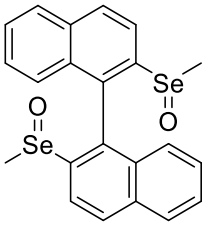

35

Compound **34** (300 mg, 0.68 mmol) was dissolved in 20 mL of 1:1 $CHCl_3$:CH_3COOH solution and H_2O_2 (0.4 mL, 13.6 mmol, 30% in water) was added dropwise. The reaction mixture was quenched with saturated KOH aq. solution at 0 °C, until pH~12. The mixture was extracted with $CHCl_3$ (3 x 10 mL), and the combined organic phases were dried with $MgSO_4$, filtered, concentrated under reduced pressure and dried on a high vacuum. Product **35** was obtained as an oil in a quantitative yield (472 mg). The product was used as a diastereoisomeric mixture in the next step.

IR (ATR) ν (cm^{-1}): 3055, 2982, 1501, 1396, 1308, 1258, 1157, 1072, 899, 876, 799, 775, 748, 687, 671, 625; ^{1}H NMR (300 MHz, $CDCl_3$) spectra of the diastereoisomeric mixture attached in the Appendix A. ^{13}C spectra not recorded due to low solubility. HRMS (APCI$^+$): m/z $[M+H]^+$ calcd for ($C_{22}H_{19}O_2{}^{78}Se_2$): 470.9731; found: 470.9745.

Synthesis of selenoxanthenoselenoxanthene 36

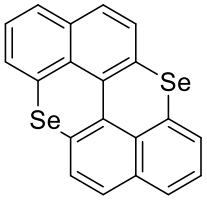

36

To a two-neck, oven dried flask fitted with a condenser compound **35** (50 mg, 0.1 mmol) was added under N_2. TfOH (0.3 mL) was added, and the mixture stirred at 80 °C overnight. Pyridine (1.5 mL) was added, and the mixture stirred overnight at 100 °C. The cooled mixture was diluted with toluene, transferred to a round bottom flask and evaporated under reduced pressure. Water was added and the mixture extracted with toluene (1 x 50 mL). The organic phase was washed with water (3 x 20 mL) and brine

(1 x 20 mL), dried with $MgSO_4$ and concentrated under reduced pressure. Pure product **36** was obtained as red needles by recrystallisation from hot toluene and hexane mixture (19 mg, 44%). Prior to photophysical characterisation compound **36** was repurified by flushing through a small column packed with neutral Alumina Brockman activity 1, using petroleum ether/toluene 10:1 as an eluent.

M.p.: 166 - 168 °C; IR (ATR) v (cm^{-1}): 3046, 2980, 2889, 1717, 1595, 1541, 1506, 1456, 1418, 1395, 1387, 1339, 1258, 1204, 1157, 1105, 1070, 957, 806, 772, 746, 627, 546; ^{1}H NMR (300 MHz, $CDCl_3$): δ = 7.46 (d, *J* = 8.5 Hz, 2H), 7.36 (dd, *J* = 7.9, 1.3 Hz, 2H), 7.28 (dd, *J* = 7.3 Hz, 1.3 Hz, 2H), 7.19 (d, *J* = 8.5 Hz, 2H), 7.14 (dd, *J* = 7.9 Hz, 7.3 Hz, 2H); ^{13}CNMR could not me recorded due to poor solubility. HRMS ($APCI^+$): m/z $[M+H]^+$ calcd for ($C_{20}H_{11}{}^{78}Se^{80}Se$): 408.9199; found: 408.9187. Crystals suitable for X-RAY diffraction were obtained by recrystallization from toluene and hexane mixture, see section 4.4.

Synthesis of 2-(methylseleno)-1,1'-biphenyl 38

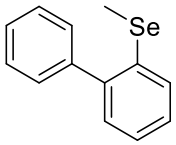

38

General procedure E applied. To a solution of 2-bromo-1,1'-biphenyl (0.74 mL, 4.3 mmol) in dry THF (10 mL) TMEDA (0.7 mL, 4.8 mmol) was added under N_2. *n*-BuLi (1.6 M solution in hexanes) (3.2 mL, 5,16 mmol) was added dropwise at -78 °C and the mixture stirred for 1h. Me_2Se_2 (0.55 mL, 5.8 mmol) was added dropwise to the slurry at -78 °C. The reaction mixture was stirred overnight while allowed to slowly return back to rt. Water (20 mL) was added, and the mixture extracted with CH_2Cl_2 (3 x 20 mL). The combined organic phases were dried with $MgSO_4$, filtered and concentrated in vacuo. Purified by silica gel chromatography with eluent petroleum ether/CH_2Cl_2 10:1 to give product **38** as a white precipitate (734 mg, 69% yield).

^{1}H NMR (300 MHz, $CDCl_3$): δ = 7.45 – 7.39 (m, 6H), 7.33 – 7.28 (m, 1H), 7.26 – 7.24 (m, 2H), 2.23 (s, 3H); ^{13}C NMR (75 MHz, $CDCl_3$) δ = 143, 141.7, 132.1, 129.9, 129.1, 128.4, 128.3, 128.2, 127.8, 125.7, 7.2; HRMS (ASAP+): m/z $[M+H]^+$ calcd for ($C_{13}H_{13}{}^{76}Se$): 244.0131; found: 244.0121; In agreement with literature data.[132]

Synthesis of 2-(methylseleninyl)-1,1'-biphenyl 39

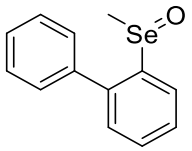

39

Compound **38** (711 mg, 2.88 mmol) was dissolved in 10 mL of 1:1 $CHCl_3$:CH_3COOH mixture and H_2O_2 (1 mL, 9.8 mmol, 30% in water) was added dropwise. The reaction mixture was quenched with saturated KOH aq. solution at 0 °C, until pH~12. The mixture was extracted with $CHCl_3$ (3 x 15 mL). The combined organic phases were dried with $MgSO_4$, filtered, concentrated under reduced pressure and dried under high vacuum. Product **39** was obtained as a white solid (736 mg, 97% yield).

M.p.: 146 - 148 °C; IR (ATR) ν (cm^{-1}): 3036, 2920, 1458, 1447, 1423, 1396, 1252, 1055, 997, 893, 829, 816, 772, 748, 743, 725, 706, 658, 613, 561, 554, 532; ^{1}H NMR (300 MHz, $CDCl_3$): δ = 8.19 (dd, *J* = 7.7, 1.5 Hz, 1H), 7.63 (td, *J* = 7.4, 1.5 Hz, 1H), 7.55 (td, *J* = 7.4, 1.5 Hz, 1H), 7.51 – 7.43 (m, 3H), 7.38 – 7.33 (m, 3H), 2.18 (s, 3H); ^{13}C NMR (75 MHz, $CDCl_3$) δ = 141.3, 140.7, 138.4, 130.9, 129.9, 129.1, 128.9, 128.8, 128.7, 125.0, 35.6; HRMS (APCI$^+$): m/z $[M+H]^+$ calcd for ($C_{13}H_{13}O^{76}Se$): 261.0159; found: 261.0158.

Synthesis of dibenzoselenophene 40

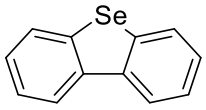

40

A two-neck, oven dried flask, fitted with a condenser was charged with compound **39** (200 mg, 0.76 mmol) under N_2. TfOH (1 mL) was added, and the mixture stirred at 80 °C overnight. Pyridine (5 mL) was added, and the mixture stirred overnight at 100 °C. After cooling down to rt the mixture was diluted with toluene, transferred to a round bottom flask and concentrated under reduced pressure. Water was added and the mixture extracted with EtOAc (3 x 10 mL). The combined organic phases were washed with water (1 x 10 mL) and brine (1 x 20 mL), dried with $MgSO_4$ and concentrated. Purified by silica gel chromatography with eluent petroleum ether, gradient to petroleum ether/ EtOAc 100:1 to give **40** as a white precipitate (158 mg, 90%).

^{1}H NMR (300 MHz, $CDCl_3$): δ = 8.14 (ddd, *J* = 7.7, 1.4, 0.5 Hz, 2H), 7.90 (ddd, *J* = 7.8, 1.3, 0.5 Hz, 2 H), 7.48 (ddd, *J* = 7.7, 7.2, 1.3 Hz, 2H), 7.40 (ddd, *J* = 7.8, 7.2, 1.4 Hz, 2H); ^{13}C NMR (75 MHz, $CDCl_3$) δ = 139.4, 138.4, 127.0, 126.2, 125.0, 123.0; LRMS ($APCI^+$): m/z $[M]^+$ calcd for ($C_{12}H_8Se$): 231.98; found: 231.98; In agreement with literature data.[133]

Synthesis of 4-(1-methyl-1H-pyrrol-2-yl)benzonitrile 42

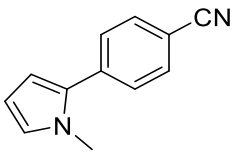

42

Synthesised according to the general procedure C with 4-chlorobenzonitrile as an aryl halide and N-methylpyrrole as a radical trap. Purified by silica gel chromatography with eluent petroleum ether/EtOAc 20:1, gradient to 15:1. Product **42** was obtained as a yellowish solid (25 mg, 69% yield).

^{1}H NMR (300 MHz, $CDCl_3$): δ = 7.67 (d, *J* = 8.7 Hz, 2H), 7.50 (d, *J* = 8.7 Hz, 2H), 6.79 (dd, *J* = 2.7, 1.8 Hz, 1H), 6.36 (dd, *J* = 3.7, 1.8 Hz, 1H), 6.24 (dd, *J* = 3.7, 2.7 Hz, 1H), 3.72 (s, 3H); ^{13}C NMR (75 MHz, $CDCl_3$) δ = 137.8, 132.7, 132.4, 128.4, 126, 119.2, 110.9, 109.8, 108.7, 35.6; LRMS (ES^+): m/z $[M+H]^+$ calcd for ($C_{12}H_{11}N_2$): 183.09; found: 183.09; In agreement with literature data.[134]

Synthesis of methyl 4-(1-methyl-1H-pyrrol-2-yl)benzoate 43

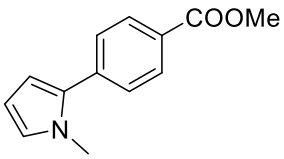

43

Synthesised according to the general procedure C with methyl 4-chlorobenzoate as an aryl halide and N-methylpyrrole as a radical trap. Purified by silica gel chromatography with eluent petroleum ether/EtOAc 20:1. Product **43** was obtained as a yellowish solid (23 mg, 53% yield).

^{1}H NMR (300 MHz, $CDCl_3$): δ = 8.06 (d, *J* = 8.7 Hz, 2H), 7.48 (d, *J* = 8.7 Hz, 2H), 6.77 (dd, *J* = 2.7, 1.8 Hz, 1H), 6.34 (dd, *J* = 3.7, 1.8 Hz, 1H), 6.23 (dd, *J* = 3.7, 2.7 Hz, 1H), 3.93 (s, 3H), 3.72 (s, 3H); ^{13}C NMR (75 MHz, $CDCl_3$) δ 167.1, 137.8, 133.6,

129.9, 128.0, 128.0, 125.3, 110.2, 108.4, 52.3, 35.6; LRMS (ES^+): m/z $[M+H]^+$ calcd for ($C_{13}H_{14}NO_2$): 216.10; found: 216.10; In agreement with literature data.[29]

Synthesis of 1-(4-(1-methyl-1H-pyrrol-2-yl)phenyl)ethan-1-one 44

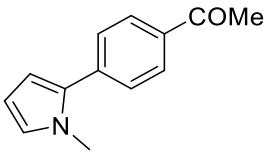

44

Synthesised according to the general procedure C with 4-bromoacetophenone as an aryl halide and N-methylpyrrole as a radical trap. Purified by silica gel chromatography with eluent petroleum ether, gradient to petroleum ether/EtOAc 10:1. Product **44** was obtained as a yellowish solid (20 mg, 50% yield).

^1H NMR (300 MHz, $CDCl_3$): δ = 7.99 (d, *J* = 8.5 Hz, 2H), 7.50 (d, *J* = 8.5 Hz, 2H), 6.78 (dd, *J* = 2.7, 1.8 Hz, 1H), 6.36 (dd, *J* = 3.7, 1.8 Hz, 1H), 6.24 (dd, *J* = 3.7, 2.7 Hz, 1H), 3.73 (s, 3H), 2.63 (s, 3H); ^{13}C NMR (75 MHz, $CDCl_3$) δ = 197.7, 138.0, 135.0, 133.5, 128.7, 128.1, 125.4, 110.3, 108.5, 35.6, 26.7; LRMS (ES^+): m/z $[M+H]^+$ calcd for ($C_{13}H_{14}NO$): 200.11; found: 200.11; In agreement with literature data.[135]

Synthesis of 6-chloro-[1,1':2',1''-terphenyl]-3-carbonitrile 52

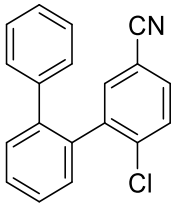

52

Synthesised according to the general procedure A using [1,1'-biphenyl]-2-ylboronic acid (915 mg, 4.62 mmol), 3-bromo-4-chlorobenzonitrile (1000 mg, 4.62 mmol), $[Pd(PPh_3)_4]$ (266 mg, 0.23 mmol), K_2CO_3 (766 mg, 5.54 mmol), toluene (23 mL) and water (3 mL). Refluxed overnight. Purified by silica gel chromatography with eluent petroleum ether, gradient to petroleum ether/EtOAc 30:1. Product **52** was obtained as a white powder (305 mg, 23% yield).

M.p.: 99 - 100 °C; IR (ATR) v (cm^{-1}): 3069, 3025, 2225, 1467, 1431, 1387, 1082, 1053, 1009, 903, 829, 780, 768, 743, 729, 703, 628, 611, 553, 529, 512, 486; ^1H NMR (300 MHz, $CDCl_3$): δ = 7.52 – 7.40 (m, 6H), 7.31 – 7.29 (d, *J* = 7.5 Hz, 1H), 7.21 – 7.19 (m, 3H), 7.10 -7.07 (m, 2H); ^{13}C NMR (75 MHz, $CDCl_3$) δ = 142.1, 141.5, 140.3, 138.9,

135.8, 135.6, 131.6, 130.5, 130.4, 130.4, 129.3, 129.1, 128.1, 127.3, 127.1, 118.0, 110.5; HRMS (APCI$^+$): m/z [M+H]$^+$ calcd for ($C_{19}H_{13}NCl$): 290.0737; found: 290.0746.

Synthesis of 2-chloro-[1,1':2',1''-terphenyl]-3-carbonitrile 53

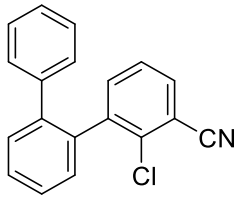

53

Synthesised according to the general procedure A using [1,1'-biphenyl]-2-ylboronic acid (297 mg, 1.5 mmol), 3-bromo-2-chlorobenzonitrile (325 mg, 1.5 mmol), [Pd(PPh_3)$_4$] (87 mg, 0.075 mmol), K_2CO_3 (249 mg, 1.8 mmol), toluene (7.5 mL) and water (1 mL). Refluxed overnight. Purified by silica gel chromatography with eluent petroleum ether, gradient to petroleum ether/EtOAc 40:1. Product **53** was obtained as a white powder (130 mg, 30%).

M.p.: 100 - 102 °C; IR (ATR) v (cm^{-1}): 3067, 3025, 2233, 1481, 1454, 1409, 1271, 805, 799, 776, 767, 761, 744, 733, 720, 703, 543, 436, 412; ^{1}H NMR (300 MHz, $CDCl_3$): δ = 7.50 – 7.35 (m, 4H), 7.26 – 7.22 (m, 2H), 7.16 – 7.11 (m, 4H), 7.03 – 6.99 (m, 2H); ^{13}C NMR (75 MHz, $CDCl_3$) δ = 142.3, 141.4, 140.4, 136.5, 136.2, 136.0, 132.9, 130.5, 130.4, 129.3, 129.0, 128.1, 127.3, 127.1, 126.7, 116.4, 114.0; HRMS (APCI$^+$): m/z [M]$^+$ calcd for ($C_{19}H_{12}NCl$): 289.0658; found: 289.0670.

Synthesis of methyl 6-chloro-[1,1':2',1''-terphenyl]-3-carboxylate 54

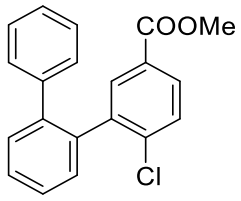

54

Synthesised according to the general procedure A using [1,1'-biphenyl]-2-ylboronic acid (198 mg, 1 mmol), methyl 3-bromo-4-chlorobenzoate (250 mg, 1 mmol), [Pd(PPh_3)$_4$] (58 mg, 0.05 mmol), K_2CO_3 (276 mg, 2 mmol), toluene (5 mL) and water (1 mL). Refluxed overnight. Purified by silica gel chromatography with eluent petroleum ether/EtOAc 30:1. Product **54** was obtained as a white powder (102 mg, 32% yield).

M.p.: 134 - 136 °C; IR (ATR) ν (cm^{-1}): 3071, 3025, 2952, 1722, 1700, 1428, 1396, 1276, 1266, 1241, 1231, 1107, 1079, 1022, 909, 852, 770, 757, 746, 699, 691, 552, 529; ^{1}H NMR (300 MHz, $CDCl_3$): δ = 7.90 (d, *J* = 2.2 Hz, 1H), 7.86 (dd, *J* = 8.3, 2.3 Hz, 1H), 7.55 – 7.43 (m, 3H), 7.39 – 7.33 (m, 2H), 7.21 – 7.13 (m, 5H), 3.89 (s, 3H); ^{13}C NMR (75 MHz, $CDCl_3$) δ = 166.3, 141.6, 140.9, 138.6, 137.2, 133.3, 130.6, 130.3, 129.6, 129.5, 129.4, 128.7, 128.4, 127.9, 127.2, 126.9, 52.4 (1 carbon peak is missing due to overlap); HRMS (EI): m/z $[M]^+$ calcd for ($C_{20}H_{15}O_2Cl$): 322.0755; found: 322.0754.

Synthesis of 2-chloro-5-nitro-1,1':2',1''-terphenyl 55

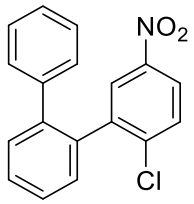

55

Synthesised according to the general procedure A using [1,1'-biphenyl]-2-ylboronic acid (198 mg, 1 mmol), 2-bromo-1-chloro-4-nitrobenzene (236 mg, 1 mmol), $[Pd(PPh_3)_4]$ (58 mg, 0.05 mmol), K_2CO_3 (276 mg, 2 mmol), toluene (5 mL) and water (1 mL). Refluxed overnight. Purified by silica gel chromatography with eluent petroleum ether, gradient to petroleum ether/EtOAc 100:1. Product **55** was obtained as a white powder (117 mg, 38% yield).

M.p.: 114 - 116 °C; IR (ATR) ν (cm^{-1}): 3075, 3032, 2916, 2851, 1566, 1516, 1481, 1458, 1342, 1076, 1053, 918, 880, 768, 737, 698, 579, 509; ^{1}H NMR (300 MHz, $CDCl_3$): δ = 8.05 – 8.01 (m, 2H), 7.57 – 7.44 (m, 4H), 7.34 (d, *J* = 7.4 Hz, 1H), 7.22 – 7.18 (m, 3H), 7.14 – 7.09 (m, 2H); ^{13}C NMR (75 MHz, $CDCl_3$) δ = 146.1, 142.1, 141.6, 140.7, 140.4, 135.9, 130.5, 130.4, 129.4, 129.3, 128.2, 127.5, 127.2, 127.1, 123.2, (1 carbon peak is missing due to overlap); HRMS ($APCI^+$): m/z $[M]^+$ calcd for ($C_{18}H_{12}ClNO_2$): 309.0557; found: 309.0557.

Synthesis of 4-chloro-3-(naphthalen-1-yl)benzonitrile 56

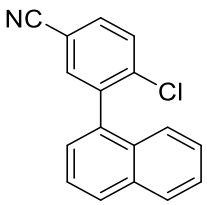

56

Synthesised according to the general procedure A using naphthalen-1-ylboronic acid (258 mg, 1.5 mmol), 3-bromo-4-chlorobenzonitrile (325 mg, 1.5 mmol), $[Pd(PPh_3)_4]$ (87 mg, 0.075 mmol), K_2CO_3 (249 mg, 1.8 mmol), toluene (7.5 mL) and water (1 mL). Refluxed overnight. Purified by silica gel chromatography with eluent petroleum ether/EtOAc 40:1, gradient to 30:1. Product **56** was obtained as a white powder (350 mg, 88% yield).

M.p.: 112 -114 °C; IR (ATR) v (cm-1): 3094, 3061, 2228, 1472, 1381, 1123, 1060, 1047, 899, 835, 800, 776, 743, 624, 605, 569, 543, 528, 519, 482, 433; ^{1}H NMR (300 MHz, $CDCl_3$): δ = 7.98 – 7.93 (m, 2H), 7.11 – 7.65 (m, 3H), 7.59 – 7.54 (m, 2H), 7.46 (ddd, *J* = 8.3, 6.8, 1.5 Hz, 1H), 7.39 – 7.35 (m, 2H); ^{13}C NMR (75 MHz, $CDCl_3$) δ = 141.1, 139.8, 135.6, 135.1, 133.6, 132.4, 131.2, 130.8, 129.3, 128.7, 127.3, 126.8, 126.4, 125.3, 125.2, 118.0, 111.1; HRMS (APCI$^+$): m/z $[M]^+$ calcd for ($C_{17}H_{10}NCl$): 263.0502; found: 263.0504.

Synthesis of 6-chloro-2'-(1H-pyrrol-1-yl)-[1,1'-biphenyl]-3-carbonitrile 57

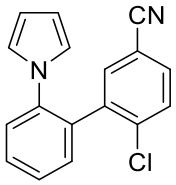

57

Synthesised according to the general procedure A using (2-chloro-5-cyanophenyl)boronic acid (272 mg, 1.65 mmol), 1-(2-bromophenyl)-1H-pyrrole (244 mg, 1.1 mmol), $[Pd(PPh_3)_2Cl_2]$ (77 mg, 0.11 mmol), K_2CO_3 (759 mg, 5.5 mmol), DME (6 mL) and water (2 mL). Refluxed overnight. Purified by silica gel chromatography with eluent petroleum ether, gradient to petroleum ether/EtOAc 30 :1. Product **57** was obtained as a white powder (130 mg, 42% yield).

M.p.: 90 - 92 °C; IR (ATR) v (cm^{-1}): 3067, 2230, 1593, 1578, 1501, 1466, 1443, 1393, 1331, 1319, 1069, 1015, 922, 837, 760, 733, 613, 498; ^{1}H NMR (400 MHz, $CDCl_3$): δ = 7.56 – 7.49 (m, 3H), 7.47 – 7.41 (m, 3H), 7.36 – 7.34 (m, 1H), 6.54 – 6.53 (m, 2H), 6.12 – 6.10 (m, 2H); ^{13}C NMR (100 MHz, $CDCl_3$) δ = 139.8, 139.6, 139.2, 134.5, 132.5, 132.3, 131.4, 130.7, 130.1, 127.1, 126.2, 121.9, 117.8, 111.1, 109.7; HRMS (ES$^+$): m/z $[M+H]^+$ calcd for ($C_{17}H_{12}ClN_2$): 279.0689; found: 279.0698.

Synthesis of 6-chloro-2'-(thiophen-3-yl)-[1,1'-biphenyl]-3-carbonitrile 58

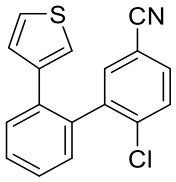

58

Synthesised according to the general procedure A using (2-chloro-5-cyanophenyl)boronic acid (283 mg, 1.56 mmol), 3-(2-bromophenyl)thiophene (249 mg, 1.04 mmol), [Pd(dppf)Cl_2] (39 mg, 0.052 mmol), K_2CO_3 (287 mg, 2.08 mmol), dioxane (7.5 mL) and water (1.5 mL). Refluxed overnight. Purified by silica gel chromatography with eluent petroleum ether, gradient to petroleum ether/EtOAc 25:1, followed by recrystallization from hexane to give product **58** (136 mg, 44% yield).

M.p.: 108 -110 °C; IR (ATR) v (cm^{-1}): 3061, 2234, 1466, 1461, 1438, 1390, 1194, 1077, 1022, 912, 828, 824, 793, 770, 765, 753, 715, 647, 624, 612, 497; ^{1}H NMR (300 MHz, $CDCl_3$): δ = 7.48 – 7.38 (m, 5H), 7.34 (ddd, *J* = 7.5, 7.2, 1.8 Hz, 1H), 7.21 – 7.18 (m, 1H), 7.08 (dd, *J* = 5.0, 3.0 Hz, 1H), 6.82 (dd, *J* = 3.0, 1.3 Hz, 1H), 6.69 (dd, *J* = 5.0, 1.3 Hz, 1H); ^{13}C NMR (75 MHz, $CDCl_3$) δ = 142.3, 140.8, 139.1, 136.1, 135.7, 135.3, 131.9, 130.7, 130.4, 130.0, 129.2, 128.3, 127.4, 125.4, 123.3, 118.0, 110.8; HRMS (APCI$^+$): m/z $[M+H]^+$ calcd for ($C_{17}H_{11}NSCl$): 296.0301; found: 296.0313.

Synthesis of 2'-bromo-2,4-dimethoxy-1,1'-biphenyl 59a

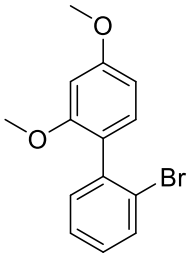

59a

Synthesised according to the general procedure A using (2,4-dimethoxyphenyl)boronic acid (328 mg, 1.8 mmol), 1-bromo-2-iodobenzene (424 mg, 1.5 mmol), [Pd(PPh_3)$_2Cl_2$] (53 mg, 0.075 mmol), K_2CO_3 (415 mg, 3 mmol), toluene (10 mL) and MeOH (5 mL). Refluxed for 4 h. Purified by silica gel chromatography with eluent petroleum ether/EtOAc 12:1. Product **59a** was obtained as a colourless oil (415 mg, 94% yield).

IR (ATR) v (cm^{-1}): 2980, 2889, 2833, 1611, 1578, 1558, 1541, 1508, 1458, 1435, 1412, 1306, 1281, 1260, 1206, 1157, 1134, 1065, 1026, 1001, 934, 826, 758; ^{1}H NMR (300

MHz, $CDCl_3$): δ = 7.56 (dd, *J* = 8.0, 1.2 Hz, 1H), 7.26 (ddd, *J* = 7.6, 7.1, 1.2 Hz, 1H), 7.20 (dd, *J* = 7.6, 2.1 Hz, 1H), 7.1 (ddd, *J* = 8.0, 7.1, 2.1 Hz, 1H), 7.03 – 7.00 (m, 1H), 6.50 – 6.47 (m, 2H), 3.79 (s, 3H), 3.69 (s, 3H); ^{13}C NMR (75 MHz, $CDCl_3$) δ = 160.9, 157.7, 139.7, 132.6, 132.1, 131.4, 128.6, 127.1, 124.9, 123.3, 104.1, 98.8, 55.7, 55.5; HRMS (ES^+): m/z $[M+H]^+$ calcd for ($C_{14}H_{14}BrO_2$): 293.0177; found: 293.0180.

Synthesis of 6-chloro-2'',4''-dimethoxy-[1,1':2',1''-terphenyl]-3-carbonitrile 59

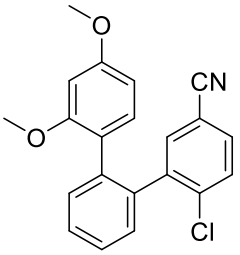

59

Synthesised according to the general procedure A using (2-chloro-5-cyanophenyl)boronic acid (212 mg, 1.17 mmol), compound **59a** (228 mg, 0.78 mmol), $[Pd(dppf)Cl_2]$ (28 mg, 0.039 mmol), K_2CO_3 (216 mg, 1.56 mmol), dioxane (5 mL) and water (1 mL). Refluxed overnight. Purified by silica gel chromatography with eluent petroleum ether/EtOAc 20 :1. Product **59** was obtained as a white powder (180 mg, 66% yield).

M.p.: 103 - 104 °C; IR (ATR) ν (cm^{-1}): 3065, 2995, 2967, 2942, 2231, 1613, 1511, 1456, 1437, 1298, 1207, 1159, 1135, 1053, 1027, 1021, 899, 840, 823, 800, 763, 636, 625, 612, 576, 561, 508, 482; ^1H NMR (300 MHz, $CDCl_3$): δ = 7.51 – 7.36 (m, 6H), 7.31 (d, *J* = 7.2 Hz, 1H), 7.05 (d, *J* = 8.3 Hz, 1H), 6.44 (d, *J* = 8.3, 2.2 Hz, 1H), 6.24 (d, *J* = 2.2 Hz, 1H), 3.78 (s, 3H), 3.48 (s, 3H); ^{13}C NMR (75 MHz, $CDCl_3$) δ = 160.7, 156.7, 142.3, 138.9, 138.0, 135.3, 131.9, 131.3, 131.2, 130.2, 129.8, 128.8, 127.1, 122.0, 118.2, 109.7, 104.3, 98.1, 55.4, 54.8 (1 carbon peak is missing due to overlap); HRMS (EI): m/z $[M]^+$ calcd for ($C_{21}H_{16}O_2NCl$): 349.0864; found: 349.0862.

Synthesis of 2-bromo-4'-(tert-butyl)-1,1'-biphenyl 60a

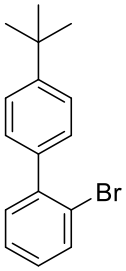

60a

Synthesised according to the general procedure A using (4-(tert-butyl)phenyl)boronic acid (320 mg, 1.8 mmol), 1-bromo-2-iodobenzene (424 mg, 1.5 mmol), $[Pd(PPh_3)_2Cl_2]$ (53 mg, 0.075 mmol), K_2CO_3 (415 mg, 3 mmol), toluene (10 mL) and MeOH (5 mL). Refluxed overnight. Purified by twice performing silica gel chromatography with eluent petroleum ether. Product **60a** was obtained as a white powder (413 mg, 95% yield).

^{1}H NMR (300 MHz, $CDCl_3$): δ = 7.68 – 7.65 (m, 1H), 7.47 – 7.43 (m, 2H), 7.39 – 7.32 (m, 4H), 7.22 – 7.16 (m, 1H), 1. 38 (s, 9H); ^{13}C NMR (75 MHz, $CDCl_3$) δ = 150.6, 142.6, 138.2, 133.3, 131.6, 129.1, 128.6, 127.5, 125.0, 122.8, 34.8, 31.5; LRMS (APCI$^+$): m/z $[M]^+$ calcd for ($C_{16}H_{17}Br$): 288.05; found: 288.05; In agreement with literature data.[136]

Synthesis of 4''-(tert-butyl)-6-chloro-[1,1':2',1''-terphenyl]-3-carbonitrile 60

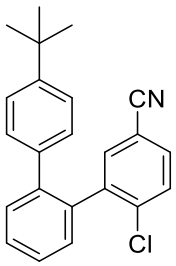

60

Synthesised according to the general procedure A using (2-chloro-5-cyanophenyl)boronic acid (190 mg, 1.05 mmol), **60a** (202 mg, 0.7 mmol), $[Pd(dppf)Cl_2]$ (77 mg, 0.105 mmol), K_2CO_3 (193 mg, 1.4 mmol), dioxane (5 mL) and water (1 mL). Refluxed for 5.5 h. Purified by silica gel chromatography with eluent petroleum ether, gradient to petroleum ether/EtOAc 25 :1. The resulting material purified by heating to 45 °C under a high vacuum (the side product sublimes). Product **60** was obtained as a white powder (163 mg, 67% yield).

M.p.: 148 -149 °C; IR (ATR) ν (cm^{-1}): 3058, 3026, 2964, 2233, 1461, 1444, 1387, 1270, 1110, 1079, 1047, 1024, 905, 838, 826, 772, 767, 743, 642, 624, 613, 583, 563, 543, 49; ^{1}H NMR (300 MHz, $CDCl_3$): δ = 7.51 – 7.36 (m, 6H), 7.30 – 7.20 (m, 3H), 7.0 (d, *J* = 8.2 Hz, 2H), 1.27 (s, 9H); ^{13}C NMR (75 MHz, $CDCl_3$) δ = 150.1, 142.3, 141.4, 139.1, 137.3, 135.8, 135.7, 131.6, 131.5, 130.6, 130.5, 129.1, 129.0, 127.1, 125.1, 110.4, 34.6, 31.4 (1 carbon peak is missing due to overlap), HRMS (APCI$^+$): m/z $[M]^+$ calcd for ($C_{23}H_{20}ClN$): 345.1284; found: 345.1287.

Synthesis of methyl 2'-bromo-[1,1'-biphenyl]-4-carboxylate 61a

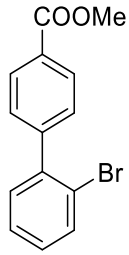

61a

Synthesised according to the general procedure A using (4-(methoxycarbonyl)phenyl)boronic acid (432 mg, 2.4 mmol), 1-bromo-2-iodobenzene (566 mg, 2 mmol), [Pd(dppf)Cl_2] (73 mg, 0.1 mmol), K_2CO_3 (553 mg, 4 mmol), toluene (15 mL) and MeOH (7.5 mL). Refluxed overnight. Purified by silica gel chromatography with eluent petroleum ether, gradient to petroleum ether/EtOAc 30:1. Product **61a** was obtained as a white powder (431 mg, 74% yield).

^{1}H NMR (300 MHz, $CDCl_3$): δ = 8.03 – 8.00 (m, 2H), 7.59 (ddd, *J* = 8.0, 1.2, 0.4 Hz, 1H), 7.42 – 7.38 (m, 2H), 7.29 (ddd, *J* = 7.6, 7.1, 1.2 Hz, 1H), 7.22 (ddd, *J* = 7.6, 2.1, 0.4 Hz, 1H); 7.14 (ddd, *J* = 8.0, 7.1, 2.1 Hz, 1H), 3.85 (s, 3H); ^{13}C NMR (75 MHz, $CDCl_3$) δ = 167.0, 145.7, 141.7, 133.4, 131.1, 129.6, 129.4, 129.4, 127.6, 122.3, 52.3 (1 carbon peak is missing due to overlap); HRMS (APCI$^+$): m/z $[M+H]^+$ calcd for ($C_{14}H_{12}BrO_2$): 291.0021; found: 291.0028; In agreement with literature data.[137]

Synthesis of methyl 2''-chloro-5''-cyano-[1,1':2',1''-terphenyl]-4-carboxylate 61

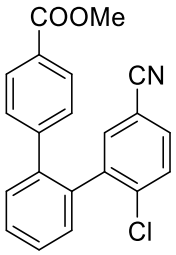

61

Synthesised according to the general procedure A using (2-chloro-5-cyanophenyl)boronic acid (272 mg, 1.5 mmol), compound **61a** (291 mg, 1 mmol), [Pd(dppf)Cl_2] (37 mg, 0.05 mmol), K_2CO_3 (276 mg, 2 mmol), dioxane (5 mL) and water (1 mL). Refluxed overnight. Purified by silica gel chromatography with eluent petroleum ether, gradient to petroleum ether/EtOAc 5:1. The resulting material was washed with petroleum ether and recrystallised from hexane to give product **61** (141 mg, 40% yield).

M.p.: 154 -156 °C; IR (ATR) v (cm^{-1}): 3067, 2955, 2230, 1713, 1605, 1470, 1435, 1393, 1312, 1281, 1192, 1180, 1119, 1103, 1080, 1049, 1022, 907, 860, 833, 748, 729, 706, 613; ^{1}H NMR (300 MHz, $CDCl_3$): δ = 7.89 (d, *J* = 8.2 Hz, 2H), 7.57 – 7.40 (m, 6H), 7.32 (d, *J* = 7.8 Hz, 1H), 7.16 (d, *J* = 8.2 Hz, 2H), 3.89 (s, 3H); ^{13}C NMR (75 MHz, $CDCl_3$) δ = 166.9, 145.1, 141.7, 140.5, 138.9, 135.8, 135.4, 132.0, 130.7, 130.6, 130.2, 129.5, 129.4, 129.3, 128.9, 128.1, 117.9, 110.8, 52.3; HRMS (ES^+): m/z $[M+Na]^+$ calcd for ($C_{21}H_{14}NO_2NaCl$): 370.0611; found: 370.0615.

Synthesis of 2'-bromo-[1,1'-biphenyl]-4-carbonitrile 62a

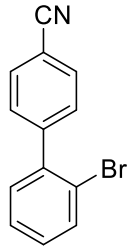

62a

Synthesised according to the general procedure A using (4-cyanophenyl)boronic acid (353 mg, 2.4 mmol), 1-bromo-2-iodobenzene (566 mg, 2 mmol), $[Pd(dppf)Cl_2]$ (73 mg, 0.1 mmol), K_2CO_3 (553 mg, 4 mmol), toluene (15 mL) and MeOH (7.5 mL). Refluxed overnight. Purified by silica gel chromatography with eluent petroleum ether, gradient to petroleum ether/EtOAc 30:1. Product **62a** was obtained as a white powder (475 mg, 92% yield).

^{1}H NMR (300 MHz, $CDCl_3$): δ = 7.77 – 7.70 (m, 3H), 7.57 – 7.53 (m, 2H), 7.45 – 7.40 (m, 1H), 7.33 – 7.26 (m, 2H); ^{13}C NMR (75 MHz, $CDCl_3$) δ = 145.7, 140.8, 133.5, 132.0, 131.0, 130.4, 129.9, 127.8, 122.2, 118.9, 111.6; LRMS ($APCI^+$): m/z $[M]^+$ calcd for ($C_{13}H_8{}^{79}BrN$): 256.98; found: 256.98; In agreement with literature data.[138]

Synthesis of 6-chloro-[1,1':2',1''-terphenyl]-3,4''-dicarbonitrile 62

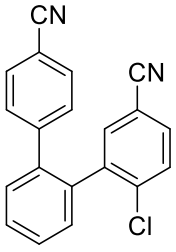

62

Synthesised according to the general procedure A using (2-chloro-5-cyanophenyl)boronic acid (408 mg, 2.25 mmol), compound **62a** (387 mg, 1.5 mmol),

[Pd(dppf)Cl_2] (55 mg, 0.075 mmol), K_2CO_3 (415 mg, 3 mmol), dioxane (5 mL) and water (1 mL). Refluxed for 3 days. Purified by silica gel chromatography with eluent petroleum ether, gradient to petroleum ether/EtOAc 20:1. The resulting material was recrystallised from hexane to give product **62** (91 mg, 19% yield).

M.p.: 142 -144 °C; IR (ATR) v (cm^{-1}): 3067, 2959, 2924, 2851, 2226, 1721, 1609, 1458, 1261, 1099, 826, 764, 613, 571; ^{1}H NMR (300 MHz, $CDCl_3$): δ = 7.59 – 7.48 (m, 5H), 7.47 – 7.41 (m, 3H), 7.35 – 7.30 (m, 1H), 7.23 – 7.19 (m, 2H); ^{13}C NMR (75 MHz, $CDCl_3$) δ = 145.3, 141.3, 139.6, 138.8, 135.8, 135.3, 132.2, 132.0, 130.8, 130.8, 130.1, 130.0, 129.5, 128.6, 118.8, 117.8, 111.1, 111.0; HRMS (APCI$^+$): m/z [M+H]$^+$ calcd for ($C_{20}H_{12}ClN_2$): 315.0689; found: 315.0693.

Synthesis of methyl 2-bromo-[1,1'-biphenyl]-4-carboxylate 63a

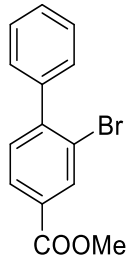

63a

Synthesised according to the general procedure B using phenylboronic acid (36 mg, 0.3 mmol), methyl 3-bromo-4-iodobenzoate (93 mg, 0.27 mmol), [Pd(PPh_3)$_2Cl_2$] (9 mg, 0.013 mmol), Et_3N (165 mg, 1.62 mmol) and emulsion (0.54 mL). Refluxed for 40 min. Diluted with CH_2Cl_2 and charged on the silica gel column with eluent system petroleum ether, gradient to petroleum ether/EtOAc 20:1. Product **63a** was obtained impure and used directly in the next step without full characterisation.

HRMS (EI$^+$): m/z [M]$^+$ calcd for ($C_{14}H_{11}BrO_2$): 289.9937; found: 289.9937.

Synthesis of methyl 2''-chloro-5''-cyano-[1,1':2',1''-terphenyl]-4'-carboxylate 63

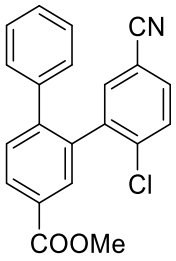

63

Synthesised according to the general procedure B using (2-chloro-5-cyanophenyl)boronic acid (63 mg, 0.345 mmol), **63a** (66 mg, ~0.23 mmol), $[Pd(dtbpf)Cl_2]$ (3 mg, 0.004 mmol), Et_3N (141 mg, 1.38 mmol) and emulsion (0.46 mL). Refluxed for 3 h. Diluted with CH_2Cl_2 and charged on the silica gel column with eluent system petroleum ether, gradient to petroleum ether/EtOAc 15:1. Product **63** was obtained as a white powder (56 mg, combined yield over two steps 59%).

M.p.: 196 -200 °C; IR (ATR) ν (cm^{-1}): 3059, 2980, 2970, 2234, 1717, 1472, 1429, 1387, 1310, 1277, 1260, 1240, 1109, 1076, 1042, 1007, 833, 781, 760, 698, 621; ^1H NMR (300 MHz, $CDCl_3$): δ = 8.10 (dd, *J* = 8.1, 1.6 Hz, 1H), 7.92 (d, *J* = 1.4 Hz, 1H), 7.48 (d, *J* = 8.1 Hz, 1H), 7.43 – 7.35 (m, 3H), 7.19 – 7.14 (m, 3H), 7.04 – 7.01 (m, 2H) 3.88 (s, 3H); ^{13}C NMR (75 MHz, $CDCl_3$) δ = 166.5, 146.0, 141.3, 139.4, 138.9, 136.0, 135.5, 132.1, 131.8, 130.7, 130.7, 130.2, 129.3, 129.2, 128.3, 127.9, 117.9, 110.8, 52.5; HRMS (ES^+): m/z $[M+H]^+$ calcd for ($C_{21}H_{15}NO_2Cl$): 348.0791; found: 348.0798.

Synthesis of triphenylene-2-carbonitrile 64

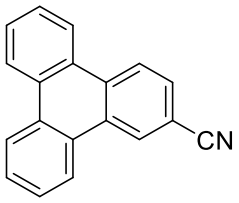

64

Synthesised according to the general procedure D with compound **52** as an aryl chloride. Purified by silica gel chromatography with eluent petroleum ether/EtOAc 95:5. Obtained material washed with cold petroleum ether to give product **64** as a yellowish solid (35 mg, 70% yield).

^1H NMR (300 MHz, $CDCl_3$): δ = 8.94 (d, *J* = 1.7 Hz, 1H), 8.72 – 8.56 (m, 5H), 7.85 (dd, *J* = 8.5, 1.7 Hz, 1H), 7.78 -7.68 (m, 4H); ^{13}C NMR (75 MHz, $CDCl_3$) δ = 132.9, 130.8, 130.1, 130.0, 129.0, 128.5, 128.4, 128.3, 128.2, 127.9, 127.8, 124.3, 124.0, 123.6, 123.5, 123.3, 119.5, 110.6 (1 carbon peak is missing due to overlap); LRMS (EI^+): m/z $[M]^+$ calcd for ($C_{19}H_{11}N$): 253.09; found: 253.08; In agreement with literature data.[139]

Synthesis of triphenylene-1-carbonitrile 65

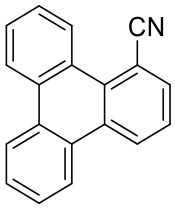

65

Synthesised according to the general procedure D with compound **53** as an aryl chloride. Purified by silica gel chromatography with eluent petroleum ether/EtOAc 200:1, gradient to 50:1. Obtained material washed with cold petroleum ether to give the product **65** as a yellowish solid (36 mg, 72% yield).

^{1}H NMR (300 MHz, $CDCl_3$): δ = 9.52 (dd, *J* = 7.4, 2.2 Hz, 1H), 8.72 (d, *J* = 8.4 Hz, 1H), 8.56 (dd, *J* = 7.3, 2.2 Hz, 1H), 8.51 (dd, *J* = 7.6, 1.8 Hz, 1H), 8.43 (dd, *J* = 7.6, 1.8 Hz, 1H), 7.96 (dd, *J* = 7.4, 1.2 Hz, 1H), 7.73 – 7.56 (m, 5H); ^{13}C NMR (75 MHz, $CDCl_3$) δ = 136.1, 131.2, 130.8, 130.6, 130.0, 128.9, 128.5, 128.4, 128.0, 127.7, 127.5, 127.3, 126.3, 125.9, 123.4, 123.3, 121.8, 107.9 (1 carbon peak is missing due to overlap); HRMS (APCI$^+$): m/z $[M+H]^+$ calcd for ($C_{19}H_{12}N$): 254.0970; found: 254.0972; In agreement with literature data.[139]

Synthesis of methyl triphenylene-2-carboxylate 66

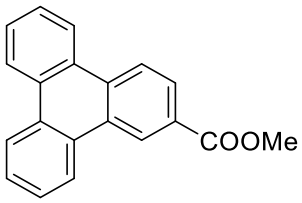

66

Synthesised according to the general procedure D with compound **54** as an aryl chloride. Purified by silica gel chromatography with eluent petroleum ether/EtOAc 20:1. Product **66** was obtained as a yellowish solid (41 mg, 72% yield).

^{1}H NMR (300 MHz, $CDCl_3$): δ = 9.28 (s, 1H), 8.70 – 8.57 (m, 5H), 8.19 (d, *J* = 8.7 Hz, 1H), 7.70 – 7.57 (m, 4H), 4.03 (s, 3H); ^{13}C NMR (75 MHz, $CDCl_3$) δ = 167.3, 133.2, 130.7, 129.9, 129.5, 129.0, 128.3, 127.8, 127.6, 127.5, 127.3, 125.5, 124.0, 123.6, 123.5, 123.5, 123.4, 52.4 (2 carbon peaks are missing due to overlap); LRMS (ES$^+$): m/z $[M+H]^+$ calcd for ($C_{20}H_{15}O_2$): 287.11; found: 287.11; In agreement with literature data.[140]

Synthesis of pyrrolo[1,2-*f*]phenanthridine-10-carbonitrile 68

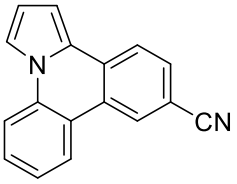

68

Synthesised according to the general procedure D with compound **57** as an aryl chloride. Purified by silica gel chromatography with eluent petroleum ether/EtOAc 20:1. Product **68** was obtained as a yellowish solid (40 mg, 83% yield).

M.p.: 192 - 193 °C; IR (ATR) v (cm^{-1}): 3140, 3113, 3075, 2222, 1609, 1543, 1493, 1447, 1350, 1238, 1099, 880, 833, 760, 745, 710, 610, 420; ^{1}H NMR (300 MHz, $CDCl_3$): δ = 8.37 (d, *J* = 1.5 Hz, 1H), 8.16 (dd, *J* = 8.2, 1.2 Hz, 1H), 7.92 (d, *J* = 8.3 Hz, 1H), 7.82 – 7.79 (m, 2H), 7.60 – 7.54 (m, 2H), 7.39 (ddd, *J* = 8.3, 7.3, 1.2 Hz, 1H), 7.02 (dd, *J* = 3.9, 1.3 Hz, 1H), 6.77 (dd, *J* = 3.9, 2.9 Hz, 1H); ^{13}C NMR (75 MHz, $CDCl_3$) δ = 133.2, 130.3, 129.9, 129.3, 127.8, 127.3, 125.0, 124.5, 124.0, 123.3, 120.0, 119.6, 115.2, 115.0, 113.1, 108.7, 105.1; (EI^+): m/z $[M]^+$ calcd for ($C_{17}H_{10}N_2$): 242.0839; found: 242.0833.

Synthesis of phenanthro[9,10-b]thiophene-9-carbonitrile 69a and phenanthro[9,10-c]thiophene-6-carbonitrile 69b

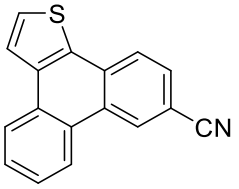

69a

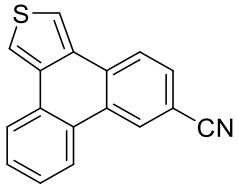

69b

Synthesised according to the general procedure D with compound **58** as an aryl chloride. Purified by silica gel chromatography with eluent petroleum ether, gradient to petroleum ether/EtOAc 50:1. Two regioisomers **69a** and **69b** were obtained (13 mg and 12 mg, respectively) as yellowish solids with a combined yield of 48%.

69a

M.p.: 160 -162 °C; IR (ATR) v (cm^{-1}): 3079, 2961, 2923, 2222, 1610, 1507, 1466, 1446, 1275, 1261, 1236, 1126, 1101, 1097, 1071, 1019, 893, 884, 824, 811, 781, 758, 728, 711, 676, 669, 649, 611, 583, 539, 501, 423, 419; ^{1}H NMR (300 MHz, $CDCl_3$): δ = 8.92 (d, *J* = 1.5 Hz, 1H), 8.58 (d, *J* = 7.5, 2.0 Hz, 1H), 8.31 (dd, *J* = 7.3, 2.0 Hz, 1H), 8.13

(dd, *J* = 8.3, 0.5 Hz, 1H), 7.98 (d, *J* = 5.4 Hz, 1H), 7.76 (dd, *J* = 8.3, 1.5 Hz, 1H), 7.76 – 7.66 (m, 3H); ^{13}C NMR (75 MHz, $CDCl_3$) δ = 137.3, 135.0, 131.4, 129.1, 129.0, 128.9, 128.4, 127.8, 127.5, 126.9, 125.1, 124.6, 123.5, 119.6, 109.3, (2 carbon peaks are missing due to overlap); HRMS (ES$^+$): m/z $[M+H]^+$ calcd for ($C_{17}H_{10}NS$): 260.0534; found: 260.0539.

69b

M.p.: 204 -206 °C; IR (ATR) v (cm^{-1}): 3107, 3089, 2224, 1608, 1534, 1477, 1468, 1237, 1229, 1187, 1048, 884, 875, 837, 799, 787, 757, 726, 719, 711, 705, 639, 613, 588, 545, 502, 424, 406, 401; ^{1}H NMR (300 MHz, $CDCl_3$): δ = 8.62 (d, *J* = 1.4 Hz, 1H), 8.29 (dd, *J* = 7.1, 2.2 Hz, 1H), 8.21 – 8.18 (m, 2H), 8.12 (d, *J* = 3.0 Hz, 1H), 8.07 (d, *J* = 3.0 Hz, 1H), 7.69 (dd, *J* = 8.2, 1.5 Hz, 1H), 7.62 – 7.53 (m, 2H); ^{13}C NMR (75 MHz, $CDCl_3$) δ = 135.3, 133.8, 131.4, 129.9, 129.6, 128.7, 128.5, 128.4, 127.7, 127.5, 125.0, 124.4, 123.5, 119.8, 117.9, 110.2 (1 carbon peak is missing due to overlap); HRMS (APCI$^+$): m/z $[M+H]^+$ calcd for ($C_{17}H_{10}NS$): 260.0534; found: 260.0545.

Synthesis of 11-(tert-butyl)triphenylene-1-carbonitrile 71

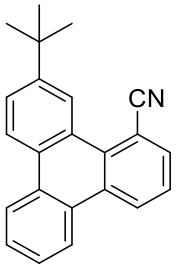

71

Synthesised according to the general procedure D with compound **60** as an aryl chloride. Purified by silica gel chromatography with eluent petroleum ether/EtOAc 40:1. Product **71** was obtained as a yellowish solid (43 mg, 69% yield).

M.p.: 200 - 202 °C; IR (ATR) v (cm^{-1}): 3076, 2965, 2906, 2868, 2224, 1492, 1478, 1456, 1408, 1402, 1364, 1264, 909, 887, 828, 777, 761, 749, 718, 631, 611, 477, 424, 420, 405; ^{1}H NMR (300 MHz, $CDCl_3$): δ = 8.92 (s, 1H), 8.72 (d, *J* = 8.7 Hz, 1H), 8.68 – 8.50 (m, 4H), 7.90 – 7.65 (m, 4H), 1.51 (s, 9H); ^{13}C NMR (75 MHz, $CDCl_3$) δ = 150.7, 133.3, 130.2, 130.2, 128.9, 128.6, 128.5, 128.5, 128.1, 128.0, 127.6, 127.2, 124.3, 123.5, 123.4, 123.3, 119.9, 119.6, 110.4, 35.3, 31.5; HRMS (APCI$^+$): m/z $[M+H]^+$ calcd for ($C_{23}H_{20}N$): 310.159; found: 310.1594.

Synthesis of methyl 10-cyanotriphenylene-2-carboxylate 75

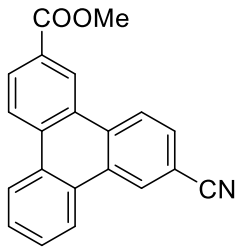

75

Synthesised according to the general procedure D with compound **61** as an aryl chloride. Purified by silica gel chromatography with eluent petroleum ether/EtOAc 20:1. Product **75** was obtained as a yellowish solid (24 mg, 38% yield).

M.p.: 248 - 250 °C; IR (ATR) v (cm^{-1}): 3096, 3035, 2951, 2227, 1715, 1617, 1420, 1286, 1260, 1241, 1190, 1110, 834, 751, 617; ^{1}H NMR (300 MHz, $CDCl_3$): δ = 9.13 (d, *J* = 1.5 Hz, 1H), 8.79 (d, *J* = 1.5 Hz, 1H), 8.62 (d, *J* = 8.6 Hz, 1H), 8.59 – 8.54 (m, 2H), 8.48 – 8.45 (m, 1H), 8.26 (dd, *J* = 8.6, 1.6 Hz, 1H), 7.78 (dd, *J* = 8.5, 1.6, Hz, 1H), 7.74 – 7.69 (m, 2H), 4.05 (s, 3H); ^{13}C NMR (75 MHz, $CDCl_3$) δ = 166.7, 134.1, 132.5, 130.1, 129.3, 129.2, 129.0, 128.9, 128.8, 128.7, 128.3, 128.0, 125.9, 124.6, 124.2, 123.7, 123.4, 119.1, 111.2, 52.6 (1 carbon peak is missing due to overlap); HRMS ($APCI^+$): m/z $[M+H]^+$ calcd for ($C_{21}H_{14}NO_2$): 312.1025; found: 312.1033.

Synthesis of methyl 11-cyanotriphenylene-2-carboxylate 76

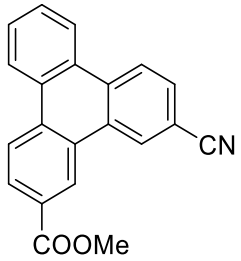

76

Synthesised according to the general procedure D with compound **63** as an aryl chloride but on 0.155 mmol (54 mg) scale of chloride instead of 0.2 mmol, with the rest of the reagents scaled down accordingly. Purified by silica gel chromatography with eluent petroleum ether, gradient to petroleum ether/EtOAc 15:1. The obtained material was washed with cold petroleum ether to give desired product **76** as a yellowish solid (32 mg, 66%).

M.p.: 264 °C (decomposition); IR (ATR) v (cm^{-1}): 3048, 3017, 2959, 2222, 1721, 1612, 1485, 1423, 1265, 1238, 1107, 976, 903, 822, 745, 706, 617, 490; ^{1}H NMR (300 MHz, $CDCl_3$): δ = 9.17 (d, *J* = 1.6 Hz, 1H), 8.93 (d, *J* = 1.6 Hz, 1H), 8.66 – 8.63 (m, 3H), 8.61 – 8.57 (m, 1H), 8.29 (d, *J* = 8.6, 1.6 Hz, 1H), 7.84 (d, *J* = 8.6, 1.6 Hz, 1H), 7.79 – 7.73 (m, 2H), 4.07 (s, 3H); ^{13}C NMR (75 MHz, $CDCl_3$) δ = 166.8, 133.5, 130.1, 129.6, 129.3, 129.2, 129.0, 128.6, 128.6, 128.0, 125.3, 124.5, 124.3, 124.2, 123.8, 119.3, 111.1, 52.7 (3 carbon peaks are missing due to overlap); HRMS (ES^+): m/z $[M+H]^+$ calcd for ($C_{21}H_{14}NO_2$): 312.1025; found: 312.1021.

Synthesis of 6,6'''-dichloro-[1,1':2',1'':2'',1'''-quaterphenyl]-3,3'''-dicarbonitrile 78

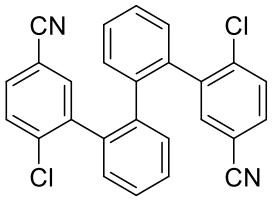

78

Synthesised according to the general procedure B using (2-chloro-5-cyanophenyl)boronic acid (694 mg, 3.83 mmol), 2,2'-dibromo-1,1'-biphenyl (398 mg, 1.28 mmol), [Pd(dtbpf)Cl_2] (33 mg, 0.051 mmol), Et_3N (777 mg, 7.7 mmol) and emulsion (2.5 mL). Refluxed for 3.5 h. Diluted with CH_2Cl_2 and filtered through a silica plug. Resulting material was recrystallised from EtOH to give compound **78** as a white, crystalline solid (358 mg, 66% yield).

M.p.: 244 - 246 °C; IR (ATR) v (cm^{-1}): 3090, 3062, 2229, 1458, 1434, 1387, 1075, 1022, 901, 822, 779, 768, 756, 611, 403; ^{1}H NMR (500 MHz, $CDCl_3$): δ = 7.55 – 7.12 (m, 12H), 6.97 – 6.86 (m, 2H); ^{13}C NMR (125 MHz, $CDCl_3$) δ = 141.3, 140.1, 139.8, 139.5, 138.6, 136.9, 136.5, 136.2, 134.7, 134.5, 132.9, 132.3, 132.2, 131.4, 130.6, 130.3, 129.3, 129.0, 128.7, 128.5, 127.7, 127.4, 118.0, 117.6, 110.9, 110.2; HRMS (ES^+): m/z $[M+H]^+$ calcd for ($C_{26}H_{15}N_2Cl_2$): 425.0612; found: 425.0616.

Synthesis of tetraphenylene-2,7-dicarbonitrile 80

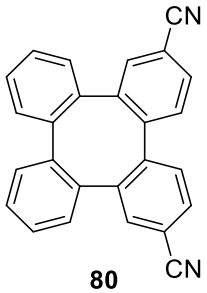

80

Synthesised according to the general procedure D, using 0.1 mmol (42.5 mg) of chloride **78**, 0.06 eq of PXX (1.7 mg), 2.8 eq of DIPEA (49 µL) and 4 mL of DMSO. Irradiated for 4 days. Purified by silica gel chromatography with eluent petroleum ether/EtOAc 20:1. Product **80** was obtained as a white solid (10 mg, 28%).

M.p.: 290 °C; IR (ATR) ν (cm^{-1}): 3059, 3024, 2959, 2230, 1601, 1470, 1393, 1261, 849, 833, 760, 745, 625, 590, 563, 548, 525; ^{1}H NMR (300 MHz, CD_2Cl_2): δ = 7.62 (dd, *J* = 7.9, 1.7 Hz, 2H), 7.50 (dd, *J* = 1.7, 0.5 Hz, 2H), 7.41 – 7.32 (m, 4H), 7.28 (dd, *J* = 7.9, 0.5 Hz, 2H), 7.22 – 7.13 (m, 4H); ^{13}C NMR (75 MHz, CD_2Cl_2) δ = 144.8, 142.9, 141.1, 139.0, 133.2, 131.5, 129.9, 129.8, 129.2, 128.9, 128.3, 118.6, 112.7; HRMS (EI^+): m/z $[M]^+$ calcd for ($C_{26}H_{14}N_2$): 354.1152; found: 354.1142. Crystals suitable for X-RAY diffraction were obtained by slow diffusion of hexane into solution of **80** in toluene.

3.4 X-Ray Data

Crystallographic data for PTXTX yellow plate polymorph (CCDC 1869244)

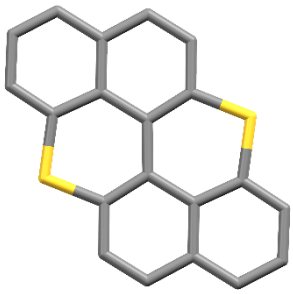

	Crystal data	
Empirical formula	$C_{20}H_{10}S_2$	
Formula weight	314.40	
Crystal system	Monoclinic	
Space group	*P* $2_1/c$	
Unit cell dimensions	a = 10.4432(7) Å	α= 90°.
	b = 3.8850(3) Å	β= 94.403(6)°.

	c = 16.2216(10) Å γ = 90°.
Volume	656.20(8) $Å^3$
Z	2
Density (calculated)	1.591 Mg/m^3
Absorption coefficient	0.396 mm^{-1}
F(000)	324
Crystal size	0.586 x 0.081 x 0.018 mm^3
Data Collection	
Temperature	150(2) K
Wavelength	0.71073 Å
Theta range for data collection	3.306 to 29.394°.
Index ranges	-14<=h<=9, -5<=k<=4, -21<=l<=19
Reflections collected	2897
Independent reflections	1535 [R(int) = 0.0309]
Completeness to theta = 25.242°	99.7%
Refinement	
Refinement method	Full-matrix least-squares on F^2
Data / restraints / parameters	1535 / 0 / 100
Goodness-of-fit on F^2	1.108
Final R indices [I>2sigma(I)]	R1 = 0.0573, wR2 = 0.1308
R indices (all data)	R1 = 0.0711, wR2 = 0.1432
Extinction coefficient	n/a
Largest diff. peak and hole	1.202 and -0.508 $e.Å^{-3}$

Crystallographic data for PTXTX red needle polymorph (CCDC 1869246)

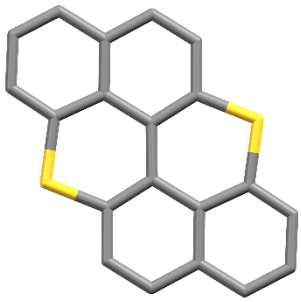

Crystal data	
Empirical formula	$C_{20}H_{10}S_2$
Formula weight	314.40
Crystal system	Monoclinic
Space group	*P* $2_1/c$

Unit cell dimensions	a = 17.8523(14) Å	α= 90°.
	b = 4.4843(2) Å	β= 112.549(9)°.
	c = 18.1505(13) Å	γ = 90°.
Volume	1341.96(17) $Å^3$	
Z	4	
Density (calculated)	1.556 Mg/m^3	
Absorption coefficient	3.501 mm^{-1}	
F (000)	648	
Crystal size	0.559 x 0.041 x 0.023 mm^3	

Data collection

Temperature	293(2) K
Wavelength	1.54184 Å
Theta range for data collection	4.917 to 74.230°.
Index ranges	-22<=h<=17, -3<=k<=5, -21<=l<=22
Reflections collected	4081
Independent reflections	2629 [R(int) = 0.0415]
Completeness to theta = 67.684°	99.3%

Refinement

Refinement method	Full-matrix least-squares on F^2
Data / restraints / parameters	2629 / 0 / 199
Goodness-of-fit on F^2	1.081
Final R indices [I>2sigma(I)]	R1 = 0.0723, wR2 = 0.1931
R indices (all data)	R1 = 0.0929, wR2 = 0.2102
Extinction coefficient	n/a
Largest diff. peak and hole	1.124 and -0.685 e.$Å^{-3}$

Crystallographic data for molecule 25 (CCDC 1869239)

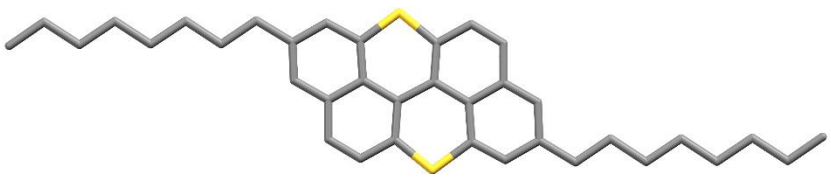

Crystal data

Empirical formula	$C_{36}H_{42}S_2$
Formula weight	538.81
Crystal system	Triclinic
Space group	*P -1*

Unit cell dimensions	a = 6.5467(6) Å	α= 03.522(12)°.
	b = 9.0261(13) Å	β= 98.696(10)°.
	c = 12.6132(18) Å	γ= 92.979(10)°.
Volume	713.37(16) $Å^3$	
Z	1	
Density (calculated)	1.254 Mg/m^3	
Absorption coefficient	1.851 mm^{-1}	
F(000)	290	
Crystal size	0.595 x 0.061 x 0.039 mm^3	

Data collection

Temperature	150(2) K
Wavelength	1.54184 Å
Theta range for data collection	3.656 to 73.764°.
Index ranges	-8<=h<=5, -9<=k<=11, -15<=l<=15
Reflections collected	4457
Independent reflections	2782 [R(int) = 0.0359]
Completeness to theta = 67.684°	99.8%

Refinement

Refinement method	Full-matrix least-squares on F^2
Data / restraints / parameters	2782 / 0 / 173
Goodness-of-fit on F^2	1.099
Final R indices [I>2sigma(I)]	R1 = 0.0774, wR2 = 0.2012
R indices (all data)	R1 = 0.0897, wR2 = 0.2071
Extinction coefficient	n/a
Largest diff. peak and hole	0.898 and -0.421 $e.Å^{-3}$

Crystallographic data for molecule 28 (CCDC 1869245)

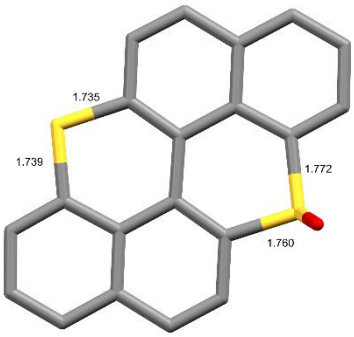

Crystal data

Empirical formula	$C_{20}H_{10}OS_2$
Formula weight	330.40

Crystal system	Orthorhombic	
Space group	*P* $2_1 2_1 2_1$	
Unit cell dimensions	a = 4.4895(4) Å	α= 90°.
	b = 14.9454(10) Å	β= 90°.
	c = 20.4702(17) Å	γ = 90°.
Volume	1373.50(19) $Å^3$	
Z	4	
Density (calculated)	1.598 Mg/m^3	
Absorption coefficient	3.509 mm^{-1}	
F(000)	680	
Crystal size	0.217 x 0.049 x 0.023 mm^3	
Data collection		
Temperature	150(2) K	
Wavelength	1.54184 Å	
Theta range for data collection	3.662 to 74.024°.	
Index ranges	-5<=h<=3, -18<=k<=18, -25<=l<=21	
Reflections collected	4652	
Independent reflections	2707 [R(int) = 0.0399]	
Completeness to theta = 67.684°	100.0%	
Absorption correction	Semi-empirical from equivalents	
Max. and min. transmission	1.00000 and 0.82231	
Refinement		
Refinement method	Full-matrix least-squares on F^2	
Data / restraints / parameters	2707 / 0 / 208	
Goodness-of-fit on F^2	1.044	
Final R indices [I>2sigma(I)]	R1 = 0.0653, wR2 = 0.1761	
R indices (all data)	R1 = 0.0713, wR2 = 0.1841	
Absolute structure parameter	0.49(4)	
Extinction coefficient	n/a	
Largest diff. peak and hole	1.063 and -0.360 $e.Å^{-3}$	

Crystallographic data for molecule 29 (CCDC 1869242)

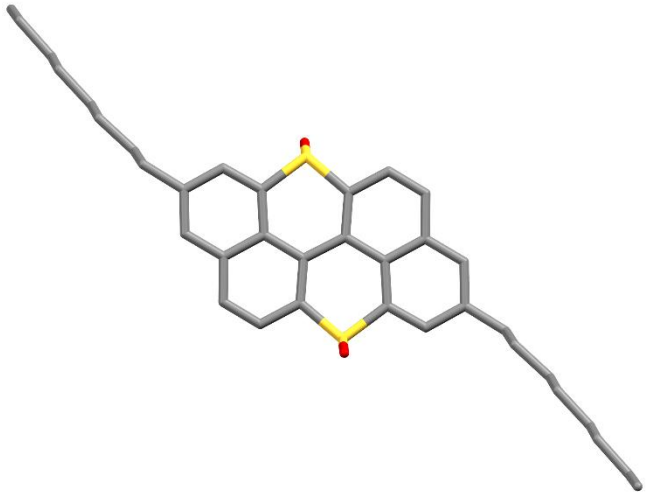

Crystal data		
Empirical formula	$C_{36}H_{42}OS_2$	
Formula weight	554.81	
Crystal system	Triclinic	
Space group	*P -1*	
Unit cell dimensions	a = 4.6395(3) Å	α= 94.112(4)°.
	b = 8.9684(5) Å	β= 92.591(4)°.
	c = 18.1464(9) Å	γ= 102.510(5)°.
Volume	733.80(7) $Å^3$	
Z	1	
Density (calculated)	1.256 Mg/m^3	
Absorption coefficient	1.841 mm^{-1}	
F(000)	298	
Crystal size	0.602 x 0.061 x 0.025 mm^3	
Data collection		
Temperature	150(2) K	
Wavelength	1.54184 Å	
Theta range for data collection	4.896 to 74.046°.	
Index ranges	-5<=h<=5, -11<=k<=10, -22<=l<=22	
Reflections collected	11402	
Independent reflections	2931 [R(int) = 0.0551]	
Completeness to theta = 67.684°	99.8%	
Refinement		
Refinement method	Full-matrix least-squares on F^2	
Data / restraints / parameters	2931 / 0 / 182	
Goodness-of-fit on F^2	1.154	
Final R indices [I>2sigma(I)]	R1 = 0.0629, wR2 = 0.1807	

R indices (all data)	R1 = 0.0707, wR2 = 0.1859
Extinction coefficient	n/a
Largest diff. peak and hole	0.359 and -0.289 e.Å^{-3}

Crystallographic data for molecule *trans*-30 (CCDC 1869243)

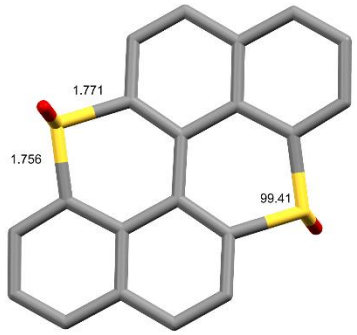

Crystal data

Empirical formula	$C_{20}H_{10}O_2S_2$	
Formula weight	346.40	
Crystal system	Monoclinic	
Space group	P 21/c	
Unit cell dimensions	a = 4.6090(6) Å	α = 90°.
	b = 12.7558(15) Å	β = 9.999(13)°.
	c = 11.9209(17) Å	γ = 90°.
Volume	700.85(16) Å^3	
Z	2	
Density (calculated)	1.641 Mg/m^3	
Absorption coefficient	0.390 mm^{-1}	
F(000)	356	
Crystal size	0.482 x 0.039 x 0.030 mm^3	

Data Collection

Temperature	298(2) K
Wavelength	0.71073 Å
Theta range for data collection	3.418 to 29.465°.
Index ranges	-6<=h<=4, -16<=k<=16, -16<=l<=10
Reflections collected	2921
Independent reflections	1535 [R(int) = 0.0318]
Completeness to theta = 25.242°	99.8%

Refinement

Refinement method	Full-matrix least-squares on F^2
Data / restraints / parameters	1535 / 0 / 110

Goodness-of-fit on F^2	1.084
Final R indices [I>2sigma(I)]	R1 = 0.0527, wR2 = 0.1046
R indices (all data)	R1 = 0.0774, wR2 = 0.1205
Extinction coefficient	n/a
Largest diff. peak and hole	0.244 and -0.250 e.Å^{-3}

Crystallographic data for trioxide (CCDC 1869241)

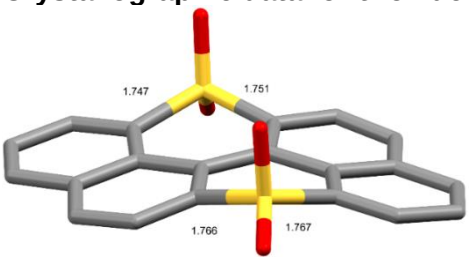

Crystal data

Empirical formula	$C_{20}H_{10}O_3S_2$	
Formula weight	362.40	
Crystal system	Triclinic	
Space group	*P -1*	
Unit cell dimensions	a = 8.0506(7) Å	α = 65.390(8)°.
	b = 9.3882(8) Å	β = 81.640(7)°.
	c = 11.1338(9) Å	γ = 73.069(8)°.
Volume	731.62(12) Å^3	
Z	2	
Density (calculated)	1.645 Mg/m^3	
Absorption coefficient	3.460 mm^{-1}	
F(000)	372	
Crystal size	0.287 x 0.130 x 0.079 mm^3	

Data collection

Temperature	150(2) K
Wavelength	1.54184 Å
Theta range for data collection	4.370 to 73.835°.
Index ranges	-10<=h<=9, -11<=k<=11, -13<=l<=13
Reflections collected	5240
Independent reflections	5240 [R(int) = ?]
Completeness to theta = 67.684°	100.0%

Refinement

Refinement method	Full-matrix least-squares on F^2
Data / restraints / parameters	5240 / 0 / 236
Goodness-of-fit on F^2	1.025

Final R indices [I>2sigma(I)]	R1 = 0.0729, wR2 = 0.1949
R indices (all data)	R1 = 0.0813, wR2 = 0.2045
Extinction coefficient	n/a
Largest diff. peak and hole	0.625 and -0.325 e.Å^{-3}

Crystallographic data for molecule 31 (CCDC 1869240)

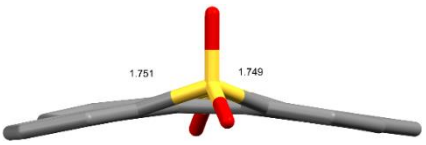

Crystal data

Empirical formula	$C_{20}H_{10}O_4S_2$	
Formula weight	378.40	
Crystal system	Triclinic	
Space group	*P -1*	
Unit cell dimensions	a = 8.5368(7) Å	α= 69.159(7)°.
	b = 8.6036(7) Å	β= 84.585(6)°.
	c = 11.2632(8) Å	γ = 76.154(7)°.
Volume	750.62(11) Å^3	
Z	2	
Density (calculated)	1.674 Mg/m^3	
Absorption coefficient	0.381 mm^{-1}	
F(000)	388	
Crystal size	0.329 x 0.158 x 0.118 mm^3	

Data collection

Temperature	150(2) K
Wavelength	0.71073 Å
Theta range for data collection	3.113 to 29.933°.
Index ranges	-10<=h<=9, -10<=k<=11, -12<=l<=15
Reflections collected	5909
Independent reflections	3512 [R(int) = 0.0291]
Completeness to theta = 25.242°	99.9%

Refinement

Refinement method	Full-matrix least-squares on F^2
Data / restraints / parameters	3512 / 0 / 235
Goodness-of-fit on F^2	1.059
Final R indices [I>2sigma(I)]	R1 = 0.0496, wR2 = 0.1147
R indices (all data)	R1 = 0.0719, wR2 = 0.1350

Extinction coefficient	n/a
Largest diff. peak and hole	0.536 and -0.407 e.Å^{-3}

Crystallographic data for molecule 32 in polymorphs: *anti*-32 (CCDC 1914850) and *syn*-32 (CCDC 1914851)

***anti*-32**

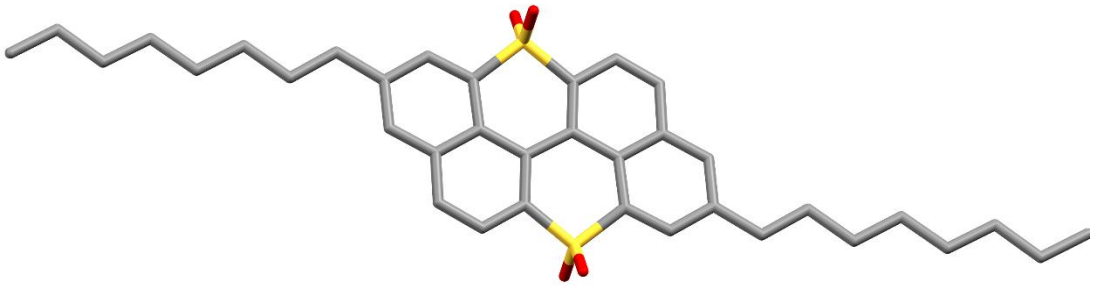

***syn*-32**

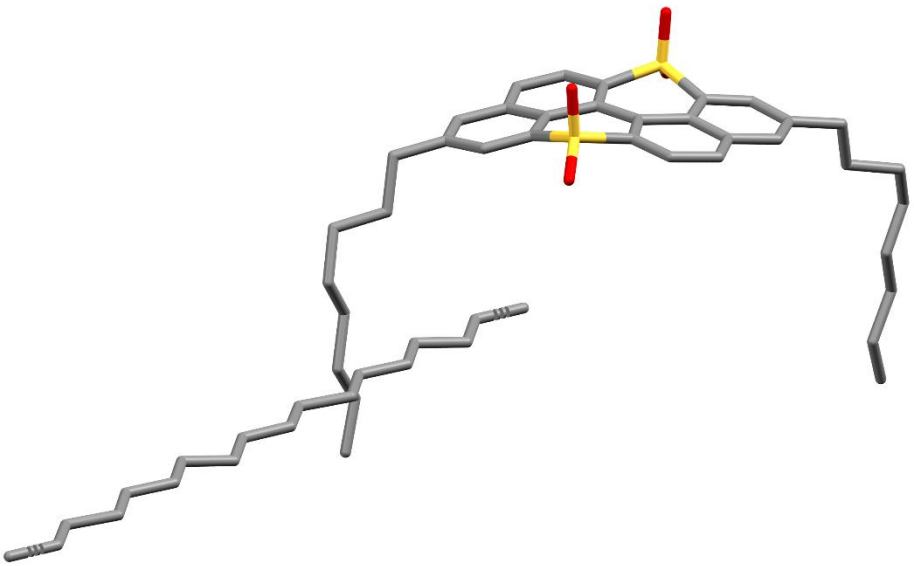

	anti-32	**syn-32**
	[$C_{36}H_{42}O_4S_2$]	[$C_{36}H_{42}O_4S_2$·1/2C_6H_{14}]
CCDC Number	1914850	1914851
Chemical Formula	$C_{36}H_{42}O_4S_2$	$C_{39}H_{49}O_4S_2$
Formula weight (g/mol)	602.81	647.70
Temperature (K)	100(2)	100(2)
Wavelength (Å)	0.700	0.700
Crystal system	Monoclinic	Monoclinic
Space Group	*P* 2_1/*c*	*C* 2/*c*
Unit cell dimensions	a = 11.610(2Å	a = 12.421(3) Å
	b = 18.059(4) Å	b = 30.614(6) Å
	c = 7.330(2) Å	c = 10.526(2) Å
	α = 90°	α = 90°

	β = 99.14(3)°	β = 94.99(3)°
	γ = 90°	γ = 90°
Volume (Å^3)	1517.3(5)	3987.4(14)
Z	2	4
Density (calculated) (g·cm^{-3})	1.319	1.079
Absorption coefficient (mm^{-1})	0.204	0.159
F(000)	644	1390
Crystal size (mm^3)	0.10 x 0.02 x 0.02	0.08 x 0.08 x 0.02
Crystal habit	Colorless rods	Colorless plates
Theta range for data collection	1.75° to 30.96°	2.32° to 24.01°
Resolution (Å)	0.68	0.86
Index ranges	-17 ≤ h ≤ 17	-14 ≤ h ≤ 14
	-26 ≤ k ≤ 26	-35 ≤ k ≤ 35
	-10 ≤ l ≤ 10	-12 ≤ l ≤ 12
Reflections collected	25318	14680
Independent reflections (data with I>2σ(I))	4894 (3827)	3270 (1534)
Data multiplicity (max resltn)	4.95 (4.22)	4.45 (4.46)
I/σ(I) (max resltn)	16.17 (8.24)	5.77 (1.34)
R_{merge} (max resltn)	0.0562 (0.1322)	0.1014 (0.5971)
Data completeness (max resltn)	96.7% (91.5%)	99.6% (99.5%)
Refinement method	Full-matrix least-squares on F^2	Full-matrix least-squares on F^2
Data / restraints / parameters	4894 / 0 / 191	3270 / 26 / 228
Goodness-of-fit on F^2	1.101	1.012
Δ/σ_{max}	0.001	0.000
Final R indices [I>2σ(I)][a]	R_1 = 0.0701,	R_1 = 0.1172,
	wR_2 = 0.1935	wR_2 = 0.2670
R indices (all data)[a]	R_1 = 0.0854,	R_1 = 0.2067,
	wR_2 = 0.2051	wR_2 = 0.3306
Largest diff. peak and hole (e·Å^{-3})	1.389 and -1.080	0.877 and -0.454
R.M.S. deviation from mean (e·Å^{-3})	0.086	0.090

Crystallographic data for molecule 36

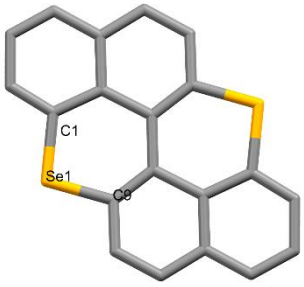

Crystal data		
Empirical formula	$C_{20}H_{10}Se_2$	
Formula weight	408.20	
Crystal system	Monoclinic	
Space group	P 21/c	
Unit cell dimensions	a = 10.419(3) Å	α= 90°.
	b = 4.0268(9) Å	β= 94.116(18)°.
	c = 16.510(3) Å	γ = 90°.
Volume	690.9(3) $Å^3$	
Z	2	
Density (calculated)	1.962 Mg/m^3	
Absorption coefficient	5.343 mm^{-1}	
F(000)	396	
Crystal size	0.181 x 0.074 x 0.046 mm^3	
Data collection		
Temperature	200(2) K	
Wavelength	0.71073 Å	
Theta range for data collection	3.922 to 29.821°.	
Index ranges	-12<=h<=13, -5<=k<=3, -22<=l<=15	
Reflections collected	3096	
Independent reflections	1653 [R(int) = 0.0472]	
Completeness to theta = 25.242°	99.7 %	
Refinement		
Refinement method	Full-matrix least-squares on F^2	
Data / restraints / parameters	1653 / 0 / 100	
Goodness-of-fit on F^2	1.240	
Final R indices [I>2sigma(I)]	R1 = 0.1021, wR2 = 0.2648	
R indices (all data)	R1 = 0.1314, wR2 = 0.2787	
Extinction coefficient	n/a	
Largest diff. peak and hole	2.897 and -1.428 $e.Å^{-3}$	

3.5 Literature

[1] A. D. McNaught, A. Wilkinson, *IUPAC. Compendium of Chemical Terminology, 2nd Ed. (the "Gold Book").*, Blackwell Scientific Publications, Oxford, **1997**.

[2] N. A. Romero, D. A. Nicewicz, *Chem. Rev.* **2016**, *116*, 10075–10166.

[3] D. Ravelli, M. Fagnoni, A. Albini, *Chem. Soc. Rev.* **2013**, *42*, 97–113.

[4] M. H. Shaw, J. Twilton, D. W. C. MacMillan, *J. Org. Chem.* **2016**, *81*, 6898–6926.

[5] S. G. E. Amos, M. Garreau, L. Buzzetti, J. Waser, *Beilstein J. Org. Chem.* **2020**, *16*, 1163–1187.

[6] M. A. Ischay, M. E. Anzovino, J. Du, T. P. Yoon, *J. Am. Chem. Soc.* **2008**, *130*, 12886–12887.

[7] D. A. Nicewicz, D. W. C. MacMillan, *Science* **2008**, *322*, 77–80.

[8] J. M. R. Narayanam, J. W. Tucker, C. R. J. Stephenson, *J. Am. Chem. Soc.* **2009**, *131*, 8756–8757.

[9] J. A. Terrett, J. D. Cuthbertson, V. W. Shurtleff, D. W. C. MacMillan, *Nature* **2015**, *524*, 330–334.

[10] Z. Dong, D. W. C. MacMillan, *Nature* **2021**, *598*, 451–456.

[11] J. D. Cuthbertson, D. W. C. MacMillan, *Nature* **2015**, *519*, 74–77.

[12] W. Chen, Z. Huang, N. E. S. Tay, B. Giglio, M. Wang, H. Wang, Z. Wu, D. A. Nicewicz, Z. Li, *Science* **2019**, *364*, 1170–1174.

[13] M. M. Hossain, A. C. Shaikh, J. Moutet, T. L. Gianetti, *Nat. Synth.* **2022**, *1*, 147–157.

[14] E. B. Corcoran, M. T. Pirnot, S. Lin, S. D. Dreher, D. A. Dirocco, I. W. Davies, S. L. Buchwald, D. W. C. Macmillan, *Science* **2016**, *353*, 279–283.

[15] Y. Du, R. M. Pearson, C. Lim, S. M. Sartor, M. D. Ryan, H. Yang, N. H. Damrauer, G. M. Miyake, *Chem. – A Eur. J.* **2017**, *23*, 10962–10968.

[16] M. S. Oderinde, M. Frenette, D. W. Robbins, B. Aquila, J. W. Johannes, *J. Am. Chem. Soc.* **2016**, *138*, 1760–1763.

[17] A. Juris, V. Balzani, P. Belser, A. von Zelewsky, *Helv. Chim. Acta* **1981**, *64*, 2175–2182.

[18] C. K. Prier, D. A. Rankic, D. W. C. MacMillan, *Chem. Rev.* **2013**, *113*, 5322–5363.

[19] Y. Xi, H. Yi, A. Lei, *Org. Biomol. Chem.* **2013**, *11*, 2387–2403.

[20] L. Flamigni, A. Barbieri, C. Sabatini, B. Ventura, F. Barigelletti, in *Photochem. Photophysics Coord. Compd. II*, Springer Berlin Heidelberg, Berlin, Heidelberg,

2007, pp. 143–203.

[21] J. D. Nguyen, E. M. D'Amato, J. M. R. Narayanam, C. R. J. Stephenson, *Nat. Chem.* **2012**, *4*, 854–859.

[22] Y. Cheng, X. Gu, P. Li, *Org. Lett.* **2013**, *15*, 2664–2667.

[23] H. W. Shih, M. N. Vander Wal, R. L. Grange, D. W. C. MacMillan, *J. Am. Chem. Soc.* **2010**, *132*, 13600–13603.

[24] P. Nuss, M. J. Eckelman, *PLoS One* **2014**, *9*, 1–12.

[25] S. Fukuzumi, H. Kotani, K. Ohkubo, S. Ogo, N. V. Tkachenko, H. Lemmetyinen, *J. Am. Chem. Soc.* **2004**, *126*, 1600–1601.

[26] H. Uoyama, K. Goushi, K. Shizu, H. Nomura, C. Adachi, *Nature* **2012**, *492*, 234–238.

[27] D. P. Hari, P. Schroll, B. König, *J. Am. Chem. Soc.* **2012**, *134*, 2958–2961.

[28] Y. X. Liu, D. Xue, J. Di Wang, C. J. Zhao, Q. Z. Zou, C. Wang, J. Xiao, *Synlett* **2013**, *24*, 507–513.

[29] P. Natarajan, A. Bala, S. K. Mehta, K. K. Bhasin, *Tetrahedron* **2016**, *72*, 2521–2526.

[30] M. H. Aukland, M. Šiaučiulis, A. West, G. J. P. Perry, D. J. Procter, *Nat. Catal.* **2020**, *3*, 163–169.

[31] I. Ghosh, T. Ghosh, J. I. Bardagi, B. Konig, *Science* **2014**, *346*, 725–728.

[32] I. Ghosh, L. Marzo, A. Das, R. Shaikh, B. König, *Acc. Chem. Res.* **2016**, *49*, 1566–1577.

[33] V. Balzani, G. Bergamini, P. Ceroni, *Angew. Chem. Int. Ed.* **2015**, *54*, 11320–11337.

[34] D. Ravelli, M. Fagnoni, A. Albini, *Chem. Soc. Rev.* **2012**, *42*, 97–113.

[35] C. S. Wang, P. H. Dixneuf, J. F. Soulé, *Chem. Rev.* **2018**, *118*, 7532–7585.

[36] M. Raicopol, L. Necula, M. Ionita, L. Pilan, *Surf. Interface Anal.* **2012**, *44*, 1081–1085.

[37] D. Xue, Z.-H. Jia, C.-J. Zhao, Y.-Y. Zhang, C. Wang, J. Xiao, *Chem. – A Eur. J.* **2014**, *20*, 2960–2965.

[38] P. Maity, D. Kundu, B. C. Ranu, *Eur. J. Org. Chem.* **2015**, *2015*, 1727–1734.

[39] C. Costentin, M. Robert, J. M. Savéant, *J. Am. Chem. Soc.* **2004**, *126*, 16051–16057.

[40] L. Wang, J. Byun, R. Li, W. Huang, K. A. I. Zhang, *Adv. Synth. Catal.* **2018**, *360*, 4312–4318.

[41] C. J. Zeman, S. Kim, F. Zhang, K. S. Schanze, *J. Am. Chem. Soc.* **2020**, *142*, 2204–2207.

[42] I. Ghosh, B. König, *Angew. Chem. Int. Ed.* **2016**, *55*, 7676–7679.

[43] A. Sciutto, A. Fermi, A. Folli, T. Battisti, J. M. Beames, D. M. Murphy, D. Bonifazi, *Chem. Eur. J.* **2018**, *24*, 4382–4389.

[44] T. Kamei, M. Uryu, T. Shimada, *Org. Lett.* **2017**, *19*, 2714–2717.

[45] C. Pezzetta, A. Folli, O. Matuszewska, D. Murphy, R. W. M. Davidson, D. Bonifazi, *Adv. Synth. Catal.* **2021**, *363*, 4740–4753.

[46] A. L. Trifonov, L. I. Panferova, V. V. Levin, V. A. Kokorekin, A. D. Dilman, *Org. Lett.* **2020**, *22*, 2409–2413.

[47] M. T. Pirnot, D. A. Rankic, D. B. C. Martin, D. W. C. MacMillan, *Science* **2013**, *340*, 1593–1596.

[48] D. E. Bartak, K. J. Houser, B. C. Rudy, M. D. Hawley, *J. Am. Chem. Soc.* **1972**, *94*, 7526–7530.

[49] C. P. Andrieux, J. M. Saeveant, D. Zann, *Nouv. J. Chim.* **1984**, *8*, 107.

[50] G. Lefèvre, A. Jutand, *Chem. Eur. J.* **2014**, *20*, 4796–4805.

[51] X. Feng, W. Pisula, K. Müllen, *Pure Appl. Chem.* **2009**, *81*, 2203–2224.

[52] M. Stępień, E. Gońka, M. Żyła, N. Sprutta, *Chem. Rev.* **2017**, *117*, 3479–3716.

[53] A. Bodzioch, E. Kowalska, J. Skalik, P. Bałczewski, *Chem. Heterocycl. Compd.* **2017**, *53*, 11–20.

[54] B. P. Mathew, M. R. Kuram, *Inorg. Chim. Acta* **2019**, *490*, 112–129.

[55] O. T. Dyan, G. I. Borodkin, P. A. Zaikin, *Eur. J. Org. Chem.* **2019**, *2019*, 7271–7306.

[56] Y. Yamamoto, A. I. Almansour, N. Arumugam, R. S. Kumar, *Arkivoc* **2015**, *2016*,

9–41.

[57] R. Scholl, J. Mansfeld, *Ber. Dtsch. Chem. Ges.* **1910**, *43*, 1734–1746.

[58] M. Grzybowski, K. Skonieczny, H. Butenschön, D. T. Gryko, *Angew. Chem. Int. Ed.* **2013**, *52*, 9900–9930.

[59] P. Kovacic, A. Kyriakis, *Tetrahedron Lett.* **1962**, *3*, 467–469.

[60] M. Müller, H. Mauermann-Düll, M. Wagner, V. Enkelmann, K. Müllen, *Angew. Chem. Int. Ed.* **1995**, *34*, 1583–1586.

[61] C. D. Simpson, J. D. Brand, A. J. Berresheim, L. Przybilla, H. J. Räder, K. Müllen, *Chem. Eur. J.* **2002**, *8*, 1424–1429.

[62] M. Müller, C. Kübel, K. Müllen, *Chem. Eur. J.* **1998**, *4*, 2099–2109.

[63] X. Feng, W. Pisula, L. Zhi, M. Takase, K. Müllen, *Angew. Chem. Int. Ed.* **2008**, *47*, 1703–1706.

[64] B. T. King, J. Kroulík, C. R. Robertson, P. Rempala, C. L. Hilton, J. D. Korinek, L. M. Gortari, *J. Org. Chem.* **2007**, *72*, 2279–2288.

[65] J. E. Rice, Z. W. Cai, *J. Org. Chem.* **1993**, *58*, 1415–1424.

[66] T. Jin, J. Zhao, N. Asao, Y. Yamamoto, *Chem. Eur. J.* **2014**, *20*, 3554–3576.

[67] N. H. Chang, X. C. Chen, H. Nonobe, Y. Okuda, H. Mori, K. Nakajima, Y. Nishihara, *Org. Lett.* **2013**, *15*, 3558–3561.

[68] N. H. Chang, H. Mori, X. C. Chen, Y. Okuda, T. Okamoto, Y. Nishihara, *Chem. Lett.* **2013**, *42*, 1257–1259.

[69] S. Yanagisawa, K. Ueda, T. Taniguchi, K. Itami, *Org. Lett.* **2008**, *10*, 4673–4676.

[70] D. S. Roman, Y. Takahashi, A. B. Charette, *Org. Lett.* **2011**, *13*, 3242–3245.

[71] S. Lin, X. He, J. Meng, H. Gu, P. Zhang, J. Wu, *Eur. J. Org. Chem.* **2017**, *2017*, 443–447.

[72] K. I. Fujita, M. Nonogawa, R. Yamaguchi, *Chem. Commun.* **2004**, *10*, 1926–1927.

[73] C. L. Sun, Y. F. Gu, W. P. Huang, Z. J. Shi, *Chem. Commun.* **2011**, *47*, 9813–9815.

[74] B. S. Bhakuni, A. Kumar, S. J. Balkrishna, J. A. Sheikh, S. Konar, S. Kumar,

Org. Lett. **2012**, *14*, 2838–2841.

[75] S. Zhou, E. Doni, G. M. Anderson, R. G. Kane, S. W. Macdougall, V. M. Ironmonger, T. Tuttle, J. A. Murphy, *J. Am. Chem. Soc.* **2014**, *136*, 17818–17826.

[76] G. Nocera, J. A. Murphy, *Synthesis* **2020**, *52*, 327–336.

[77] A. Studer, D. P. Curran, *Angew. Chem. Int. Ed.* **2011**, *50*, 5018–5022.

[78] F. B. Mallory, C. S. Wood, J. T. Gordon, *J. Am. Chem. Soc.* **1964**, *86*, 3094–3102.

[79] F. B. Mallory, C. W. Mallory, in *Organic Reactions Vol. 30* (Ed.: W.G. Dauben), John Wiley & Sons, Inc., Hoboken, **1984**, pp. 1–456.

[80] K. B. Jørgensen, *Molecules* **2010**, *15*, 4334–4358.

[81] R. D. Broene, F. Diederich, *Tetrahedron Lett.* **1991**, *32*, 5227–5230.

[82] T. Sato, S. Shimada, K. Hata, *Bull. Chem. Soc. Jpn.* **1971**, *44*, 2484–2490.

[83] T. Sato, S. Shimada, K. Hata, *Bull. Chem. Soc. Jpn.* **1969**, *42*, 766–772.

[84] Q. Chen, S. Thoms, S. Stöttinger, D. Schollmeyer, K. Müllen, A. Narita, T. Basché, *J. Am. Chem. Soc.* **2019**, *141*, 16439–16449.

[85] I. Schnapperelle, T. Bach, *Chem. Eur. J.* **2014**, *20*, 9725–9732.

[86] M. Daigle, A. Picard-Lafond, E. Soligo, J.-F. Morin, *Angew. Chem. Int. Ed.* **2016**, *55*, 2042–2047.

[87] Z. Li, R. J. Twieg, *Chem. Eur. J.* **2015**, *21*, 15534–15539.

[88] H. Cano-Yelo, A. Deronzier, *J. Chem. Soc., Perkin Trans. 2* **1984**, 1093–1098.

[89] P. Natarajan, N. Kumar, M. Sharma, *Org. Chem. Front.* **2016**, *3*, 1265–1270.

[90] T. Osawa, T. Kajitani, D. Hashizume, H. Ohsumi, S. Sasaki, M. Takata, Y. Koizumi, A. Saeki, S. Seki, T. Fukushima, T. Aida, *Angew. Chem. Int. Ed.* **2012**, *51*, 7990–7993.

[91] S. Ukai, K. Hirose, *Chem. Pharm. Bull.* **1968**, *16*, 195–201.

[92] M. Gupta, S. K. Pal, *Langmuir* **2016**, *32*, 1120–1126.

[93] M. Saleh, M. Baumgarten, A. Mavrinskiy, T. Schäfer, K. Müllen, *Macromolecules* **2010**, *43*, 137–143.

[94] K. Togashi, S. Nomura, N. Yokoyama, T. Yasuda, C. Adachi, *J. Mater. Chem.* **2012**, *22*, 20689.

[95] S. K. Pal, S. Setia, B. S. Avinash, S. Kumar, *Liq. Cryst.* **2013**, *40*, 1769–1816.

[96] H. Y. Peng, C. K. Lam, T. C. W. Mak, Z. Cai, W. T. Ma, Y. X. Li, H. N. C. Wong, *J. Am. Chem. Soc.* **2005**, *127*, 9603–9611.

[97] B. L. Edelbach, D. A. Vicic, R. J. Lachicotte, W. D. Jones, *Organometallics* **1998**, *17*, 4784–4794.

[98] B. L. Edelbach, R. J. Lachicotte, W. D. Jones, *J. Am. Chem. Soc.* **1998**, *120*, 2843–2853.

[99] J. J. Eisch, A. M. Piotrowski, K. I. Han, C. Krüger, Y. H. Tsay, *Organometallics* **1985**, *4*, 224–231.

[100] H. Schwager, S. Spyroudis, K. P. C. Vollhardt, *J. Organomet. Chem.* **1990**, *382*, 191–200.

[101] D. Masselot, J. P. H. Charmant, T. Gallagher, *J. Am. Chem. Soc.* **2006**, *128*, 694–695.

[102] B. Wan, Y. Zhang, *Synthesis* **2021**, *53*, 3299–3306.

[103] H. Jiang, Y. Zhang, D. Chen, B. Zhou, Y. Zhang, *Org. Lett.* **2016**, *18*, 2032–2035.

[104] U. R. Von, V. G. Wittig, **1967**, *108*, 91–108.

[105] A. Rajca, H. Wang, P. Bolshov, S. Rajca, *Tetrahedron* **2001**, *57*, 3725–3735.

[106] J. F. Cui, H. Huang, H. N. C. Wong, *Synlett* **2011**, 1018–1022.

[107] C. W. Lai, C. K. Lam, H. K. Lee, T. C. W. Mak, H. N. C. Wong, *Org. Lett.* **2003**, *5*, 823–826.

[108] D. Blakemore, in *RSC Drug Discovery Series*, **2016**, pp. 1–69.

[109] F. Batool, A. H. Emwas, X. Gao, M. A. Munawar, G. A. Chotana, *Synthesis* **2017**, *49*, 1327–1334.

[110] K. M. Clapham, A. S. Batsanov, M. R. Bryce, B. Tarbit, *Org. Biomol. Chem.* **2009**, *7*, 2155–2161.

[111] D. Bulfield, S. M. Huber, *J. Org. Chem.* **2017**, *82*, 13188–13203.

[112] G. La Sorella, G. Strukul, A. Scarso, *Green Chem.* **2015**, *17*, 644–683.

[113] M. Rooney, S. Mattiello, R. Stara, A. Sanzone, P. Brazzo, M. Sassi, L. Beverina, *Dyes Pigm.* **2018**, *149*, 893–901.

[114] D. J. K. Robert M. Silverstein, Francis X. Webster, *J. Mol. Struct.* **2005**, 512.

[115] A. Sciutto, A. Fermi, A. Folli, T. Battisti, J. M. Beames, D. M. Murphy, D. Bonifazi, *Chem. Eur. J.* **2018**, *24*, 4382–4389.

[116] A. Sanzone, A. Calascibetta, E. Ghiglietti, C. Ceriani, G. Mattioli, S. Mattiello, M. Sassi, L. Beverina, *J. Org. Chem.* **2018**, *83*, 15029–15042.

[117] H. Irngartinger, W. R. K. Reibel, *Acta Crystallogr. Sect. B Struct. Crystallogr. Cryst. Chem.* **1981**, *37*, 1724–1728.

[118] D. V. Preda, L. T. Scott, *Org. Lett.* **2000**, *2*, 1489–1492.

[119] J. W. Han, X. S. Peng, H. N. C. Wong, *Natl. Sci. Rev.* **2017**, *4*, 892–916.

[120] *CrysAlisPro, Agilent Technologies, Version 1.171.37.33 c (Release 27-03-2014 CrysAlis171 .NET)*, **n.d.**

[121] G. M. Sheldrick, *SHELX-2013: Program for the Solution of Crystal Structures*, University Of Göttingen, **2013**.

[122] A. Lausi, M. Polentarutti, S. Onesti, J. R. Plaisier, E. Busetto, G. Bais, L. Barba, A. Cassetta, G. Campi, D. Lamba, A. Pifferi, S. C. Mande, D. D. Sarma, S. M. Sharma, G. Paolucci, *Eur. Phys. J. Plus* **2015**, *130*, 43.

[123] W. Kabsch, *Acta Crystallogr. Sect. D* **2010**, *66*, 125–132.

[124] G. Sheldrick, *Acta Crystallogr. Sect. A* **2015**, *71*, 3–8.

[125] G. Sheldrick, *Acta Crystallogr. Sect. C* **2015**, *71*, 3–8.

[126] P. Emsley, B. Lohkamp, W. G. Scott, K. Cowtan, *Acta Crystallogr. Sect. D* **2010**, *66*, 486–501.

[127] G. A. Crosby, J. N. Demas, *J. Phys. Chem.* **1971**, *75*, 991–1024.

[128] N. Armaroli, F. Diederich, C. O. Dietrich-Buchecker, L. Flamigni, G. Marconi, J. F. Nierengarten, J. P. Sauvage, *Chem. Eur. J.* **1998**, *4*, 406–416.

[129] Y. Rio, G. Accorsi, H. Nierengarten, C. Bourgogne, J. M. Strub, A. Van Dorsselaer, N. Armaroli, J. F. Nierengarten, *Tetrahedron* **2003**, *59*, 3833–3844.

[130] H. He, L.-Y. Chen, W.-Y. Wong, W.-H. Chan, A. W. M. Lee, *Eur. J. Org. Chem.* **2010**, *2010*, 4181–4184.

[131] R. Mariz, A. Poater, M. Gatti, E. Drinkel, J. J. Bürgi, X. Luan, S. Blumentritt, A. Linden, L. Cavallo, R. Dorta, *Chem. Eur. J.* **2010**, *16*, 14335–14347.

[132] M. Tiecco, L. Testaferri, M. Tingoli, D. Chianelli, M. Montanucci, *J. Org. Chem.* **1983**, *48*, 4289–4296.

[133] K. Nishino, Y. Ogiwara, N. Sakai, *Chem. Eur. J.* **2018**, *24*, 10971–10974.

[134] B. Yiğit, N. Gürbüz, M. Yiğit, Z. Dağdeviren, İ. Özdemir, *Inorg. Chim. Acta* **2017**, *465*, 44–49.

[135] D. S. Lee, C. S. Kim, N. Iqbal, G. S. Park, K. S. Son, E. J. Cho, *Org. Lett.* **2019**, *21*, 9950–9953.

[136] T. F. Wang, C. L. Lin, C. N. Chen, T. C. Wang, *J. Chinese Chem. Soc.* **2007**, *54*, 811–816.

[137] J. Song, F. Wei, W. Sun, K. Li, Y. Tian, C. Liu, Y. Li, L. Xie, *Org. Lett.* **2015**, *17*, 2106–2109.

[138] M. Nishimura, M. Ueda, N. Miyaura, *Tetrahedron* **2002**, *58*, 5779–5787.

[139] P. H. Gore, F. S. Kamounah, A. Y. Miri, *Tetrahedron* **1979**, *35*, 2927–2929.

[140] J. Tu, G. Li, X. Zhao, F. Xu, *Tetrahedron Lett.* **2019**, *60*, 44–47.

Chapter 4 Appendix A

Characterisation of 2,2’-bis(methylthio)-1,1’-binaphthalene 1

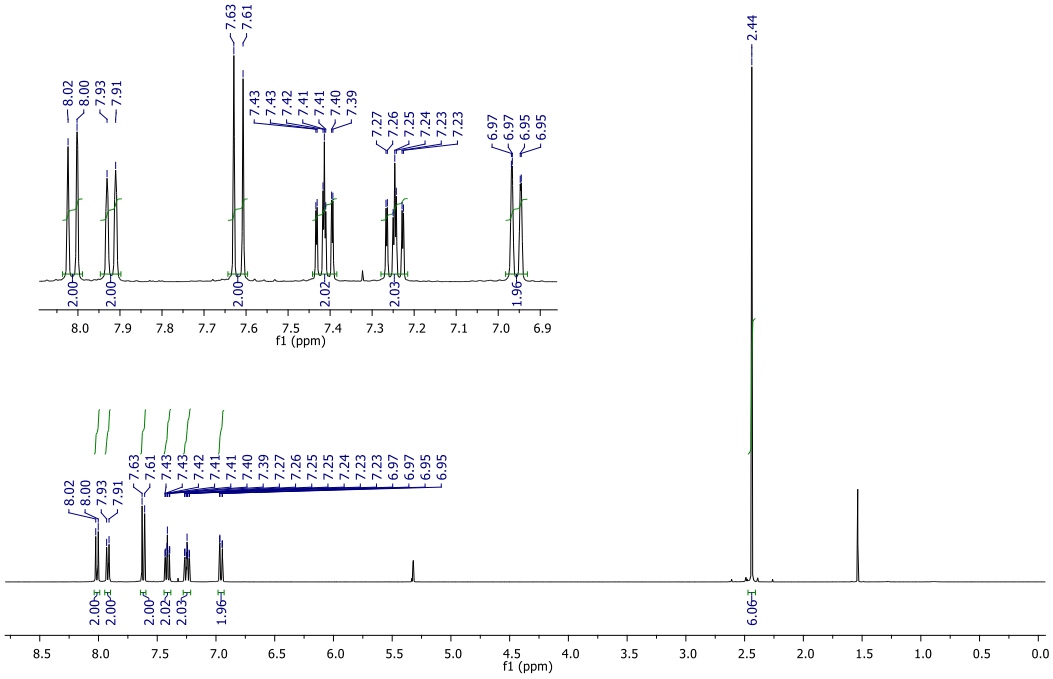

Figure A.1. ^{1}H NMR, 400 MHz, CD_2Cl_2.

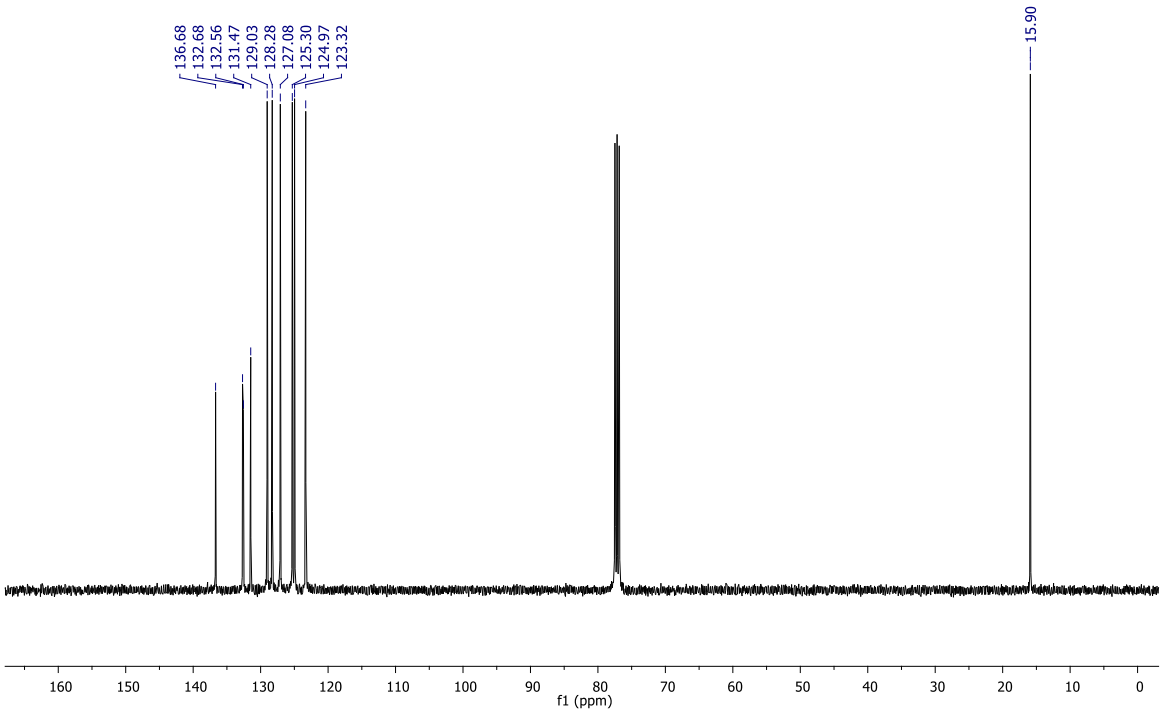

Figure A.2. ^{13}C NMR, 100 MHz, $CDCl_3$.

Elemental Composition Report **Page 1**

Single Mass Analysis
Tolerance = 5.0 PPM / DBE: min = -1.5, max = 100.0
Element prediction: Off
Number of isotope peaks used for i-FIT = 3

Monoisotopic Mass, Even Electron Ions
2 formula(e) evaluated with 1 results within limits (up to 10 closest results for each mass)
Elements Used:
C: 0-22 H: 0-19 S: 0-2

03-Oct-2017
DB_MS17933_ESP 24 (0.191)

Synapt G2-Si Cardiff University (EP/L027240/1)
1: TOF MS ES+
6.66e+004

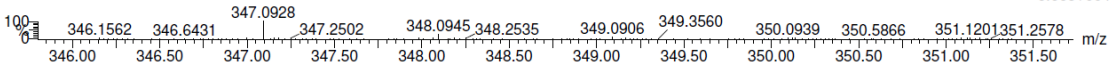

Minimum:				-1.5				
Maximum:		1000.0	5.0	100.0				
Mass	Calc. Mass	mDa	PPM	DBE	i-FIT	Norm	Conf(%)	Formula
347.0928	347.0928	0.0	0.0	13.5	570.6	n/a	n/a	C22 H19 S2

Figure A.3. HRMS, ES+, TOF.

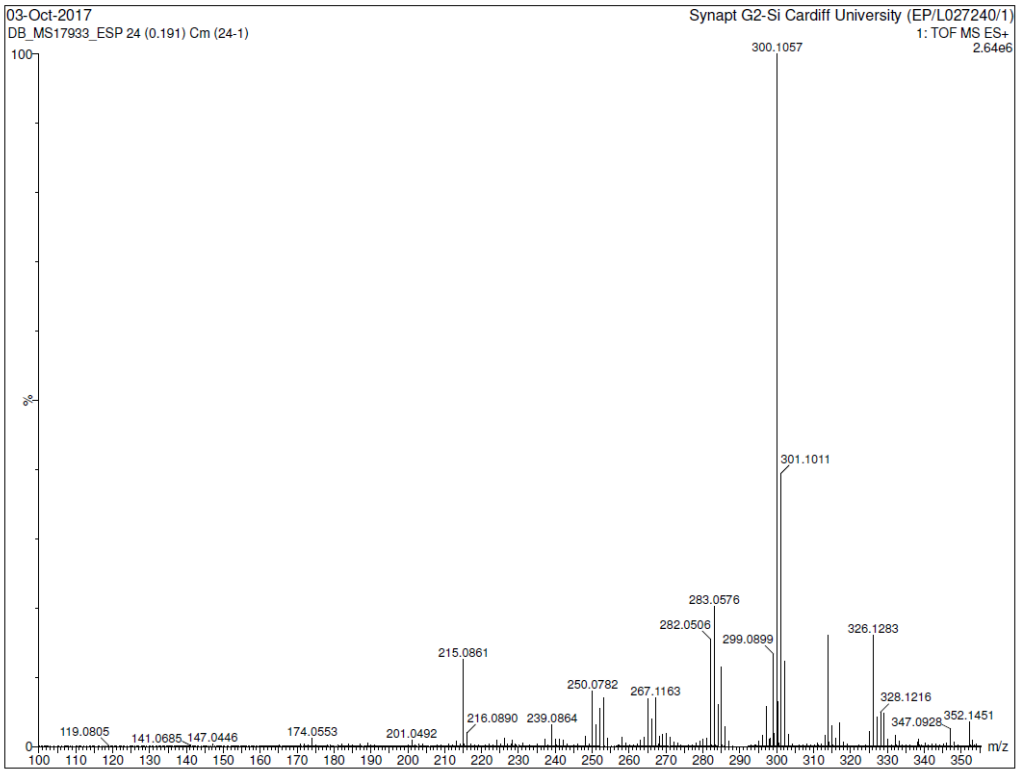

Figure A.4. HRMS, ES+, TOF.

Characterisation of 2,2'-bis(methylsulfinyl)-1,1'-binaphthalene 2

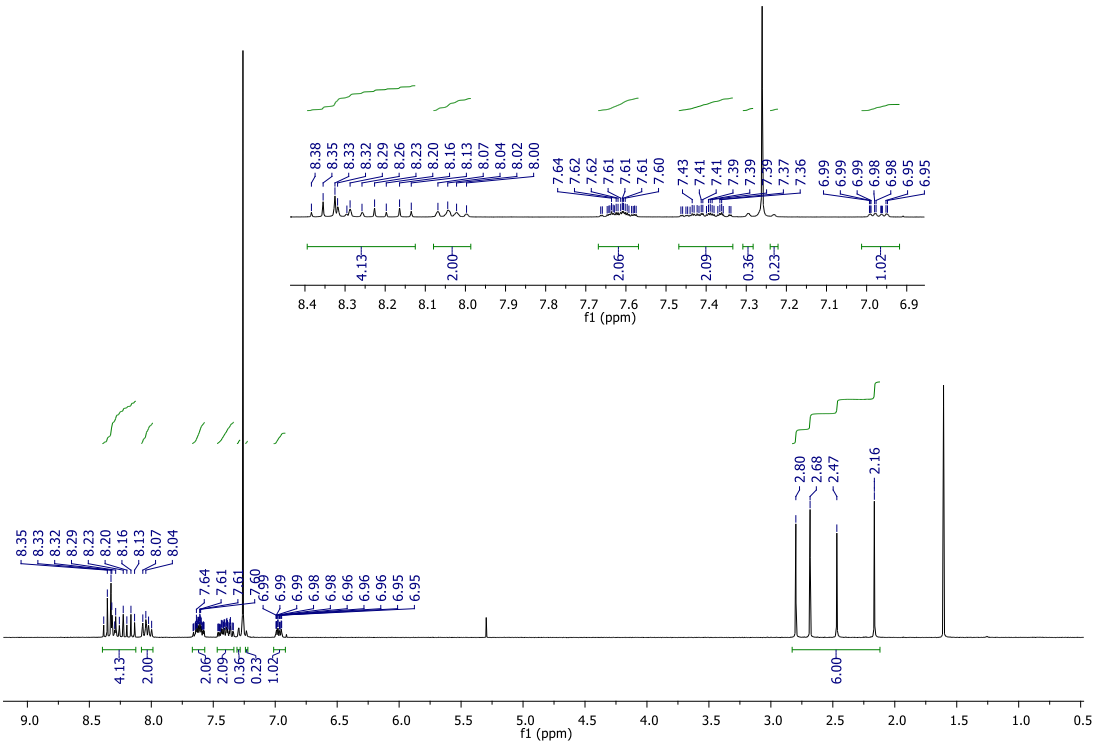

Figure A.5. ^{1}H NMR, 300 MHz, $CDCl_3$.

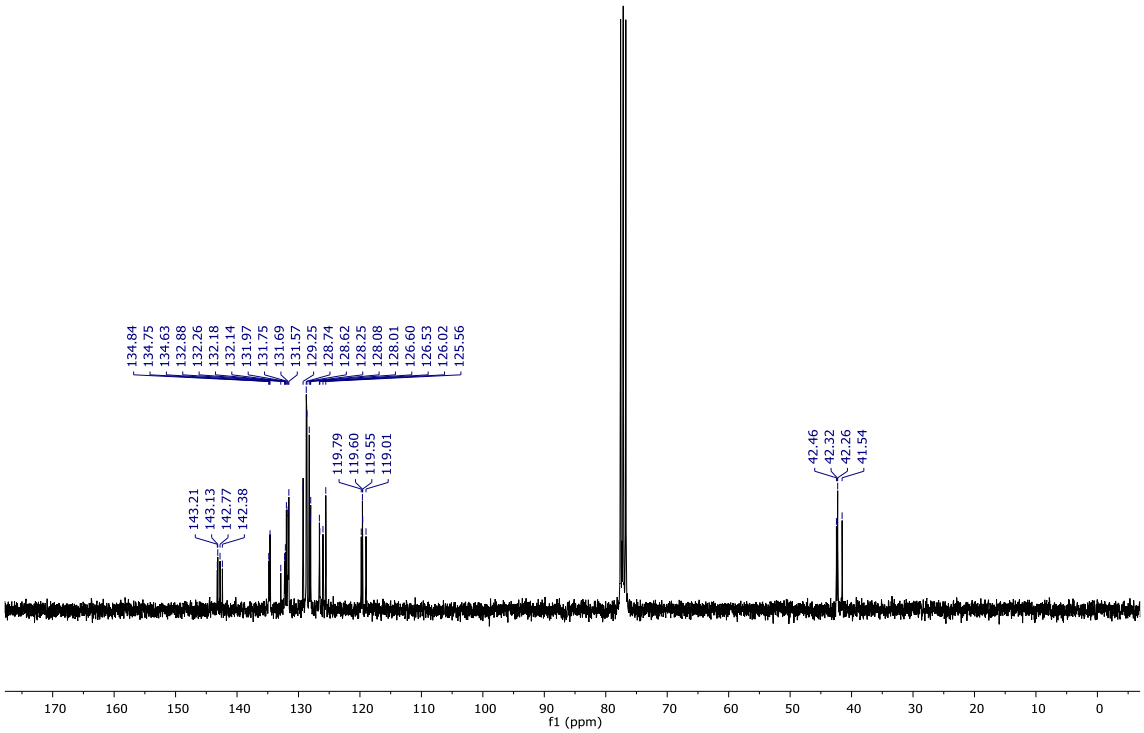

Figure A.6. ^{13}C NMR, 75 MHz, $CDCl_3$.

Elemental Composition Report **Page 1**

Single Mass Analysis
Tolerance = 5.0 PPM / DBE: min = -1.5, max = 100.0
Element prediction: Off
Number of isotope peaks used for i-FIT = 3

Monoisotopic Mass, Odd and Even Electron Ions
6 formula(e) evaluated with 1 results within limits (up to 50 best isotopic matches for each mass)
Elements Used:
C: 0-22 H: 0-19 O: 0-2 S: 0-2

Minimum:				-1.5				
Maximum:		5.0	5.0	100.0				
Mass	Calc. Mass	mDa	PPM	DBE	i-FIT	Norm	Conf(%)	Formula
379.0829	379.0826	0.3	0.8	13.5	803.8	n/a	n/a	C22 H19 O2 S2

Figure A.7. Elemental composition report.

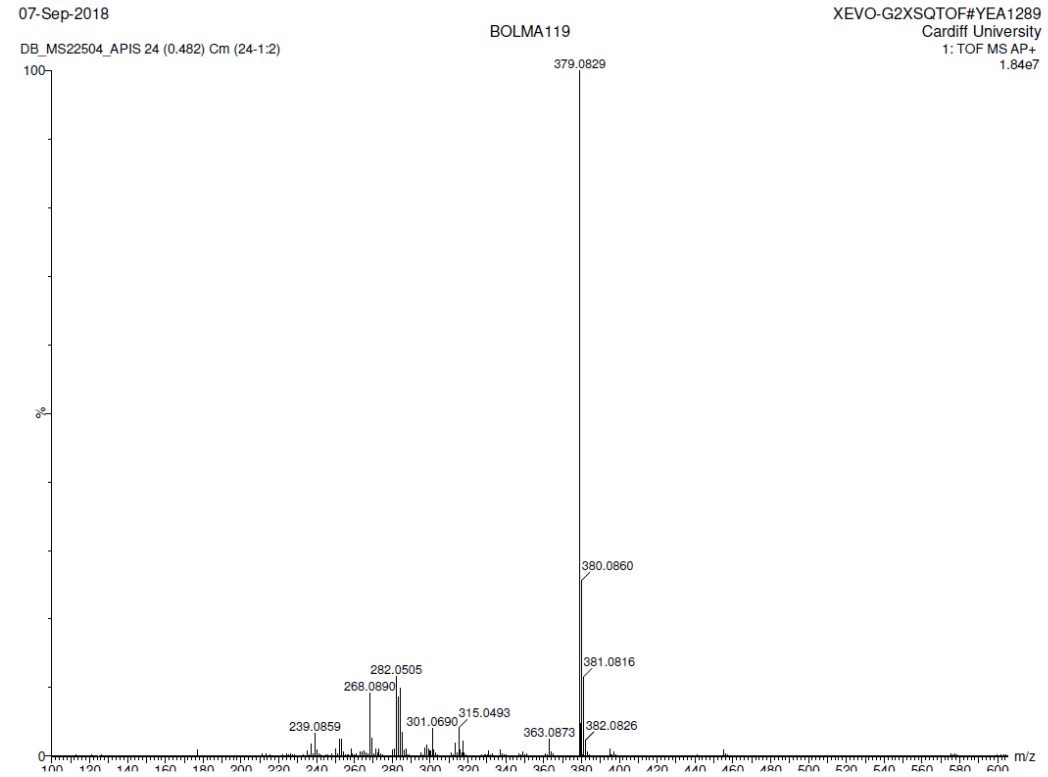

Figure A.8. HRMS, APCI+, TOF.

Characterisation of thioxanthenothioxanthene PTXTX

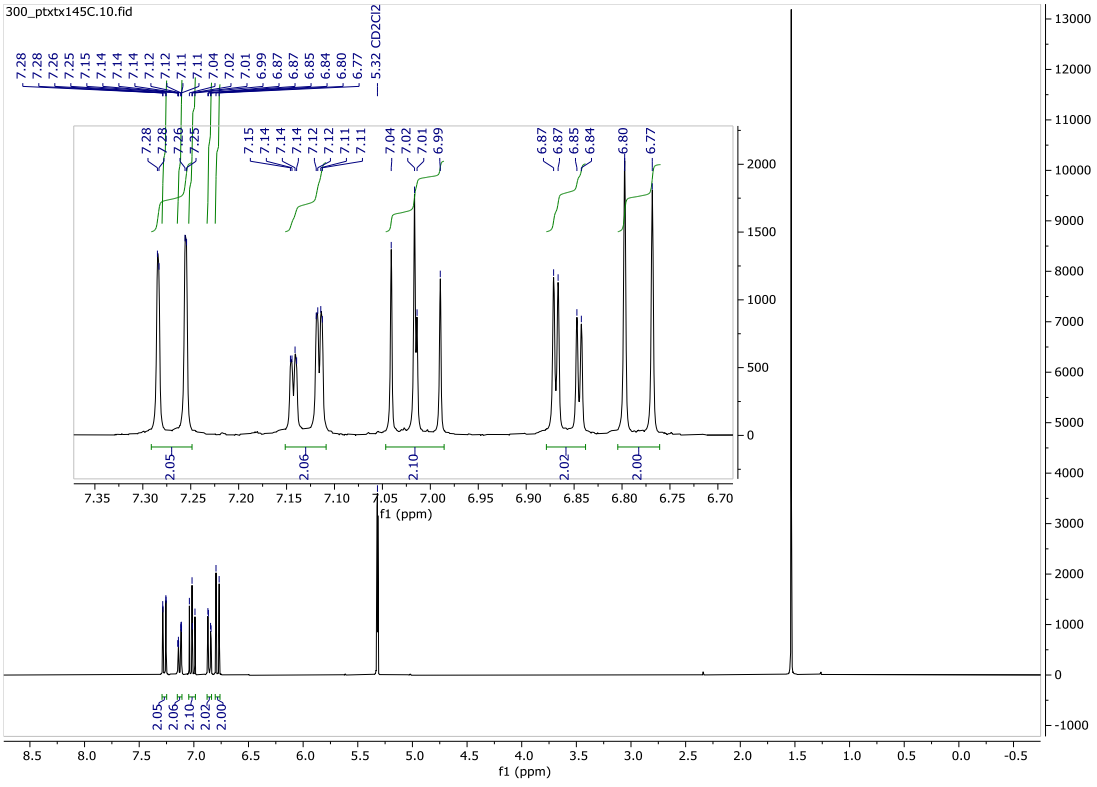

Figure A.9. ^{1}H NMR, 300 MHz, CD_2Cl_2.

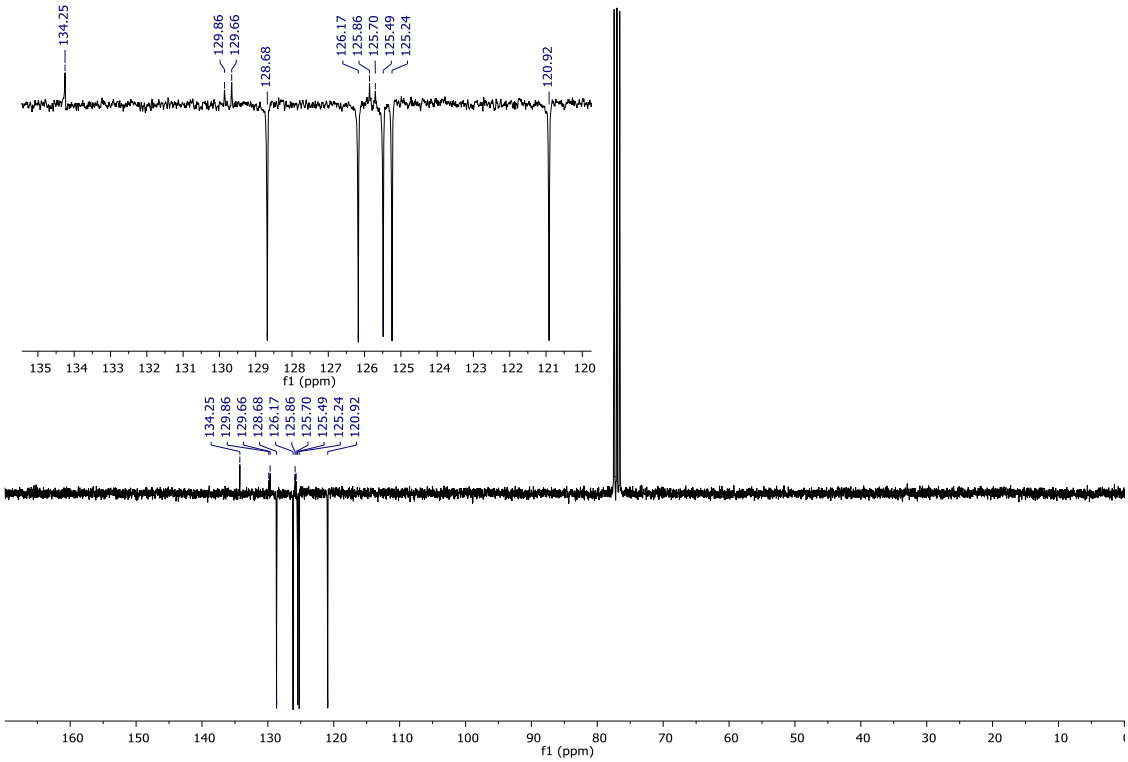

Figure A.10. ^{13}C NMR, 75 MHz, $CDCl_3$.

Elemental Composition Report **Page 1**

Single Mass Analysis
Tolerance = 5.0 PPM / DBE: min = -1.5, max = 100.0
Element prediction: Off
Number of isotope peaks used for i-FIT = 3

Monoisotopic Mass, Even Electron Ions
2 formula(e) evaluated with 1 results within limits (up to 10 closest results for each mass)
Elements Used:
C: 0-20 H: 0-11 S: 0-2

02-Oct-2017
DB_MS17929_AP 36 (0.156)

Synapt G2-Si Cardiff University (EP/L027240/1)
1: TOF MS AP+
6.54e+003

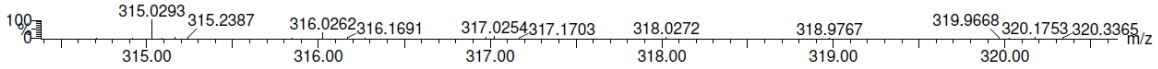

Minimum:				-1.5				
Maximum:		1000.0	5.0	100.0				
Mass	Calc. Mass	mDa	PPM	DBE	i-FIT	Norm	Conf(%)	Formula
315.0293	315.0302	-0.9	-2.9	15.5	80.5	n/a	n/a	C20 H11 S2

Figure A.11. Elemental composition report.

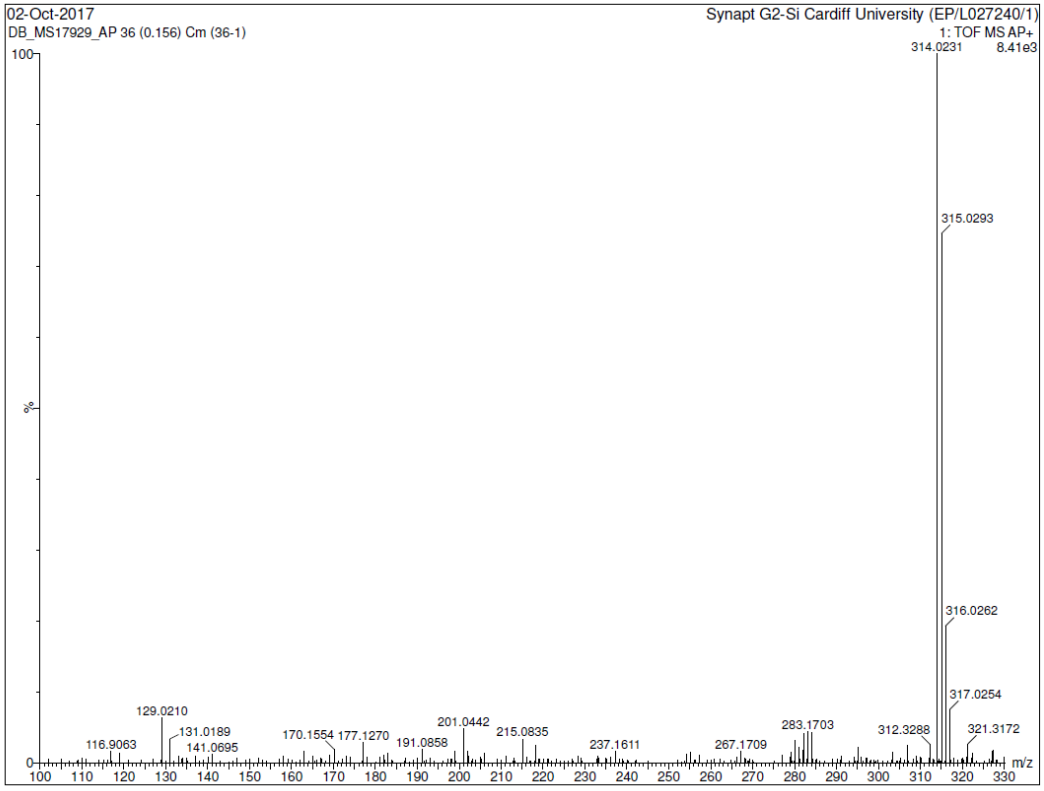

Figure A.12. HRMS, APCI+, TOF.

Characterisation of 1,1'-Binaphthalene-2,2'-diyl-O,O'-bis(N,N'-dimethylthiocarbamate) 3

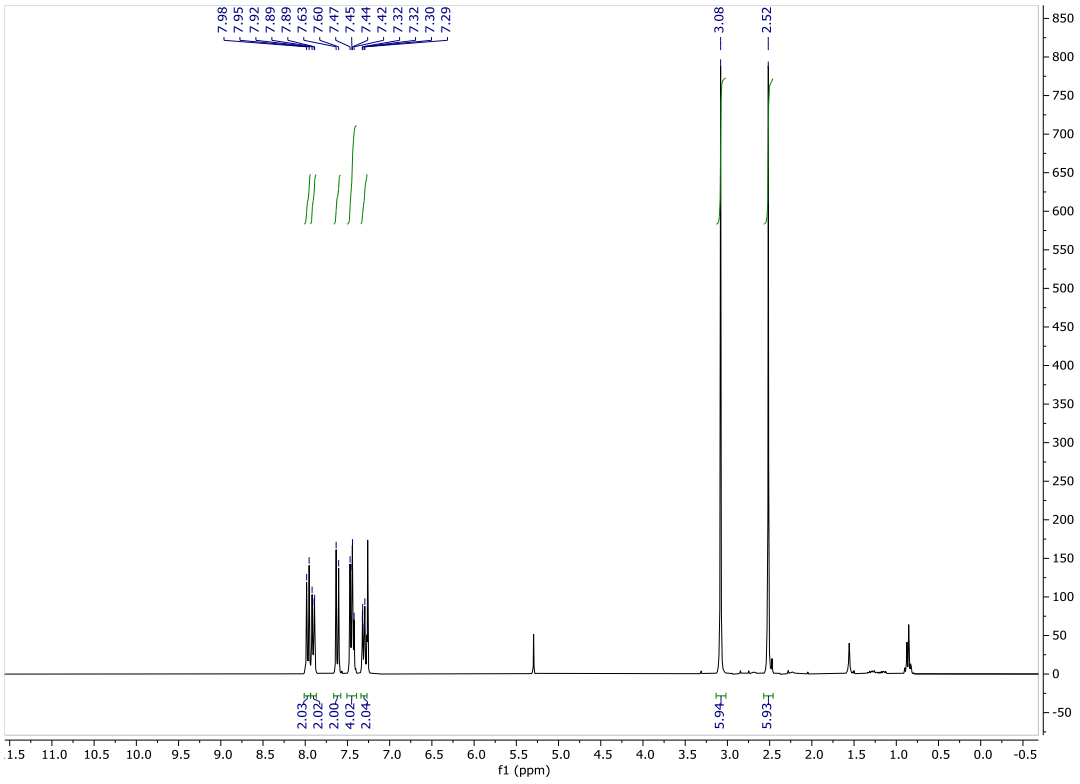

Figure A.13. ^{1}H NMR, 300 MHz, $CDCl_3$.

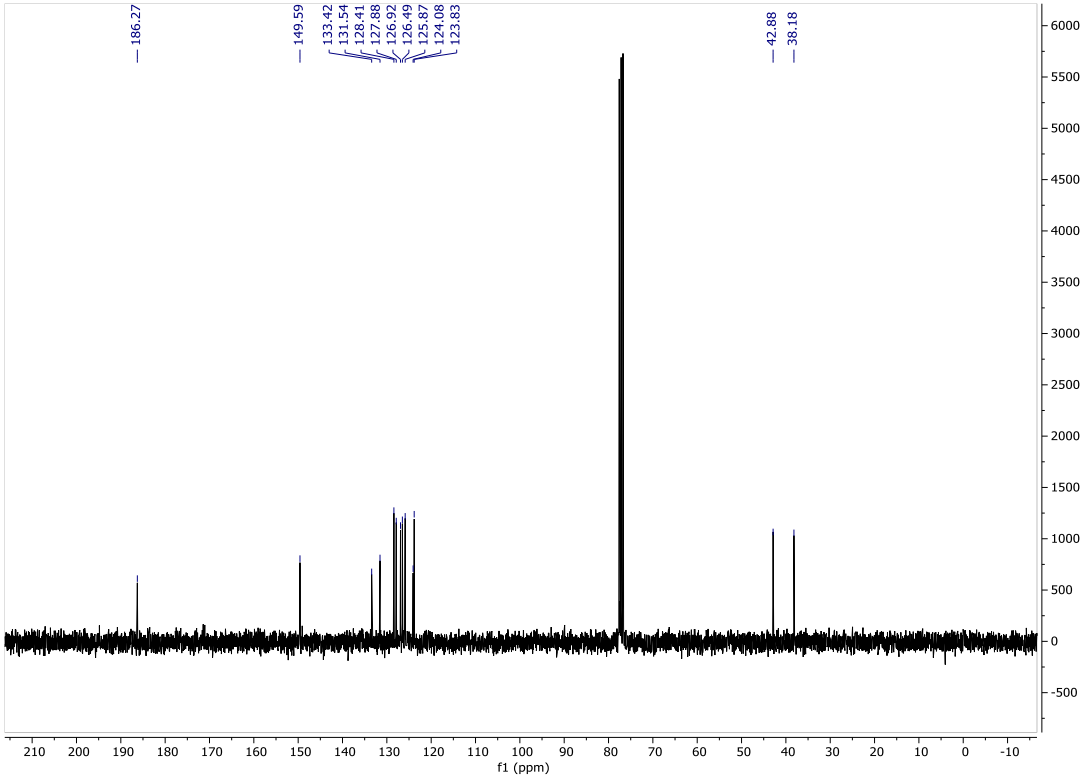

Figure A.14. ^{13}C NMR, 75 MHz, $CDCl_3$.

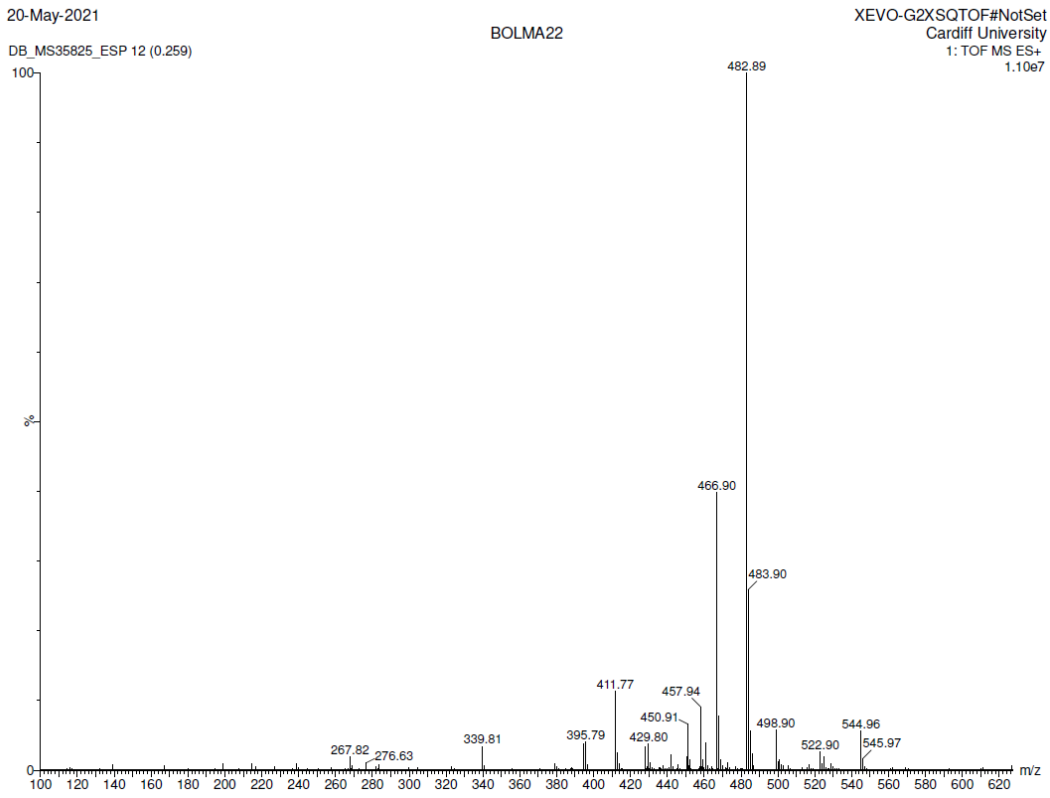

Figure A.15. LRMS, ES+, TOF.

Characterisation of 1,1'-Binaphthalene-2,2'-diyl-S,S'-bis(N,N'-dimethylthiocarbamate) 4

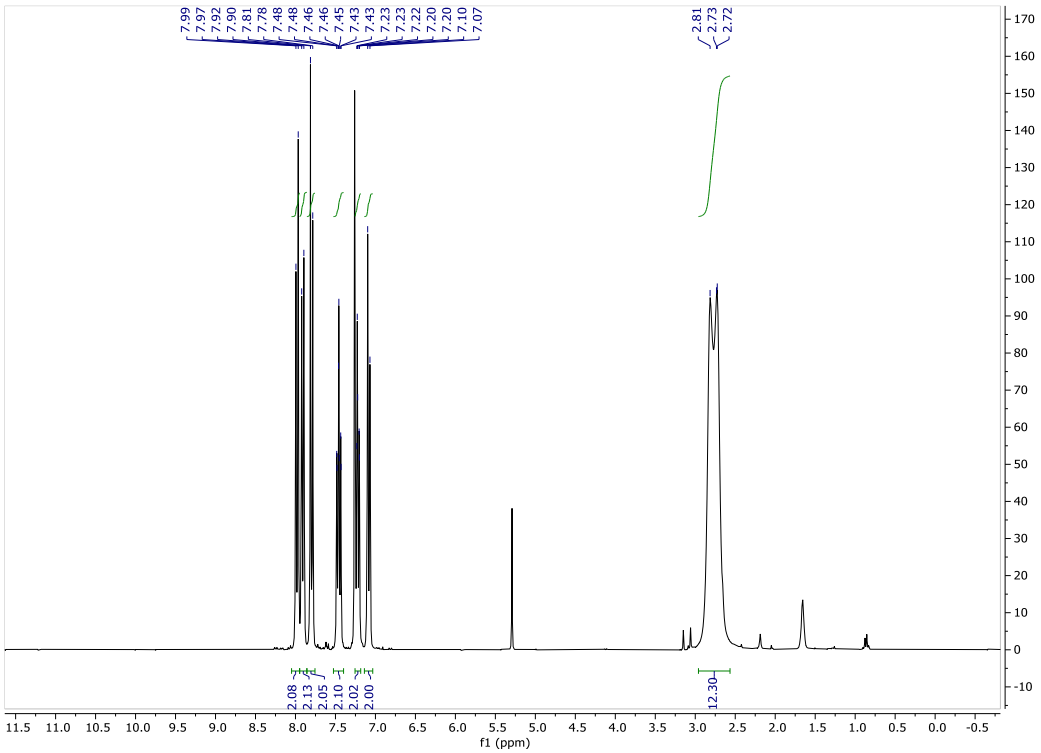

Figure A.16. ^{1}H NMR, 300 MHz, $CDCl_3$.

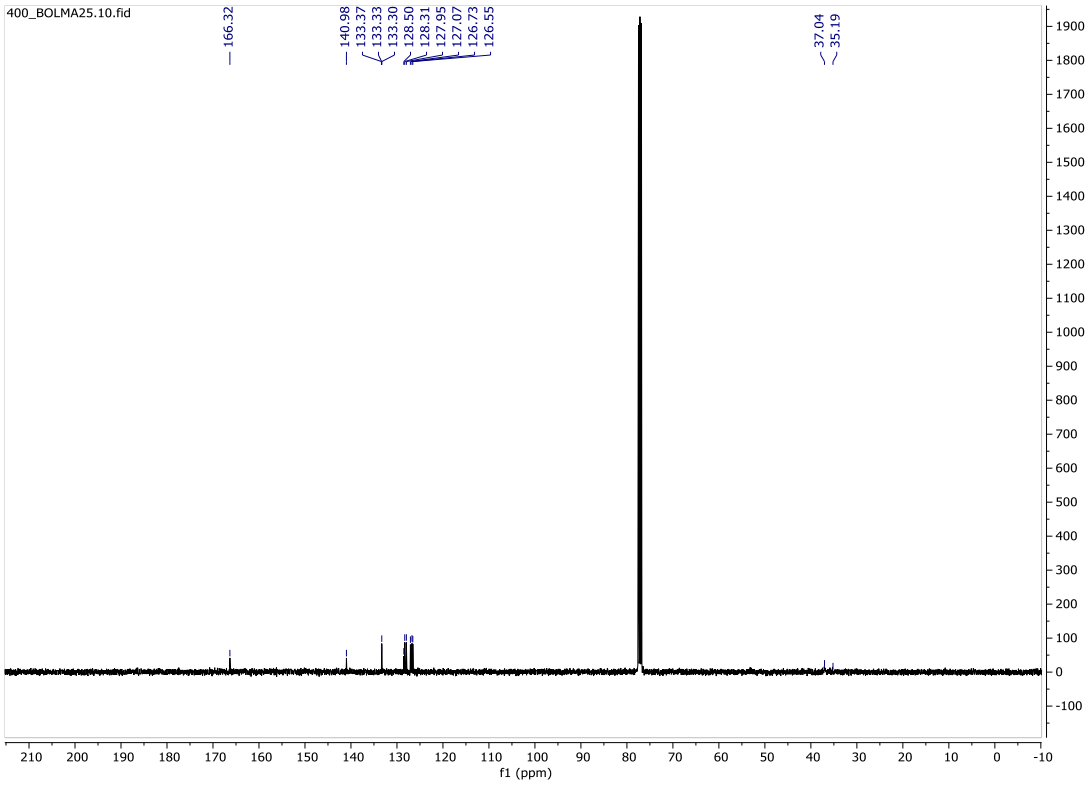

Figure A.17. ^{13}C NMR, 100 MHz, $CDCl_3$.

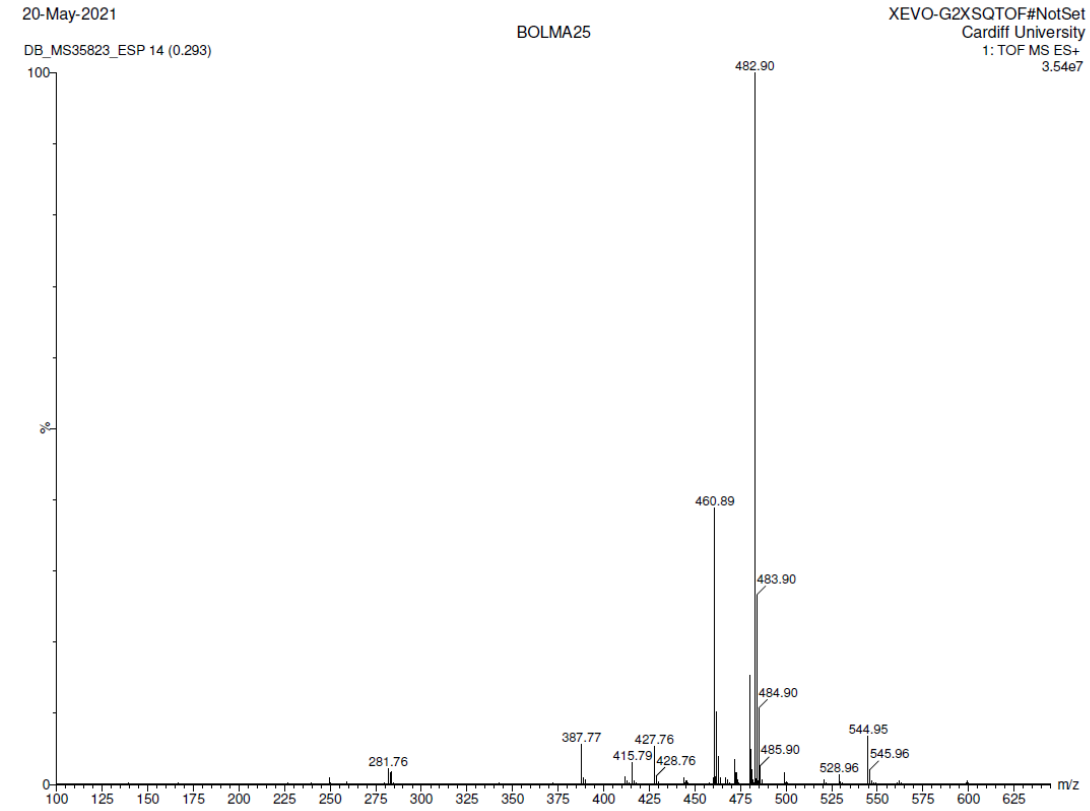

Figure A.18. LRMS, ES+, TOF.

Characterisation of 1,1'-Binaphthalene-2,2'-dithiol 6

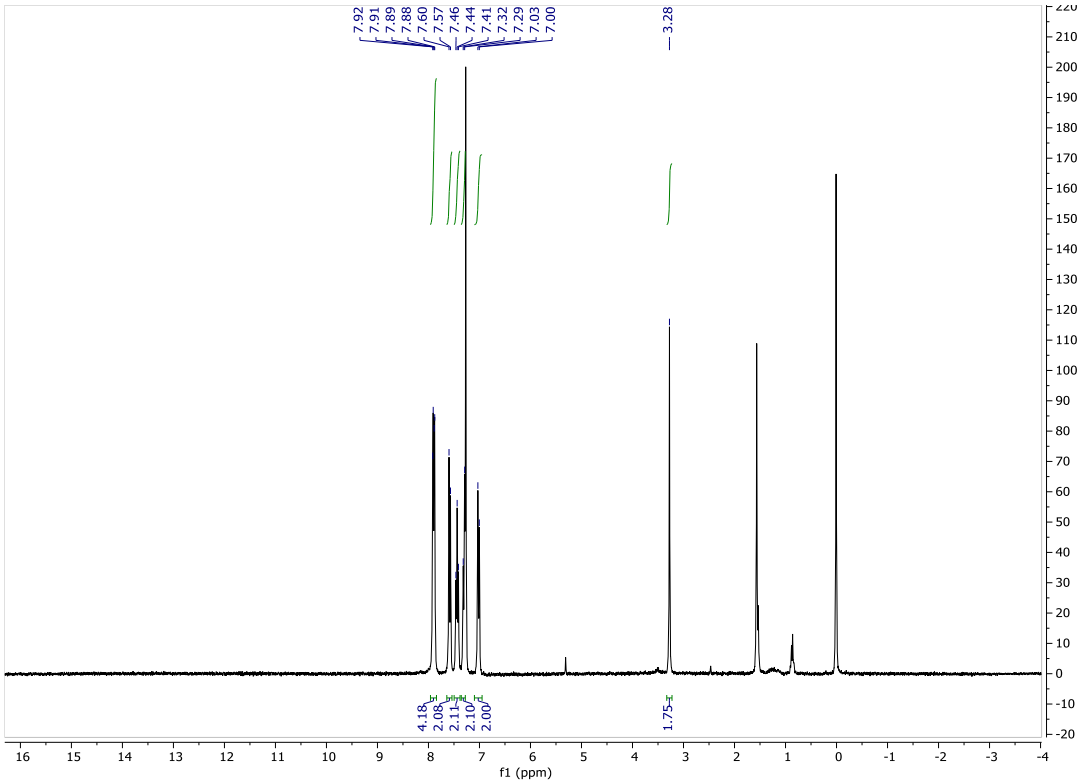

Figure A.19. ^{1}H NMR, 300 MHz, $CDCl_3$.

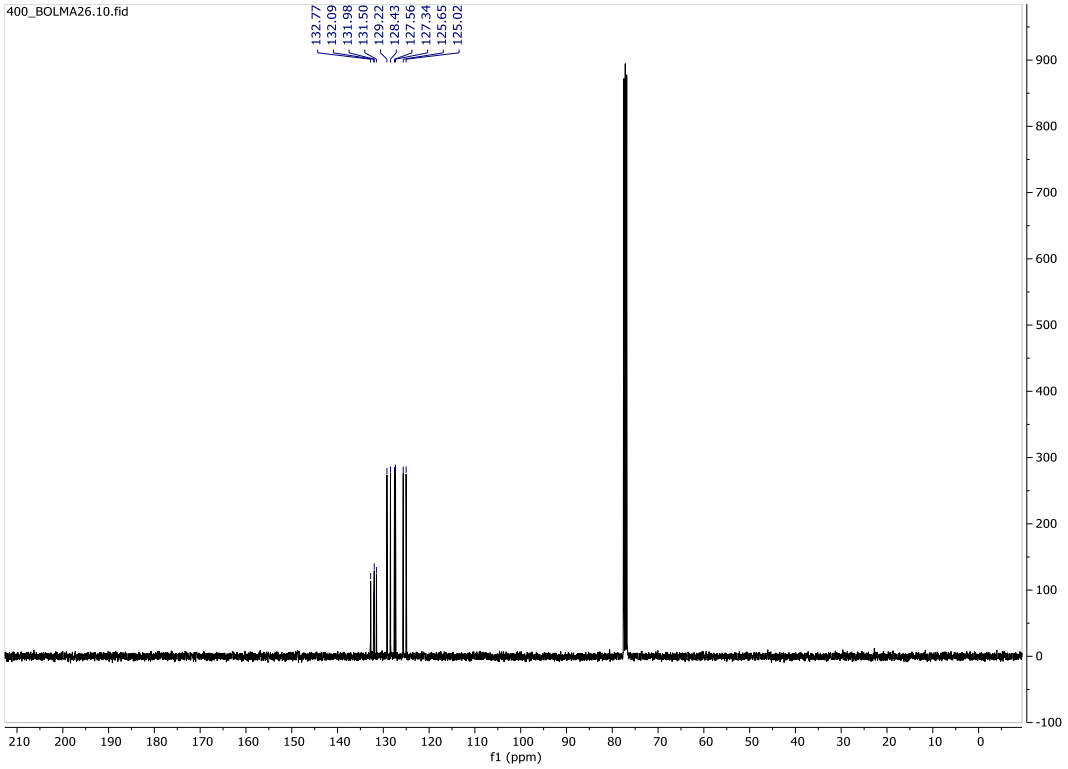

Figure A.20. ^{13}C NMR, 100 MHz, $CDCl_3$.

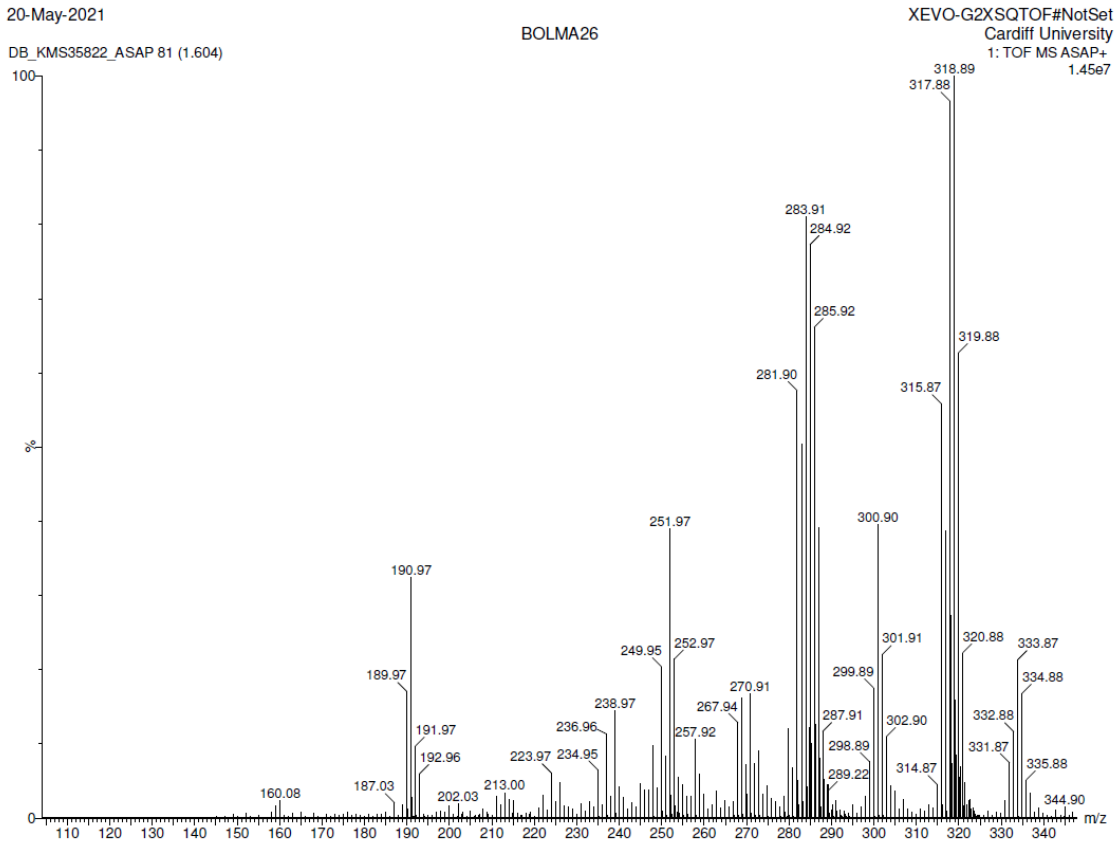

Figure A.21. LRMS, ASAP+, TOF.

Characterisation of 2,2'-bis(phenylthio)-1,1'-binaphthalene 8

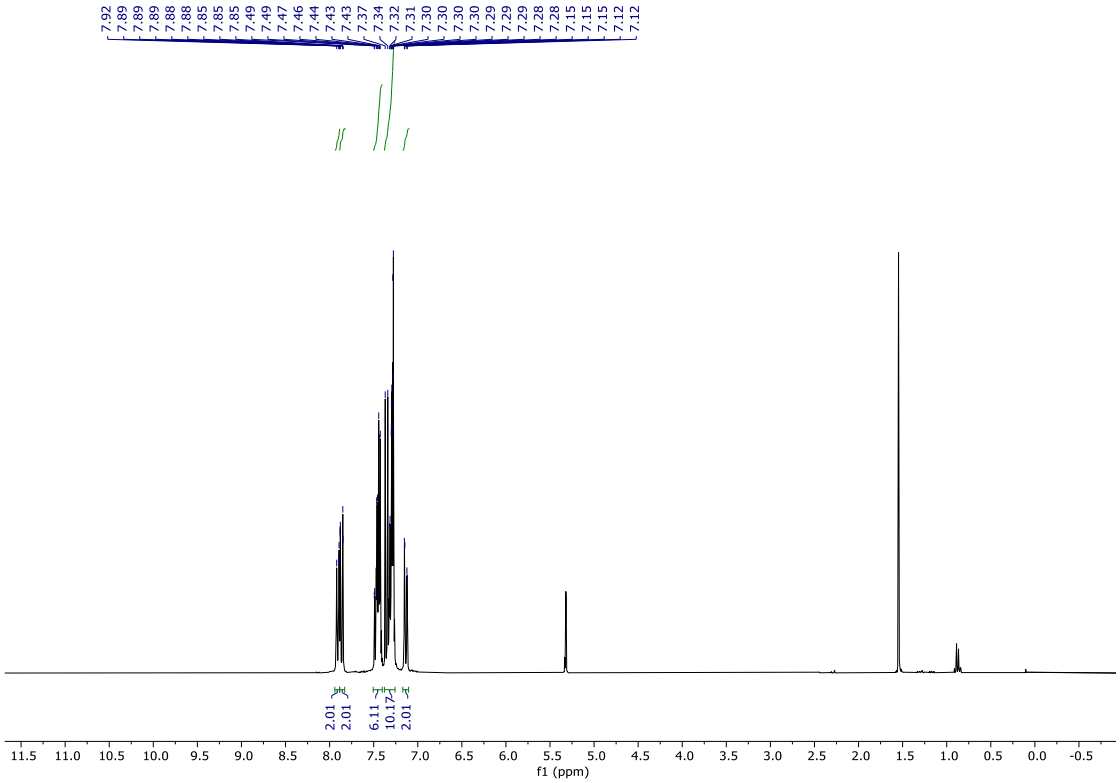

Figure A.22. ^{1}H NMR, 300 MHz, CD_2Cl_2.

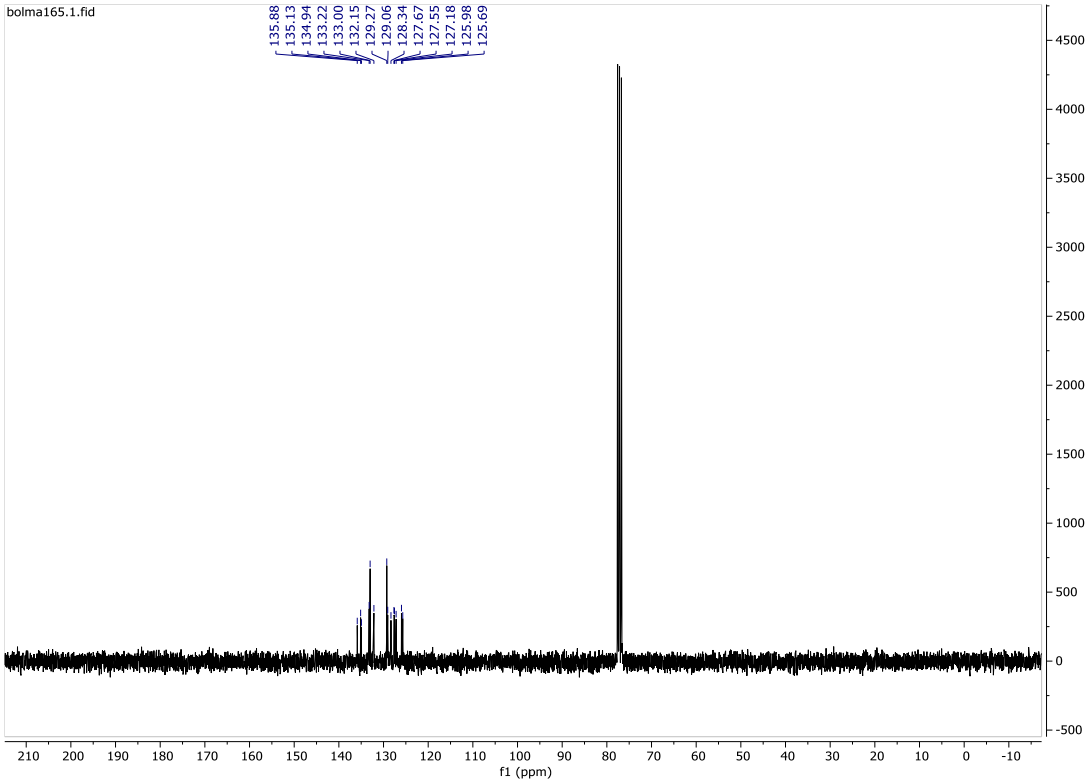

Figure A.23. ^{13}C NMR, 75 MHz, $CDCl_3$.

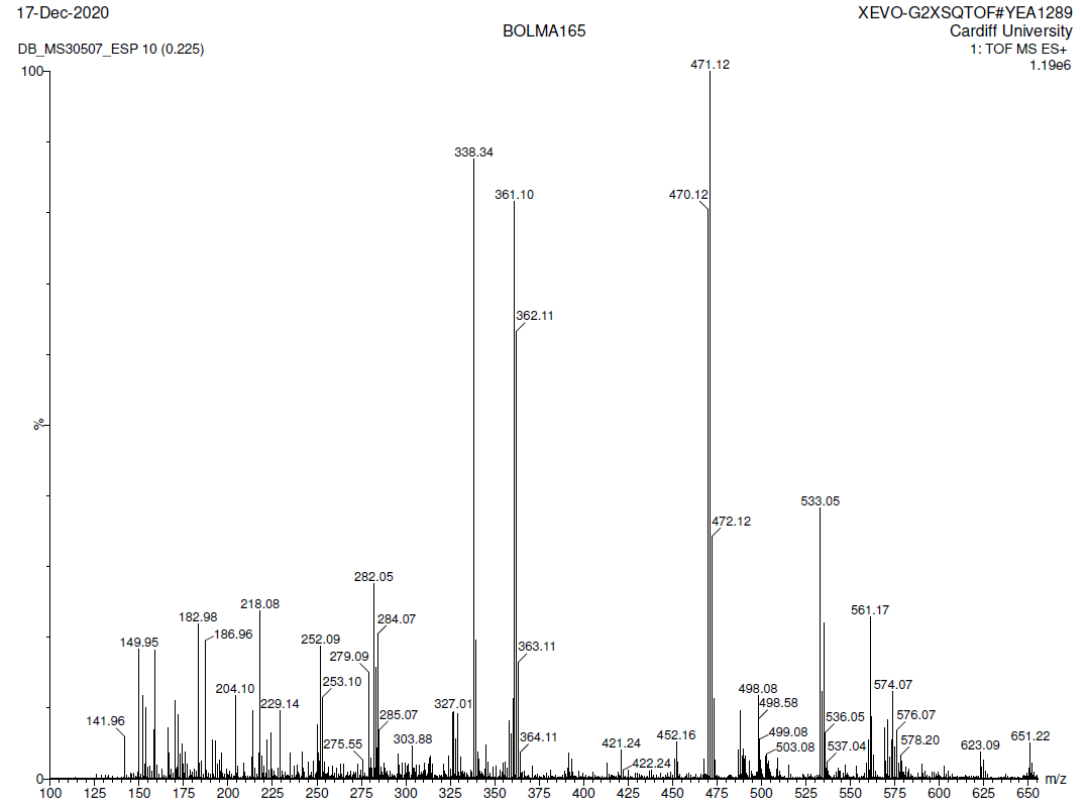

Figure A.24. LRMS, ES+, TOF.

Characterisation of 6,6'-dibromo-2,2'-bis(methylsulfinyl)-1,1'-binaphthalene 11

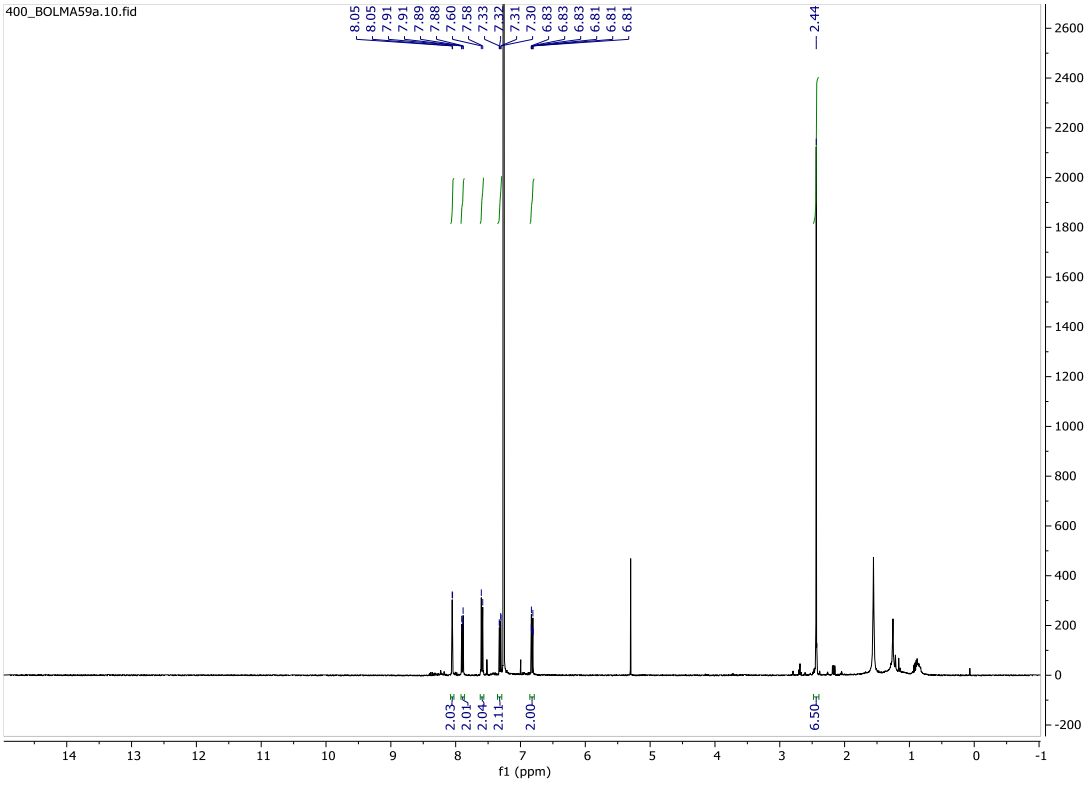

Figure A.25. ^{1}H NMR, 400 MHz, $CDCl_3$.

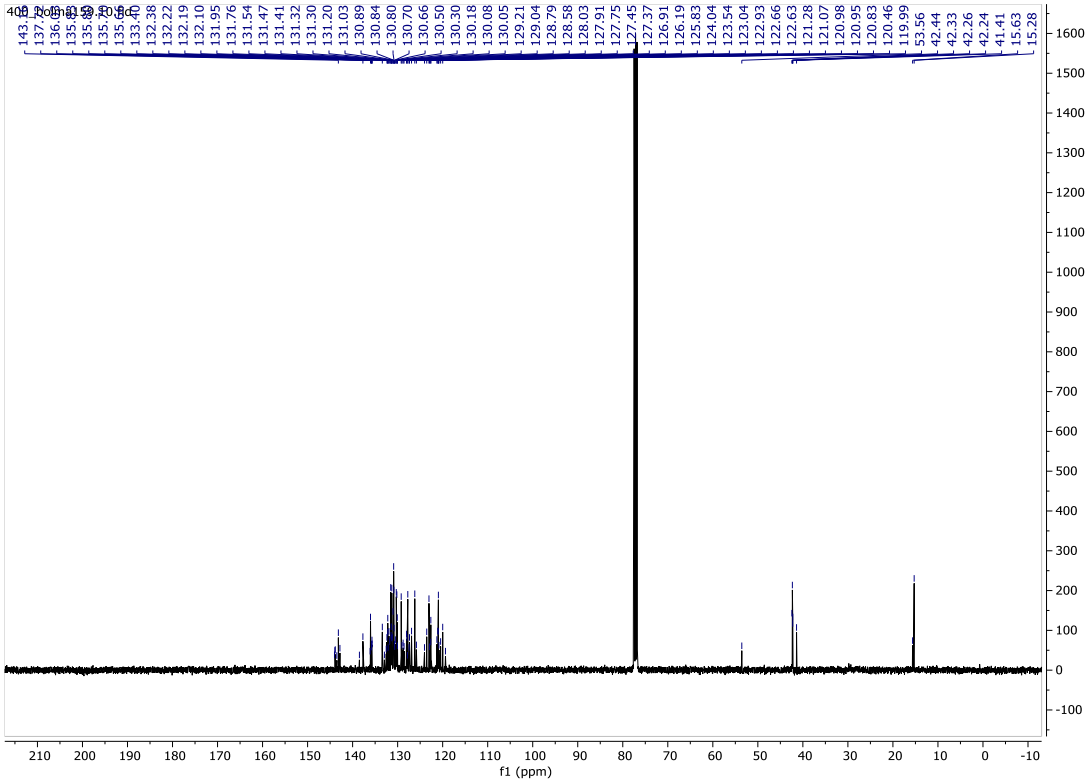

Figure A.26. ^{13}C NMR, 100 MHz, $CDCl_3$.

Elemental Composition Report Page 1

Single Mass Analysis
Tolerance = 5.0 PPM / DBE: min = -1.5, max = 100.0
Element prediction: Off
Number of isotope peaks used for i-FIT = 3

Monoisotopic Mass, Odd and Even Electron Ions
24 formula(e) evaluated with 1 results within limits (up to 50 best isotopic matches for each mass)
Elements Used:
C: 0-22 H: 0-17 O: 0-2 S: 0-2 Br: 0-2

Minimum:				-1.5				
Maximum:		5.0	5.0	100.0				
Mass	Calc. Mass	mDa	PPM	DBE	i-FIT	Norm	Conf(%)	Formula
534.9047	534.9037	1.0	1.9	13.5	470.9	n/a	n/a	C22 H17 O2 S2 Br2

Figure A.27. Elemental composition report.

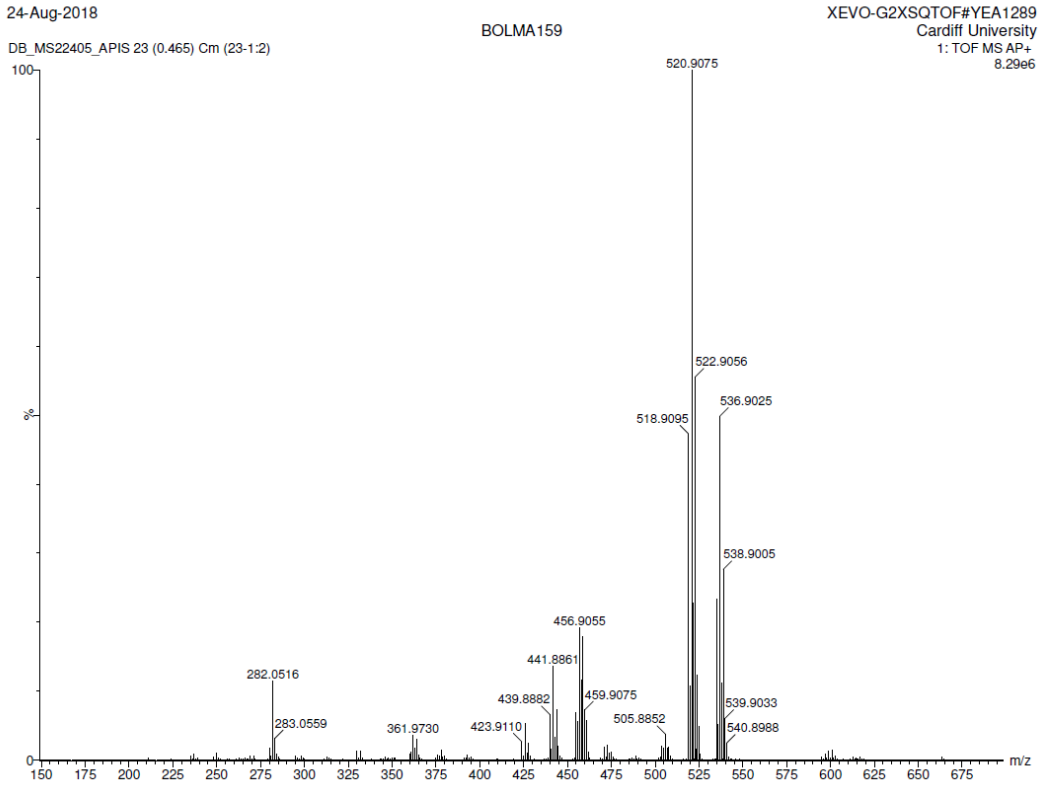

Figure A.28. HRMS, APCI+, TOF.

Characterisation of (6,6'-dibromo-[1,1'-binaphthalene]-2,2'-diyl)bis(methylsulfane) 12

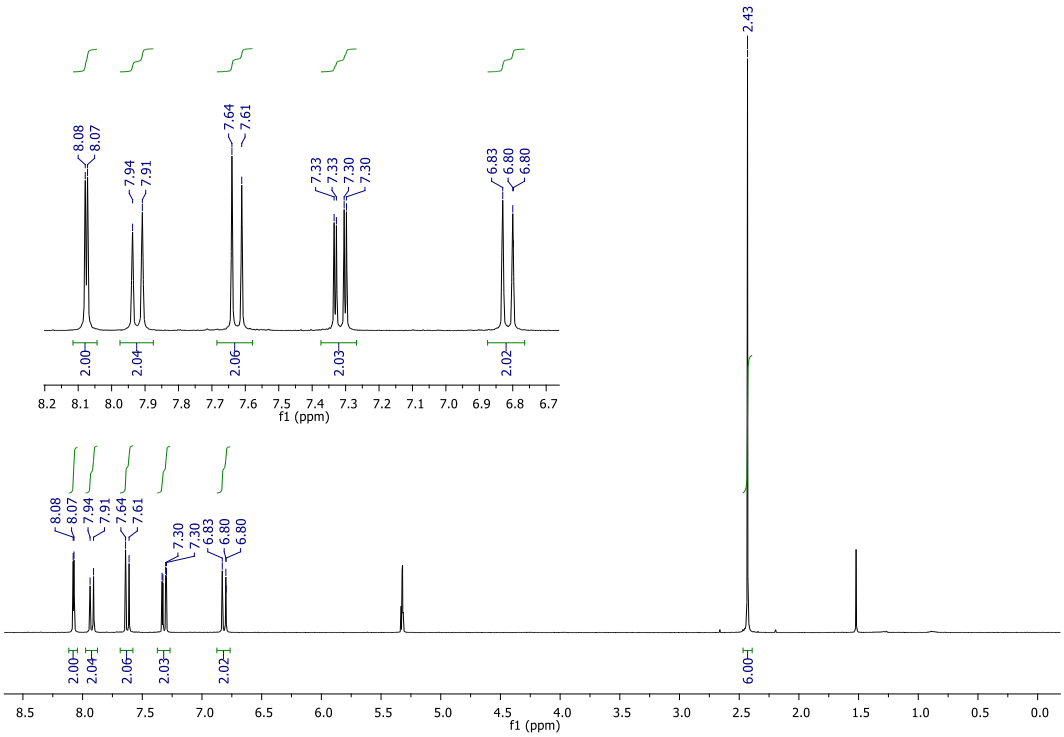

Figure A.29. ^{1}H NMR, 300 MHz, CD_2Cl_2.

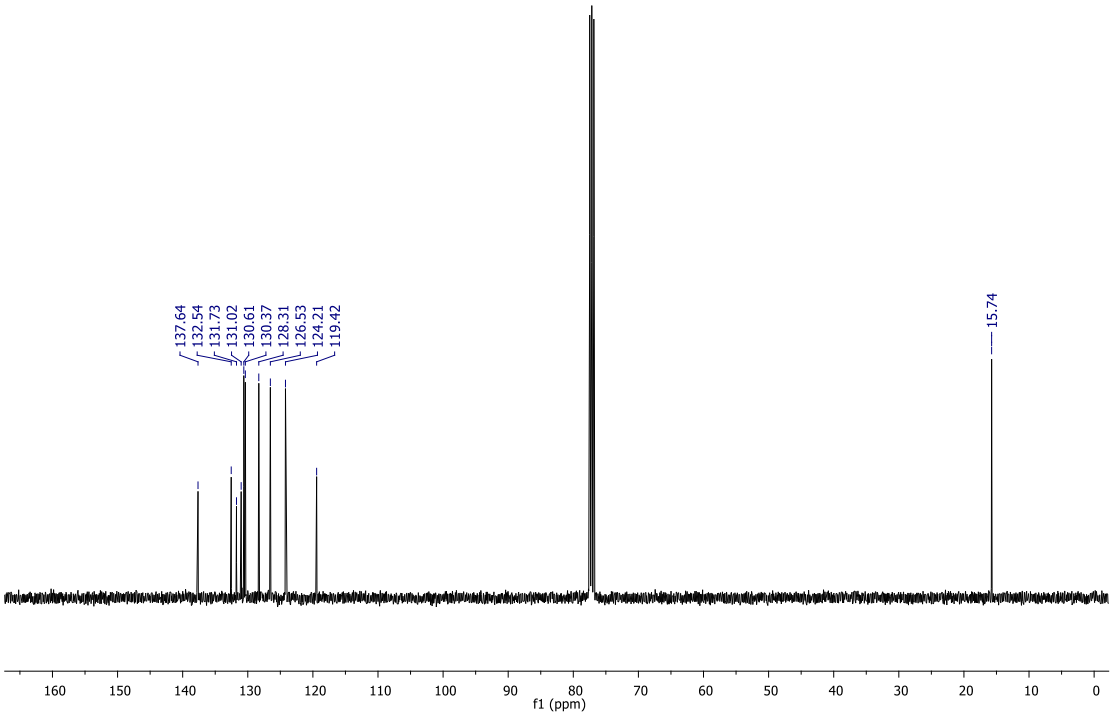

Figure A.30. ^{13}C NMR, 100 MHz, $CDCl_3$.

Elemental Composition Report **Page 1**

Single Mass Analysis
Tolerance = 5.0 PPM / DBE: min = -1.5, max = 50.0
Element prediction: Off

Monoisotopic Mass, Odd and Even Electron Ions
54 formula(e) evaluated with 1 results within limits (all results (up to 1000) for each mass)
Elements Used:
C: 0-22 H: 0-16 S: 0-2 79Br: 0-2 81Br: 0-8

03-Oct-2017
DB_MS17938B 434 (7.234) Cm (434-35:169)

BOLMA49

School of Chemistry Cardiff University
TOF MS EI+
8.95e+003

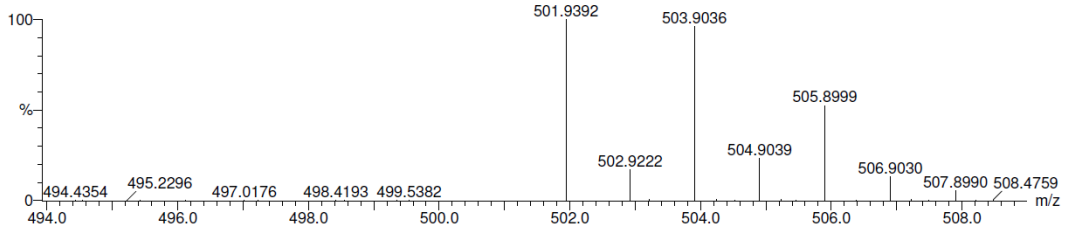

Minimum:				-1.5		
Maximum:		5.0	5.0	50.0		
Mass	Calc. Mass	mDa	PPM	DBE	i-FIT	Formula
503.9036	503.9040	-0.4	-0.8	14.0	8.5	C22 H16 S2 79Br 81Br

Figure A.31. Elemental composition report.

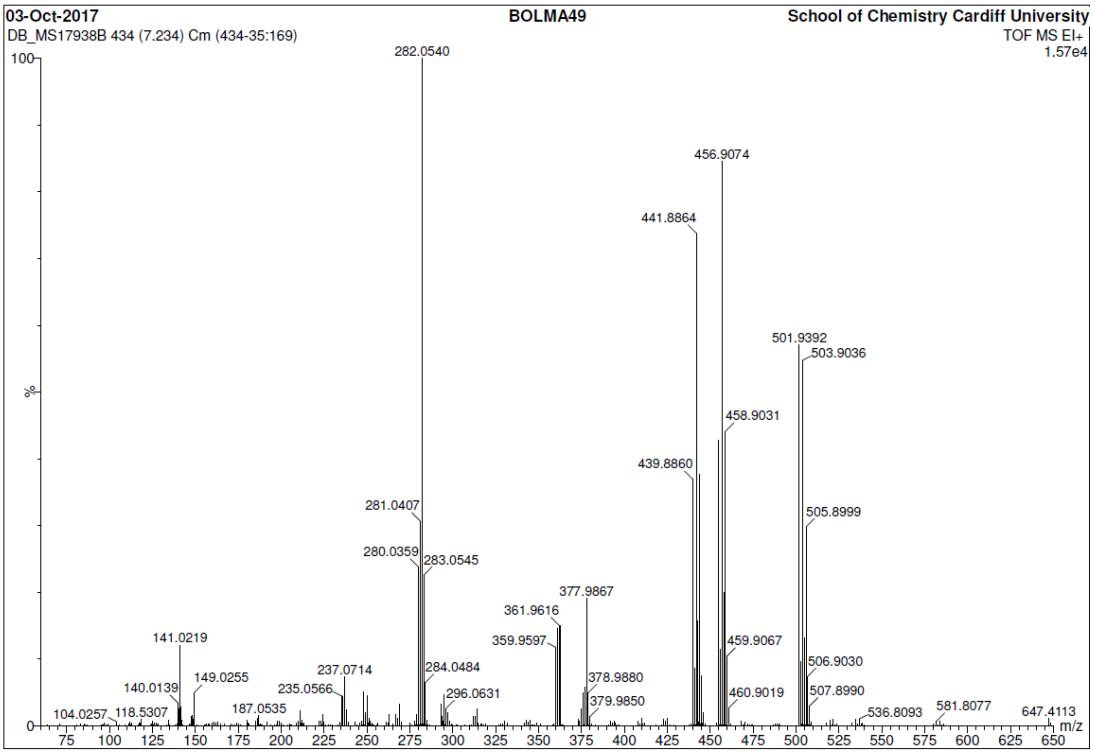

Figure A.32. HRMS, EI+, TOF.

Characterisation of 6,6'-dimesityl-[1,1'-binaphthalene]-2,2'-diyl)bis(methylsulfane) 13

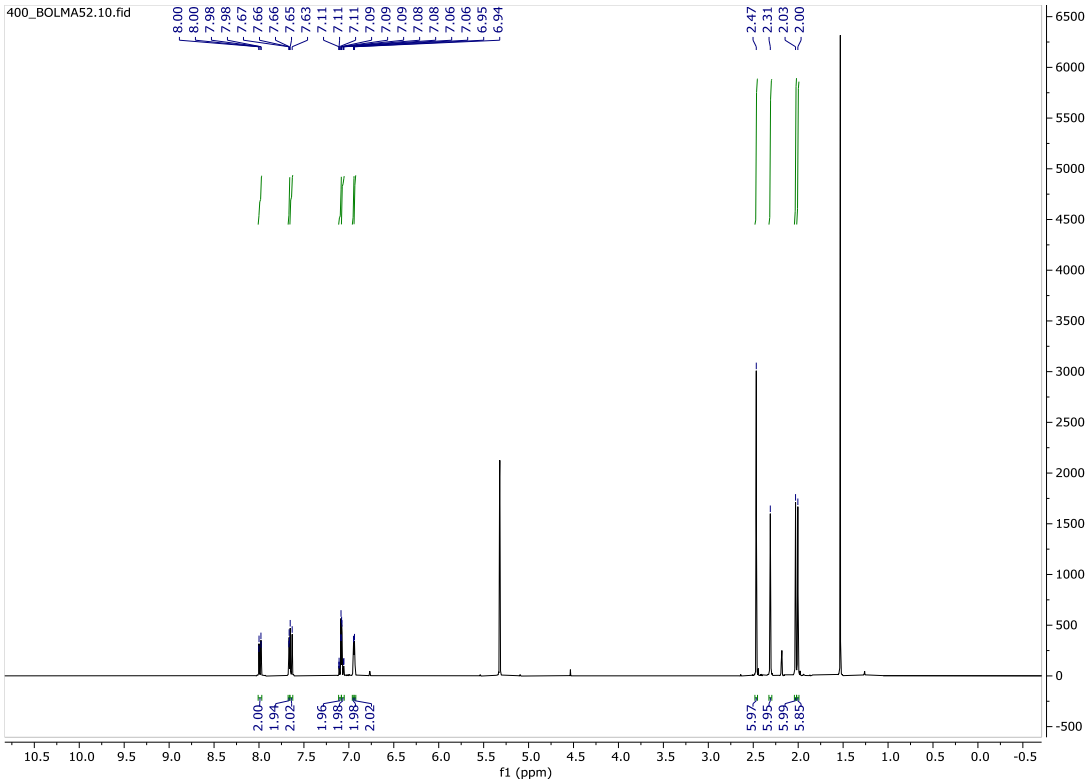

Figure A.33. ^{1}H NMR, 400 MHz, CD_2Cl_2.

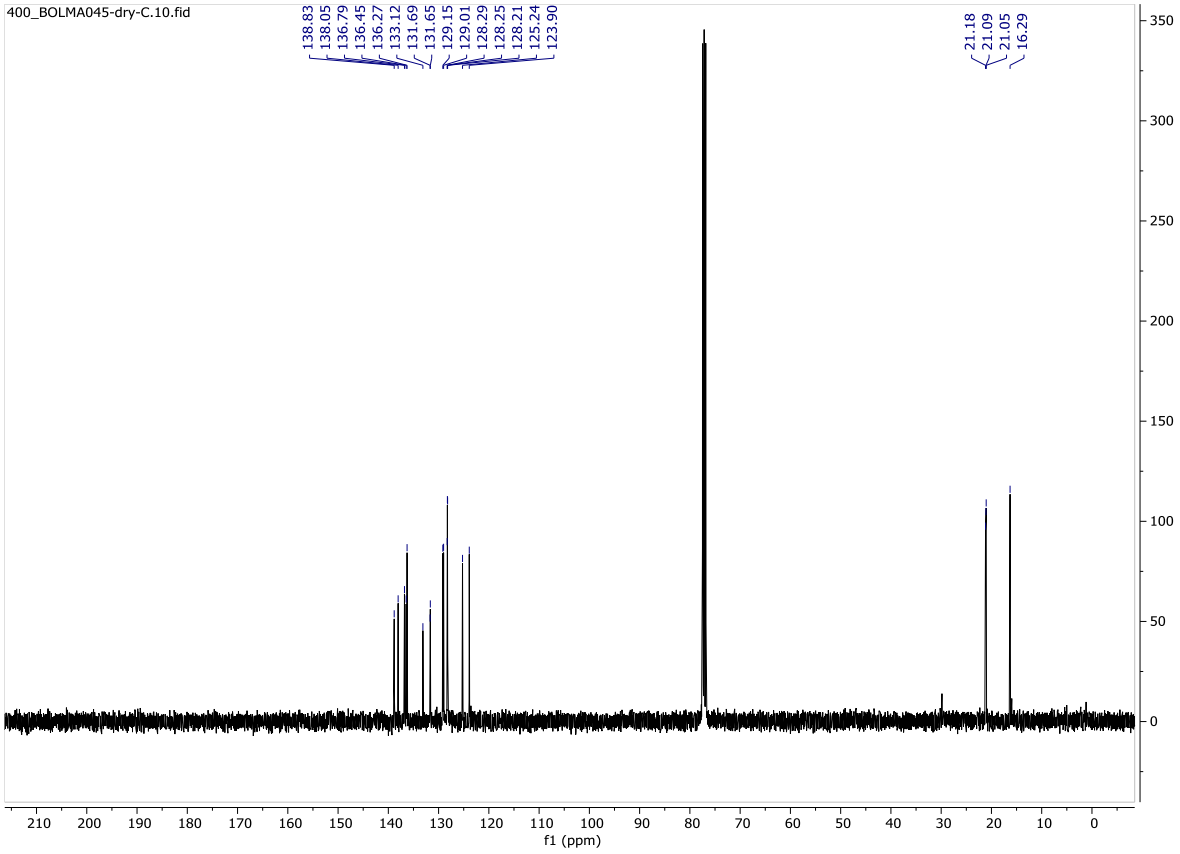

Figure A.34. ^{13}C NMR, 100 MHz, $CDCl_3$.

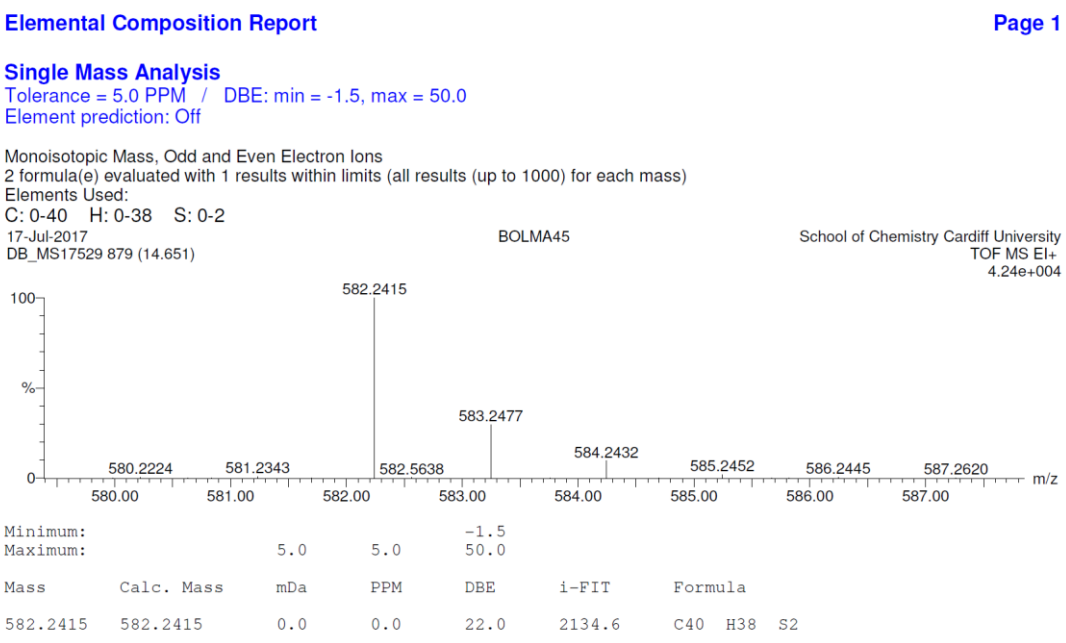

Figure A.35. Elemental composition report.

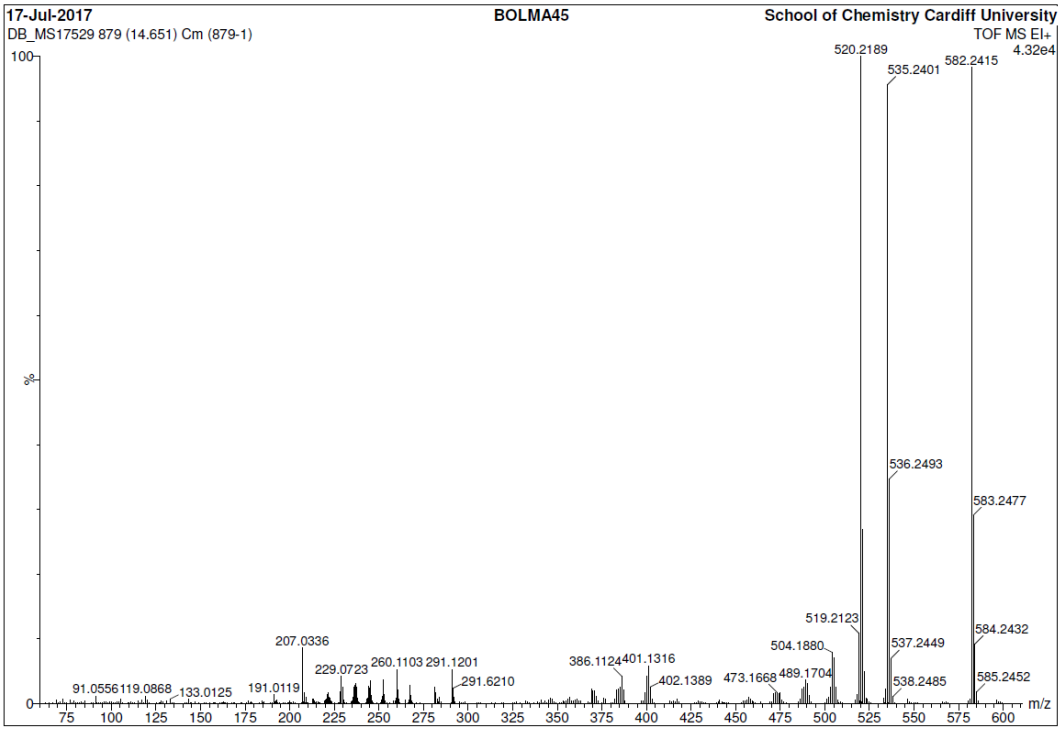

Figure A.36. HRMS, EI+, TOF.

Characterisation of 6,6'-dimesityl-2,2'-bis(methylsulfinyl)-1,1'-binaphthalene 14

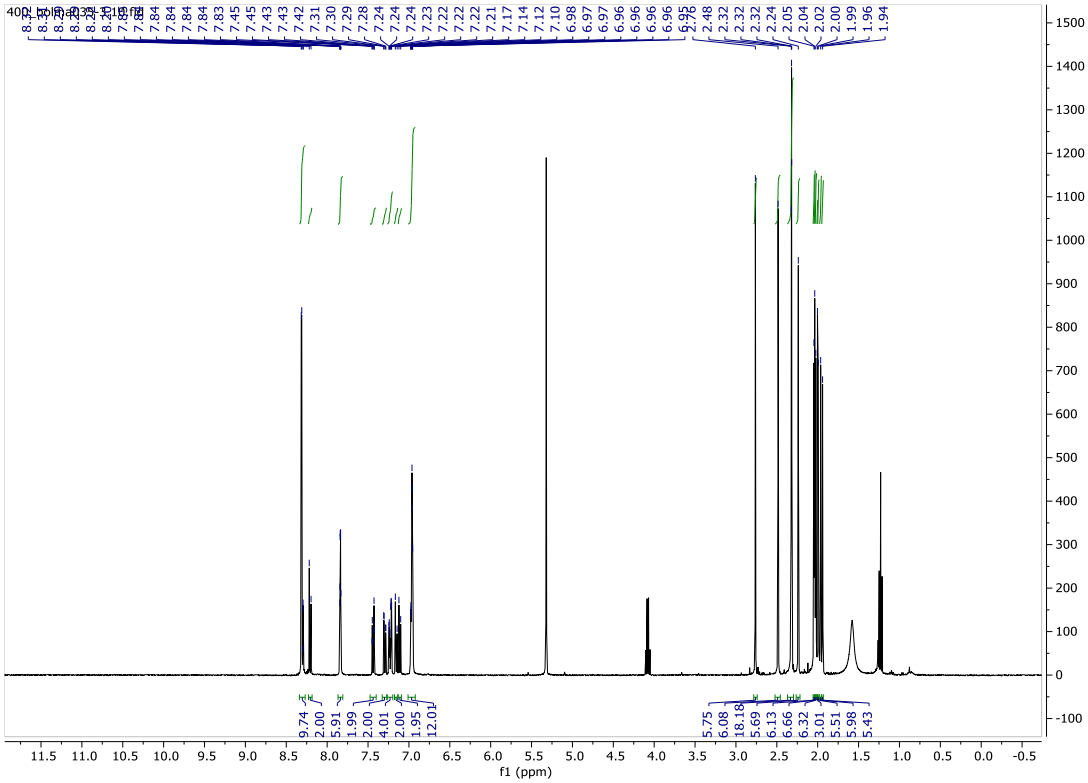

Figure A.37. ^{1}H NMR, 400 MHz, CD_2Cl_2.

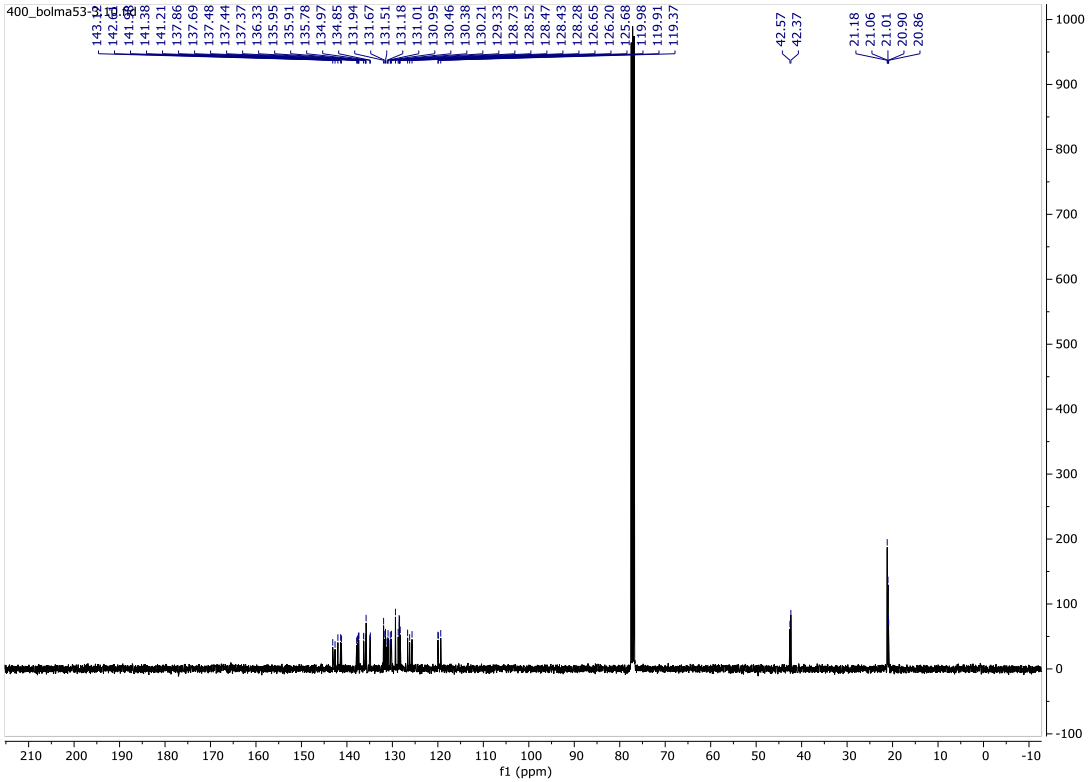

Figure A.38. ^{13}C NMR, 100 MHz, $CDCl_3$.

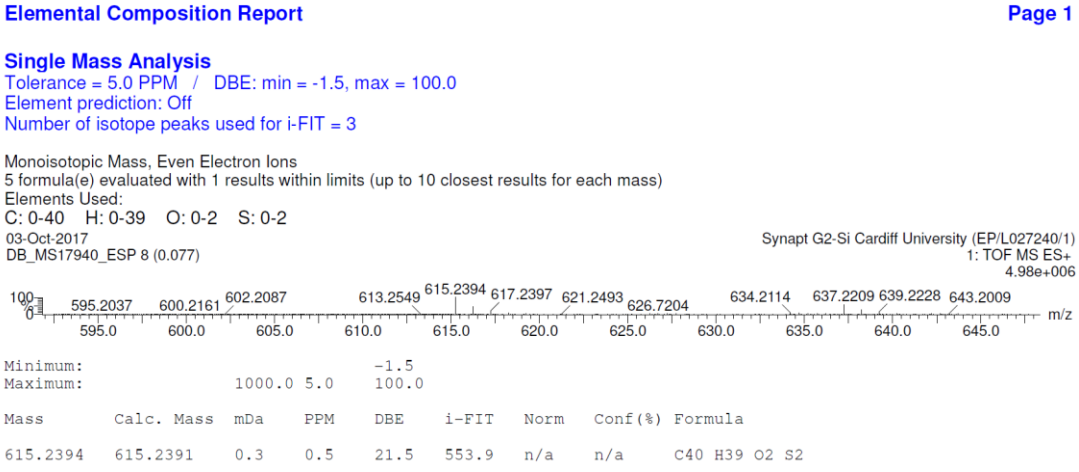

Elemental Composition Report **Page 1**

Single Mass Analysis
Tolerance = 5.0 PPM / DBE: min = -1.5, max = 100.0
Element prediction: Off
Number of isotope peaks used for i-FIT = 3

Monoisotopic Mass, Even Electron Ions
5 formula(e) evaluated with 1 results within limits (up to 10 closest results for each mass)
Elements Used:
C: 0-40 H: 0-39 O: 0-2 S: 0-2

03-Oct-2017
DB_MS17940_ESP 8 (0.077)

Synapt G2-Si Cardiff University (EP/L027240/1)
1: TOF MS ES+
4.98e+006

595.2037 600.2161 602.2087 613.2549 615.2394 617.2397 621.2493 626.7204 634.2114 637.2209 639.2228 643.2009 m/z

Minimum:				-1.5				
Maximum:		1000.0	5.0	100.0				
Mass	Calc. Mass	mDa	PPM	DBE	i-FIT	Norm	Conf(%)	Formula
615.2394	615.2391	0.3	0.5	21.5	553.9	n/a	n/a	C40 H39 O2 S2

Figure A.39. Elemental composition report.

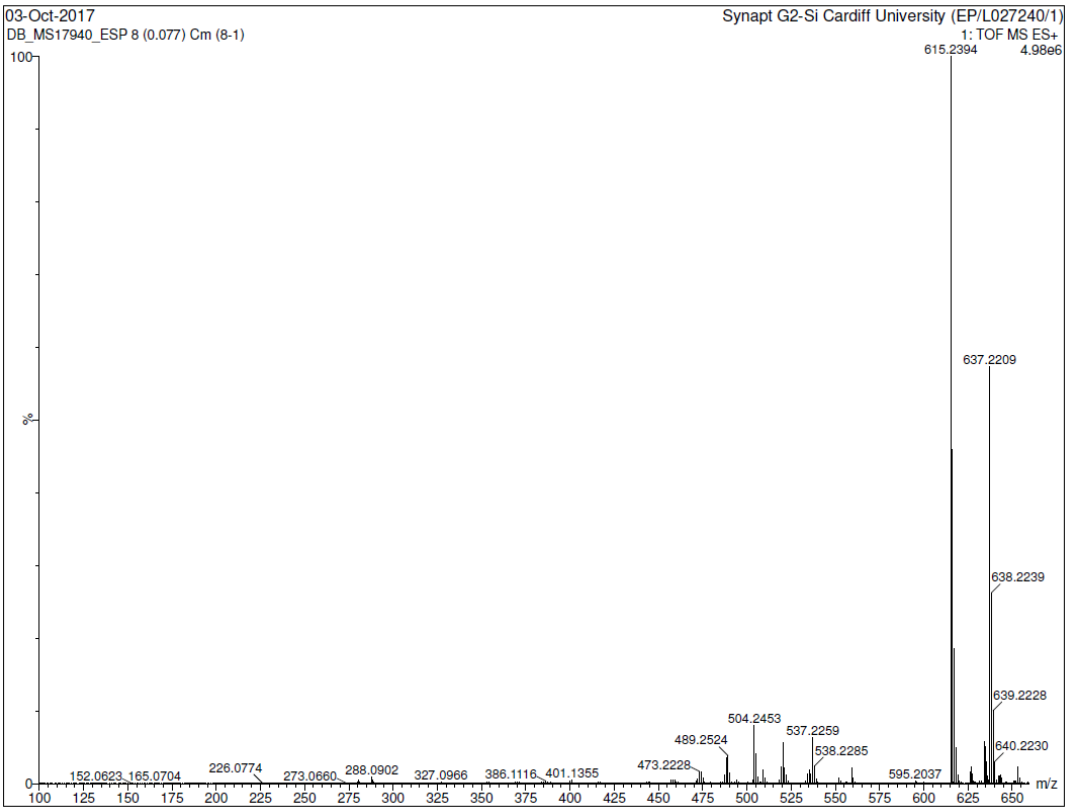

Figure A.40. HRMS, ES+, TOF.

Characterisation of 2,8-dimesitylthioxantheno[2,1,9,8-klmna]thioxanthene 15

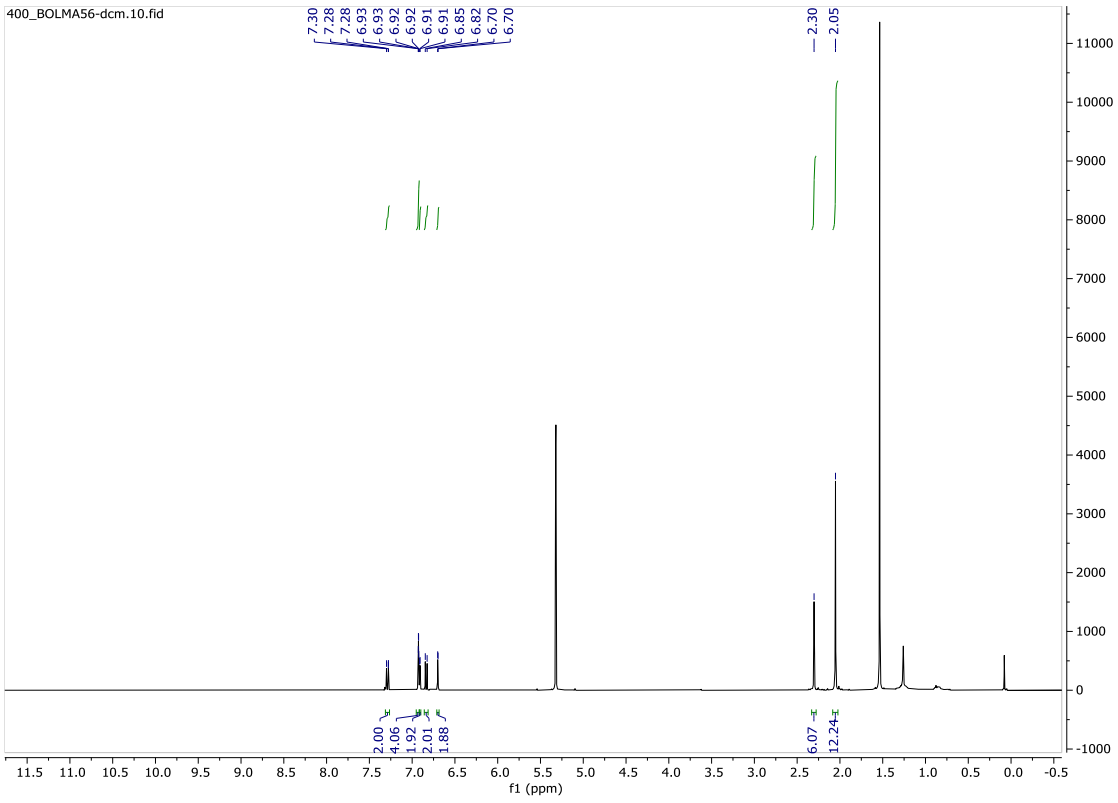

Figure A.41. ^{1}H NMR, 400 MHz, CD_2Cl_2.

Elemental Composition Report **Page 1**

Single Mass Analysis
Tolerance = 5.0 PPM / DBE: min = -1.5, max = 100.0
Element prediction: Off
Number of isotope peaks used for i-FIT = 3

Monoisotopic Mass, Even Electron Ions
2 formula(e) evaluated with 1 results within limits (up to 10 closest results for each mass)
Elements Used:
C: 0-38 H: 0-31 S: 0-2

03-Oct-2017
DB_MS17941_ESP 53 (0.405)

Synapt G2-Si Cardiff University (EP/L027240/1)
1: TOF MS ES+
2.93e+003

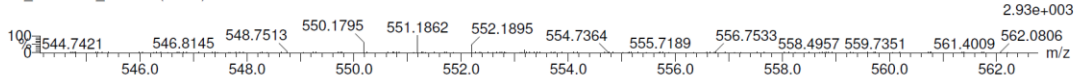

Minimum:				-1.5				
Maximum:		1000.0	5.0	100.0				
Mass	Calc. Mass	mDa	PPM	DBE	i-FIT	Norm	Conf(%)	Formula
551.1862	551.1867	-0.5	-0.9	23.5	187.8	n/a	n/a	C38 H31 S2

Figure A.42. Elemental composition report.

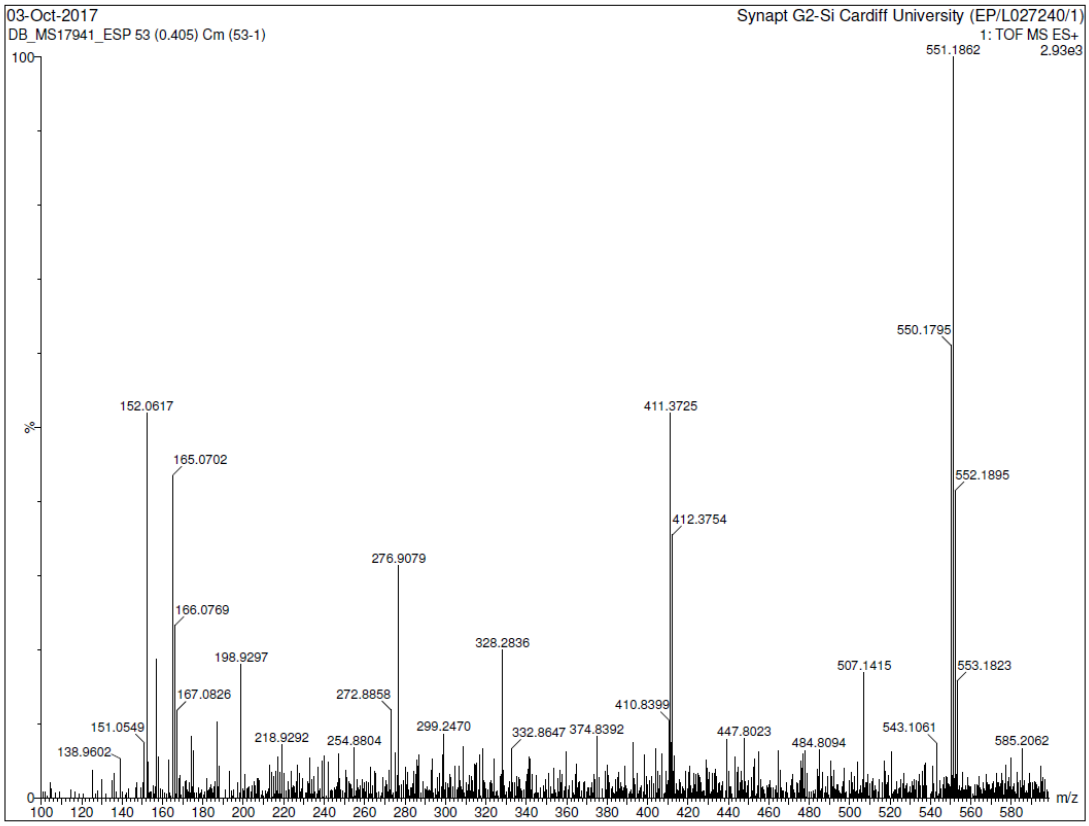

Figure A.43. HRMS, ES+, TOF.

Characterisation of 2,8-dibromothioxanthenothioxanthene 16

Elemental Composition Report **Page 1**

Single Mass Analysis
Tolerance = 5.0 PPM / DBE: min = -1.5, max = 100.0
Element prediction: Off
Number of isotope peaks used for i-FIT = 3

Monoisotopic Mass, Odd and Even Electron Ions
22 formula(e) evaluated with 1 results within limits (up to 50 closest results for each mass)
Elements Used:
C: 0-20 H: 0-8 S: 0-2 79Br: 0-2 81Br: 0-2

Minimum:				-1.5				
Maximum:		5.0	5.0	100.0				
Mass	Calc. Mass	mDa	PPM	DBE	i-FIT	Norm	Conf(%)	Formula
471.8425	471.8414	1.1	2.3	16.0	633.7	n/a	n/a	C20 H8 S2 79Br 81Br

Figure A.44. Elemental composition report.

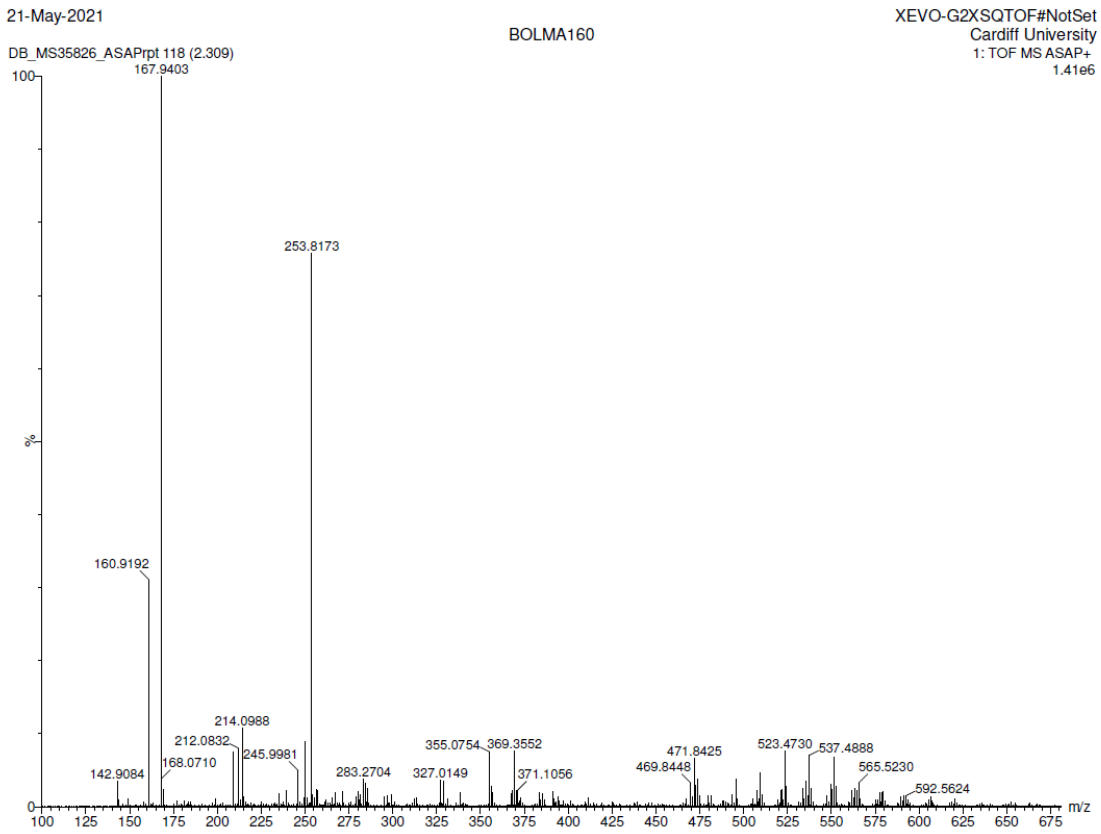

Figure A.45. HRMS, ASAP+, TOF.

Characterisation of (6,6'-bis(4-(tert-butyl)phenyl)-[1,1'-binaphthalene]-2,2'-diyl)bis(methylsulfane) 17

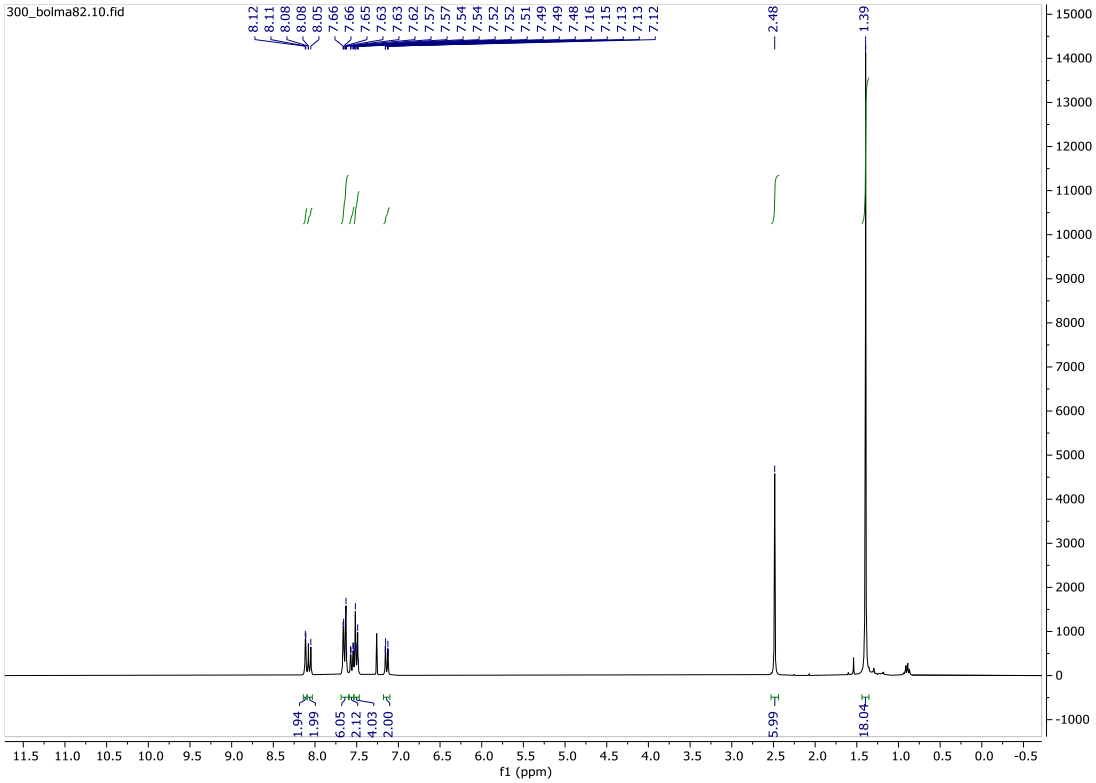

Figure A.46. ^{1}H NMR, 300 MHz, $CDCl_3$.

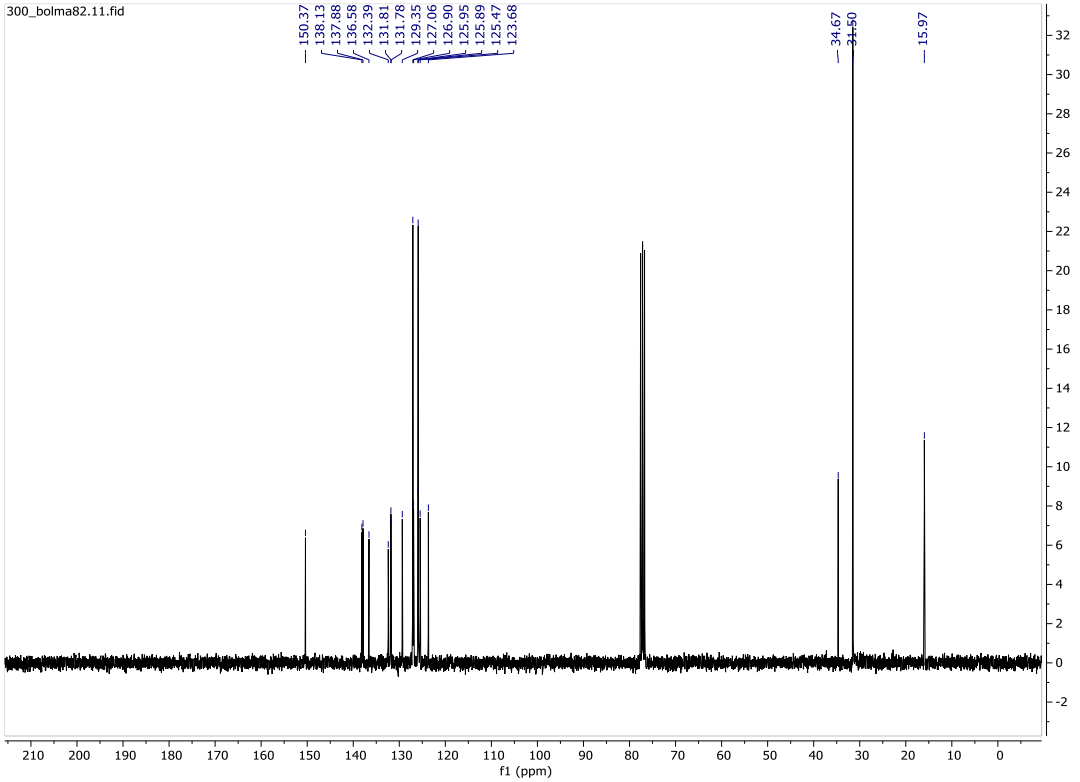

Figure A.47. ^{13}C NMR, 75 MHz, $CDCl_3$.

Elemental Composition Report **Page 1**

Single Mass Analysis
Tolerance = 5.0 PPM / DBE: min = -1.5, max = 100.0
Element prediction: Off
Number of isotope peaks used for i-FIT = 3

Monoisotopic Mass, Even Electron Ions
2 formula(e) evaluated with 1 results within limits (up to 50 closest results for each mass)
Elements Used:
C: 0-42 H: 0-43 S: 0-2

Minimum:				-1.5				
Maximum:		5.0	5.0	100.0				
Mass	Calc. Mass	mDa	PPM	DBE	i-FIT	Norm	Conf(%)	Formula
611.2783	611.2806	-2.3	-3.8	21.5	637.3	n/a	n/a	C42 H43 S2

Figure A.48. Elemental composition report.

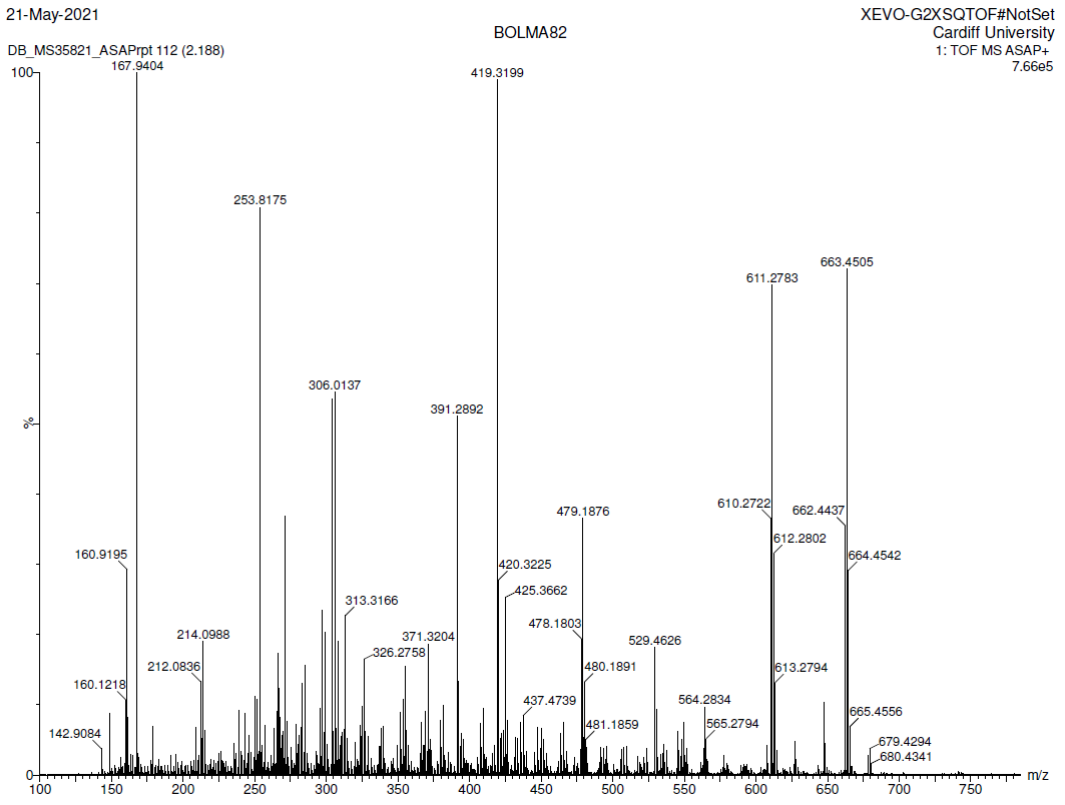

Figure A.49. HRMS, ASAP+, TOF.

Characterisation of 6,6'-bis(4-(tert-butyl)phenyl)-2,2'-bis(methylsulfinyl)-1,1'-binaphthalene 18

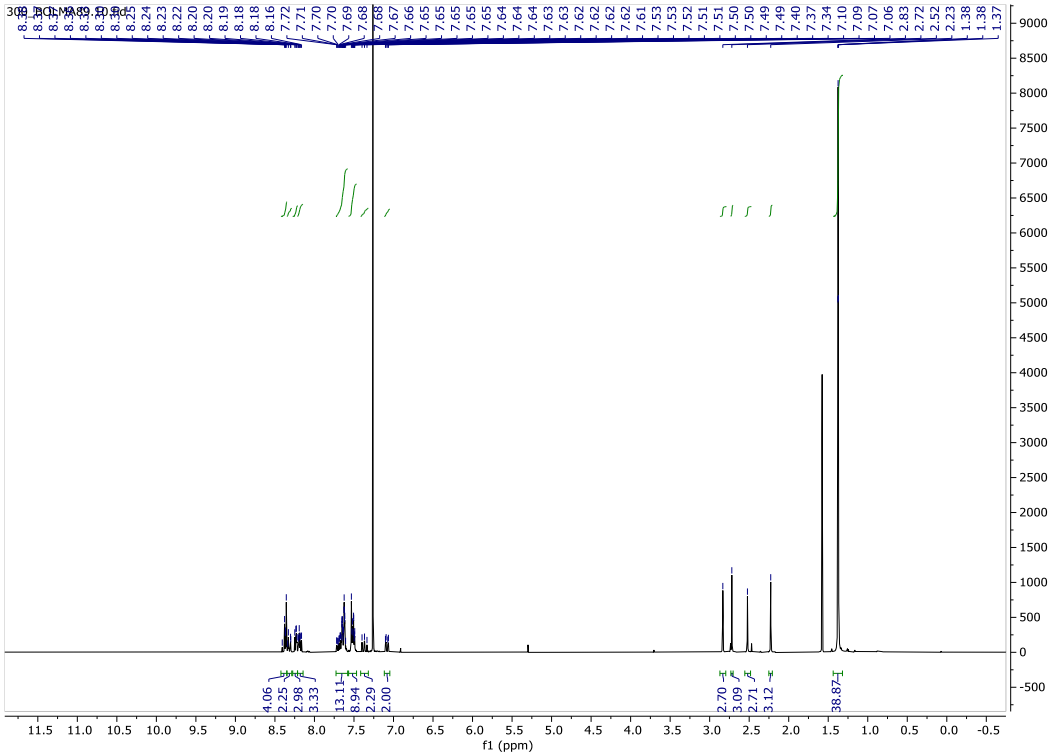

Figure A.50. ^{1}H NMR, 300 MHz, $CDCl_3$.

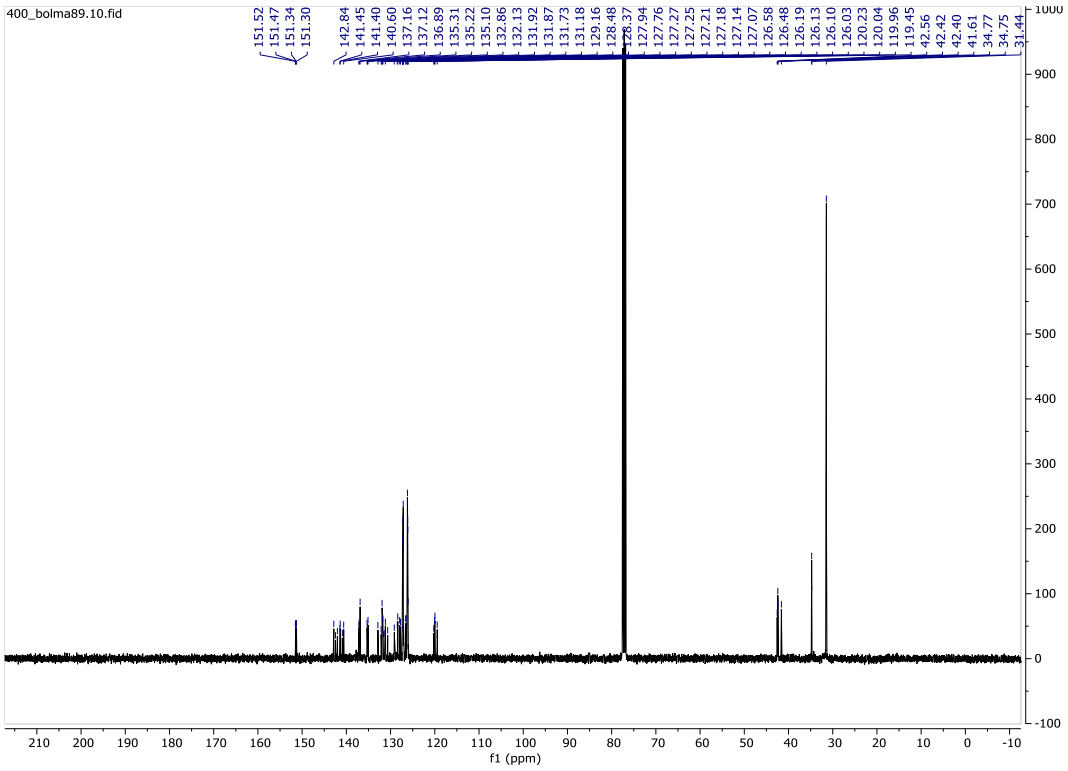

Figure A.51. ^{13}C NMR, 100 MHz, $CDCl_3$.

Elemental Composition Report **Page 1**

Single Mass Analysis
Tolerance = 5.0 PPM / DBE: min = -1.5, max = 100.0
Element prediction: Off
Number of isotope peaks used for i-FIT = 3

Monoisotopic Mass, Odd and Even Electron Ions
5 formula(e) evaluated with 1 results within limits (up to 50 closest results for each mass)
Elements Used:
C: 0-42 H: 0-43 O: 0-2 S: 0-2

Minimum:				-1.5				
Maximum:		5.0	5.0	100.0				
Mass	Calc. Mass	mDa	PPM	DBE	i-FIT	Norm	Conf(%)	Formula
643.2700	643.2704	-0.4	-0.6	21.5	677.9	n/a	n/a	C42 H43 O2 S2

Figure A.52. Elemental composition report.

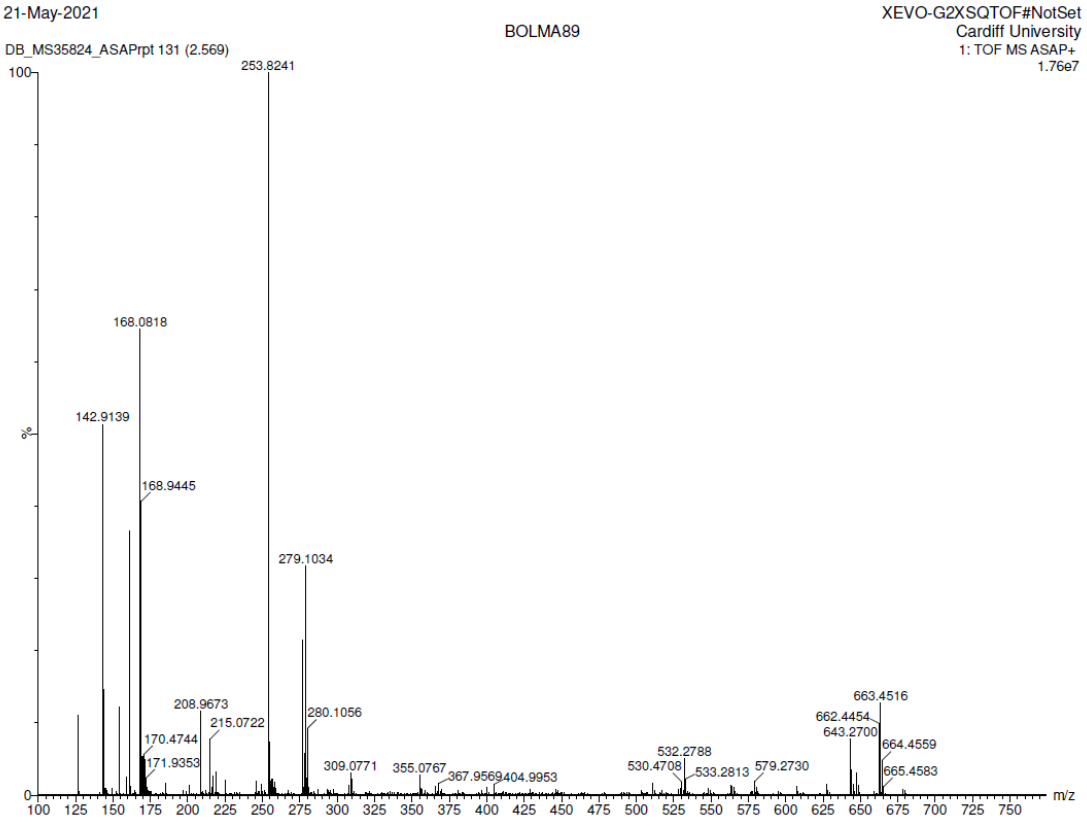

Figure A.53. HRMS, ASAP+, TOF.

Characterisation of (6,6'-bis(4-(trifluoromethyl)phenyl)-[1,1'-binaphthalene]-2,2'-diyl)bis(methylsulfane) 20

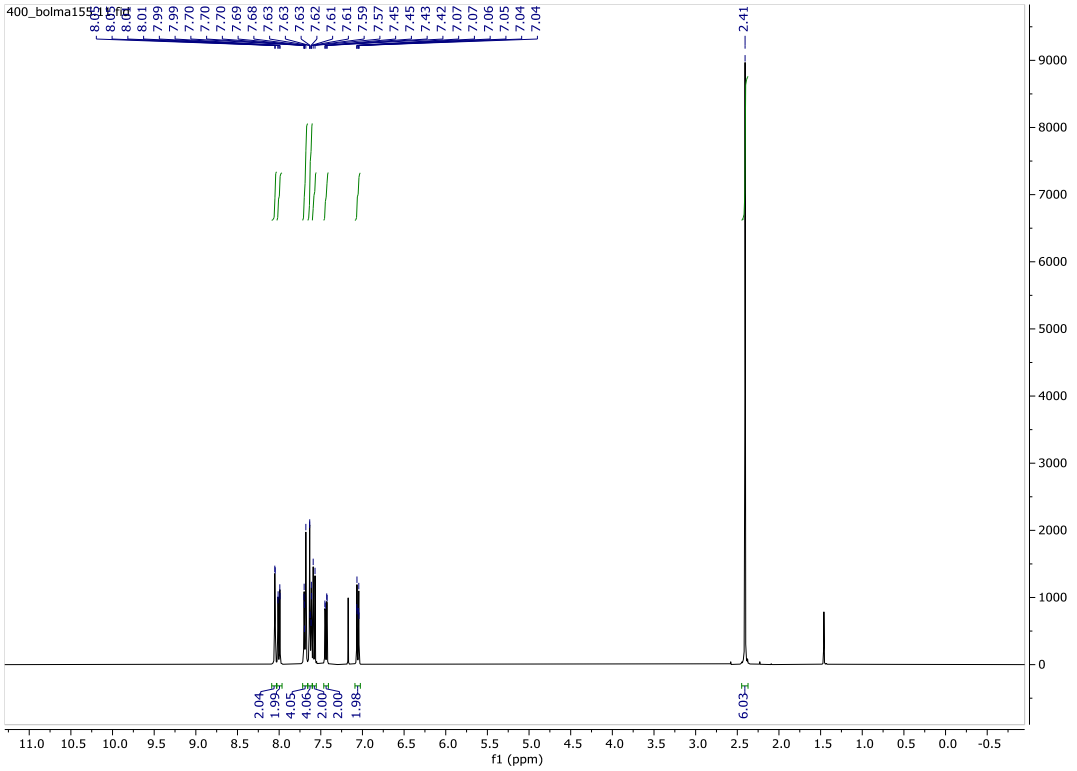

Figure A.54. ^{1}H NMR, 400 MHz, $CDCl_3$.

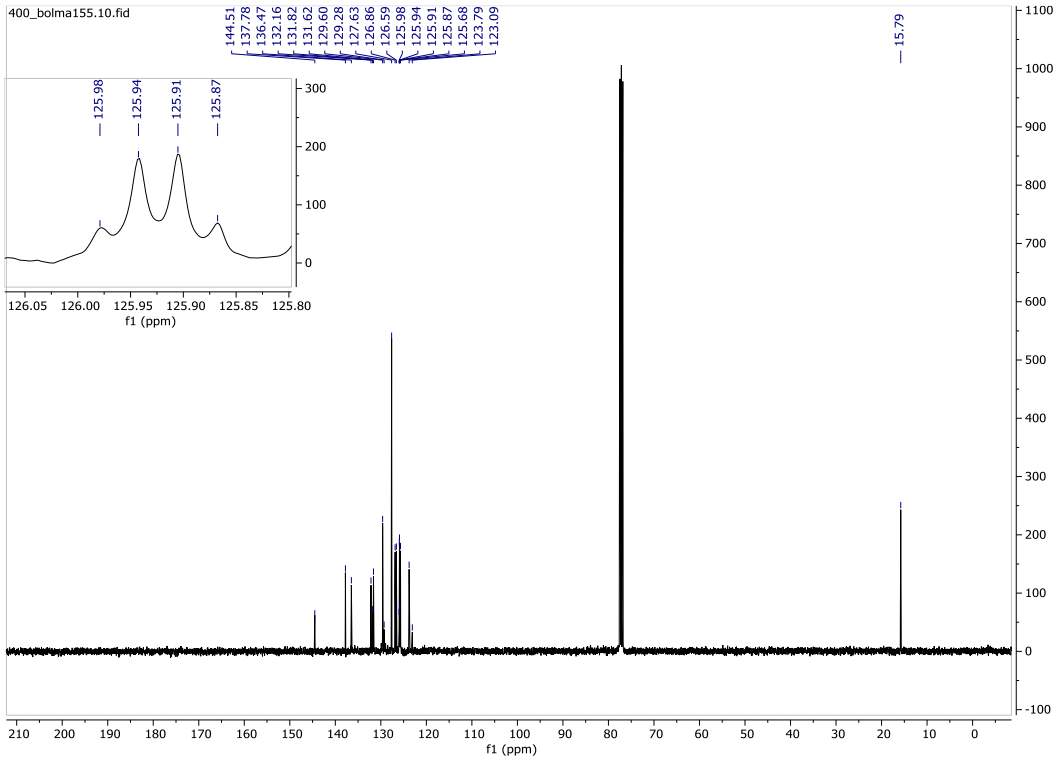

Figure A.55. ^{13}C NMR, 100 MHz, $CDCl_3$.

Elemental Composition Report **Page 1**

Single Mass Analysis
Tolerance = 5.0 PPM / DBE: min = -1.5, max = 50.0
Element prediction: Off

Monoisotopic Mass, Odd and Even Electron Ions
16 formula(e) evaluated with 1 results within limits (up to 50 best isotopic matches for each mass)
Elements Used:
C: 0-36 H: 0-24 S: 0-2 F: 0-6

20-Aug-2018 BOIMA155 School of chemistry Cardiff University
DB_MS22364 55 (1.817) Cm (55-42:46) TOF MS EI+
1.12e+004

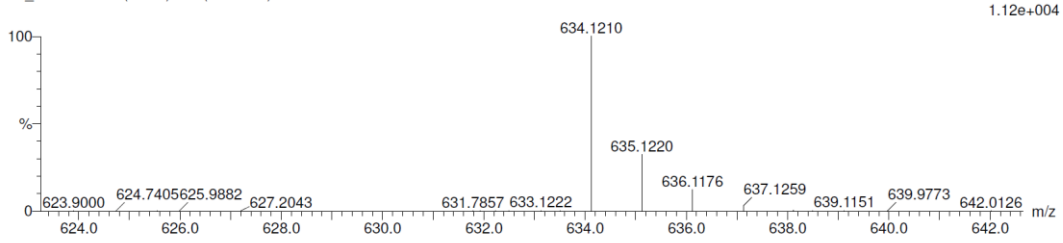

Minimum:				-1.5		
Maximum:		5.0	5.0	50.0		
Mass	Calc. Mass	mDa	PPM	DBE	i-FIT	Formula
634.1210	634.1224	-1.4	-2.2	22.0	175.2	C36 H24 S2 F6

Figure A.56. Elemental composition report.

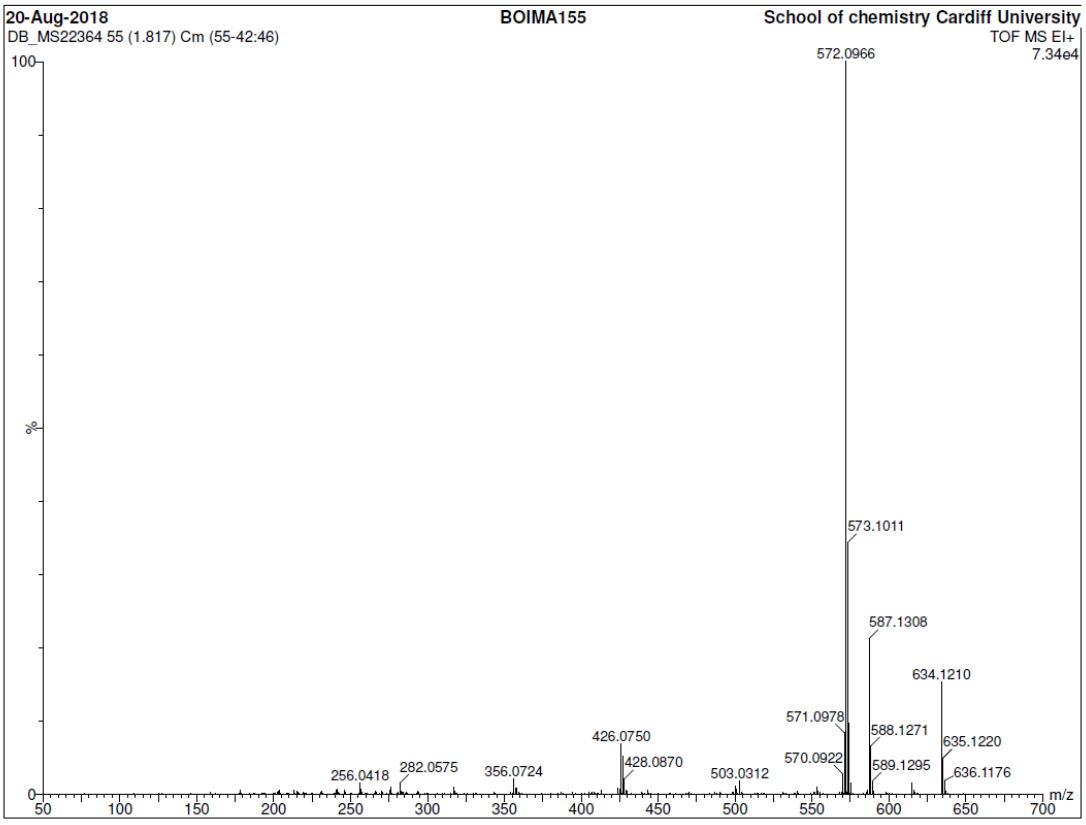

Figure A.57. HRMS, EI+, TOF.

Characterisation of 2,2'-bis(methylsulfinyl)-6,6'-bis(4-(trifluoromethyl)phenyl)-1,1'-binaphthalene 21

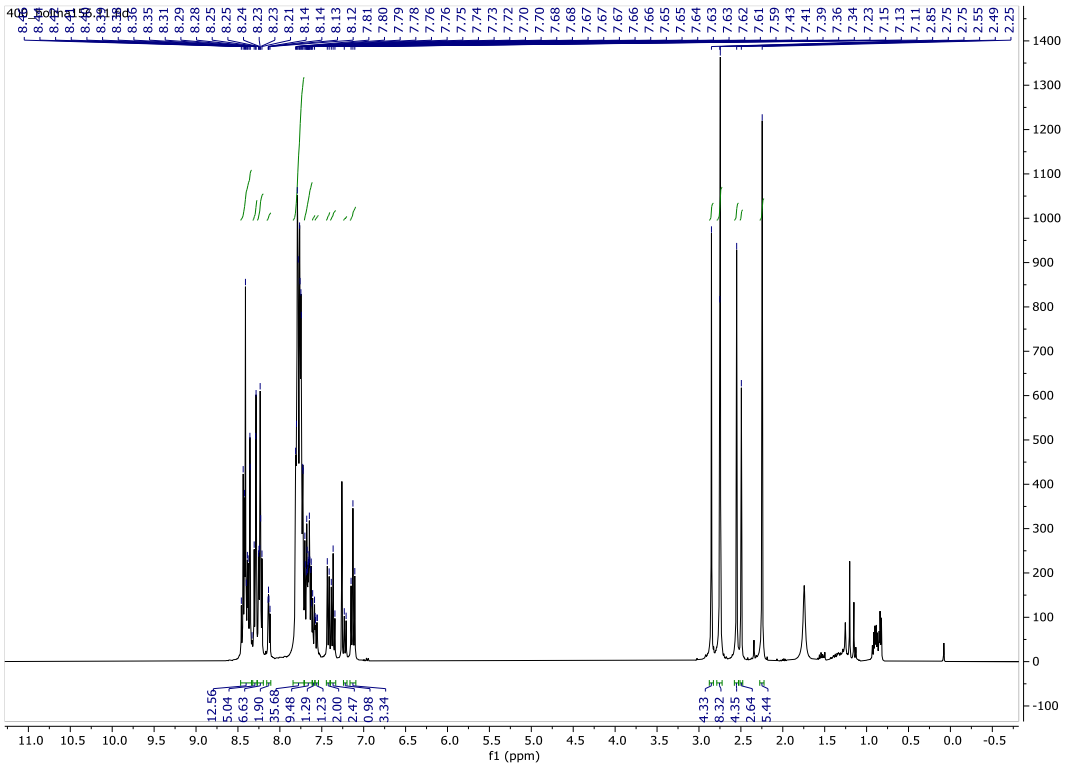

Figure A.58. ^{1}H NMR, 400 MHz, $CDCl_3$.

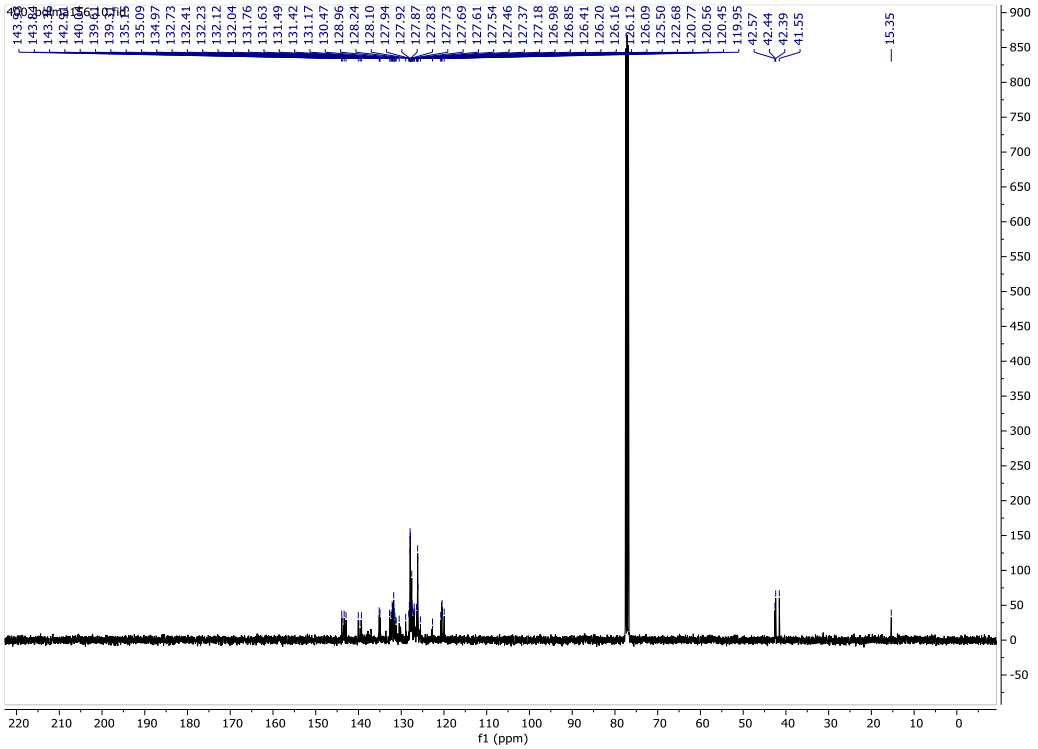

Figure A.59. ^{13}C NMR, 100 MHz, $CDCl_3$.

Elemental Composition Report **Page 1**

Single Mass Analysis
Tolerance = 5.0 PPM / DBE: min = -1.5, max = 100.0
Element prediction: Off
Number of isotope peaks used for i-FIT = 3

Monoisotopic Mass, Odd and Even Electron Ions
53 formula(e) evaluated with 1 results within limits (up to 50 best isotopic matches for each mass)
Elements Used:
C: 0-36 H: 0-25 O: 0-2 F: 0-6 S: 0-2

Minimum:				-1.5				
Maximum:		5.0	5.0	100.0				
Mass	Calc. Mass	mDa	PPM	DBE	i-FIT	Norm	Conf(%)	Formula
667.1197	667.1200	-0.3	-0.4	21.5	679.6	n/a	n/a	C36 H25 O2 F6 S2

Figure A.60. Elemental composition report.

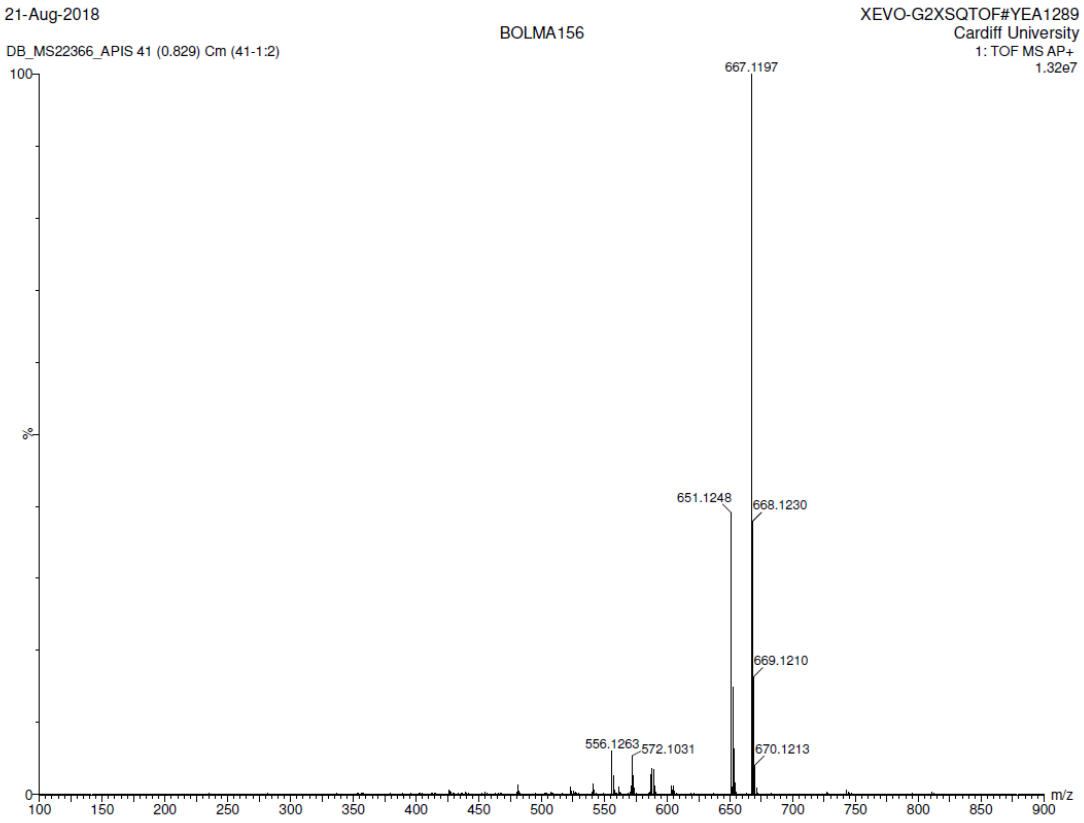

Figure A.61. HRMS, APCI+, TOF.

Characterisation of 2,8-bis(4-(trifluoromethyl)phenyl)thioxanthenothioxanthene 22

Elemental Composition Report **Page 1**

Single Mass Analysis
Tolerance = 5.0 PPM / DBE: min = -1.5, max = 100.0
Element prediction: Off
Number of isotope peaks used for i-FIT = 3

Monoisotopic Mass, Odd and Even Electron Ions
16 formula(e) evaluated with 1 results within limits (up to 50 closest results for each mass)
Elements Used:
C: 0-34 H: 0-17 F: 0-6 S: 0-2

Minimum:				-1.5				
Maximum:		5.0	5.0	100.0				
Mass	Calc. Mass	mDa	PPM	DBE	i-FIT	Norm	Conf(%)	Formula
603.0665	603.0676	-1.1	-1.8	23.5	443.7	n/a	n/a	C34 H17 F6 S2

Figure A.62. Elemental composition report.

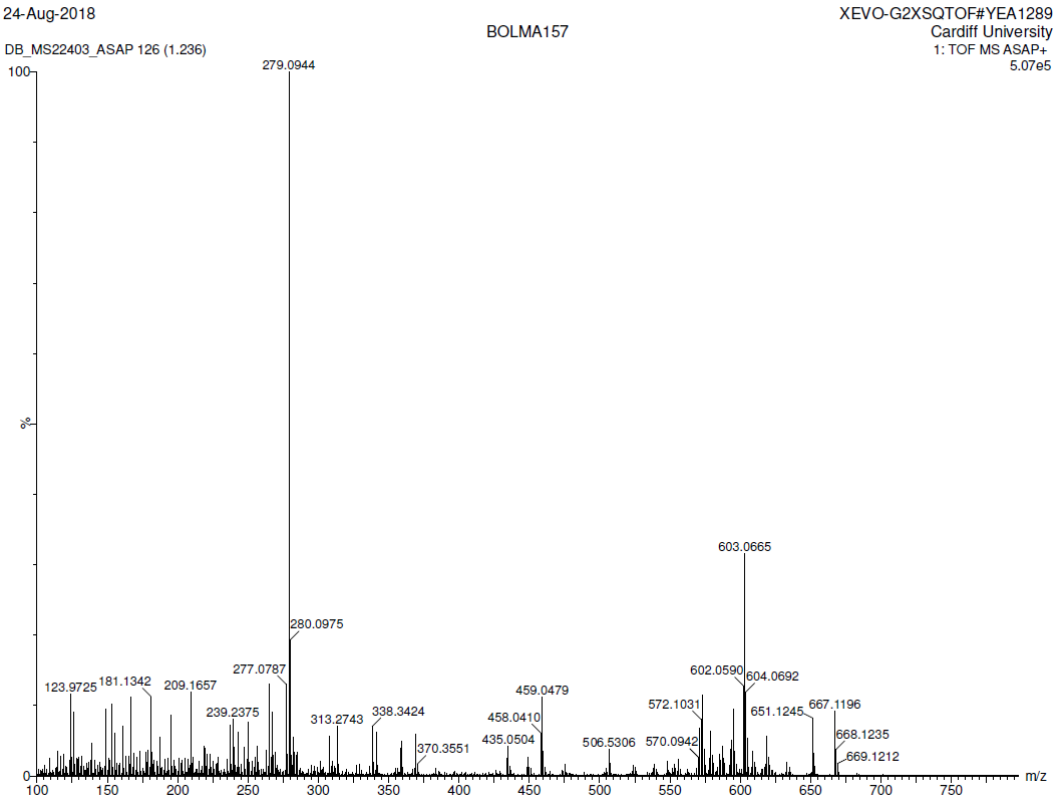

Figure A.63. HRMS, APCI+, TOF.

Characterisation of (6,6'-dioctyl-[1,1'-binaphthalene]-2,2'-diyl)bis(methylsulfane) 23

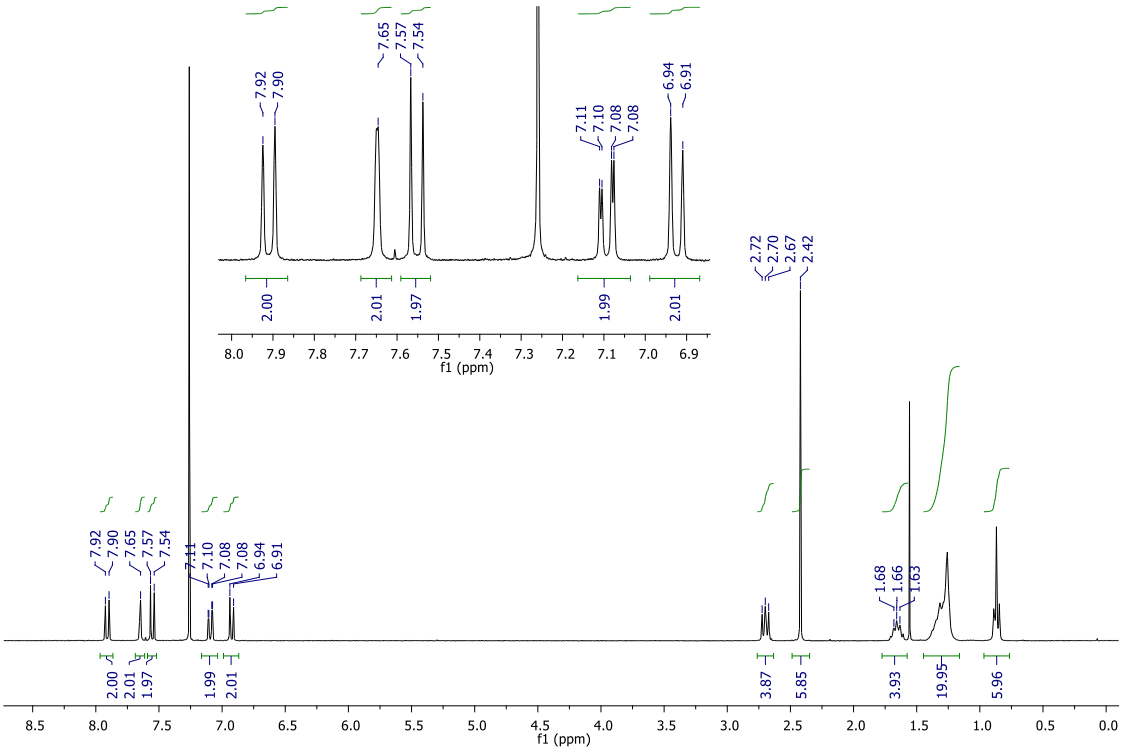

Figure A.64. ^{1}H NMR, 300 MHz, $CDCl_3$.

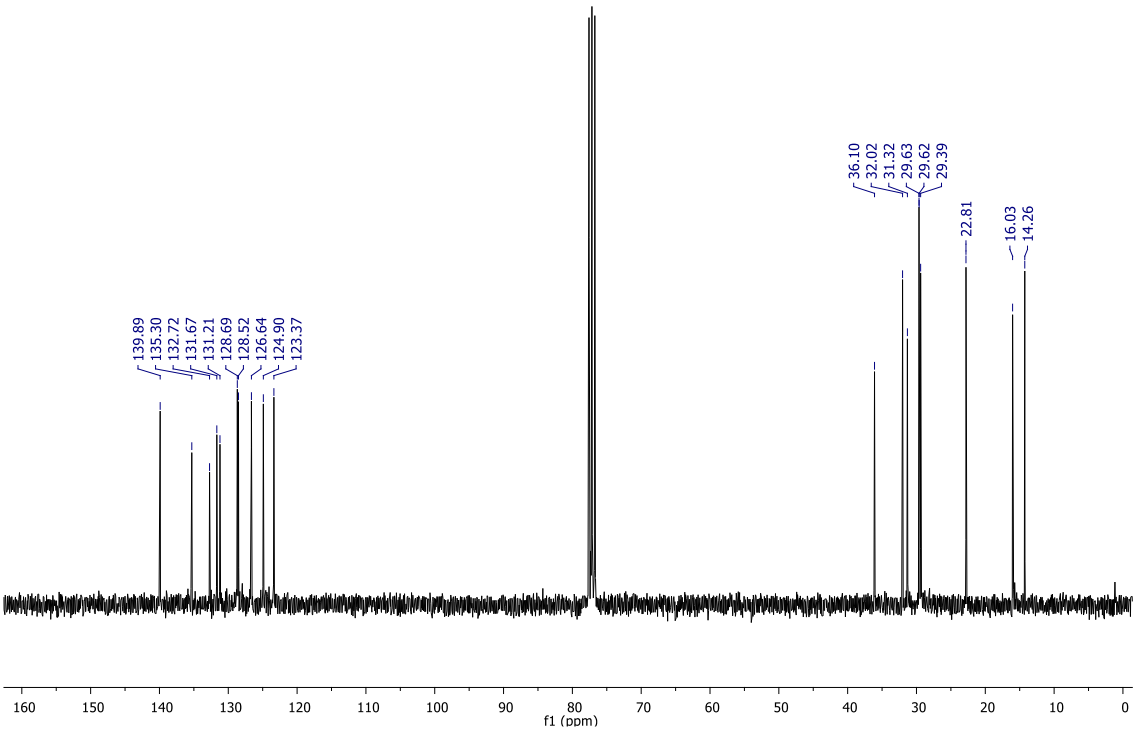

Figure A.65. ^{13}C NMR, 75 MHz, $CDCl_3$.

Elemental Composition Report **Page 1**

Single Mass Analysis
Tolerance = 5.0 PPM / DBE: min = -1.5, max = 100.0
Element prediction: Off
Number of isotope peaks used for i-FIT = 3

Monoisotopic Mass, Odd and Even Electron Ions
2 formula(e) evaluated with 1 results within limits (up to 50 best isotopic matches for each mass)
Elements Used:
C: 0-38 H: 0-51 S: 0-2

Minimum:				-1.5				
Maximum:		5.0	5.0	100.0				
Mass	Calc. Mass	mDa	PPM	DBE	i-FIT	Norm	Conf(%)	Formula
571.3435	571.3432	0.3	0.5	13.5	683.1	n/a	n/a	C38 H51 S2

Figure A.66. Elemental composition report.

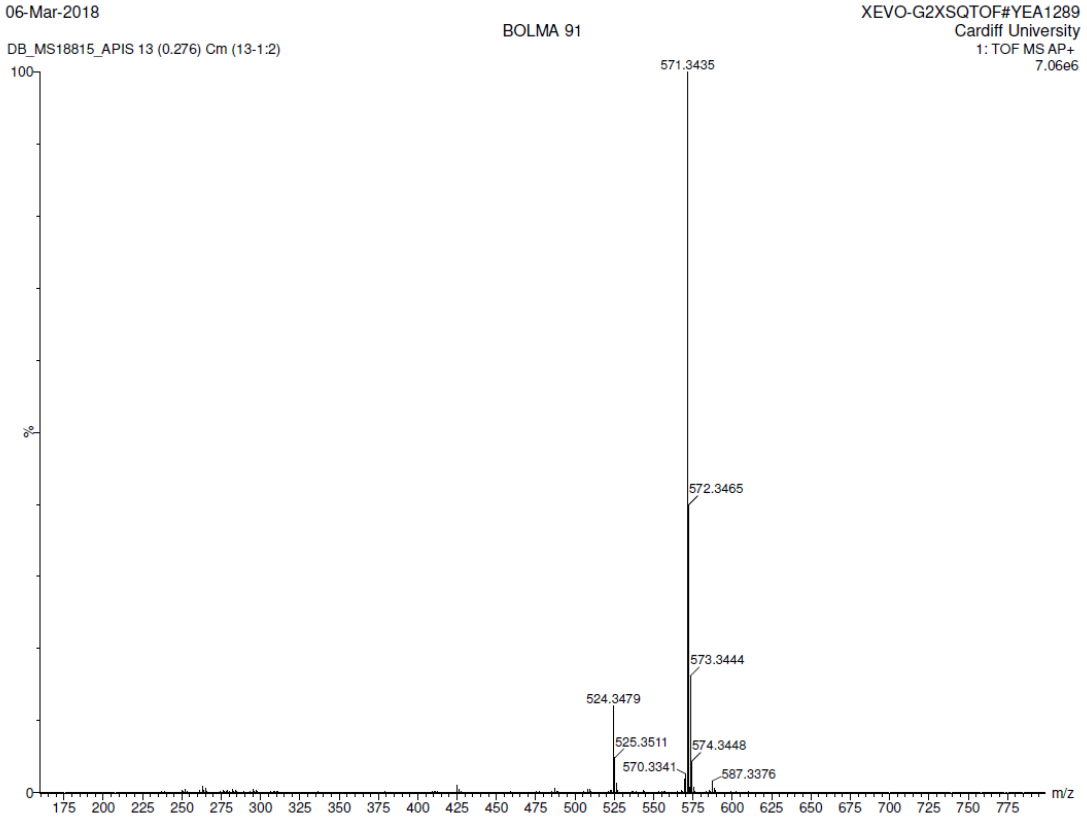

Figure A.67. HRMS, APCI+, TOF.

Characterisation of 2,2'-bis(methylsulfinyl)-6,6'-dioctyl-1,1'-binaphthalene 24

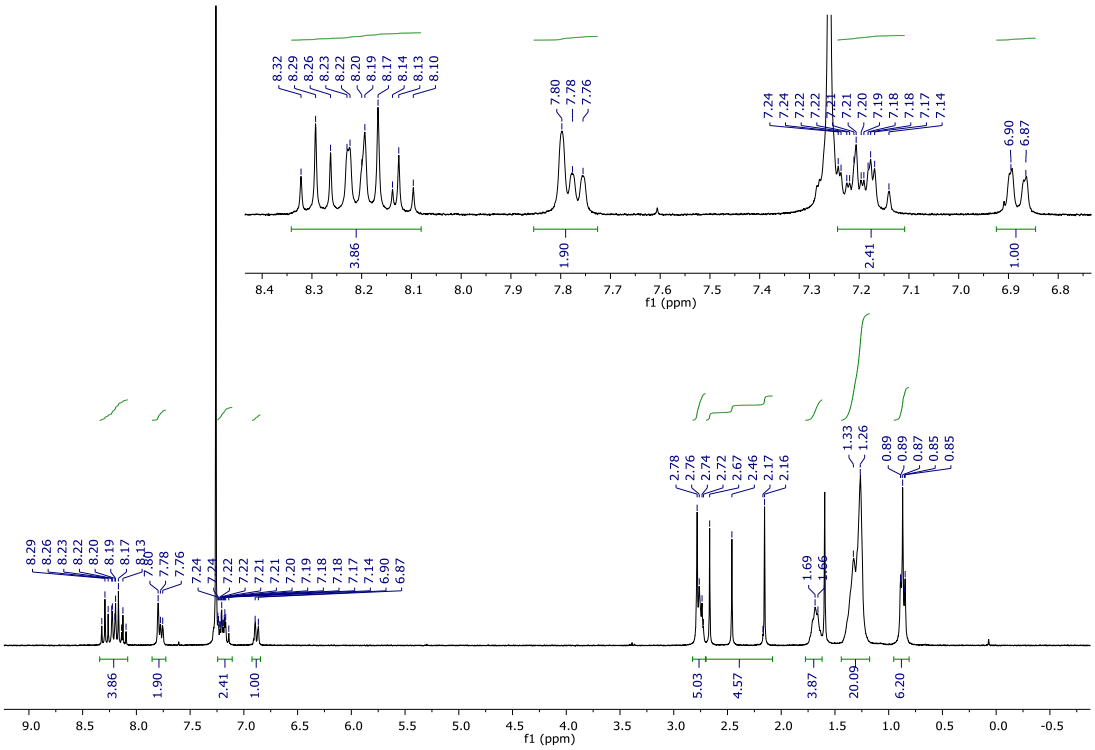

Figure A.68. ^{1}H NMR, 300 MHz, $CDCl_3$.

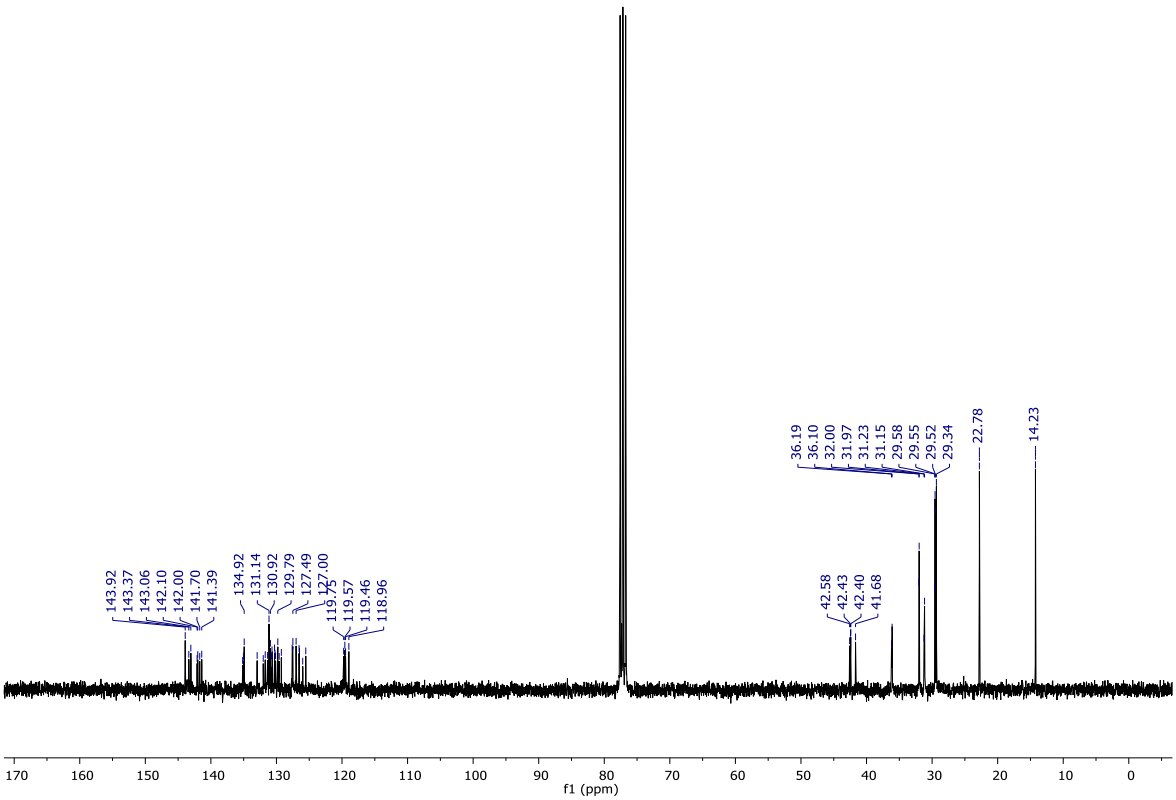

Figure A.69. ^{13}C NMR, 75 MHz, $CDCl_3$.

Elemental Composition Report **Page 1**

Single Mass Analysis
Tolerance = 5.0 PPM / DBE: min = -1.5, max = 100.0
Element prediction: Off
Number of isotope peaks used for i-FIT = 3

Monoisotopic Mass, Odd and Even Electron Ions
6 formula(e) evaluated with 1 results within limits (up to 50 best isotopic matches for each mass)
Elements Used:
C: 0-38 H: 0-51 O: 0-2 S: 0-2

Minimum:				-1.5				
Maximum:		5.0	5.0	100.0				
Mass	Calc. Mass	mDa	PPM	DBE	i-FIT	Norm	Conf(%)	Formula
603.3340	603.3330	1.0	1.7	13.5	660.2	n/a	n/a	C38 H51 O2 S2

Figure A.70. Elemental composition report.

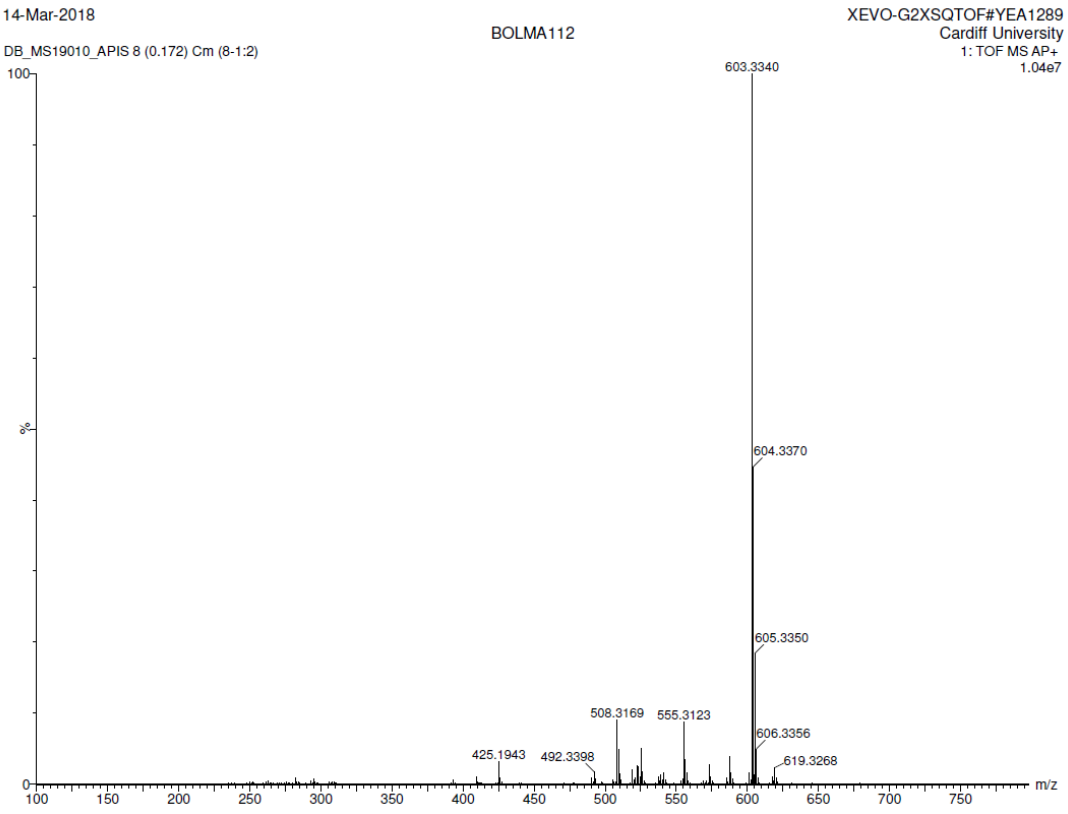

Figure A.71. HRMS, APCI+, TOF.

Characterisation of 2,8-dioctylthioxanthenothioxanthene 25

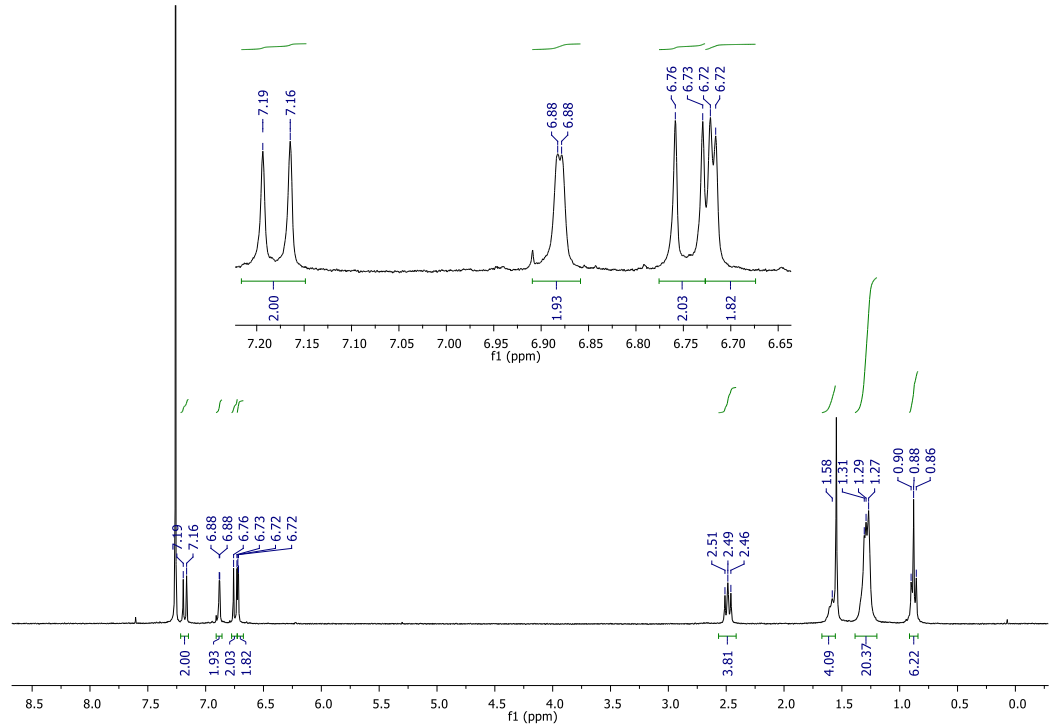

Figure A.72. ^{1}H NMR, 300 MHz, $CDCl_3$.

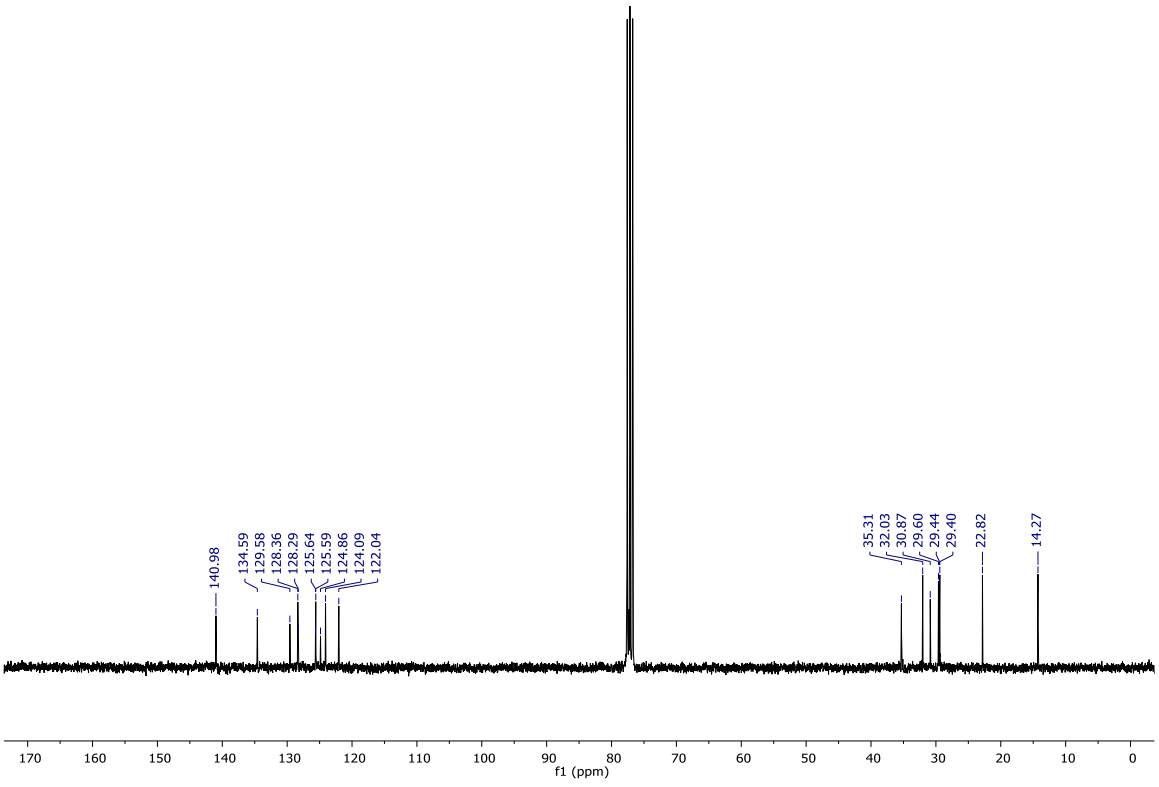

Figure A.73. ^{13}C NMR, 75 MHz, $CDCl_3$.

Elemental Composition Report **Page 1**

Single Mass Analysis
Tolerance = 20.0 PPM / DBE: min = -1.5, max = 50.0
Element prediction: Off

Monoisotopic Mass, Odd and Even Electron Ions
2 formula(e) evaluated with 1 results within limits (all results (up to 1000) for each mass)
Elements Used:
C: 0-36 H: 0-42 S: 0-2

19-Apr-2018 BOCMA123 School of Chemistry Cardiff University
DB_MS19405 159 (2.650) Cm (159-2:9) TOF MS EI+
4.78e+004

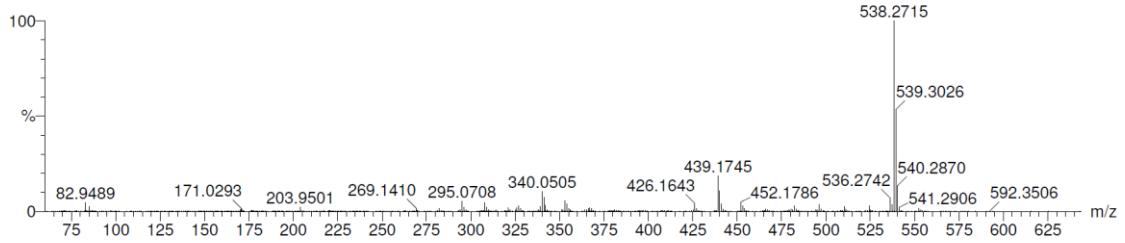

Minimum:				-1.5		
Maximum:		5.0	20.0	50.0		
Mass	Calc. Mass	mDa	PPM	DBE	i-FIT	Formula
538.2715	538.2728	-1.3	-2.4	16.0	1022.2	C36 H42 S2

Figure A.74. Elemental composition report.

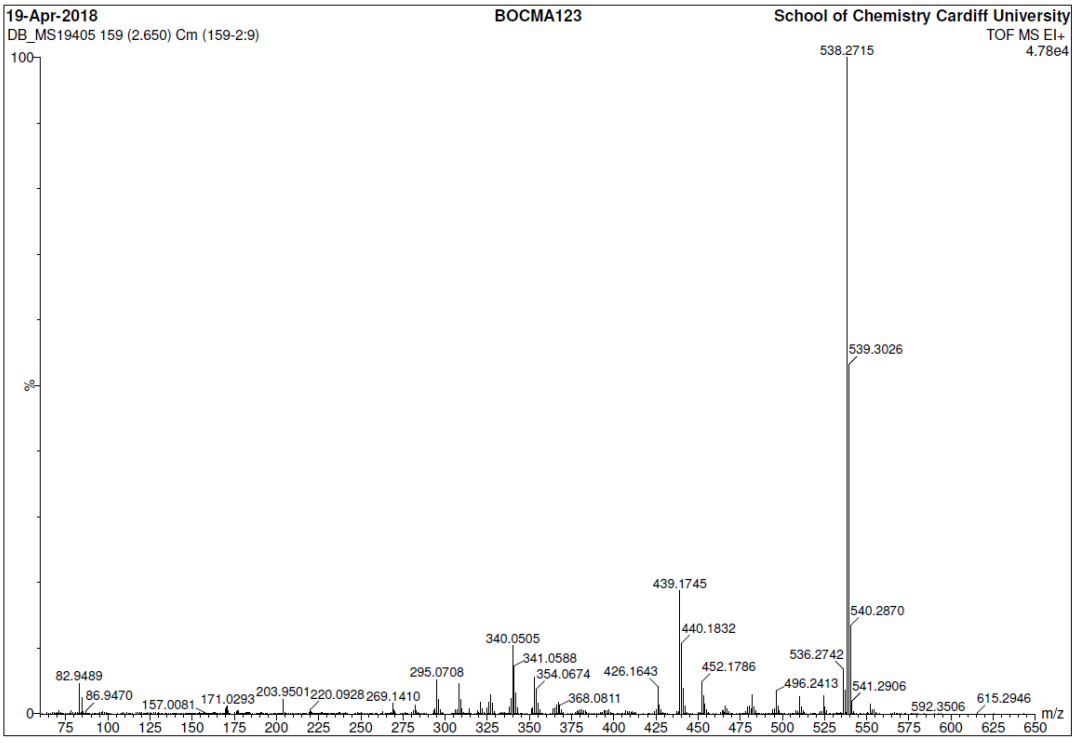

Figure A.75. HRMS, EI+, TOF.

Characterisation of thioxanthenothioxanthene-6-oxide 28

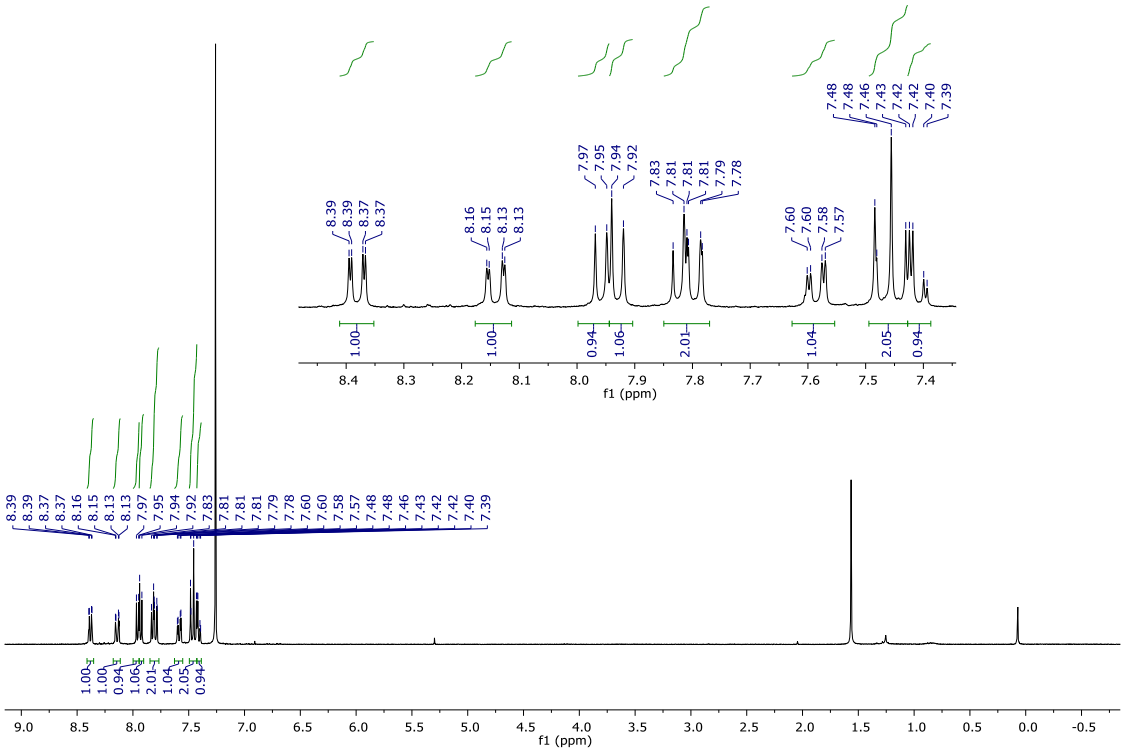

Figure A.76. ^{1}H NMR, 300 MHz, $CDCl_3$.

Elemental Composition Report **Page 1**

Single Mass Analysis
Tolerance = 5.0 PPM / DBE: min = -1.5, max = 50.0
Element prediction: Off
Number of isotope peaks used for i-FIT = 3

Monoisotopic Mass, Odd and Even Electron Ions
4 formula(e) evaluated with 1 results within limits (up to 50 best isotopic matches for each mass)
Elements Used:
C: 0-20 H: 0-11 O: 0-1 S: 0-2

Minimum:				-1.5				
Maximum:		5.0	5.0	50.0				
Mass	Calc. Mass	mDa	PPM	DBE	i-FIT	Norm	Conf(%)	Formula
331.0255	331.0251	0.4	1.2	15.5	827.9	n/a	n/a	C20 H11 O S2

Figure A.77. Elemental composition report.

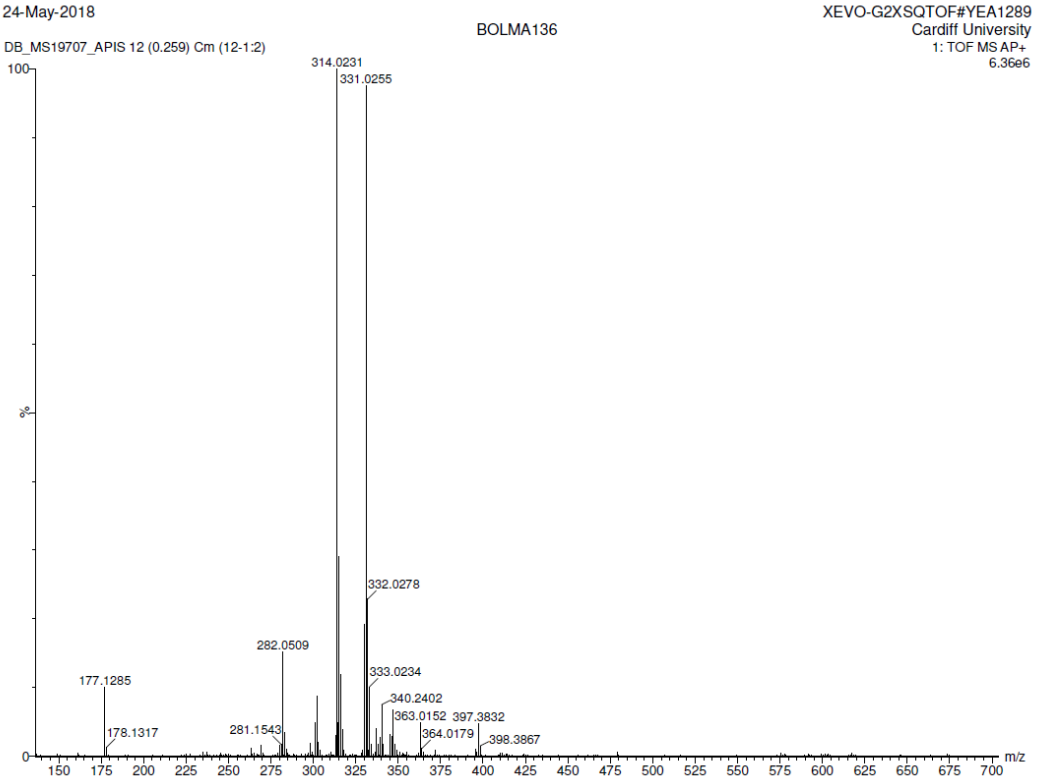

Figure A.78. HRMS, APCI+, TOF.

Characterisation of 2,8-dioctylthioxanthenothioxanthene-6-oxide 29

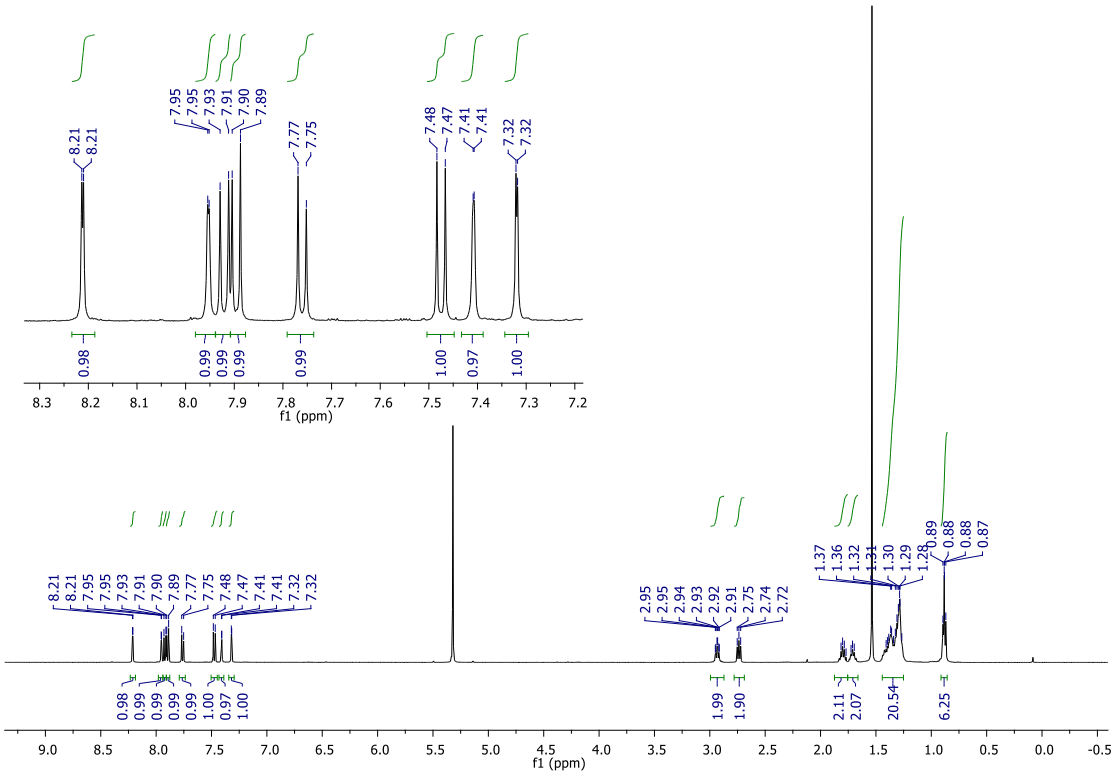

Figure A.79. ^{1}H NMR, 500 MHz, CD_2Cl_2.

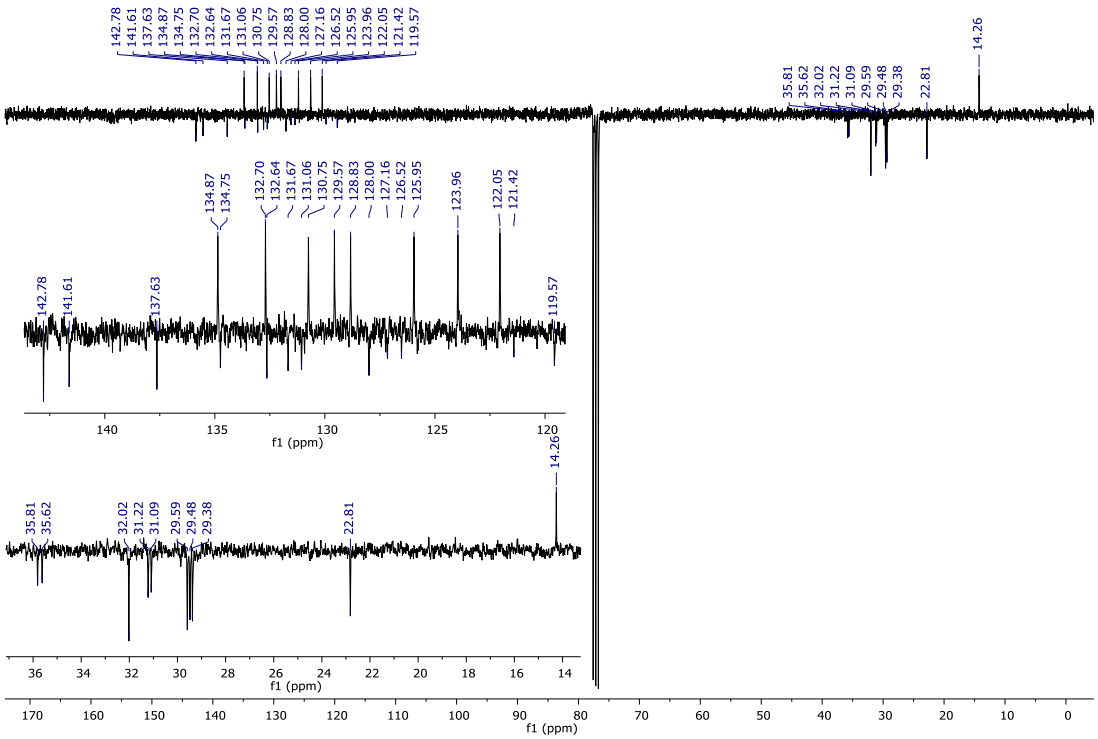

Figure A.80. ^{13}C NMR, 75 MHz, $CDCl_3$.

Elemental Composition Report **Page 1**

Single Mass Analysis
Tolerance = 5.0 PPM / DBE: min = -1.5, max = 50.0
Element prediction: Off
Number of isotope peaks used for i-FIT = 3

Monoisotopic Mass, Odd and Even Electron Ions
4 formula(e) evaluated with 1 results within limits (up to 50 best isotopic matches for each mass)
Elements Used:
C: 0-36 H: 0-43 O: 0-1 S: 0-2

Minimum:				-1.5				
Maximum:		5.0	5.0	50.0				
Mass	Calc. Mass	mDa	PPM	DBE	i-FIT	Norm	Conf(%)	Formula
555.2758	555.2755	0.3	0.5	15.5	753.0	n/a	n/a	C36 H43 O S2

Figure A.81. Elemental composition report.

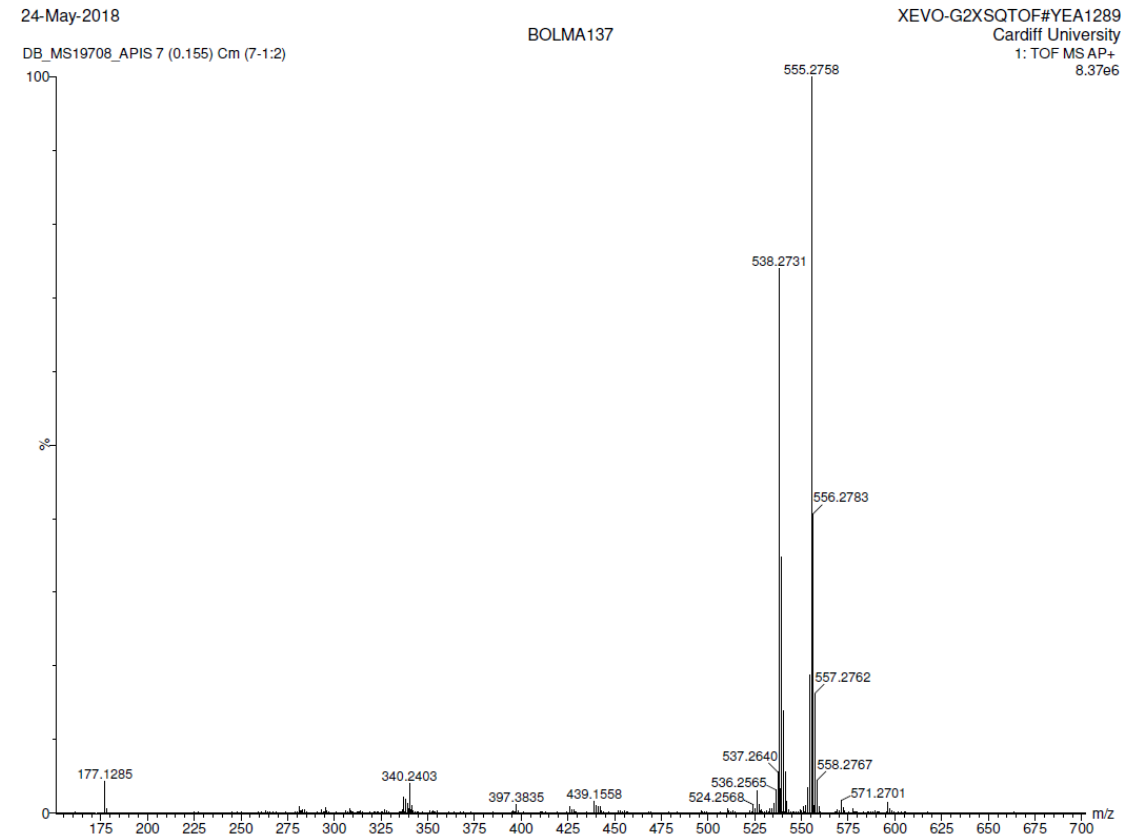

Figure A.82. HRMS, APCI+, TOF.

Characterisation of thioxanthenothioxanthene-6,12-dioxide 30

Mixture of diastereoisomers

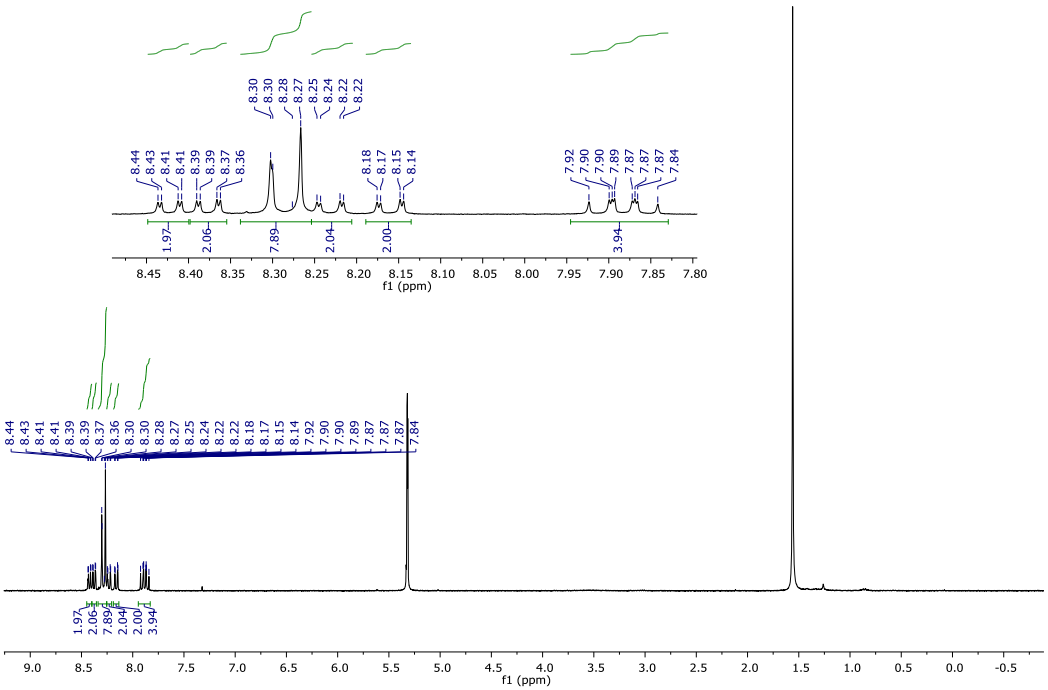

Figure A.83. ^{1}H NMR, 300 MHz, CD_2Cl_2.

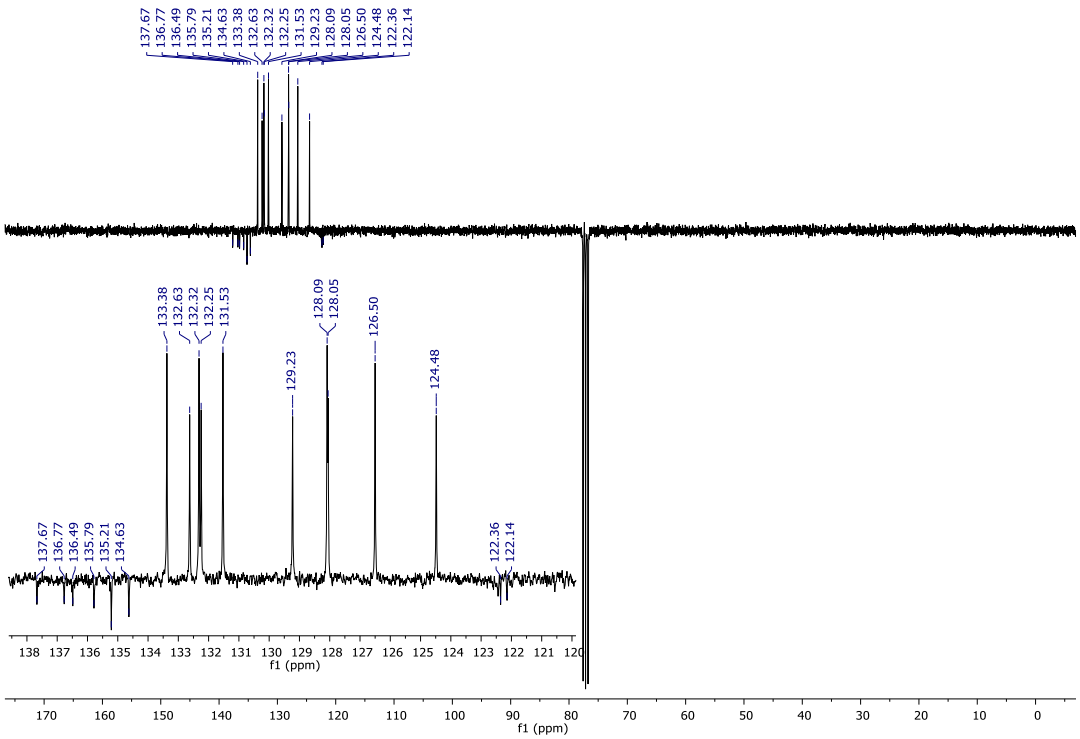

Figure A.84. ^{13}C NMR, 75 MHz, $CDCl_3$.

Elemental Composition Report **Page 1**

Single Mass Analysis
Tolerance = 5.0 PPM / DBE: min = -1.5, max = 100.0
Element prediction: Off
Number of isotope peaks used for i-FIT = 3

Monoisotopic Mass, Odd and Even Electron Ions
6 formula(e) evaluated with 1 results within limits (up to 50 best isotopic matches for each mass)
Elements Used:
C: 0-20 H: 0-11 O: 0-2 S: 0-2

Minimum:				-1.5				
Maximum:		5.0	5.0	100.0				
Mass	Calc. Mass	mDa	PPM	DBE	i-FIT	Norm	Conf(%)	Formula
347.0211	347.0200	1.1	3.2	15.5	760.4	n/a	n/a	C20 H11 O2 S2

Figure A.85. Elemental composition report.

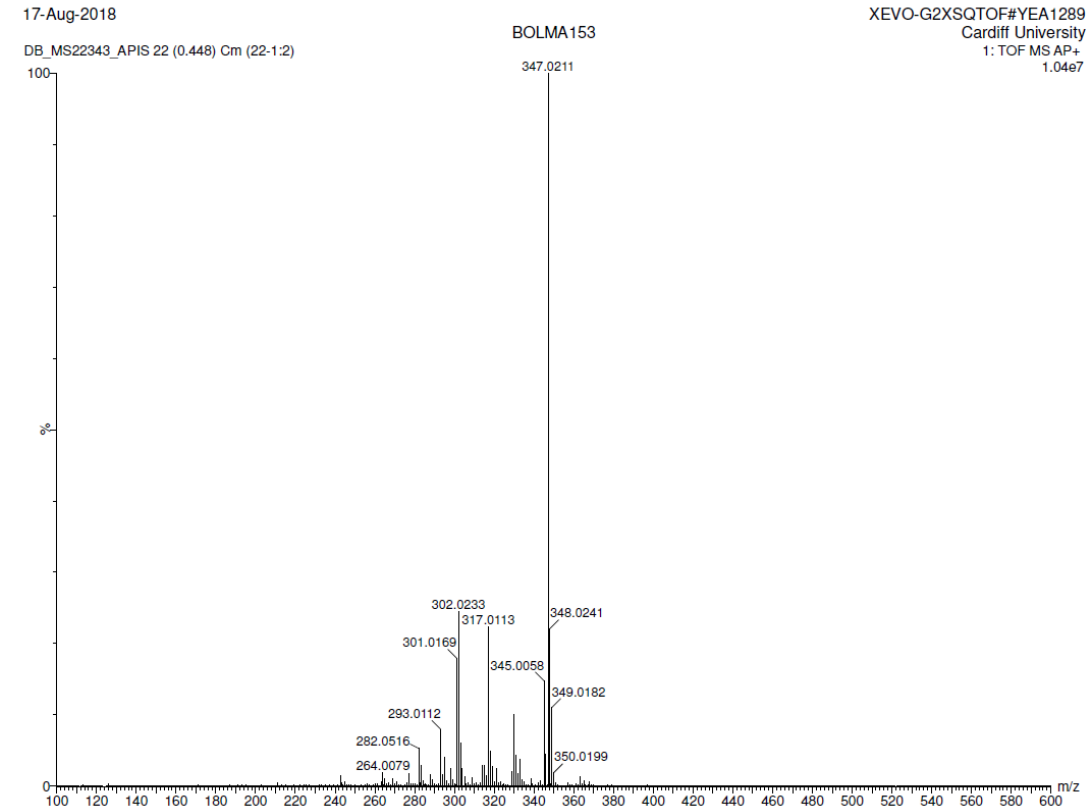

Figure A.86. HRMS, APCI+, TOF.

Isomer *trans*-30

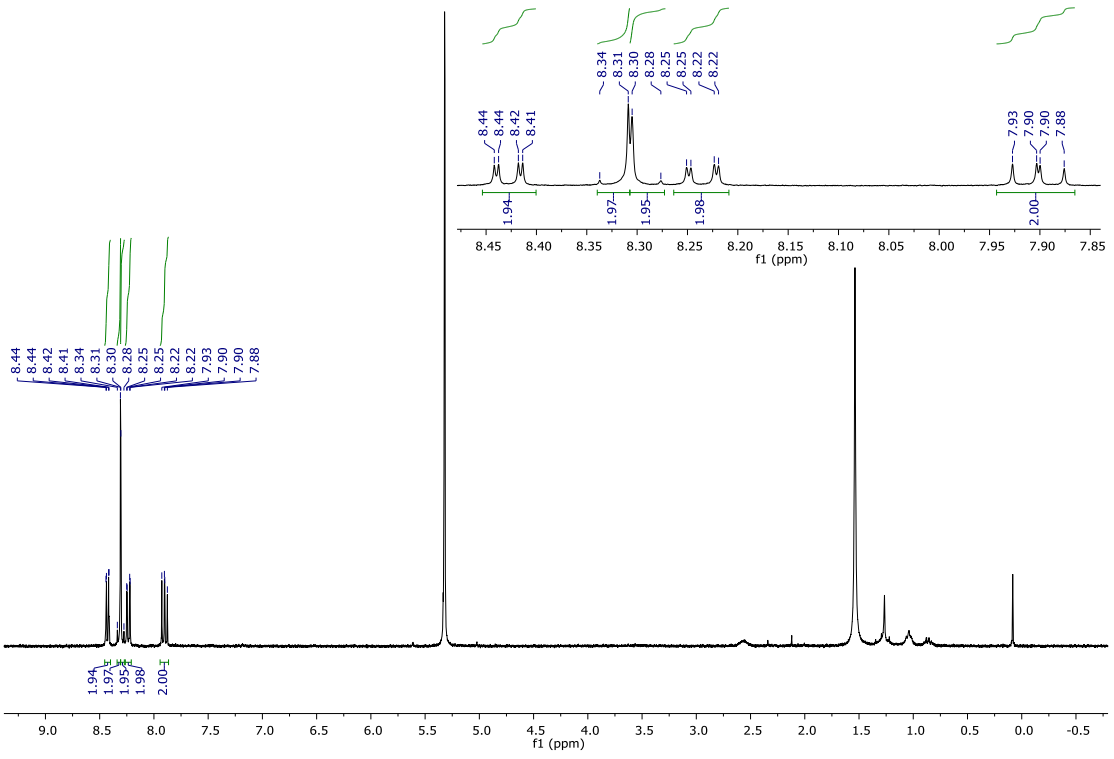

Figure A.87. ^{1}H NMR, 300 MHz, CD_2Cl_2.

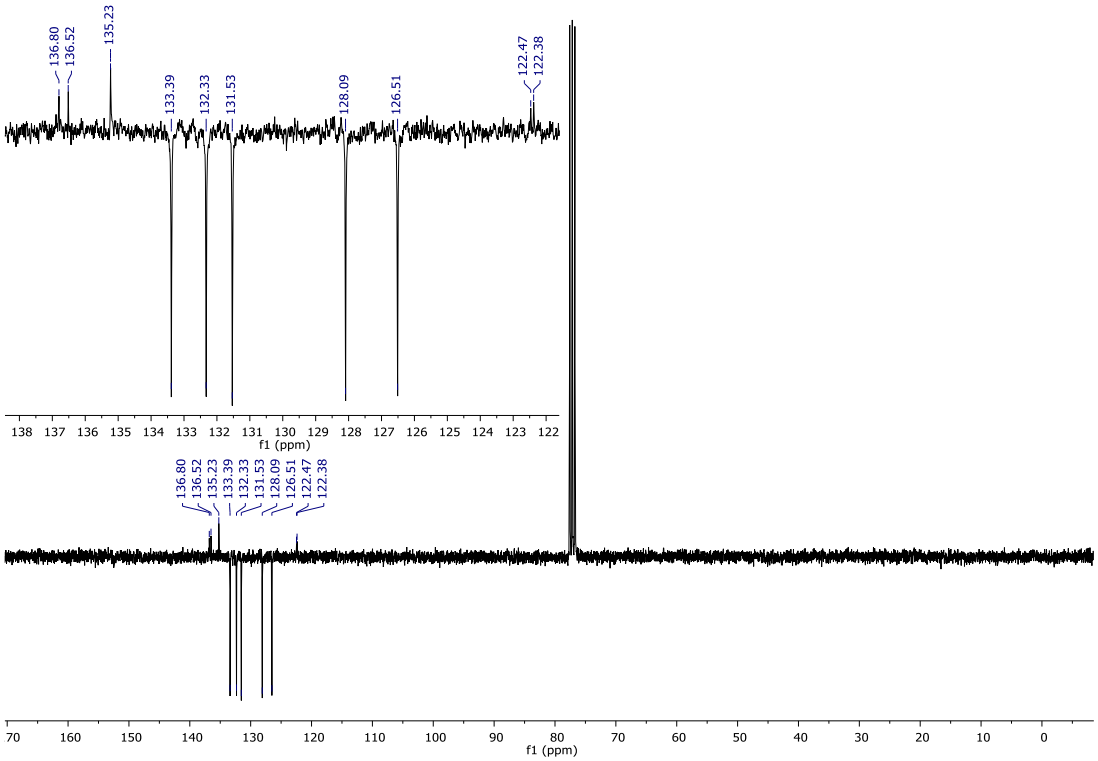

Figure A.88. ^{13}C NMR, 75 MHz, $CDCl_3$.

Elemental Composition Report **Page 1**

Single Mass Analysis
Tolerance = 5.0 PPM / DBE: min = -1.5, max = 50.0
Element prediction: Off
Number of isotope peaks used for i-FIT = 3

Monoisotopic Mass, Odd and Even Electron Ions
6 formula(e) evaluated with 1 results within limits (up to 50 best isotopic matches for each mass)
Elements Used:
C: 0-20 H: 0-11 O: 0-2 S: 0-2

Minimum:				-1.5				
Maximum:		5.0	5.0	50.0				
Mass	Calc. Mass	mDa	PPM	DBE	i-FIT	Norm	Conf(%)	Formula
347.0190	347.0200	-1.0	-2.9	15.5	535.6	n/a	n/a	C20 H11 O2 S2

Figure A.89. Elemental composition report.

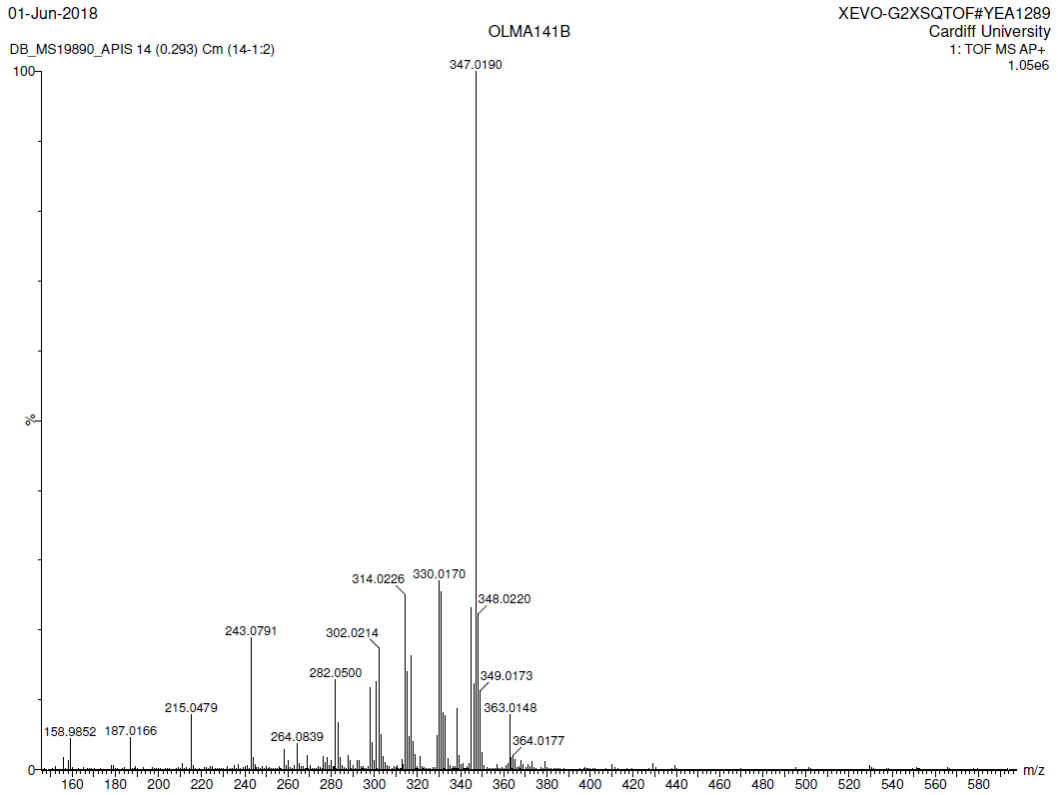

Figure A.90. HRMS, APCI+, TOF.

Characterisation of 2,8-dioctylthioxanthenothioxanthene-6,6,12,12-tetraoxide 32

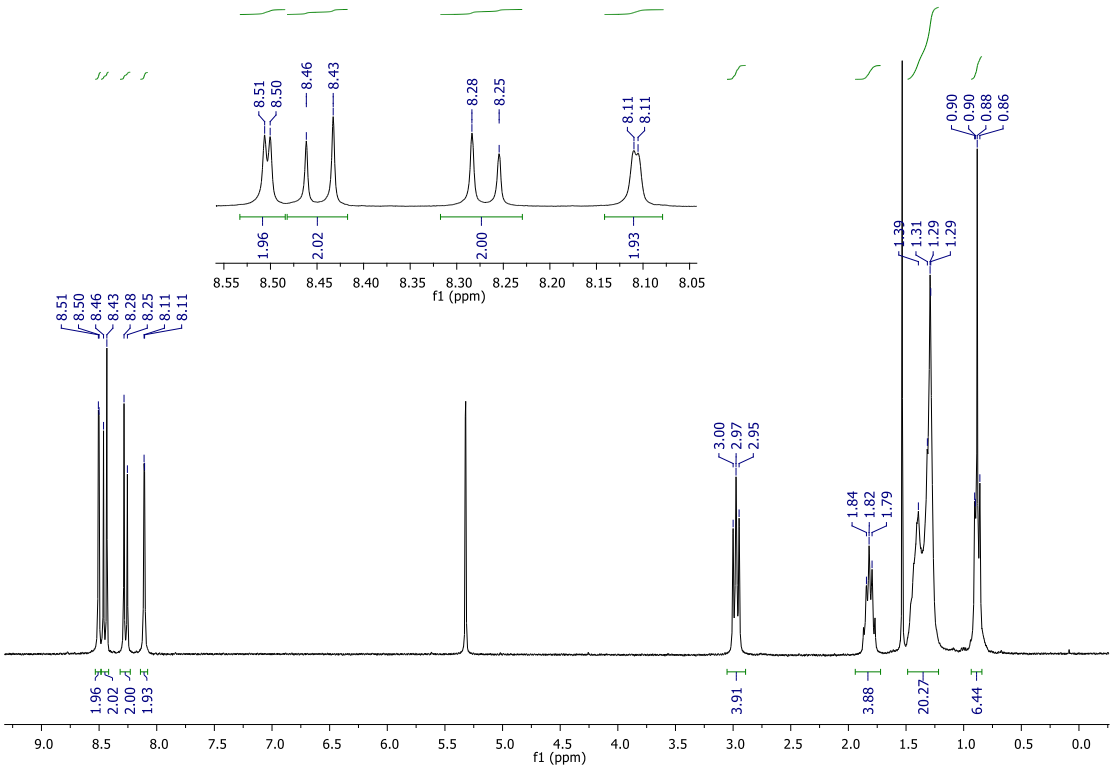

Figure A.91. ^{1}H NMR, 300 MHz, CD_2Cl_2.

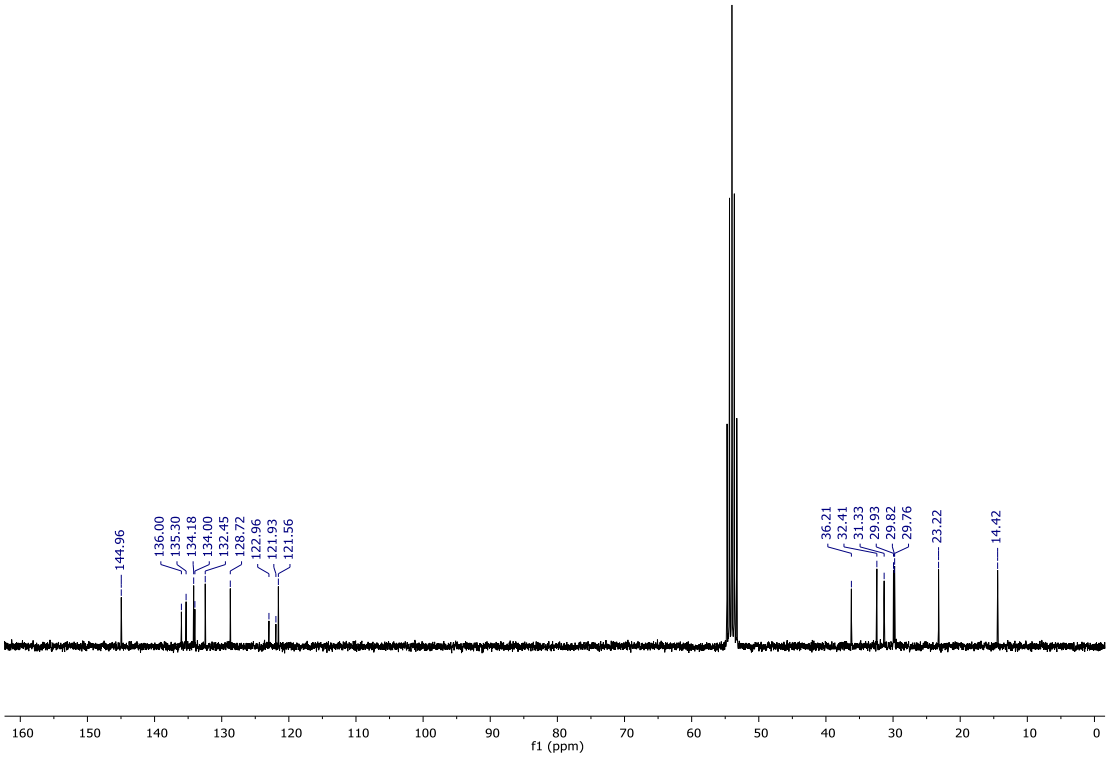

Figure A.92. ^{13}C NMR, 75 MHz, CD_2Cl_2.

Elemental Composition Report **Page 1**

Single Mass Analysis
Tolerance = 5.0 PPM / DBE: min = -1.5, max = 50.0
Element prediction: Off
Number of isotope peaks used for i-FIT = 3

Monoisotopic Mass, Odd and Even Electron Ions
12 formula(e) evaluated with 1 results within limits (up to 50 best isotopic matches for each mass)
Elements Used:
C: 0-36 H: 0-43 O: 0-4 S: 0-2

Minimum:				-1.5				
Maximum:		5.0	5.0	50.0				
Mass	Calc. Mass	mDa	PPM	DBE	i-FIT	Norm	Conf(%)	Formula
603.2603	603.2603	0.0	0.0	15.5	554.2	n/a	n/a	C36 H43 O4 S2

Figure A.93. Elemental composition report.

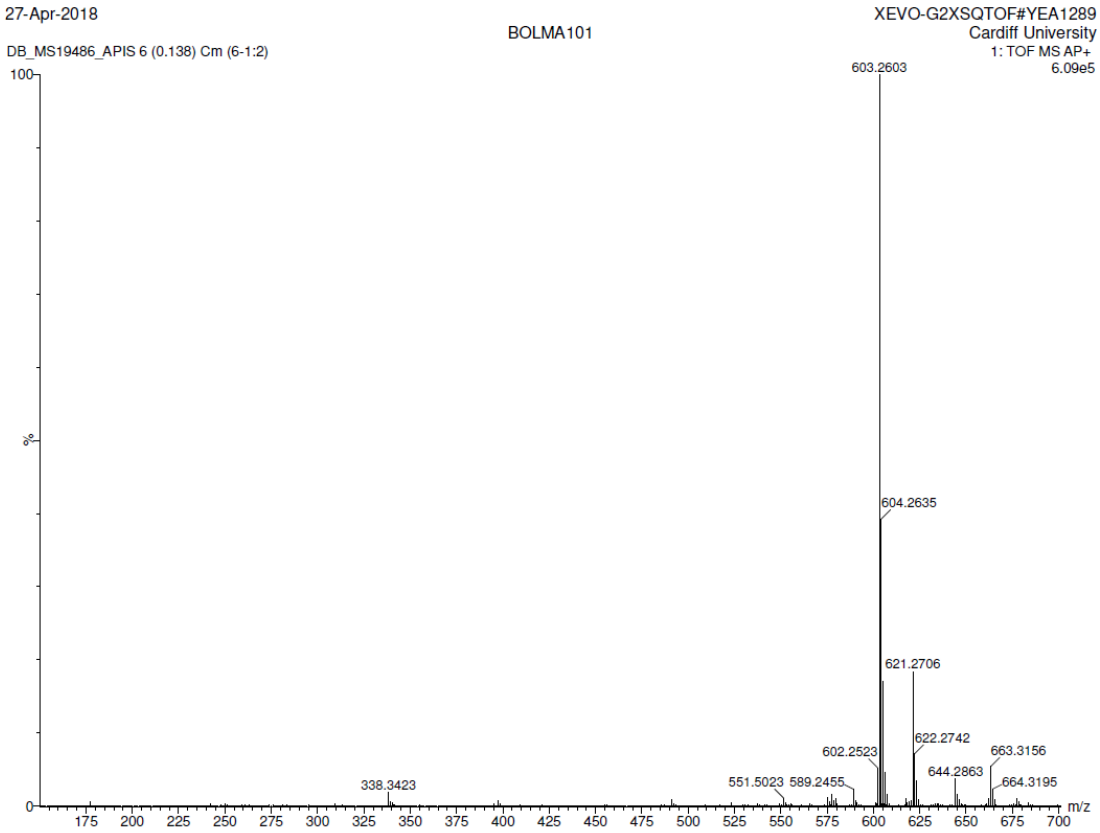

Figure A.94. HRMS, APCI+, TOF.

Characterisation of 2,2'-bis(methylselanyl)-1,1'-binaphthalene 34

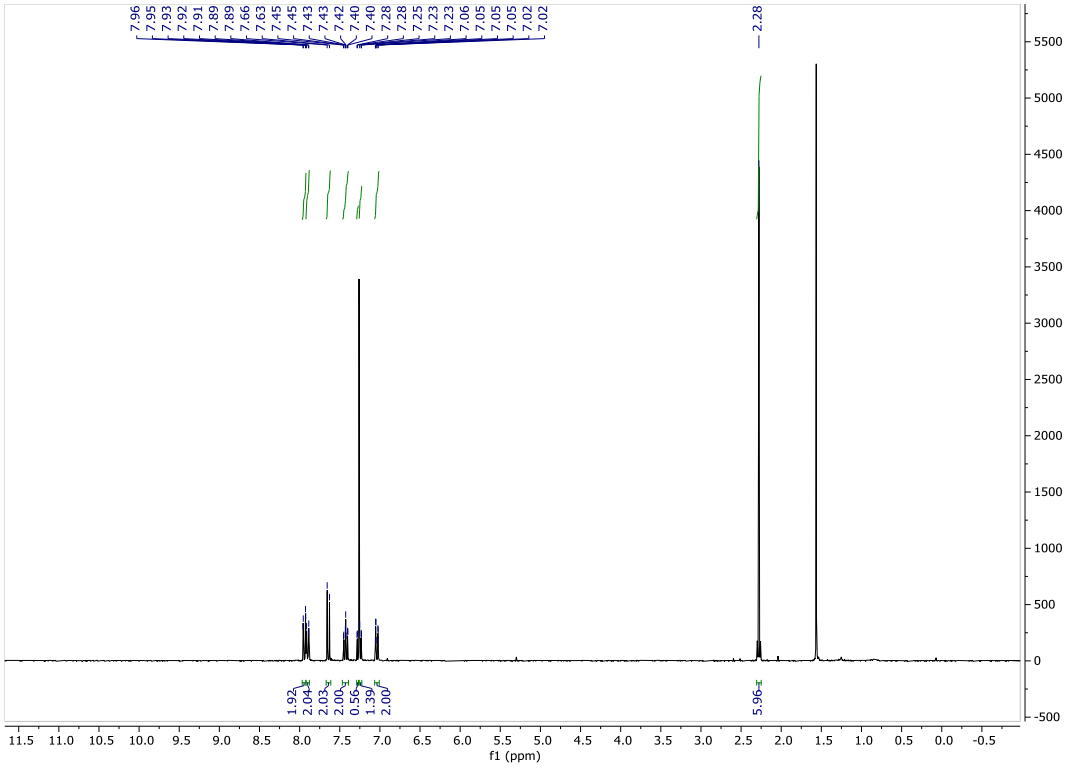

Figure A.95. ^{1}H NMR, 300 MHz, $CDCl_3$.

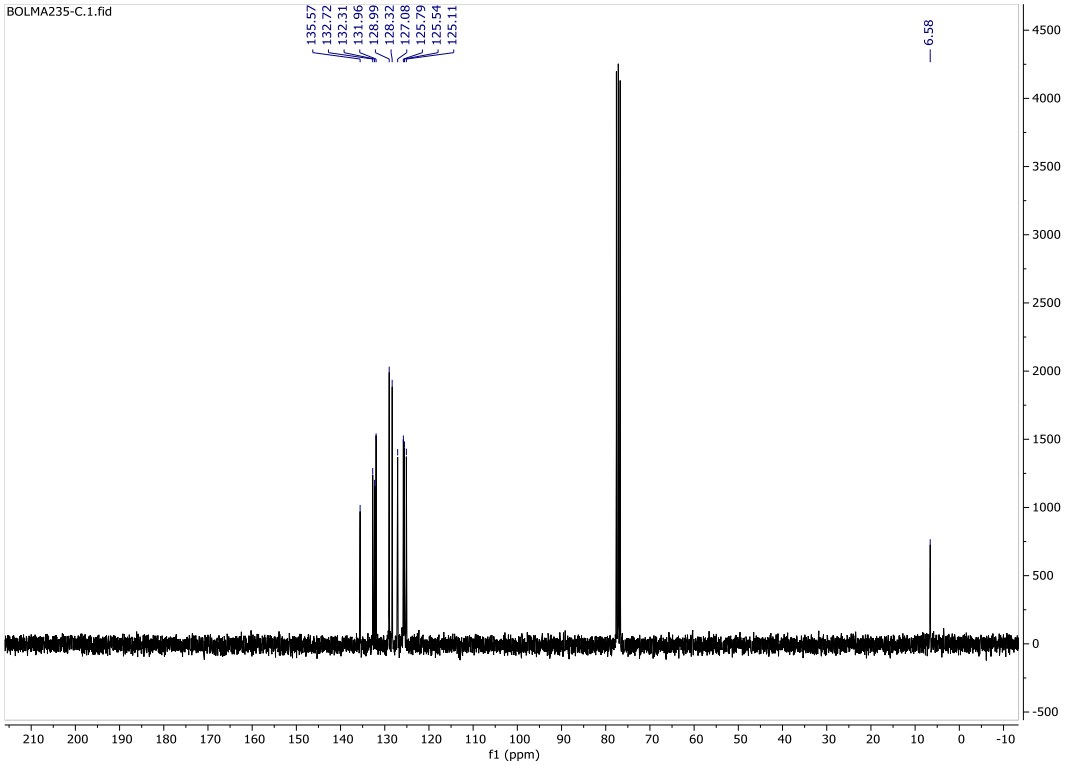

Figure A.96. ^{13}C NMR, 75 MHz, $CDCl_3$.

Elemental Composition Report **Page 1**

Single Mass Analysis
Tolerance = 5.0 PPM / DBE: min = -1.5, max = 200.0
Element prediction: Off
Number of isotope peaks used for i-FIT = 3

Monoisotopic Mass, Odd and Even Electron Ions
3 formula(e) evaluated with 1 results within limits (up to 50 closest results for each mass)
Elements Used:
C: 0-22 H: 0-19 78Se: 0-2

Minimum:				-1.5				
Maximum:		5.0	5.0	200.0				
Mass	Calc. Mass	mDa	PPM	DBE	i-FIT	Norm	Conf(%)	Formula
438.9840	438.9833	0.7	1.6	15.5	614.3	n/a	n/a	C22 H19 78Se2

Figure A.97. Elemental composition report.

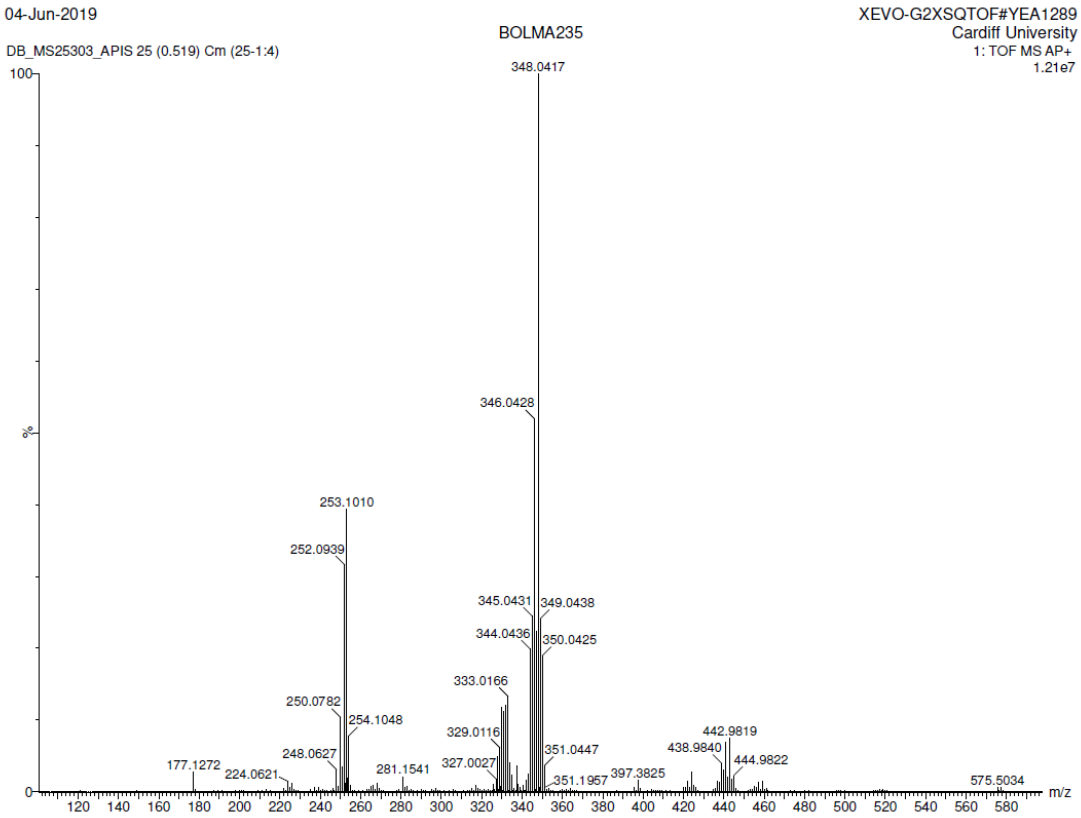

Figure A.98. HRMS, APCI+, TOF.

Characterisation of 2,2'-bis(methylseleninyl)-1,1'-binaphthalene 35

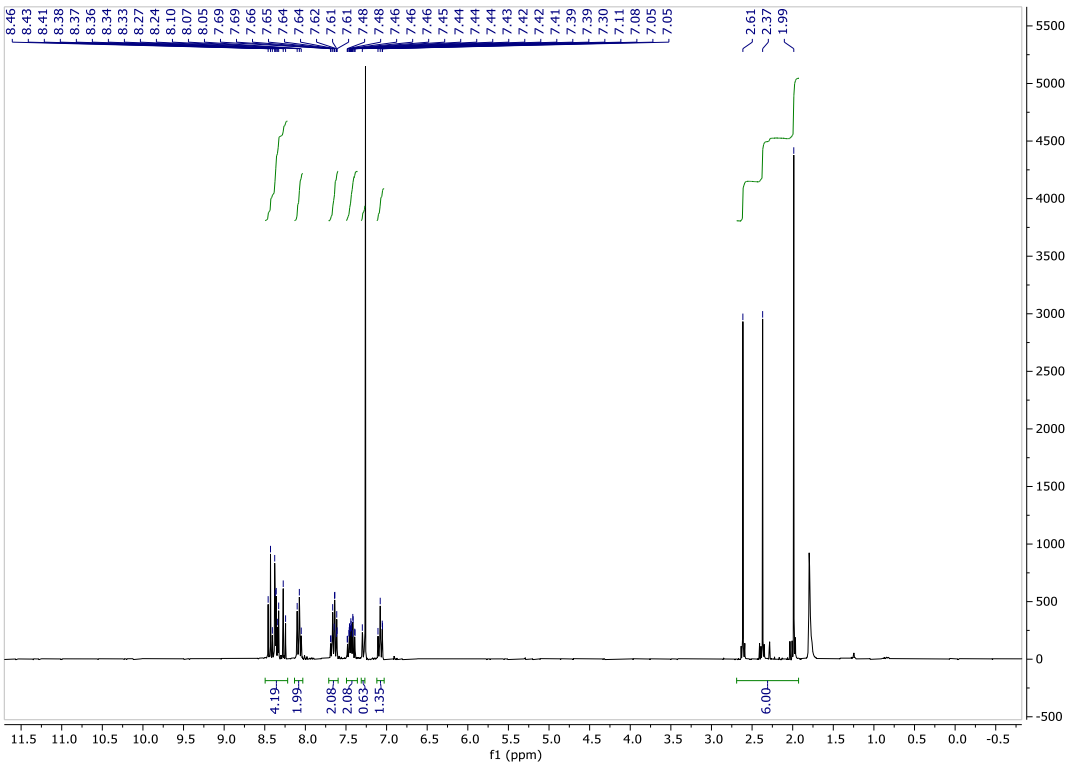

Figure A.99. ^{1}H NMR, 300 MHz, $CDCl_3$.

Elemental Composition Report **Page 1**

Single Mass Analysis
Tolerance = 5.0 PPM / DBE: min = -1.5, max = 200.0
Element prediction: Off
Number of isotope peaks used for i-FIT = 3

Monoisotopic Mass, Odd and Even Electron Ions
7 formula(e) evaluated with 1 results within limits (up to 50 closest results for each mass)
Elements Used:
C: 0-22 H: 0-19 O: 0-2 78Se: 0-2

Minimum:				-1.5				
Maximum:		5.0	5.0	200.0				
Mass	Calc. Mass	mDa	PPM	DBE	i-FIT	Norm	Conf(%)	Formula
470.9745	470.9731	1.4	3.0	15.5	822.4	n/a	n/a	C22 H19 O2 78Se2

Figure A.100. Elemental composition report.

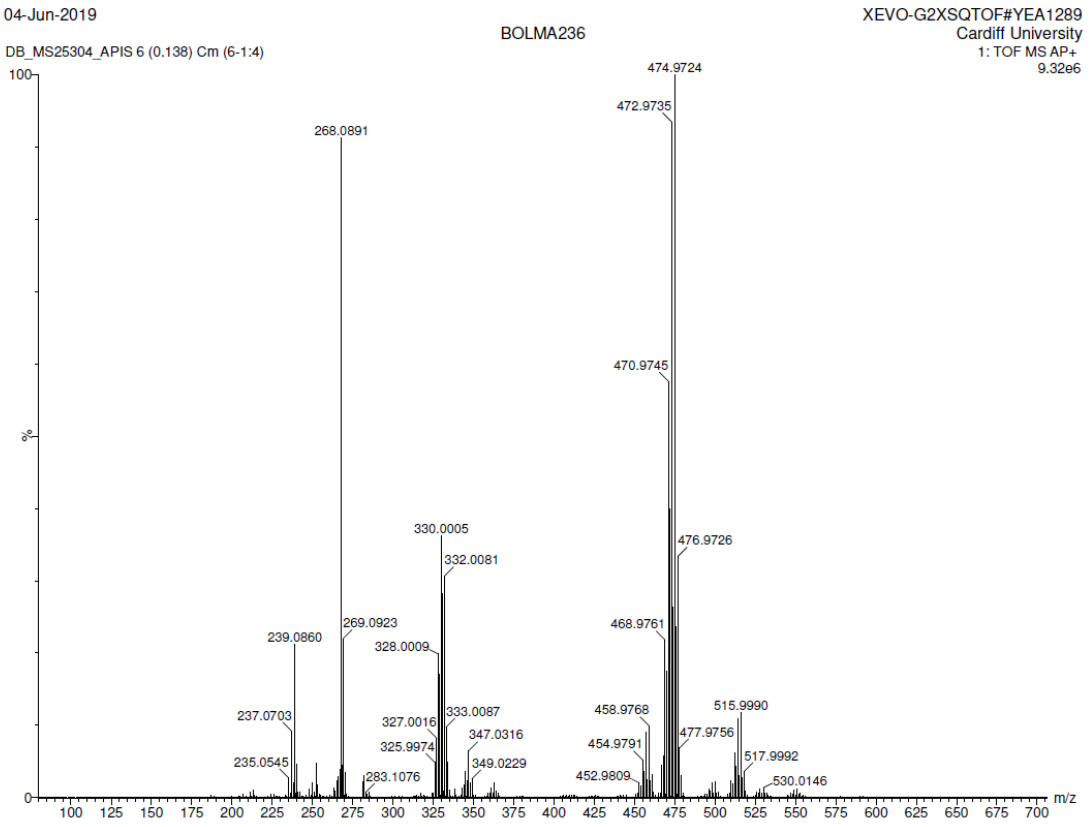

Figure A.101. HRMS, APCI+, TOF.

Characterisation of selenoxanthenoselenoxanthene 36

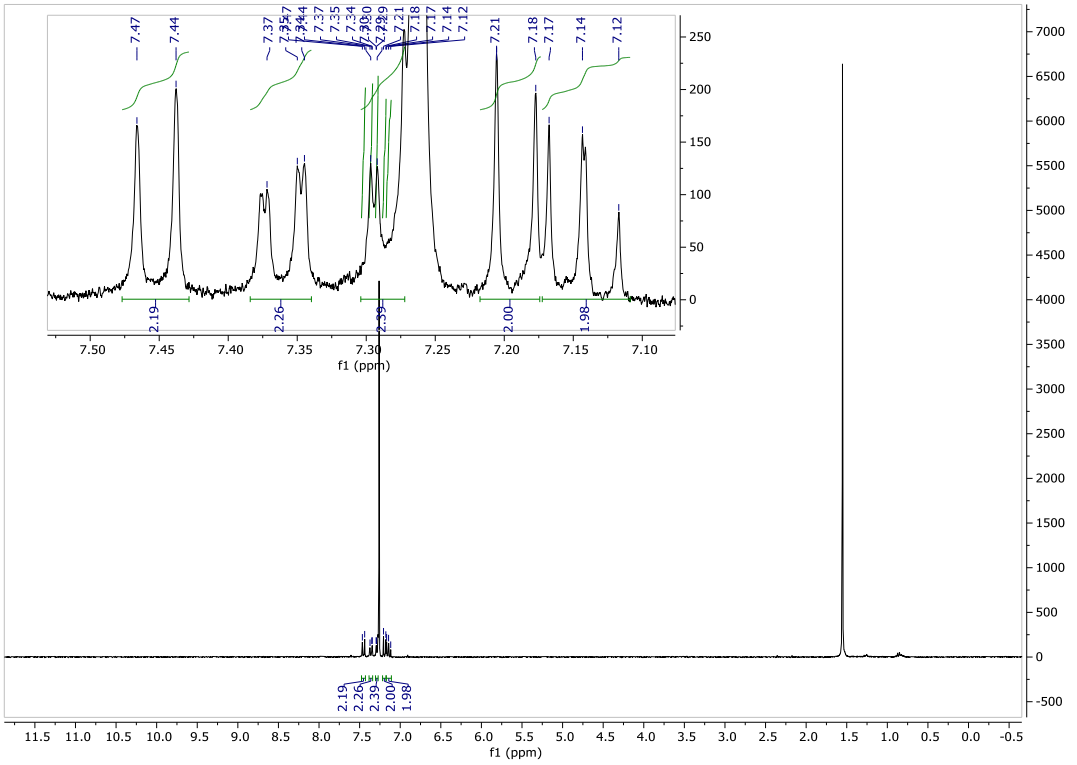

Figure A.102. ^{1}H NMR, 300 MHz, $CDCl_3$.

Elemental Composition Report **Page 1**

Single Mass Analysis
Tolerance = 5.0 PPM / DBE: min = -1.5, max = 200.0
Element prediction: Off
Number of isotope peaks used for i-FIT = 3

Monoisotopic Mass, Odd and Even Electron Ions
4 formula(e) evaluated with 1 results within limits (up to 50 closest results for each mass)
Elements Used:
C: 0-20 H: 0-11 78Se: 0-1 80Se: 0-1

Minimum:				-1.5				
Maximum:		5.0	5.0	200.0				
Mass	Calc. Mass	mDa	PPM	DBE	i-FIT	Norm	Conf(%)	Formula
408.9187	408.9199	-1.2	-2.9	17.5	512.2	n/a	n/a	C20 H11 78Se 80Se

Figure A.103. Elemental composition report.

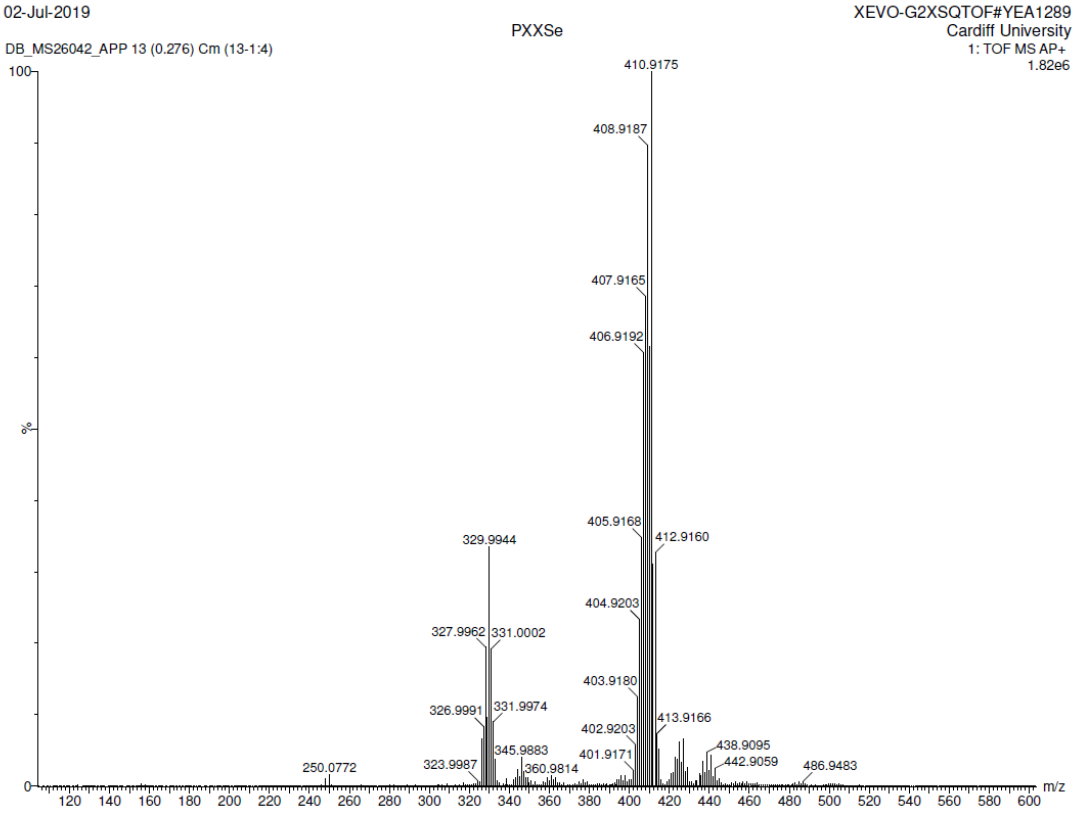

Figure A.104. HRMS, APCI+, TOF.

Characterisation of 2-(methylseleno)-1,1'-biphenyl 38

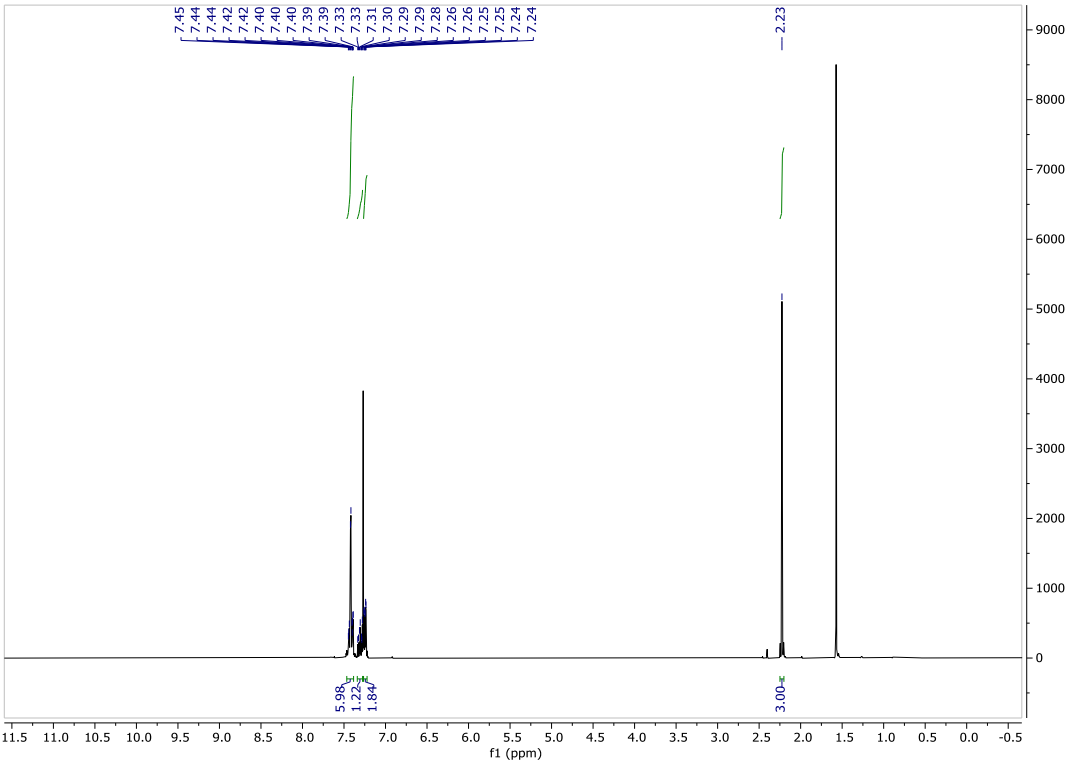

Figure A.105. ^{1}H NMR, 300 MHz, $CDCl_3$.

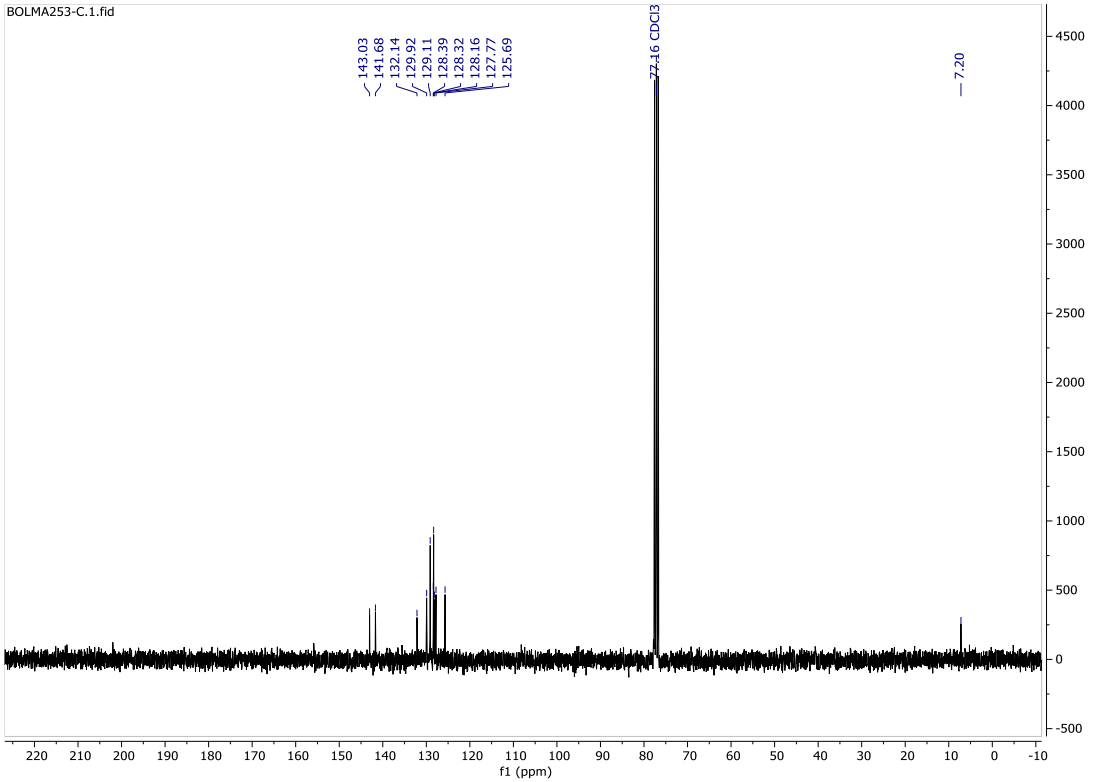

Figure A.106. ^{13}C NMR, 75 MHz, $CDCl_3$.

Elemental Composition Report **Page 1**

Single Mass Analysis
Tolerance = 5.0 PPM / DBE: min = -1.5, max = 200.0
Element prediction: Off
Number of isotope peaks used for i-FIT = 3

Monoisotopic Mass, Odd and Even Electron Ions
3 formula(e) evaluated with 1 results within limits (up to 50 closest results for each mass)
Elements Used:
C: 0-13 H: 0-12 76Se: 0-2

Minimum:				-1.5				
Maximum:		5.0	5.0	200.0				
Mass	Calc. Mass	mDa	PPM	DBE	i-FIT	Norm	Conf(%)	Formula
244.0121	244.0131	-1.0	-4.1	9.0	135.2	n/a	n/a	C13 H12 76Se

Figure A.107. Elemental composition report.

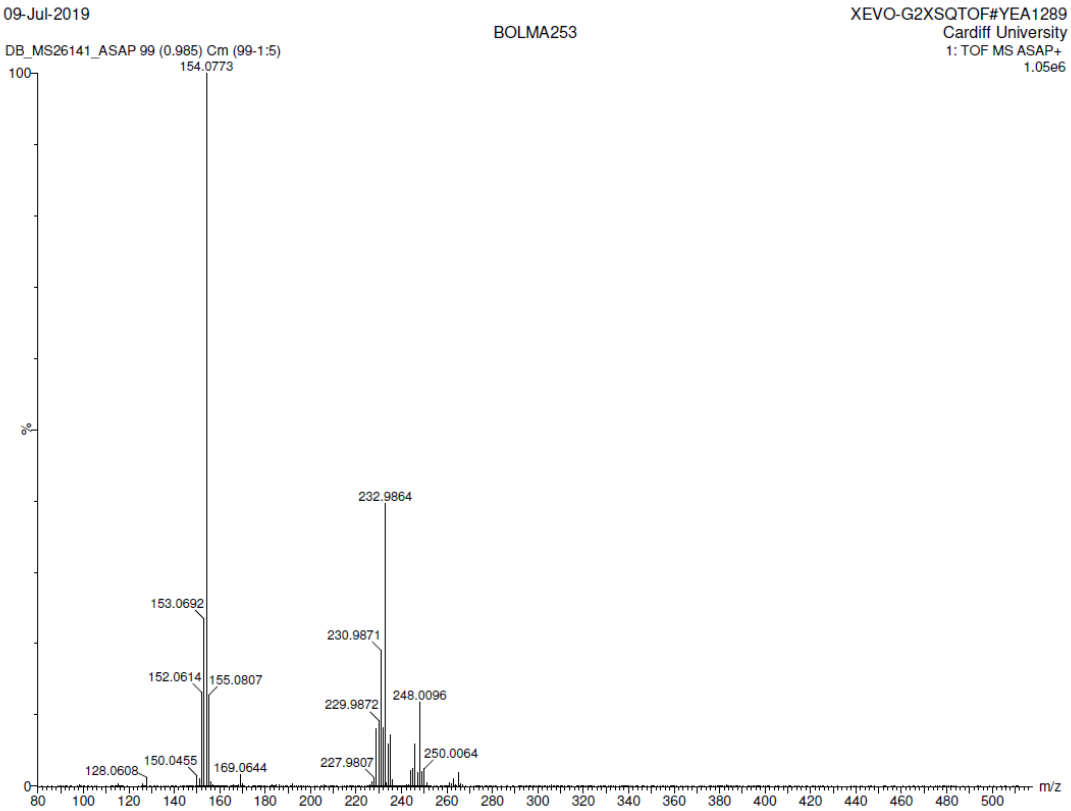

Figure A.108. HRMS, ASAP+, TOF.

Characterisation of 2-(methylseleninyl)-1,1'-biphenyl 39

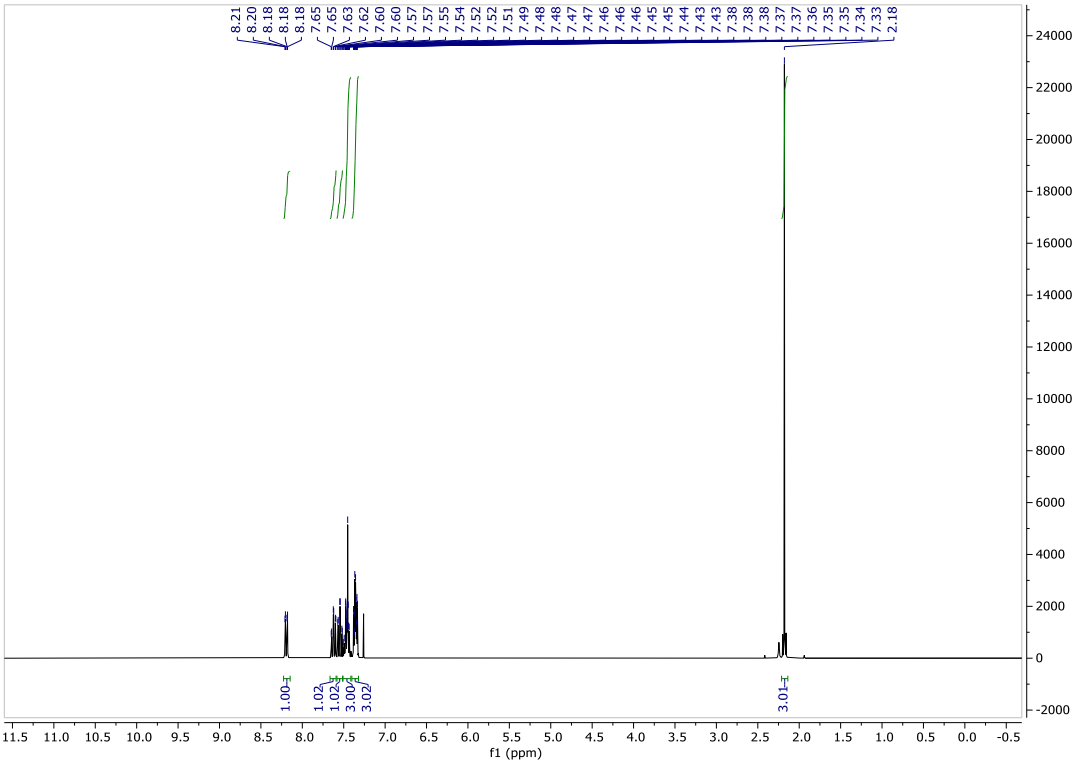

Figure A.109. ^{1}H NMR, 300 MHz, $CDCl_3$.

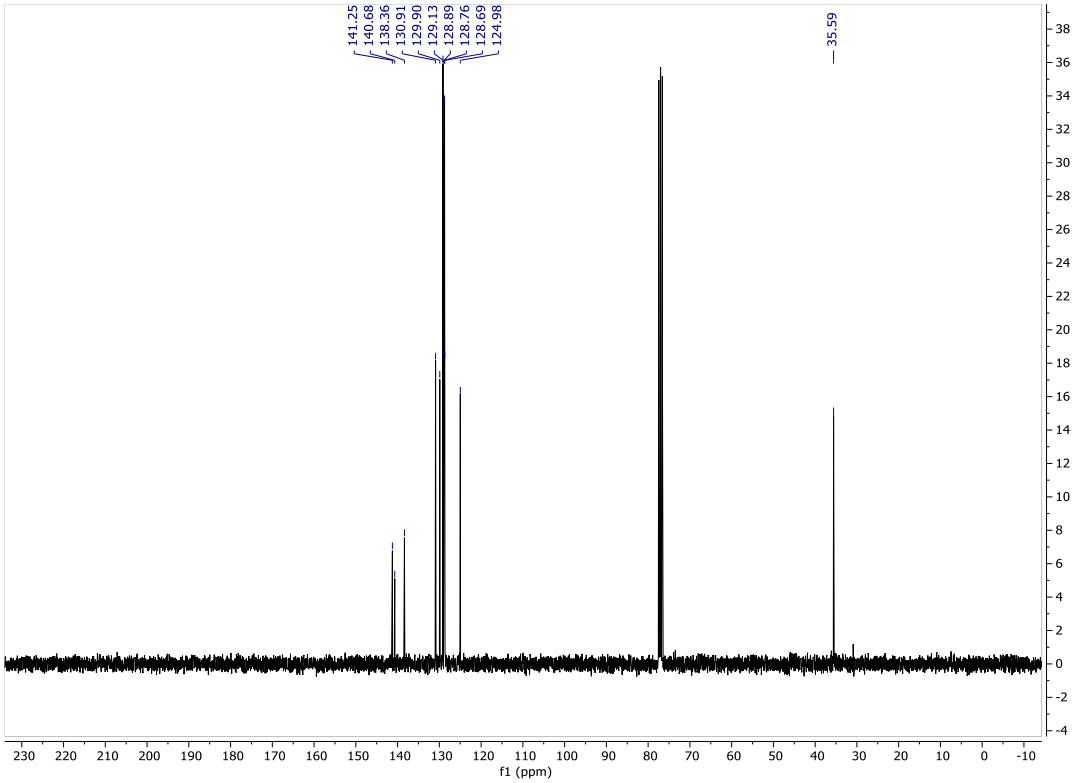

Figure A.110. ^{13}C NMR, 75 MHz, $CDCl_3$.

Elemental Composition Report **Page 1**

Single Mass Analysis
Tolerance = 5.0 PPM / DBE: min = -1.5, max = 200.0
Element prediction: Off
Number of isotope peaks used for i-FIT = 3

Monoisotopic Mass, Odd and Even Electron Ions
6 formula(e) evaluated with 1 results within limits (up to 50 closest results for each mass)
Elements Used:
C: 0-13 H: 0-13 O: 0-1 76Se: 0-2

Minimum:				-1.5				
Maximum:		5.0	5.0	200.0				
Mass	Calc. Mass	mDa	PPM	DBE	i-FIT	Norm	Conf(%)	Formula
261.0158	261.0159	-0.1	-0.4	8.5	531.5	n/a	n/a	C13 H13 O 76Se

Figure A.111. Elemental composition report.

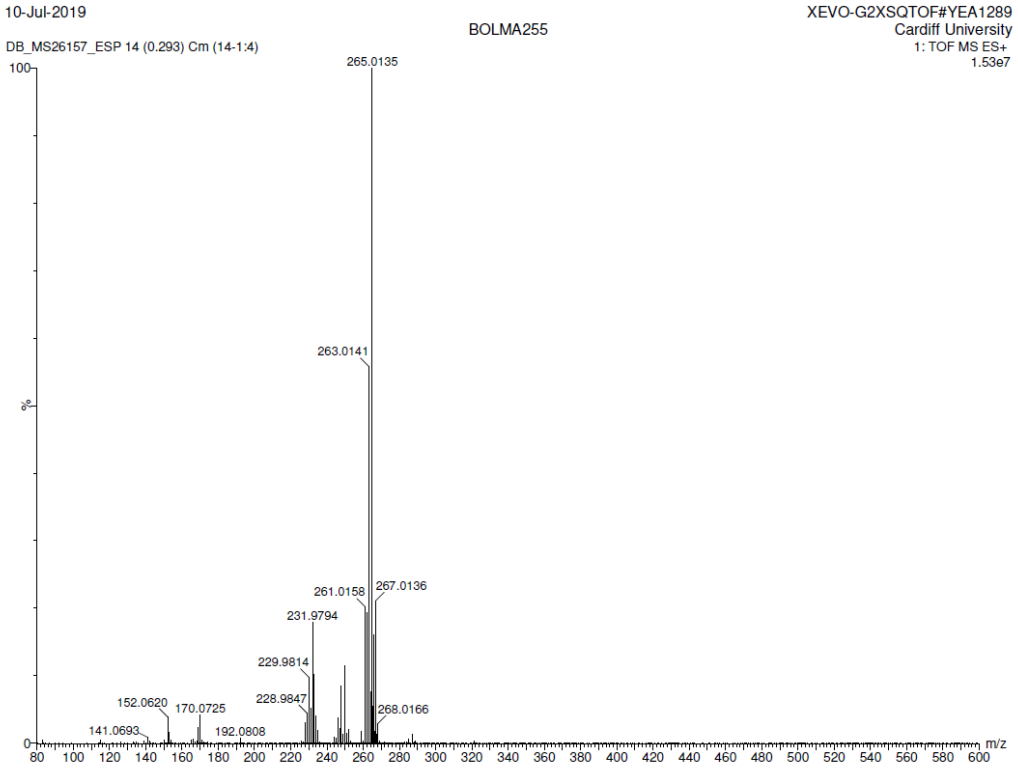

Figure A.112. HRMS, ES+, TOF.

Characterisation of dibenzoselenophene 40

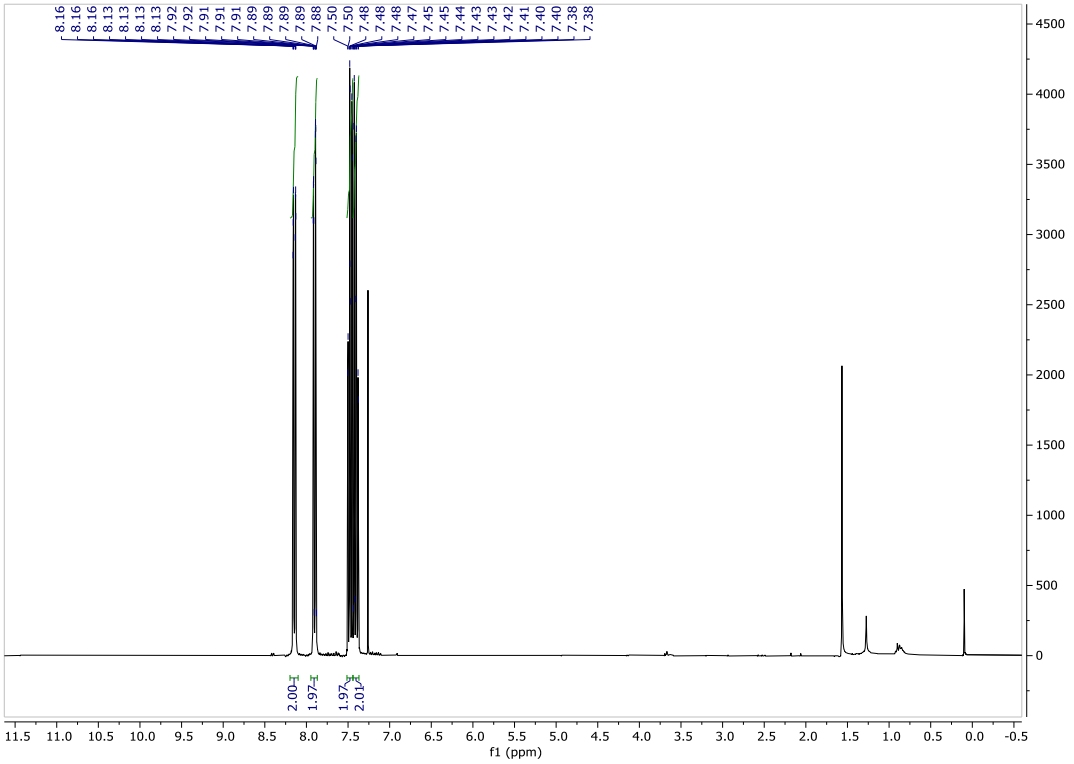

Figure A.113. ^{1}H NMR, 300 MHz, $CDCl_3$.

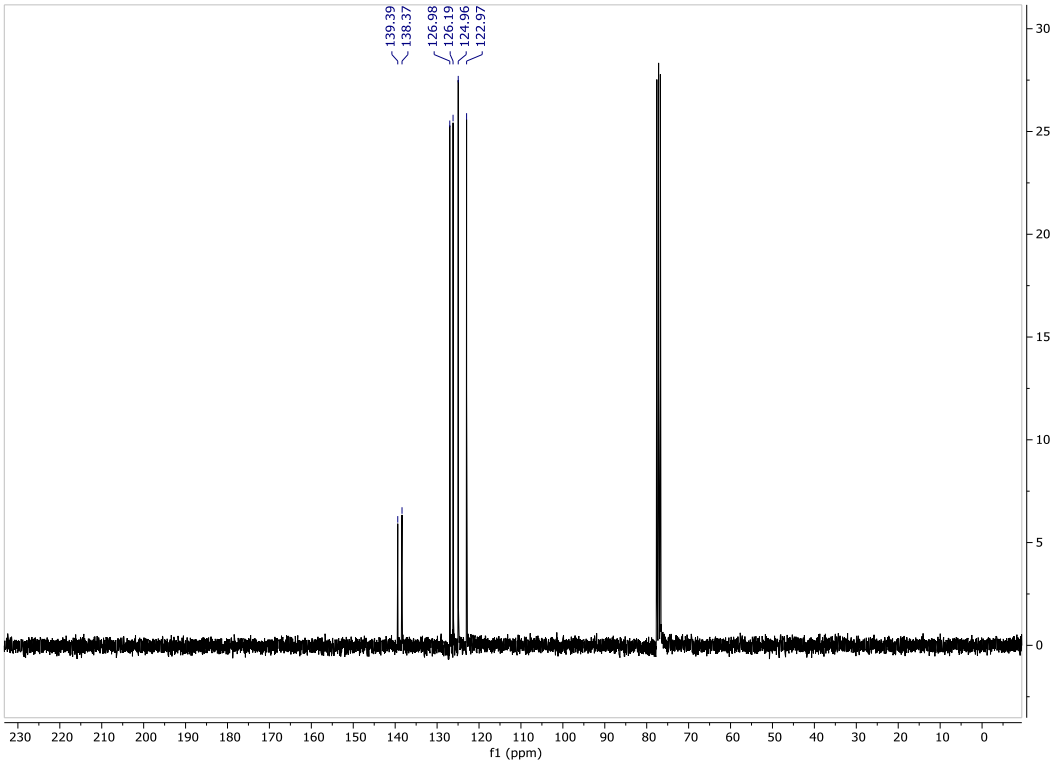

Figure A.114. ^{13}C NMR, 75 MHz, $CDCl_3$.

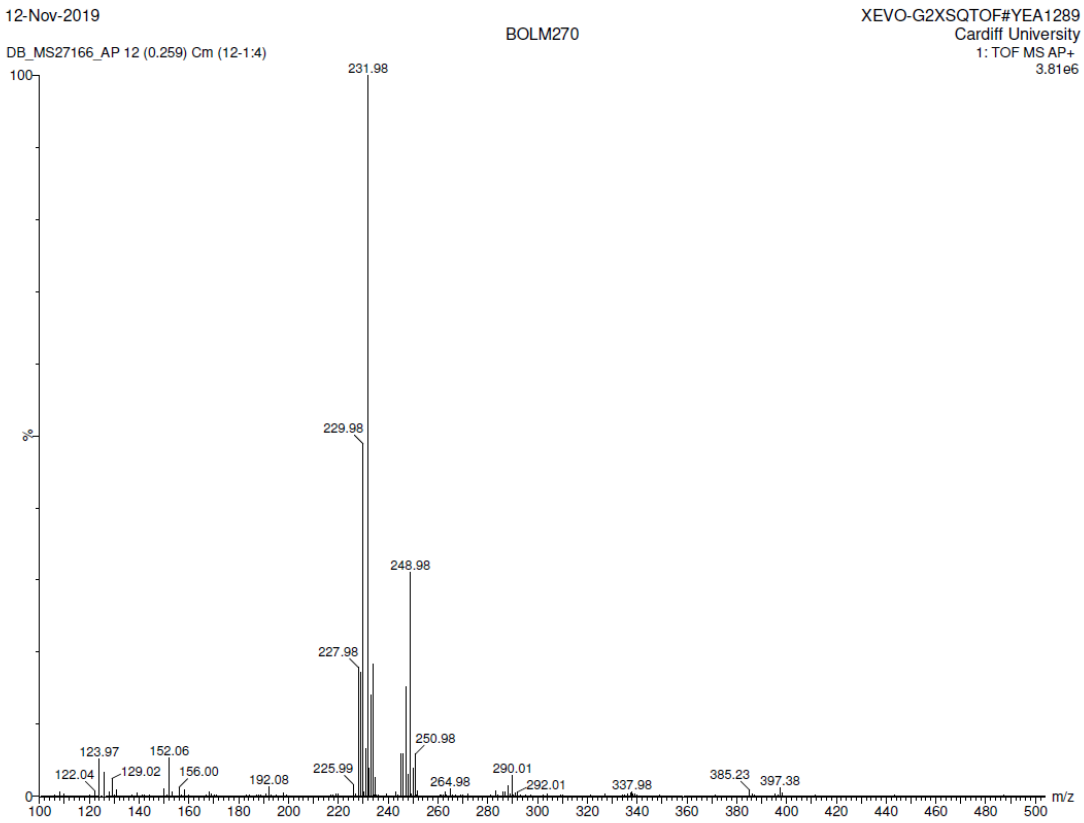

Figure A.115. LRMS, APCI+, TOF.

Characterisation of 4-(1-methyl-1H-pyrrol-2-yl)benzonitrile 42

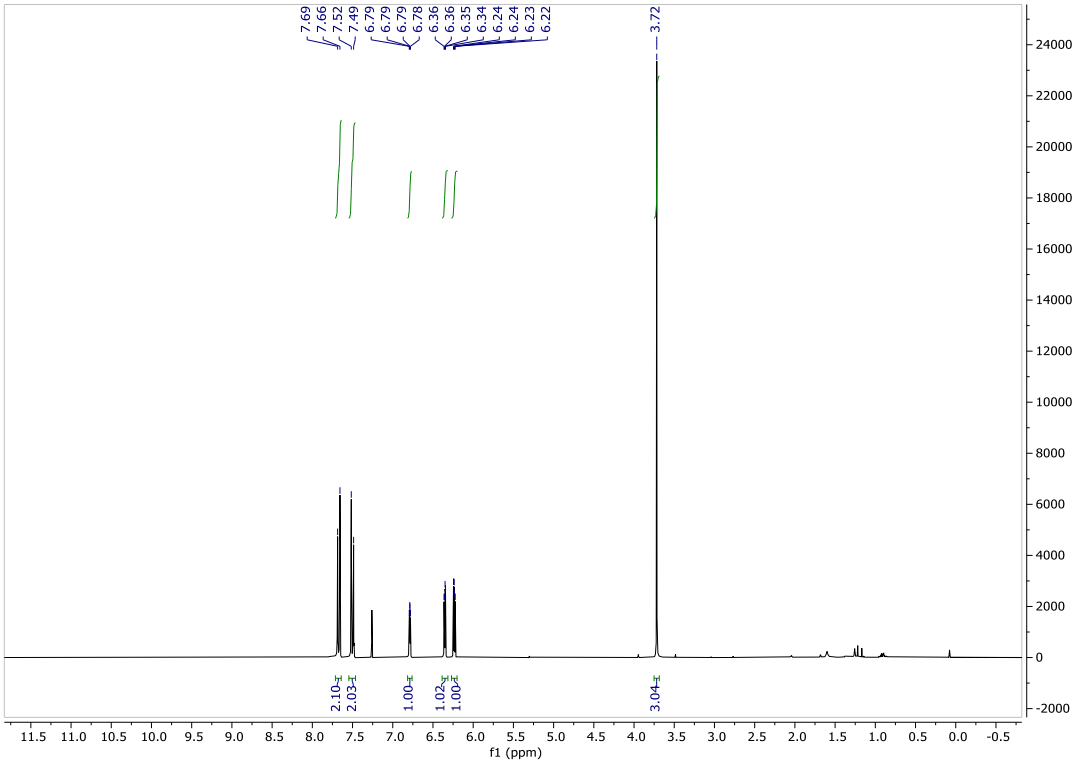

Figure A.116. ^{1}H NMR, 300 MHz, $CDCl_3$.

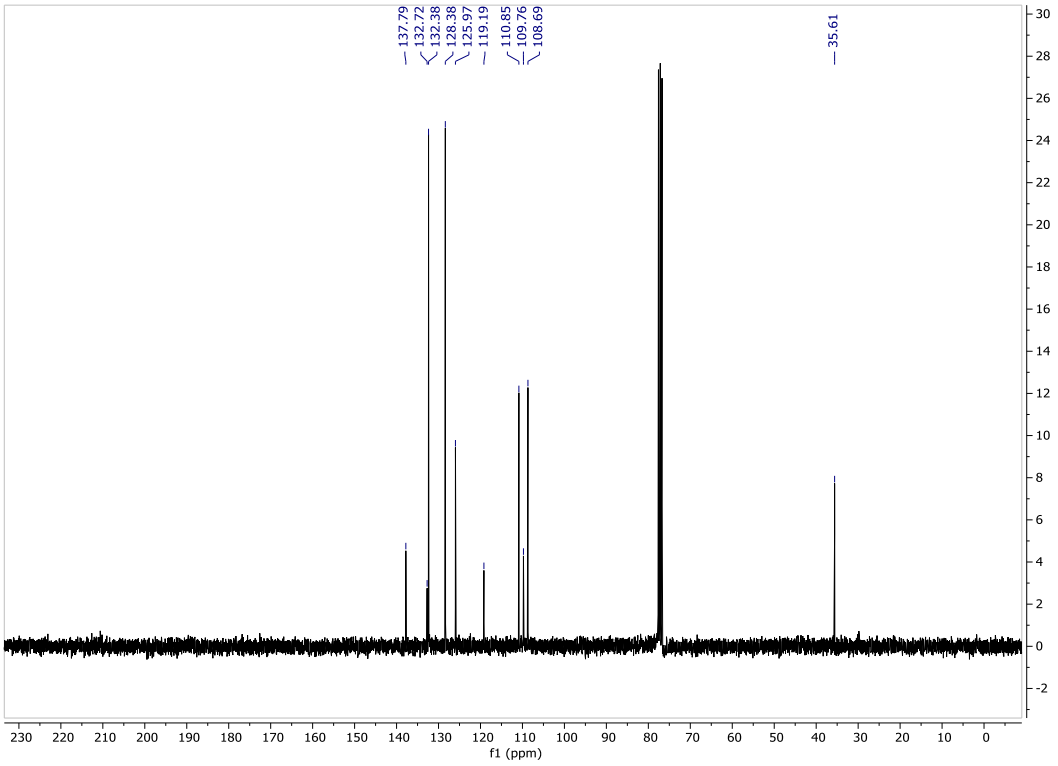

Figure A.117. ^{13}C NMR, 75 MHz, $CDCl_3$.

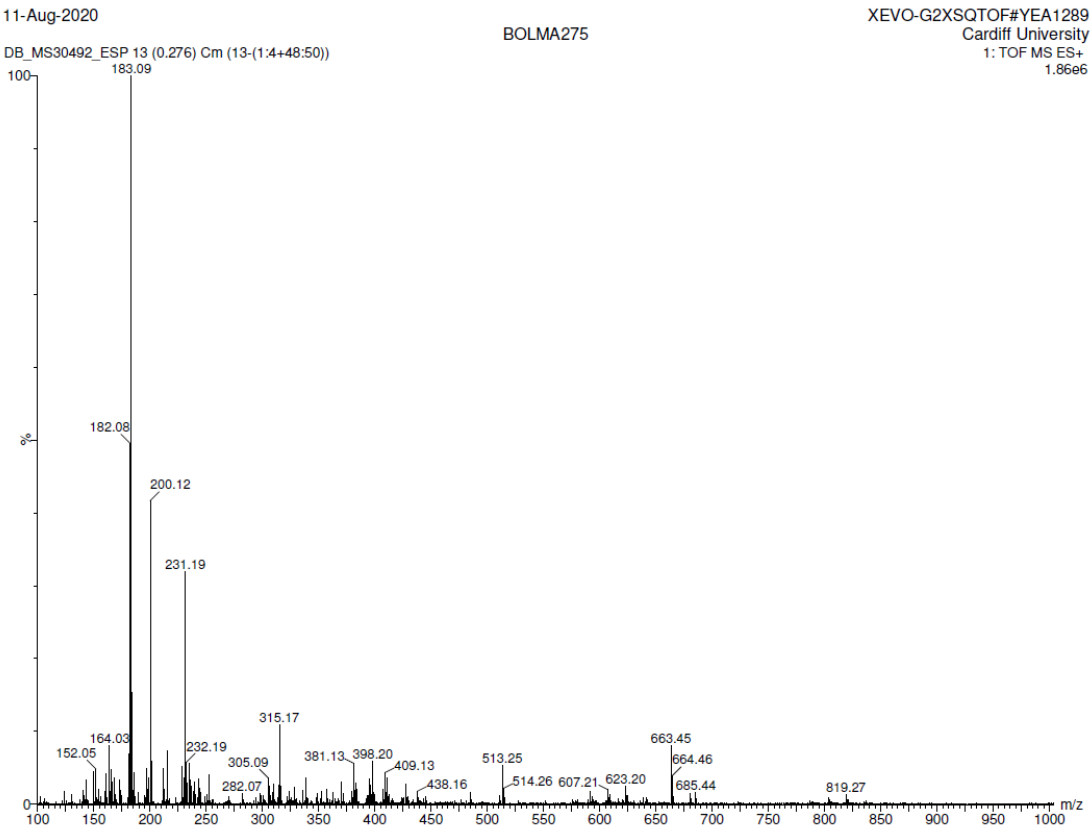

Figure A.118. LRMS, ES+, TOF.

Characterisation of methyl 4-(1-methyl-1H-pyrrol-2-yl)benzoate 43

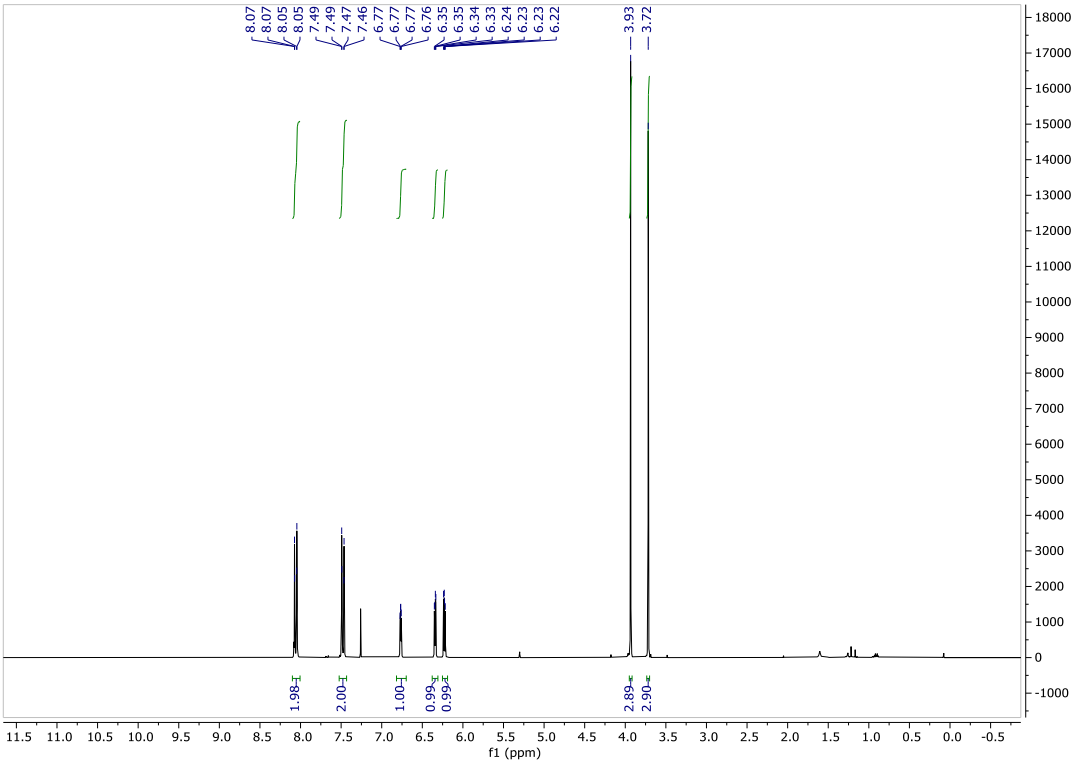

Figure A.119. ^{1}H NMR, 300 MHz, $CDCl_3$.

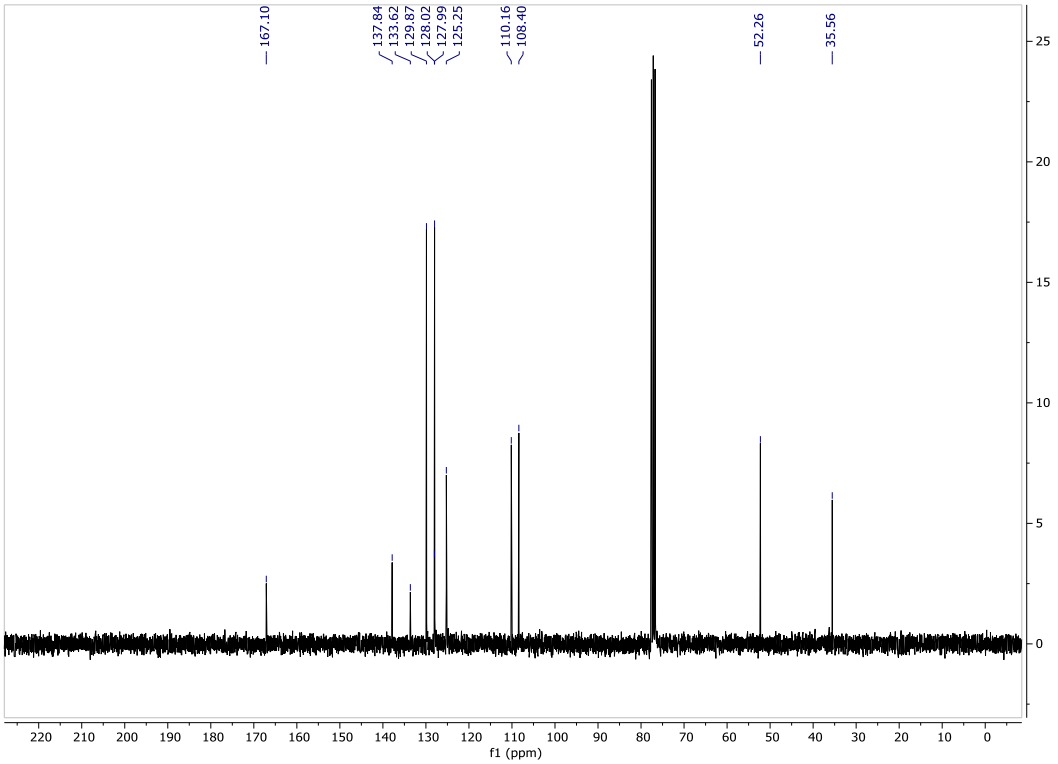

Figure A.120. ^{13}C NMR, 75 MHz, $CDCl_3$.

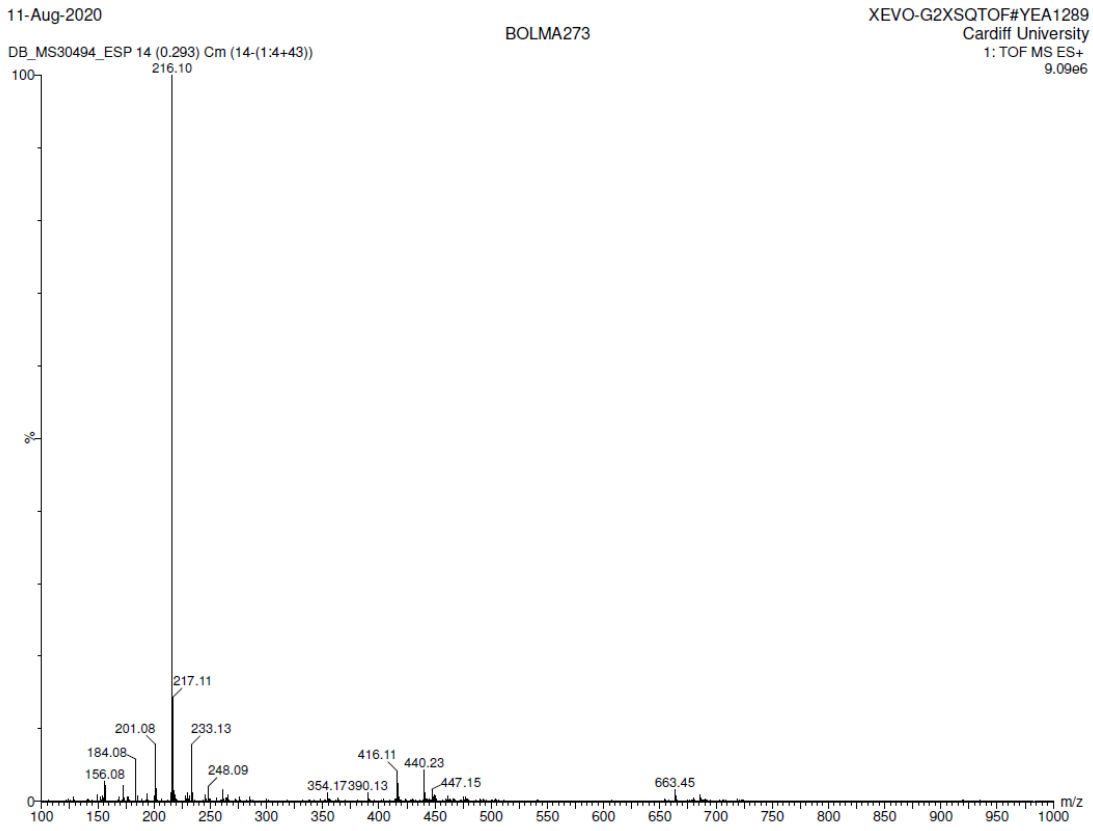

Figure A.121. LRMS, ES+, TOF.

Characterisation of 1-(4-(1-methyl-1H-pyrrol-2-yl)phenyl)ethan-1-one 44

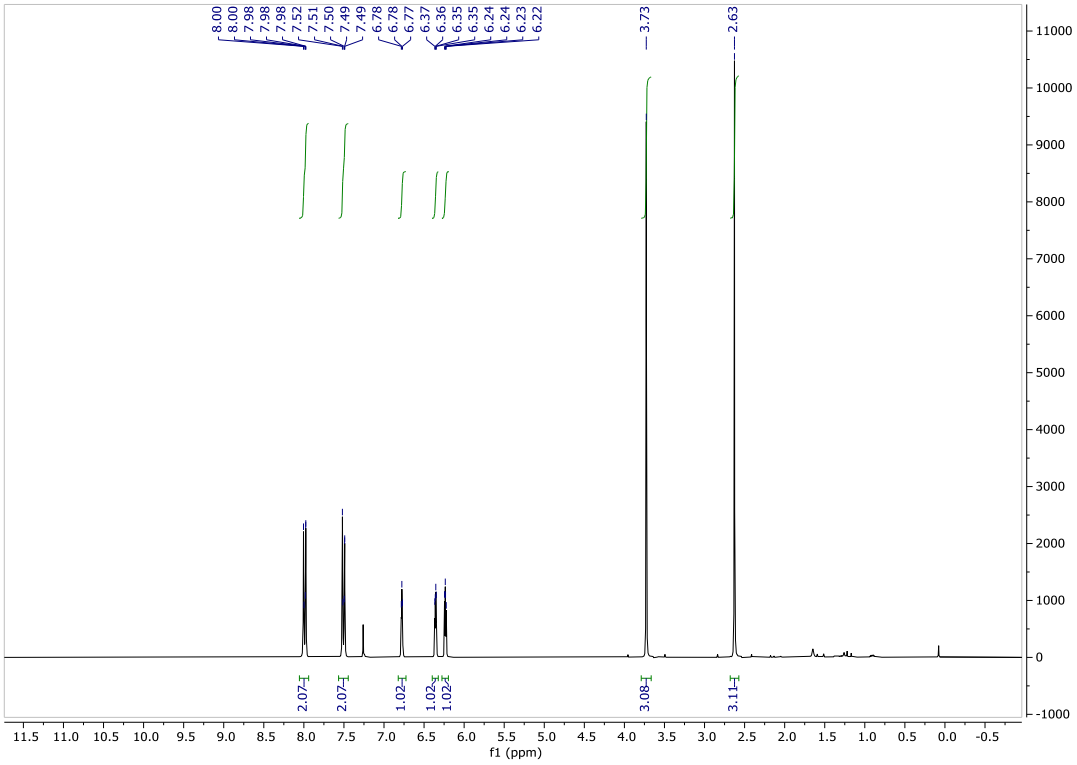

Figure A.122. ^{1}H NMR, 300 MHz, $CDCl_3$.

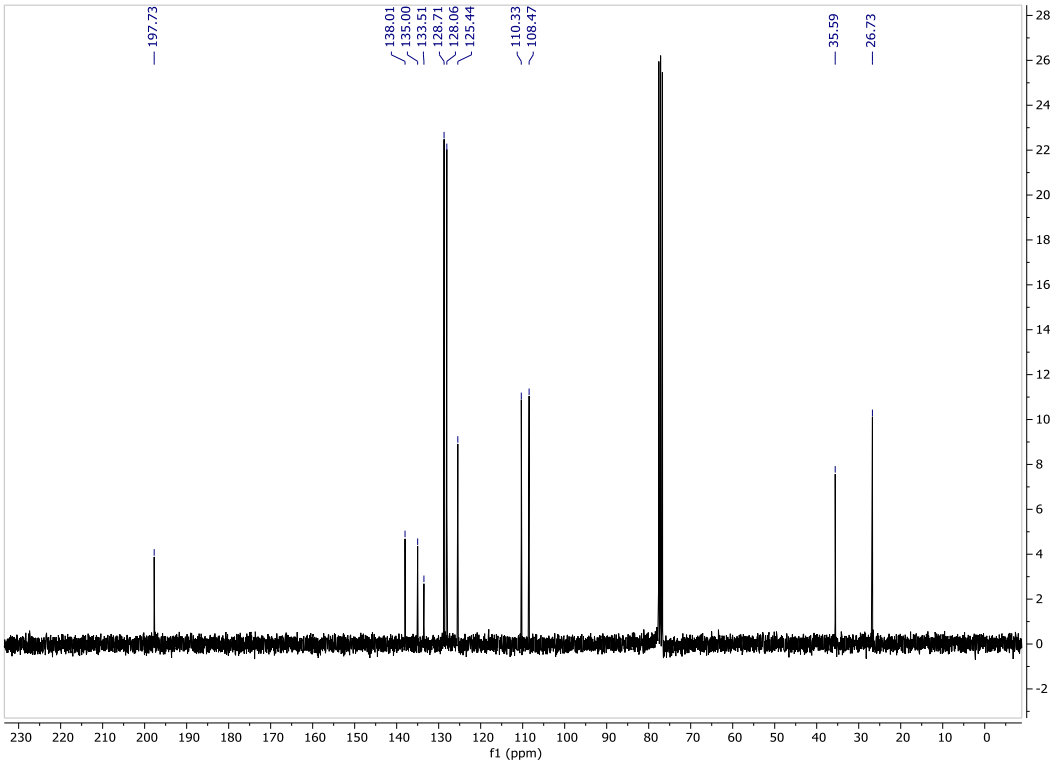

Figure A.123. ^{13}C NMR, 75 MHz, $CDCl_3$.

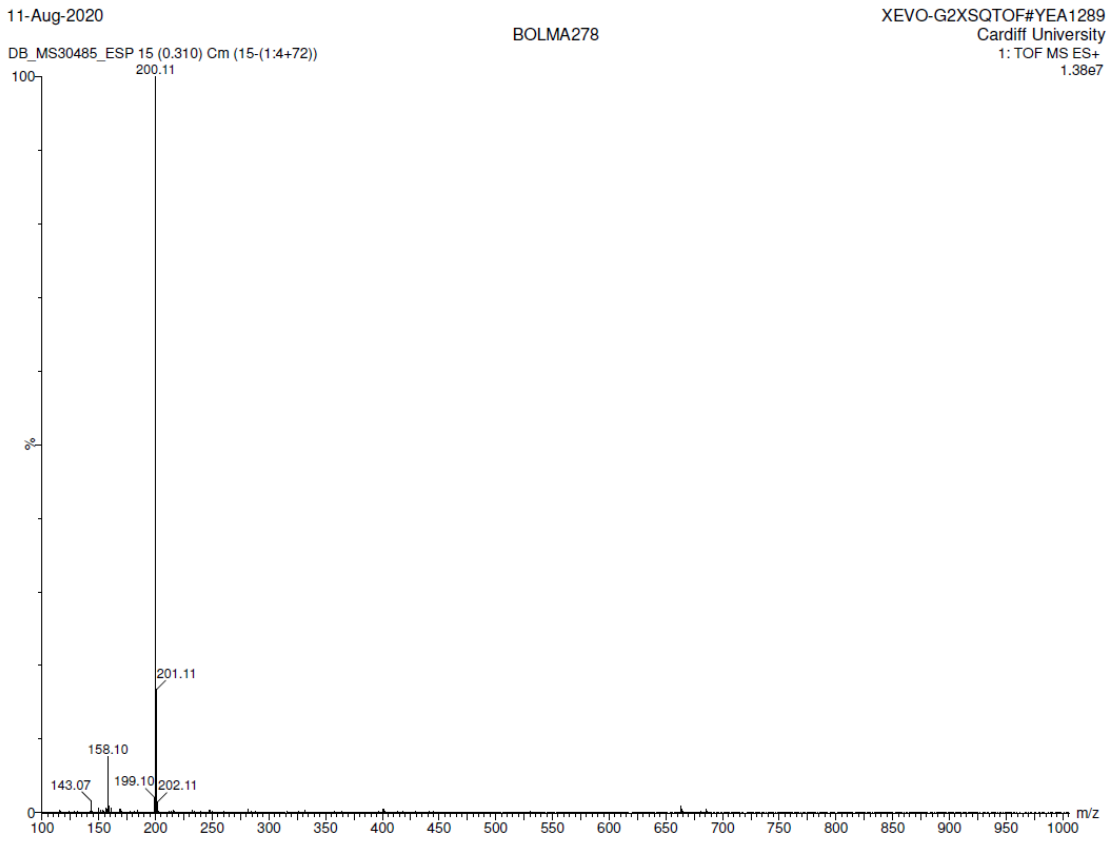

Figure A.124. LRMS, ES+, TOF.

Characterisation of 6-chloro-[1,1':2',1''-terphenyl]-3-carbonitrile 52

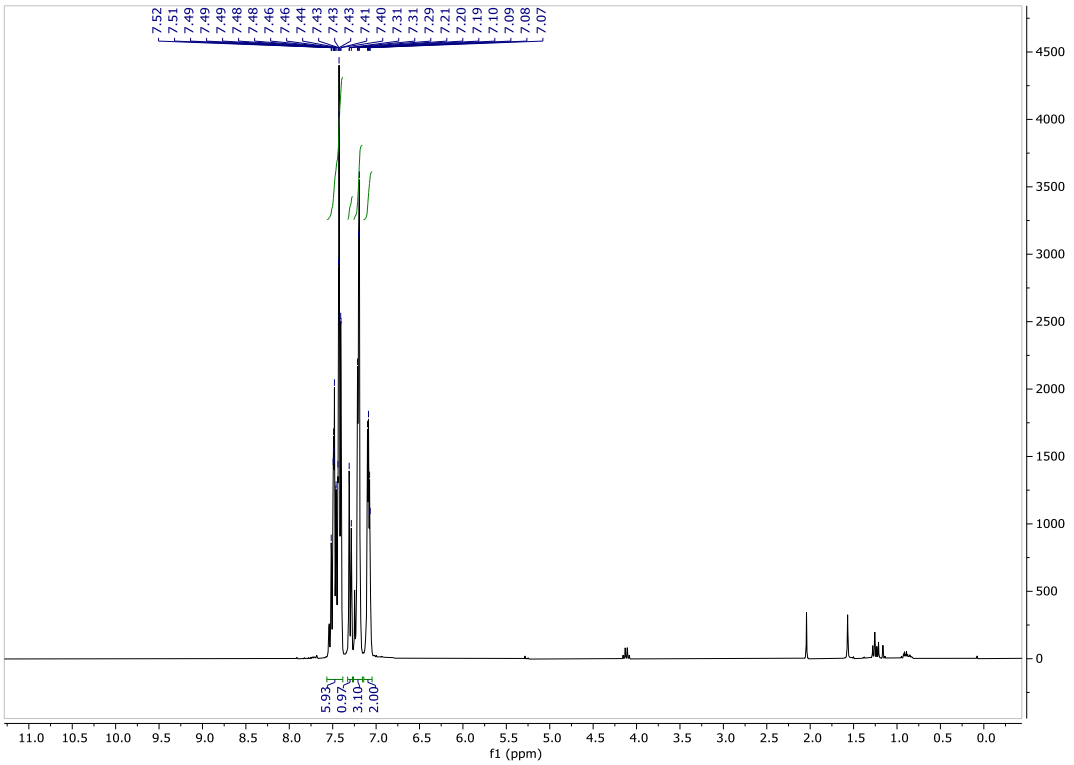

Figure A.125. ^{1}H NMR, 300 MHz, $CDCl_3$.

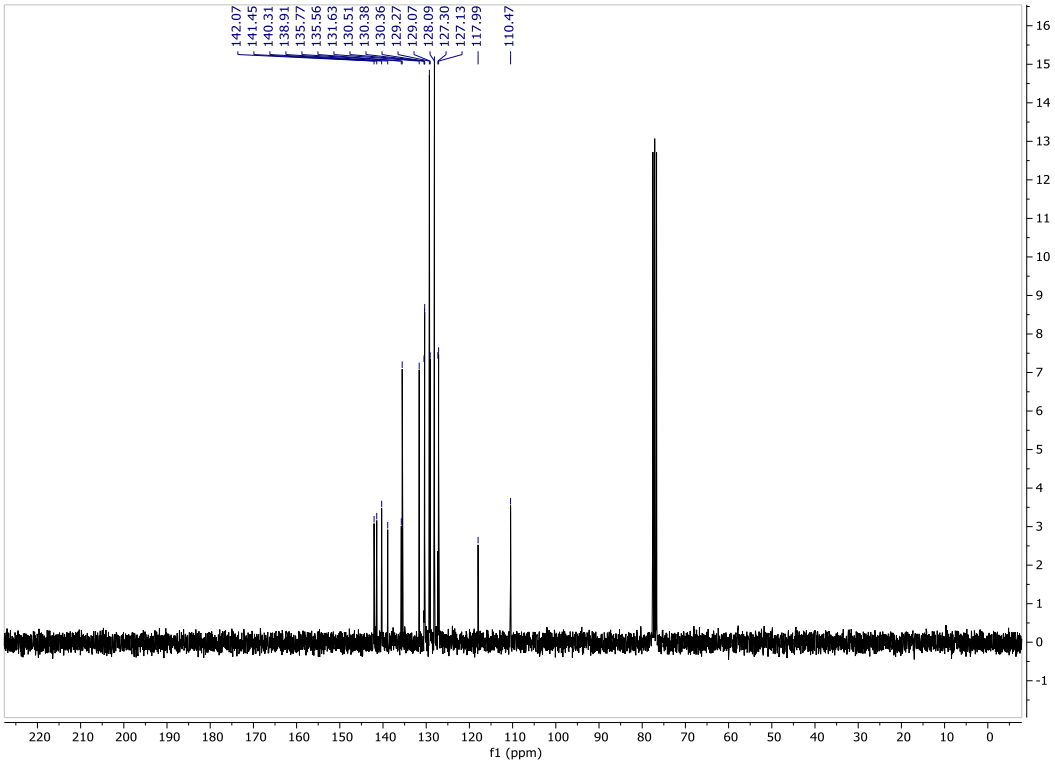

Figure A.126. ^{13}C NMR, 75 MHz, $CDCl_3$.

Elemental Composition Report **Page 1**

Single Mass Analysis
Tolerance = 5.0 PPM / DBE: min = -1.5, max = 200.0
Element prediction: Off
Number of isotope peaks used for i-FIT = 3

Monoisotopic Mass, Odd and Even Electron Ions
2 formula(e) evaluated with 1 results within limits (up to 50 closest results for each mass)
Elements Used:
C: 0-19 H: 0-13 N: 0-1 Cl: 0-1

Minimum:				-1.5				
Maximum:		5.0	5.0	200.0				
Mass	Calc. Mass	mDa	PPM	DBE	i-FIT	Norm	Conf(%)	Formula
290.0746	290.0737	0.9	3.1	13.5	989.2	n/a	n/a	C19 H13 N Cl

Figure A.127. Elemental composition report.

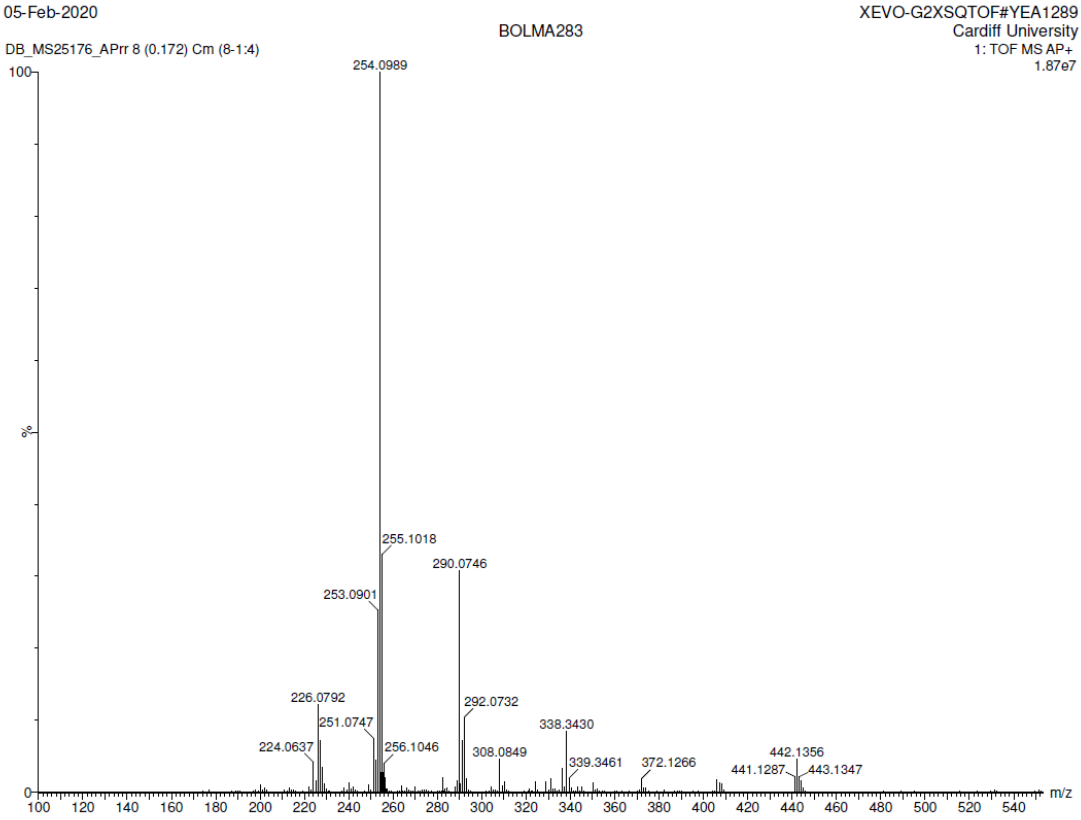

Figure A.128. HRMS, APCI+, TOF.

Characterisation of 2-chloro-[1,1':2',1''-terphenyl]-3-carbonitrile 53

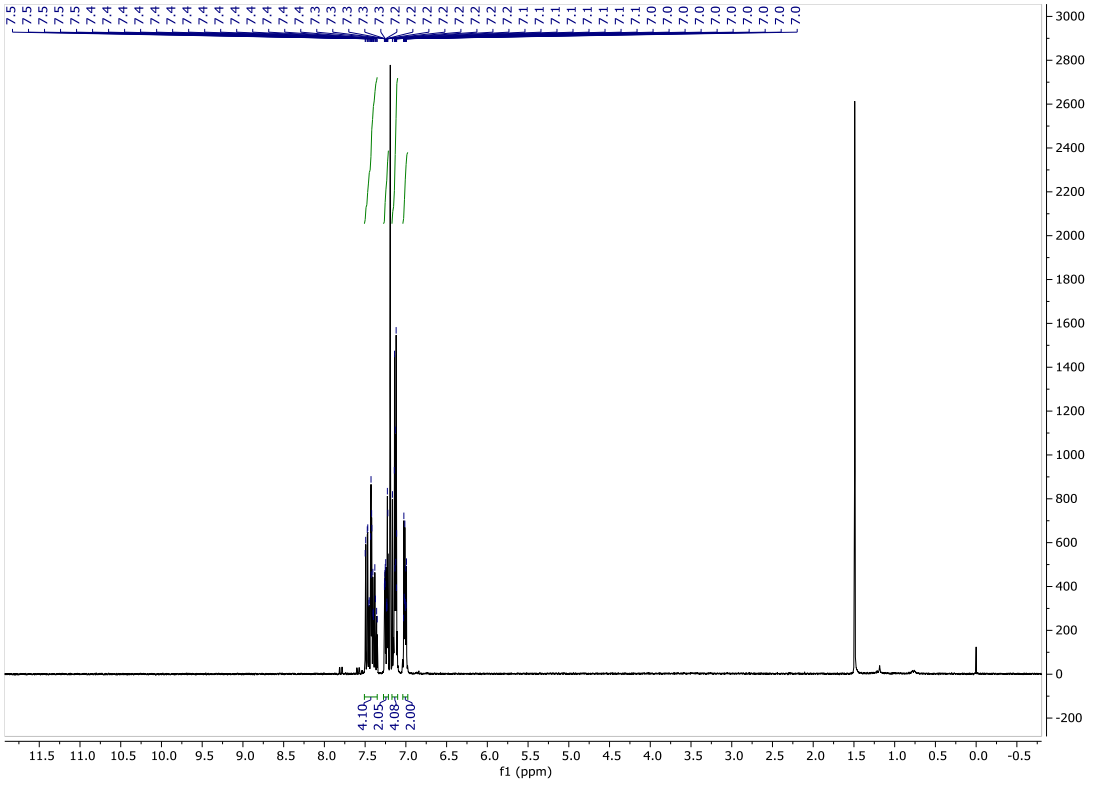

Figure A.129. ^{1}H NMR, 300 MHz, $CDCl_3$.

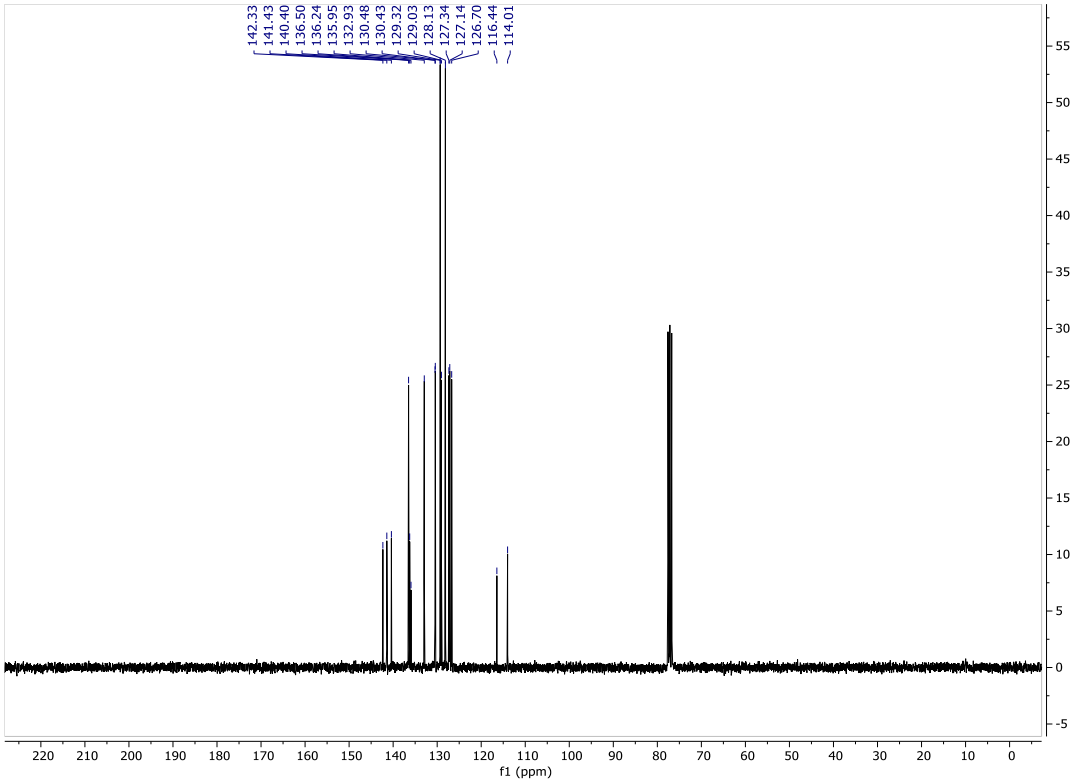

Figure A.130. ^{13}C NMR, 75 MHz, $CDCl_3$.

Elemental Composition Report **Page 1**

Single Mass Analysis
Tolerance = 5.0 PPM / DBE: min = -1.5, max = 200.0
Element prediction: Off
Number of isotope peaks used for i-FIT = 3

Monoisotopic Mass, Odd and Even Electron Ions
2 formula(e) evaluated with 1 results within limits (up to 50 closest results for each mass)
Elements Used:
C: 0-19 H: 0-12 N: 0-1 Cl: 0-1

Minimum:				-1.5				
Maximum:		5.0	5.0	200.0				
Mass	Calc. Mass	mDa	PPM	DBE	i-FIT	Norm	Conf(%)	Formula
289.0670	289.0658	1.2	4.2	14.0	1189.9	n/a	n/a	C19 H12 N Cl

Figure A.131. Elemental composition report.

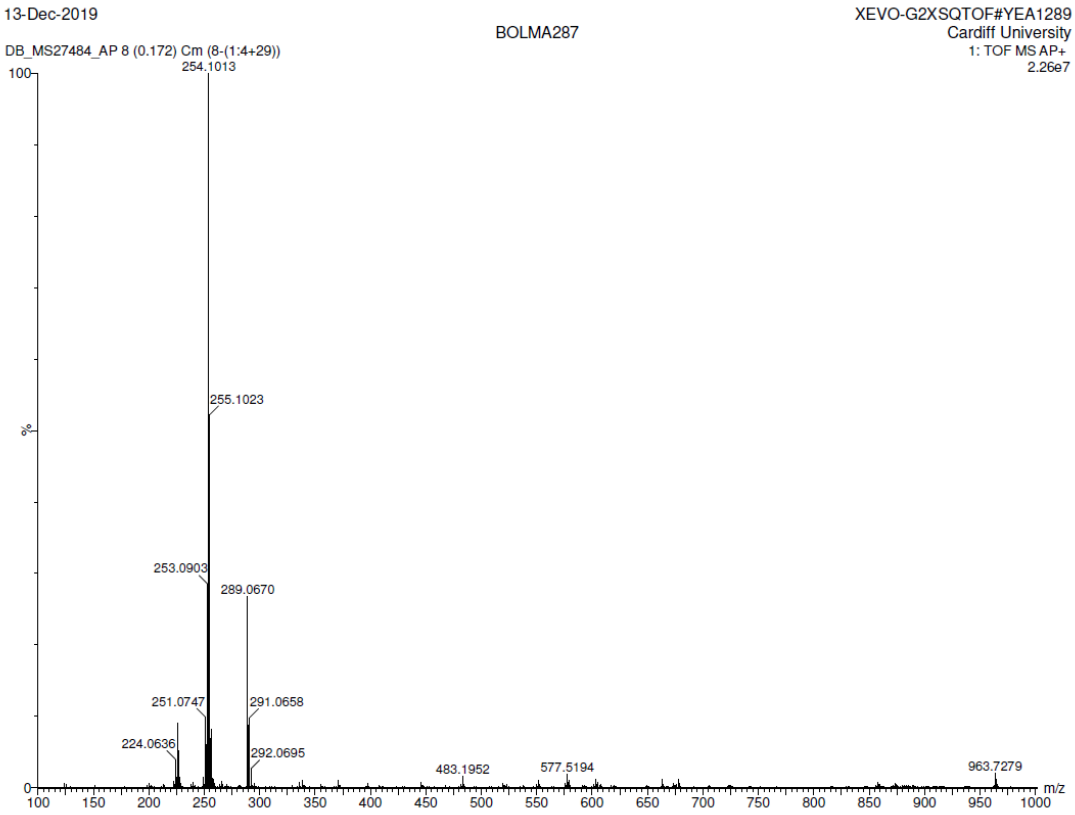

Figure A.132. HRMS, APCI+, TOF.

Characterisation of methyl 6-chloro-[1,1':2',1''-terphenyl]-3-carboxylate 54

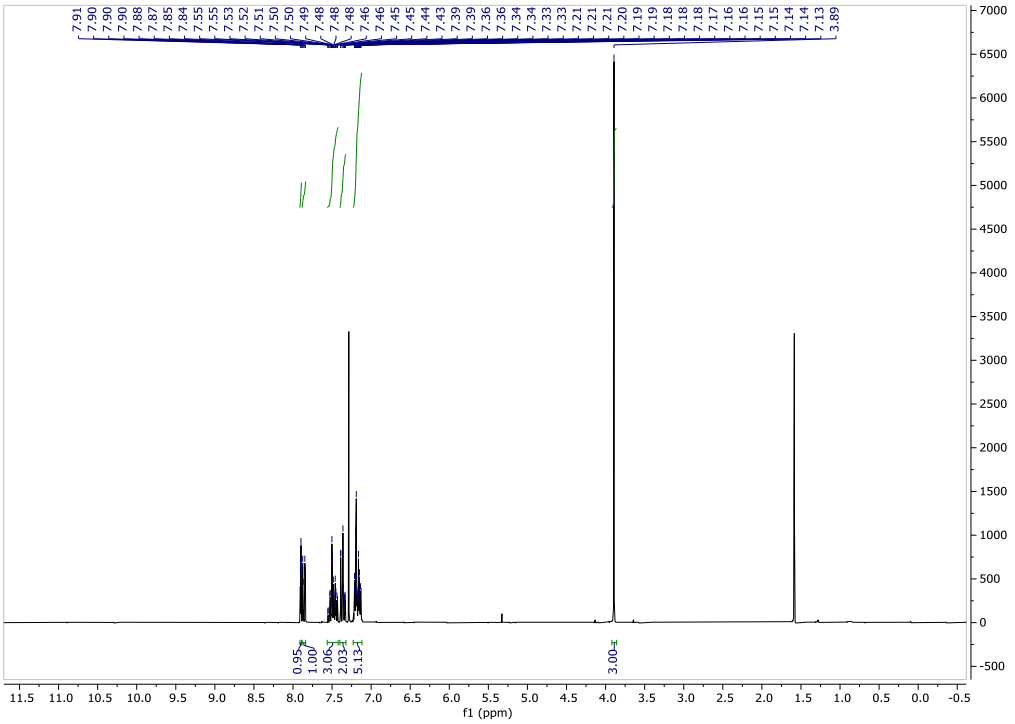

Figure A.133. ^{1}H NMR, 300 MHz, $CDCl_3$.

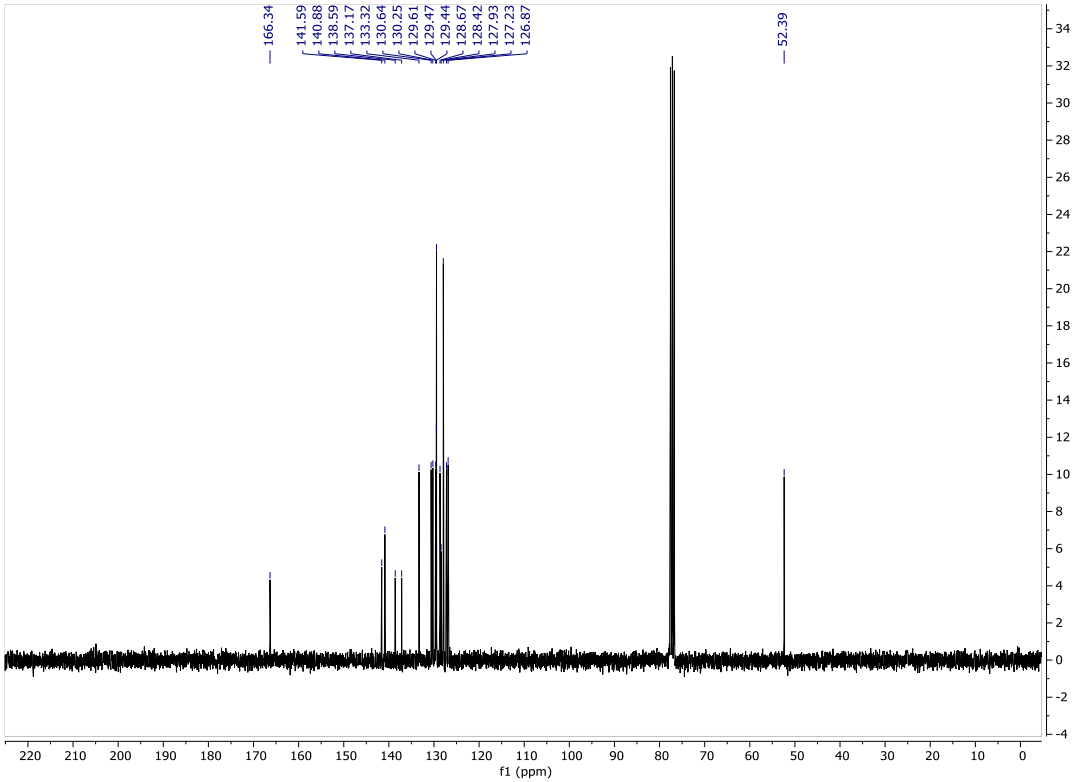

Figure A.134. ^{13}C NMR, 75 MHz, $CDCl_3$.

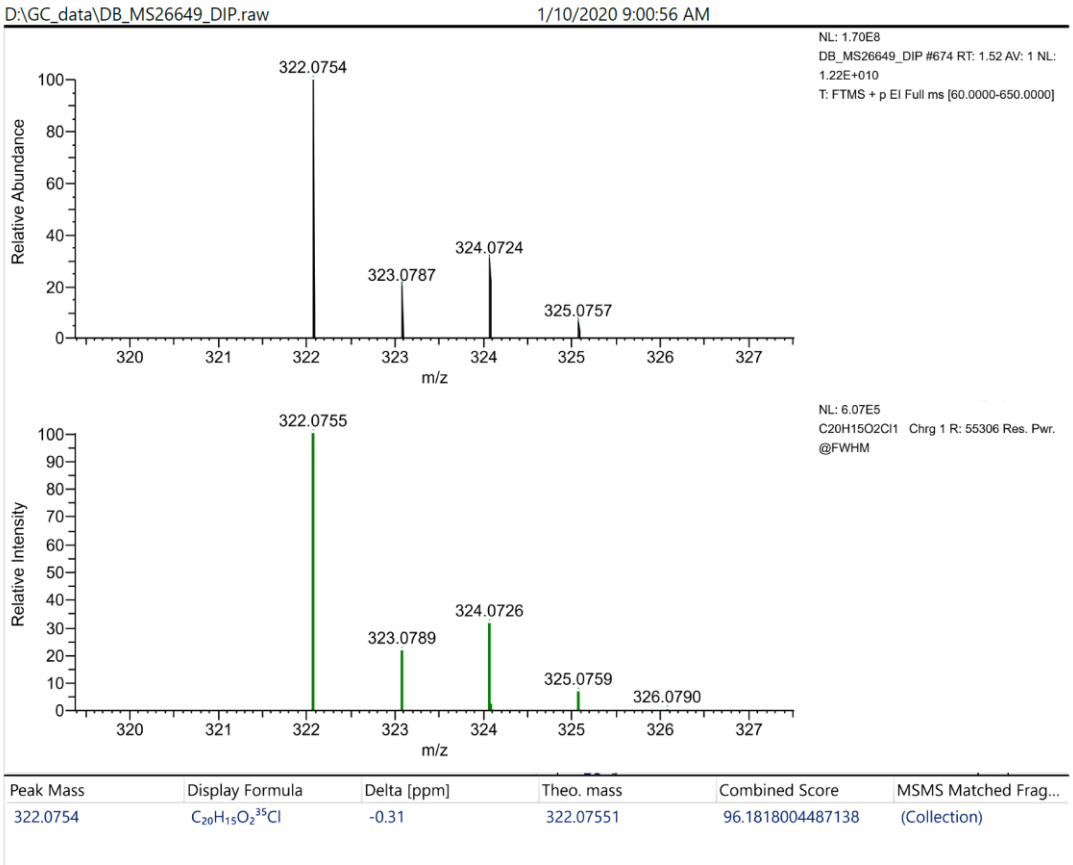

Figure A.135. Elemental composition report.

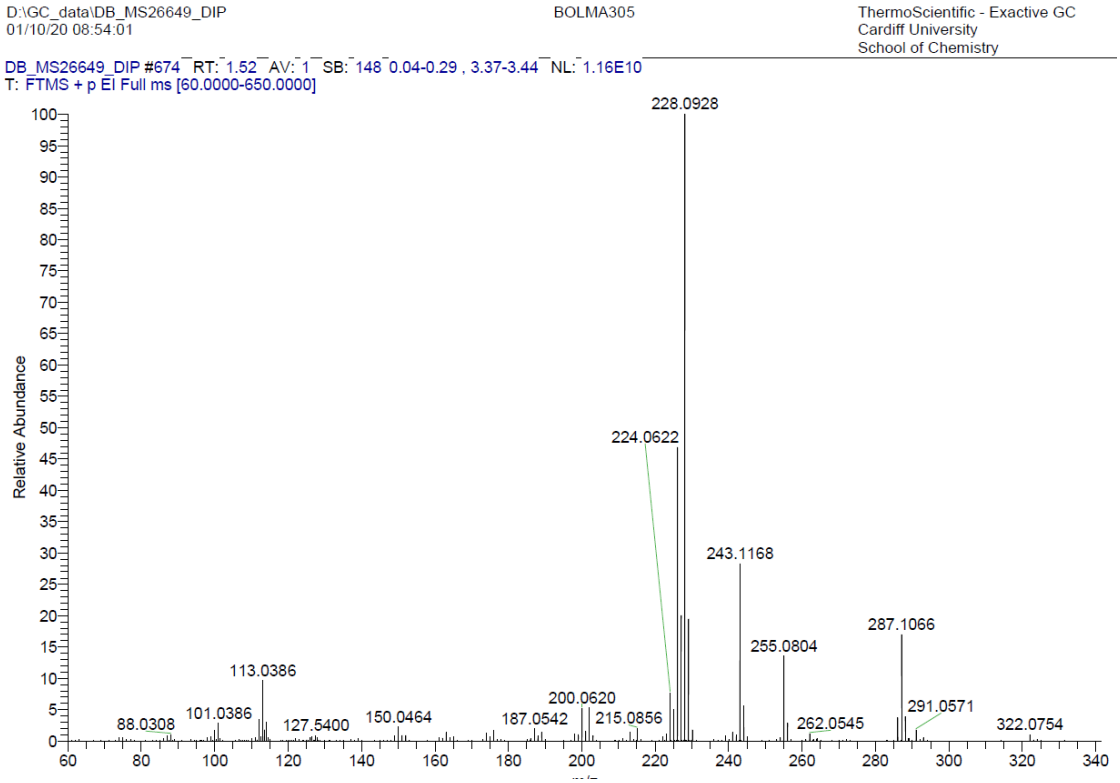

Figure A.136. HRMS, EI+, TOF.

Characterisation of 2-chloro-5-nitro-1,1':2',1''-terphenyl 55

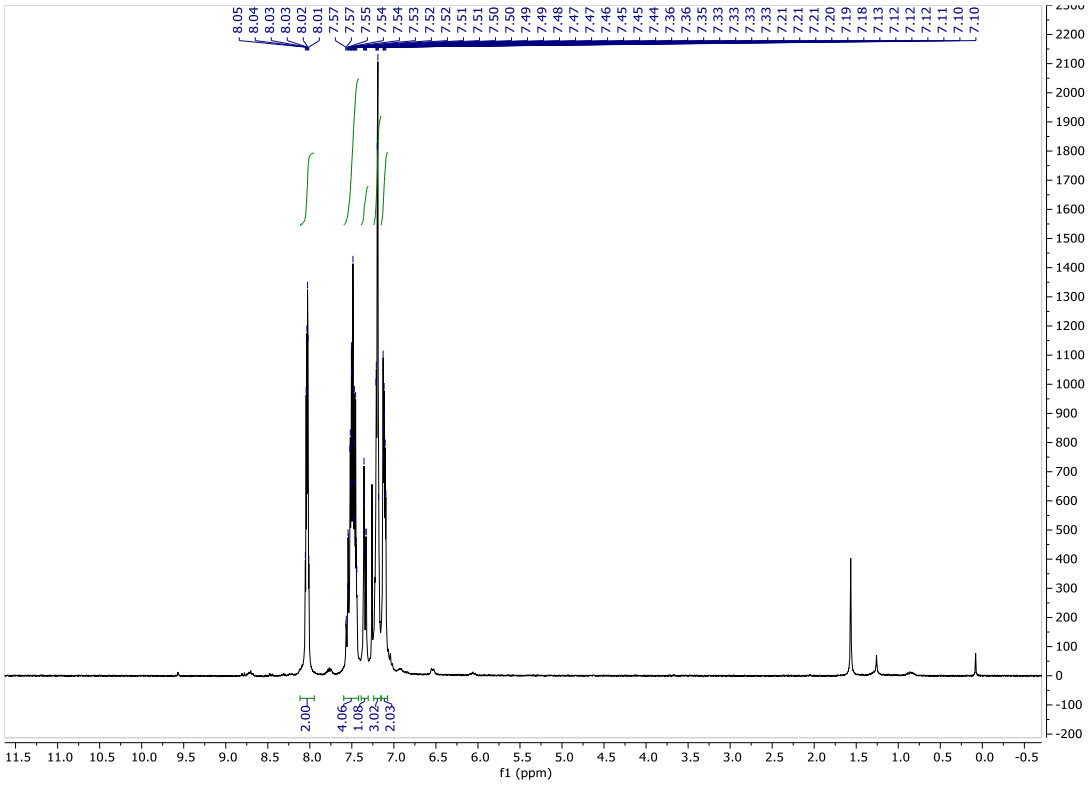

Figure A.137. ^{1}H NMR, 300 MHz, $CDCl_3$.

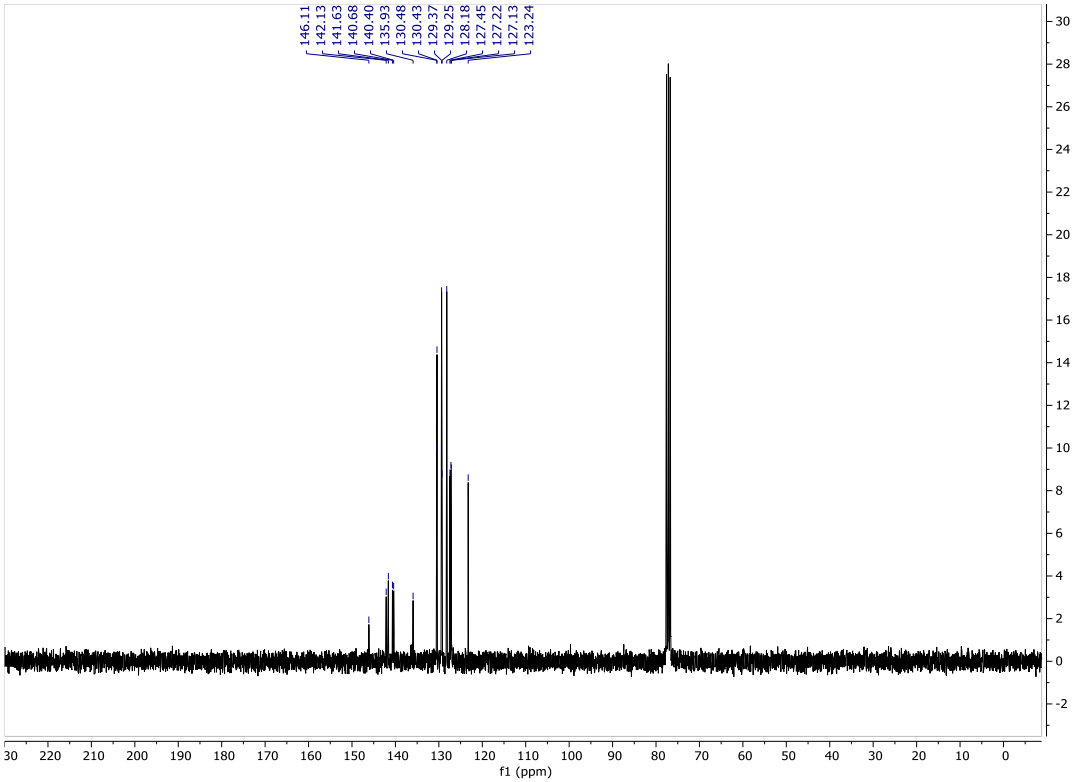

Figure A.138. ^{13}C NMR, 75 MHz, $CDCl_3$.

Elemental Composition Report **Page 1**

Single Mass Analysis
Tolerance = 5.0 PPM / DBE: min = -1.5, max = 200.0
Element prediction: Off
Number of isotope peaks used for i-FIT = 3

Monoisotopic Mass, Odd and Even Electron Ions
7 formula(e) evaluated with 1 results within limits (up to 50 closest results for each mass)
Elements Used:
C: 0-20 H: 0-12 N: 0-1 O: 0-2 Cl: 0-1

Minimum:				-1.5				
Maximum:		5.0	5.0	200.0				
Mass	Calc. Mass	mDa	PPM	DBE	i-FIT	Norm	Conf(%)	Formula
309.0557	309.0557	0.0	0.0	13.0	780.0	n/a	n/a	C18 H12 N O2 Cl

Figure A.139. Elemental composition report.

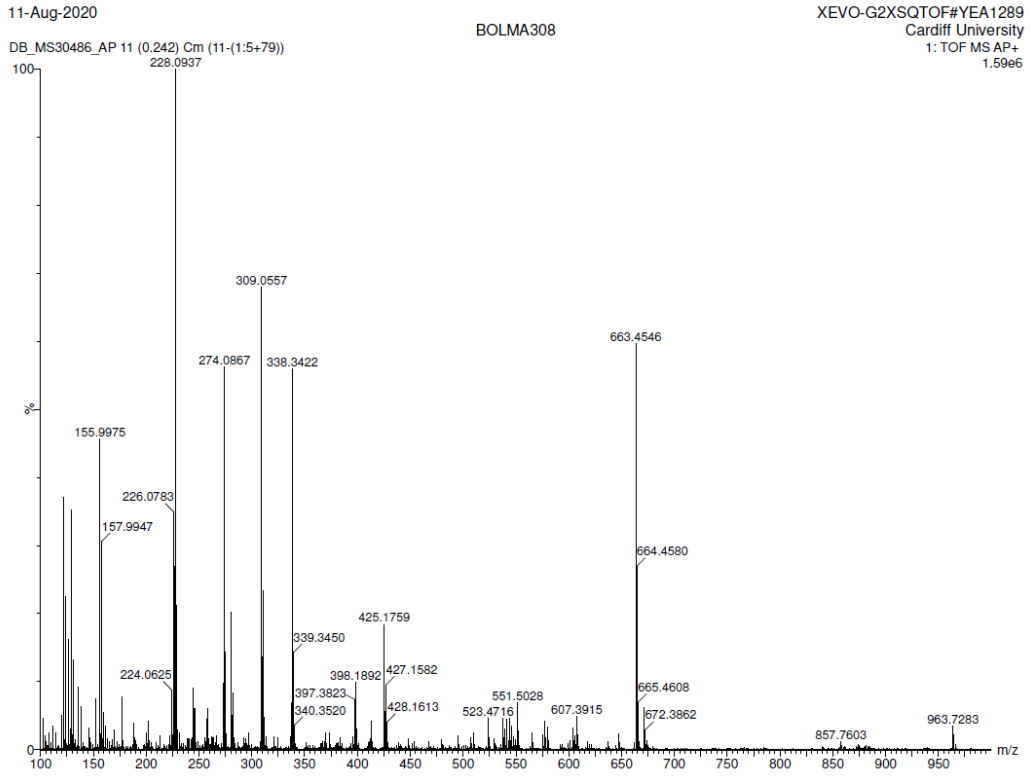

Figure A.140. HRMS, APCI+, TOF.

Characterisation of 4-chloro-3-(naphthalen-1-yl)benzonitrile 56

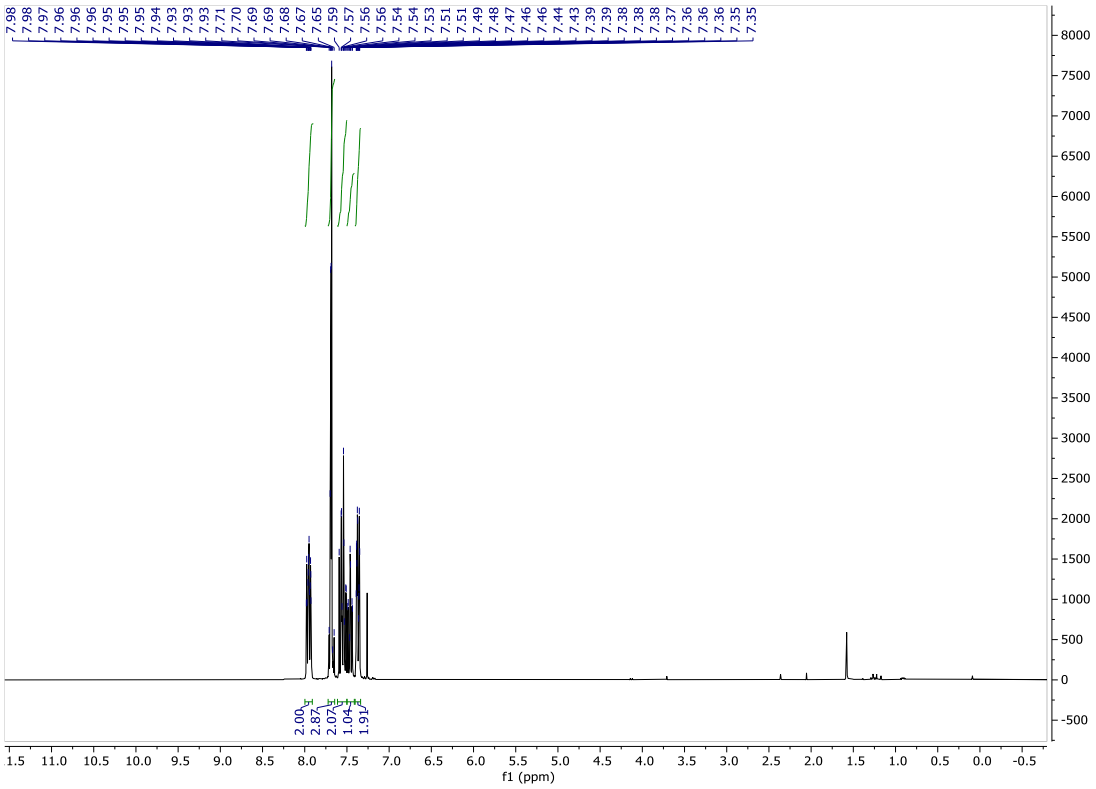

Figure A.141. ^{1}H NMR, 300 MHz, $CDCl_3$.

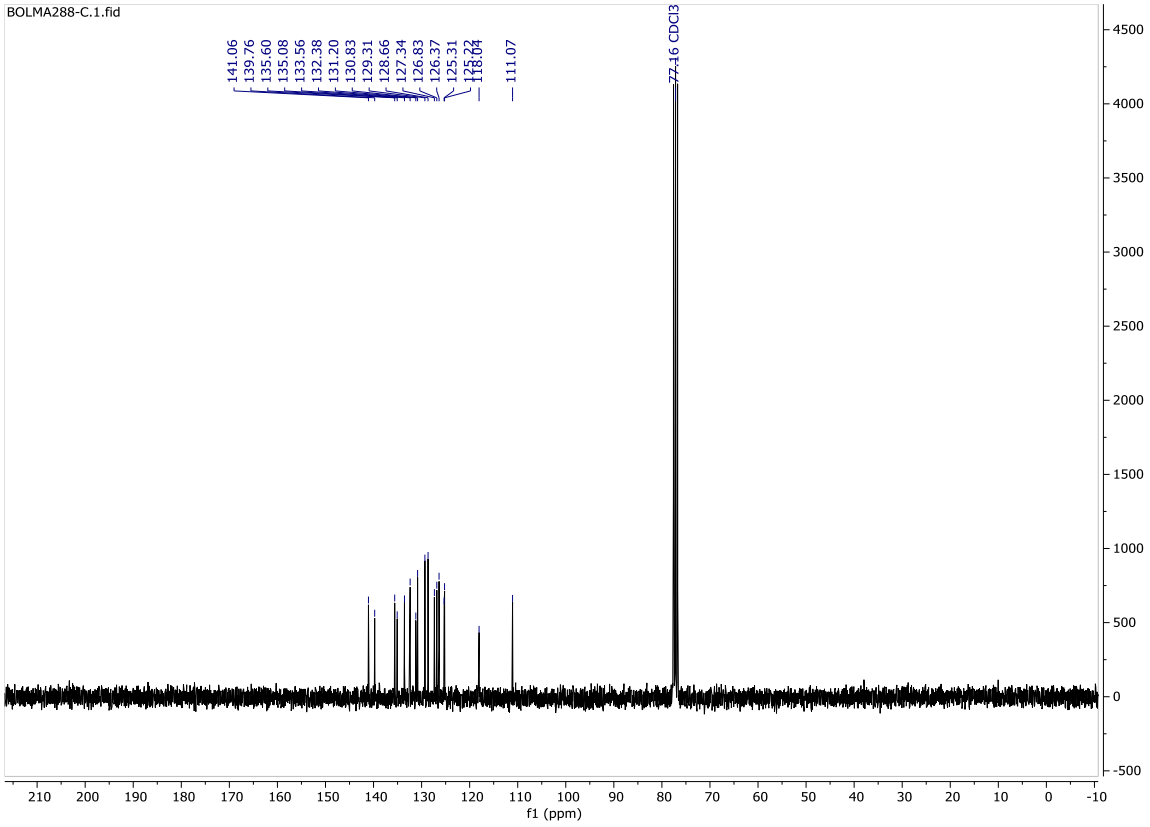

Figure A.142. ^{13}C NMR, 75 MHz, $CDCl_3$.

Elemental Composition Report **Page 1**

Single Mass Analysis
Tolerance = 5.0 PPM / DBE: min = -1.5, max = 200.0
Element prediction: Off
Number of isotope peaks used for i-FIT = 3

Monoisotopic Mass, Odd and Even Electron Ions
2 formula(e) evaluated with 1 results within limits (up to 50 closest results for each mass)
Elements Used:
C: 0-17 H: 0-11 N: 0-1 Cl: 0-1

Minimum:				-1.5				
Maximum:		5.0	5.0	200.0				
Mass	Calc. Mass	mDa	PPM	DBE	i-FIT	Norm	Conf(%)	Formula
263.0504	263.0502	0.2	0.8	13.0	1143.4	n/a	n/a	C17 H10 N Cl

Figure A.143. Elemental composition report.

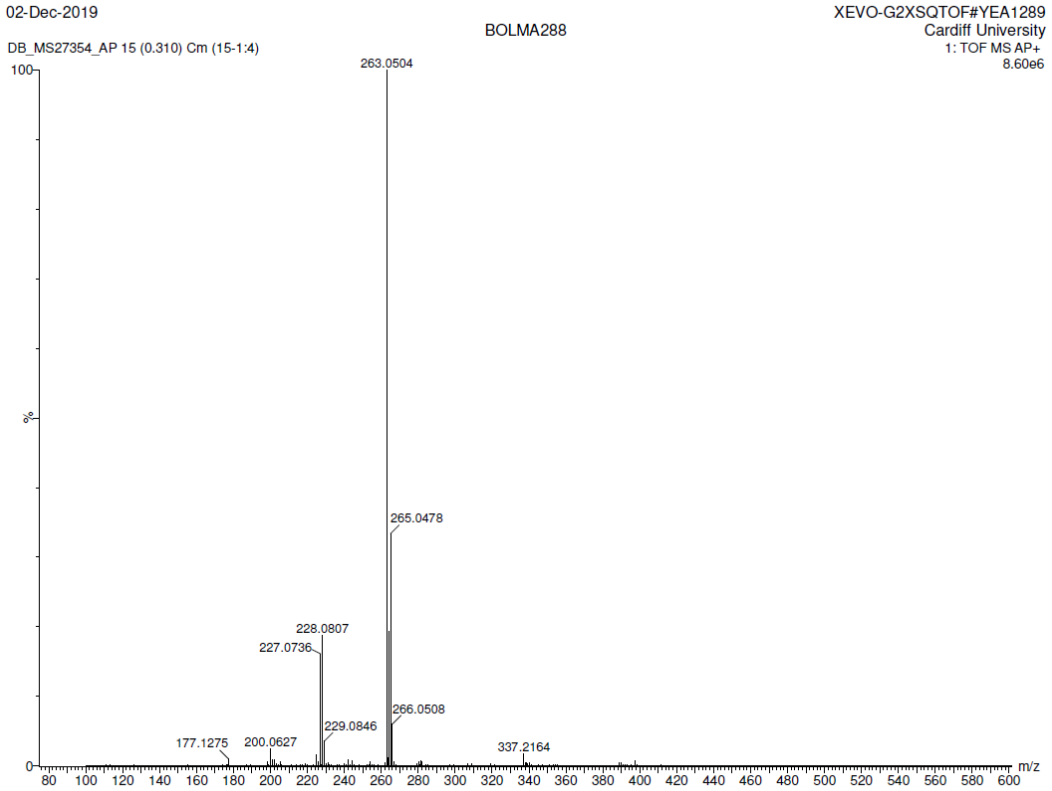

Figure A.144. HRMS, APCI+, TOF.

Characterisation of 6-chloro-2'-(1H-pyrrol-1-yl)-[1,1'-biphenyl]-3-carbonitrile 57

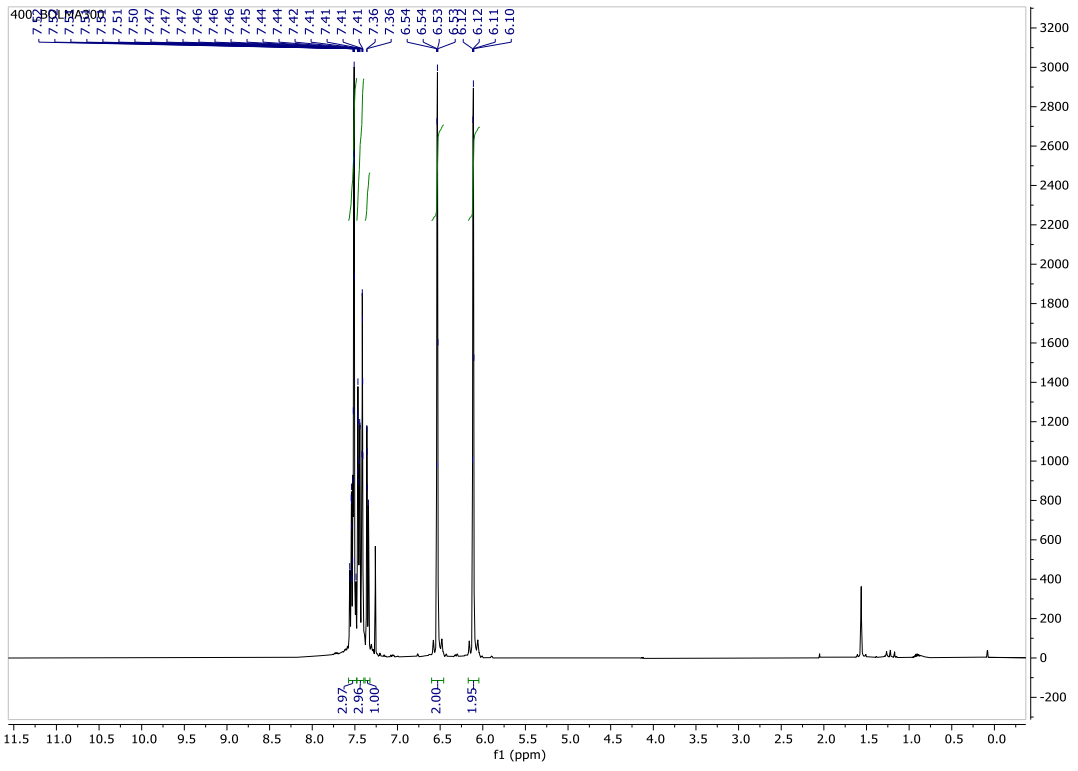

Figure A.145. ^{1}H NMR, 400 MHz, $CDCl_3$.

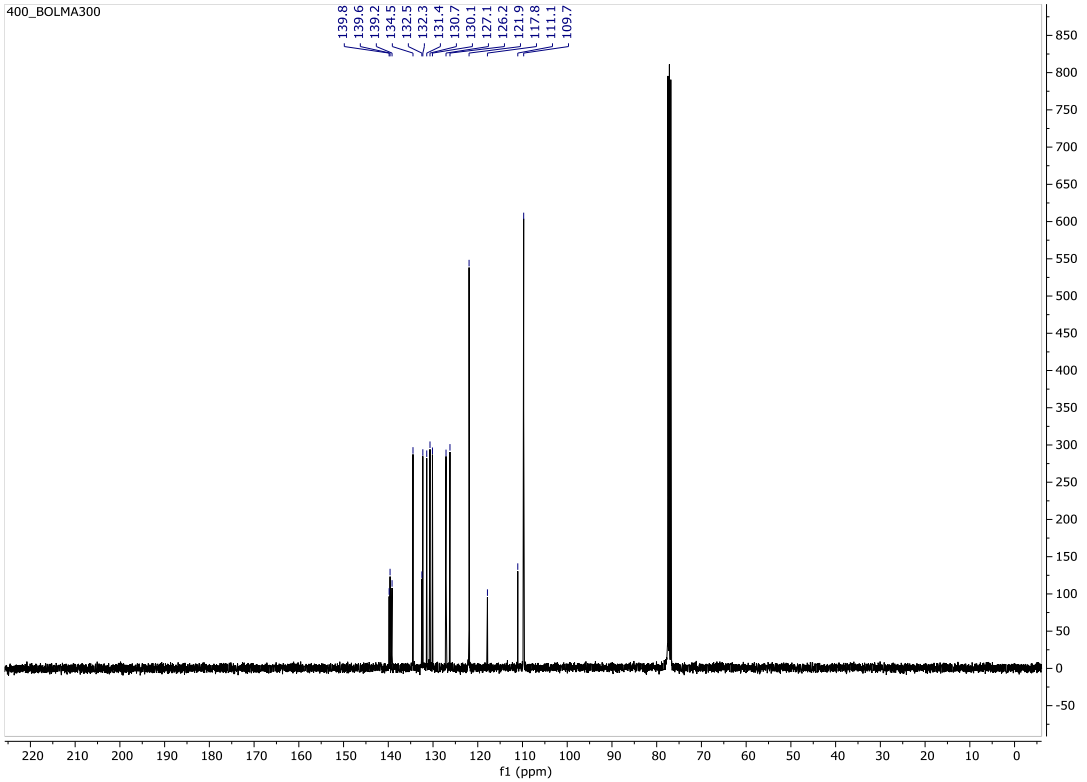

Figure A.146. ^{13}C NMR, 100 MHz, $CDCl_3$.

Elemental Composition Report **Page 1**

Single Mass Analysis
Tolerance = 5.0 PPM / DBE: min = -1.5, max = 200.0
Element prediction: Off
Number of isotope peaks used for i-FIT = 3

Monoisotopic Mass, Odd and Even Electron Ions
3 formula(e) evaluated with 1 results within limits (up to 50 closest results for each mass)
Elements Used:
C: 0-17 H: 0-12 N: 0-2 Cl: 0-1

Minimum:				-1.5				
Maximum:		5.0	5.0	200.0				
Mass	Calc. Mass	mDa	PPM	DBE	i-FIT	Norm	Conf(%)	Formula
279.0698	279.0689	0.9	3.2	12.5	1230.7	n/a	n/a	C17 H12 N2 Cl

Figure A.147. Elemental composition report.

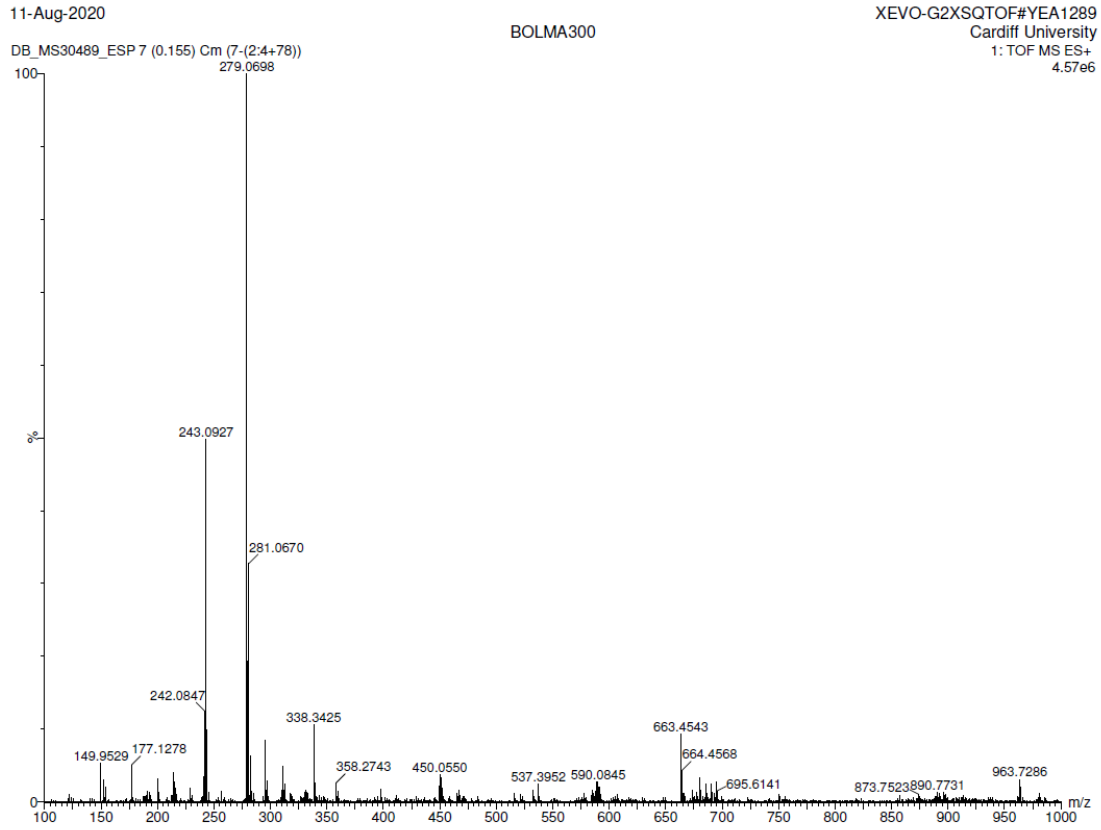

Figure A.148. HRMS, ES+, TOF.

Characterisation of 6-chloro-2'-(thiophen-3-yl)-[1,1'-biphenyl]-3-carbonitrile 58

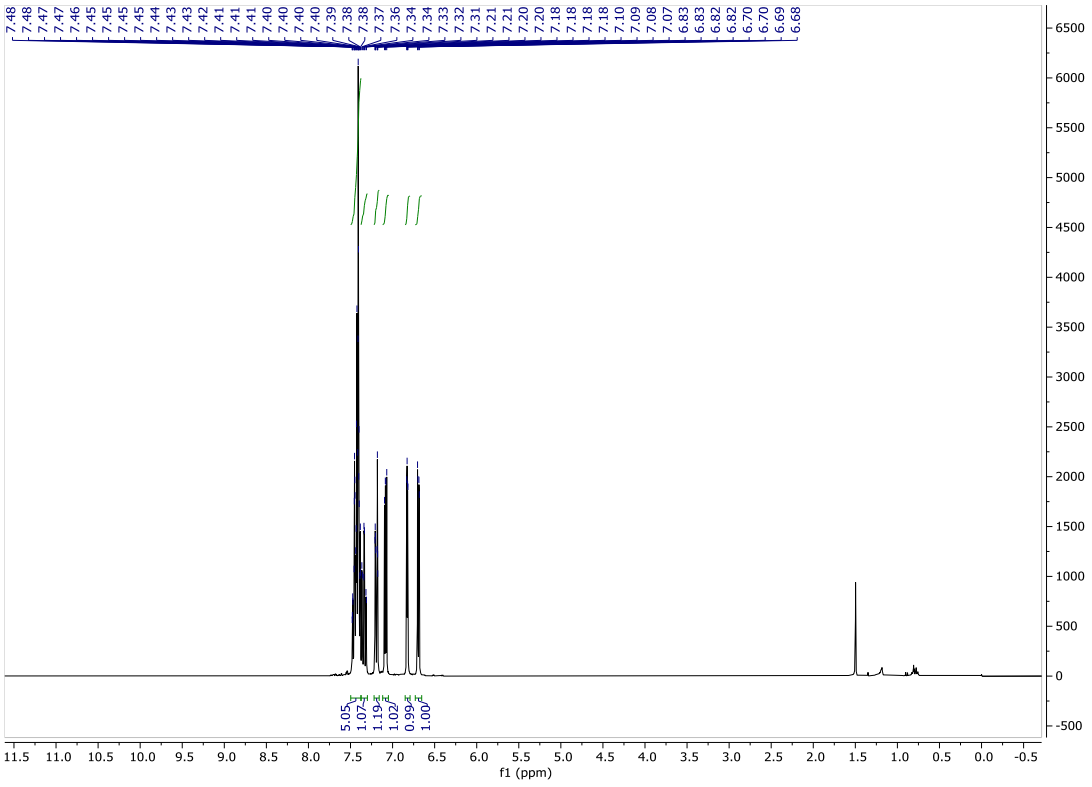

Figure A.149. ^{1}H NMR, 300 MHz, $CDCl_3$.

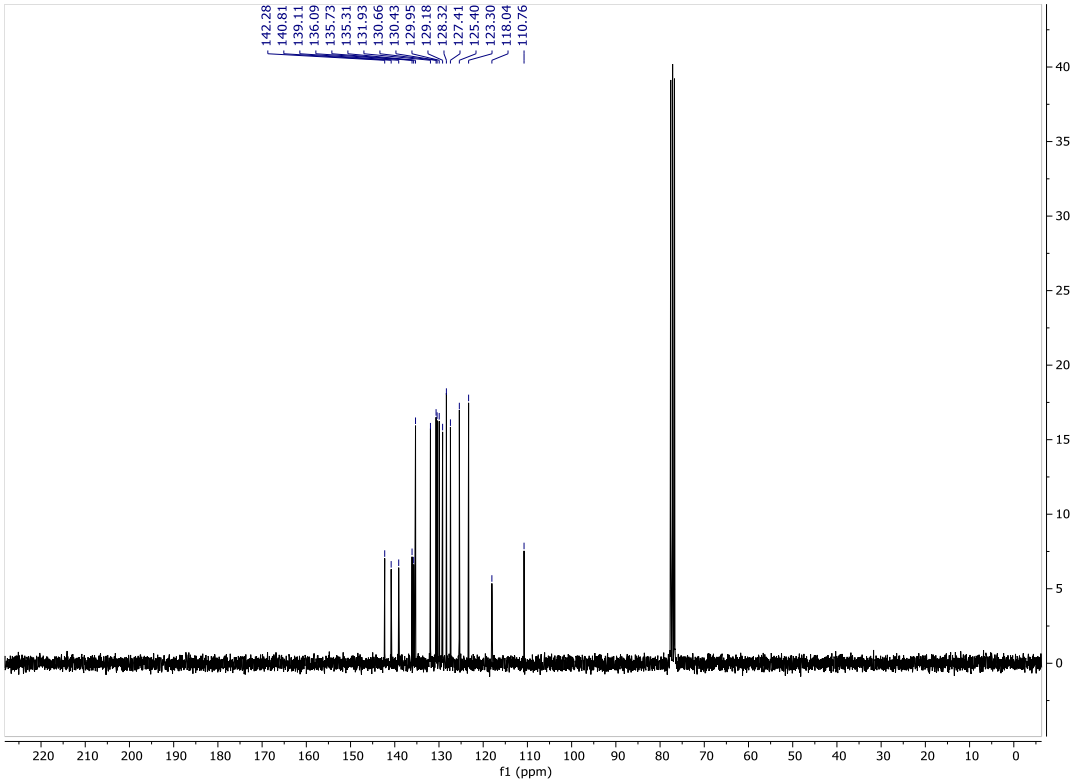

Figure A.150. ^{13}C NMR, 75 MHz, $CDCl_3$.

Elemental Composition Report **Page 1**

Single Mass Analysis
Tolerance = 5.0 PPM / DBE: min = -1.5, max = 200.0
Element prediction: Off
Number of isotope peaks used for i-FIT = 3

Monoisotopic Mass, Odd and Even Electron Ions
5 formula(e) evaluated with 1 results within limits (up to 50 closest results for each mass)
Elements Used:
C: 0-17 H: 0-11 N: 0-1 S: 0-1 Cl: 0-1

Minimum:				-1.5				
Maximum:		5.0	5.0	200.0				
Mass	Calc. Mass	mDa	PPM	DBE	i-FIT	Norm	Conf(%)	Formula
296.0313	296.0301	1.2	4.1	12.5	1070.3	n/a	n/a	C17 H11 N S Cl

Figure A.151. Elemental composition report.

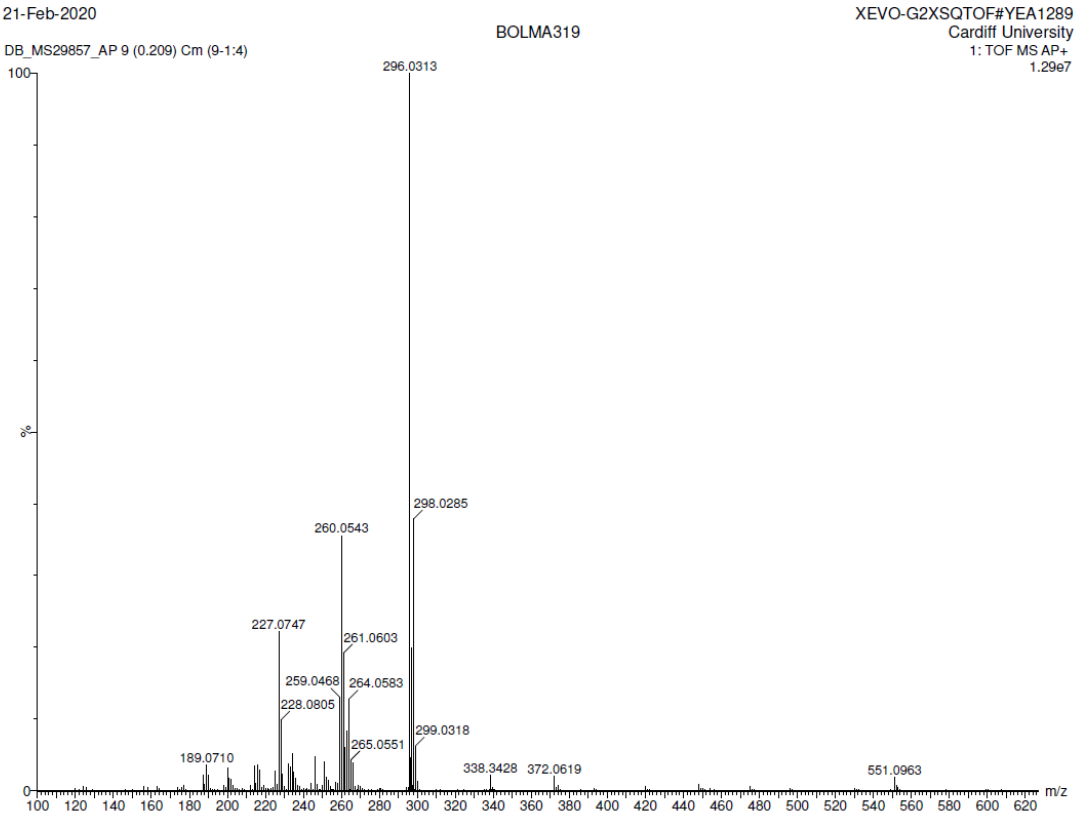

Figure A.152. HRMS, APCI+, TOF.

Characterisation of 2'-bromo-2,4-dimethoxy-1,1'-biphenyl 59a

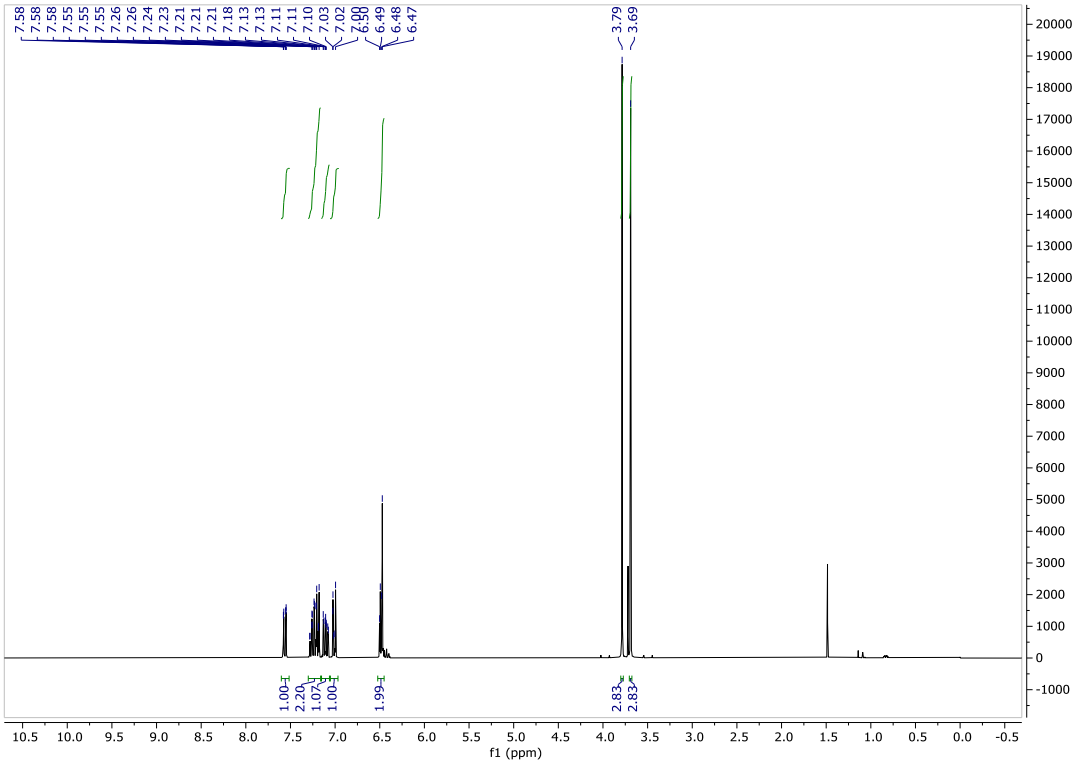

Figure A.153. ^{1}H NMR, 300 MHz, $CDCl_3$.

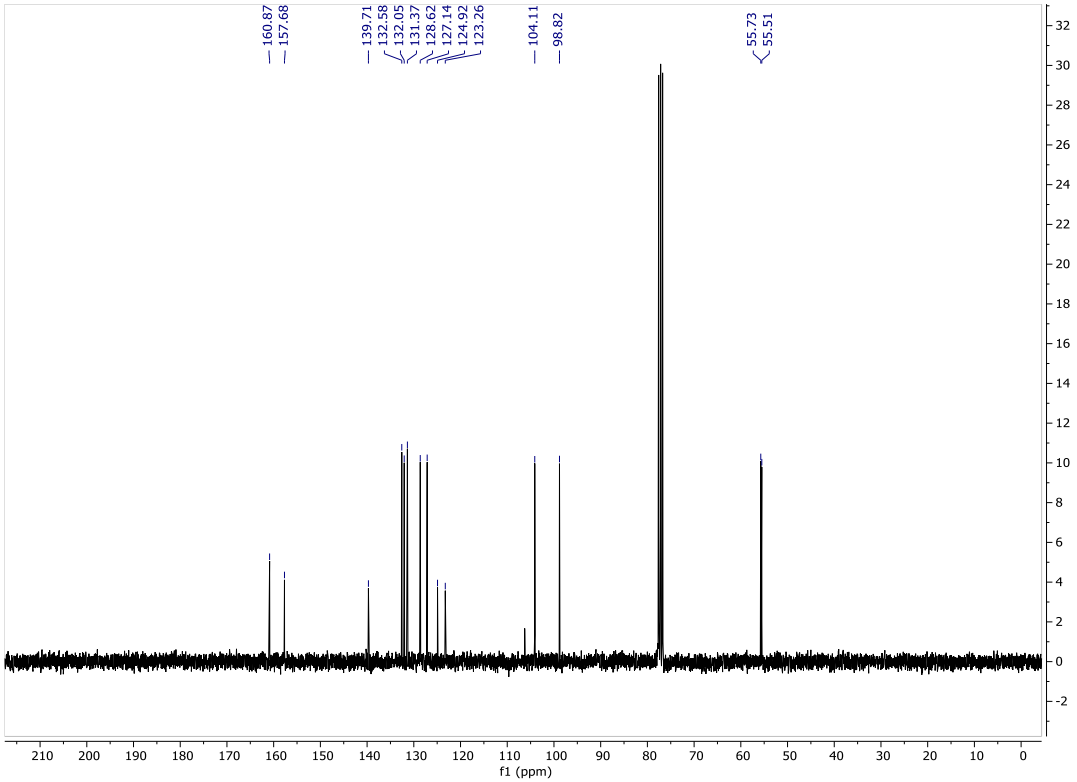

Figure A.154. ^{13}C NMR, 75 MHz, $CDCl_3$.

Elemental Composition Report **Page 1**

Single Mass Analysis
Tolerance = 5.0 PPM / DBE: min = -1.5, max = 200.0
Element prediction: Off
Number of isotope peaks used for i-FIT = 3

Monoisotopic Mass, Odd and Even Electron Ions
9 formula(e) evaluated with 1 results within limits (up to 50 closest results for each mass)
Elements Used:
C: 0-14 H: 0-14 B: 0-1 O: 0-2 Br: 0-1

Minimum:				-1.5				
Maximum:		5.0	5.0	200.0				
Mass	Calc. Mass	mDa	PPM	DBE	i-FIT	Norm	Conf(%)	Formula
293.0180	293.0177	0.3	1.0	7.5	175.3	n/a	n/a	C14 H14 O2 Br

Figure A.155. Elemental composition report.

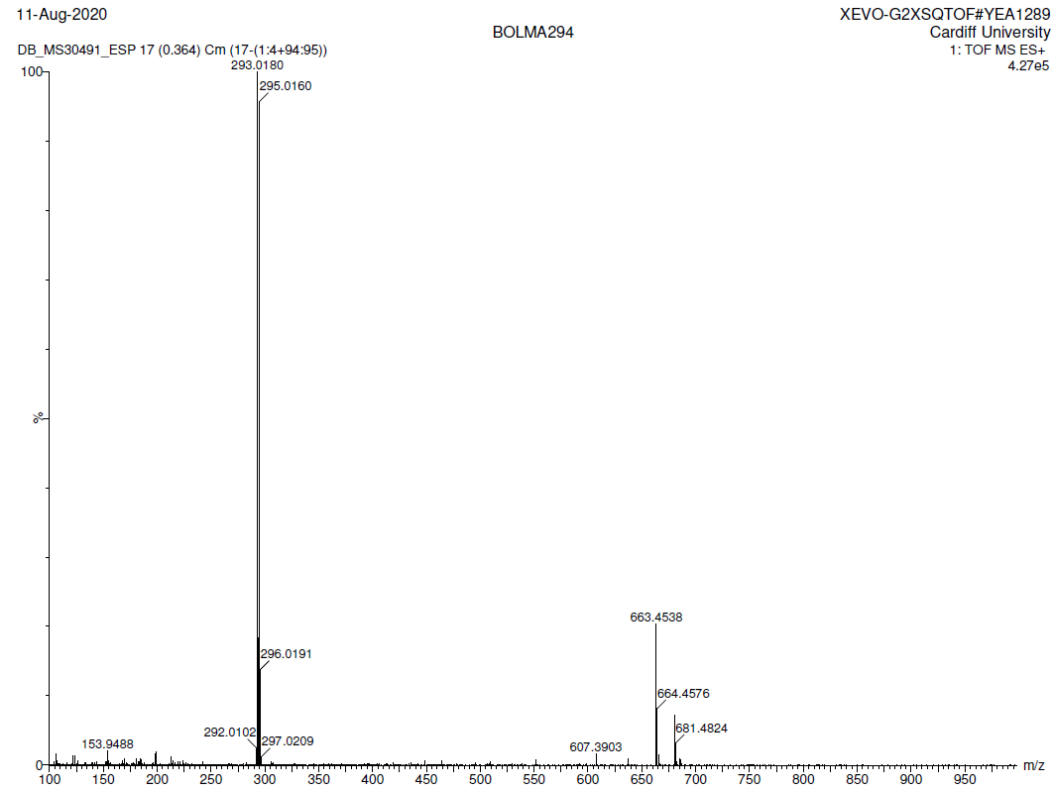

Figure A.156. HRMS, ES+, TOF.

Characterisation 6-chloro-2'',4''-dimethoxy-[1,1':2',1''-terphenyl]-3-carbonitrile 59

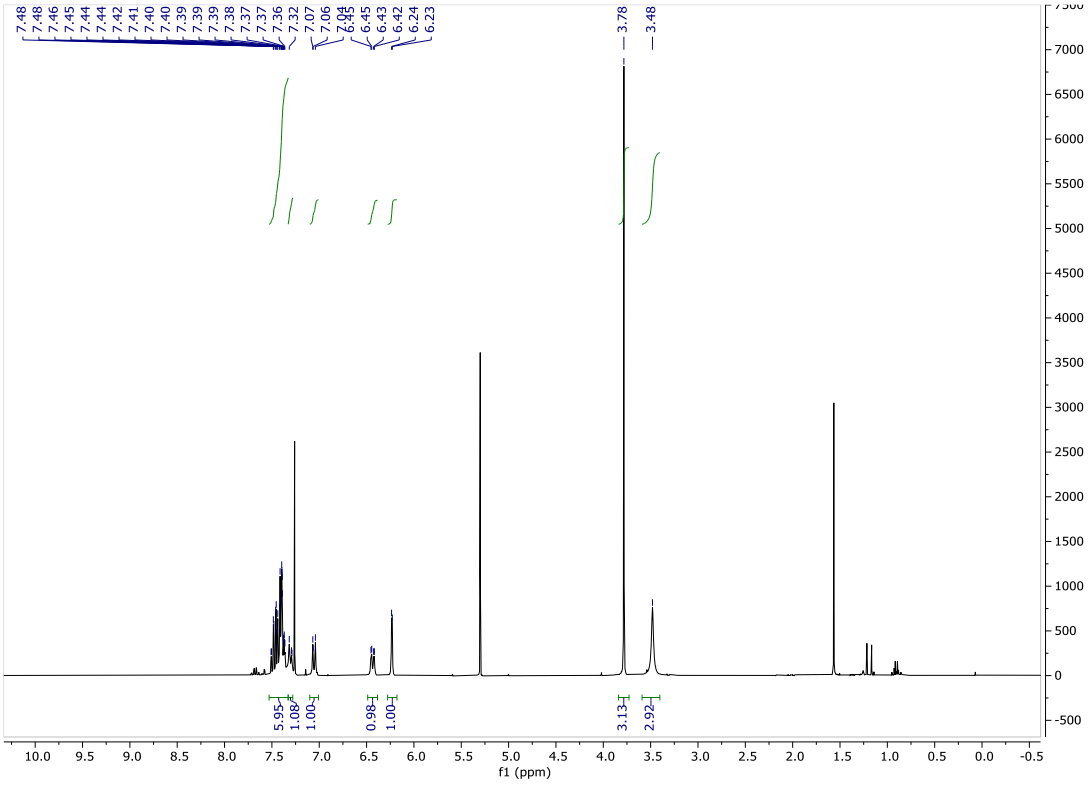

Figure A.157. ^{1}H NMR, 300 MHz, $CDCl_3$.

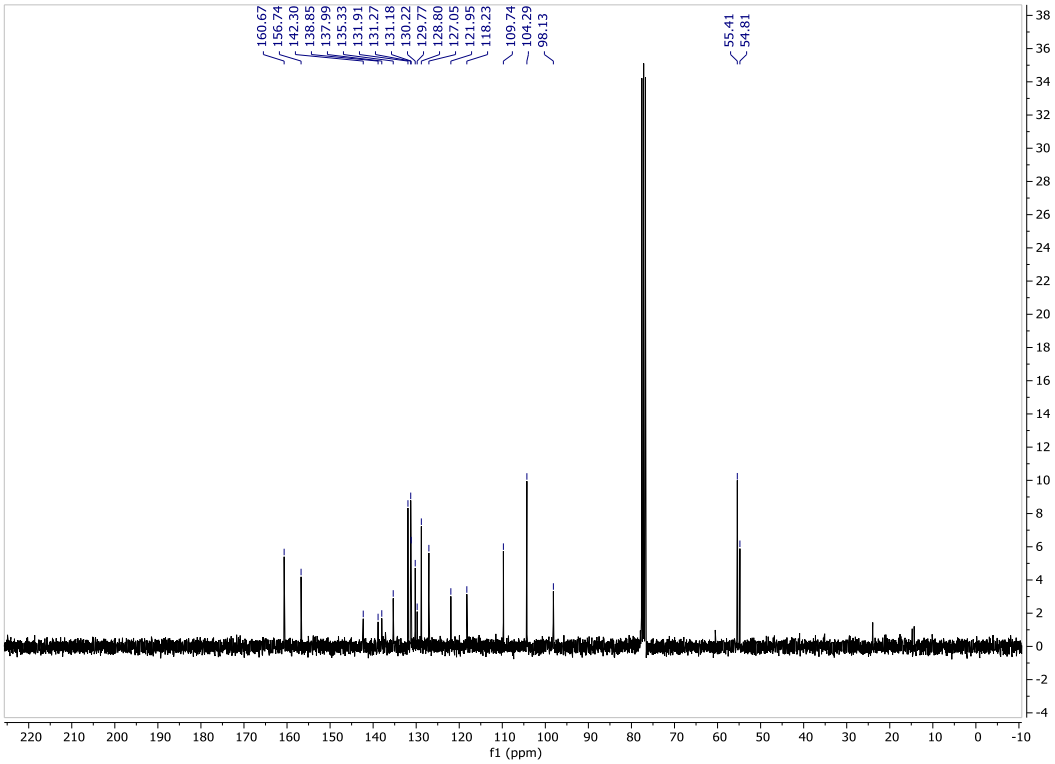

Figure A.158. ^{13}C NMR, 75 MHz, $CDCl_3$.

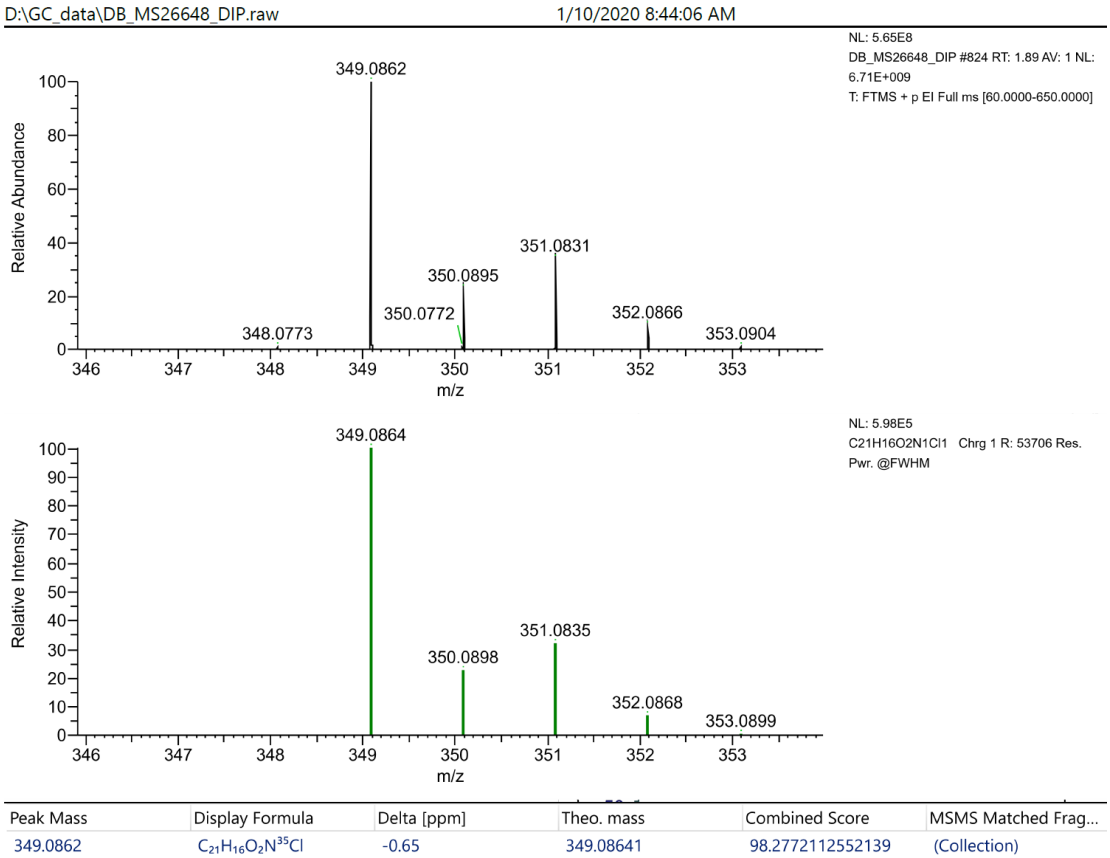

Peak Mass	Display Formula	Delta [ppm]	Theo. mass	Combined Score	MSMS Matched Frag...
349.0862	$C_{21}H_{16}O_2N^{35}Cl$	-0.65	349.08641	98.2772112552139	(Collection)

Figure A.159. Elemental composition report.

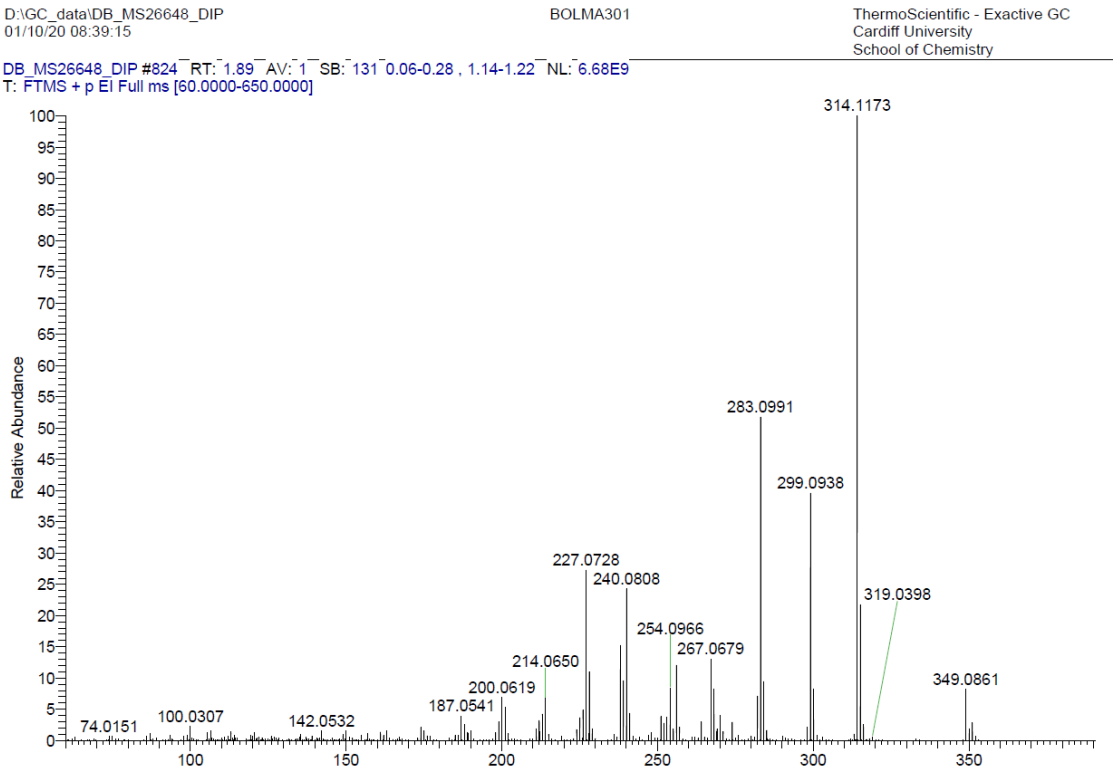

Figure A.160. HRMS, EI+, TOF.

Characterisation of 2-bromo-4'-(tert-butyl)-1,1'-biphenyl 60a

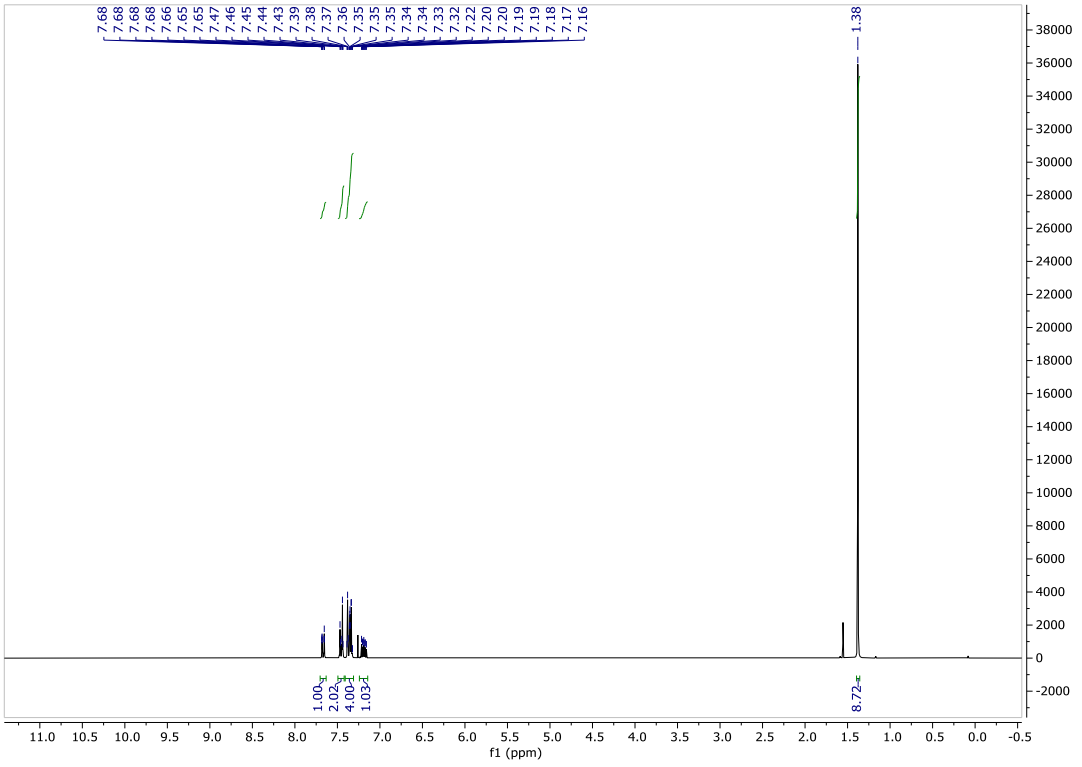

Figure A.161. ^{1}H NMR, 300 MHz, $CDCl_3$.

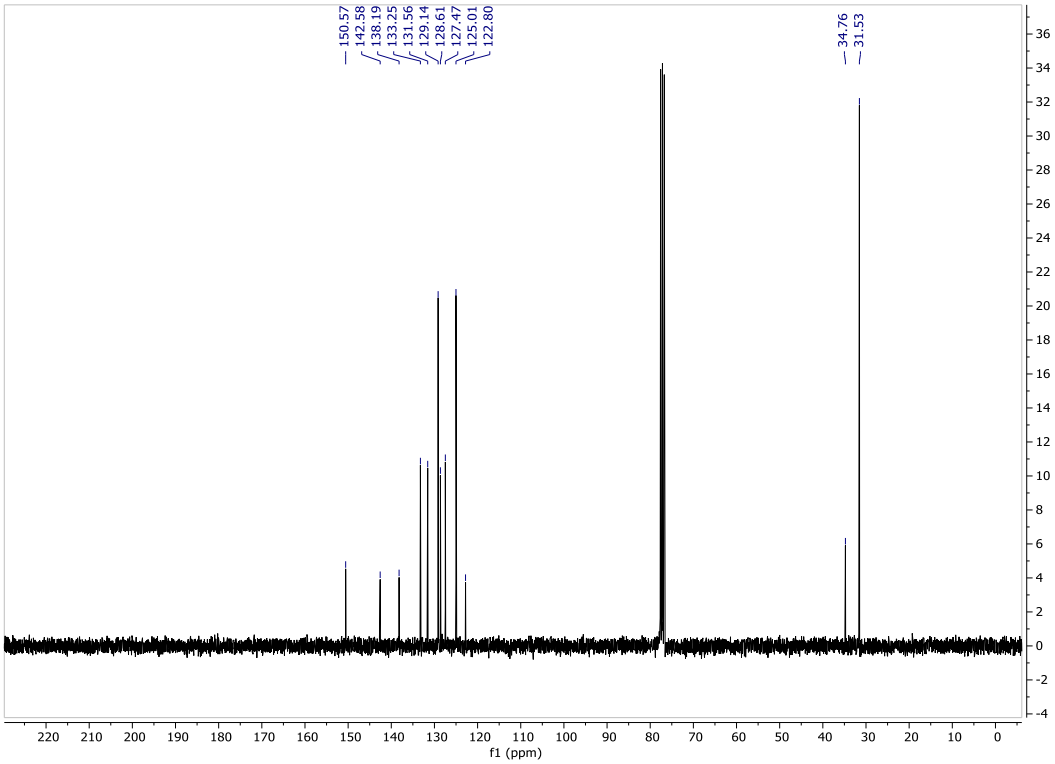

Figure A.162. ^{13}C NMR, 75 MHz, $CDCl_3$.

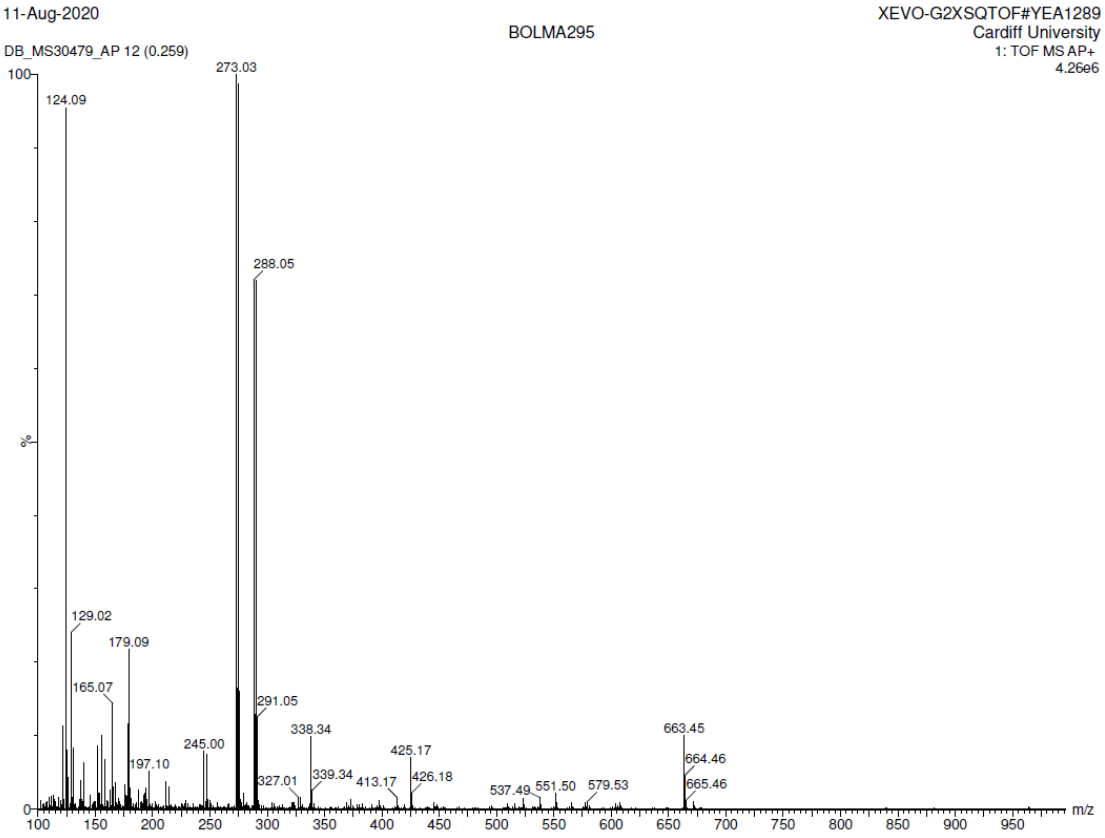

Figure A.163. LRMS, APCI+, TOF.

Characterisation of 4''-(tert-butyl)-6-chloro-[1,1':2',1''-terphenyl]-3-carbonitrile 60

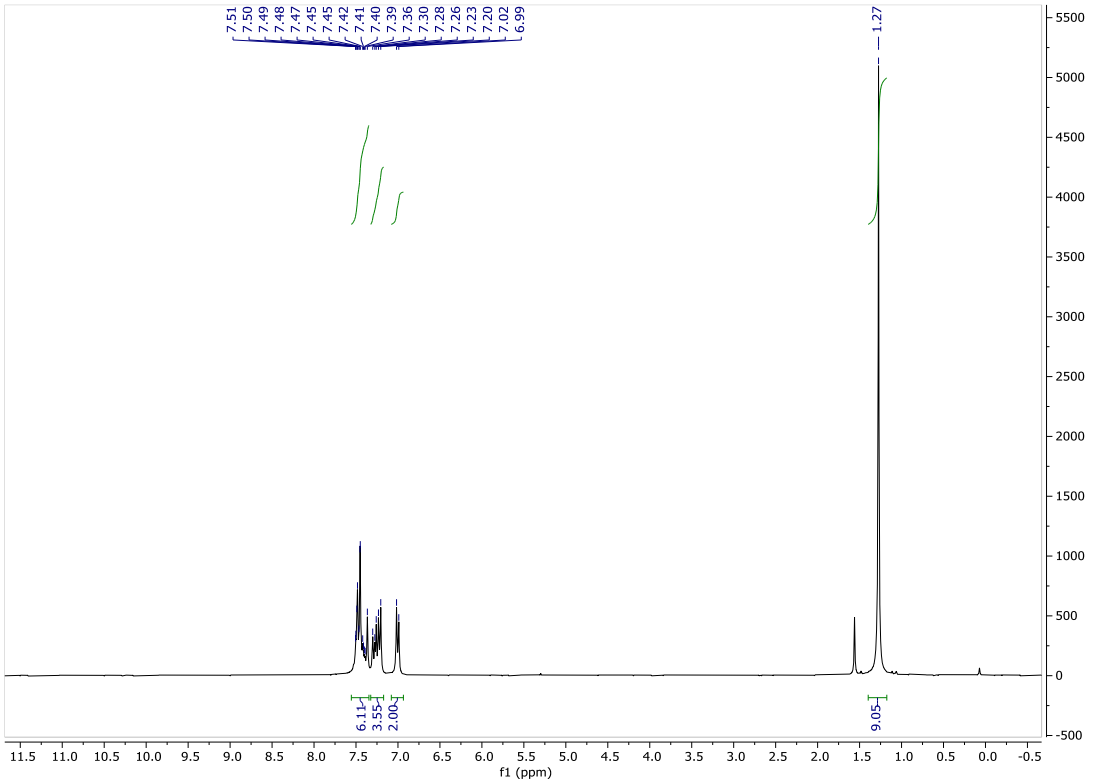

Figure A.164. ^{1}H NMR, 300 MHz, $CDCl_3$.

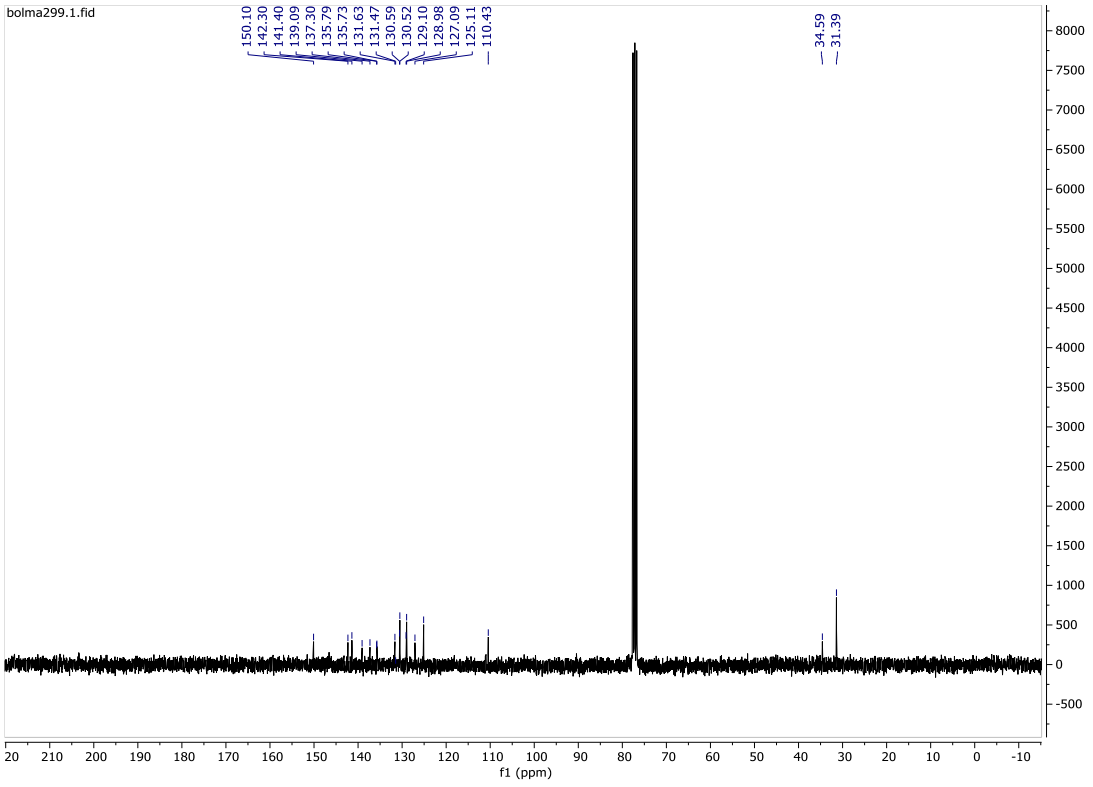

Figure A.165. ^{13}C NMR, 75 MHz, $CDCl_3$.

Elemental Composition Report **Page 1**

Single Mass Analysis
Tolerance = 5.0 PPM / DBE: min = -1.5, max = 200.0
Element prediction: Off
Number of isotope peaks used for i-FIT = 3

Monoisotopic Mass, Odd and Even Electron Ions
2 formula(e) evaluated with 1 results within limits (up to 50 closest results for each mass)
Elements Used:
C: 0-23 H: 0-21 N: 0-1 Cl: 0-1

Minimum:				-1.5				
Maximum:		5.0	5.0	200.0				
Mass	Calc. Mass	mDa	PPM	DBE	i-FIT	Norm	Conf(%)	Formula
345.1287	345.1284	0.3	0.9	14.0	935.7	n/a	n/a	C23 H20 N Cl

Figure A.166. Elemental composition report.

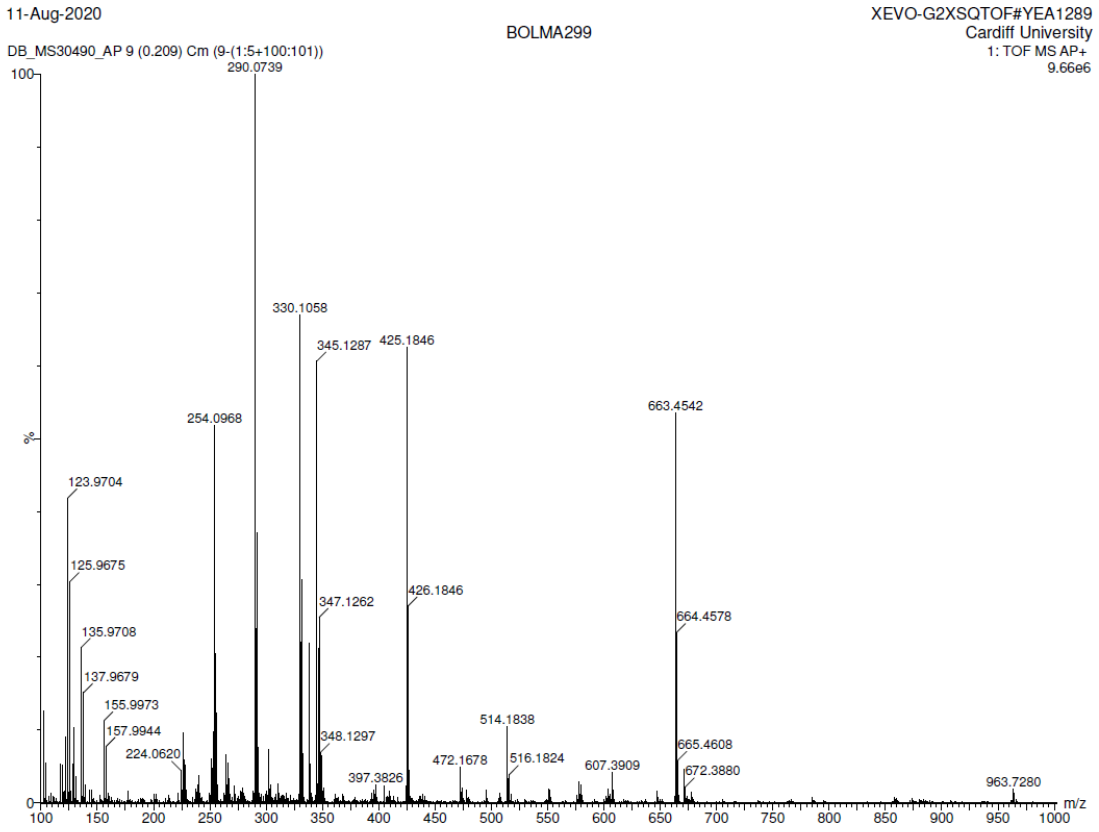

Figure A.167. HRMS, APCI+, TOF.

Characterisation of methyl 2'-bromo-[1,1'-biphenyl]-4-carboxylate 61a

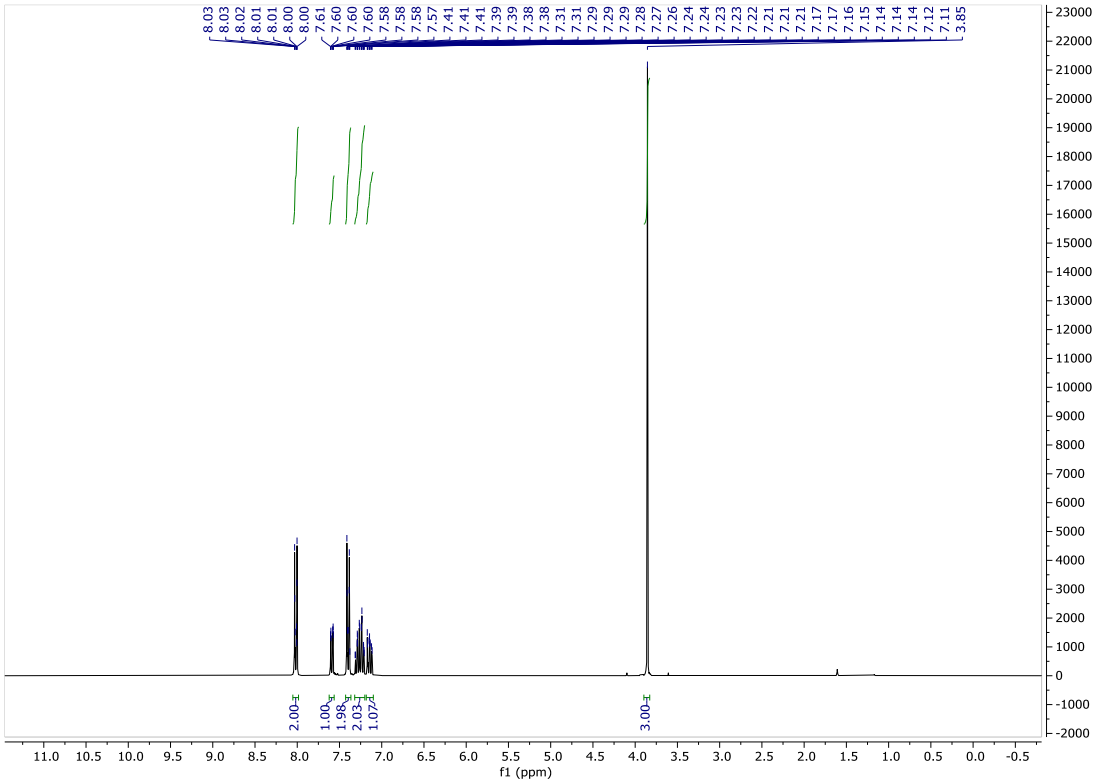

Figure A.168. ^{1}H NMR, 300 MHz, $CDCl_3$.

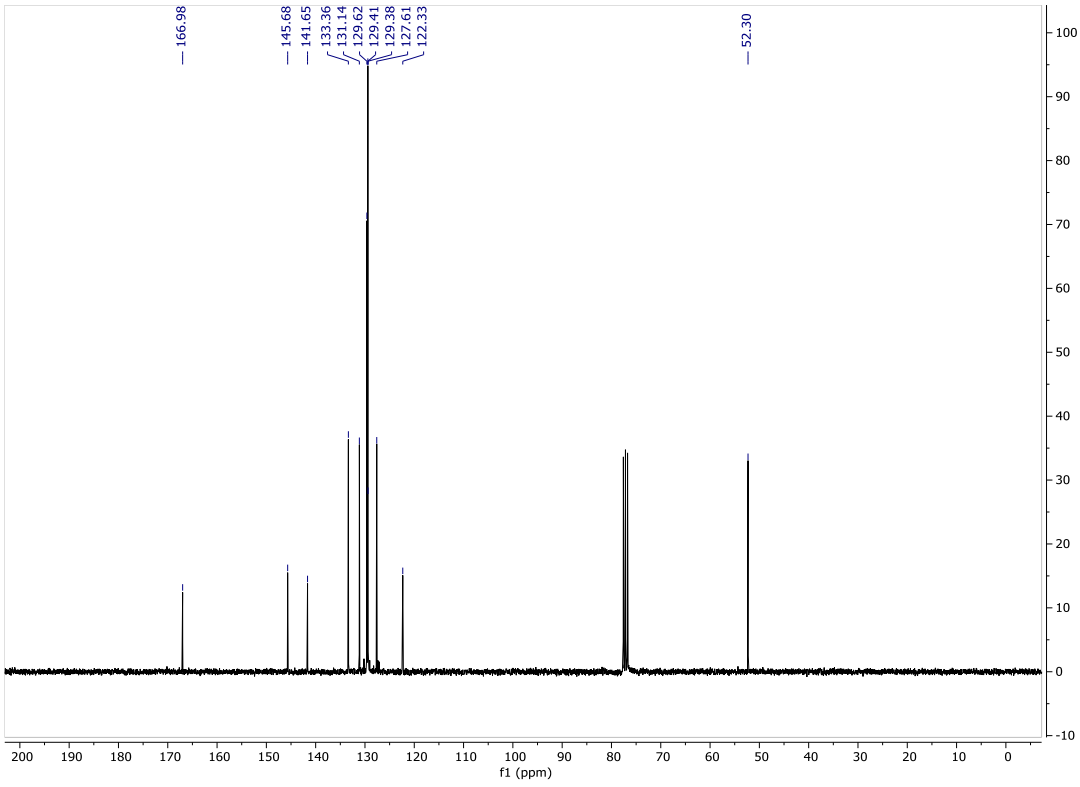

Figure A.169. ^{13}C NMR, 75 MHz, $CDCl_3$.

Elemental Composition Report **Page 1**

Single Mass Analysis
Tolerance = 5.0 PPM / DBE: min = -1.5, max = 200.0
Element prediction: Off
Number of isotope peaks used for i-FIT = 3

Monoisotopic Mass, Odd and Even Electron Ions
5 formula(e) evaluated with 1 results within limits (up to 50 closest results for each mass)
Elements Used:
C: 0-14 H: 0-12 O: 0-2 Br: 0-1

Minimum:				-1.5				
Maximum:		5.0	5.0	200.0				
Mass	Calc. Mass	mDa	PPM	DBE	i-FIT	Norm	Conf(%)	Formula
291.0028	291.0021	0.7	2.4	8.5	453.8	n/a	n/a	C14 H12 O2 Br

Figure A.170. Elemental composition report.

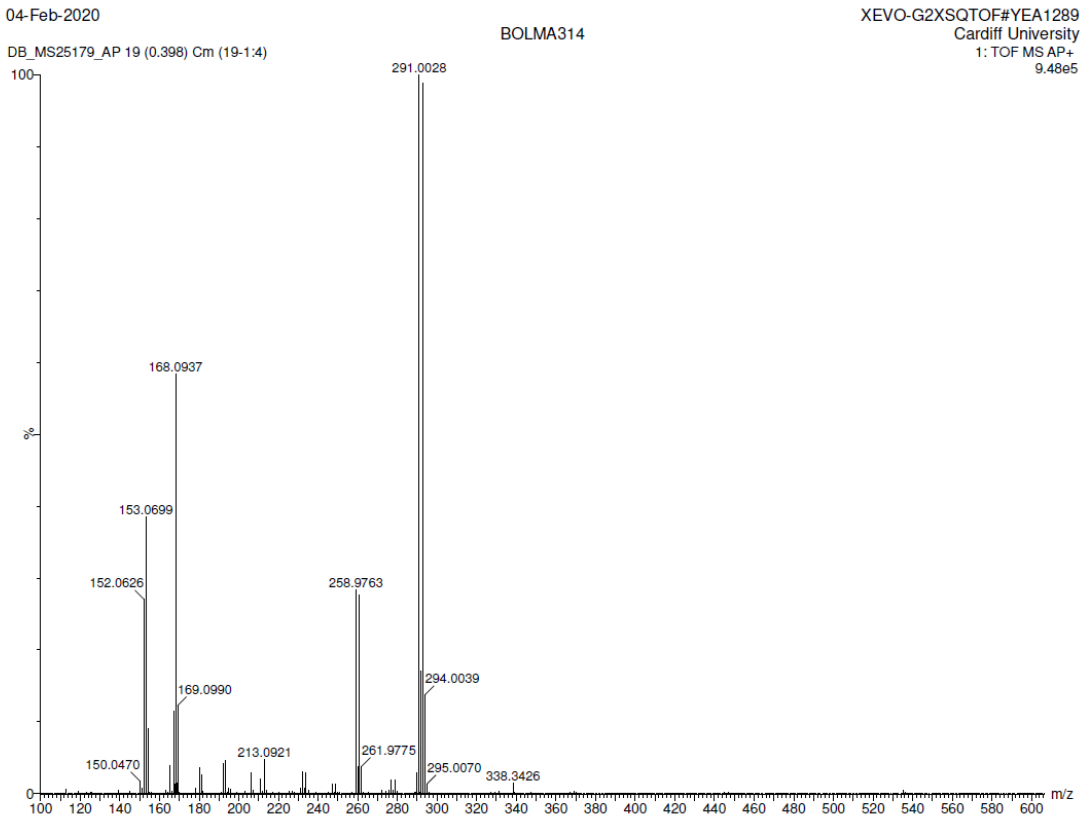

Figure A.171. HRMS, APCI+, TOF.

Characterisation of methyl 2''-chloro-5''-cyano-[1,1':2',1''-terphenyl]-4-carboxylate 61

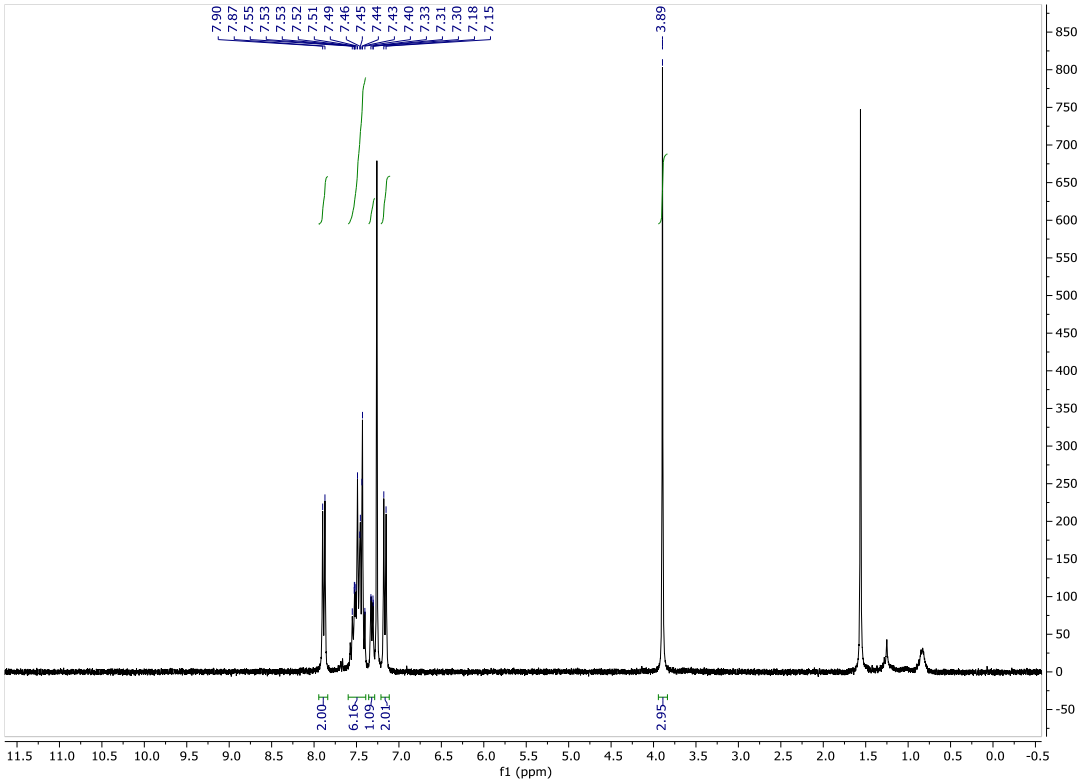

Figure A.172. ^{1}H NMR, 300 MHz, $CDCl_3$.

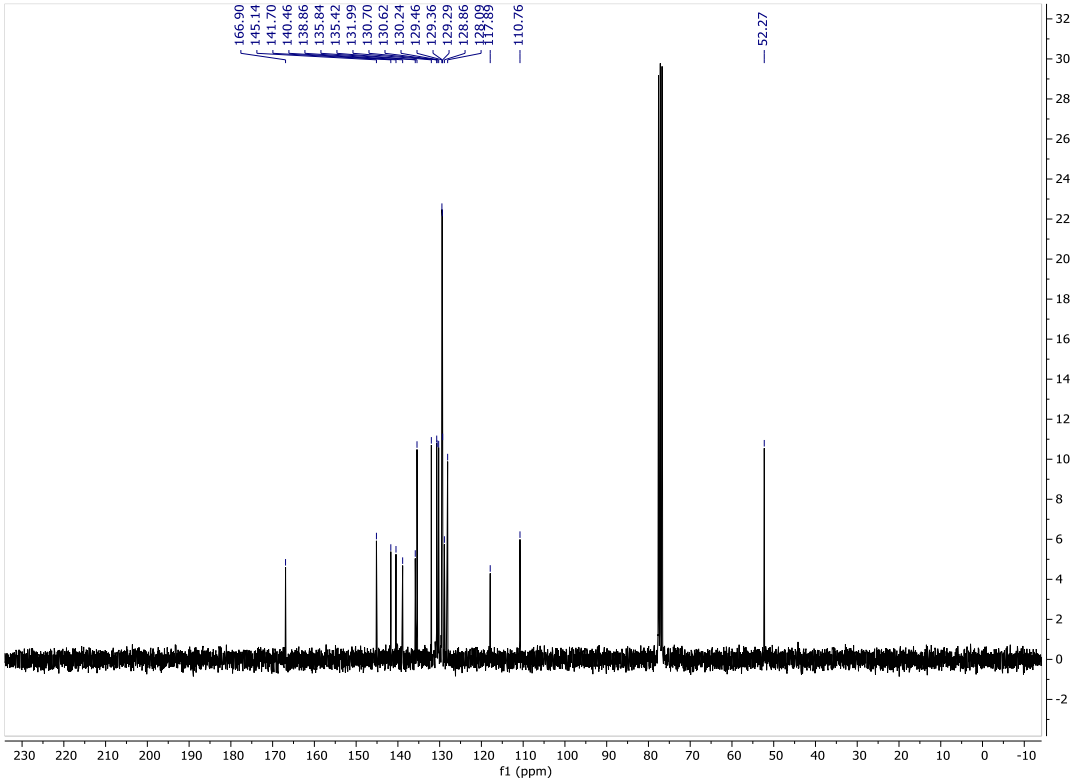

Figure A.173. ^{13}C NMR, 75 MHz, $CDCl_3$.

Elemental Composition Report **Page 1**

Single Mass Analysis
Tolerance = 5.0 PPM / DBE: min = -1.5, max = 200.0
Element prediction: Off
Number of isotope peaks used for i-FIT = 3

Monoisotopic Mass, Odd and Even Electron Ions
16 formula(e) evaluated with 1 results within limits (up to 50 closest results for each mass)
Elements Used:
C: 0-21 H: 0-14 N: 0-1 O: 0-2 23Na: 0-1 Cl: 0-1

Minimum:				-1.5				
Maximum:		5.0	5.0	200.0				
Mass	Calc. Mass	mDa	PPM	DBE	i-FIT	Norm	Conf(%)	Formula
370.0615	370.0611	0.4	1.1	14.5	465.9	n/a	n/a	C21 H14 N O2 23Na Cl

Figure A.173. Elemental composition report.

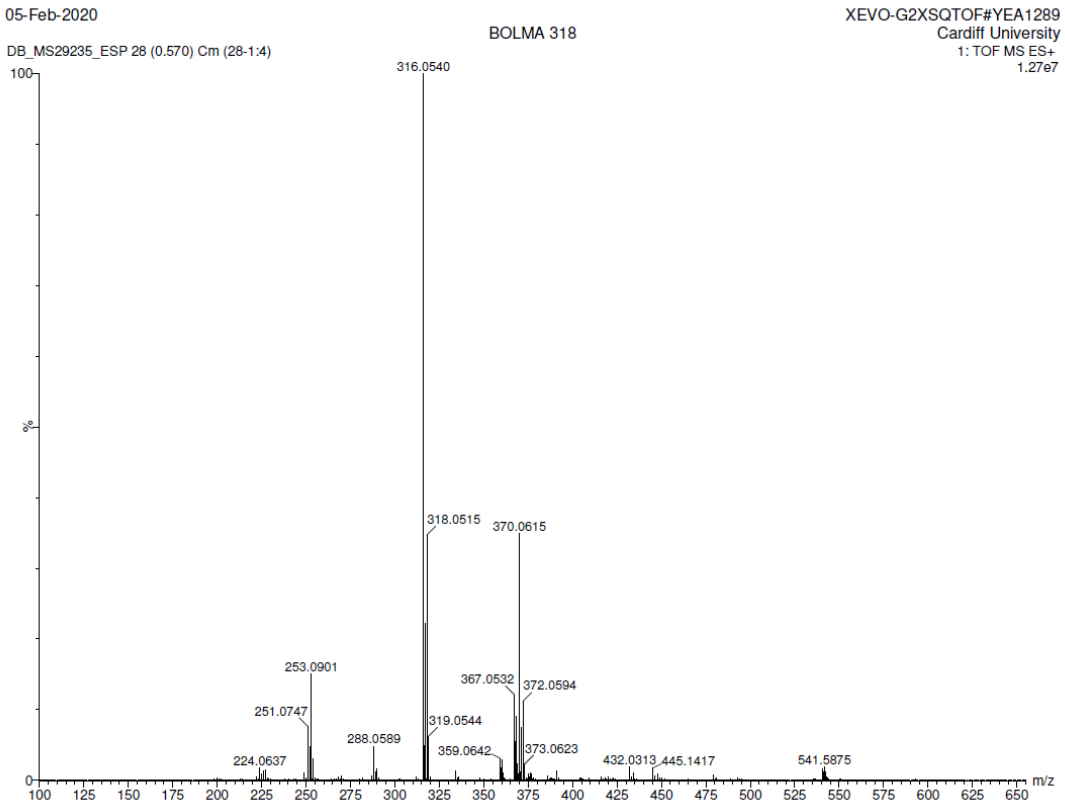

Figure A.174. HRMS, ES+, TOF.

Characterisation of 2'-bromo-[1,1'-biphenyl]-4-carbonitrile 62a

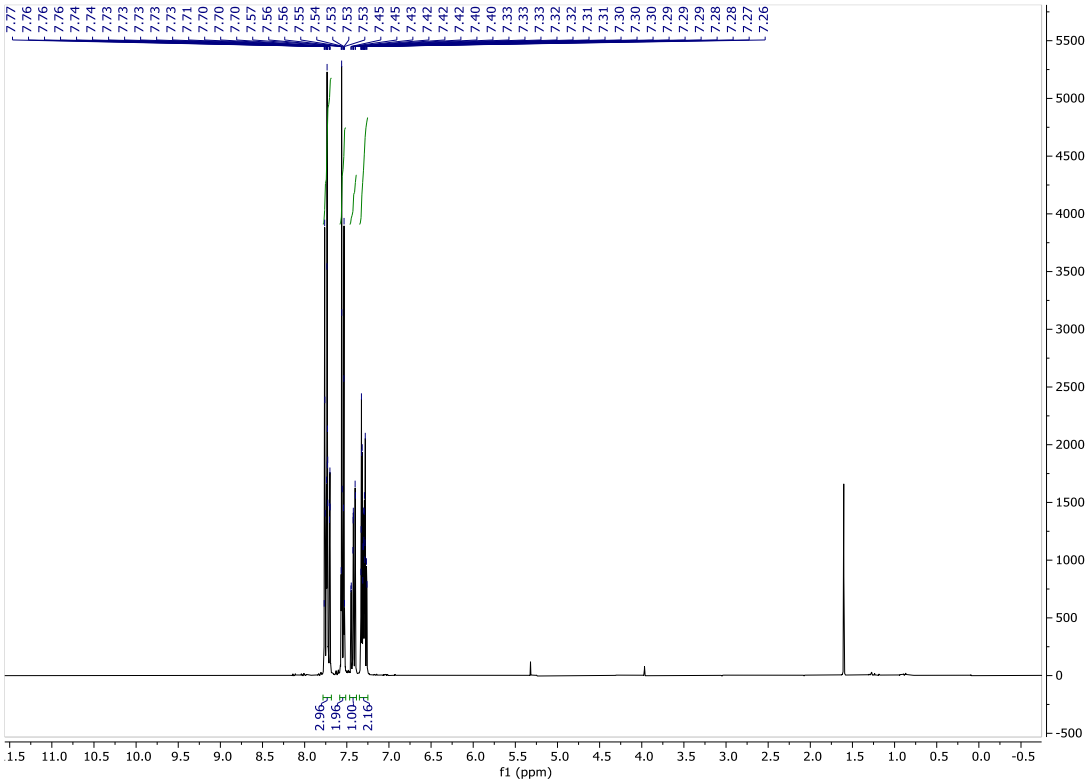

Figure A.175. ^{1}H NMR, 300 MHz, $CDCl_3$.

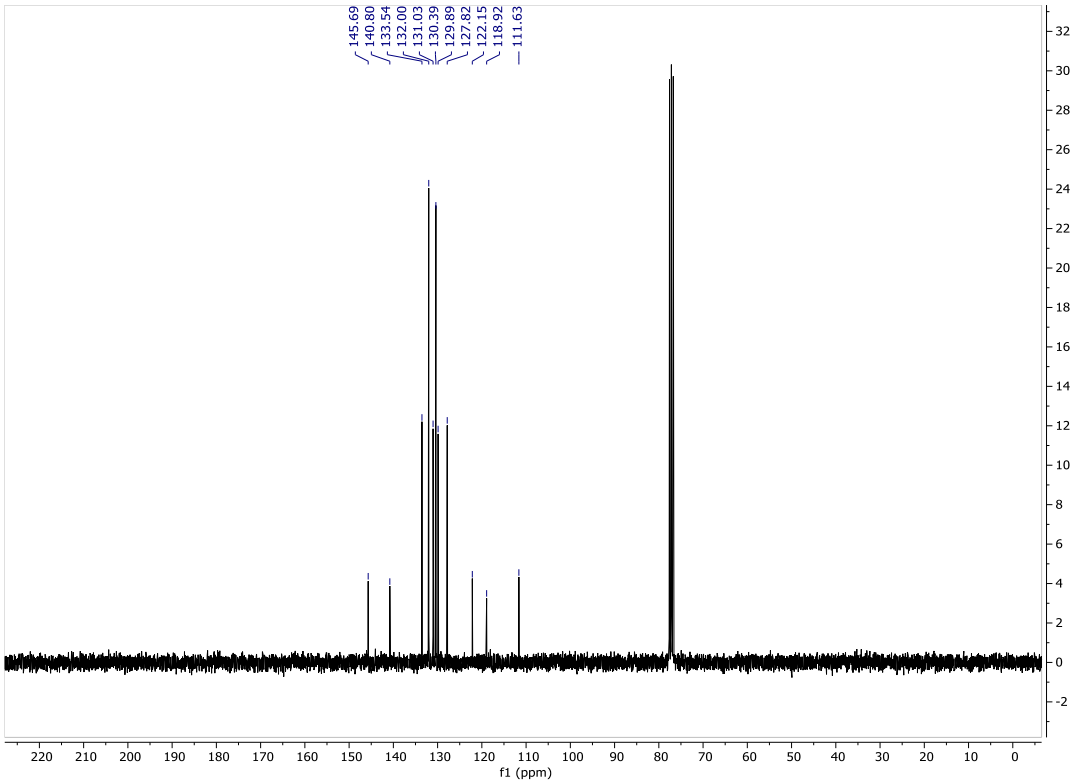

Figure A.176. ^{13}C NMR, 75 MHz, $CDCl_3$.

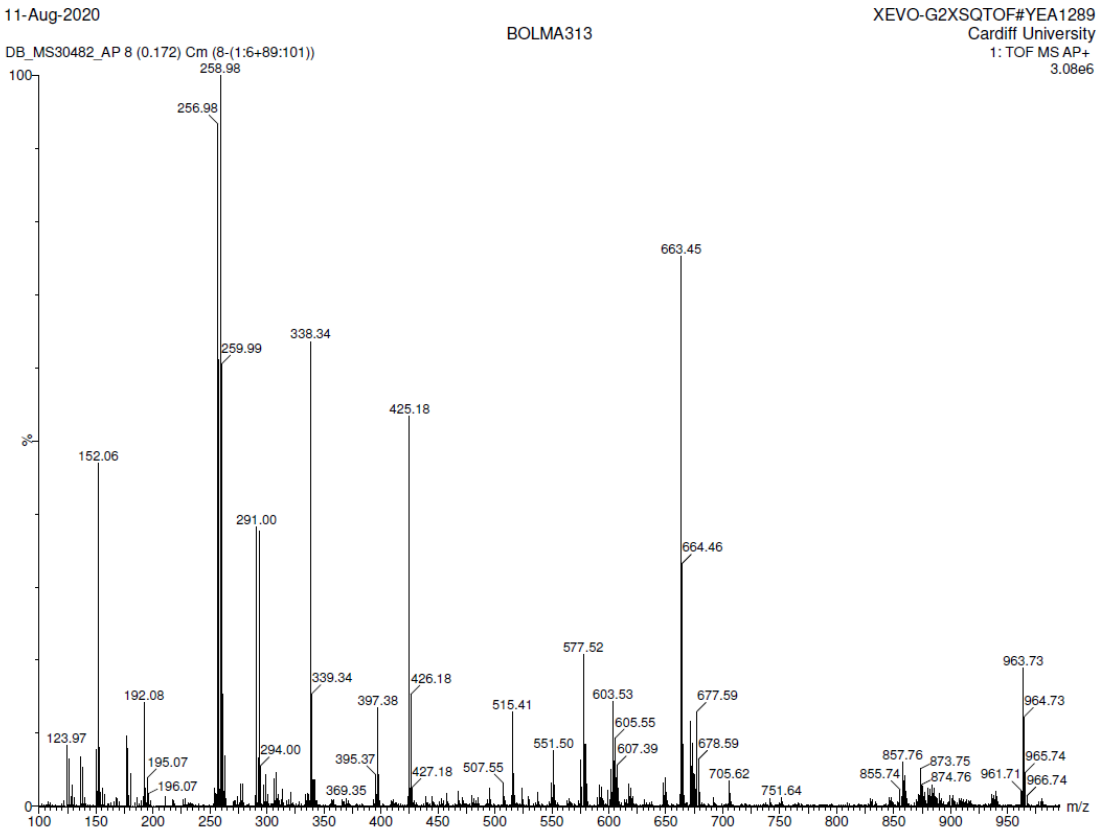

Figure A.177. LRMS, APCI+, TOF.

Characterisation of 6-chloro-[1,1':2',1''-terphenyl]-3,4''-dicarbonitrile 62

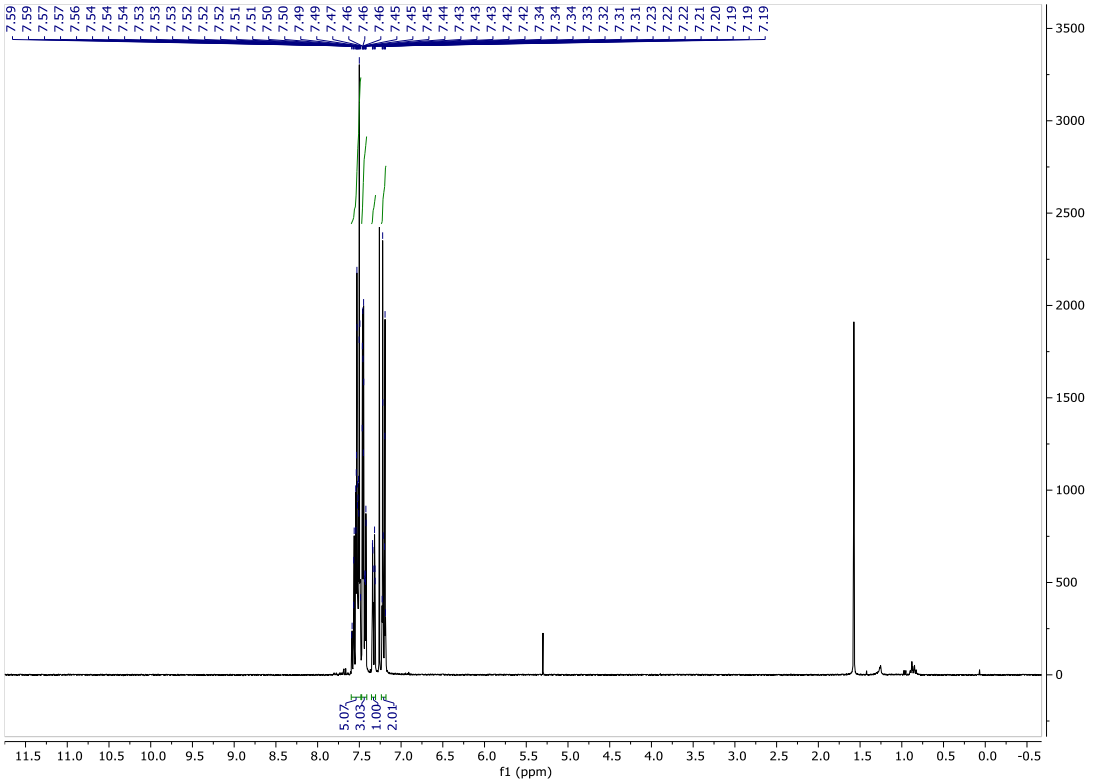

Figure A.178. ^{13}C NMR, 75 MHz, $CDCl_3$.

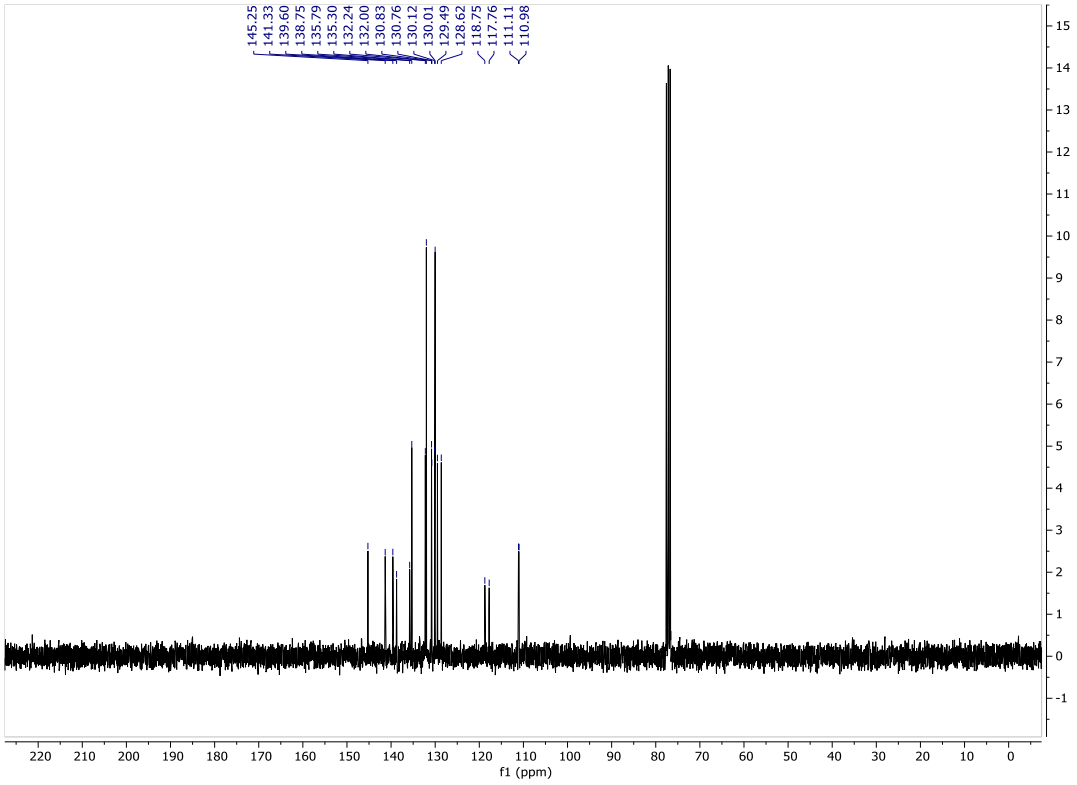

Figure A.179. ^{13}C NMR, 75 MHz, $CDCl_3$.

Elemental Composition Report **Page 1**

Single Mass Analysis
Tolerance = 5.0 PPM / DBE: min = -1.5, max = 200.0
Element prediction: Off
Number of isotope peaks used for i-FIT = 3

Monoisotopic Mass, Even Electron Ions
3 formula(e) evaluated with 1 results within limits (up to 50 closest results for each mass)
Elements Used:
C: 0-20 H: 0-12 N: 0-2 Cl: 0-1

Minimum:				-1.5				
Maximum:		5.0	5.0	200.0				
Mass	Calc. Mass	mDa	PPM	DBE	i-FIT	Norm	Conf(%)	Formula
315.0693	315.0689	0.4	1.3	15.5	1231.7	n/a	n/a	C20 H12 N2 Cl

Figure A.180. Elemental composition report.

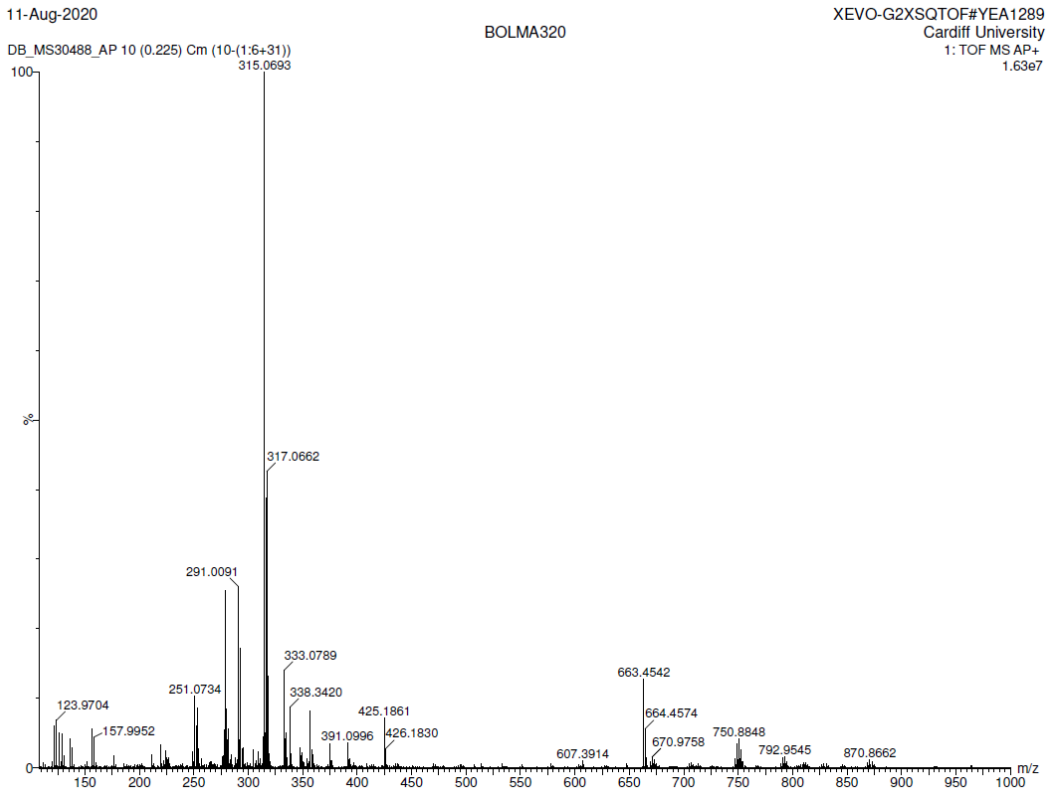

Figure A.181. LRMS, APCI+, TOF.

Characterisation of methyl 2-bromo-[1,1'-biphenyl]-4-carboxylate 63a

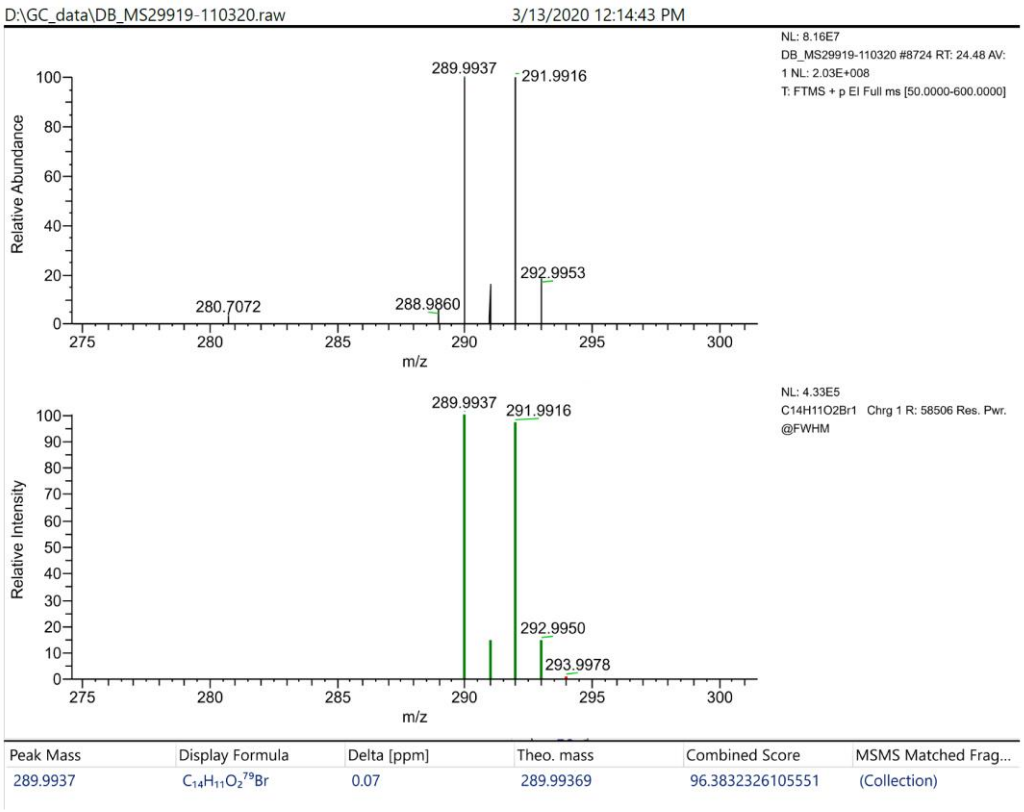

Peak Mass	Display Formula	Delta [ppm]	Theo. mass	Combined Score	MSMS Matched Frag...
289.9937	$C_{14}H_{11}O_2{}^{79}Br$	0.07	289.99369	96.3832326105551	(Collection)

Figure A.182. Elemental composition report.

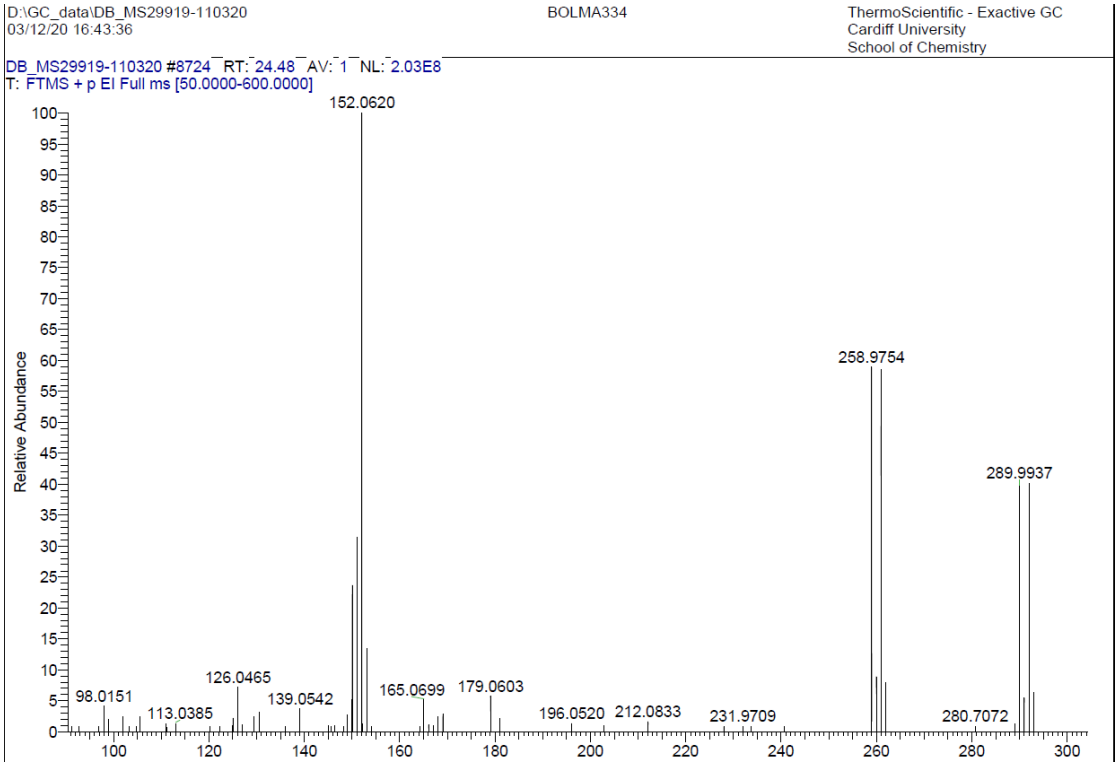

Figure A.183. HRMS, ES+, TOF.

Characterisation of methyl 2''-chloro-5''-cyano-[1,1':2',1''-terphenyl]-4'-carboxylate 63

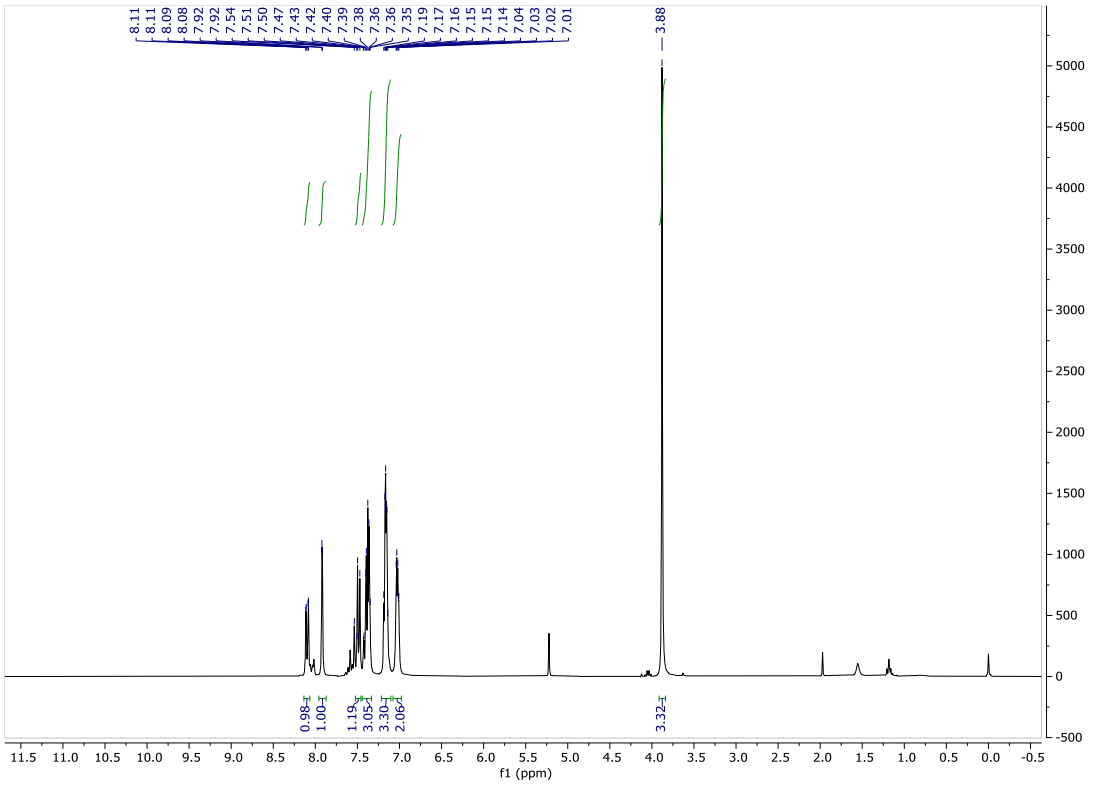

Figure A.184. ^{1}H NMR, 300 MHz, $CDCl_3$.

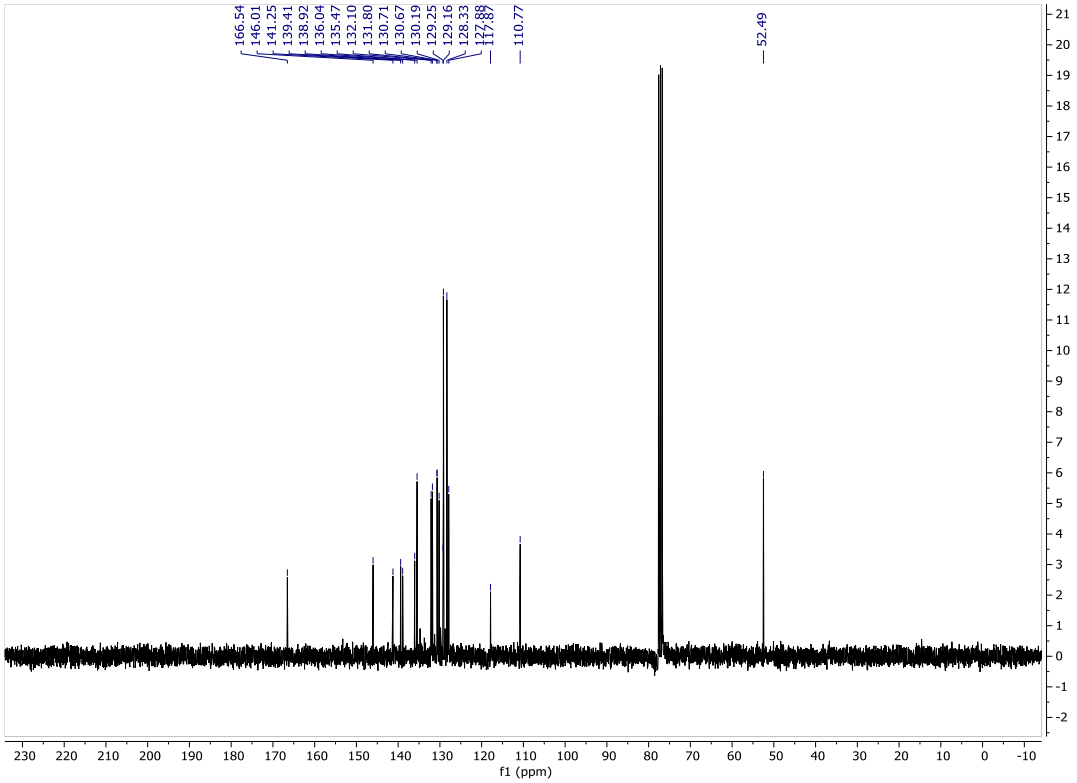

Figure A.185. ^{13}C NMR, 75 MHz, $CDCl_3$.

Elemental Composition Report **Page 1**

Single Mass Analysis
Tolerance = 5.0 PPM / DBE: min = -1.5, max = 200.0
Element prediction: Off
Number of isotope peaks used for i-FIT = 3

Monoisotopic Mass, Odd and Even Electron Ions
7 formula(e) evaluated with 1 results within limits (up to 50 closest results for each mass)
Elements Used:
C: 0-21 H: 0-15 N: 0-1 O: 0-2 35Cl: 0-1

Minimum:				-1.5				
Maximum:		5.0	5.0	200.0				
Mass	Calc. Mass	mDa	PPM	DBE	i-FIT	Norm	Conf(%)	Formula
348.0798	348.0791	0.7	2.0	14.5	1066.8	n/a	n/a	C21 H15 N O2 35Cl

Figure A.186. Elemental composition report.

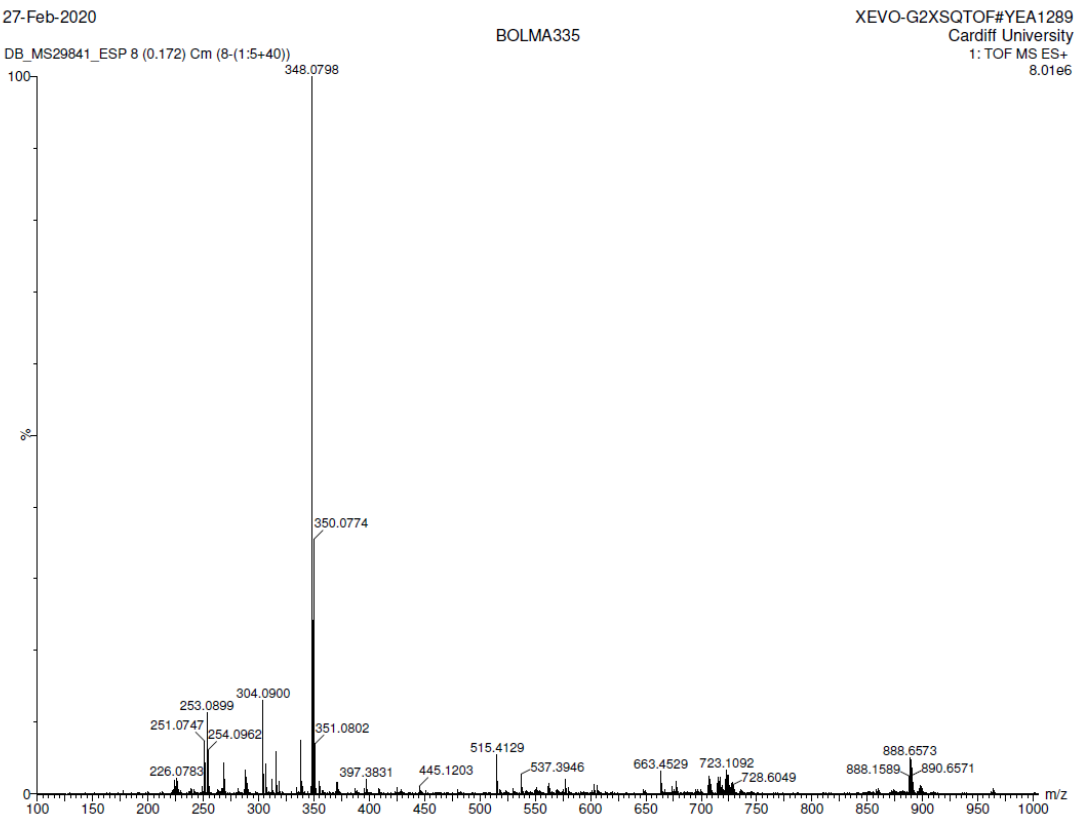

Figure A.187. HRMS, ES+, TOF.

Characterisation of triphenylene-2-carbonitrile 64

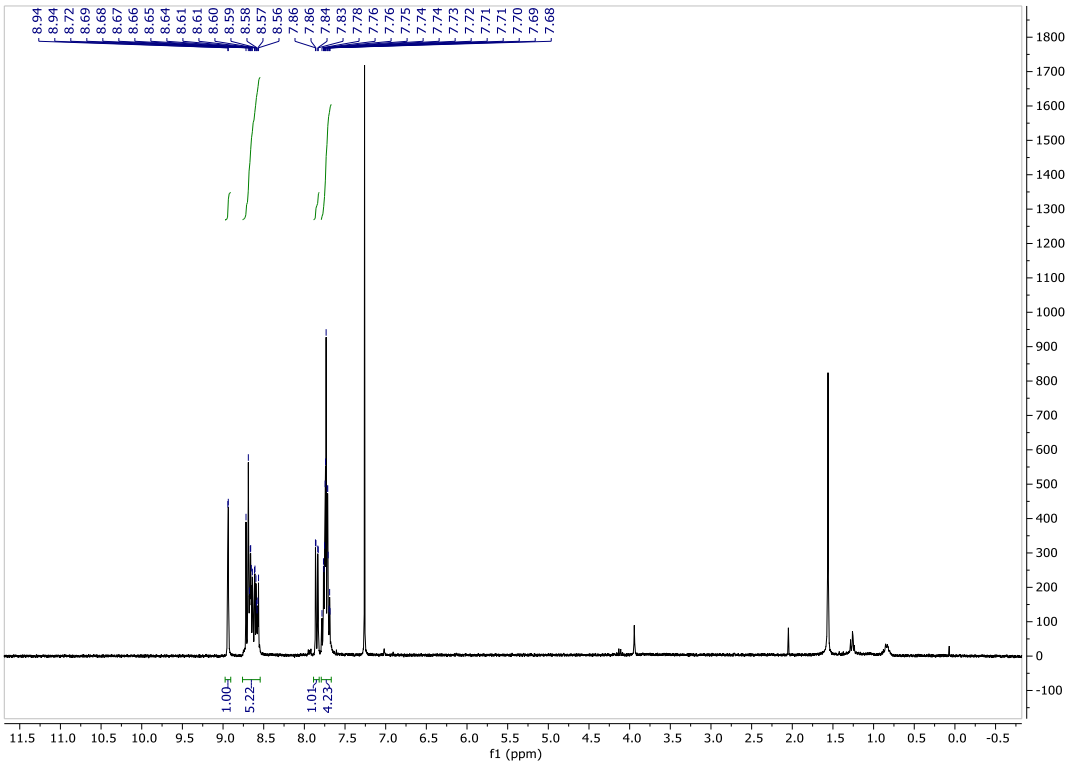

Figure A.188. ^{1}H NMR, 300 MHz, $CDCl_3$.

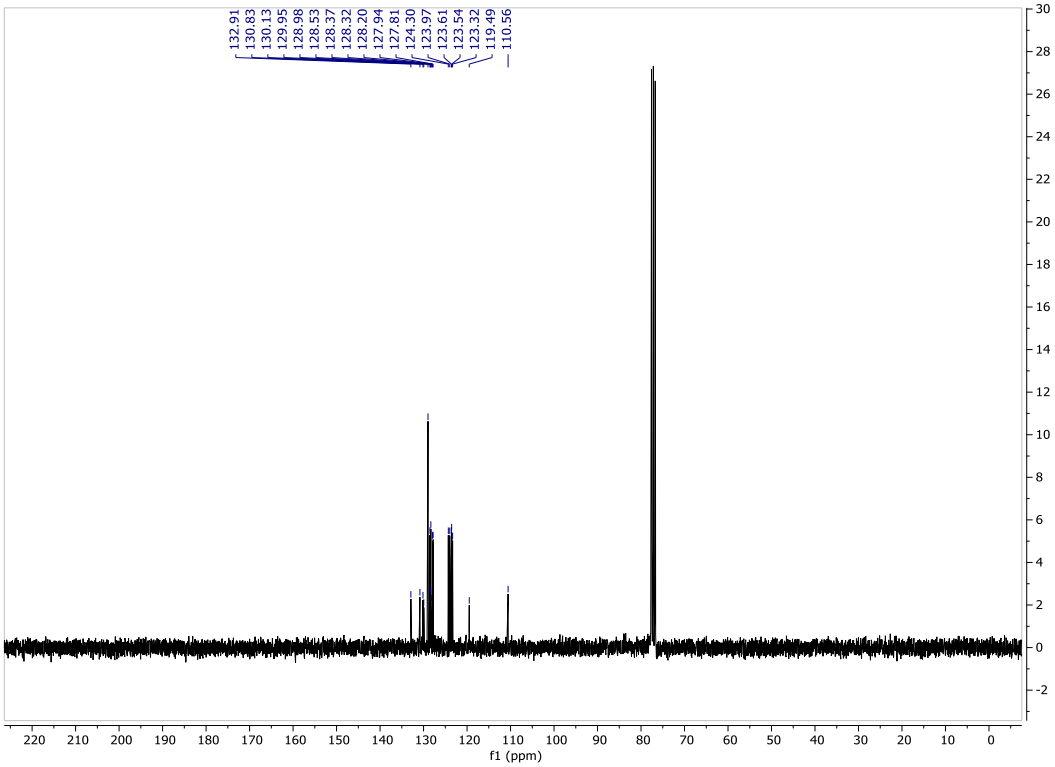

Figure A.189. ^{13}C NMR, 75 MHz, $CDCl_3$.

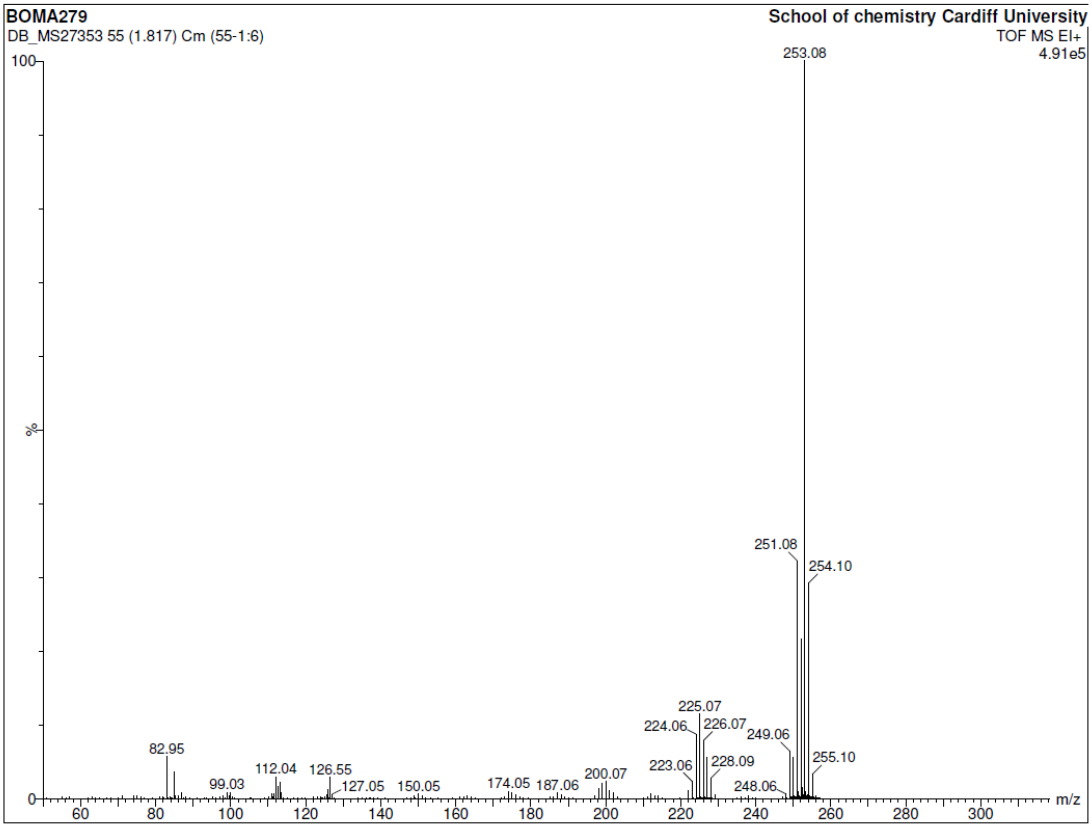

Figure A.190. LRMS, EI+, TOF.

Characterisation of triphenylene-1-carbonitrile 65

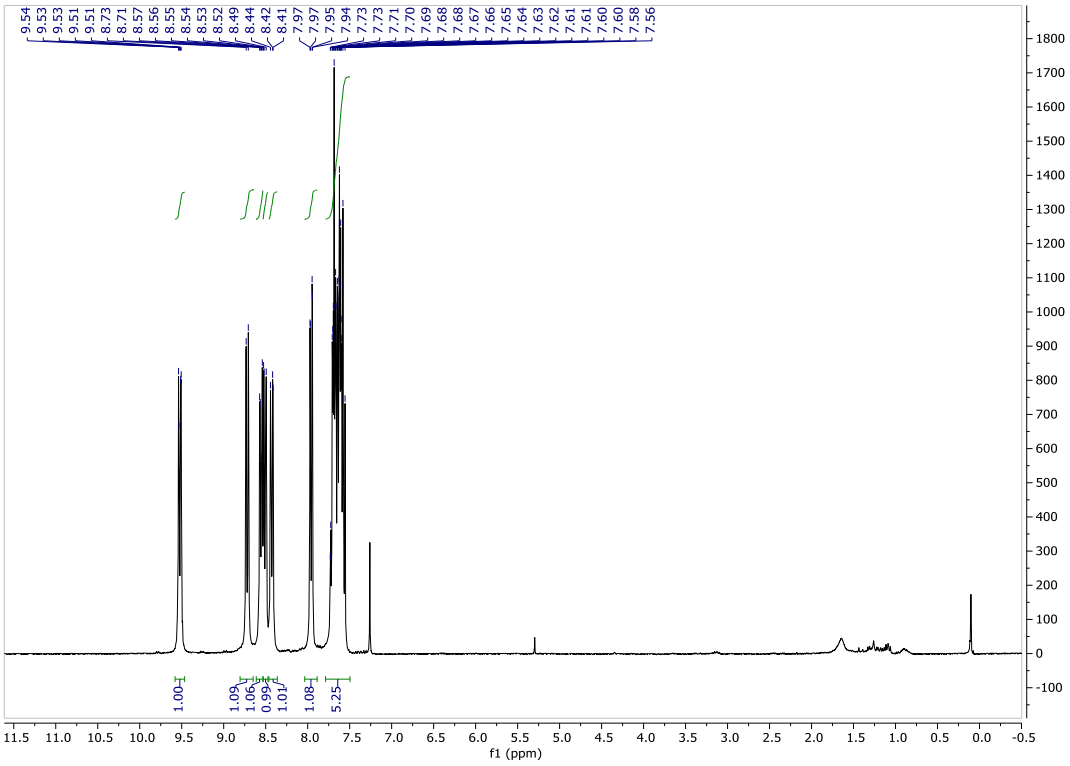

Figure A.191. ^{1}H NMR, 300 MHz, $CDCl_3$.

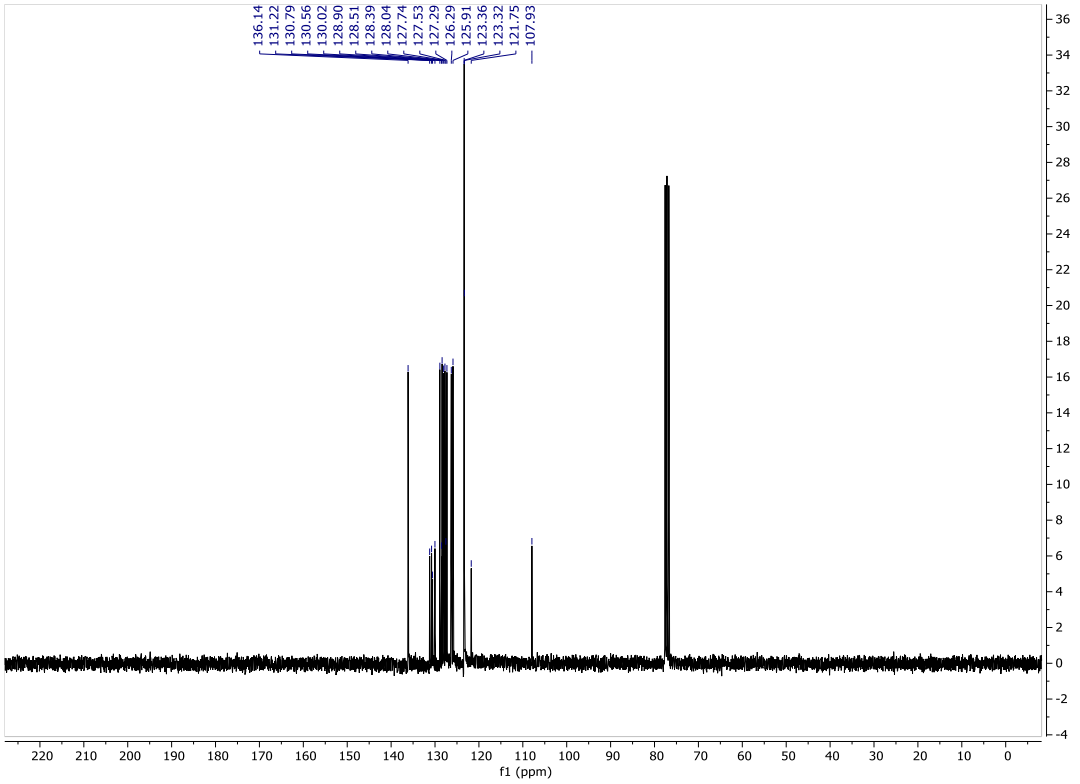

Figure A.192. ^{13}C NMR, 75 MHz, $CDCl_3$.

Elemental Composition Report **Page 1**

Single Mass Analysis
Tolerance = 5.0 PPM / DBE: min = -1.5, max = 200.0
Element prediction: Off
Number of isotope peaks used for i-FIT = 3

Monoisotopic Mass, Odd and Even Electron Ions
1 formula(e) evaluated with 1 results within limits (up to 50 closest results for each mass)
Elements Used:
C: 0-19 H: 0-12 N: 0-1

Minimum:				-1.5				
Maximum:		5.0	5.0	200.0				
Mass	Calc. Mass	mDa	PPM	DBE	i-FIT	Norm	Conf(%)	Formula
254.0972	254.0970	0.2	0.8	14.5	171.8	n/a	n/a	C19 H12 N

Figure A.193. Elemental composition report.

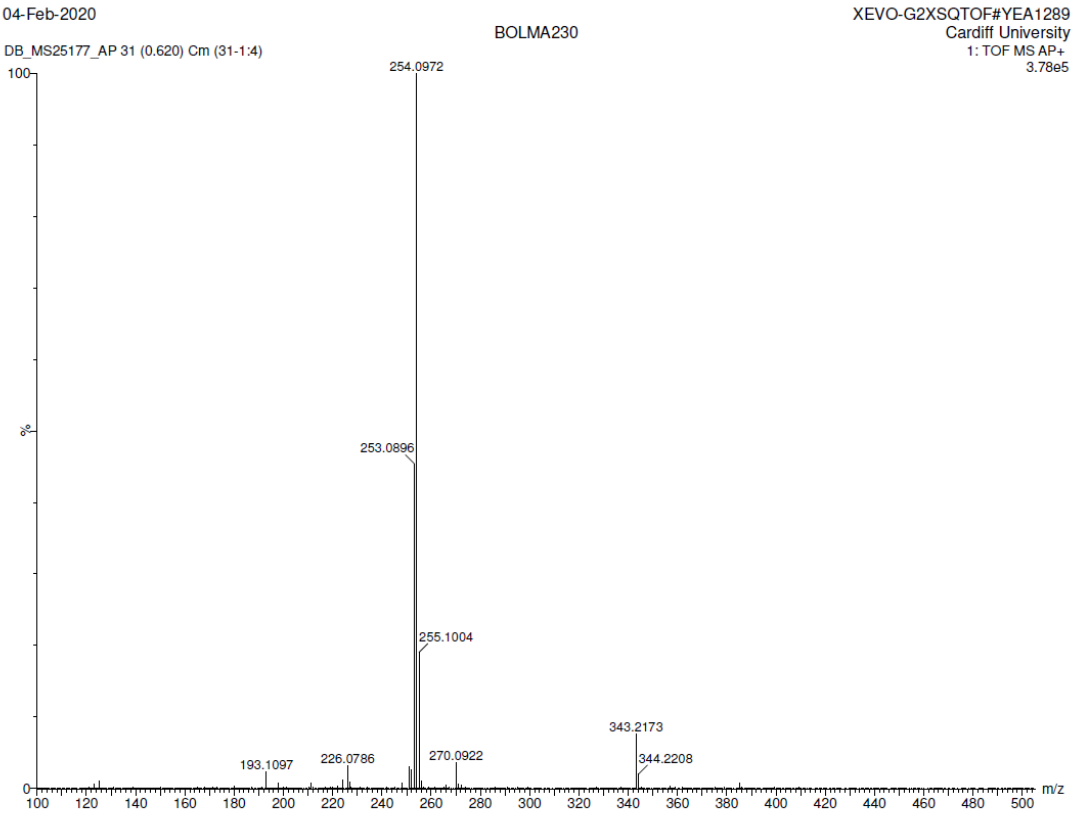

Figure A.194. HRMS, APCI+, TOF.

Characterisation of methyl triphenylene-2-carboxylate 66

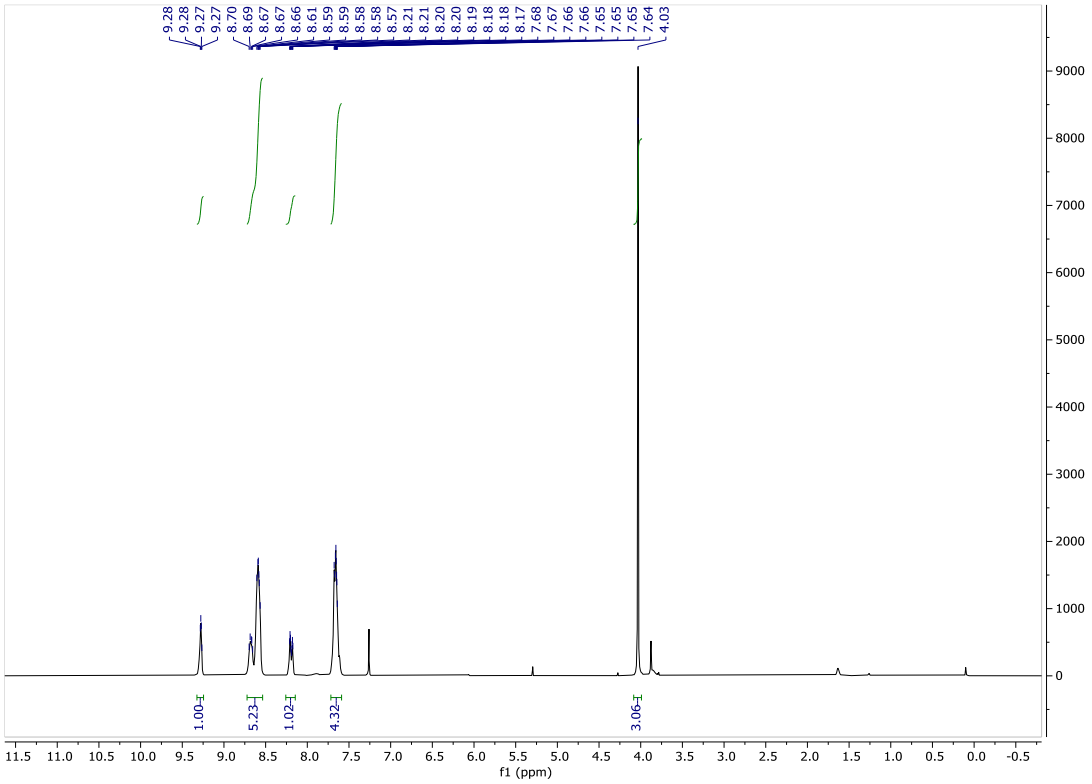

Figure A.195. ^{1}H NMR, 300 MHz, $CDCl_3$.

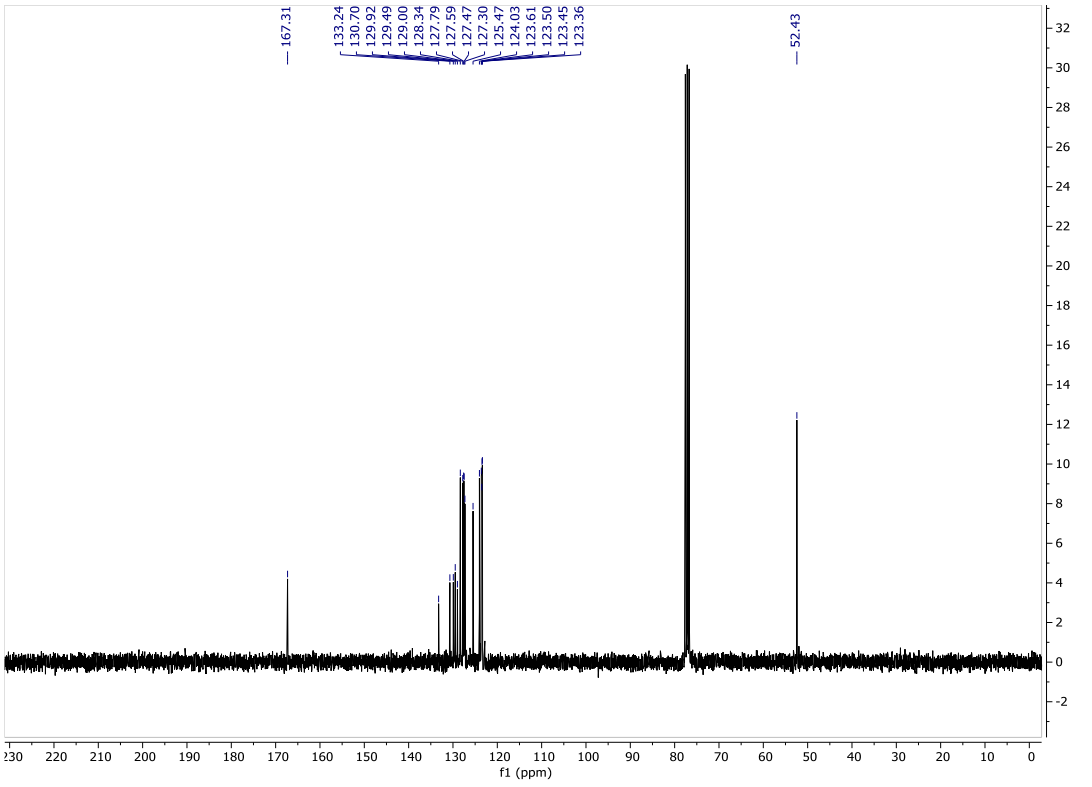

Figure A.196. ^{13}C NMR, 75 MHz, $CDCl_3$.

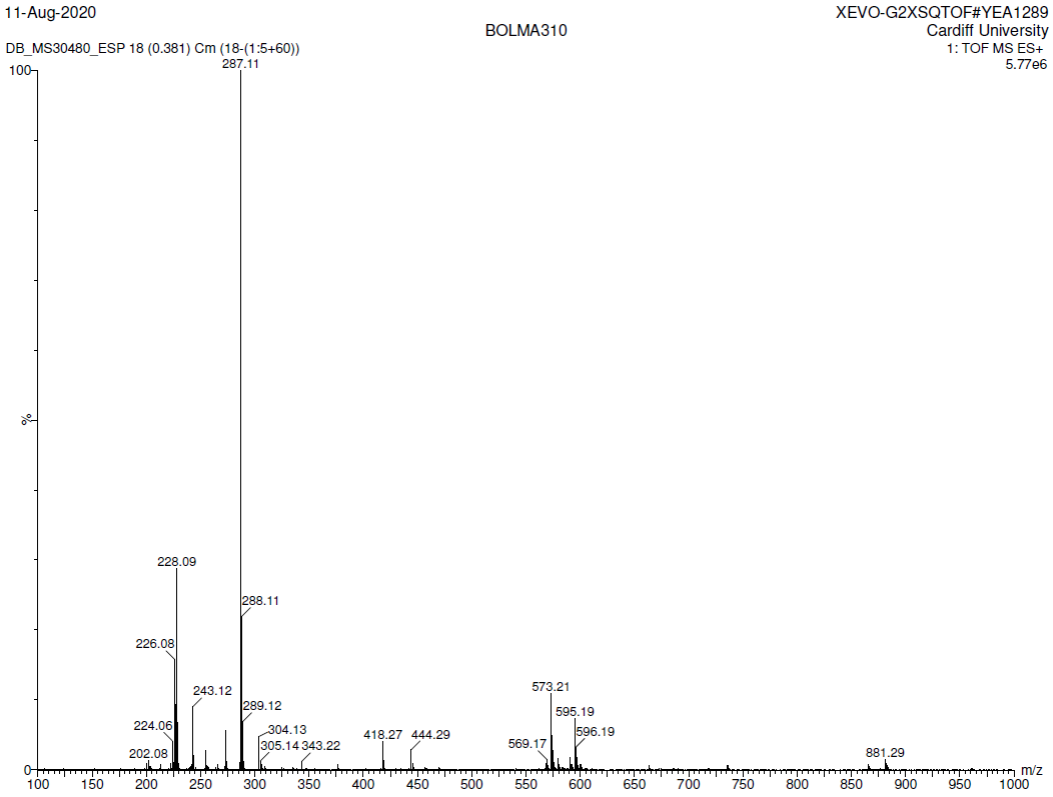

Figure A.197. LRMS, ES+, TOF.

Characterisation of pyrrolo[1,2-*f*]phenanthridine-10-carbonitrile 68

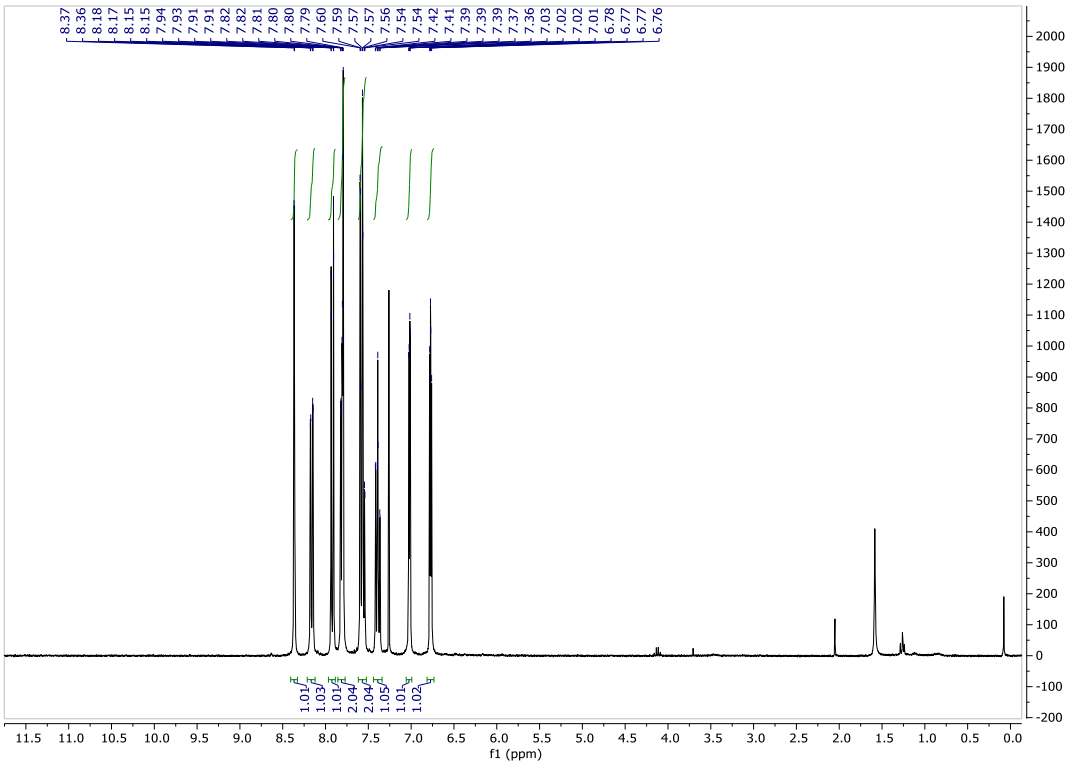

Figure A.198. ^{1}H NMR, 300 MHz, $CDCl_3$.

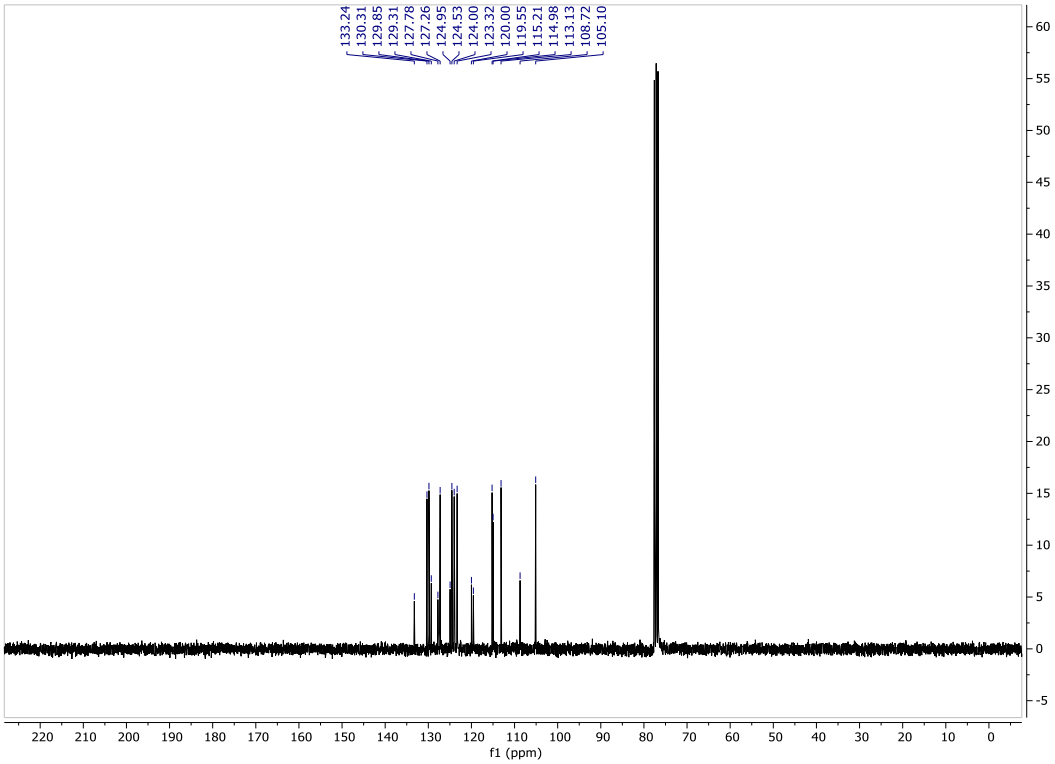

Figure A.199. ^{13}C NMR, 75 MHz, $CDCl_3$.

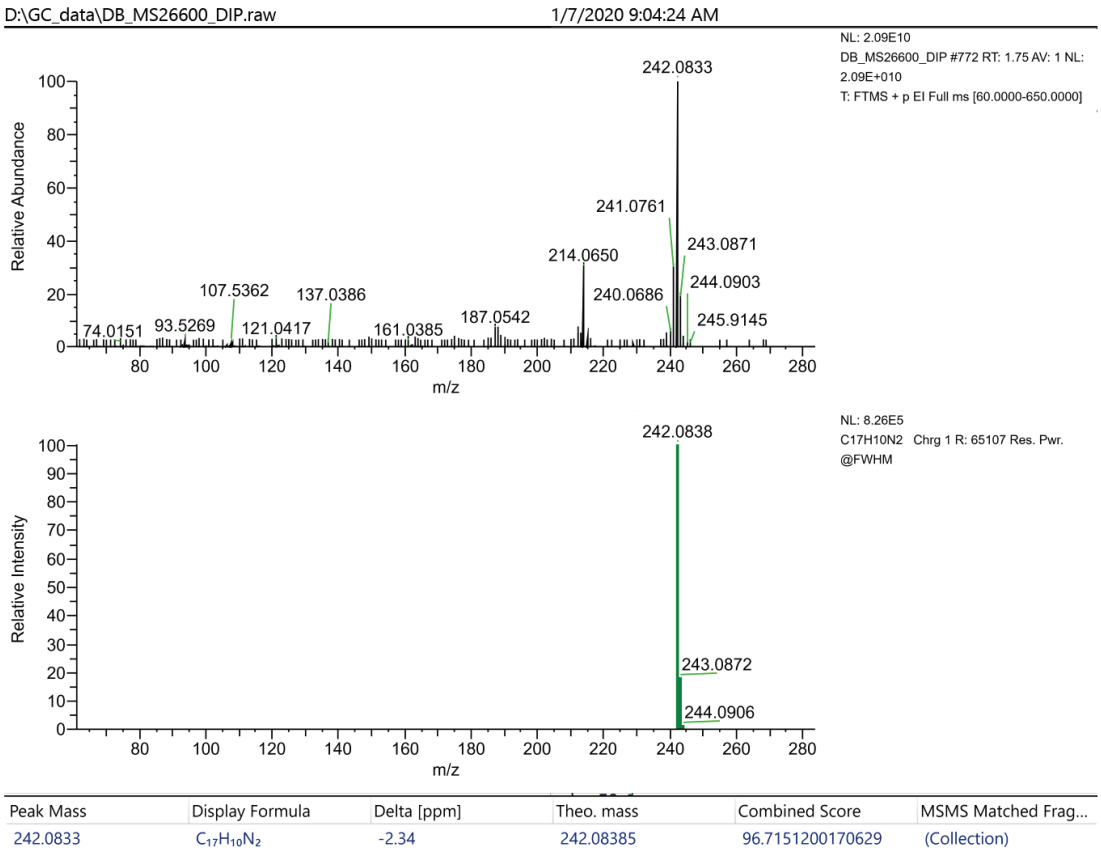

Peak Mass	Display Formula	Delta [ppm]	Theo. mass	Combined Score	MSMS Matched Frag...
242.0833	$C_{17}H_{10}N_2$	-2.34	242.08385	96.7151200170629	(Collection)

Figure A.200. Elemental composition report.

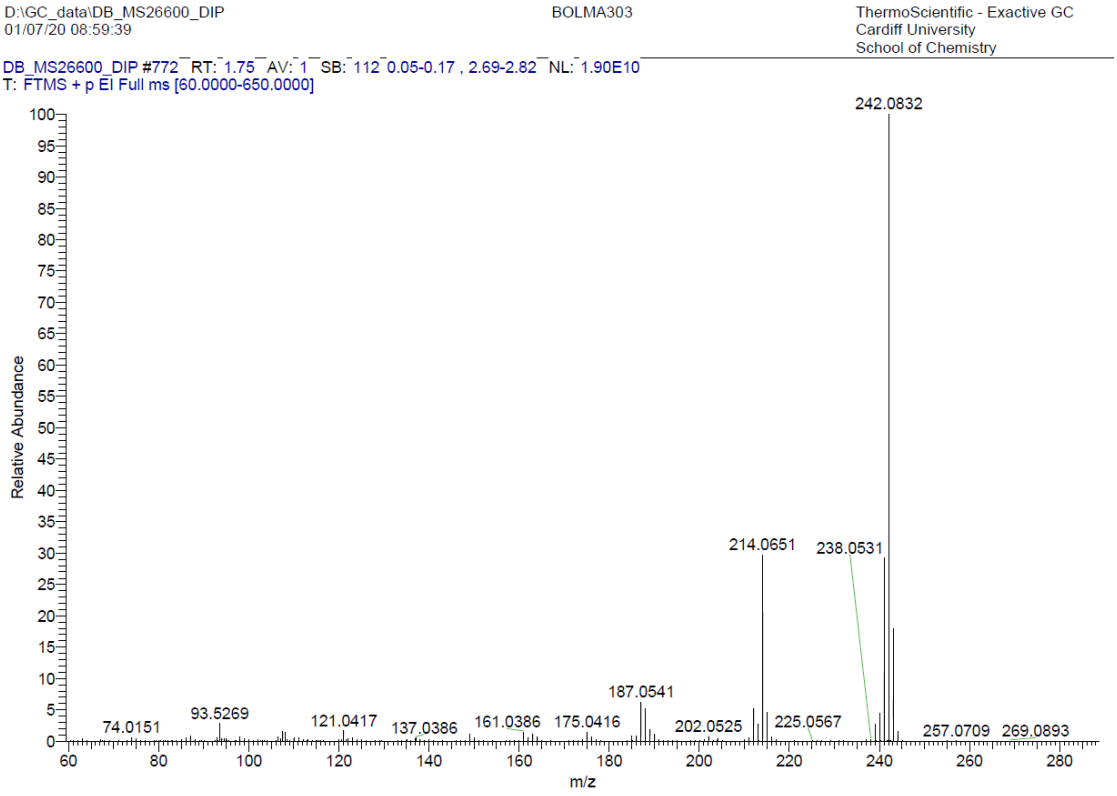

Figure A.201. HRMS, EI+, TOF.

Characterisation of phenanthro[9,10-b]thiophene-9-carbonitrile 69a

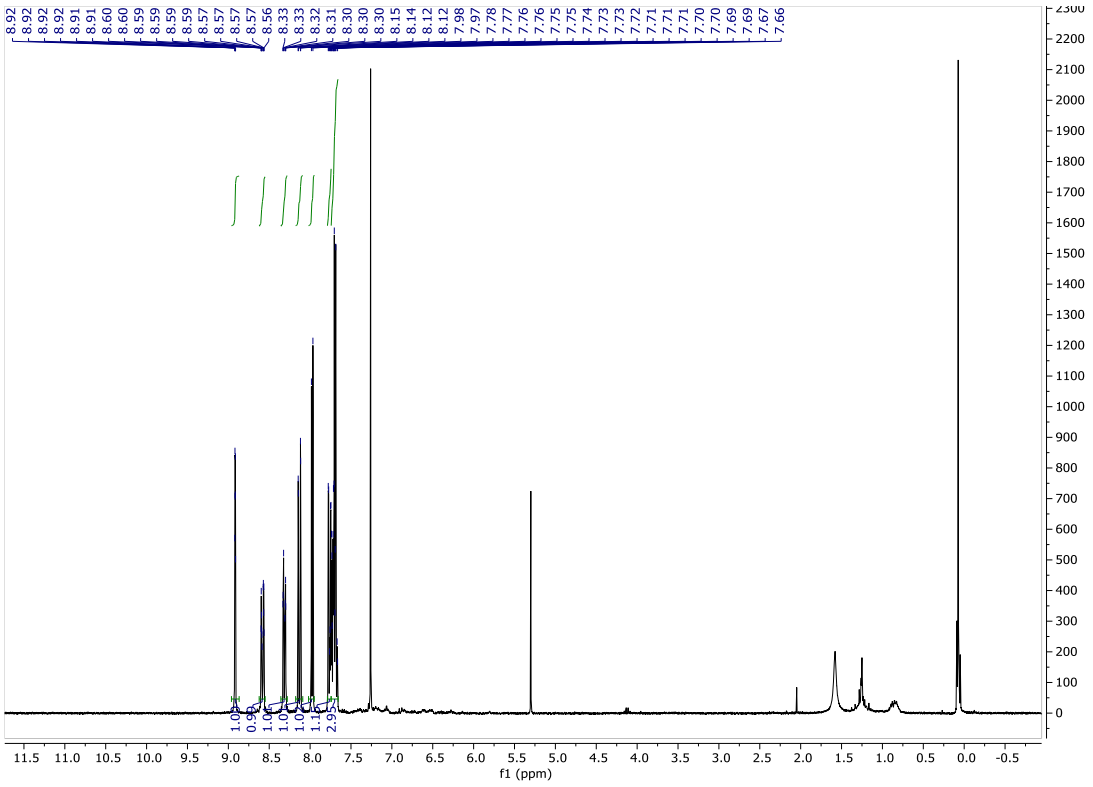

Figure A.202. ^{1}H NMR, 300 MHz, $CDCl_3$.

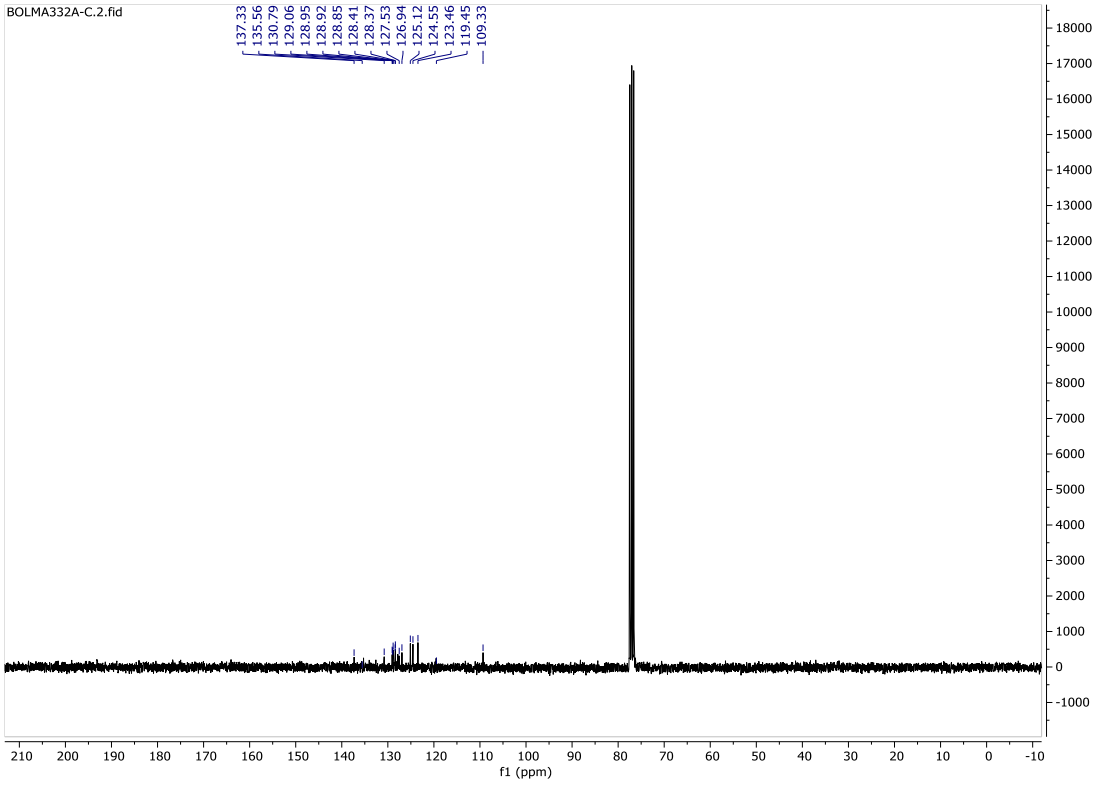

Figure A.203. ^{13}C NMR, 75 MHz, $CDCl_3$.

Elemental Composition Report **Page 1**

Single Mass Analysis
Tolerance = 5.0 PPM / DBE: min = -1.5, max = 200.0
Element prediction: Off
Number of isotope peaks used for i-FIT = 3

Monoisotopic Mass, Odd and Even Electron Ions
3 formula(e) evaluated with 1 results within limits (up to 50 closest results for each mass)
Elements Used:
C: 0-17 H: 0-12 N: 0-2 S: 0-1

Minimum:				-1.5				
Maximum:		5.0	5.0	200.0				
Mass	Calc. Mass	mDa	PPM	DBE	i-FIT	Norm	Conf(%)	Formula
260.0539	260.0534	0.5	1.9	13.5	662.1	n/a	n/a	C17 H10 N S

Figure A.204. Elemental composition report.

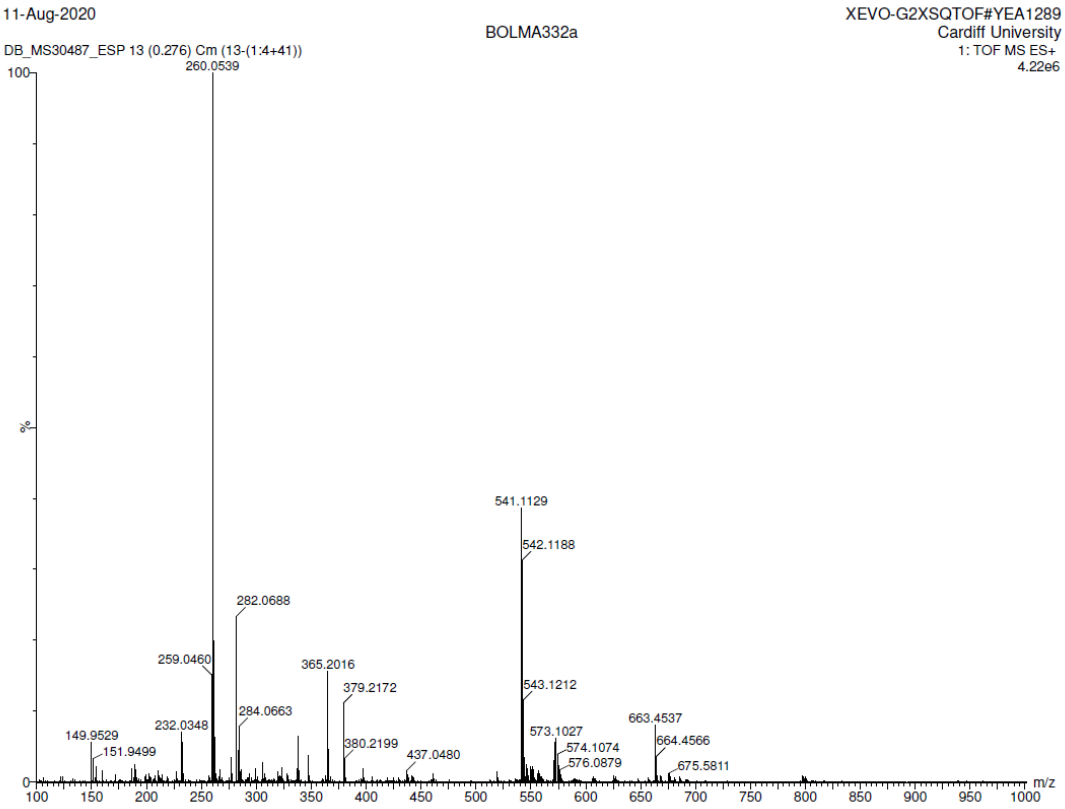

Figure A.205. HRMS, ES+, TOF.

Characterisation of phenanthro[9,10-c]thiophene-6-carbonitrile 69b

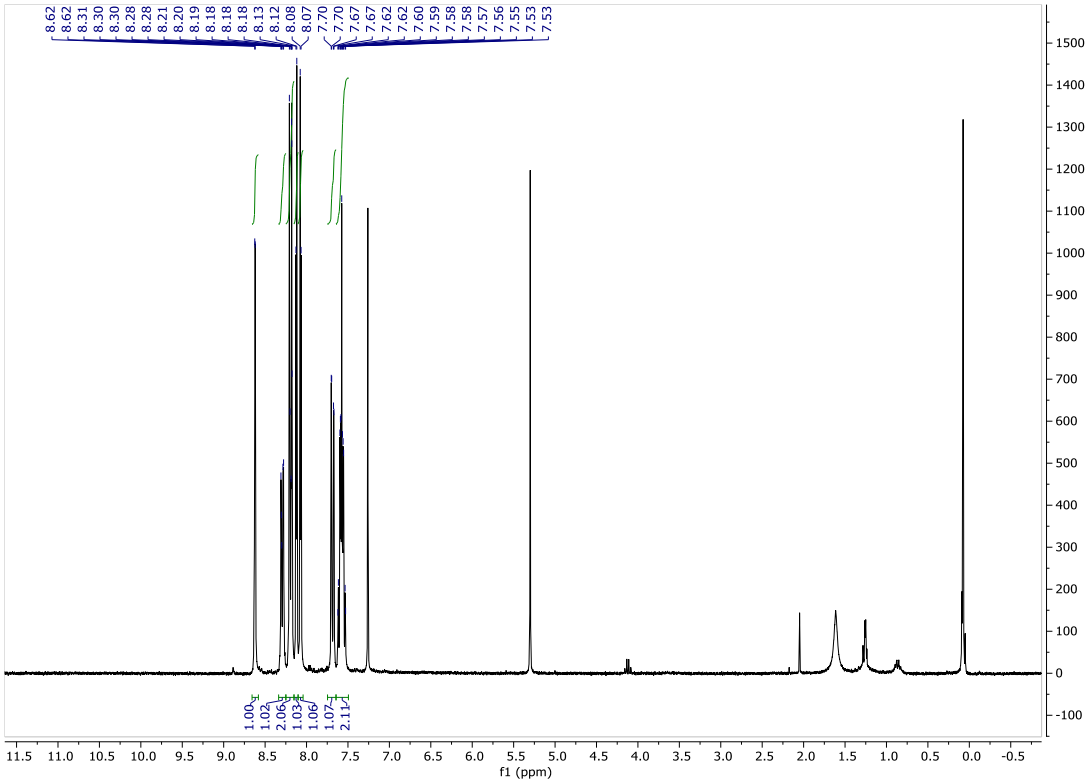

Figure A.206. ^{1}H NMR, 300 MHz, $CDCl_3$.

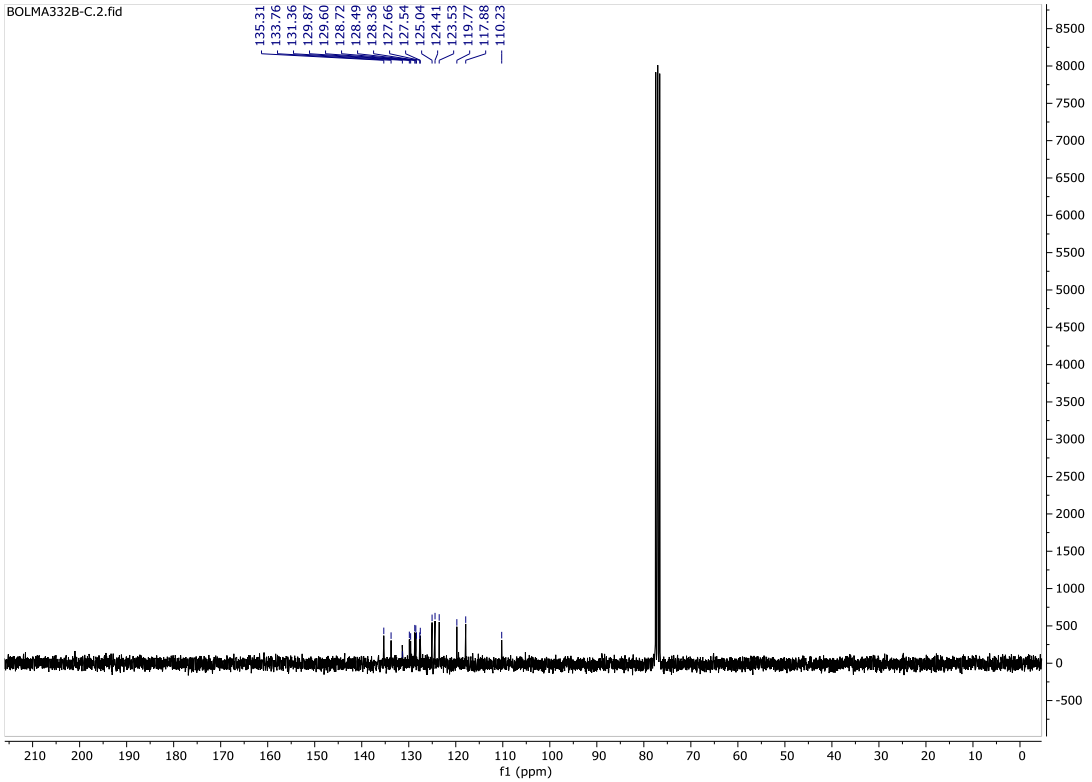

Figure A.207. ^{13}C NMR, 75 MHz, $CDCl_3$.

Elemental Composition Report **Page 1**

Single Mass Analysis
Tolerance = 5.0 PPM / DBE: min = -1.5, max = 200.0
Element prediction: Off
Number of isotope peaks used for i-FIT = 3

Monoisotopic Mass, Odd and Even Electron Ions
2 formula(e) evaluated with 1 results within limits (up to 50 closest results for each mass)
Elements Used:
C: 0-17 H: 0-10 N: 0-1 S: 0-1

Minimum:				-1.5				
Maximum:		5.0	5.0	200.0				
Mass	Calc. Mass	mDa	PPM	DBE	i-FIT	Norm	Conf(%)	Formula
260.0545	260.0534	1.1	4.2	13.5	1048.8	n/a	n/a	C17 H10 N S

Figure A.208. Elemental composition report.

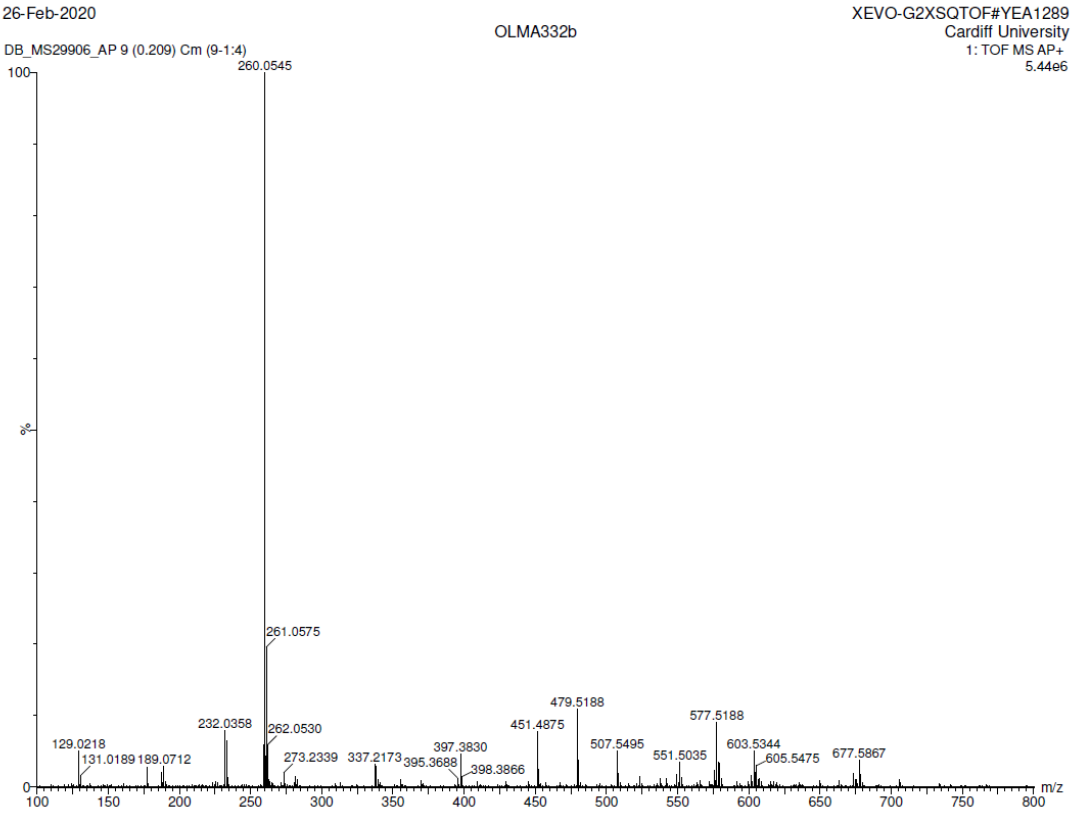

Figure A.209. HRMS, APCI+, TOF.

Characterisation of 11-(tert-butyl)triphenylene-1-carbonitrile 71

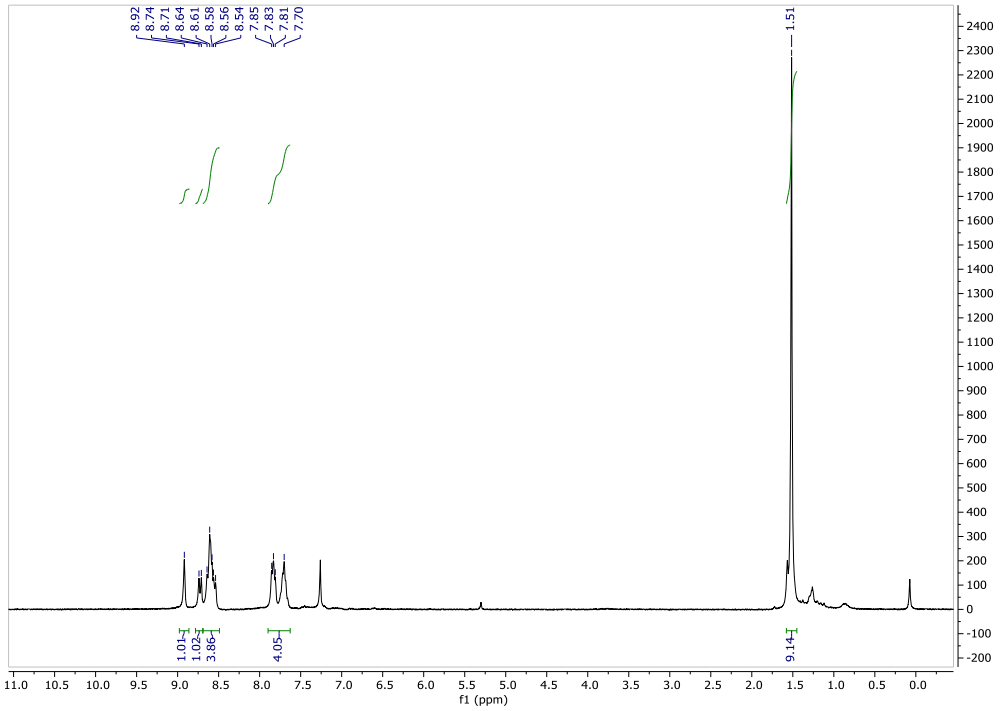

Figure A.210. ^{1}H NMR, 300 MHz, $CDCl_3$.

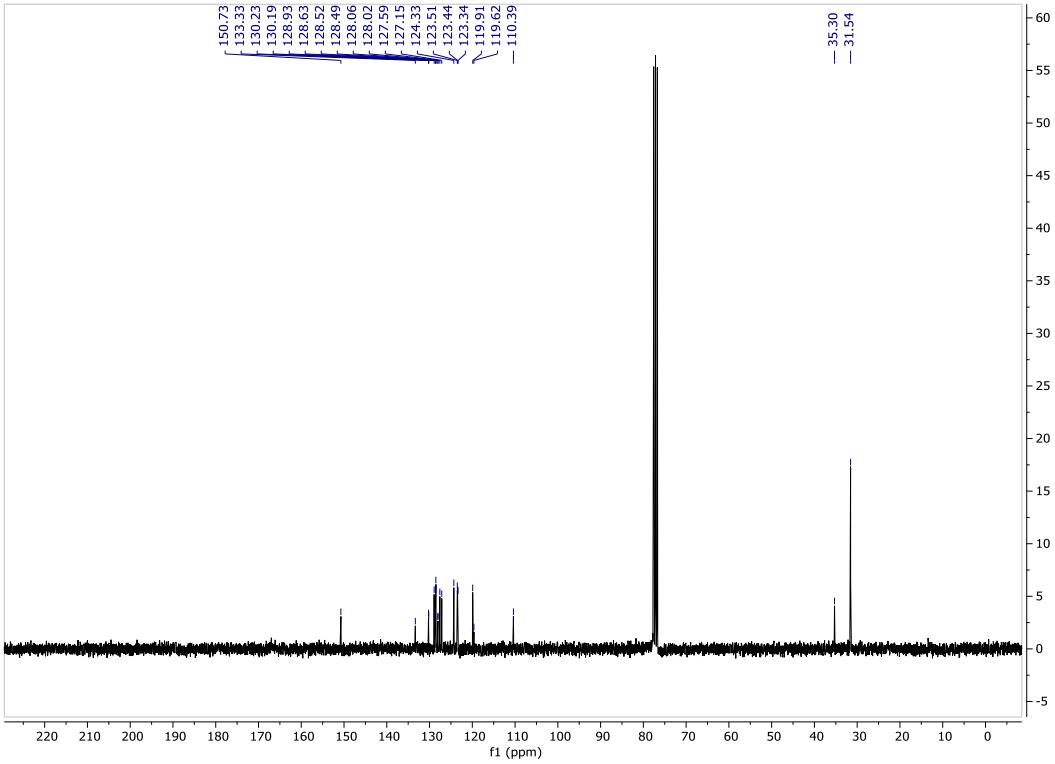

Figure A.211. ^{13}C NMR, 75 MHz, $CDCl_3$.

Elemental Composition Report **Page 1**

Single Mass Analysis
Tolerance = 5.0 PPM / DBE: min = -1.5, max = 200.0
Element prediction: Off
Number of isotope peaks used for i-FIT = 3

Monoisotopic Mass, Odd and Even Electron Ions
1 formula(e) evaluated with 1 results within limits (up to 50 closest results for each mass)
Elements Used:
C: 0-23 H: 0-20 N: 0-1

Minimum:				-1.5				
Maximum:		5.0	5.0	200.0				
Mass	Calc. Mass	mDa	PPM	DBE	i-FIT	Norm	Conf(%)	Formula
310.1594	310.1596	-0.2	-0.6	14.5	161.8	n/a	n/a	C23 H20 N

Figure A.212. Elemental composition report.

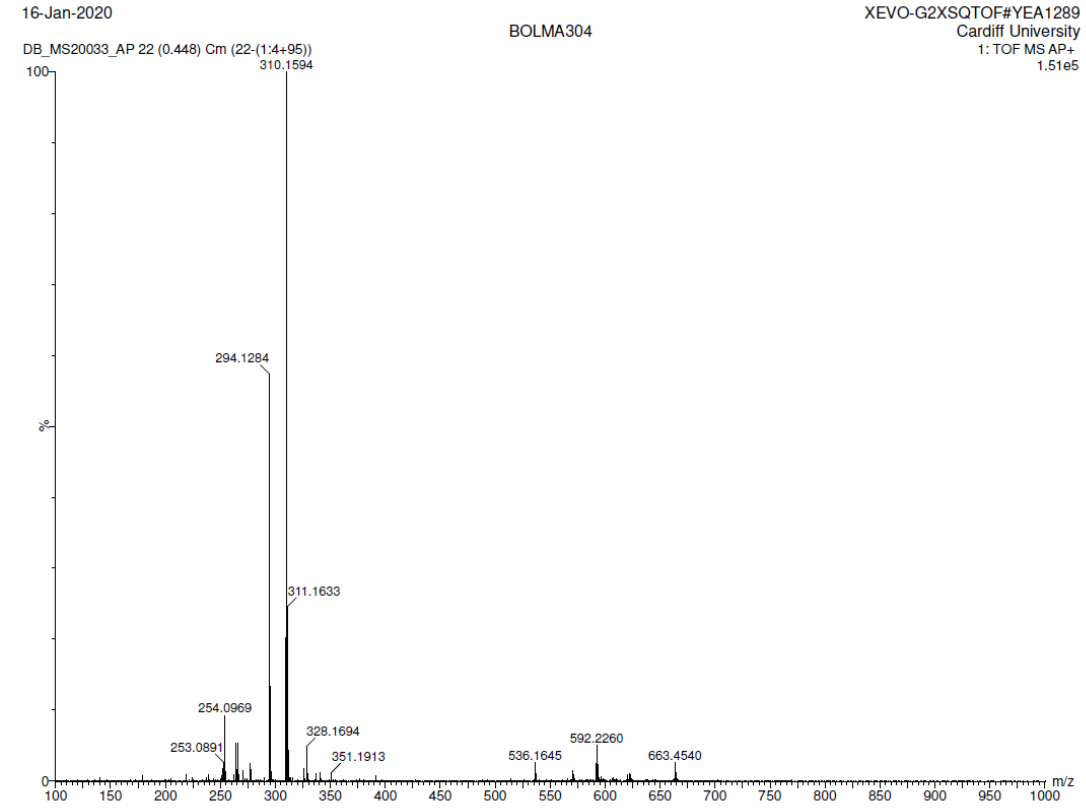

Figure A.212. HRMS, APCI+, TOF.

Characterisation of methyl 10-cyanotriphenylene-2-carboxylate 75

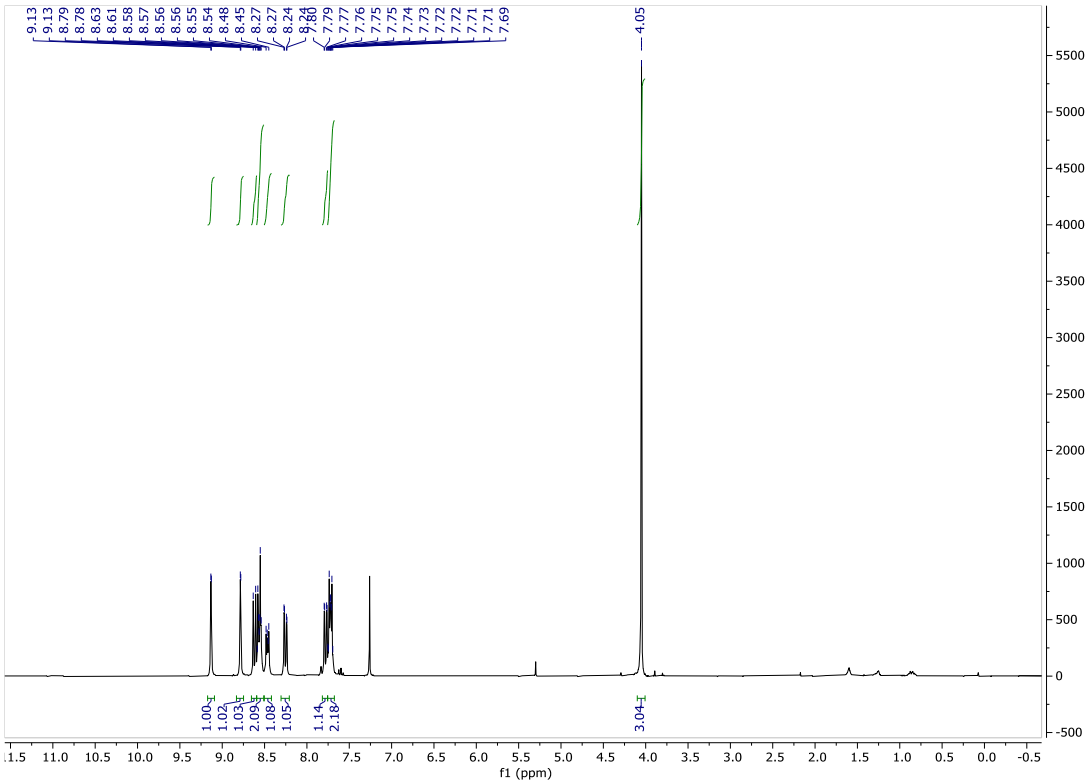

Figure A.213. ^{1}H NMR, 300 MHz, $CDCl_3$.

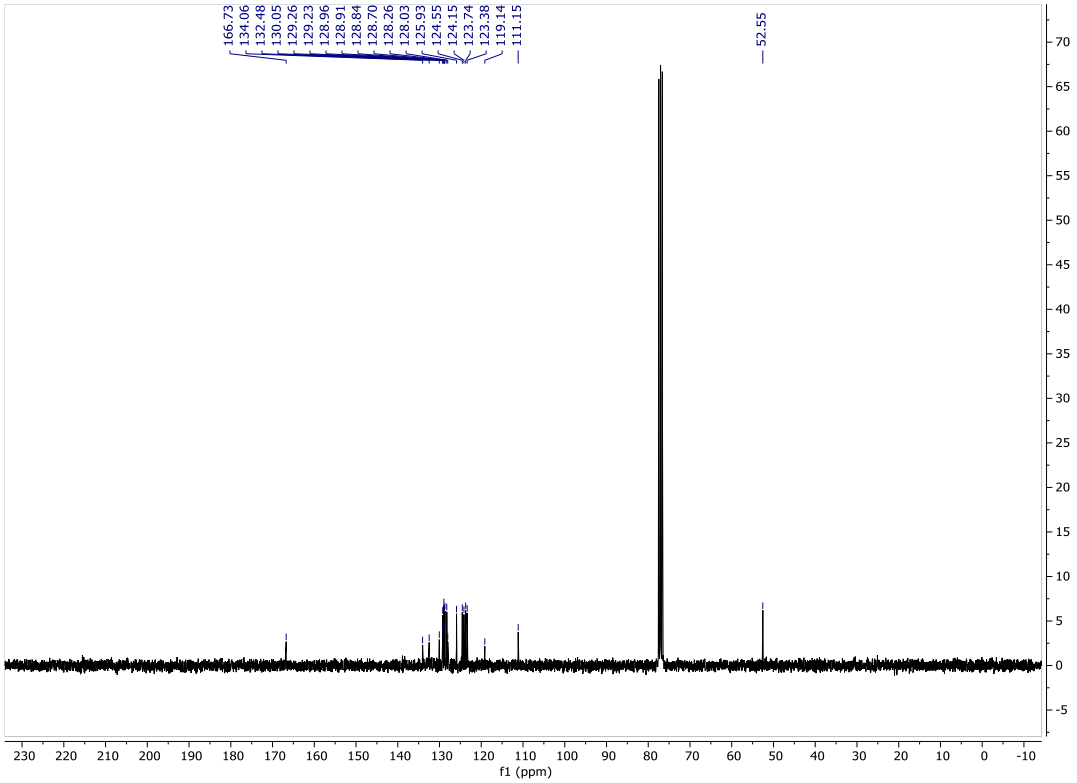

Figure A.214. ^{13}C NMR, 75 MHz, $CDCl_3$.

Elemental Composition Report **Page 1**

Single Mass Analysis
Tolerance = 5.0 PPM / DBE: min = -1.5, max = 200.0
Element prediction: Off
Number of isotope peaks used for i-FIT = 3

Monoisotopic Mass, Odd and Even Electron Ions
2 formula(e) evaluated with 1 results within limits (up to 50 closest results for each mass)
Elements Used:
C: 0-21 H: 0-14 N: 0-1 O: 0-2

Minimum:				-1.5				
Maximum:		5.0	5.0	200.0				
Mass	Calc. Mass	mDa	PPM	DBE	i-FIT	Norm	Conf(%)	Formula
312.1033	312.1025	0.8	2.6	15.5	981.0	n/a	n/a	C21 H14 N O2

Figure A.215. Elemental composition report.

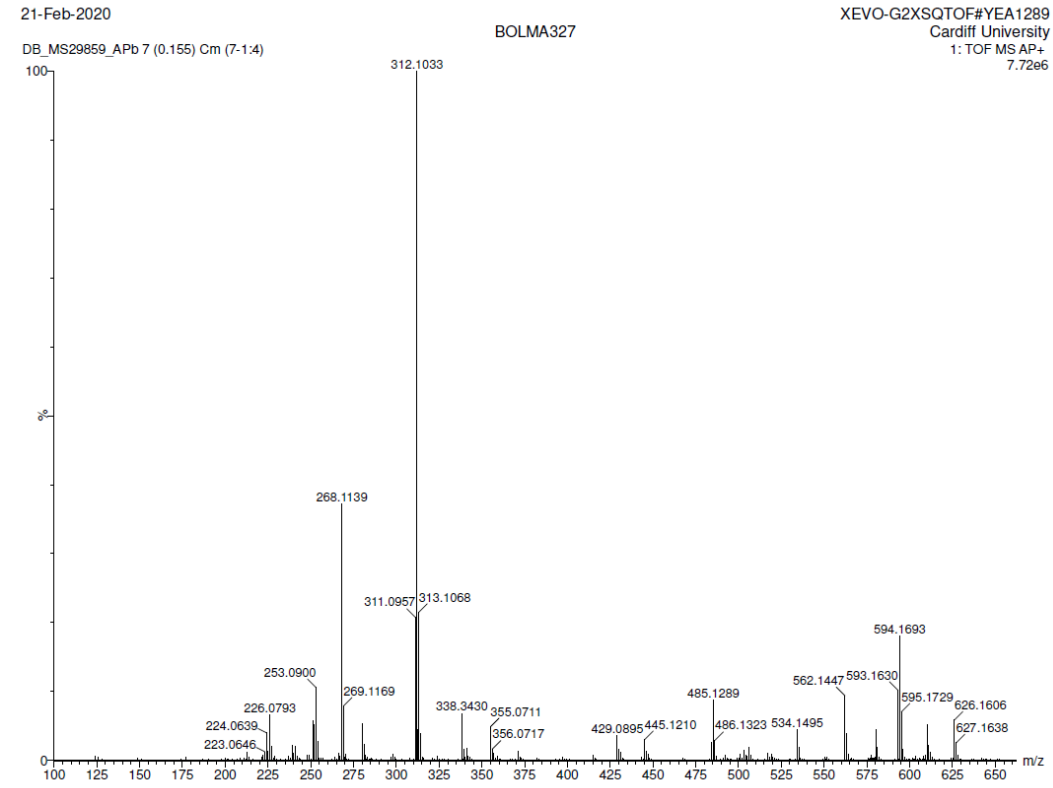

Figure A.216. HRMS, APCI+, TOF.

Characterisation of methyl 11-cyanotriphenylene-2-carboxylate 76

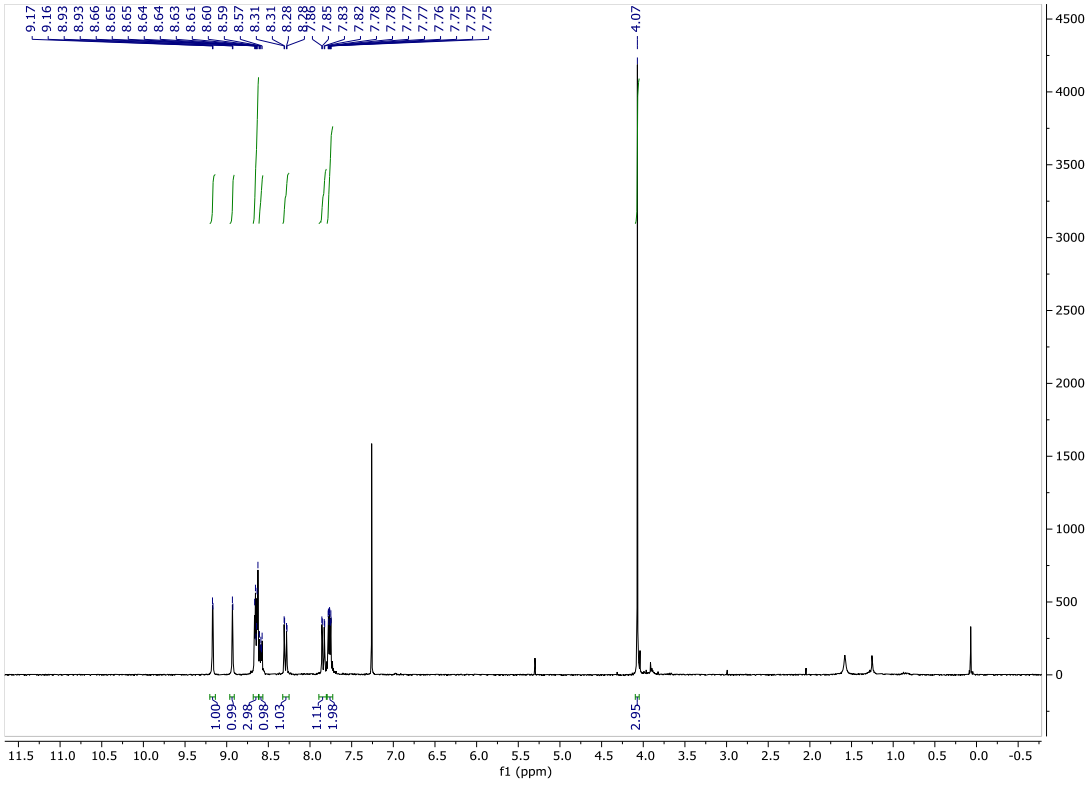

Figure A.217. ^{1}H NMR, 300 MHz, $CDCl_3$.

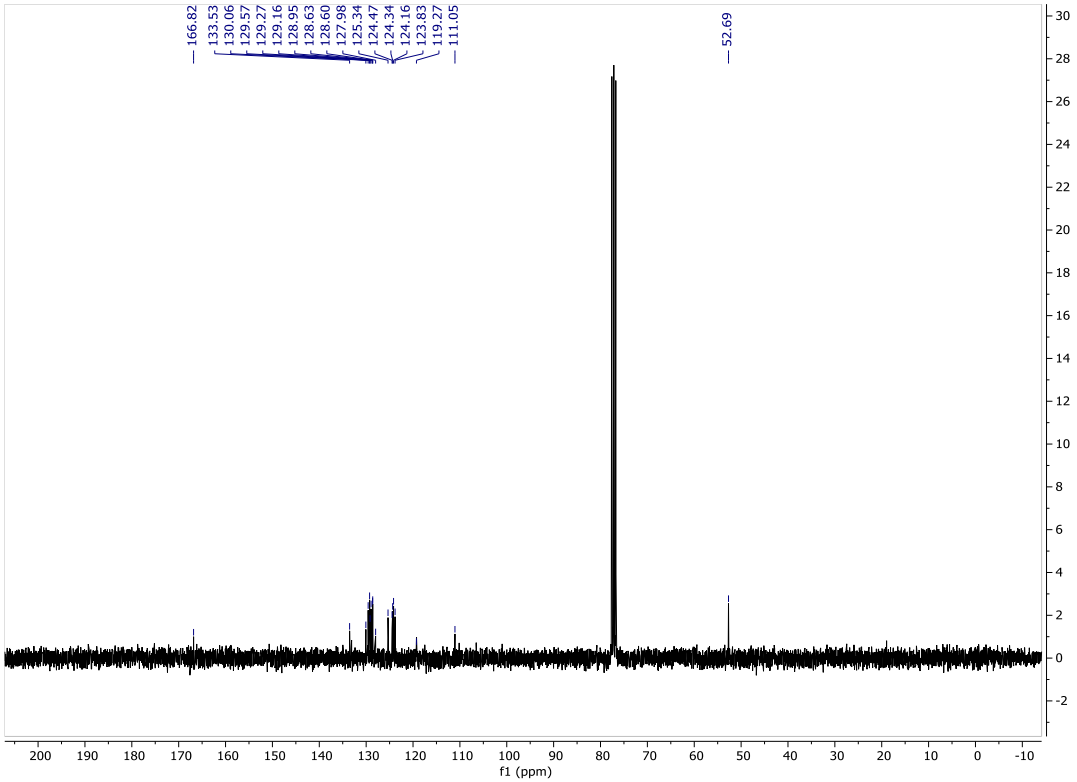

Figure A.218. ^{13}C NMR, 75 MHz, $CDCl_3$.

Elemental Composition Report **Page 1**

Single Mass Analysis
Tolerance = 5.0 PPM / DBE: min = -1.5, max = 50.0
Element prediction: Off
Number of isotope peaks used for i-FIT = 3

Monoisotopic Mass, Odd and Even Electron Ions
20 formula(e) evaluated with 1 results within limits (up to 50 closest results for each mass)
Elements Used:
C: 0-21 H: 0-14 N: 0-1 O: 0-5 23Na: 0-1

17-Dec-2020 BVDLNA336 Cardiff Uni Synapt G2-Si
DB_MS30508_ESP 24 (0.245) 1: TOF MS ES+
1.58e+006

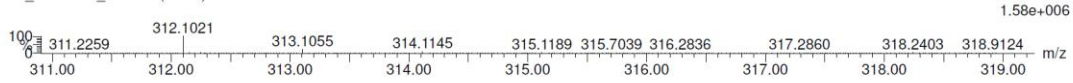

Minimum:				-1.5				
Maximum:		20.0	5.0	50.0				
Mass	Calc. Mass	mDa	PPM	DBE	i-FIT	Norm	Conf(%)	Formula
312.1021	312.1025	-0.4	-1.3	15.5	1006.5	n/a	n/a	C21 H14 N O2

Figure A.219. Elemental composition report.

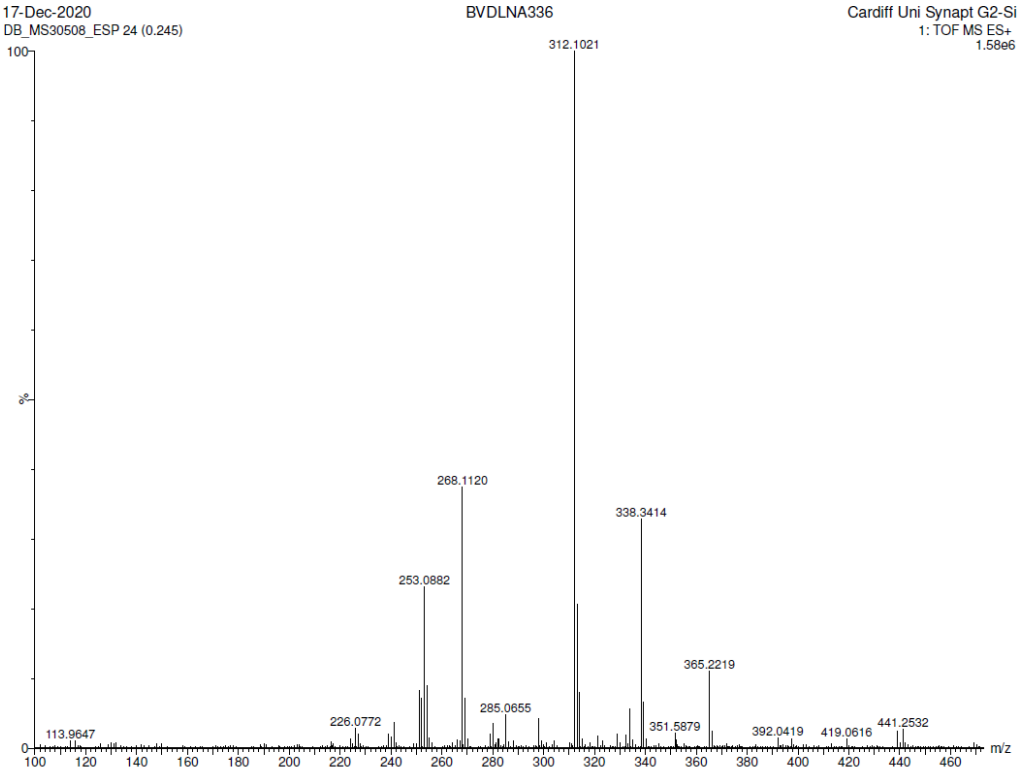

Figure A.220. HRMS, ES+, TOF.

Characterisation of 6,6'''-dichloro-[1,1':2',1'':2'',1'''-quaterphenyl]-3,3'''-dicarbonitrile 78

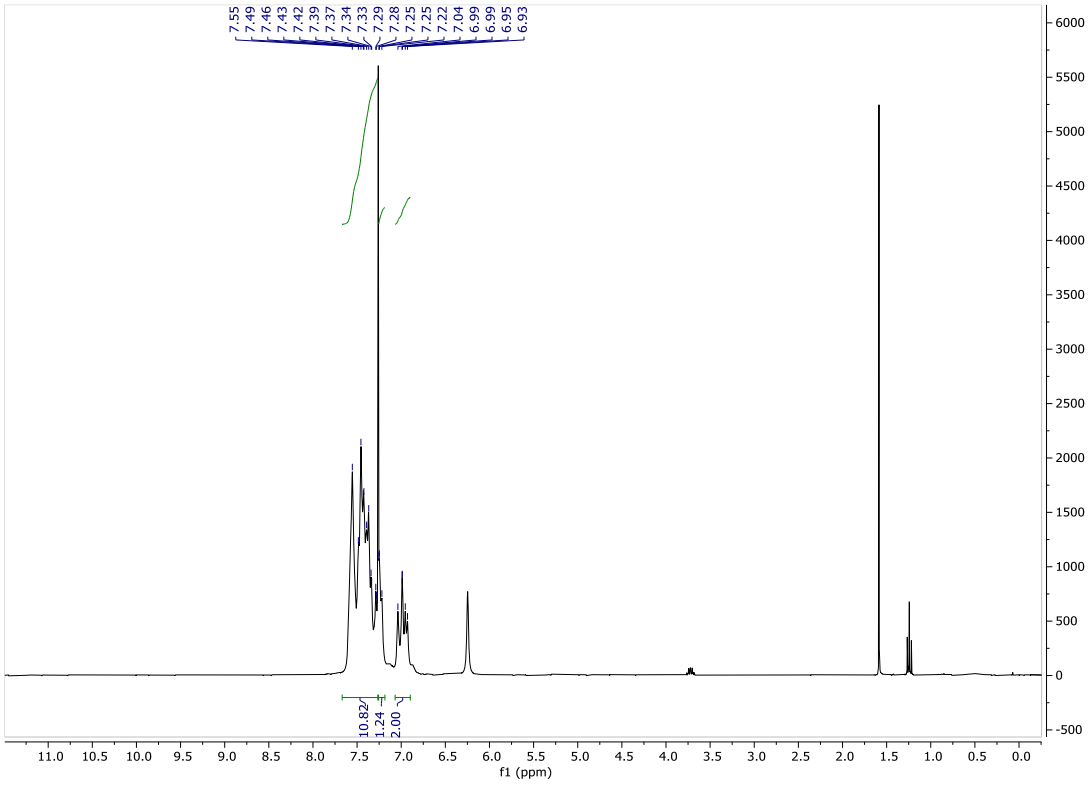

Figure A.221. ^{1}H NMR, 500 MHz, $CDCl_3$.

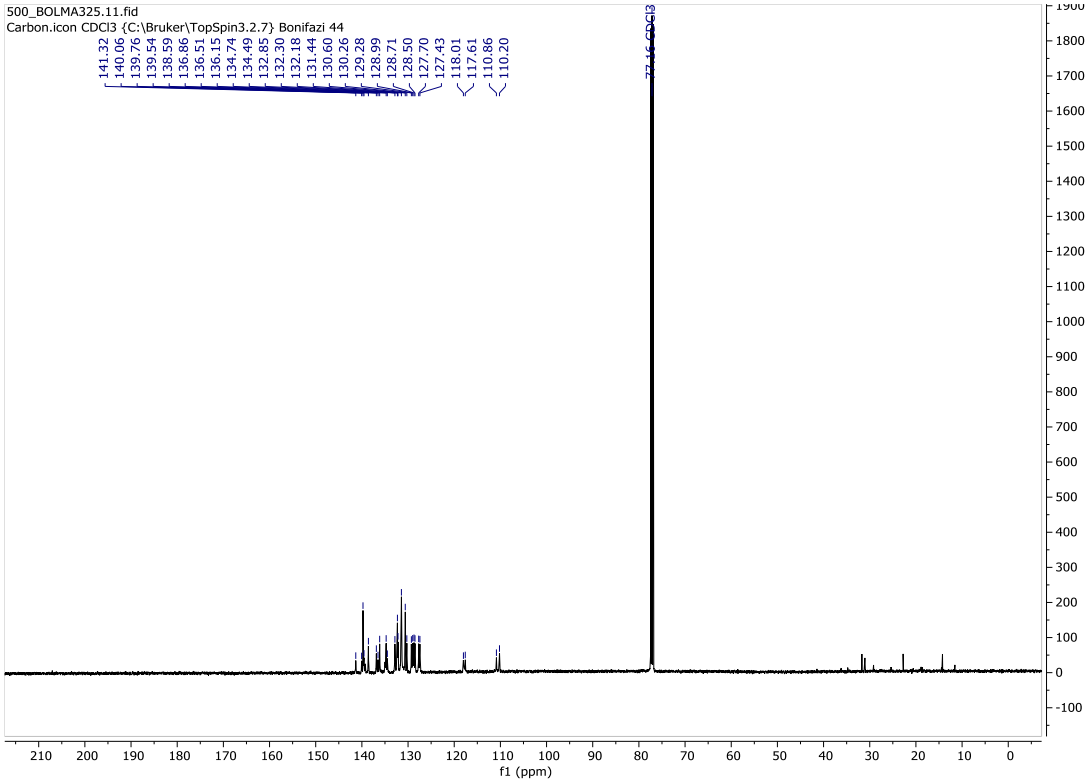

Figure A.222. ^{13}C NMR, 125 MHz, $CDCl_3$.

Elemental Composition Report **Page 1**

Single Mass Analysis
Tolerance = 5.0 PPM / DBE: min = -1.5, max = 200.0
Element prediction: Off
Number of isotope peaks used for i-FIT = 3

Monoisotopic Mass, Odd and Even Electron Ions
5 formula(e) evaluated with 1 results within limits (up to 50 closest results for each mass)
Elements Used:
C: 0-26 H: 0-15 N: 0-2 Cl: 0-2

Minimum:				-1.5				
Maximum:		5.0	5.0	200.0				
Mass	Calc. Mass	mDa	PPM	DBE	i-FIT	Norm	Conf(%)	Formula
425.0616	425.0612	0.4	0.9	19.5	859.7	n/a	n/a	C26 H15 N2 Cl2

Figure A.223. Elemental composition report.

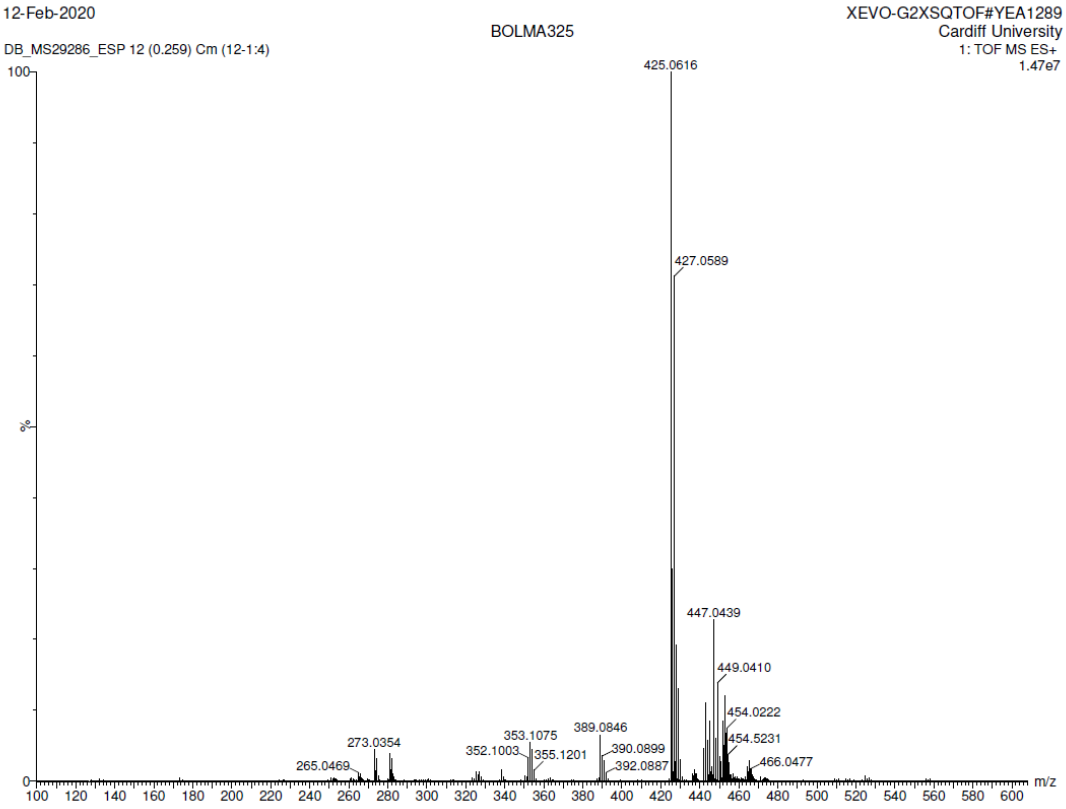

Figure A.224. HRMS, ES+, TOF.

Characterisation of tetraphenylene-2,7-dicarbonitrile 80

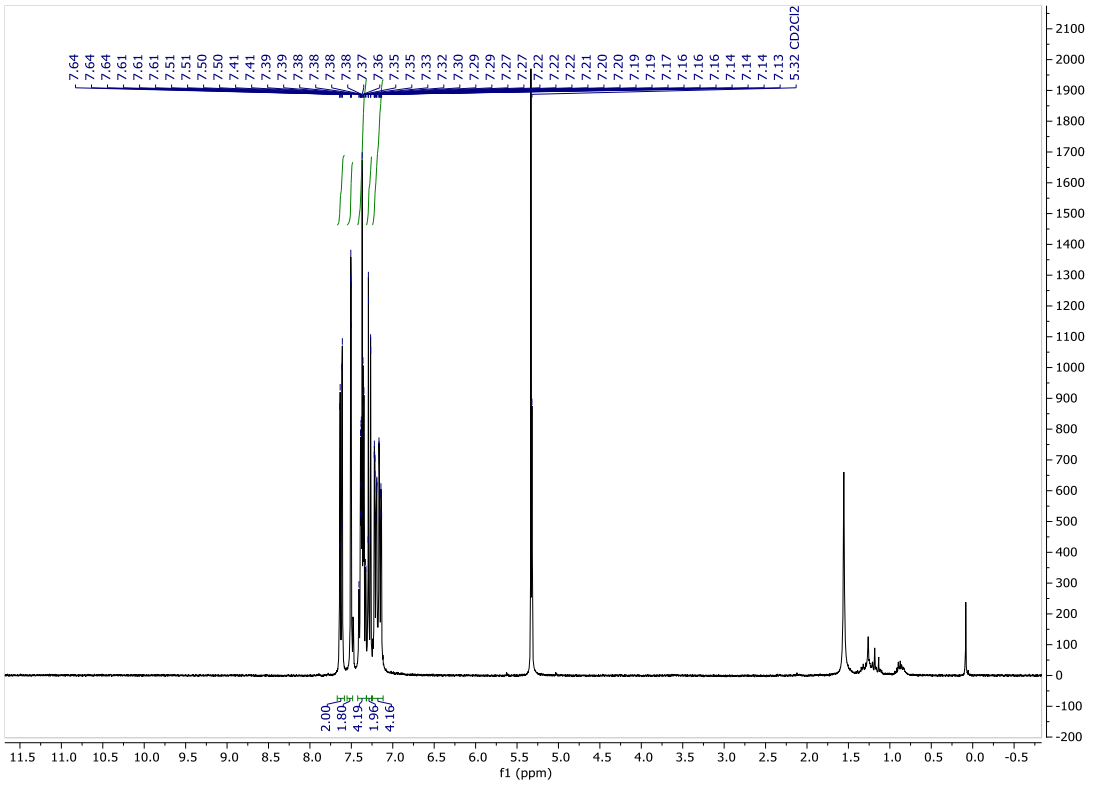

Figure A.225. ^{1}H NMR, 300 MHz, CD_2Cl_2.

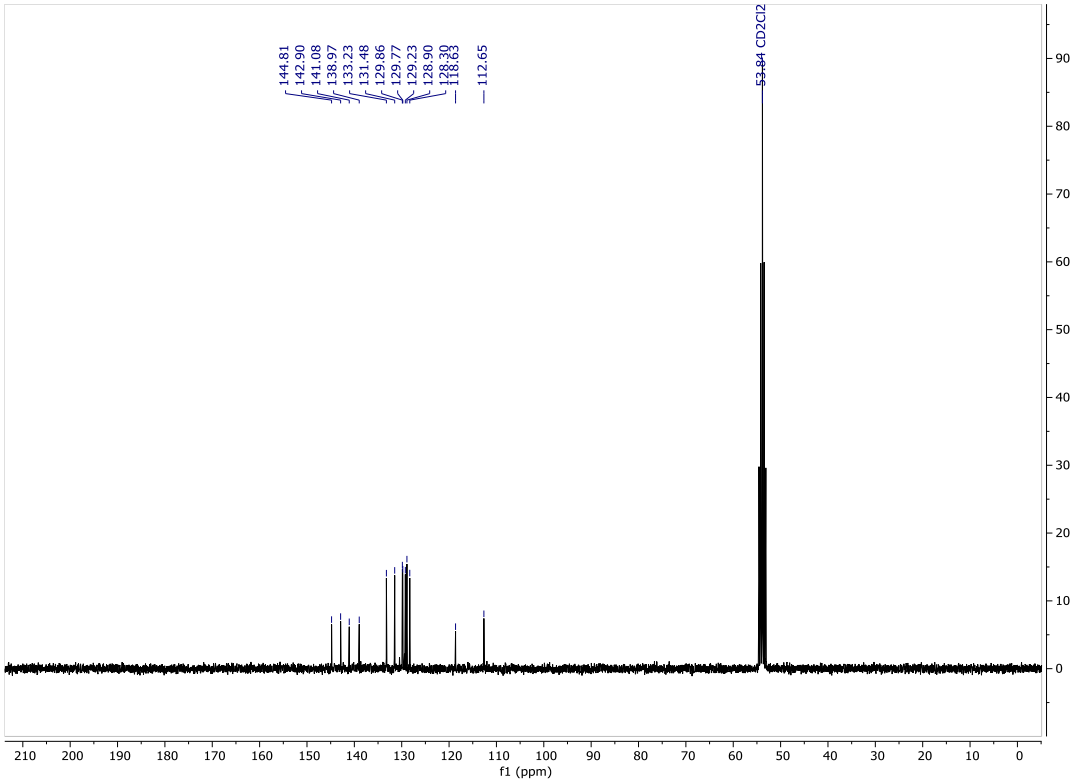

Figure A.226. ^{13}C NMR, 75 MHz, CD_2Cl_2.

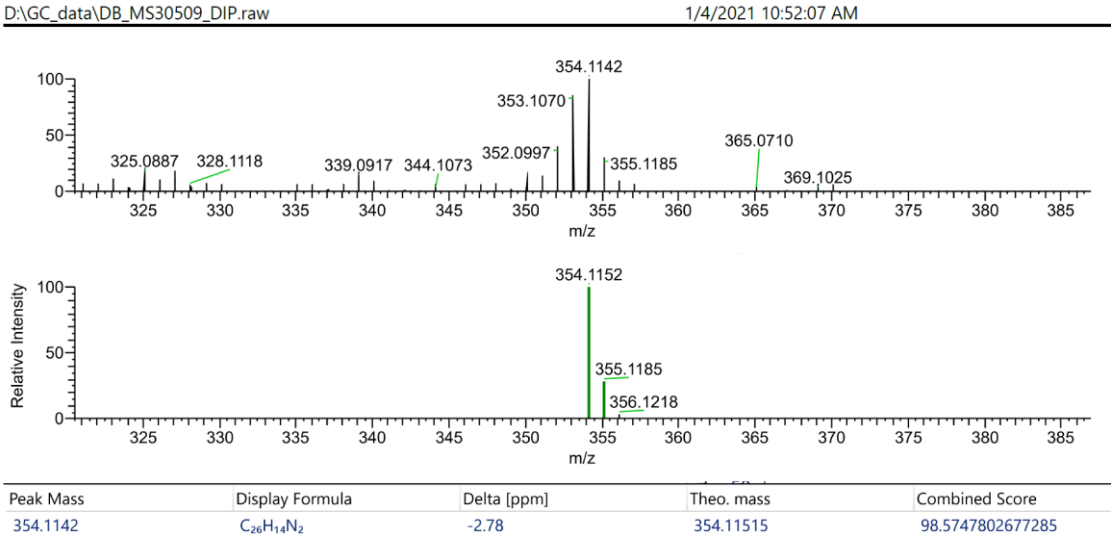

Peak Mass	Display Formula	Delta [ppm]	Theo. mass	Combined Score
354.1142	$C_{26}H_{14}N_2$	-2.78	354.11515	98.5747802677285

Figure A.227. Elemental composition report.

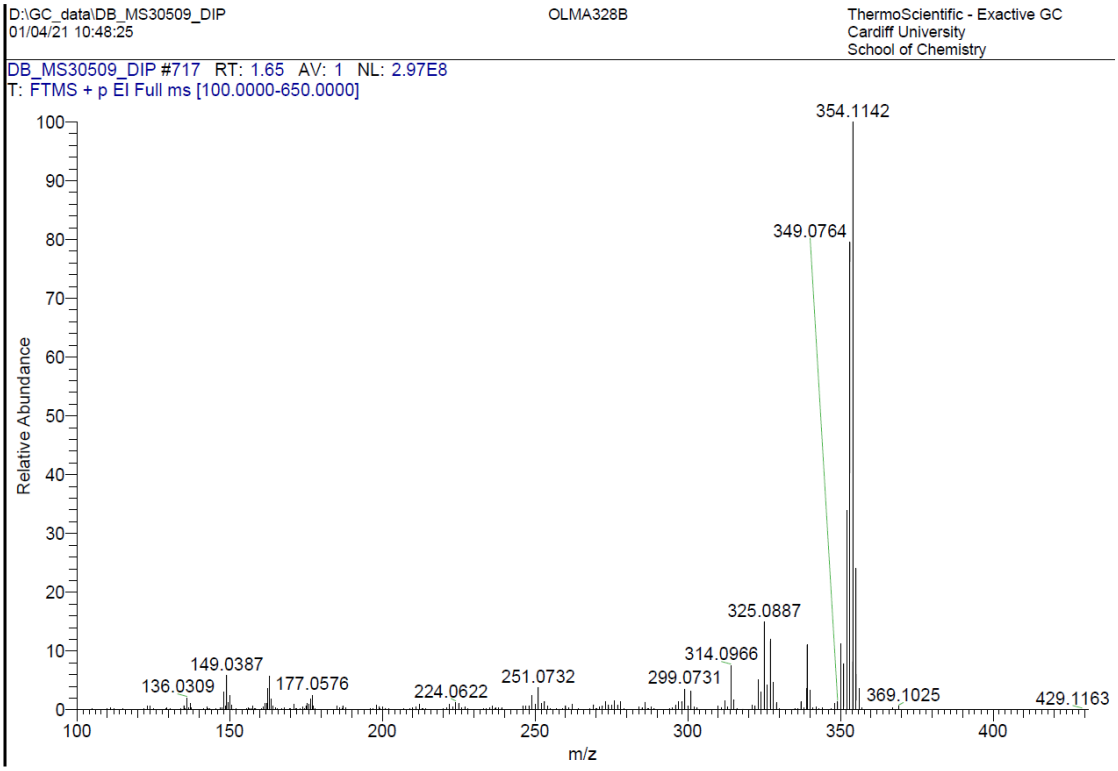

Figure A.228. HRMS, EI+, TOF.